SAPIENZA
UNIVERSITÀ DI ROMA

PhD School of Pharmaceutical Sciences XXVI cicle

"Sapienza" University of Rome

DESIGN, SYNTHESIS AND BIOLOGICAL EVALUATION OF NOVEL EPIGENETIC MODULATORS

Doctoral Dissertation

Submitted by

Donatella Labella

Department of Chemistry and Drug Technologies

Faculty of Medicine and Pharmacy

"Sapienza" University of Rome

Supervisors

Professor Antonello Mai Ph.D. (tutor and main supervisor)
Department of Drug Chemistry and Technology, "Sapienza" University of Rome, P.le Aldo Moro, 5 - 00185 – Rome, Italy.

Adjunct Professor Clemens Steegborn Ph.D. (foreign supervisor)
Department of Biochemistry, University of Bayreuth, NWIII, 95440 Bayreuth, Germany.

The present doctoral dissertation is based on the following original publications and early stage research projects listed below:

LIST OF PUBLICATIONS

1. Upadhyay, A. K., Rotili, D., Han, J. W., Hu, R., Chang, Y., Labella, D., Zhang, X., Yoon, Y. S., Mai, A., Cheng, X. An analog of BIX-01294 selectively inhibits a family of histone H3 lysine 9 Jumonji demethylases. *J. Mol. Biol.* **2012,** 416, 319-327.

2. Valente, S., Trisciuoglio, D., Tardugno, M., Benedetti, R., Labella, D., Secci, D., Mercurio, C., Boggio, R., Tomassi, S., Di Maro, S, Novellino, E., Altucci, L., Del Bufalo, D., Mai, A., Cosconati, S. tert-Butylcarbamate-containing histone deacetylase inhibitors: apoptosis induction, cytodifferentiation, and antiproliferative activities in cancer cells. *ChemMedChem* **2013**, 8, 800-811.

3. Rotili, D., Tomassi, S., Conte, M., Benedetti, R., Tortorici, M., Ciossani, G., Valente, S., Marrocco, B., Labella, D., Novellino, E., Mattevi, A., Altucci, L., Tumber, A., Yapp, C., King, O. N. F., Hopkinson, R. J., Kawamura, A., Schofield, C. J., Mai. A. Pan-histone demethylase inhibitors simultaneously targeting Jumonji C and lysine specific demethylases display high anticancer activities. *J. Med. Chem.*, accepted.

4. Valente, S., Liu, Y., Schnekenburger, M., Zwergel, C., Cosconati, S., Gros, C., Tardugno, M., Labella, D., Florean, C., Minden, S., Hashimoto, H., Chang,Y., Zhang, X., Kirsch, G., Novellino, E., Arimondo, P.B., Miele, E., Ferretti, E., Gulino, A., Diederich, M., Cheng, X., Mai, A. Selective non-nucleoside inhibitors of human dna methyltransferases active in cancer including cancer stem cells, *J. Med. Chem.*, accepted.

5. Rotili, D., Tarantino, D., Marrocco, B., Gros, C., Masson, V., Gregoire, J-M., Ausseil, F., Chang, Y., Labella, D., Cosconati, S., Di Maro, S., Novellino, E., Schnekenburger, M., Grandjenette, C., Bouvy, C., Diederich, M., Cheng, X., Arimondo, P. B., Mai. A. Identification of Quinazoline Analogues as Novel DNA methyltransferase 3A Inhibitors. *J. Med. Chem.* submitted.

In the aforementioned publications the present PhD student Labella Donatella has cured the main part of synthetic work. Modelling and docking simulations, crystallographic investigations, enzymatic and cellular assays have been carried out by the other co-authors.

Abbreviations

2OG, 2-oxoglutarate;

8HQ, 8-hydroxyquinoline;

AdoHcy, *S*-adenosyl-homocysteine

AdoMet, *S*-adenosyl-L-methionine;

AML, acute myeloid leukemia;

APHAs, aroylpyrrolylhydroxamates;

APL, acute promyelocytic leukemia;

AR, androgen receptor;

AZA, Azacytidine;

BAH, bromo-adjacent homology;

BSA, bovine serum albumin;

CaMKs, calmodulin-dependent kinases;

CE; capillary electrophoresis;

CIM, cellular invasion/migration;

CMML, chronic myelomonocytic leukemia;

CoREST, corepressor of RE1 silencing transcription factor;

CPS1, carbamoyl phosphate synthetase 1;

CR, caloric restriction;

CSCs, cancer stem cells;

DAC, Decitabine;

DAPI, 4',6-diamidino-2-phenylindole;

DLT, dose limiting toxicity;

DMEM, Dulbecco's modified eagle medium;

DMLs, designed multiple ligands;

DNMTi, DNA methyltransferase inhibitors;

DNMTs, DNA methyltransferases;

DSB, DNA doublestrand break;

EDCI, 1-ethyl-3-(3-dimethylaminopropyl)carbodiimide;

EIG, enzyme inhibiting group;

ELISA, enzyme-linked immunosorbent assay;

EMT, epithelial-mesenchymal transition;

EZH2, enhancer of zeste 2;

FACS, fluorescence-activated cell sorting;

FAO, fatty acid oxidation;

FBS, fetal bovine serum;

FIH, factor inhibiting HIF;

FOXO, forkhead box O;

Fmoc, 9-fluorenylmethoxycarbonyl;

FRET, fluorescence resonance energy transfer;

GDH, glutamate dehydrogenase;

GLP, G9a-like protein;

HATs, histone acetyltransferases;

HCC, hepatocellular carcinoma;

HCT116, human colorectal carcinoma cell line;

HeLa, Henrietta Lacks cells;

HDACi, HDAC inhibitors;

HIF, hypoxia inducible factor;

HKs, histone kinases;

HMTs, histone methyltransferases;

HPLC, high performance liquid chromatography;

HS, hydrophobic spacer;

Hr, human recombinant;

JmjC, Jumonji C;

KDMs, lysine demethylases;

KO, knockdown;

LNCaP, lymph node carcinoma of the prostate;

LSC, leukemia stem cells;

LSDs, lysine specific demethylases;

LPS, lipopolysaccharide;

LXR, liver's X receptor;

MAOs, mono amine oxidases;

MBDs, methylated DNA-binding proteins;

MCD, malonyl CoA deacarboxylase;

MDS, myeloid dysplasic syndrome;

MEF2, myocyte enhancing factor-2;

MbSCs, medulloblastoma stem cells;

MePR, mesenchymal progenitor cells;

MMP, matrix metalloproteinase;

MTT, 3-(4,5-dimethylthiazol-2-yl)-2,5-diphenyltetrazolium bromide;

MYPT1, myosin phosphatase 1;

NAM, nicotinamide;

N-CoR, nuclear receptor co-repressor;

NES, nuclear export signal;

NLS, nuclear location signal;

NSCLC, non-small-cell lung cancer;

NSD, nuclear receptor SET-Domain;

OAADPr, O-acetyl-ADP-ribose;

OSCC, oral squamous cell carcinoma;

OTC, ornithine transcarbomoylase;

PARP1, poly ADP-ribose polymerase 1;

PBMCs, peripheral blood mononuclear cells;

PC3, prostate cancer cell line;

PCNA, proliferating cell nuclear antigen;

PBMC, peripheral blood mononuclear cell;

PBS, phosphate buffered saline;

PBST, phosphate buffered saline with tween;

PDB, protein data bank;

PDGF, platelet-derived growth factor;

PFS, progression free survival;

PHD2, prolyl hydroxylase domain 2;

PI, propidium iodide;

PMSF, phenylmethylsulfonyl fluoride;

PRCs, polycomb repressive complexes;

PRMT1, protein arginine methyltransferase 1;

PyBOP, benzotriazol-1-yl-oxytripyrrolidinophosphonium hexafluorophosphate;

RB1, retinoblastoma protein 1;

RMPI, roswell park memorial institute medium;

ROI, regions-of-interests;

ROS, reactive oxygen species;

RTCA, real-time cell analyzer;

SAM, S-adenosyl-L-methionine;

SAH, S-Adenosyl-L-Homocysteine;

SMRT, silencing mediator for retinoic acid and thyroid hormone receptors;

STAT3, signal trasducer and activator of transcription 3;

TCA, trichloroacetic acid;

TRD, target recognition domain;

TRF, targeting replication foci;

TSA, trichostatin A;

TSSs, transcription start sites;

TSG, Tumor Suppressor Genes;

TXNIP, thioredoxin-interacting protein;

succPRX1, succinylated Peroxiredoxin 1;

UBHAs, aminoanilides;

UHRF1, ubiquitin-like, containing PHD and RING finger domains 1;

VPA, valproic acid.

Table of contents

1. Epigenetics

As many evidence suggest, the DNA code its self is not the only one to guide the gene expression. Nowadays it is well know that this activity depends on a numerous biological phenomena that have been lumped into the category of epigenetics. The first definition of epigenetics is reliable to Conrad Waddington (1905-1975) that defined epigenetics as "*the branch of biology which studies the causal interactions between genes and their products, which bring the phenotype into being*".[1] Epigenetics is like the bridge between genotype and phenotype: even though the vast majority of cells in a multicellular organism share an identical genotype, organismal development generates a diversity of cell types with disparate, yet stable, profiles of gene expression and distinct cellular functions.[2] Nevertheless, the definition of epigenetics has evolved over time as it is implicated in a wide variety of biological processes: the current definition is "*the study of heritable changes in gene expression that occur independently of changes in the primary DNA sequence*".[3] Most of these changes are established during differentiation and are stably maintained through multiple cycles of cell division, enabling cells to have distinct identities while containing the same genetic information. This heritability of gene expression patterns is mediated, as we will see in detail below, by two major mechanisms, sometimes strictly interdependent, covalent modifications of histone proteins (chromatin remodeling) and methylation of cytosine bases in DNA.[4,5] Failure of the proper maintenance of heritable epigenetic marks can result in inappropriate activation or inhibition of various signaling pathways and lead to disease states such as cancer.[6,7,8] Some researchers are investigating whether subtle modifications to the genome that do not alter its DNA sequence (i.e., epigenetic changes) may also underline common diseases such as diabetes, obesity, heart disease, and a host of psychiatric disorders like manic depression and schizophrenia. Many features of these conditions, such as the differences between pairs of twins in which only one suffers from schizophrenia, cannot be explained readily by DNA-sequence variation. Although some psychiatric disorders seem to run in families, the chance of succumbing depends in some cases on whether this story is on the mother's or the father's side, suggesting that parental imprinting is involved. Moreover, in the mentioned case of twins, substantial differences in their patterns of DNA methylation have been found.[9,10] These findings have led to a global initiative to understand the role of epigenetics in the initiation and propagation of those diseases. The fact that epigenetic aberrations, unlike genetic mutations, are potentially reversible and can be restored to their normal state by epigenetic therapy makes such initiatives promising and therapeutically relevant.

2. DNA methylation

Epigenetics acts mainly through three different mechanisms: DNA methylation, chromatin remodeling and histone modification.

DNA methylation is probably the most extensively studied epigenetic mark. It plays an important part in genomic imprinting, in DNA repair, in X-chromosome inactivation, and in the silencing of retrotransposons, repetitive elements and tissue-specific genes. DNA methylation in humans occurs almost exclusively in the context of CpG dinucleotides clustered in ~1 kb regions, termed CpG islands.[11-13] In addition, it also occurs at regions of lower CpG density that lie in close proximity (~2 kb), termed "CpG island shores".[14,15] Only < 80% of the methylatable CpG population, which represent over 50% of promoters, is methylated. Different CpG sites are methylated in different tissues, creating a pattern of methylation that is gene and tissue specific.[16] This pattern creates a layer of information that confers upon a genome its specific cell type identity.

Moreover, DNA methylation patterns in vertebrates are distinguished by their tight correlation with chromatin structure. Active regions of the chromatin, which enable gene expression, are associated with hypomethylated DNA, whereas hypermethylated DNA is packaged in inactive chromatin.

Therefore, DNA methylation is a highly effective mechanism for silencing of gene expression in vertebrates and plants, either by interfering with the binding of transcription factors, or by attracting methylated DNA-binding proteins (MBDs), able to recruit other proteins and histone modifying enzymes, which leads to formation of a closed chromatin configuration and silencing of gene expression.[17,18]

Noteworthy, DNA methylation patterns are altered in the progression of cancer. Both the hypomethylation and hypermethylation of different regions of the genome play a crucial role in tumorigenesis. During the development of tumors, a genome-wide demethylation occurs and this can promote genomic instability possibly by activating silenced retrotransposons.[19] On the other hand, focal hypermethylation of CpG islands has been intensively studied in cancer. Nearly all types of cancers have transcriptional inactivation of tumor suppressor genes due to DNA hypermethylation.[6] However, the exact mechanism responsible for the appearance of DNA methylation in a given promoter is not fully understood.

The establishment and maintenance of DNA methylation patterns are governed by catalytically active DNA methyltransferase (DNMT) enzymes.[20]

2.1. Chemistry of DNA methylation

Methylation of DNA occurs immediately after replication by a transfer of a methyl moiety from the donor S-adenosyl-L-methionine (SAM, or AdoMet) in a reaction catalyzed by DNMT. In mammals, DNMTs preferentially methylate position 5 of a cytosine in a 5'-CpG-3' (CpG dinucleotide) context, although non- CpG methylation (CpA, CpT or CpC) has been described.[21]

First, it has been shown that the targeted cytosine is flipped out of the DNA double helix into the catalytic site of the enzymes.[22] The thiolate of the catalytic cysteine in motif IV performs a nucleophilic attack on the 6-position of the cytosine, leading to the formation of the corresponding enamine (Figure 2.1). The tripeptide in motif VI, containing a glutamine residue, allows the subsequent protonation in N3-position. A nucleophilic attack of the enamine on the SAM cofactor is followed by deprotonation of the C5 by a base (depending on the DNMT) in the active site, releasing a molecule of S-Adenosyl-L-Homocysteine (SAH). The methyl group creates a steric clash that favors the β-elimination, allowing the recycling of the enzyme and release of the methylated DNA substrate.[23] The added methyl group now allows the recruitment of regulatory proteins with affinity for methylcytosines.

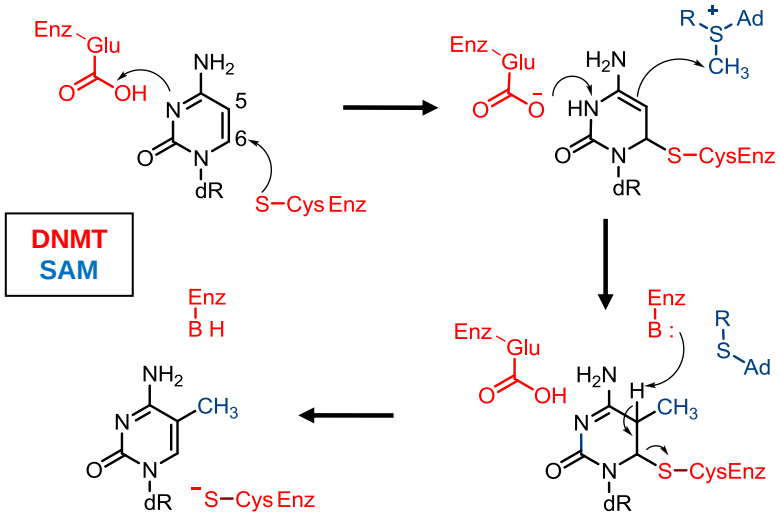

Figure 2.1. Mechanism of reaction catalyzed by cytosine C5 DNA methyltransferases.

2.2. DNA Methyltransferases (DNMTs)

In mammals, DNA nucleotide methyltransferases (DNMTs) include four members, in two families that are structurally and functionally distinct. The DNMT3 family establishes the initial CpG methylation pattern, whereas DNMT1 maintains this pattern during chromosome replication and repair.[24,25] The DNMT3 family includes two active methyltransferases, DNMT3A and DNMT3B, and one regulatory factor, DNMT3-Like protein (DNMT3L).

DNMT1 shows preference for hemimethylated DNA *in vitro*, which is consistent with its role as a maintenance DNMT, whereas DNMT3A and DNMT3B methylate unmethylated and methylated DNA at an equal rate, which is consistent with a *de novo* DNMT role.[26]

DNMT2 appears to provide an example of divergent evolution: it was named based on its high sequence and structural similarity to known DNA MTases, but it actually methylates cytosine 38 in the anticodon loop of $tRNA^{Asp}$.

The catalytically active DNMTs share common features, especially a regulating N-terminal domain and a catalytic C-terminal domain, particularly conserved among different species, including ten sequence motifs (I to X), which form the binding site for the cofactor S-Adenosyl-L-Methionine (SAM).[27,28] Motif IV includes the proline-cysteine dipeptide bearing a catalytic thiolate group. Motif VI contains the glutamine residue allowing the protonation of the 3-position of the cytosine and motif IX maintains the recognition site of the targeted cytosine base (Figure 2.2).[29]

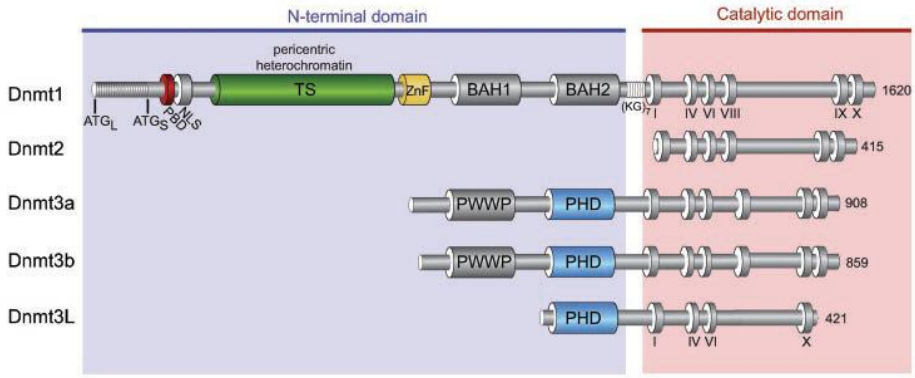

Figure 2.2. Schematic representation of the human DNMT1, TRDMT1 and DNMT3s.

On the other hand, the N-terminal part of DNMTs binds to DNA and has several protein recognition domains, guiding the DNMTs to the nucleus, to chromatin and to numerous proteins, hence tightly linking chromatin modulation and DNA methylation.

2.3. Mammalian DNMTs: characterization and biological role

2.3.1. DNMT1

The DNMT1 (Figure 2.3) was the first DNMT to be purified and characterized.[30,31] This enzyme, the most abundant of all the DNMTs in somatic cells, has 1616 amino acids and can be found as three isoforms in almost every eukaryotes: DNMT1s (somatic cells), DNMT1o (oocyte) and DNMT1p (pachytene).[32, 33] As it has a greater affinity for hemimethylated DNA than unmethylated, it intervenes mainly after DNA replication to methylate the newly synthesized strand.[34,35] Therefore DNMT1 is called "the maintenance methyltransferase".[36]

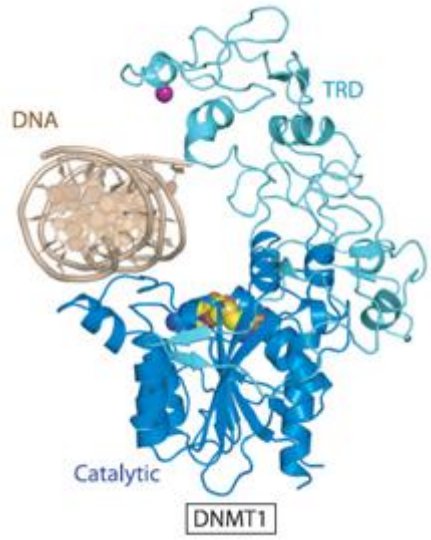

Figure 2.3. ***The crystal structure of the mDNMT1(650–1602)–DNA 19-nucleotide oligomer complex.*** The CXXC, BAH1, and BAH2 domains and CXXC-BAH1 linker of mDNMT1 have been removed for clarity. The bound DNA is in light brown, with the TRD and catalytic core in light and dark blue, respectively.

Disruption of the *Dnmt1* gene in mice can lead to significant demethylation of the genome and strong embryonic lethality. In non-tumoral cells, conditional or total knockout of DNMT1 leads to apoptosis,[37] severe mitotic defects [38] and tumorigenesis through chromosomal instability.[39,40] These results indicate that DNMT1 is essential, both during developmental stages and in somatic cells, to ensure cell proliferation and survival. In cancer cells, disruption of DNMT1 can stop tumor growth and reverse the non-differentiation state, without enhancing the invasiveness of cells, thus providing a very interesting therapeutic target.[41]

DNMT1 is responsible for the maintenance DNA methylation via two different mechanisms: (i) through its direct interaction with the replication fork and (ii) as an interacting partner of UHRF1 (ubiquitin-like, containing PHD and RING finger domains 1).[42] Indeed, at the beginning of the S phase in somatic cells, DNMT1 is transported to the nucleus, thanks to a nuclear location signal (NLS), and more precisely to the replication foci through a specific sequence located within its N-terminal domain (Targeting Replication Foci: TRF) and its PCNA (Proliferating Cell Nuclear Antigen) binding domain (PBD). It then binds to hemimethylated DNA.[43,44] The cytosine to be methylated is flipped out into the catalytic pocket and the methyl group of the SAM cofactor is transferred to position 5. Once the first CpG has been entirely methylated, DNMT1 moves along the newly synthesized DNA strand to further methylate.

The second mechanism implies UHRF1, a protein that has a specific affinity for hemimethylated CpG sites and recruits DNMT1 at these sites. Overall, the maintenance of DNA methylation patterns possesses a gross error frequency of circa 5% per CpG site and per cellular division. This leaves to cells some flexibility for subtle but probable important changes in their methylation pattern. This is balanced

by DNMT3A and 3B that help DNMT1 in the maintenance of the methylation profile during replication.[45]

DNMT1 has a number of sequence motifs shared with other proteins but of unknown or unconfirmed function. DNMT1 contains two bromo-adjacent homology (BAH) domains, which are also found in origin recognition complex proteins and other proteins involved in chromatin regulation. The BAH motif has been proposed to act as a protein-protein interaction module. Near the center of the N-terminal domain is a cysteine-rich region that binds zinc ions, present in all confirmed mammalian cytosine methyltransferases, known mammalian proteins affecting cytosine methylation, as well as the methyl-binding domain (MBD) proteins MBD1 and CpG binding protein.[46]

2.3.2. DNMT2/TRDMT1

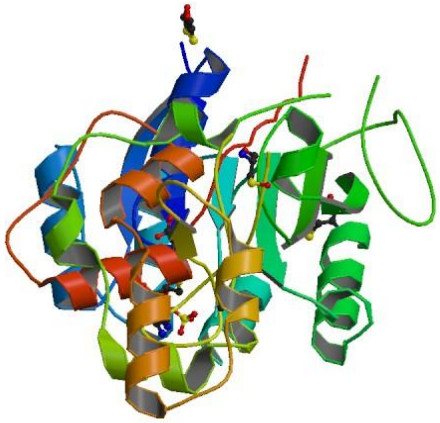

Figure 2.4. Structure of human DNMT2

The DNMT2 enzyme (Figure 2.4) was originally assigned as a member of the DNA methyltransferase family on the basis of its very high degree of similarity in sequence and structure to eukaryotic and prokaryotic DNA-(cytosine C5)-methyltransferases. DNMT2 is strongly conserved and can be found in species ranging from *Schizosaccharomyces pombe* to humans, suggesting a very important role in cellular homeostasis.

The former DNMT2 has been recently renamed as TRDMT1 since it does not methylate DNA but rather a cytosine 38 in the anticodon loop of $tRNA^{Asp}$.[47,48] It has only a very small DNA methyltransferase activity *in vitro* and *in vivo*, suggesting that the N-terminal domain is not absolutely required for this activity, but more for its regulation.[49]

Whereas depletion of DNMT1, DNMT3A, DNMT3B and even DNMT3L genes lead to abnormal phenotypes (male sterility, developmental problems) or even to embryonic death,[50] the depletion of the TRDMT1 gene does not lead to any phenotypic modification. It is, thereby, hypothesized that this enzyme might be

particularly useful not during the embryonic development, but rather during species evolution.

2.3.3. DNMT3 family

The mammalian genome encodes two functional cytosine methyltransferases of the DNMT3 family, DNMT3A and DNMT3B, which primarily methylate CpG dinucleotides, and a third homologue, DNMT3L, which lacks cytosine methyltransferase activity and functions as a regulatory factor in germ cells. DNMT3A has been identified as responsible for the imprinting of genes and methylates mainly pericentromeric regions of the DNA, while DNMT3B seems to methylate centromeric regions.[51] Furthermore, mutations on this latter lead, among other defects, to immunodeficiency syndromes and centromeric instabilities. DNMT3L lacks the catalytic motif and thus shows no methylation activity by itself (Figure 2.2).[52,53] Actually, it is a cofactor of DNMT3A and interacts with histone modifying proteins thus keeping DNA methylation connected to histone modifications. The X-ray crystal structure of the mouse catalytic DNMT3A/3L complex showed the formation of a tetramer: DNMT3L-3A-3A-3L, suggesting the simultaneous methylation of two CpG sites at one helix turn away from one another (circa 10 bp).[54] In addition, it was shown that the complex oligomerizes on the DNA[55] and that DNMT3A/3B are the only DNMTs to possess the proline-tryptophane-tryptophane-proline (PWWP) sequence, which allows them to directly bind DNA.[56] Finally, DNMTs can interact with one another. For example, the N-terminal part of DNMT1 can bind to DNMT3A/3B N-terminal part, conferring to DNMT1 a *de novo* methylation activity.[57,58] Similarly, DNMT3 enzymes can act as maintenance methyltransferases, in a DNMT1 deficient background.[59] Therefore the strict separation of maintenance and *de novo* activity between DNMT1 and DNMT3 is controversial and tend to be reconsidered.[60,61]

2.4. Structure of DNMT1-DNA complexes

The crystal structure of an enzymatically active mouse DNMT1 (mDNMT1; residues 650 to 1602) in complex with S-adenosyl homocysteine (AdoHcy) and a 19-base pair (bp) DNA duplex was solved (3.0 Å resolution). The DNA contained two unmethylated dinucleotide CpG, separated by 8 base pairs. From Figure 2.5, [62] we can clearly detect the CXXC domain (red), BAH1 and BAH2 domains (purple and orange respectively), and the C- terminal methyltransferase catalytic domain (light blue) as also the DNA's 19 bp. The catalytic domain forms the core of the complex and contacts both BAH domainsand the DNA. The CXXC and BAH1 domains are at opposite ends of the methyltransferase domain and are connected by a long linker segment (blu). The BAH1 and BAH2 domains are separated by an a-helical linker (grey), with both BAH domains positioned on the surface far from the bound DNA. There are four Zn^{2+} cations in the structure of the complex, two in coordination within the Cys of CXXC domain, whereas two others involved in coordination with Cys/His of BAH1 and the target recognition domain (TRD) of the methyltransferase.

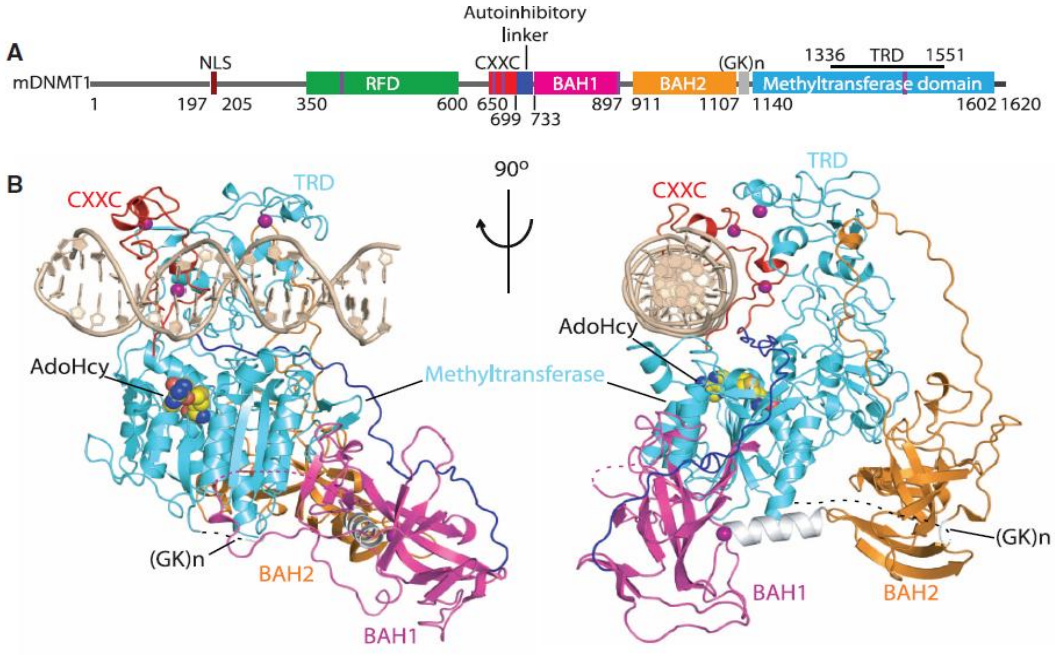

Figure 2.5. mDNMT1(650–1602)-DNA (19-nucleotide oligomer) complex with AdoHcy.

Mouse DNMT1 and human DNMT1 (hDNMT1) exhibit 85% sequence identity. The methyltransferase domain is repositioned relative to the CXXC domain and DNA by a 1-bp translation along the DNA axis (Figure 2.6).

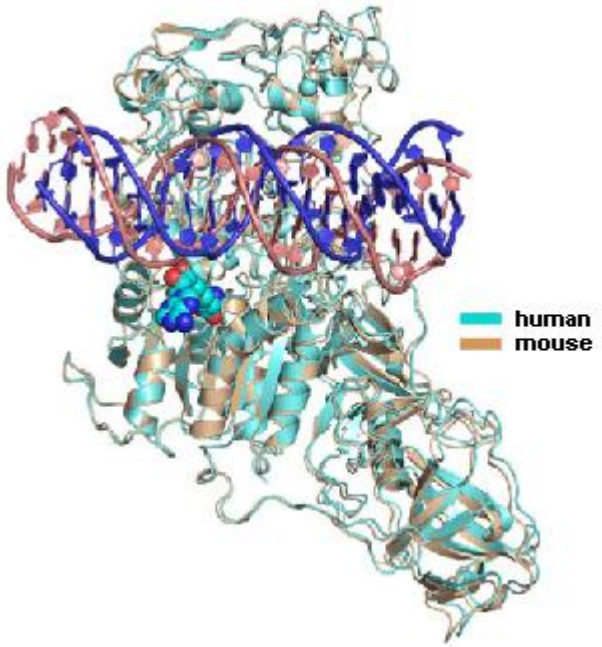

Figure 2.6. Comparison crystal structure human DNMT1 and mouse DNMT1.

All sequence-specific contacts with DNA are made through the CXXC domainin the DNMT1-DNA complex. The CXXC domain targets both the minor and major grooves of the DNA over a CpG-containing 4-bp footprint. The loop segment (Arg^{684}-Ser^{685}-Lys^{686}-Gln^{687}) from the CXXC domain penetrates into the major

groove (Figure 2.7A and 2.7B) and forms base-specific and phosphodiester intermolecular interactions (Figure 2.7C). The guanine bases in the CpG dinucleotide are recognized by side-chain interactions involving Lys^{686} and Gln^{687} of the CXXC domain, whereas the cytosine bases in the CpG dinucleotide are recognized by backbone interactions involving Ser^{685} and Lys^{686} of the CXXC domain. DNA recognition is further anchored by salt bridges between arginine side chains of the CXXC domain and the phosphodiester backbone of the DNA. The CXXC domain has been reported to specifically bind unmethylated CpG dinucleotides.

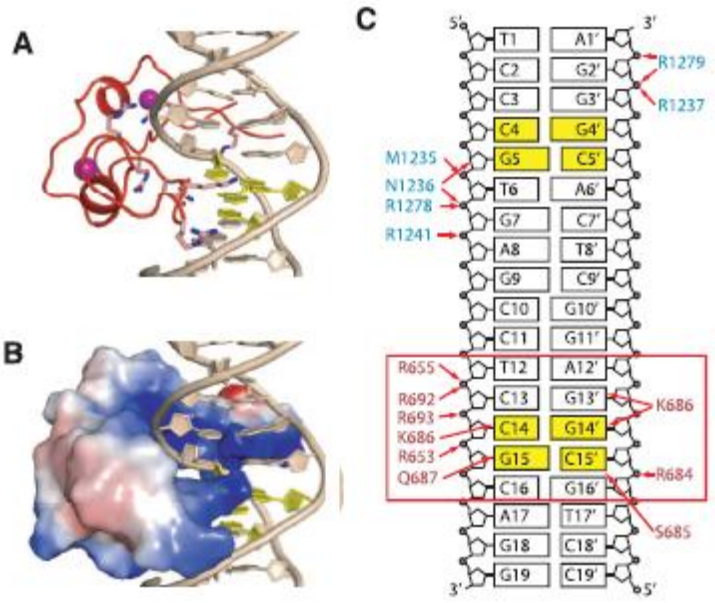

Figure 2.7. A) Ribbon representation of how CXXC domain bound to DNA. B) electrostatic surface representation of CXXC domain bound to DNA. C) intermolecular interaction in the mDNMT1-DNA complex.

2.4.1 Autoinhibitory regulation of DNMT1

The most important finding of Song et al., through the analysis of the crystal structure mDNMT1-DNA/ hDNMT1-DNA (supported by enzymatic assays) is that DNMT1 show an autoinhibitory regulation. The unmethylated DNA is excluded from the active site by the binding of the CXXC domain, because the acidic autoinhibitory CXXC-BAH1 linker move directly between the DNA and the active site, inhibiting the entrance of the DNA in the catalytic pocket. Moreover the BAH2-TRD loops block the TRD in a retracted position and prevents it from binding the DNA major groove. Unmethylated CpG sites are protected from *de novo* methylation through binding by the CXXC domain as CpG dinucleotides emerge from the replication complex (Figure 2.8).[62]

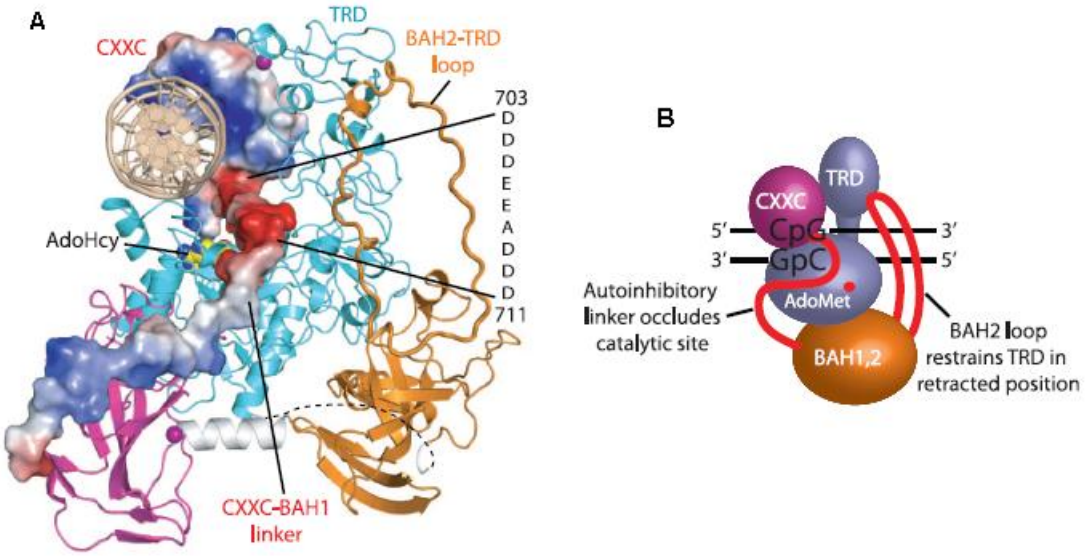

Figure 2.8. A) Representation of mDNMT1-CXXC domain and the CXXC-BAH1 linker in the complex mDNMT1 (1650-1602)-DNA 19-nucleotide oligomer. B) Proposed autoinhibitory regulation of DNMT1.

2.5. DNA methylation and pathologies

Considering their role in the regulation of gene transcription, DNA methylation (as the other epigenetic marks) is essential for crucial processes such as embryonic development or differentiation and is involved in various pathologies, from neurodegenerative diseases to cancers.[63] With the increasing accessibility to genome-wide techniques to study DNA methylation, numerous pathologies have been linked to epigenetic disruptions, particularly diseases that are influenced by the environment. Indeed, since DNA methylation is required in the memory process, it has recently been proved to have an important role, not only in Alzheimer's disease,[64] but also in psychiatric diseases (depression, bipolar disorder, schizophrenia).[65] DNA methylation is clearly involved in auto-immune diseases [66] and even in some genetic disorders (Facioscapulohumeral muscular dystrophy, Crohn disease, atherosclerosis.).[67,68]

Moreover, aberrant DNA methylation patterns have been extensively described in numerous cancers. It has been shown that cancer cells display a global hypomethylation[69] and at the same time a hypermethylation of certain gene promoters.[70] On the one hand, hypomethylation leads to chromosomal instability, since repeated sequences are no longer methylated. On the other hand, hypermethylation leads to silencing of Tumor Suppressor Genes (TSG). As mentioned above, the reversibility of DNA methylation represents an interesting strategy in oncology. Hence, the use of specific inhibitors of DNMT (DNMTi) might reactivate TSG and induce the reprogramming of cancer cells, leading to their proliferation arrest and ultimately to their death (Figure 2.9).[71]

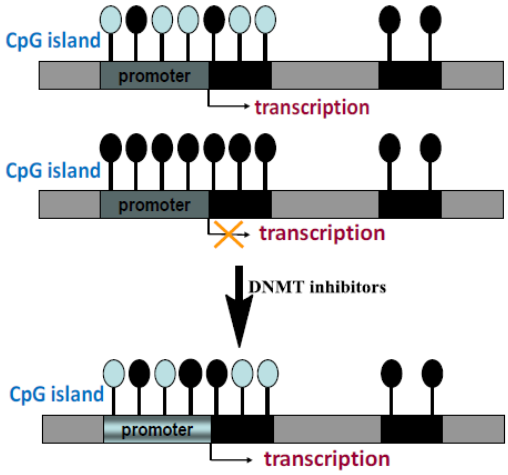

Figure 2.9. Stability and reversibility of epigenetic mutations.

Nevertheless, depleting either one DNMT is sufficient to suppress *in vitro* cell growth. In addition, several studies clearly demonstrated that DNMT1 depletion is sufficient to lead to tumor suppressor genes re-expression and cell growth arrest in various *in vitro* cancer cells such as lung, esophagus, stomach, breast, cervix, brain, head and neck.[72,73]

Overall, these data strongly argue in favor of a selective inhibition of DNMT to achieve an antitumor effect.

2.6. DNMT inhibitors (DNMTi)

As elucidated above, tumor suppressor genes hypermethylation is often involved in cancers and, due to its reversibility, their demethylation can be an interesting therapeutic strategy. Many DNMT inhibitors have been described and are divided into two families: the nucleoside analogues, that have been known and studied for many years, and the non-nucleoside inhibitors, which structure varies according to their inhibitory mechanism.

2.6.1. Nucleoside analogues

2.6.1.1. First generation molecules: Azacytidine, Decitabine and Zebularine

Until now, several DNMT1 inhibitors have been identified. They can be divided into different groups. The first one includes cytidine analogs like 5-azacytidine, 5-aza-2'-deoxycytidine and zebularine (Figure 2.10).[74]

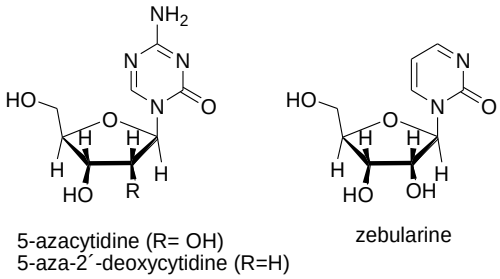

Figure 2.10. Nucleoside analogues inhibitors of DNMTs.

The nucleoside analogues 5-azacytidine (5-Aza-CR) and 5- aza-2'-deoxycytidine (5-Aza-CdR), known clinically as azacytadine (Vidaza®) and decitabine (Dacogen®), respectively, are the two most potent DNMTi. In this molecules, the carbon atom in position 5 is replaced by a nitrogen atom and linked to a ribose or a deoxyribose, respectively (Figure 2.10).

To be active, these compounds need to be integrated into the genome during the S phase (replication) of the cell cycle, allowing a certain specificity towards rapid proliferating cancer cells (Figure 2.11).

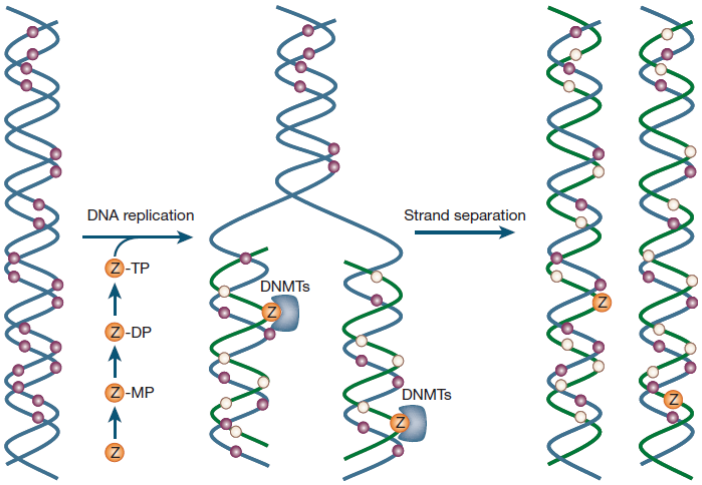

Figure 2.11. Mechanism of action of nucleoside analogue inhibitors. Deoxynucleoside analogues are depicted by Z. Pink circles, methylated CpG; cream circles, unmethylated CpG.

Once into the DNA, the cytosine analogues are recognized by the DNMTs and undergo the same reaction as normal cytosines, with the formation of the covalent intermediate between the catalytic cysteine of the enzyme and 6-position of cytosine analogues. However, unlike with cytosine, the β-elimination reaction can no longer occur because of the presence of the nitrogen atom in 5-position, resulting in a covalent irreversible complex. The enzyme is thereby trapped by the suicide inhibitor, triggering its proteasomal degradation.

At higher doses, these compounds are cytotoxic, therefore they are used at low doses in order to achieve only the demethylation effect with little cytotoxicity. Besides the DNMT inhibition, the ribose analogues are also incorporated into RNA, decreasing the incorporation into DNA and disrupting protein synthesis. This might explain why decitabine is more active than azacytidine, but also why it has also less significant secondary effects, given that the latter can be incorporated not only in dividing cells, but also in quiescent cells.

Together with the HDACi (Histone deacetylase inhibitors), these two compounds are the only "epidrugs" that have been approved, so far, against Myeloid Dysplasic Syndrome (MDS), Acute Myeloid Leukemia (AML) and Chronic Myelomonocytic Leukemia (CMML) for Vidaza® by FDA in 2004 and the European Medicines Agency (EMA), and against MDS and AML for Dacogen® by FDA in 2006. However, these two DNMT inhibitors are not selective towards the different DNMTs and have strong secondary effects, e.g. renal toxicity and myelotoxicity.[75]

Moreover, 5-Aza-CR and 5-Aza-CdR are readily hydrolyzed in aqueous solution and subject to deamination by cytidine deaminase. The instabilities of these compounds inevitably present a challenge to their clinical applications. To improve the stability and efficacy of 5-Azanucleosides, several other cytidine analogues have been developed. For example, zebularine (a cytidine analogue that lacks an amino group in the 4 position of the pyrimidine ring) can inhibit DNMTs and cytidine deaminase after oral administration.[76] The inefficient metabolic activation of this compound has, however, delayed its clinical use as a single agent.

Compared to the suicide analogues, zebularine is used at higher concentrations to obtain the same demethylation levels in cells but is associated with lower cytotoxicity. Nevertheless, no new information related to a possible clinical development of zebularine has been published recently. Moreover, recent studies have shown that, depending on the used nucleoside analogue (azacytidine, decitabine or zebularine), demethylation patterns of tumor suppressor genes promoters are different, reflecting complex and partially overlapping mechanisms of action.

The use of these drugs raises questions regarding their potential to affect non-cancerous cells epigenetically. However, normal cells divide at a slower rate than malignant cells and incorporate less of these drugs into their DNA resulting in less of an effect on DNA methylation. Also, long-term negative effects of DNA methylation inhibitors in patients have not been found to date.[77]

2.6.1.2. Second generation molecules: pro-drugs

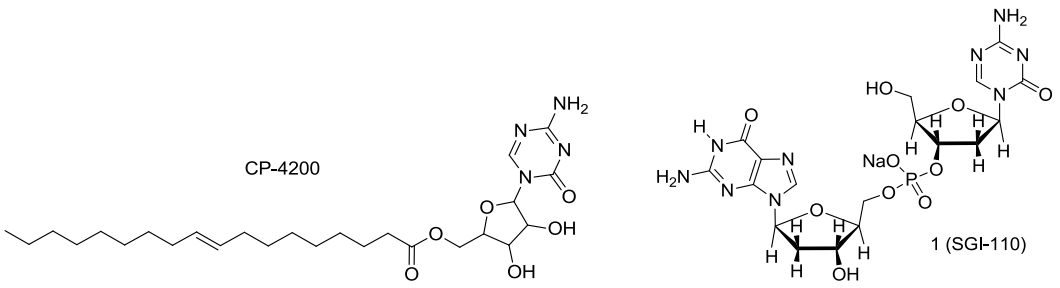

Figure 2.12. Second generation nucleosidic inhibitors of DNMTs.

Despite the advantages of 5-Aza-CR and 5-Aza-CdR, significant challenges stem from the instability of both compounds in aqueous solutions as well as in vivo deamination by cytidine deaminase. Efforts to circumvent problems of metabolic instability have yielded to two different pro-drugs (Figure 2.12).

CP-4200 (Figure 2.12) is an elaidic acid ester of azacytidine that has been synthesized with the intention of rendering drug uptake less dependent unconventional nucleoside transport systems. CP-4200 effectively depletes DNMT1 protein, which suggests that the added metabolic steps required for the activation of CP-4200 do not reduce the concentration of the active metabolite in human cancer cells. Overall, the epigenetic modulatory effects of CP-4200 seemed to be similar to that of azacytidine. It was demonstrated that CP-4200 acts as a pro-drug of azacytidine, presenting the advantage of a delayed delivery of the chemically instable azacytidine.[78]

SGI-110 (formerly S-110, Figure 2.12) is a second generation DNMT inhibitor that acts as a decitabine pro-drug. Deamination of 5-aza-CdR by cytidine deaminase rapidly depletes the plasma level of the drug, resulting in low bioavailability that has been frequently pointed out as one of the major drawbacks of 5-aza-CdR. SGI-110 dinucleotide is resistant to cytidine deaminase deamination due to the substrate specificity of the enzyme, which potentially increase the halflife of the drug, enhance bioavailability, and make the drug more efficacious.[79] SGI-110 is currently in Phase II clinical trials for the treatment of MDS and AML.[80]

Despite the successes of these nucleoside-like inhibitors, their lack of specificity and their strong secondary effects lead to an urgent need for novel more selective DNMT inhibitors.

2.6.2. Non-nucleoside analogues

There is a significant need for DNMT inhibitors that do not rely on DNA incorporation for activity. A recent study using a panel of human cancer cell lines showed a 1000-fold variability in 5-Aza-2′-deoxycytidin (DAC) potency, attributed to differential incorporation of DAC into DNA. As DNA hypomethylation correlates with clinical benefit of DAC in MDS,[81] it is possible that some element of MDS resistance to AZA and DAC stems from the ability of tumor cells to block the

import, phosphorylation, and incorporation of the drugs into DNA. Non-incorporating inhibitors could bypass these hurdles by targeting DNMT directly. Differently from nucleoside analogues, non-nucleoside inhibitors exhibit a wide structural diversity, and can be divided in the following groups.

2.6.2.1. Natural compounds: flavonoids, Psammaplin A and Curcumin

Flavonoids are polyphenolic compounds, mainly extracted from plant, and have enhanced considerable interest recently due to their potential antiviral, anti-inflammatory and antitumor activity.

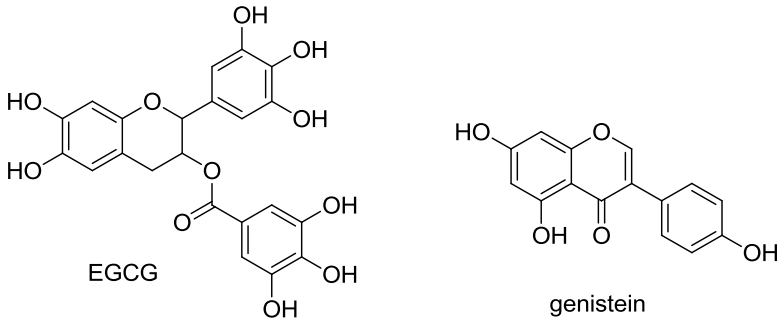

Figure 2.13. Flavonoids as DNMT inhibitors.

One of well-known polyphenol molecule is Genistein (Figure 2.13). It was first isolated from Dyer's Broom (*Genista tinctoria*) in 1899 by Perkin and Newbury, then Baker and Robinson characterized and first synthesized the isoflavone nucleus in 1928.[82] Initially, Genistein has been considered a phytoestrogenic molecule, then a potential anticancer agent because it showed *in vitro* activity against diverse enzymes such as topoisomerase I or II, histidine kinase, tyrosine kinases and protooncogene HER-2.

Another important studied flavonoid is (-) epigallocatechin-3-O-gallate (EGCG, Figure 2.13), a major component of green tea extracts. EGCG is generally considered to be the biologically most active compound *in vitro*. The changes in the activities of various protein kinases, growth factors, and transcription factors represent a common mechanism involved in cellular effects of tea polyphenols. In addition to modification of intracellular signaling by activation of cellular receptors, it was shown that EGCG can enter the cells and directly interact with their molecular targets within cells.[83]

Recently, EGCG and Genistein have been reported as enzymatic and cellular DNMT inhibitors: EGCG directly inhibited DNMT activity and partially reversed RAR-β methylation status, Genistein (20-50 mmol/L) dose-dependently inhibited DNMT activity, showing competitive and noncompetitive inhibition with respect to the substrate poly(dI-dC)· and noncompetitive inhibition with respect to SAM. Genistein was a weaker DNMT inhibitor than EGCG, yet it was just as active or more active in demethylating hypermethylated genes and reactivating their expression. One possible reason is that Genistein is more stable than EGCG in the cell culture medium,

reaching so higher intracellular concentrations than EGCG. Another possibility is that Ggenistein is also an inhibitor of histone deacetylase (HDAC). The extent of demethylation was enhanced by extending the treatment period with EGCG or Genistein or by its combination with a HDAC inhibitor.[84]

The supposed mechanism of action of flavonoids is that they inhibit enzymatic DNA methylation in vitro largely by increasing the formation of *S*-adenosyl-L-homocysteine (a potent noncompetitive inhibitor of DNMTs) during the catechol-*O*-methyltransferase-mediated *O* methylation of this flavonoids. In comparison, the strong inhibitory effect of EGCG on DNMT-mediated DNA methylation is independent of its own methylation and is largely due to its direct inhibition of the DNMTs.[85]

These two flavonoids are now regarded more as chemopreventive drugs than actual treatment drugs, even though their metabolisms drastically decrease their biodisponibility, hence lowering their potential activity.

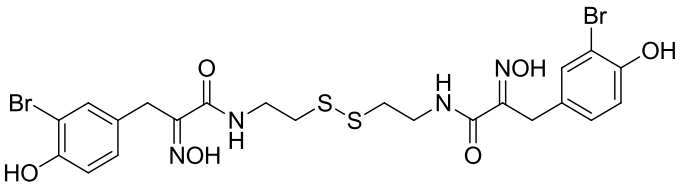

Figure 2.14. Structure of Psammaplin A.

Psammaplin A (Figure 2.14) is a natural compound extracted for the first time in 1987 from a sponge, the *Psammaplin Aplysilla*. This dimer of two derivatives of 3-bromotyrosine was synthesized primary in 1992 by Hoshino et al. and show both antibacterial and antitumor properties.[86]

Psammaplin A was described as inhibitor of almost ten different enzymes, such as leucine aminopeptidase, DNA gyrase, topoisomerase II, HDACs and DNMTs.[87]

It has been shown that several natural derivatives of psammaplin A, have an activity against DNMT1 and HDACs. Moreover Psammaplin A have antiproliferative properties also on MDA-MB- 435 and A549 cell lines (breast and lung cancer, respectively) with promising results, indeed it inhibits cell growth at low doses (IC_{50}= 2 μM). Nevertheless, no DNA demethylation has been highlighted in HCT116 cells,[88] and, in a recent study, Psammaplin A exhibited no activity on DNMT1 at 30 and 120 μM.[89]

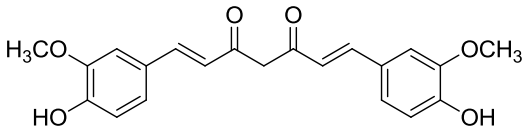

Figure 2.15. Structure of curcumin.

Molecular docking of the interaction between curcumin and DNMT1 suggested that curcumin (Figure 2.15) covalently blocks the catalytic thiolate of DNMT1 to

exert its inhibitory effect on DNA methylation. This was validated by showing that curcumin inhibits the activity of M. SssI with an IC_{50} of 30 nM, but no inhibitory activity of hexahydrocurcumin up to 100 μM. [90] Finally, curcumin at doses higher than 3 mM induced a decrease of global DNA demethylation of leukemia MV4-11 cells.

However, recent studies showed no curcumin-dependent demethylation, which suggested that curcumin has little or no pharmacologically relevant activity as a DNMT inhibitor.[91,92] The fact that the number of studies showing positive effects of curcumin is much higher than that showing negative effects, it may just indicate that there are more researchers evaluating the beneficial effects of curcumin than evaluating its toxicity. Future research is needed to establish the benefit-risk profile of curcumin. Recently, the activity of novel curcumin analogues EF31 and UBS109 as demethylating agents were investigated, by El-Rayes et al., in two pancreatic cell lines.[93] They selected the pancreatic cell lines based on baseline level of DNA methylation. MiaPaCa-2 cells have high levels of DNA methylation associated with loss of tumor suppressor gene SPARC, p16 and E-cadherin. In contrast, PANC-1 cell lines have low levels of baseline DNA methylation and expression of SPARC, p16, and E-cadherin. The EF31 and UBS109 show several folds more potency than curcumin and inhibit DNMT-1, NF-κB and HSP90. In addition, UBS109 and EF31 analogues have better solubility and bioavailability. The unique properties of UBS109 and EF31 make them promising therapeutic agents better than the parent compound curcumin.

2.6.2.2. Inhibitors identified by virtual screening: nanaomycin A and RG108

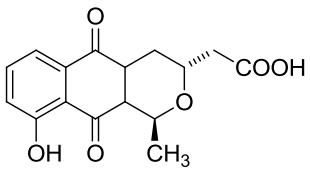

Figure 2.16. Structure of nanaomycin A.

Nanaomycin A (Figure 2.16) is a quinone antibiotic isolated from a *Streptomyces* strain, in 1975. Its DNMT1 potential inhibitory properties have been deduced after a virtual in silico screening,[94] but exhibited no activity when evaluated on DNMT1 biochemical assay. During further investigations, nanaomycin A demonstrated a selective inhibition of DNMT3B. Subsequent cellular characterization was undertaken, specifically cytotoxicity evaluations and DNA methylation level examination on three cancer cell lines (A549, HCT116 and HL60, lung, colon and leukemia cell lines, respectively). Molecular docking calculation using a homology model of DNMT3B resulted in a possible model of nanaomycin A into the catalytic domain. However, despite the effects observed on the enzyme and a weak but significant demethylation of the RASSF1A promoter region, the authors concluded

that DNMT3B inhibition is not the only mechanism of action of nanaomycin A and may share other cellular targets.[95]

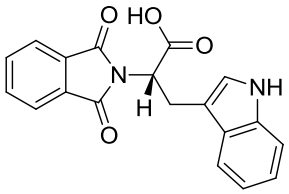

Figure 2.17. Structure of the phtalimido-L-tryptophan RG108.

RG108 is a small-molecule inhibitor of DNMT1 that was discovered using a computational screening approach.[96] The compound blocked DNA methyltransferase activity in vitro and in cells inhibited the methylation of tumor-suppressor gene promoter DNA, but not DNA in centromeric satellite elements, suggesting a context-dependent DNA methylation inhibition.[97] RG108, unlike the nucleoside analogs AZA, DAC, zebularine, procaine, and EGCG, did not demonstrate cytotoxic or genotoxic effects on cells even at high concentrations.[98] A broad application of RG108 is however limited due to its high hydrophobicity.[99]

2.6.2.3. Drugs used for other indications: hydralazine, procain, procainamide, SGI-1027.

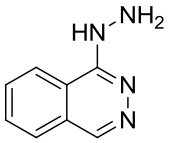

Figure 2.18. Structure of the antihypertensive hydralazine.

Hydralazine (Figure 2.18) is a cardiovascular drug that was shown to inhibit DNA methylation in cells,[100-102] although not in an *in vitro* biochemical assay.[102] Despite its frequent use for numerous years, its mechanism remains unknown. Indeed, hydralazine induces the erythematosus lupus in treated patients and this autoimmune disease is associated with a hypomethylation of T cells, confirmed on T cells in culture.[103] The DNMT inhibitory activity of hydralazine is controversial, as a subsequent study was unable to reproduce DNMT inhibitory activity in cells.[104,105] Clinical studies of hydralazine in combination with a histone deacetylase inhibitor (valproate) in MDS are undergoing, currently in phase II.[106] Moreover, hydralazine is currently tested in phase III on patients that have developed brain or ovary tumors.[107] Hydralazine is therefore, a promising molecule in anti-cancer treatments.

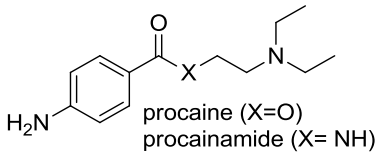

Figure 2.19. Structures of procaine and procainamide.

Procainamide (Figure 2.19) is another cardiovascular drug with apparent activity against DNMT in cells.[100,101] Like hydralazine, however, the DNA methylation inhibition of procainamide in cells has been disputed.[103] Procaine, a closely related molecule, has also been reported to inhibit DNA methylation in cells,[108] although this effect was not confirmed by an independent follow-up study.[109]

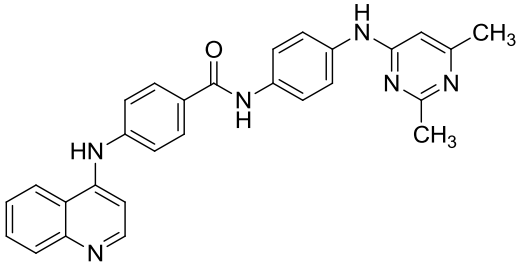

Figure 2.20. Structure of SGI-1027.

SGI-1027 (Figure 2.20), a quinoline-based compound, has demonstrated inhibitory activity against DNMT1, DNMT3A, and DNMT3B in biochemical assays and resulted in decreased methylation at tumor suppressor gene CpG islands and corresponding gene upregulation.[110]

Quinolinium bisquaternary salts related to SGI-1027 are known to bind reversibly but strongly in the minor groove of DNA.[111,112] The non quaternized, weakly basic compound SGI-1027 also binds reversibly but much less strongly to DNA, is indefinitely stable in aqueous solution, is highly lipophilic and has a low polar surface suggesting a good distribution and cell uptake abilities.

SGI-1027 is not a competitive inhibitor of DNA but of the cofactor SAM, all DNMTs are inhibited by SGI-1027 due to the very conserved motifs I and X (involved in the recognition of the SAM cofactor).

3. The role of covalent histone modifications and chromatin remodeling

Another very important mechanism in the epigenetic regulation of gene expression is the chromatin remodelling. The basic unit of chromatin is the nucleosome, which consists of 146 base pairs of DNA wrapped around an octamer of core histones, including two molecules of H2A, H2B, H3 and H4 (Figure 3.1).[113,114]

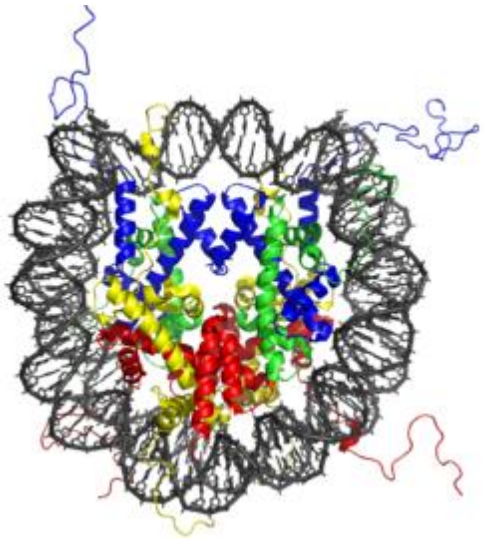

Figure 3.1. The crystal structure of the nucleosome core particle consisting of H2A , H2B , H3 and H4 core histones, and DNA. The view is from the top through the superhelical axis.

Chromatin can transit between 'open' (euchromatin) and 'closed' (heterochromatin) states. Heterochromatin mediates transcriptional repression, whereas transcriptionally active genes are in areas of open chromatin (Figure 3.2).[115,116] It is important to remember that nucleosomes are not static, and their dynamic nature, allowing nucleosomal DNA to transiently unwrap and rebind the histone octamer, can give transcription factor access to DNA, albeit at various rates.

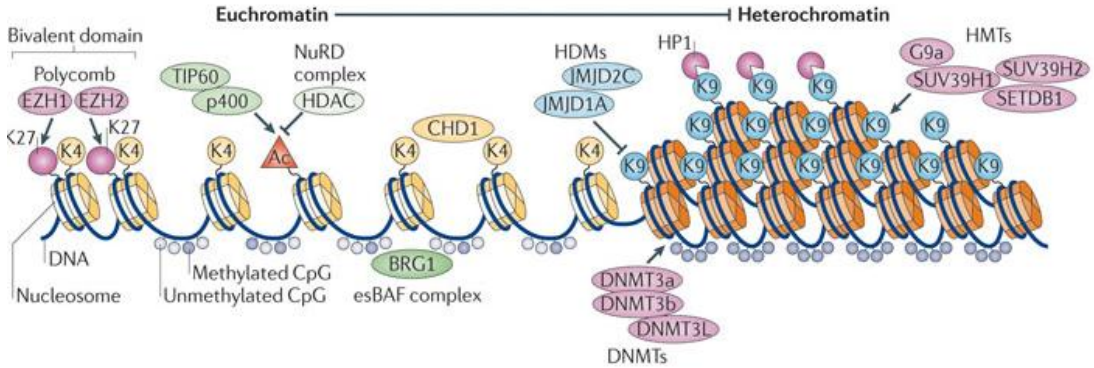

Figure 3.2. Heterochromatin (transcriptional repression) and euchromatin (transcriptional activation).

Nuclear histones, are integral and dynamic components of the machinery responsible for regulating not only gene transcription, but also other DNA-templated processes such as replication, repair, recombination and chromosome segregation. There are four families of chromatin-remodeling enzymes, based on shared structural or functional domains outside the enzymatic core: SWI/SNF, ISWI, CHD, and inositol-requiring 80 (INO80). The SWI/SNF family includes RSC and functions in the sliding and eviction of nucleosomes. ISWI remodelers function in nucleosome assembly and spacing. ISWI is also proposed to have functions in higher-level chromatin organization. CHD remodelers are associated with nucleosome sliding, eviction, spacing, and nucleosome assembly. The INO80 family is specialized for restructuring the nucleosome, including the sick with rat8ts (SWR1) family member, which is achieved by replacement of H2A-H2B dimers with dimers containing the histone variant H2A.Z and H2B.[117,118]

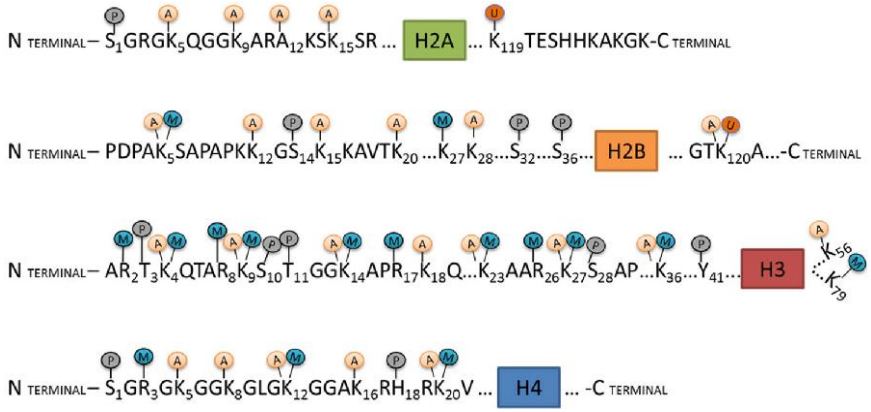

Figure 3.3. Major modifications on histones: acetylation (A), methylation (M), phosphorylation (P) and ubiquitination (U).

An extensive literature shows an elaborate collection of post-translational modifications including acetylation, phosphorylation, methylation, ubiquitylation and ADP-ribosylation that take place on the 'tail' domains of histones.[119-121] These tails, which protrude from the surface of the chromatin polymer and are protease sensitive, comprise ~25-30% of the mass of individual histones,[122] thus providing an exposed surface for potential interactions with other proteins.[123,124] Histone tails of H3 and H4 particularly are targeted from the mentioned covalent modifications. These modifications performed by histone acetyltransferases (HATs), deacetylases (HDACs), methyltransferases (HMTs) and kinases (HKs) offer a mechanism by which upstream signalling pathways can converge on common targets to regulate gene expression. Because of their implications in the pathogenesis and treatment of human diseases, a deeper understanding of the coordinated and antagonistic functions of chromatin remodeling and modifying enzymes is likely to have significant human health impacts.

4. Histone phosphorylation

Histone phosphorylation controls many important cellular processes, including transcription, apoptosis, DNA repair, and chromosome condensation. Histone phosphorylation involving Ser-10 of histone H3 is critical during interphase because it confers transcriptional activation on a number of genes depending on upstream signaling pathways, the location of Ser-10 residue in close proximity to other modifiable residues in the H3 tail enables a variety of crosstalk between phosphorylation and other modifications such as methylation and acetylation.

For gene activation, it is well known that H3S10 phosphorylation inhibits H3K9 methylation, facilitates H3K4 methylation, and enhances H3K14 acetylation, which allows further chromatin decondensation. A variety of H3S10 kinases, including Aurora B, are involved in this crosstalk.[125]

Furthermore there is a strong crosstalk between phosporylation and methylation during AR-dependent gene activation process in prostate cancer. Importantly, PKCβ-dependent phosphorylation of H3T6 prevents LSD1 from demethylating H3K4 and accelerates the demethylation of H3K9 by altering substrate specificity of LSD1.[126]

5. Histone ubiquitylation

Unlike the small covalent additions ubiquitin adds approximately 8.5 kDa to the overall mass of a histone (~11–15 kDa). Currently, histone ubiquitination has only been observed within the C-terminal domains and only at a single lysine residue within histones H2A (K119) and H2B (K120) in vivo.[127-129] The addition of ubiquitin occurs through a multistep process that involves three distinct enzymatic reactions. Alterations in the enzymes that regulate histone ubiquitination and deubiquitination pathways directly impact higher-order chromatin structure.[130,131] Ubiquitination of mammalian H2B occurs at K120 and is predominantly regulated through the enzymatic activities of ubiquitin-conjugating enzyme E2A (UBE2A or RAD6A) and the RNF20/RNF40 ubiquitin ligase complex.[132,133] Altered expression of UBE2A and RNF20/RNF40 is suggested to be a pathogenic event that contributes to the development and progression of various tumor types. Recently the ubiquitination of H2B has been implicated in DNA doublestrand break (DSB) repair. Furthermore, cells in which either RNF20 or RNF40 were independently or simultaneously silenced exhibited significant increases in DSBs which strongly implicates H2Bub1 in DNA DSB repair.[134]

6. Histone acetylation

Acetylation of the lysine ε-amino group, first discovered on histones, is a dynamic post-translational modification regulated by the opposing activities of lysine acetyltransferases (HATs) and histone deacetylases (HDACs).[135,136]

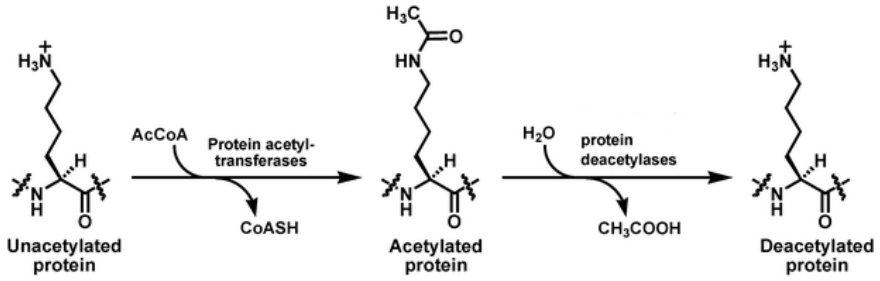

Figure 6.1. Acetylation/deacetylation reactions on lysine ε-amino groups.

The substrates for HATs and HDACs are the ε-amino groups of lysine residues in the N-terminal regions of histones. A highly acetylated core histones is associated to transcriptionally active genes whereas transcriptional repression is associated with low levels of histone acetylation. Inside the nucleosome, hypoacetylated histones (positevily charged) are tightly bound to the phosphate backbone of DNA, maintaining chromatin in a transcriptionally silent state. Acetylation, however, neutralizes the positive charge on histones, disrupting higher-order structures in chromatin, thereby enhancing access of transcription factors, transcriptional regulatory complexes and RNA polymerases to promoter regions of DNA.[137-139]

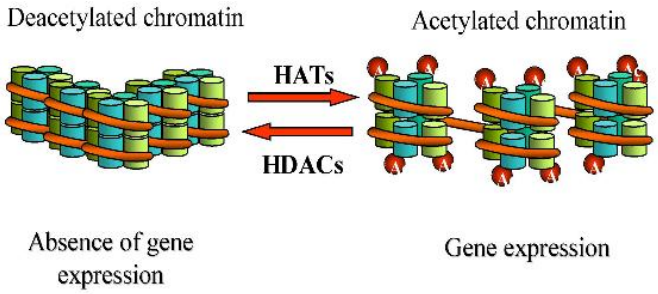

Figure 6.2. Status acetylation of histone.

6.1. Histone acetyltransferase

Allfrey and colleagues, back in 1964, showed that histones can be modified by the addition of acetyl groups. Over the course of the next 15 years, a number of studies correlated the acetylation of histones with gene activity, but only in the 90's the enzymes that mediate histone acetylation and deacetylation have been identified and characterized.[140]

Histone acetyltransferases are a diverse set of enzymes that can be grouped on the basis of their catalytic domains. Gcn5 is the founding member of the Gcn5 *N*-

acetyltransferases (GNATs), and this family includes Gcn5, PCAF, Elp3, Hat1, Hpa2 and Nut1. The MYST HATs are named for the founding members of this family: Morf, Ybf2 (Sas3), Sas2 and Tip60.[141] These two families of HATs are the predominant ones, but other proteins including p300/CBP (CREB: cyclic AMP response element-binding), Taf1 and a number of nuclear receptor co-activators, have also been shown to possess intrinsic HAT activity.

The multiprotein complexes in which HATs reside also vary. Different HAT complexes are composed of various unique subunits. The combinations of these subunits contribute to the unique features of each HAT complex. For example, some subunits have domains that cooperate to recruit the HAT to the appropriate location in the genome; these include bromodomains, chromodomains, WD40 repeats, Tudor domains and PHD fingers. For example, Gcn5 contains a bromodomain that is important for the binding, recognition and retention of SAGA on acetylated promoter nucleosomes.

The discovery that the tumour suppressor p53 is acetylated by p300/CBP, a member of the orphan class of HATs, showed that some HATs can also acetylate non-histone substrates.[142] It is now known that binding of p53 to p300/CBP through its PXXP proline rich domain mediates the DNA-dependent acetylation of p53, thereby stabilizing the acetylated p53-p300/CBP complex.[143]

HATs can function in both transcriptional activation and repression, further analyses are needed to understand how these single enzymes associated with other proteins, can regulate this swicth.

6.2. Histone deacetylase

Until now eighteen mammalian deacetylase enzymes have been identified, and these can be divided into four classes: class I, II, IV and III, based on their sequence homology to their yeast orthologues Rpd3, HdaI and Sir2, respectively.[144-146]

Class I (HDAC1, 2, 3, 8) are expressed ubiquitously in various cell lines and they are all located in nucleus. Based on sequence homology among their deacetylase domains, class II is further divided into two subclasses: IIa (HDAC4, HDAC5, HDAC7 and HDAC9 are believed to shuttle between nucleus and cytoplasm) and IIb (HDAC6 and HDAC10 contain two catalytic domains and are also shown to shuttle between nucleus and cytoplasm, but mainly in cytoplasm).[147-149] As for class IV, there is only one member, HDAC11, about which little is known.[150] All these 11 isoforms are dependent on Zn^{2+} for them deacetylase activity.[151]

These enzymes possess a highly conserved catalytic domain of approximately 390 amino acids but the class II proteins are two to three times larger in size than the class I proteins (120-130 kDa and 42-55 kDa, respectively) and there are certain conserved sequence motifs in the catalytic domain that differ between the two classes.

CLASS	HDAC	INTERACTION	CELLULAR LOCALIZATION	TISSUE EXPRESSION
I	HDAC1	DNMT1, ATM, BRCA1, MECP2, MyoD, p53, pRb, NF-kB	Nuclear	Ubiquitous
	HDAC2	DNMT1, BRCA1, pRb, NF-kB, GATA-2, Bcl-6	Nuclear	Ubiquitous
	HDAC3	pRb, NF-kB	n/c	Ubiquitous
	HDAC8	a-SMA	n/c	Ubiquitous
IIA	HDAC4	14-3-3, MEF2, calmodulin, GCMa, GATA-1, HP-1	Shuttling n/c	Heart, muscle, brain
	HDAC5	14-3-3, MEF2, calmodulin, Smad7, HP-1, GCMa	Shuttling n/c	Heart, muscle, brain
	HDAC7	14-3-3, MEF2, calmodulin, FLAG1&2, HIFa, Bcl-6	Shuttling n/c	Heart, placenta, pancreas, muscle
	HDAC9	FOX3P	Shuttling n/c	Muscle, brain
IIB	HDAC6	a-tubulin, HSP90, SHP, Smad7	Cytoplasmic	Kidey, liver, heart, pancreas
	HDAC10	HSP90, PP1, LcoR	Cytoplasmic	Sleen, kidney, liver
IV	HDAC11	HDAC6	n/c	Heart, muscle, kidney, brain

n/c: nuclear and cytoplasmic

Table 6.1. HDAC isoforms.

Members of class I and II HDACs are subunits of multiprotein nuclear complexes that play a crucial role in repression of DNA transcription. HDAC1 and 2 have been found in the CoREST complex that inactivates the expression of neuronal genes in

non-neuronal tissues and also as components of NURD and SIN3 repressor complexes.[152,153]

The cellular trafficking of class IIa members (HDAC4, 5, 7, 9) are defined by intrinsic nuclear import and export signals as well as binding sites for 14-3-3 proteins, indeed these isoforms contain three conserved 14-3-3 binding sites. Binding of the 14-3-3 proteins stimulate the nuclear export or cytoplasmatic retention of the class IIa HDACs in a phosphorylation dependent manner that consequently regulates the activity of transcription factors like the myocyte enhancing factor-2 (MEF2).[150,154,155] Moreover the phosphorylation of these 14-3-3 binding sites depend on several signalling pathways including salt-inducible kinases,[156] microtubule affinity-regulating kinases [157] and Ca^{2+}/calmodulin-dependent kinases (CaMKs).[154]

In addition, class II HDACs differ from class I proteins depending on their tissue expression, subcellular localization and consequently biological roles. Class I HDACs are ubiquitously expressed, whereas class II enzymes display tissue-specific expression in humans and mice.[158,159]

The Class III isoforms is known also as Sirtuin family. Humans contain seven different sirtuins, all share a conserved catalytic core domain, of about 275 amino acids, and operate by a very different mechanism that requires NAD^+ as cosubstrate.[160]

Sequence-based phylogenetic analysis revealed that mammalian sirtuins can be divided into four classes: SIRT1- SIRT3 belong to class I, SIRT4 to class II, SIRT5 to class III, and SIRT6 and SIRT7 to class IV.[161]

Despite these structural and mechanistic differences, HDAC and Sirtuin have been shown to silence transcription at specific promoters or chromosomal domains by localized histone deacetylation and function in other cellular processes with non-histone substrates.

6.2.1. Class I HDACs

Class I HDACs are components of multiprotein complexes. HDAC1 and HDAC2 show a high degree of omology, with an overall sequence identity of approx. 85%, have undergone little functional divergence, although specific and distinct roles have also been identified for each of them.[162,163]

In a recent series of 140 colorectal cancer samples, high HDAC1, 2, 3 expression levels implicated significantly reduced patient survival, with HDAC2 expression being an independent prognostic factor.[164] In hepatocellular carcinoma, high HDAC1 expression was associated with cancer cell invasion into the portal vein.[165] Most of the studies show that HDAC1 overexpression appears especially common in cancers of the gastrointestinal system and is associated with enhanced proliferation, invasion, advanced disease and poor prognosis. However, these studies mostly investigated only HDAC1 and not other HDAC family member. In cancer cells, HDAC1 is involved in controlling cell proliferation, knocking down HDAC1 resulted in inhibition of cell proliferation of HeLa cells, whereas knockdown of HDAC4 and 7 did not lead to decreased cell numbers.[166] Knockdown of HDAC1 results in arrest

either at the G(1) phase of the cell cycle or at the G(2)/M transition, causes loss of mitotic cells, cell growth inhibition, and an increase in the percentage of apoptotic cells in osteosarcoma and breast cancer cells. On the contrary, HDAC2 knockdown showed no such effects in these cells.[167]

In colorectal cancer, at the early polyp stage, the upregulation of HDAC2 is stronger than that of HDAC1. Similarly, in cervical dysplasia and invasive carcinoma, HDAC2 expression is more intense compared to that of HDAC1. The knockdown of HDAC2, in the cervical cancer cells caused a differentiated phenotype, subsequently induces apoptosis associated with increased p21Cip1/WAF1 expression that was independent of p53.[168] In breast cancer cells if HDAC2 is knockdown, the functional DNA binding activity of p53 increases leading to inhibition of proliferation and induction of cellular senescence.[169]

HDAC1 and HDAC2 form homo- and heterodimers between each other. The dimer is a requirement for HDAC activity.[162,170,171] HDAC1 and HDAC2 not only are protein modifiers, but they are widely post- translationally modified. HDAC1 and HDAC2 are regulated differently because HDAC1 can be acetylated and HDAC2 cannot. This differential regulation of HDAC1 and HDAC2 is due to a sequence difference at the C terminus of the two proteins. A major role for the acetylation of HDAC1 is exerted by lysine 432, which is an arginine at the corresponding position in HDAC2. More importantly, the acetylation of HDAC1 inhibits the activity of itself and also the activity of HDAC2. Dissociation of the dimer with a HDAC1 N-terminal peptide will inhibit HDAC activity. HDAC1 and HDAC2 heterodimer levels seem to depend on the cell type, because it was shown that 40% to 60% of HDAC1 and HDAC2 proteins were found to be free from each other in mouse embryonic fibroblasts [172] whereas 80% to 90% of HDAC1 and HDAC2 proteins were associated with each other in the nucleus of human breast cancer MCF-7 cells.[173]

HDAC1 and HDAC2, together with the retinoblastoma-associated proteins RbAP46 and RbAP48, are part of the catalytic core of many multiprotein transcriptional complexes, and this association is fundamental for their enzymatic activity.[174] The Sin3a bind a spectrum of different cofactors such as Sds3 and SAP proteins.[175,176]

The NuRD complex is the only complex holding both HDAC- and ATP-dependent chromatin-remodeling activities, which are carried out by HDAC1 and/or HDAC2 and Mi-2a and/or Mi-2b, respectively. Other components of this complex have been identified, such as the methyl-CpG-binding domain-containing proteins (MBD2 -able to recognize methylated DNA) and the three members of the metastasis associated protein family (MTA1, MTA2 or MTA3). Lysine-specific demethylase 1 (KDM1/ LSD1) has also been identified as a component of NuRD.[177-179]

On the other hand, the REST/CoREST complex has more specific functions: it recruits HDAC1 and HDAC2 to suppress the transcription of neural genes in non-neural tissues. As a component of the CoREST complex and as a consequence of histone H3 deacetylation, KDM1/LSD1 promotes demethylation of H3 dimethylated on lysine 4 (H3K4me2), an event that facilitates the formation of a repressive

chromatin structure. Interestingly, CoREST appears to be involved in the negative regulation of synaptic plasticity and memory formation by HDAC2.[180,181]

Both activity and complex-formation are regulated by phosphorylation. Phosphorylation of HDAC1 and/or HDAC2 in interphase cells is required for the formation of HDAC corepressor complexes. In a recent study, Davie et al. demostrate that during mitosis, HDAC2 and, to a lesser extent, HDAC1 phosphorylation levels dramatically increase. When HDAC1 and -2 are displaced from the chromosome during metaphase, they dissociate from each other, but each enzyme remains in association with components of the HDAC corepressor complexes Sin3, NuRD, and CoREST as homodimers. Enzyme inhibition studies and mutational analyses show that protein kinase CK2-catalyzed phosphorylation of HDAC1 and -2 is crucial for the dissociation of these two enzymes.[182]

Together with HDAC1 and 2, HDAC3 expression was significantly associated with poor prognosis in large series of gastric, prostate and colorectal cancer samples. HDAC3 shares 63% identical amino acids with HDAC1/HDAC2 and has 43% overall sequence identity to HDAC8. The non-conserved C-terminal region of HDAC3 is required for both deacetylase activity and transcriptional repression. In addition the nuclear localization signal (NLS) that other class I HDACs possess, has a NES (nuclear export signal) associated to its ability to localize both to the nucleus as well as to the cytoplasm. HDAC3 is the catalytic component of the N-CoR (nuclear receptor co-repressor) and SMRT (silencing mediator for retinoic acid and thyroid hormone receptors) complex. Both act as co-repressors and have a conserved deacetylase- activating domain for HDAC3 activation.[183,184]

Of all the class I HDACs, HDAC8 is the most recently identified and comprises the NLS in the center of the catalytic domain and locates to the nucleus (when overexpressed) in human cells and also has a cytosolic localization in smooth muscle cells.[185]

Recombinantly purified HDAC8 catalyzes deacetylation and displays substrate selectivity in the absence of additional protein cofactors suggesting that HDAC8 can catalyze deacetylation in vivo in the absence of a protein complex. Distinguishing between HDAC8 substrates and binding partners in the cell is currently difficult.[186]

HDAC8 is able to deacetylate all core histone in vitro, is inhibited by TSA[187] and it has recently been found to be a non-nuclear marker of smooth muscle differentiation and associates with smooth muscle α-actin (α-SMA).[188] HDAC8 may exhibit specific intracellular localization within smooth muscle cells and have a major regulatory function in controlling their contractile capacities. It is currently unclear whether Hsp20 or cofilin are acetylated and/or substrates for HDAC8. However, HDAC8 associates better with the nonacetylated form of myosin heavy chain, suggesting that this protein is not an HDAC8 substrate. Because HDAC8 enhances cell contractility and associates with three proteins important for actin function, it is likely that HDAC8 is a component of a complex that modulates actin dynamics.[188]

6.2.2. Class II HDACs

Class IIa HDACs (HDAC4, HDAC5, HDAC7 and HDAC9) are characterized by the presence in their regulatory N-terminal domains of two or three conserved serine residues subject to reversible phosphorylation. Phosphorylation leads to the binding of the 14-3-3 proteins, the nuclear export of HDACs and the derepression of their target genes. A range of kinases and phosphatases acting downstream of diverse biological pathways have been shown to regulate the nucleo-cytoplasmic distribution of class IIa HDACs.[189]

HDAC4, 5 and 7 have their catalytic domain on the C-terminal half of the protein, and the NLS is situated close to the N-terminus. Binding domains for C-terminal binding protein (CtBP), myocyte enhancer factor 2 (MEF2) and 14-3-3 proteins are conserved in all three HDACs on the N-terminus.

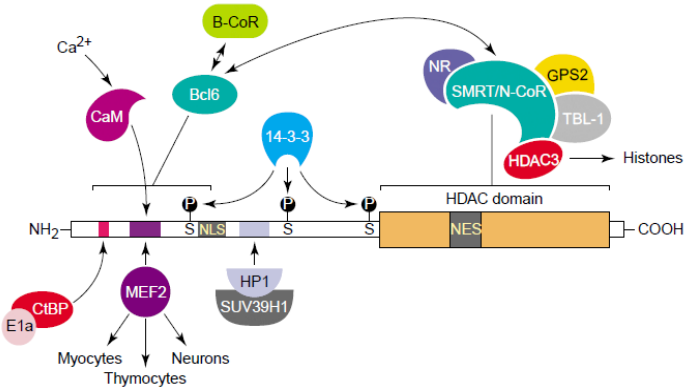

Figure 6.3. Interaction partners of class IIa histone deacetylases (HDACs).

The initial examination of the sequences surrounding the conserved phosphorylation residues in class IIa HDACs revealed that they are closely related to consensus phosphorylation sites for the calcium/calmodulin-dependent protein kinases (CaMKs). CaMK I and CaMK IV phosphorylate all four class IIa HDACs and in cell-culture models CaMKs induced the re-localization of class IIa HDACs from the nucleus to the cytoplasm.[190]

In cardiomyocytes, CaMK IIδ is the specific and endogenous HDAC4 kinase. HDAC4 and HDAC5 form homo-oligomers and hetero-oligomers, and by interacting with each other acquires CaMK II responsiveness, either by phosphorylation of HDAC4 or by transphosphorylation of HDAC5.[191] CaMK II is involved with HDACs in other tissues as well. In the nervous system, HDAC4 is highly expressed in the brain, it is mainly localized in the cytoplasm of cultured cerebellar granule neurons but translocates to the nucleus under neuronal death conditions. Moreover the treatment with a proapoptotic CaMK inhibitor (KN-93) stimulates HDAC4 nuclear accumulation. These experiments suggest that CaMK induces neuronal survival by phosphorylating HDAC4 and leading to its cytoplasmic localization.[192] Recently Hardingham et al., demonstrate that the association of HDAC class IIa with the co-

repressor Silencing Mediator Of Retinoic and Thyroid Hormone Receptors (SMRT) allows the nuclear export of these enzymes and not the direct phosporylation due to CaMK.[193]

Class IIa HDACs interact with various transcription factors but the biological relevance of these associations has been established only for the MEF2-regulated processes.[194,195] MEF2 plays a central role in the development and adaptive response of diverse tissues and organs, it is also selectively targeted for mutations in several types of cancers.[196-198] Class IIa HDACs do not bind directly to DNA but depend on their interaction with the sequence-specific transcription factor MEF2 for genomic targeting.[199,200] This interaction is mediated by a short amphipathic helix conserved in the N-terminal regulatory domain of class IIa HDACs. Crystallography analyses and in vitro biochemical studies reveal that the amphipathic helix binds to a highly conserved hydrophobic groove on the MADS-box/MEF2 domain of MEF2.[201] These studies suggest that small molecules binding to the hydrophobic pocket of MEF2 could block the recruitment of class IIa HDACs to DNA, thereby inhibiting the function of class IIa HDACs.[202]

HDAC4, which is expressed in prehypertrophic chondrocytes, regulates chondrocyte hypertrophy and endochondral bone formation by interacting with and inhibiting the activity of Runx2 (transcription factor necessary for chondrocyte hypertrophy). Overexpression of HDAC4 in proliferating chondrocytes in vivo inhibits chondrocyte hypertrophy and differentiation, mimicking a Runx2 loss of function phenotype. These results suggest that HDAC4 is a central regulator of chondrocyte hypertrophy and skeletogenesis.[203] Moreover, HDAC4 inhibit fusion protein PLZF-RARα (promyelocytic leukemia zinc finger-retinoic acid receptor alpha) in APL (acute promyelocytic leukemia).[204] Evidence also suggest that HDAC4 is the mediator which induced neuronal cell death in normal neurons.[192]

When HDAC5, as well as HDAC9, were knocked down, severe cardiac responses are observed, such as hypertrophy and fibrosis. So they might play a crucial role in heart development.[205,206]

HDAC7 is reported as a thymus-specific isoform. In developing thymocytes, Nur77 which is associated with apoptosis and negative selection, is inhibited.[207] Nevertheless, Chang S et al. reported that HDAC7 disruption led to blood vessels rupture, resulting in embryonic lethality. The process of maintaining vascular integrity by HDAC7 is achieved by repressing MMP10 (matrix metalloproteinase-10).[208] Knockdown of HDAC7 result in significant G1/S arrest in different cancer cell lines.[209] The expression of HDAC7 protein plays an important role in the apoptosis and vascular tubulogenesis of hepatocellular carcinoma by upregulation of P21 and HIF-1α (hypoxia inducible factor-1α) and downregulation of cyclin E and MMP10.[210]

The phylogenetic tree shows that HDAC9 splice variants are clustered as a separate group related to HDAC4, 5, 7 within class II of the classical HDAC family. The HDAC9 catalytic domain is located on the N-terminus, as for the class I HDACs.[211] There are three known splice variants, HDAC9a, HDAC9b and

HDRP/HDAC9c. HDAC9c/HDRP lacks the catalytic domain and is 50% similar to the N-terminus of HDAC4 and HDAC5. By analogy with HDAC4, 5 and 7, HDRP is able to recruit HDAC3, thus circumventing the lack of a catalytic domain. In addition, HDAC9 is also able to interact with MEF2, CaMK and 14-3-3 proteins, indicating that HDAC9 may have an important function in muscle differentiation.

HDAC6 is evolutionarily most closely related to HDAC10, indeed they belong to the so called Class IIb. HDAC6 contains two tandem deacetylase domains and a C-terminal zinc finger. HDAC6 has emerged as a major cytoplasmic deacetylase functioning as an α-tubulin deacetylase [212] and HSP90 deacetylase thereby regulating cell motility, adhesion and chaperone function.[213] In 2010, Mandana et al. reported that when HDAC6 is selectively inhibited by tubacin, cell death induced by etoposide and SAHA (suberoylanilide hydroxamic acid) would be significantly enhanced in LNCaP (human prostatic adenocarcinoma cell line) and MCF-7 (breast cancer cell line) tumor cells.[214] In addition, HDAC6 exerts cellular functions independently from its deacetylase activity. The binding to ubiquitin via its zinc finger domain regulates aggresome function, autophagy, heat shock factor-1 (HSF-1) and platelet derived growth factor (PDGF) function.[215,216]

HDAC10 is structurally related to HDAC6, but contains one additional catalytically inactive domain. HDAC10 was found in both the nucleus and cytoplasm. When it is knockdown, TXNIP (thioredoxin-interacting protein) expression is significantly increasing in SNU-620 gastric cancer cells, while HDAC1, 2 and 6 not. TXNIP is the endogenous inhibitor of a cellular antioxidant TRX (thioredoxin). In addition, HDAC10 inhibition induce release of cytochrome C and activate apoptotic signaling molecules through accumulation of ROS (reactive oxygen species).[217]

6.2.3. Class IV HDAC

HDAC11 has sequence similarity to classes I and II HDACs. Aside from its evolutionary conservation's implying a vital role across species and a study suggesting a role in the decision between immune activation and immune tolerance, little is known of HDAC11 functions.[148,218] Recently has been reported that HDAC11 is overexpressed in several carcinomas as compared to corresponding healthy tissues. HDAC11 depletion is sufficient to cause cell death and to inhibit metabolic activity in HCT-116 colon, PC-3 prostate, MCF-7 breast and SKOV-3 ovarian cancer cell lines. The antitumoral effect induced can be mimicked by enforced expression of a catalytically impaired HDAC11 variant, suggesting that inhibition of the enzymatic activity of HDAC11 by small molecules could trigger the desired phenotypic changes.[219]

6.2.4. Class III HDACs: Sirtuin family

The sirtuins are a family of proteins homologous to yeast silent information regulator 2 (Sir2) that in 1984 was cloned and characterized as a gene required for maintaining silent chromatin in yeast.[220] The discovery of the longevity-promoting effect of Sir2

in yeast, in higher eukaryotes nematode worm and in the fruit fly led to start a search of mammalians homologues.[221,222] Sirtuins were initially thought to function as mono-ADP-ribosyl transferases, it is widely accepted that their primary function is lysine deacetylation. Because of their unique NAD^+ dependence, they have been grouped in a class of their own, HDAC Class III. Recent research has also shown that some isoforms can in fact desuccinylate and demalonylate lysine residues in proteins.[160] Sirtuin appear to play important roles in many physiological and pathological processes.

6.2.4.1. Mammalian Sirtuins: function, classification and localization

In mammals the sirtuin family comprises seven proteins (SIRT1-SIRT7), which vary in tissue specificity, subcellular localization, enzymatic activity and targets. Sirtuins carry a conserved catalytic domain consisting of about 275 residues. Based on phylogenetic analysis mammalian Sirtuins are grouped into four different classes (I-IV).[160,223] SIRT1, SIRT2 and SIRT3 belong to class I along with most eukaryotic Sirtuins such as Sir2.1 from *Drosophila melanogaster* and the founding member yeast Sir2, HST1 and 2 from yeast. SIRT4 belongs to class II, SIRT5 to class III, and SIRT6 and SIRT7 are placed in class IV. Additionally, a novel class ("U") has been created to include sirtuins with unique features, such as gram-positive bacteria and Termoga maritime sirtuins. Mammalian Sirtuins are localized in different compartment of the cells (Figure 6.4).[224,225] SIRT1 is predominantly localized in the nucleus but is also present in the cytosol and mithochondria.[226] Under specific circumstances, in particular when the insulin pathway is inhibited, the shuttling from nuclear to cytosol it is allowed.[227] SIRT2 is mainly cytosolic but is also present in the nucleus during the transition from G2 phase to M phase of the cell cycle.[228] SIRT3, SIRT4 and SIRT5 have a mitochondrial targeting sequence, and are localized in different compartments of this organelle.[229,230] SIRT6 is mainly nuclear [231] and SIRT7 is present in the nucleolus.[232]

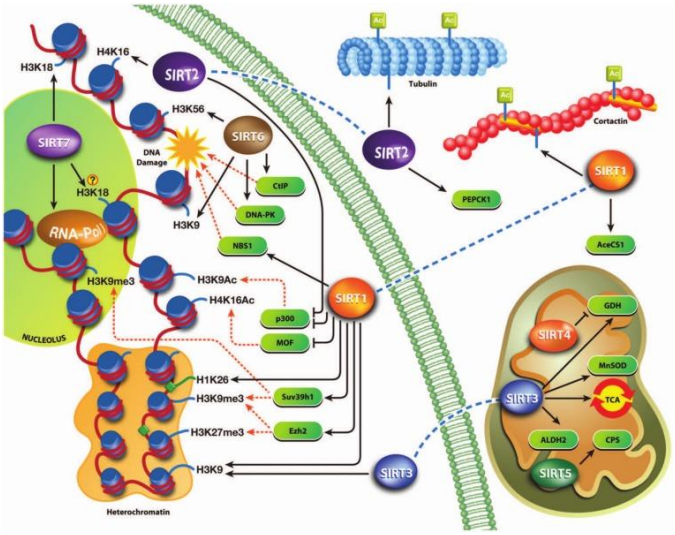

Figure 6.4. Mammalian sirtuin localization and target in the cell.

Potential sirtuins substrates range from histone to various acetylated proteins involved in cell metabolism, apoptosis and regulation of gene transcription.
SIRT1, the most-studied mammalian sirtuin, was originally described to just deacetylate histones (H3, H4) but soon after was also shown to deacetylate other protein targets. The first non-histone target described for SIRT1 was p53, which is deacetylated on lysine 382 and repressed resulting in impaired apoptosis.[233] This suggested that increased SIRT1 activity could be tumorigenic, but actually seems true the contrary.[234] The PGC1α (peroxisome proliferator-activated receptor-γ co-activator 1 α) is a transcriptional co-regulator that regulate mitochondrial biogenesis and activity. When PGC1α is deacetylated by SIRT1, its activation induce a downstream pathways that control mitochondrial gene expression.[235] Moreover SIRT1 controls the acetylation of forkhead box O (FOXO) transcription factors, which is linked to glucose and lipidic metabolism and stress responses. As a fact, SIRT1 promotes insulin secretion and pancreatic beta cell survival by suppressing uncoupling protein (UCP2) expression and interact with FOXO. SIRT1 knockout animals showed a lower level of ATP in pancreatic β-cells as a result of increased UCP2 level and they exhibited a decrease insulin secretion in response to glucose.[236,237] Lipid metabolism (HDL biogenesis) in the liver is also stimulated by SIRT1-dependent Liver's X receptor (LXR) deacetylation suggesting a mechanism that affects atherosclerosis and other aging-associated diseases.[238]

With regard to SIRT2, in vitro studies demonstrated that SIRT2, similarly to SIRT1, preferentially deacetylates histone H4.[239] In the cytosol, SIRT2 is associated with microtubules, where it deacetylates α-tubulin. During the mitotic phase, SIRT2 increases and colocalizes with chromatin during the transition from G2 to M phase, suggesting that this sirtuin is involved in the regulation of the cell cycle in response to stress.[240-242] More detailed studies on sirtuins show that SIRT2 plays an important role in glial cells development, microtubule dynamics in oligodendrocytes and maintenance of axonal integrity, which makes this isoform an attractive therapeutic target in neurodegenerative diseases.[243,244]

The most characterized mitochondrial sirtuin is SIRT3. Lombard et al. show that the absence of SIRT3 leads to protein hyperacetylation in mitochondrial fractions of liver and other tissues.[245] Functional association analyses of the targeted proteins revealed that SIRT3 is involved in the regulation of all major mitochondrial processes, including protection from reactive oxygen species (ROS), maintenance of mtDNA integrity and metabolic pathways.[246] For example, mitochondrial acetyl-CoA production is stimulated by SIRT3-mediated deacetylation, and hence catalytic activation of acetyl-CoA synthase 2.[247,248] Acetyl-CoA can then enter the Krebs cycle, which is further regulated by SIRT3-dependent deacetylation of succinate dehydrogenase.[249] During calorie restriction period, the liver releases a large amount of acetate into the blood. The heart and the muscles express acetyl-CoA synthase 2 and use acetate in an efficient way as an energy source. Deacetylation of acetyl-CoA synthetase switches on its activity so it is relevant that SIRT3 is indeed activated during CR.[250] Several other SIRT3 targets involved in metabolism have been recently

described. Hallows et al. identified the urea cycle enzyme ornithine transcarbomoylase (OTC) and other enzymes involved in β-oxidation as likely SIRT3 targets. Fasted mice lacking SIRT3 revealed alterations in β-oxidation and in the urea cycle; this study also suggest that under low energy input conditions, SIRT3 modulates mitochondria by promoting amino acid catabolism and β-oxidation.[250] Even if the knowledge about SIRT3-dependent deacetylation has expanded rapidly, it's still questionable why this enzyme has such a broad spectrum of targets.[251]

SIRT4 exhibits an efficient ADP-ribosyltransferase activity on histones and bovine serum albumin but no detectable deacetylation activity. Although this may be due to a very specific substrate spectrum for the deacetylation reaction, another NAD^+-dependent enzymatic activity, namely mono-ADP-ribosylation, was identified for SIRT4. SIRT4 is expressed in islets of Langerhans and colocalizes with insulin-expressing beta cells. SIRT4 is reported to down-regulate insulin secretion.[252,253] Glutamate dehydrogenase (GDH) is a substrate of SIRT4.[254] By ADP-ribosylating GDH, SIRT4 suppresses its activity and prevents the usage of amino acids as an energy source. During calorie restriction SIRT4 expression is decreased, consequently GDH is activated and it induces the usage of glutamate and glutamine in order to generate ATP. GDH can also be deacetylated by SIRT3, although the functional link between acetylation and ADP-ribosylation of this important enzyme is not yet well understood. Nasrin et al. investigated whether the depletion of SIRT4 would enhance liver and muscle metabolism. When SIRT4 is knockdown (KO) there is a significant increase in gene expression of mitochondrial and fatty acid metabolism enzymes in hepatocytes. Fatty acid oxidation (FAO) was increased in SIRT4 KO primary hepatocytes and this effect was dependent on SIRT1-SIRT4 KO, in primary myotubes, resulted in increased FAO, cellular respiration, and pAMPK levels. In conclusion taken together these findings, SIRT4 inhibition increases fat oxidative capacity in liver (in contrast with the functions of SIRT1 and SIRT3) and mitochondrial function in muscle.[254] In a study of Laurent et al. has been highlighted a novel function for SIRT4 in the regulation of lipid metabolism. SIRT4 represses fatty acid oxidation in skeletal muscle and stimulates lipogenesis in white adipose tissue, indicating that SIRT4 can regulate the balance between fat oxidation and fat synthesis. SIRT4 directly binds, deacetylates (K471) and represses malonyl CoA deacarboxylase (MCD). Malonyl CoA is the carbon skeleton for lipogenesis and also inhibits fat oxidation. The K471 is at close distance to the malonyl CoA entry point of MCD and its acetylation might help gate the ligand entry. When SIRT4 is knockdown in mice, they display a deregulation of crucial physiologic aspects of lipid metabolism.[255]

SIRT5 appears to primarily remove acylation marks in proteins other than acetyl groups. Originally, SIRT5 was found to be a NAD^+-dependent deacetylase and involved in the regulation of the urea cycle by deacetylation of carbamoylphosphate synthase 1 (CPS1).[256,257] The urate oxidase is also a SIRT5 substrate and its deacetylation stimulate purine catabolism in mice via deacetylation of urate oxidase, but the urate oxidase is not expressed in hominoid primates including humans.[258,259]

SIRT5 revealed a weak deacetylation activity, in line with the lack of hyperacetylation in mitochondrial fractions from SIRT5 knockout mice. SIRT5 reveal rather deacylase activity with higher affinity for malonylated and succinylated targets.[223] Du et al. show that while CPS1 is both acetylated and succinylated at three lysine residues (K44, K287, and K1291), in the absence of SIRT5 succinylation of K1291 increases, whereas succinylation of K44 and K287 or acetylation of K44, K287, and K1291 remain unchanged. These new succinylation data suggests that SIRT5 regulates the enzymatic activity of CPS1 by desuccinylating K1291. Because acetylation and succinylation can occur on the same CPS1 lysine residues, further studies are needed to resolve which modification is regulatory. The preference for succinyl and malonyl groups is due to the presence of an arginine residue (Arg105) and tyrosine residue (Tyr102) in the acyl pocket of Sirt5. Analogous to the deacetylation reaction, the deacylation reaction releases O-malonyl-ADPR or O-succinyl- ADPR as products. Sirt5 deficiency in mice leads to hyperammonemia after a period of caloric restriction. This effect is due to the lack of Sirt5-dependent deacylation and thereby activation of its first and so far only identified physiological substrate carbamoyl phosphate synthetase 1 (CPS1). Sirt5 activity is triggered by higher NAD^+ availability in times of nutrient deprivation, when amino acids are catabolized as an alternative energy source and CPS1 is needed to detoxicate the by-product ammonia through catalyzing the first step of the urea cycle.[260,261]

SIRT6 was originally found to have both deacetylase and mono-ADP-ribosyl transferase catalytic activities.[262] It is capable to deacetylate H3K9-Ac and H3K56-Ac substrates. On the contrary, its mono ADP-ribosyl transferase activity is poorly understood, and it's only known substrates are itself and poly ADP-ribose polymerase 1 (PARP1).[263] Recently, Gil et al. show that the binding to nucleosomes significantly enhances SIRT6 deacetylation of H3K9 and H3K56. Thus, these findings suggest that its binding to the nucleosome in vivo might convert it into an active structure.[264] A recent study by Jiang et al. show that SIRT6 hydrolyses long-chain fatty acyl groups from lysine residues. SIRT6 was tested with acylated histone H3K9 substrates. The longer the aliphatic tail was, the stronger was the catalytic efficiency of SIRT6. Palmitoyl, octanoyl and butyryl are all better substrates than acetylated H3K9-Ac substrates.[265] A number of evidence correlates SIRT6 to metabolism, aging and genome stability. SIRT6 regulates the expression of glycolitic genes like the glucose transporter GLUT1 mediated by hypoxia-inducible factor 1α (HIF1α).[266] SIRT6 deficiency promotes tumorigenesis by promoting increased glycolysis.[267] SIRT6 is involved in several DNA repair pathways, for example it regulates the DNA double-strand break repair by deacetylating the histone H3K9Ac.[268]

The enzymatic activity, molecular targets, and physiological functions of SIRT7 are poorly defined. SIRT7 was reported to activate RNA polymerase I transcription, although its protein substrate is still uncertain.[232] A recent study has shown that SIRT7 deacetylates histone H3 acetylated at lysine 18 (H3K18ac), hypoacetylation of H3K18 compromising transcription of genes that are linked to oncogenic

transformation.[269] Consistent with an important role of SIRT7 in cell proliferation and tumor initiation, SIRT7 was found to be upregulated in human hepatocellular carcinomas, whereas suppression of SIRT7 reduced tumor growth in a mouse xenograft model.[270] Recently Chen et al. have identified PAF53 as a new nonhistone substrate of SIRT7. PAF53 is a subunit of Pol I that is not shared by Pol II and III, providing a class-specific mechanism for SIRT7-dependent regulation of RNA polymerase activity.[271] SIRT7 may also deacetylate p53: SIRT7 knockout mice display cardiac hypertrophy, which is linked to p53 hyperacetylation.[272] However, further studies will have to determine whether p53 is indeed deacetylated by both SIRT1 and SIRT7 and, if so, whether and how these two sirtuins interconnect on this target.

HDAC III	Sirtuin	Localization	Substrates	Catalytic activity	Function
Class I	SIRT1	Cytosol, nucleus	PGC1α, eNOS, FOXO, p53, MyoD, NF-kB, histone H3 and H4	NAD^+-dependent protein deacetylation	Cell survival, insulin, signaling, inflammation, metabolism regulation oxidative stress response, lifespan regulation
	SIRT2	Cytosol, nucleus	α-tubulin, histone H4	NAD^+-dependent protein deacetylation	Cell cycle regulation, nervous system development
	SIRT3	MItochondria, nucleus	AceC2, IDH2, ShdhA	NAD^+-dependent protein deacetylation	Regulation of mitochondrial energetic metabolism
Class II	SIRT4	Mitochondria	GDH, MCD	Mono- ADP-ribosyl transferase, NAD^+-dependent protein deacetylation	Regulation of mitochondrial energetic metabolism/ lipid metabolism, insulin secretion
Class III	SIRT5	Mitochiondria	Histone H4, CPS1, cyt c	NAD^+-dependent protein deacylation	Urea cycle regulation, apoptosis

Class IV	SIRT6	Nucleus	Histone H3K9, PARP1	NAD^+-dependent protein deacetylation, Mono-ADP-ribosyl transferase	Genome stability, DNA repair, nutrient-dependent metabolism regulation
	SIRT7	Nucleoli	RNA pol I, p53, histone H3K18	NAD^+-dependent protein deacetylation	Regulation of rRNA trascription, cell cycle regulation

Table 6.2. Characterization of seven mammalian sirtuins.[273] Abbreviation: AceC2, acetylcoenzyme synthetase2; CPS1, carbamoyl synthetase 1; cyt, cytocrome; FOXO, forkhead transcription factors; GDH, glutamate dehydrogenase; IDH2, isocitrate dehydrogenase; MCD, malonyl CoA deacarboxylase; MyoD, Myogenic differentiation 1 factor; eNOS, epithelial nitric oxide synthase; NF-kB nuclear factor kB; PGC1α, Peroxisome proliferator-activated receptor gamma co activator 1- alpha; ShdhA, succinate dehydrogenase flavoprotein.

6.2.4.2. Structural features of Sirtuins

Primary sequence alignment of sirtuins shows that they share a highly conserved catalytic core and N- and C-terminal segments with divergent lengths and sequences. The overall structures of these core domains, determined by X-ray, are highly similar displaying a conserved large Rossmann fold domain for NAD^+ binding and a more variant small domain, unique for each sirtuins, that contains a zinc-binding ribbon module. The two domains are connected by four loops that arise from the Rossmann fold and include a flexible loop called the co-substrate binding loop. Both the connection and the position of the small domain with respect to the large domain varies among different Sirtuins and is often influenced by the presence of ligands and other small molecules which can affect the co-substrate loop. The most interesting part of the Sirtuin structure is the cleft between the large and small domain. The substrate and NAD^+ insert from opposite sides into a hydrophobic tunnel within the cleft, where catalysis takes place (Figure 6.5).[274]

The zinc ion does not directly participate to the catalysis, as for the other classical HDACs, because it is too remote from the active site but seems to be required for structural stability, indeed the zinc atom coordinate with four conserved Cysteins holding the three β-strands together. There is a lack of deacetylase activity by removing the zinc through mutation of the coordinating cysteine or by using chelating reagent due to partial collapse of the structure, matter of fact the subsequent supplementation of zinc restores activity.[275]

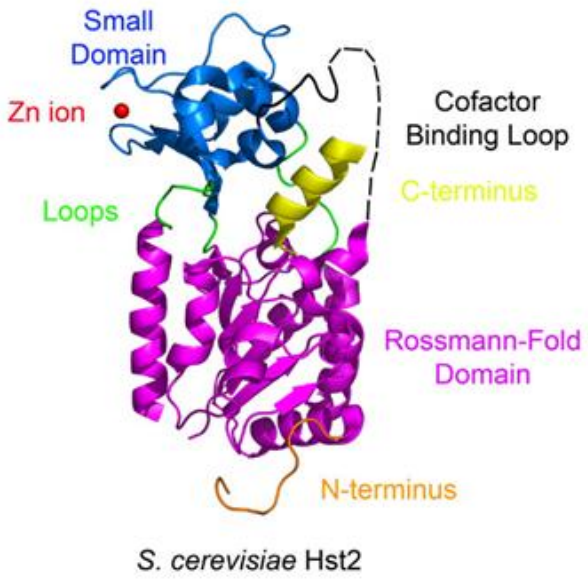

Figure 6.5. Overall sirtuin structure represented by Hst2.

The large domain has a classical open α/β Rossmann-fold structure for NAD^+ to bind. It consists of a central β-sheet with six parallel β-strands sandwiched by several α-helices on each side (the number of those helices depends upon the different sirtuins).[276] The four loops that connect the small and large domains form the cleft that acts as the enzyme active site. The elongated NAD^+ molecule inserts its nicotinamide ribose moiety into the cleft, lays the pyrophosphate group along the edge of the β-sheet in a positively charged groove, and places the adenine base in a pocket remote from the cleft. The orientation of NAD^+ here is inverted compared with most Rossmann fold-containing enzymes, where the adenine base of NAD^+ binds to the C-terminal half, and the nicotinamide group of NAD^+ binds to the N-terminal half of the β-sheet.[277] The peptide/substrate orientation and backbone interactions observed in several crystal structures of sirtuins suggests that sirtuins discriminate between different substrates and on the protein level there might be other interactions between sirtuins (especially the N and C-terminal domains) and its substrates that can lead to a substrate specificity. The nicotinamide ring of NAD^+ while bound in the strained conformation makes contacts with the co-substrate binding loop and lead to a decrease in the deacetylation activity of the Sirtuin, highlighting its importance.[278] When there is no NAD^+ present, the co-substrate loop adopts a relaxed/ open state, but switches to an ordered/ closed state when the acetyllysine and NAD^+ are present in the cleft.

6.2.5. Histone deacetylase and cancer

Mutation and/or aberrant expression of various HDACs have often been observed in human disease, in particular cancer, making them an important target in cancer therapy. Indeed, in 2005 Esteller and colleagues have reported that a lost of

acetylation of histone H4 at lysine 16 is a common event in human cancer in particulary in tumorogenesis.[279]

Class I subfamily of HDACs are deregulated in many cancers. In several studies analyzing patient cancer samples, overexpression of HDAC1 has been found in gastric, breast, pancreatic, hepatocellular, lung and prostate carcinomas.[280,281] Other studies have reported a high expression of HDAC1, HDAC2 and HDAC3 in colorectal and gastric cancer, in renal cell cancer even in classical Hodgkin's lymphoma.[164,282,283] HDAC2 is also aberrantly expressed in lung cancer tissues.[284] Taken together, these studies point out that overexpression of class I HDACs, in particular HDAC1, is a cancer marker associated with poor prognosis. In contrast to other members of the class I subfamily, HDAC8 expression seems to be cancer-type specific. Oehme et al. have reported overexpression of HDAC8 in childhood neuroblastoma.[285] In these patients, HDAC8 expression correlates with advance stage disease, poor prognosis and poor survival. There are hundreds of studies that link class I HDACs with cancer. siRNA-mediated knockdown of HDAC1 and HDAC3 in HeLa cells results in inhibition of cell proliferation, whereas knockdown of HDAC4 and HDAC7 has no effect.[166] In breast cancer cell lines, overexpression of HDAC1, HDAC6 or HDAC8 increases cell invasion and the level of matrix metalloproteinase-9 (MMP9).[286] Recently, HDAC1 has been reported to be overexpressed in a subset of hepatocellular and liver cancer cell lines. HDAC1 inactivation results in the regression of tumor cell growth, the induction of autophagic cell death and the increase of p21 and p27 gene expression.[287]

In recent years class IIa HDACs have started to be linked to several types of cancer. In contrast to class I HDACs, some members of the class IIa subfamily seem to exert a dual role in cancer.

HDAC4 along with HDAC9 and SIRT5 are found to be overexpressed in patients with Waldenstrom's macroglobulinemia.[288] HDAC4 expression is also upregulated in breast cancer samples compared with renal, bladder and colorectal cancer.[289] However, HDAC4 has not only been reported to be over-represented in cancer, several studies demonstrate that HDAC4 dysfunction and downregulation are associated with cancer development. Indeed Stark et al. in 2007 have observed a HDAC4 homozygous deletion in melanoma cell lines and Sjoblom et al. have found HDAC4 mutations in breast cancer cells.[290,291]

HDAC5 and HDAC9 are overexpressed in high-risk medulloblastoma patients, demonstrating a clear relationship between their expression and poor survival. The knockdown of these two enzymes in medulloblastoma cells is sufficient to promote cell death, but their molecular role in this type of cancer is still to be clarified.[292] HDAC5, together with HDAC3, is also aberrantly expressed in hepatocellular carcinoma (HCC). Treatment with the HDAC inhibitor panobinostat is found to be highly efficient in preclinical models of HCC, confirming the importance of these HDACs in HCC progression.[293]

High levels of cytoplasmic HDAC7 have been reported in pancreatic cancer patients and in children with acute lymphoblastic leukemia.[294,295] In contrast, Skov and

colleagues have reported HDAC7 to be significantly downregulated in myeloproliferative neoplasms.[296]

Overexpression of HDAC6 have been associated with tumorigenesis.[297] Significantly higher HDAC6 expression was found in oral squamous cell carcinoma, versus normal oral squamous tissue, and HDAC6 expression was augmented in advanced stage cancers compared to early stage.[298] In breast cancer, HDAC6 expression was associated with better survival and was higher in small tumors, in estrogen and progesterone receptor-positive tumors.[299] However, in another study analyzing breast cancer tissues, HDAC6 protein expression revealed no significant use as prognostic indicator for breast cancer progression.[300] HDAC6 deacetylates the chaperone Hsp90, resulting in the inhibition of steroid receptor mediated transcriptional activation. This mechanism has been reported to affect the growth of prostate cancer cells and breast stem cells.[301,302] Two other studies by Kaluza and Li reported that HDAC6 promotes angiogenesis by regulating the polarization and migration of vascular epithelial cells, in particularly by deacetylating the cortactin.[303,304]

When tubacin, a HDAC6 specific inhibitor is used in the treatment of acute lymphoblastic leukemia cells there is an anti-proliferative effect, enhancing the effects of chemotherapy *in vitro* and *in vivo*.[305] A similar mechanism has been attributed to the induction of apoptosis after treatment of multiple myeloma cells with the HDAC6 inhibitor ACY-1225.[306] In conclusion, targeting HDAC6 with specific HDAC inhibitorss should be considered for treating cancer cells, alone or in combination with other chemotherapeutic agents.

Sirtuins, as in the case for other HDACs, seem to play both a pro-oncogenic as well as a tumor suppressor role in cancer. Similarly to classical HDACs, aberrant expression of several sirtuins is found in many types of cancer.

SIRT1 upregulation in breast cancer cells is associated with inactivation of tumor suppressor hypermethylated in cancer 1 (HIC1) by DNA hypermethylation.[307] In addition, SIRT1 can promote cell migration by directly interacting and deacetylating cortactin.[308] SIRT1 activator SRT1720 promotes the migration and pulmonary metastasis of subcutaneously-implanted breast cancer cells in mice, further supporting the cancer promoting effect of SIRT1 in breast cancer.[309] There is also a body of evidence, particularly from mouse model studies, pointing to a tumor suppressor role of SIRT1. For example SIRT1 expression is significantly downregulated in human head and neck squamous cell carcinoma (HNSCC). High SIRT1 expression is associated with good prognosis for HNSCC patients.[310]

Similar to SIRT1, SIRT2 may have both tumor suppression and promotion function. SIRT2 expression is reduced in gliomas, in esophageal adenocarcinomas, gastric adenocarcinomas, HNSCC and in human breast cancer.[311-313] On the other hand, SIRT2 knockdown leads to both necrotic and apoptotic cell death in C6 glioma cells.[314] Similarly, in response to SIRT2 downregulation, cervical carcinoma HeLa cells undergo apoptosis.[315]

SIRT3 plays crucial roles in metabolism and oxidative stress response, and is considered a mitochondrial tumor suppressor. SIRT3 levels are reduced in colon,

human breast carcinoma and HNSCC.[316,317] Mechanistically, SIRT3 may inhibit tumor growth by reducing production of reactive oxygen species (ROS) through regulating electron transport, superoxide dismutase, mitochondrial IDH2, and FOXO3a.[318] Anyway, potential roles of SIRT3 in tumor promotion have also been reported. SIRT3 expression is higher in oral squamous cell carcinoma (OSCC) and in human lymph-node-positive breast cancer.[319,320] The selective inhibition of SIRT3 in OSCC cells inhibits cell growth and sensitizes OSCC cells to radiation and cisplatin treatments in vitro.[319]

SIRT4 in cancer is a potential tumor suppressor.[321] SIRT4 expression is found to be significantly lower in human bladder, breast, colon, gastric, ovarian, and thyroid carcinomas, relative to normal tissues. In his recent study, Jeong has reported that the loss of SIRT4 led to increased glutamine-dependent cell proliferation and stress-induced genomic instability, resulting in tumorigenic phenotypes. Indeed SIRT4 knockout mice spontaneously develop lung tumors. This study highlights a crucial role of SIRT4 in linking the glutamine metabolism with tumorigenesis.[321]

The biological significance of demalonylation and desuccinylation of carbamoyl phosphate synthetase 1 by SIRT5 remains unknown.[322] To date, there are no studies evaluating the role of SIRT5 in tumorigenesis.

There is a growing evidence suggesting SIRT6 as tumor suppressor. SIRT6 deacetylates histone H3K9 and H3K56.[323] H3K56 has been shown to be hyperacetylated in skin, thyroid, liver and breast cancer.[324] Overexpression of SIRT6 leads to a massive apoptosis in a variety of cancer cell lines but not in normal cells.[325] In any case, there are some evidence incongruent with SIRT6 tumor suppression function. Indeed, there is a study by Bauer et al. that report how SIRT6 enhance cytokine production and migration in pancreatic cells by regulating the Ca^{2+} responses.[326]

Several groups show that SIRT7 expression is upregulated in human cancers of liver, thyroid, breast.[232,327,328] In 2006 Ford et al. have demonstrated that knockdown of SIRT7 inhibits cell growth and induces apoptosis.[232] Barber et al. have confirmed that knockdown of SIRT7 in cancer cell lines reduces cell growth both in vitro and in vivo, and moreover have demonstrated a novel oncogenic mechanism of SIRT7 by deacetylating H3K18.[329] Interestingly, many different cancers display global hypoacetylation of H3K18, but further *in vivo* studies are needed to evaluate the role of SIRT7 in cancer.

Very few studies have reported a potential role for class IV HDAC11 in cancer. HDAC11 is involved in Hodgkin lymphoma (HL); indeed by using small interfering RNAs (siRNAs) that selectively inhibit HDAC11 expression, induced apoptosis in HL cell lines and boost the production of tumor necrosis-α (TNF-α).[330] Future studies should be undertaken tot elucidate the pathways controlled by HDAC11 in other tumor entities.

6.2.6. Mechanism of deacetylation

In 1999, was reported the crystal structure of a bacterial HDAC homolog, HDLP (histone-deacetylase-like protein), bound to the HDAC inhibitor trichostatin A (TSA) (Figure 6.6).[331] The catalytic domain of HDLP is very closely related to both classes I and II of HDACs, and thus the mechanism of deacetylation is presumably conserved as well. HDLP has a single domain structure related to the open α/ β class of folds. It contains a central eight-stranded parallel β sheet, with four α helices packed on either face. Eight additional α helices and large loops in the β sheet further extend the structure and result in the formation of a deep narrow pocket with an adjacent internal cavity. TSA binds to this pocket, which thus represents the active site of the enzyme. HDLP requires Zn^{2+} for activity, this cation is positioned near the bottom of the pocket and is coordinated by several histidine and aspartate residues. The channel leads to the active site being surrounded by hydrophobic residues, which is presumably where the aliphatic chain of the acetyl-lysine residue is nestled.

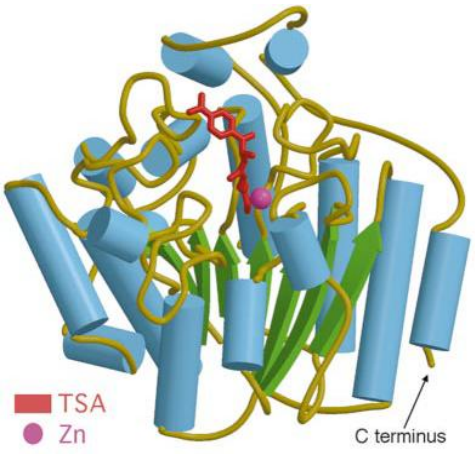

Figure 6.6. Crystal structure of HDLP bound to an HDAC inhibitor, trichostatin A.

The cocrystallization of TSA with HDLP (Figure 6.7) allows an analysis of the structural properties of this HDAC inhibitor.[332] The hydroxamic acid coordinates the zinc cation in a bidentate fashion and hydrogen bonds with some of the active site residues. Fitting into the channel, the aliphatic chain makes several van der Waals contacts with the channel residues, the cap group contacts residues on the rim of the pocket and possibly mimics the amino acids adjacent to the acetylated lysine residue in the histone. The binding of TSA causes a conformational change in the Tyr91 and thereby allows tighter packing of the cap group. The proposed deacetylase mechanism is consistent with the contacts TSA or SAHA make in the active site. Specifically, the carbonyl oxygen of the *N*-acetyl amide bond could bind the zinc, and the carbonyl carbon could be positioned in close proximity to the water molecule. The zinc ion could polarize the carbonyl group so that the carbon is a better electrophile, and could also help orient the water molecule.

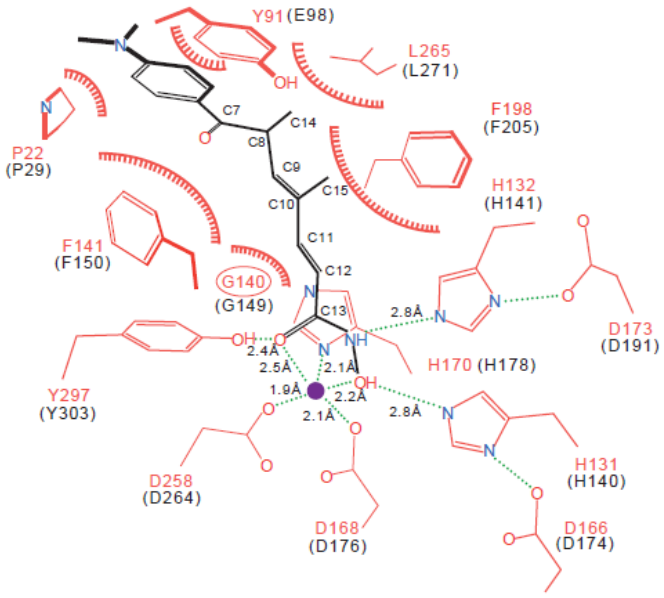

Figure 6.7. Cocrystallization of TSA with HDLP

The nucleophilicity of the water molecule would be increased by the negative charge of the buried Asp 166-His 131 charge-relay system to which the water is hydrogen bonded. The nucleophilic attack of the water on the carbonyl carbon would result in a tetrahedral carbon. This oxyanion intermediate could be stabilized by two zinc-oxygen interactions, and possibly by a hydrogen bond from the Tyr 297 hydroxyl group. In the final step, the carbon-nitrogen bond of the intermediate would break, and the nitrogen of the scissile bond would accept a proton from the exposed Asp 173-His 132 charge relay, yielding the acetate and lysine products (Figure 6.8).[332-336]

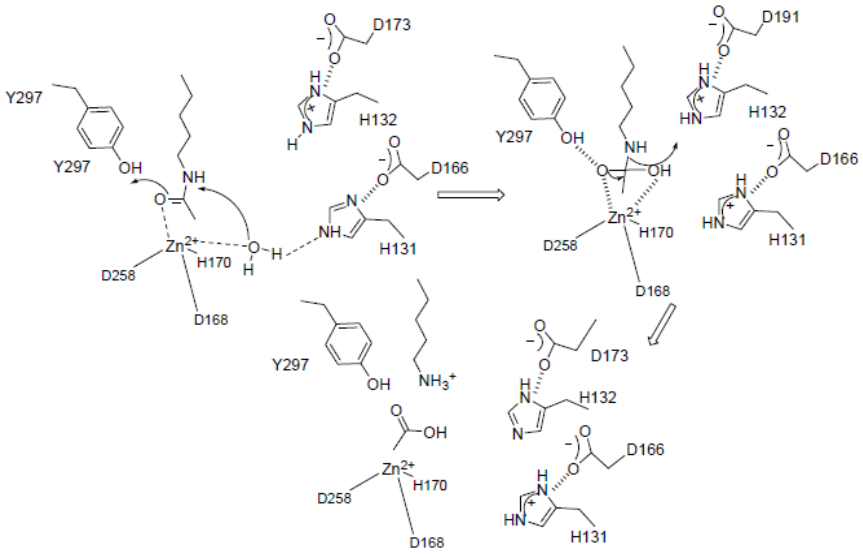

Figure 6.8. Proposed mechanism for HDAC deacetylation.

Sirtuins have been shown to possess both deacylase activity and ADP-ribosyl transferase activity. The Sirtuin mechanism is unique due to the involvement of two substrates and release of three products (Figure 6.9).[337] Several biochemical and structural data suggest multiple enzyme/intermediate and enzyme/transition state complexes.[274,338] The deacetylation is considered as the main function of the Sirtuins and the ADP-ribosyl transferase activity is often considered as a secondary reaction but the ADP-ribosyl transferase mechanism is still subject to debate.[338]

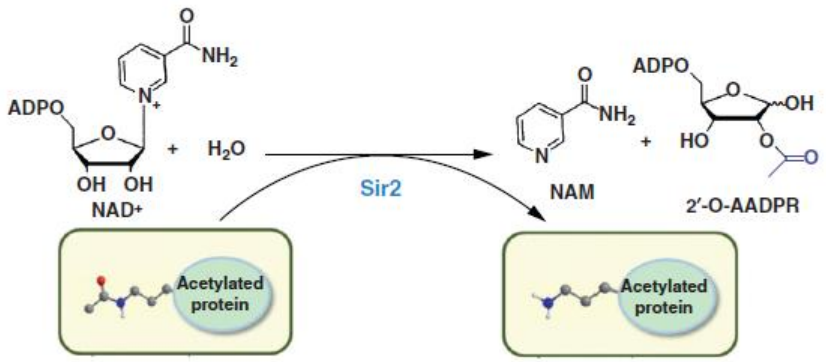

Figure 6.9. NAD^+ dependent reaction catalyzed by sirtuin enzymes. NAD^+ is consumed as a substrate, along with an acetylated protein substrate and a water molecule. Upon reaction, the acetyl-group at the N-(ε)-position is removed and nicotinamide and 2´-O-AADPR are formed as co-products.

In Figure 6.10, it is shown the deacetylation mechanism, ADPR-peptidyl-imidate mechanism, proposed by Sauve and colleagues. Central to the mechanism is an 1-α-O-ADPR-peptidylimidate intermediate formed by ADP ribosylation of the acetyllysine oxygen. The imidate complex can react reversibly to reform NAD^+ or react forward to form 2´-AADPR product. Equilibrative binding of nicotinamide causes the imidate to be in two forms, one with nicotinamide bound and the other with nicotinamide dissociated. Both forms are proposed to be competent to form the subsequent tetrahedral intermediate formed by reaction of the 2´-OH with the imidate carbon. To verify which decomposition form is promoted they used ^{18}O water that can lead to two possible decompositions, one of which is observed, leading to formation of 2´-AADPR. The other non-observed decomposition generates 1´-α-AADPR.[337] Direct observation of the imidate species on a sirtuin enzyme still remains to be obtained.

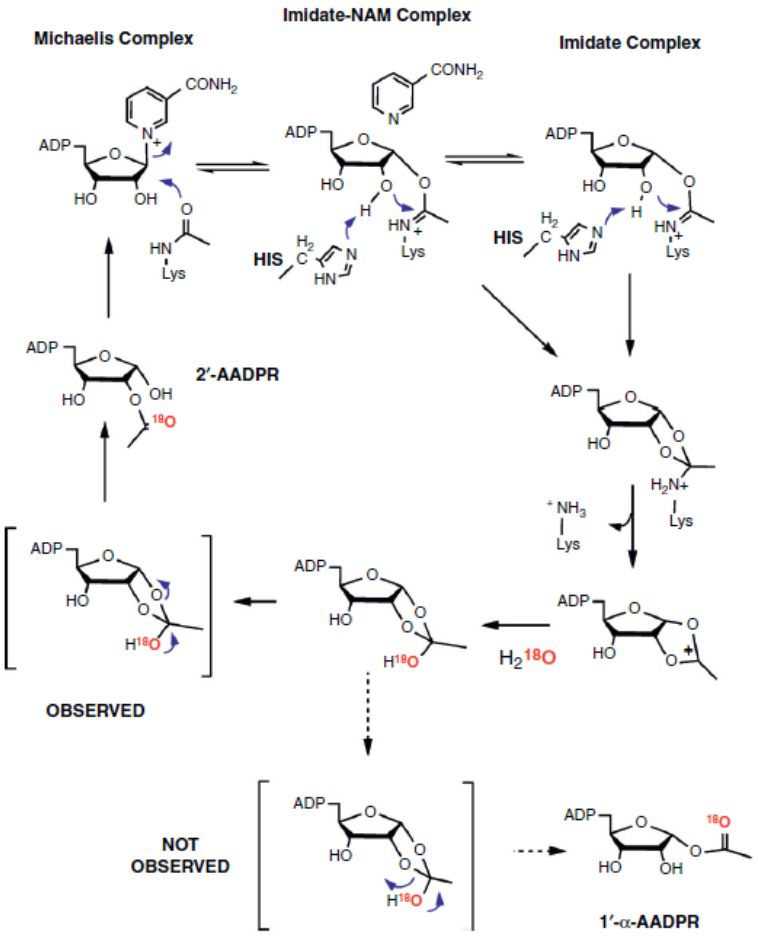

Figure 6.10. Sirtuin deacetylation: proposed ADPR-peptidyl-imidate mechanism

6.2.7. HDAC inhibitors

From the TSA/HDLP complex data,[331] described above, it is possible to elaborate a structural model (common pharmacophore) for class I/II HDAC inhibition. This pharmacophore consists of a metal binding domain (zinc binding group ZBG), which interacts with the active site, a linker domain, which occupies the channel, and a surface recognition domain, which interacts with residues on the rim of the active site (Figure 6.11).

In all known natural or synthetic inhibitors it is possible to see an extremely variable cap group. This moiety contacts residues on the rim of the catalytic pocket and is generally connected to an electronegative group that is able to interact by hydrogen bond with other residues.

Such portion is bound to an hydrocarbon linker interacting with the channel residues of the active site of the enzyme and finishing with the enzyme inhibiting group, that in many cases chelate the zinc cation near the bottom of the catalytic pocket. The cap groups can be, for example, represented by substituted benzene rings, pyridine, pyridylmethyl groups, a portion of tricyclic systems or of cyclic tetrapeptides. The electronegative group is generally a ketone, an amide, a reverse amide, a carbamate, or a sulfonamide. The linker is a saturated or unsaturated aliphatic chain, which mimics that of the lysine substrate, with an optimal length of 4-6 carbon residues. In some cases, it is possible to find an aromatic or heteroaromatic ring inserted into the hydrocarbon chain. To date, the most useful ZBG is the hydroxamic acid moiety but also ethyl ketone, trifluoromethyl ketone, α-ketoamide, 2-aminoanilide, thiol and its acetyl derivative (which *in vivo* is rapidly hydrolyzed) are effectively able to chelate the zinc ion.

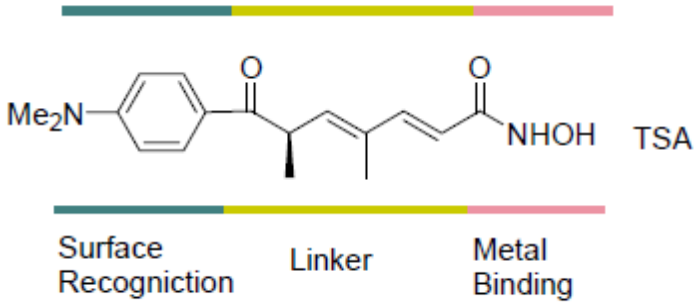

Figure 6.11. Pharmacophore model for HDAC inhibitors based on TSA structure.

HDAC inhibitors can be structurally grouped into at least four classes:
- hydroxamates,
- cyclic peptides,
- aliphatic acids,
- benzamides.

6.2.7.1. Hydroxamates

Hydroxamates were the first compounds to be identified as histone deacetylase inhibitors, and these agents helped to define the pharmacophore model for HDAC inhibitors (Figure 6.12). The linker domain can consist of linear or cyclic structures, either saturated or unsaturated, and the surface recognition domain is generally a hydrophobic group, most often aromatic.

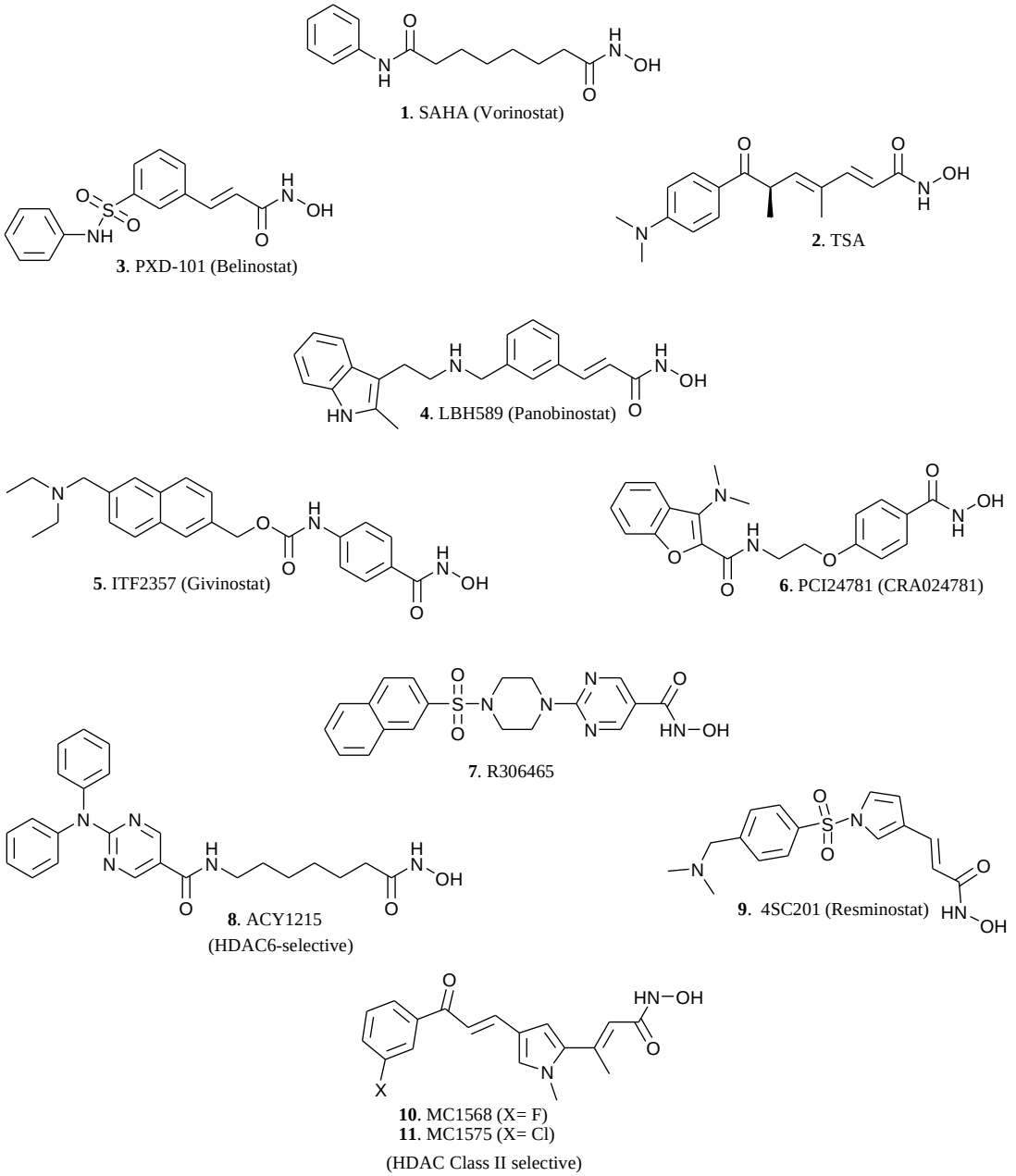

Figure 6.12. HDACi: Hydroxamic acids.

TSA (**2**) and its glucopyranosyl derivative trichostatin C were first isolated from cultures of *Streptomyces hygroscopicus* as antifungal antibiotics active against *Trichophyton* species.[332] Many years later, the trichostatins were found to have potent antiproliferative and differentiating activity at nanomolar concentrations

against Friend murine erythroleukemia cells in culture. Between the two possible enantiomers the (*R*)-TSA is 70 fold more pontent of (*S*)-TSA. In later studies, TSA was active in a number of normal and tumour cell lines, arresting the growth of rat fibroblast cells in G1 and G2 phases of the cell cycle. Nuclear histones from cells treated with TSA were highly acetylated and this was not due to increased acetylation but rather, to decreased deacetylation. In experiments using partially purified mouse HDAC, TSA was a potent, reversible, noncompetitive inhibitor with K_i = 3.4 nM, closely related to the effective antiproliferative concentration in cell lines. Furthermore, the K_i was 10-fold higher for HDAC purified from a mutant cell line resistant to TSA, suggesting that HDAC was the likely primary target of TSA.[334-336]

SAHA (suberoylanilide hydroxamic acid **1**) is the prototype of a series of synthetic hydroxamic acid-based HDAC inhibitors with nanomolar potency. Structure-activity studies have shown that the hydroxamic acid is the crucial moiety to obtain high inhibiting activity, since substitution or modification at this site reduces their anti-HDAC effect.[331] SAHA (Zolinza ®) is the first of the new HDACi to be approved by the Food and Drug Administration for clinical use in cancer patients for the treatment of cutaneous T-cell lymphoma. It is reported to be active in patients with solid tumors and with Hodgkin's disease at non-toxic doses. A recent study show that Vorinostat monotherapy demonstrate minimal activity in a group of patients with acute myeloid leukemia. Although clinical results with Vorinostat used as a single agent have been unsuccessful in treatment of solid malignancies, preclinical data strongly suggest combination with conventional cancer therapies would be beneficial.[339]

A phase I/II multicenter study was conducted in advanced HCC with PXD-101 (Belinostat **3**) by Yeo et al.. In phase I 18 patients were accrued with no dose limiting toxicities (DLTs) observed at 1400mg/m^2/day intravenously for 5 days every 3 weeks. Therefore, this dose was selected for phase II development with 42 patients enrolled. Pharmacokinetics showed that Belinostat does not have saturable kinetics, despite liver impairment at the doses studied, and it undergoes rapid clearance, with modest interindividual variability. The most frequent higher toxicities included abdominal pain, hyperbilirubinemia, anemia and vomiting. However, it is noted that the short PFS (Progression Free Survival) and the phase II design of this study preclude definitive assessment of antitumor activity of Belinostat.[340] In another phase II study, Belinostat was used in patients with advanced thymoma or thymic carcinoma. It was administered intravenously at 1 g/m^2 on days 1 to 5 of a 21-day cycle until disease progression or development of intolerance. Treatment was well tolerated, with nausea, vomiting, and fatigue being the most frequent adverse effects. Over 41 patients, two patients achieved partial response (both had thymoma), 25 had stable disease, and 13 had progressive disease; there were no responses among patients with thymic carcinoma. In conclusion Belinostat has modest antitumor

activity in this group of heavily pretreated thymic malignancies, however additional testing of belinostat in this disease is warranted.[341]

LBH-589 (Panobinostat **4**) is a cinnamic hydroxamic acid-based HDACi, developed by Novartis, with a structure similar to Vorinostat. It was in phase II trial for the treatment of patients with refractory metastatic renal cell carcinoma. They were treated with 45 mg orally twice a week, and were reevaluated after 8 weeks. Panobinostat was generally well tolerated but had no activity in this group of patients with refractory renal carcinoma.[342] LBH-589 is also in phase I clinical trials for cutaneous T-cell lymphoma as an oral agent administered three times a week. It has a longer half life than Vorinostat. Responses were seen in 6 or 10 patients including two complete responses and one partial response. Toxicities were similar to those observed with Vorinostat.[343]

ITF2357 (Givinostat **5**) is a synthetic HDACi containing a hydroxamic acid moiety linked to an aromatic ring. *In vitro* and *in vivo* studies involving human tumor cell lines have shown that ITF2357 (used alone or in combination with other agents) has cytotoxic effects and inhibitory effects on proinflammatory cytokines.[344,345] In a phase II open-label nonrandomized clinical study involving heavily pretreated, relapsed, or refractory Hodgkin's lymphoma patients, preliminary data showed that the oral application of ITF2375 had antitumor activity with an acceptable safety profile. The toxicity profile included leucopenia, thrombocytopenia, fatigue, diarrhea and cardiac QT persistence leading to drug discontinuation in 20% of treated patients.[346]

PCI-24781 (**6**) is a broad-spectrum phenyl hydroxamate. Preclinical studies involving combination with radiotherapy have suggested it may act in DNA-repair mechanisms, leading to apoptosis.[347] In a phase I clinical study involving refractory advanced solid tumors, patients were relatively successful, with adverse side effects including anemia, thrombocytopenia, diarrhea, nausea, vomiting, and fatigue.[348]

Phase I study of R306465 (**7**) about its absorption, breakdown, elimination in patients with advanced solid malignancies was completed in October 2006, but no further clinical study had been conducted later.[349]

ACY1215 (**8**) is a HDAC6-selective inhibitor, a series of studies are carried out in combination with bortezomib and dexamethasone in multiple myeloma.[306,350]

4SC201 (Resminostat **9**) has been used in a phase I trial in patients with advanced refractory solid tumors.[351,352] Nausea, vomiting and fatigue represented the most common drug-related toxicities. The recommended dose for phase II evaluation was 600 mg once daily in a 14 day cycle. Resminostat is currently being tested in phase I/II clinical trials in hepatocellular carcinoma in monotherapy or in combination with Sorafenib [353] and as a second-line treatment option in patients with KRAS tumor mutations in combination with the FOLFIRI regimen colorectal cancer,[354] but data have not yet been published.

Since 2001 a new class of HDAC inhibitors, namely aroyl-pyrrolyl-hydroxy-amides (APHAs), have been described by Mai et al.[355] Performing some chemical modification, they were able to synthesize two compound MC1568 (**10**) and MC1575 (**11**), gained in potency and selectivity, indeed these two molecule are class II selective inhibitors. Illy and colleagues, reported that in human umbilical vein ECs (HUVECs) NO inhibited serum-induced histone acetylation and enhanced histone deacetylase (HDAC) activity. In particular by immunofluorescence and Western blot analyses it was found that NO induced class II HDAC4 and 5 nuclear shuttling and that class II HDACs selective inhibitor MC1568 rescued serum-dependent histone acetylation above control level in NO-treated HUVECs. In contrast, class I HDACs inhibitor MS-275 had no effect, indicating a specific role for class II HDACs in NO-dependent histone deacetylation.[356] In 2012 Venza et al. showed that MC1568 and MC1575 inhibited IL-8 levels and cell proliferation in melanoma cells, suggesting that class II-specific HDACis may constitute a novel therapeutic strategy for improving the treatment of this cancer.[357]

6.2.7.2. Cyclic peptides

The cyclic peptide class is a structurally complex group of HDACi, which includes the natural product depsipeptide (Romidepsin, FK-228, **15**, Gloucester Pharmaceutical Inc.), Apicidin (**13**), and the cyclic hydroxamic acid- containing peptide group of molecules, all active at nanomolar concentrations. All compounds are conforming to the pharmacophore model for HDAC inhibitors and possess a macrocycle containing hydrophobic amino acids in the surface recognition domain, an alkyl chain in the linker domain, and a functional group in the metal binding domain (Figure 6.13).

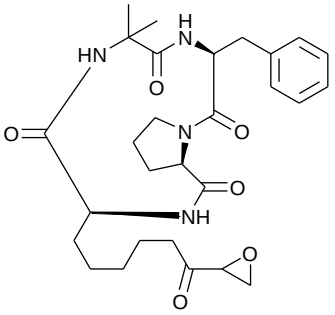

12. Chlamydocin

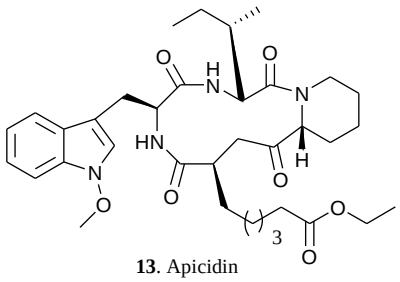

13. Apicidin

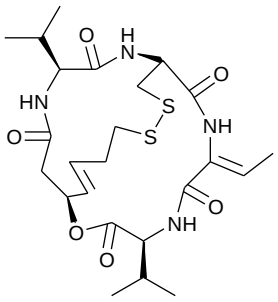

15. FK228 (Romidepsin)

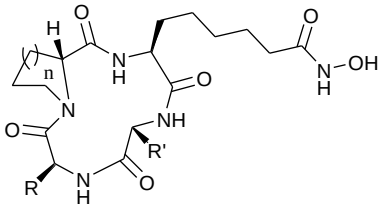

14. CHAPs

Figure 6.13. Cyclic peptides

The first examples of the cyclic peptide class arose from the screening of natural products for antiparasitic or antiproliferation activity, bearing (*S*)-2-amino-9,10-epoxy-8-oxodecanoic acid on the surface, as for Chlamydocin (**12**). Later studies demonstrate that the potentially reactive epoxy ketone moiety is not required for HDAC inhibition.[358]

Apicidin (**13**), a fungal metabolite, contains an (*S*)-2-amino-8-oxodecanyl side chain lacking the epoxide group.[359] Apicidin has broad spectrum activity (ranging from 4 to 125 ng/mL) against the apicomplexan family of parasites, presumably via inhibition of protozoan histone deacetylases (IC_{50}=1-2 nM), and demonstrates efficacy against *Plasmodium berghei* malaria in mice. Colletti and coworkers conducted SAR studies on the side chain of apicidin. They found that reduction of

the C-8 keto group to alcohol or CH_2 group or conversion to olefin or epoxide resulted in the attenuation of the anti-HDAC activity of apicidin. However, substitution of the ethyl ketone moiety of apicidin side chain with hydroxamic acid, epimeric epoxide, and hydroxyketone resulted in analogs with improved HDAC activity relative to apicidin. Some of these derivates were tested for HDAC inhibition using partially purified extracts of both human HeLa cells and *Eimeria tenella* protozoa, and they showed a picomolar cytotoxic activity.[360]

Komatsu and colleagues, synthetized a series of hybrids between TSA and cyclic tetrapeptides defined as Cyclic Hydroxamic-Acid containing Peptides (CHAPs **14**). All CHAPs synthesized in this study were potent inhibitors of HDAC1 with chlamydocin-type CHAP showing the highest inhibition of HDAC1 (IC_{50}= 0.44 nM) among all of them. Concerning their selectivity, these compounds showed 86-fold higher selectivity for HDAC1 versus HDAC6.[361]

FK-228 (Romidepsin **15**) is the most well studied depsipeptide HDACi to date. FK-228 and his closely related FR901375, are naturally occurring depsipeptides isolated from *Chromobacterium violaceum.*[362] FK-228 has a unique structural feature which includes a 16-membered cyclic depsipeptide bridged by a 15-membered macrocyclic disulfide ring. FK-228 is a stable prodrug which is activated by glutathione reductase *in vivo* by reduction of the disulfide bond to reveal a butenyl thiol moiety which then interacts with zinc at the HDAC active site.[363] It shows high selectivity toward class I HDACs compared to HDAC4 and HDAC6. In November 2009, FK228 has been approved by FDA for the treatment of relapsed and refractory cutaneous T-cell lymphoma. In contrast to SAHA, FK228 is approved as second-line therapy. Promising results have been demonstrated in Phase II testing of peripheral T-cell lymphoma subtypes. Future directions include expanded indications in T-cell lymphomas as well as novel combinations with other HDAC inhibitors and other therapeutic agents.[364]

6.2.7.3. Aliphatic acids

The aliphatic acids, such as butyrate, phenylbutyrate, and valproic acid, are relatively weak inhibitors of the HDACs, with activity at millimolar concentrations (Figure 6.14).

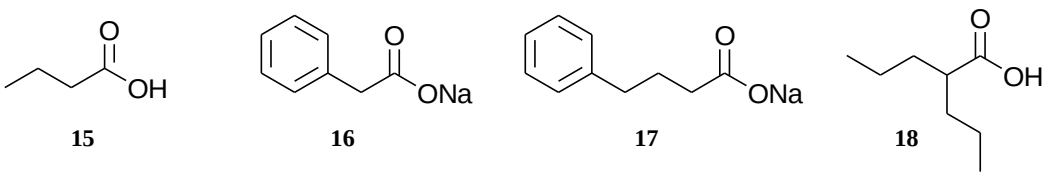

15 **16** **17** **18**

Figure 6.14. Aliphatic acids.

The butyric acid (**15**), a product generated in man by metabolism of fatty acids and bacterial fermentation of fiber in the colon, has long been known to be an antiproliferative and differentiating agent.[365] In 1933, it was first reported his anticancer activity on solid tumors, afterwards additional observations highlighted that it possessed differentiating activity at high micromolar concentrations on several cancer cell types.[366] It was later determined that butyric acid is a millimolar HDAC inhibitor, and this observation is thought to explain its mechanism of action.

Others short-chain fatty acids such as sodium phenylacetate (**16**), sodium phenylbutyrate (**17**), and the anticonvulsant valproic acid (**18**) have also been identified as antiproliferative agents and HDAC inhibitors.[367] Despite poor enzymatic inhibitory activity, a number of carboxylates, including butyric (**19**) and phenylbutyric acid (**20**), have undergone phase II clinical trials for cancer treatment alone and in combination with other agents.[368] However, the application of these acids in cancer therapy has been limited by their low potency (requiring millimolar drug concentrations in plasma) and rapid clearance, requiring continuous administration of high doses to achieve suitable plasma concentrations.

Valproic acid (VPA) is a short-chain fatty acid that has been used in clinic for the treatment of epilepsy. VPA, after the finding as HDACi,[369] has been extensively tested as a monotherapy, but also in combination with other anticancer modalities. In phase I clinical trials, patients with acute myeloid leukemia or myelodysplastic showed an improvement of 24%. In separate studies, to patients who had acute myeloid leukemia or high-risk myelodysplastic syndrome were administered the combination therapy of the azacitidine, all-*trans* retinoic acid, and VPA. The study reported significant clinical activity and a safe combination. Phase I clinical studies have also been performed on solid malignancies.[370,371]

6.2.7.4. Benzamides

Among non hydroxamate HDAC inhibitors there are *O*-Aminoanilides (Figure 6.15), indeed Suzuki and co-workers identified MS-275 (**19**) from a set of synthetic benzamide derivatives.[372] MS-275 inhibited HDACs with an IC_{50} of 4.8 μM and showed significant oral anticancer activity without severe side effects in animal models.[373] Phase I clinical studies were performed in patients with relapsed or refractory acute myeloid leukemia or refractory solid tumors. Results demonstrated safety and were well tolerated up to 8 mg/m^2. Dose-limiting toxicities were reversible with no long-term adverse outcomes. Common low-grade toxicities included nausea/vomiting, constipation, fatigue, and cytopenias. HDAC inhibition was observed in peripheral blood mononuclear cells (PBMCs), and pharmacokinetic analysis suggested a 39 to 80-hour half-life.[374-376]

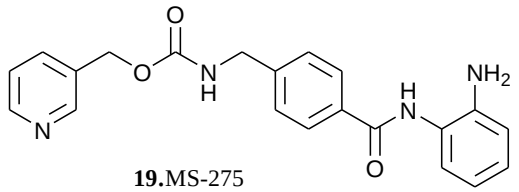

19.MS-275

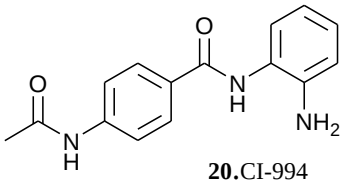

20.CI-994

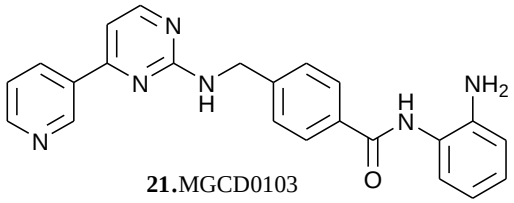

21.MGCD0103

Figure 6.15. Benzamides.

CI-994 (**20**) is an acetylated derivative of dinaline that inhibits HDAC1 with IC_{50} of 0.57 μM and causes G1 cell cycle arrest. Several data using CI-994 in the treatment of advanced NSCLC (Non-small-cell lung cancer) patients are available. In a phase II trial, CI-994 at the continuously oral daily dose of 8 mg/m^2, was administered to 32 pretreated NSCLC patients. Two patients achieved a partial response, eight a stable disease lasting more than 8 weeks. CI-994 treatment was well-tolerated.[377] Further evaluation investigated CI-994 in a phase II randomized trials in NSCLC patients but in association with gemcitabin.[378] Currently CI-994 is in Phase III clinical trial in patients with lung cancer.[339]

MGCD0103 (Mocetinostat **21**) MGCD010 is an isoform-selective aminophenyl benzamide that inhibits HDAC classes I and IV, with almost no effect on class II.[379] The compound is currently in Phase I combination clinical trial with Docetaxel for solid tumors, Phase I/II combination trials with Azacitidina for hematological malignancies and with Gemcitabine for pancreatic cancer and Phase II clinical trials in hematological malignancies.[339]

6.2.7.5. Sirtuin inhibitors

Initially research's effort to find out sirtuin inhibitors were focus on the evaluation of substrate or product mimetics. Nicotinamide (**20**), one product of sirtuins deacetylation reaction, is a physiological inhibitor of Sir2 with a K_i value of 50 μM. In a screening of nicotinamide analogs no potent inhibitor was identified.[380]

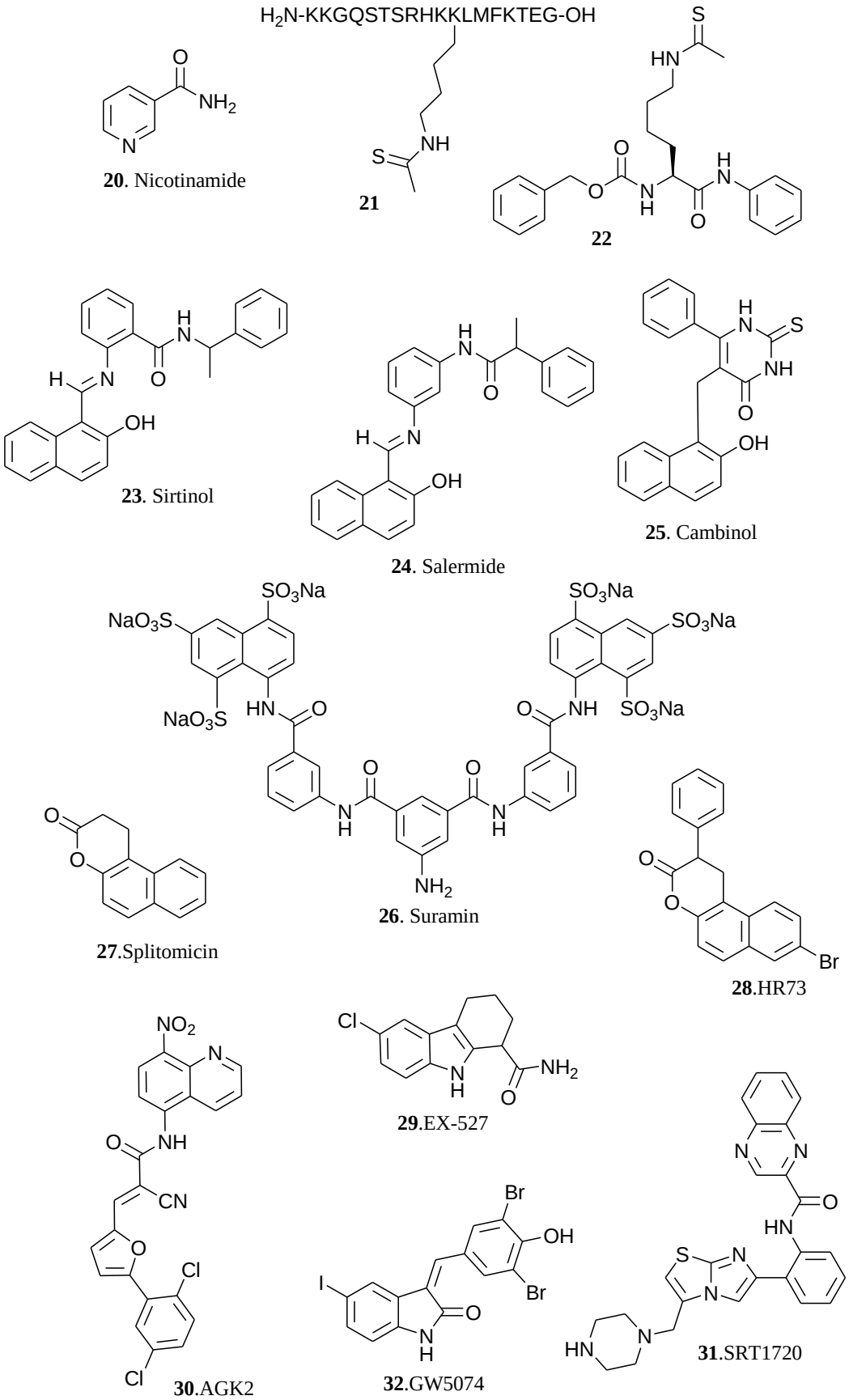

Figure 6.16. Sirtuin inhibitors.

Inhibitors based on peptides have been actively pursued. Zheng and coworkers incorporate an *N*-thiocetyl lysine into an 18-residue peptide derived from C-terminal region of human p53 protein, leading to **21** (Figure 6.16) which inhibited SIRT1with an IC_{50}= 2 μM.[381] Thioacetyllysine derived inhibitors have been demonstrated to be potent general sirtuin inhibitors as shown by numerous studies. The mechanism of action for inhibitors bearing a thioacetyl lysine was investigated by mass spectrometry and crystal structure studies. Incubation of enzyme with NAD^+ and thioacetyllysine peptide led to slower enzymatic turnovers; it has been proposed that the thioacetyl analogues follow the same reaction coordinate as their acetyl counterparts but form stalled thioimidate intermediate.[382] Kiviranta et al. in their study investigated short peptides based on the protein sequence of human p53 and α-tubulin bearing the *N*-thioacetyl lysine, and possessing a sub-micromolar IC_{50}. Generally were more potent the petides derived from the p53 sequence. Remarkably truncation of the pentapeptides into a tripeptides enhanced the selectivity toward SIRT2.[383] Suzuki and colleagues discovered a non- peptide sirtuin inhibitor (**22**) in which the peptide backbone was simplified and replaced by a *N*-thioacetyl lysine. This compound selectively inhibited SIRT1 in the micromolar range and induced a dose- response acetylation of p53 in HCT116 cells.[384]

In a cell-based screen, Grozinger et al. discovered another sirtuin inhibitor, Sirtinol (2-[(2-hydroxynaphthalen-1-ylmethylene)-amino]-N-(1-phenyl-ethyl)-benzamide) (**23**) that inhibited both yeast Sir2 and human SIRT2 activity *in vitro*. The 2-hydroxyl-1-napthol moiety was demonstrated to be sufficient for inhibition.[385] Sirtinol induced senescence-like growth arrest in human breast cancer MCF-7 and lung cancer H1299 cells.[386] Moreover, Sirtinol treatment also reduced inflammation in human dermal microvascular endothelial cells, modulating the expression of adhesion molecules and monocyte adhesion in primary human dermal microvascular endothelial cells.[387]

Through an extensive SAR study, Mai and colleagues identified Salermide (**24**), a reverse amide *m*-sirtinol analogue, with a more potent inhibitory effect than sirtinol against human SIRT1 and SIRT2. Salermide was well tolerated by mice at concentrations up to 100 μM and induced p53-independent apoptosis in cancer but not in normal cells, by reactivation of proapoptotic genes that had been epigenetically repressed exclusively in cancer cells by SIRT1.[388]

Cambinol (**25**) showed micromolar inhibitor activity against SIRT1 and SIRT2 without relevant activities toward SIRT3 and SIRT5. It was well tolerated in mice and inhibited growth of Burkitt lymphoma xenografts, inducing apoptosis via hyperacetylation of BCL6 oncoprotein and p53.[389] A SAR study indicated that the β-naphthol moiety is crucial to cambinol's inhibitory activity. Incorporation of either methyl or fluoro substituents on the phenyl ring of cambinol resulted in SIRT1 selective inhibitors with equal cambinol's potency. Substitutions on the N-1 position provided SIRT2 selective inhibitors.[390]

Suramin (**26**) was discovered as a potent SIRT1 inhibitor during a screening for sirtuin activators using a fluorescence based deacetylation assay.[391] Suramin is a symmetric polyanionic naphthylurea. Further structure–activity studies identified several suramin analogues as selective inhibitors of SIRT1 and SIRT2 with nanomolar potency.[392] Unlike cambinol, Suramin is a more potent inhibitor towards SIRT5 NAD^+-dependent deacetylase activity, with an IC_{50} value of 22 μM. The X-ray structure of SIRT5 bound to suramin suggested that the interaction between suramin, the nicotinamide binding pocket and the acetyllysine binding cleft is responsible for its inhibitory effect on this enzyme.[393]

Splitomicin (**27**) was discovered in a cell-based screening for inhibitors of the yeast Sir2 and showed an IC_{50} of 60 μM.[394] However, splitomicin showed rather weak inhibition on human SIRT1. HR73 (**28**), a splitomicin analog which contains a phenyl group at position 2, was reported to inhibit SIRT1 with an IC_{50} value of less than 5 μM.[395] These observations suggest that position 2 of splitomicin is a promising site for further SAR study.

EX-527 (**29**) is an indol derivative discovered by in vitro HST screening using a fluorescent assay. It inhibits SIRT1 (IC_{50}= 98nM) 100-fold more potently than SIRT2 and SIRT3.[396] EX-527, as expected, increased the acetylation level of p53, but it failed to affect cell survival after DNA damage.[397] Evaluation of the stereochemistry of position 1 indicated that the *S* enantiomer is the active isomer. In addition, EX-527 showed no activity against NADase, and NAD^+-hydrolyzing enzyme. In a recent study, Gertz et al. explain the mechanism of Sirtuin inhibition by Ex-527, collecting a set of Sirtuin/ligand crystal structures together with activity and binding data.[398]

Kazantsev and colleagues identified, through an *in vitro* screening employing fluorometric assays, a selective SIRT2 inhibitor AGK2 (**30**) with IC_{50}= 3.5 μM. A follow-up assay showed hyperacetylation of α-tubulin, a SIRT2 physiological substrate, upon cell treatment with AGK2. In a Parkinson disease model, AGK2 rescued dopamine neurons from α-synuclein toxicity in a dose-dependent manner. This study suggests that pharmacological inhibition of SIRT2 is a promising strategy for the treatment of Parkinson's disease.[399,400]

SRT1720 (**31**), was initially described as an activator for human SIRT1. Recentlty, Nguyen et al. confirm that SRT1720 is able to inhibit human SIRT3 with an IC_{50}= 11μM.[401] To identify the hSIRT3 binding site for SRT1720 and to reveal the compound's inhibition mechanism, the crystal structure hSirt3/carba-NAD^+/SRT1720 complex was solved. The complex structure indicates the compound' s molecular inhibition mechanism, rationalizing its un-competitive inhibition behavior with NAD^+. SRT1720 forms a tightly packed π-stacking sandwich with Phe157 and NAD^+. All these findings can provide a structural basis for compound improvement and selective hSIRT3 inhibitors.[402]

Based on the rationale that ATP and NAD^+ share the adenosine moiety, Jung and collegues tested a series of known kinase and phosphatase inhibitors, using a homogeneous fluorescent assay, and identified several sirtuin inhibitors including GW5074 (**32**).[403] In a recent study, carried out by Suenkel et al., it has been found that GW5074 is able to inhibit Sirt5 desuccinylation activity with an IC_{50} of 20 μM; so a first pharmacological scaffold has been identified in order to develop Sirt5 specific inhibitors.[404]

7. Histone methylation

Histone methylation occurs on all basic residues: arginines, lysines and histidines. Lysines can be mono-, di- or trimethylated on their ε-amine group,[405,406] arginines can be monomethylated, symmetrically dimethylated or asymmetrically dimethylated on their guanidinyl group, and histidines have been reported to be monomethylated, although this methylation appears to be rare and has not been further characterized.[407,408] The most extensively studied histone methylation sites include histone H3 lysine 9 (H3K9), H3K4, H3K27, H3K36, H3K79 and H4K20. Sites of arginine (R) methylation include H3R2, H3R8, H3R17, H3R26 and H4R3. However, many other basic residues beside the histone proteins H1, H2A, H2B, H3 and H4 have also recently been identified as methylated by mass spectrometry and quantitative proteomic analyses. Histone methylation had been thought to be an irreversible process until the discovery of an H3K4 demethylase, lysine-specific demethylase 1A (KDM1A or LSD1), revealed that histone methylation is, in fact, reversible.[409,410] Up to now, a large number of methyltransferases and demethylases have been identified. Unlike acetylation, which eliminates the lysine's positive charge and generally correlates with transcriptional activation, lysine methylation preserves the positive charge on the lysine side chain and can act as either activating or repressing signal, depending on the sites of methylation.[411] This chapter will focus specifically on the histone lysine methylation and demethylation pathways.

7.1. Histone lysines methyltransferases

Three families of enzymes have been identified thus far that catalyse the addition of methyl groups donated from *S*-adenosylmethionine (SAM) to histones. The SET-domain-containing proteins and DOT1-like proteins, have been shown to methylate lysines, and members of the protein arginine *N*-methyltransferase (PRMT) family have been shown to methylate arginines (Table 7.1). These histone methyltransferases have been reported to methylate histones that are incorporated into chromatin and also free histones and non-histone proteins. Except for the H3K79-specific DOT1L methylase, all known lysine methyltransferases (KMTs) have a conserved catalytic SET (Suppressor of variegation, Enhancer of Zeste, Trithorax) domain harboring the enzymatic activity.

Histone and residue	*Homo sapiens*		
	me3	**me2**	**me1**
H3R2		CARM1 PRMT6 PRMT5 PRMT7	CARM1 PRMT2 PRMT5 PRMT7
H3K4	SETD1A SETD1B ASH1L MLL MLL2 MLL3 MLL4 SMYD3 PRMD9	SETD1A SETD1B MLL MLL2 MLL3 MLL4 SMYD3	SETD1A SETD1B ASH1L MLL MLL2 MLL3 MLL4 SETD7
H3R8		PRMT5(s)	PRMT5
H3H9	SUV39H1 SUV39H2 SETDB1 PRDM2	SUV39H1 SUV39H2 SETDB1 G9a EHMT1 PRMD2	SETDB1 G9a EHMT1 PRMD2
H3R17		CARM1(a)	CARM1
H3R26		CARM1(a)	CARM1
H3K27	EZH2 EZH1	EZH2 EZH1	
H3K36	SETD2	NSD3 NSD2 NSD1 SMYD2 SETD2	SETD2 NSD3 NSD2 NSD1
H3K79	DOT1L	DOT1L	DOTL1
HAR3		PRMT1(a) PRMT6(A) PRMT5(s) PRMT7(s)	PRMT1 PRMT6 PRMT5 PRMT7
H4K20	SUV420H1 SUV420H2	SUV420H1 SUV420H2	SETD8

Table 7.1. Histone (H) methyltransferases for various lysine (K) and arginine (R) residues. Trimethylation (me3); dimethylation (me2); monomethylation (me1); asymmetric (a) or symmetric (s) dimethylation.

7.1.2. MLL1

The mixed lineage leukemia (MLL1) gene is a frequent target for recurrent chromosomal translocations found in lymphoid and myeloid leukemias.[412] MLL is a large multi-domain protein with several putative DNA-binding domains at the N-terminus and a C-terminal SET domain specific for H4K3me1/2/3. More than 50 functionally diverse MLL-fusion proteins have been identified in human leukemias. MLL-fusion proteins may induce leukemogenesis by misregulating genes important for proliferation and differentiation of hematopoietic cells. During normal

hematopoiesis, expression of HoxA7, HoxA9 and HoxA10 promote stem cell self-renewal, and the downregulation of these genes correlates with terminal differentiation.[413] In mouse and human leukemias however, these genes are frequently overexpressed together with Meis1, HOX co-factor. Indeed, in mice MLL-fusion mediated transformation requires HoxA7 and HoxA9, and forced expression of HoxA9 and Meis1 is sufficient to induce acute myeloid leukemia.[414]
The most frequent MLL translocation partners, are AF4, AF9, ENL, AF10 and AF6. AF10 has been found to interact with the non-SET histone methyltransferase DOT1L. DOT1L and its HMT activity are required for transformation by MLL-AF10. Direct fusion of enzymatical active DOT1L to MLL enables immortalization of myeloid progenitor cells. In cells transformed by either MLL-AF10 or MLL-DOT1L, HoxA9, HoxA7 and Meis1 are upregulated. Indeed, HoxA9 is required for immortalization of bone marrow progenitor cells. Upregulation of HoxA9 coincides with H3K79 hypermethylation and reduced H3K4me2 levels associated with the HoxA9 gene, suggesting that mistargeting of DOT1L contributes to upregulation of leukemia-relevant genes. [415]
Beside MLL1, the mammalian MLL family consists of four other members, MLL2-5. The family shares a distinct SET domain, which in MLL1-4 encodes the H3K4 methylation activity. MLL1 and MLL2 are highly homologous and form similar KMT complexes, which are distinct from MLL3/MLL4 complexes. Mutations and amplifications in MLL2, MLL3 and MLL4 have also been implicated in tumorigenesis. MLL5 is a distantly related family member and it seems to lack KMT activity. [416,417]

7.1.2. The NSD family

The NSD (Nuclear receptor SET-Domain) family is implicated in different human malignancies. The NSD proteins are related to the Saccharomyces cerevisae SET2 HMT, which has been shown to repress transcription through the interaction with the phosphorylated C-terminal domain of RNA polymerase II.[418] The members of this family NSD1 and NSD2 catalyze H3K36 methylation a modification that is enriched in the body of actively transcribed genes.[419] Together with the results suggesting that SET2 works as a transcriptional repressor, these data suggest that H3K36 methylation participates in suppressing erroneous transcriptional initiation inside actively transcribed genes.
NSD1 is a large protein containing several motifs involved in transcriptional regulation, including a SET domain and five PHD fingers. Still there is a lack of information regarding the mechanism and role of this protein in cell proliferation and differentiation. However NSD1 is required for normal development, since homozygous mutant *Nsd1*$^{-/-}$ embryos die during gastrulation displaying high levels of apoptosis.[420] Recently has been demonstrated that in mice the NUP98-NSD1 fusion protein can be a driving oncogene in acute myeloid leukemia.[421] Expression of the fusion protein is sufficient for sustaining the self-renewal of myeloid stem cells *in*

vitro and to enforce the expression of the HoxA7, HoxA9, HoxA10 and the Meis1 proto-oncogenes.

The NSD2 protein contains a SET domain, a PHD finger, a PWWP domain and an HMG box. Various activities have been associated with NSD2, including the ability to trimethylate H3K4 and H4K20, to mono- and trimethylate H3K27, and to mono-, di- and trimethylate H3K36. Of these activities, the trimethylation of H3K36 appears best supported by *in vivo* observations. In contrast to S. cerevisae SET2, NSD2 protein showed a really weak interaction with RNA polymerase II but interacted with several developmental transcription factors and chromatin modifying enzymes such as HDAC1, HDAC2, SIN3A and LSD1. These data suggest that NSD2 is part of a co-repressor complex, which regulate cell fate decisions.[422,423]

NSD3 is genetically amplified in a few cases of breast carcinomas and expressed in acute myeloid leukemia as fusion protein NUP98–NSD3. The high homology in the conserved domains between NSD3 and its two relatives, suggests that NSD3 most likely catalyzes the methylation of H3K36.[424,425]

7.1.3. Polycomb group proteins

At the molecular level, PcG proteins act through the concerted function of at least two distinct classes of multimeric complexes, termed Polycomb Repressive Complexes (PRCs). The catalytic subunit of this complex is EZH2 (Enhancer of Zeste 2) which is highly conserved and can catalyze di- and trimethylation of H3K27 but is dependent on the other complex members EED and SUZ12.[426,427] PRC1 consists of Ring1B, Bmi1, PH1 and CBX4, it binds to the H3K27 methylation mark and mediates H2A ubiquitination. Together, through the histone modification, PRC1 and PRC2 implement and maintain transcription silencing. EZH2 was found to be significantly upregulated in metastatic prostate cancer suggesting that EZH2 levels could serve as a prognostic indicator of clinical outcome of prostate cancer patients. EZH2 was also significantly increased in invasive carcinoma and breast cancer metastases compared to normal breast tissues.[428] More recently, somatic mutations in EZH2 leading to the replacement of a single tyrosine in the SET domain of EZH2 protein (Tyr 641) have been found in the follicular lymphoma and the germinal centre B cell subtype of diffuse large B-cell lymphoma cases.[429]

7.1.4. G9a and other histone methyltransferases

G9a and GLP are members of the Suv39h subgroup of SET domain-containing molecules, and together they are the key HKMTs for H3K9me1 and H3K9me2. G9a is a major H3K9me1 and H3K9me2 HKMT of euchromatin. It is also involved in H3K9me3 modification *in vivo* and it has been shown recently that G9a is indeed involved in H1 and H3K27 methylation *in vivo*.[430-432] GLP was in initially described as a gene encoding a G9a like protein. Later various studies have demonstrated that GLP and G9a possess the same substrate specificities on histones. Tachida and colleagues reported that the double knock out of G9a and GLP does not further

reduce H3K9me1 and H3K9me2 levels. Moreover, through biochemical characterization of G9a and GLP, they showed that G9a and GLP can form a homomeric and heteromeric complex via their SET domains and that the G9a-GLP heteromeric complex seems to be the functional H3K9 HKMT *in vivo*.[430] In Neurospora, H3K9 methylation controls DNA methylation.[433] There are different studies that report functional links between H3K9 methylation and DNA methylation in mammals as well.[434] G9a and GLP have also both been found to be up-regulated in various types of human cancer cells, indeed knockdown of G9a suppresses tumor cell growth in vitro and the invasion of cancer cells in nude mice.[435,436]

Suv39h1 represents the first histone methyltransferase that was identified and characterized in 2000.[437] Suv39h1 is one of the two mammalian orthologs of the Drosophila Su(var)3-9. The other homolog has been named Suv39h2 and both Suv39h1 and Suv39h2 direct trimethylation of H3K9 at pericentric heterochromatin.[438,439] Differential expression profiles of Suv39h1 were found in colorectal cancers versus normal colorectal mucosa.[289,440] Moreover in a study of NiIeles et al. is reported that the interaction of Suv39h1 with the retinoblastoma protein (pRB) is disrupted in cancers with RB1 mutations.[441]

The pRB-interacting zing finger gene (RIZ1) is a tumor suppressor that also methylates histone H3K9. The protein was initially identified as an interaction partner of the retinoblastoma protein (PR). An intact PR domain is known to be important for RIZ1 tumor suppressor function in mice.[442] Naturally occurring mutations in the PR domain that altered its tumor suppressor function also inactivated its HMT activity suggesting a role for the HMT activity of RIZ1 in many human cancers including liver,breast and gastric cancers.[443,444]

7.2 Histone lysine demethylases

Lysine-specific demethylases (KDMs) work in coordination with histone lysine methylases to maintain global histone methylation patterns (Figure 7.1).[444]

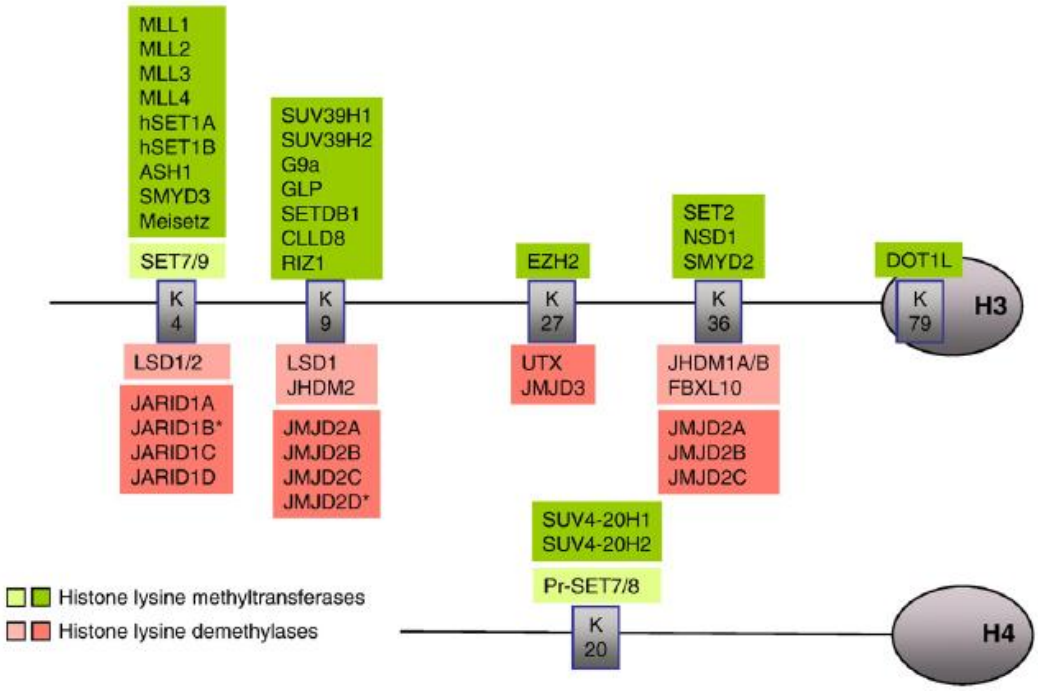

Figure 7.1. Histone lysine methylation patters. Lighter shades: monomethylation by KMTs or demethylation of mono and di-methylated lysine. Darker shades: mono-, di-, tri-methylation by KMTs or demthylation of di- and tri-methylated lysine residues by KDMs.

Thus far two evolutionarily conserved families of histone demethylases, which utilize different reaction mechanisms to establish demethylation, have been identified. One are the amine oxidases LSD1/2 and the other the iron- and α-ketoglutarate dependent JmJC-domain containing proteins (Table 7.2).[444]

Histone demethylases	Other names	Histone substrates	Association with human disease
LSD1	KDM1A, AOF2, BHC110	H3K4me2/1 H3K9me2/1	-Overexpressed in prostate cancer, undifferentiated malignant neuroblastoma, oestrogen-receptor-negative breast cancer, bladder cancer, lung carcinoma and colorectal carcinoma -Silenced or downregulated in breast cancer
LSD2	KDM1B, AOF1	H3K4me2/1	Amplified and overexpressed in urothelial carcinoma
JMJD1A	KDM3A, JHDM2A, TSGA	H3K9me2/me1	Overexpressed in malignant colorectal cancer, metastasized prostate adenocarcinoma, renal cell carcinoma and hepatocellular carcinoma
JMJD1B	KDM3B	H3K9me2/me1	-
JMJD1C		H3K9me2/me1	Target of MLL–AF4
JMJD2A	KDM4A, JHDM3A	H3K9me3/2 H3K36me3/2 H1.4K26me3/2	-Silenced or downregulated in bladder cancer -Overexpressed in breast cancer
JMJD2B	KDM4B, JHDM3B	H3K9me3/me2 H3K36 me3/me2 H1.4K26 me3/me2	Overexpressed in malignant peripheral nerve sheath tumour
JMJD2C	KDM4C, JHDM3C, GASC1	H3K9me3/me2 H3K36me3/me2 H1.4K26me3/me2	-Amplified in oesophageal cancer, breast cancer and medulloblastoma -Translocated in lymphoma1
JMJD2D	KDM4D, JHDM3D	H3K9me3	-
JMJD3	KDM6B	H3K27me3/me2	-Overexpressed in various cancers including lung and liver carcinomas and several haematological malignancies -Overexpressed in neutrophils of patients with ANCA-associated vasculitis -Overexpressed in primary Hodgkin's lymphoma
UTX	KDM6A	H3K27me2, H3K27me3	-Mutated in multiple tumour types including multiple myeloma, oesophageal squamous cell carcinoma, renal clear cell carcinoma, transitional cell carcinoma and chronic myelomonocytic leukaemia -Overexpressed in breast cancer -Deleted in Kabuki syndrome
UTY	-	-	-
JMJD4	-	-	-
JMJD5	KDM8	H3K36me2	-
JMJD6	-	H3R2, H4R3	-

JMJD7	-	-	-
JMJD8	-	-	-
FBXL11	KDM2A, JHDM1A	H3K36me2/1	-
FBXL10	KDM2B, JHDM1B	H3K36me2/1 H3K4me3	Overexpressed in various leukaemias and bladder carcinoma
KIAA1718	KDM7A, JHDM1D	H3K9me2/1 H3K27me2/1	-
PHF2	JHDM1E	H3K9me2	Mutated, silenced or downregulated in breast carcinoma as well as head and neck squamous cell carcinoma
PHF8	JHDM1F	H3K9me2/1 H4K20me1	Mutation and deletion associated with X-linked mental retardation and cleft lip/palate
JARID1A	KDM5A, JARID1A, RBP2	H3K4me3/2	-Silenced, downregulated or deleted in melanoma -Translocated in acute leukaemia -Mutated in ankylosing spondylitis
JARID1B	KDM5B, PLU1	H3K4me3/2	Overexpressed in bladder cancer, prostate cancer and breast cancer
JARID1C	KDM5C, SMCX	H3K4me3/2	-Mutated in intellectual disability -Mutated in autism -Mutated in renal carcinoma
JARID1D	KDM5D, SMCY	H3K4me3/2	Deleted in prostate cancer
JARID2	-	-	-
HIF1AN	-	-	-
HSPBAP1	-	-	-
HR	-	-	-
NO66	-	H3K4me3/2 H3K36me3/2	Overexpressed in non-small-cell lung cancer
MINA	-	-	Overexpressed in non-small-cell lung cancer

Table 7.2. Histone Lysine Demethylases (KDMs): specificity and role in human diseases.
ANCA, anti-neutrophil cytoplasmic antibody; FBXL10, F-box and leucine-rich repeat protein 10; HIF1AN, hypoxia-inducible factor 1α inhibitor; HR, hairless homolog; HSPBAP1, HSPB1 (27 kDa heat shock protein)-associated protein 1; JARID, Jumonji/ARID domain-containing protein; JMJD, Jumonji domain-containing protein; LSD1, lysine-specific demethylase 1; MINA, MYC-induced nuclear antigen; MLL, mixed lineage leukaemia; NO66, nucleolar protein 66; PHF2, PHD finger protein 2; UTX, ubiquitously transcribed TPR protein on the X chromosome; UTY, ubiquitously transcribed TPR protein on the Y chromosome.

7.2.1. LSD demethylases

LSD1 is a FAD-dependent amine oxidase which was first characterized by Shi et al. in 2004.[410] This enzyme is able to remove methyl groups from histone 3 lysine 4 when mono- or di-methylated (H3K4me1/2) at the ε-position, but not the trimethylated lysine. One year later from its discovery, Metzger et al. demonstrate that the substrate specificity of LSD1 can change to mono- or di-methyl H3K9 (H3K9me1/2) when co-localizing with the androgen receptor (AR).[445] In addition,

LSD1 can demethylate non-histone targets, such as K370me1 and K370me2 on p53,[446] Lys1096 on DNA methyltransferase 1 (DNMT1)[447] and Lys185 on E2F1.[448] The other LSD family member, LSD2, has so far only been shown to demethylate H3K4me1 and H3K4me2.[449]

7.2.1.2. LSD1

LSD1 is typically associated with a transcriptional corepressor protein (CoREST) and histone deacetylase (HDAC) 1 or 2, forming a stable core subcomplex recruited by many chromatin remodeling multiprotein complexes.[450] However, LSD1 is also involved in some gene activation processes, thus highlighting its multifaceted function in chromatin regulation. Moreover LSD1 participates in several growth promoting pathways, and it is upregulated in certain high-risk tumors.[451,452] An important feature in the LSD1-mediated demethylation process is the mechanism for substrate recognition. The crystal structure of the LSD1-CoREST-histone peptide ternary complex reveals that the peptide binds to the amine oxidase domain (Figure 7.2),[453] adopting a folded conformation that enables the binding site to accommodate the relatively long stretch of the N-terminal H3 tail. Biochemical evidence indicates that substrate recognition by LSD1 requires a peptide comprising at least the first 20 N-terminal amino acids of H3. This ability of recognizing a "long" and "heavily charged" segment of the histone N-terminal tail enables LSD1 to detect the presence of multiple post-translational modifications written in the H3 tail. Indeed some evidence show that the charge distribution on the histone N-terminal tail appears to be determinant in the readout of the histone code by LSD1, for example Lys9 deacetylation significantly improves LSD1 activity mainly through an increase in substrate affinity.[454]

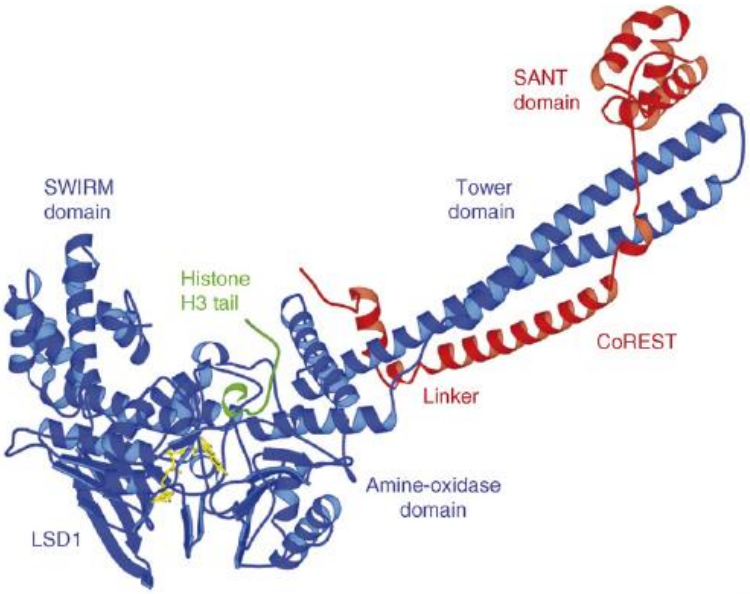

Figure 7.2. Structural biology of LSD1 in complex with CoREST and a peptide substrate.

As a member of monoamine oxidase (MAO) family, LSD1 catalyzes the specific demethylation of mono- or dimethylated histone H3 lysine 4 (H3K4) and H3 lysine 9 (H3K9) via a redox process. The reason why LSD1 is not able to demethylate a trimethyl lysine is caused by the FAD dependent catalytic mechanism. This is limited by the initial step, the oxidation of the ε-amine to form an iminium intermediate with the concurrent reduction of the flavin. The intermediate can then be attacked by a water molecule close to the iminium ion to react to an unstable hemiaminal intermediate which decomposes into formaldehyde and the demethylated H3K4. The reduced FADH2 is reoxidized by oxygen in a subsequent step to form FAD and hydrogen peroxide. The lysine residue requires a lone electron pair that can be protonated and then form the iminium intermediate. Thus, a trimethylated lysine cannot be demethylated by LSD1/2 (Figure 7.3).[455]

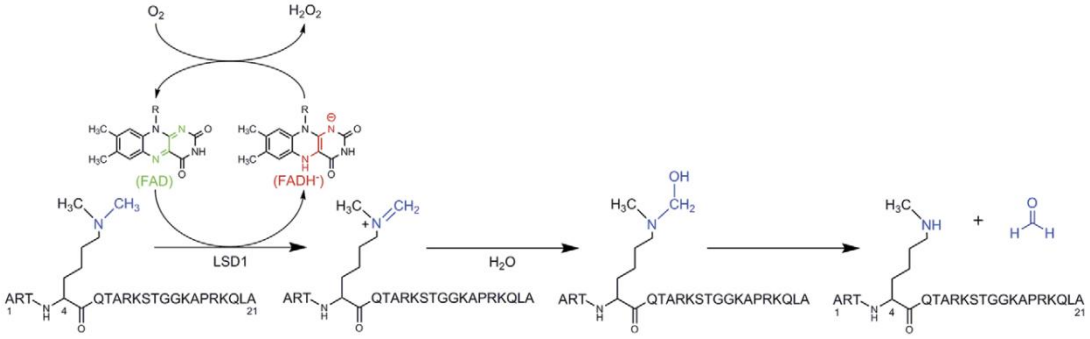

Figure 7.3. LSD1 reaction mechanism.

7.2.1.2.1. LSD1 crystal structure

In 2006 Chen et al. solved the crystal structure of LSD1.[456] The structure of LSD1 contains three domains. Two of them, the SWIRM (residues 172-270) and AOL (residues 271-417 and 523-833) domains, pack together through extensive interactions resulting in a globular structure. The SWIRM domain consists mostly of α-helices and is a newly identified structural module often found in chromatin-associated proteins. The AOL domain folds into a compact structure that exhibits a topology found in several flavin-dependent oxidases. It contains a large insertion (residues 418-522) that forms an additional domain and adopts a tower-like structure (Tower domain) protruding away from the AOL domain by 75 Å. The Tower consists of a pair of long helices that adopts a typical antiparallel coiled-coil conformation (Figure 7.4A and 7.4B).[457]

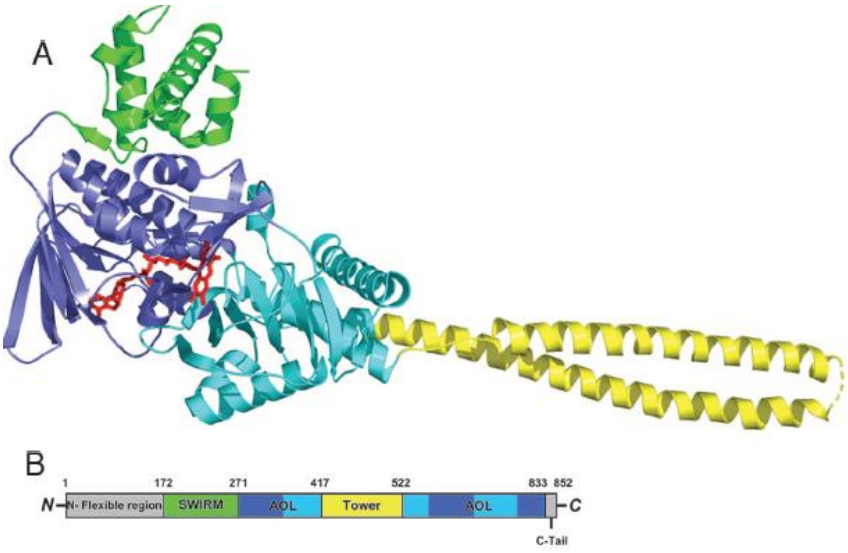

Figure 7.4. (A) Ribbon diagram of the LSD1 structure. (B) Domain organization of LSD1.

The **SWIRM domain** of LSD1 is characterized by a long helix, SWα4, in the center surrounded by five other helices, moreover it has an additional two-stranded β-sheet formed between the SWα4-SWα5 loop and the C terminus of the SWIRM domain (Figure 7.5A).

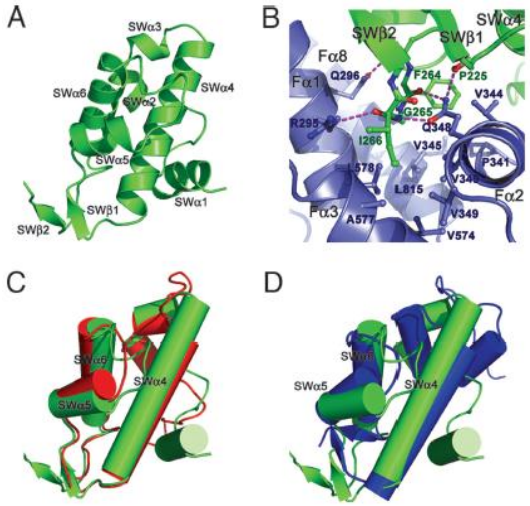

Figure 7.5. A) Ribbon diagram of the SWIRM domain. B) A three-amino-acid motif (F264G265I266) of the SWIRM domain mediates the interactions between the SWIRM (blue) and AOL (green) domains. C) and D) Superposition of the LSD1 SWIRM domain (green) with those of Swi3 (red) and Ada2α (blue).

The LSD1 SWIRM domain is structurally most similar to those of the chromatin-remodeling proteins Swi3 and ADA2α. The three SWIRM domains have very similar hydrophobic core packing but SWα1 and SWα2, which are not conserved, are positioned further away from the hydrophobic core (Figure 7.5C and D). The SWIRM domain is located far away from both the FAD-binding site and the catalytic center of LSD1 (Figure 7.4A). The β-sheet helps anchor the SWIRM and AOL domains by forcing the SWα6–SWα2 loop to protrude out into a hydrophobic pocket formed by helices Fα1, Fα2, Fα3, and Fα8 of the AOL domain (Figure 7.5B). A three-amino-acid motif (F264-G265-I266) between SWα6 and SWα2 anchors the binding through extensive interactions with the AOL domain, involving both hydrophobic contacts and hydrogen bonding interactions (Figure 7.5B). The side chains of F264 and I266 and the main chain Cα atom of G265 stack against a hydrophobic pocket from the AOL domain. These hydrophobic contacts are reinforced by extensive hydrogen-bonding interactions between the backbone of this motif and the side chains of R295 and Q348. The SWIRM-AOL packing buries a total surface area of 1.115 $Å^2$, and the residues that form the interface are highly conserved across species.

The **AOL domain** of LSD1 folds into two well defined subdomains, one to bind the FAD and the other one to identify and interact with the substrate (Figure 7.6).

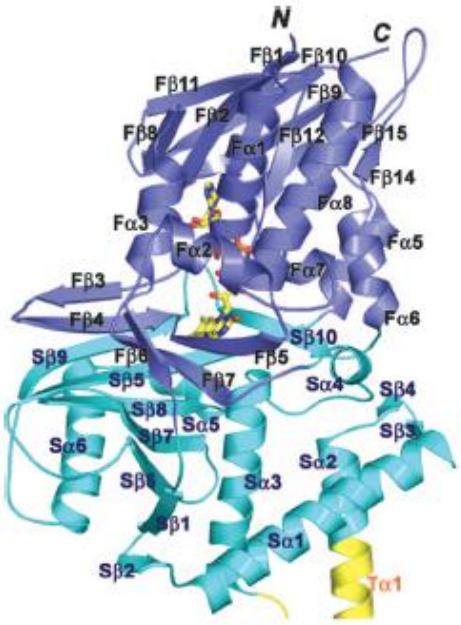

Figure 7.6. Ribbon diagram of the AOL domain in LSD1.

The FAD-binding subdomain has three fragments (residues 271-356, 559-657, and 770-833) and adopts a mixed α–β structure. The substrate-binding subdomain comprises three fragments (residues 357-417, 523-558, and 658-769) and is characterized by a six-stranded mixed β-sheet flanked by six α-helices. The two subdomains create a big cavity that defines the enzyme activity center at their interface. The catalytic cavity is framed by many structural elements that surround the catalytic center: a six-stranded β-sheet (Sβ1 and Sβ6-Sβ9) and a long helix (Sα3) form the left side and the bottom surfaces, respectively, whereas a short one-turn helix (Sα4), a two-stranded β-sheet (Fβ5-Fβ7), and several loops with variable lengths cover the rest of the cavity (Figure 7.6). The cavity goes deep into the protein, extending for a length of 23 Å from its entrance to the core of the catalytic site where the flavin ring is located (Figure 7.7). Inside the active site cavity, there are four major invaginations with distinct chemical properties that could be used for the specific binding of side chains. Furthermore, it seems plausible that these pockets can sense not only the histone tail sequence but also its chemical modifications.[410] The first pocket exposes the isoalloxazine ring of the FAD cofactor and forms the catalytic chamber of LSD1.

The residues that create this hydrophobic chamber and lie close to the isoalloxazine ring are Val317, Gly330, Ala331, Met332, Val333, Phe538, Leu659, Asn660, Lys661, Trp695, Ser749, Ser760 and Tyr761 (Figure 7.8). These residues are required for the exact positioning of both the FAD cofactor and the substrate lysine. In other oxidases, the isoalloxazine ring is usually found in conjunction with a positively charged residue, which is required for proper FAD binding and stabilization of the anionic form of the reduced cofactor. In LSD1 the residue that fulfils this function is Lys661. The remaining three pockets of the active site cavity are probably required for the binding of histone tail residues directly adjacent to the substrate lysine. Compared with other flavin-dependent oxidases, as PAO (maize polyamine oxidase), LSD1 has a unique structural feature.

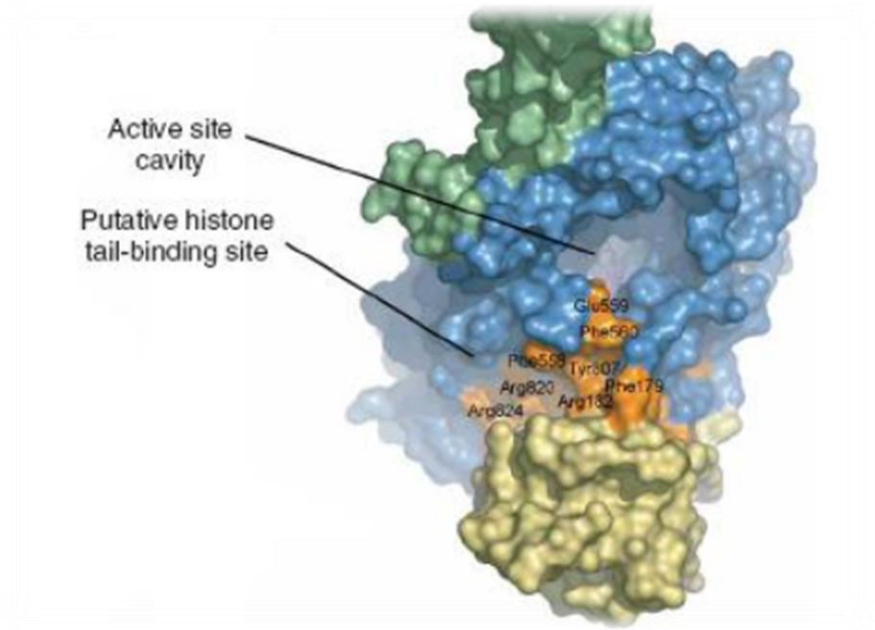

Figure 7.7. Three-dimensional representation of the catalytic cavity.

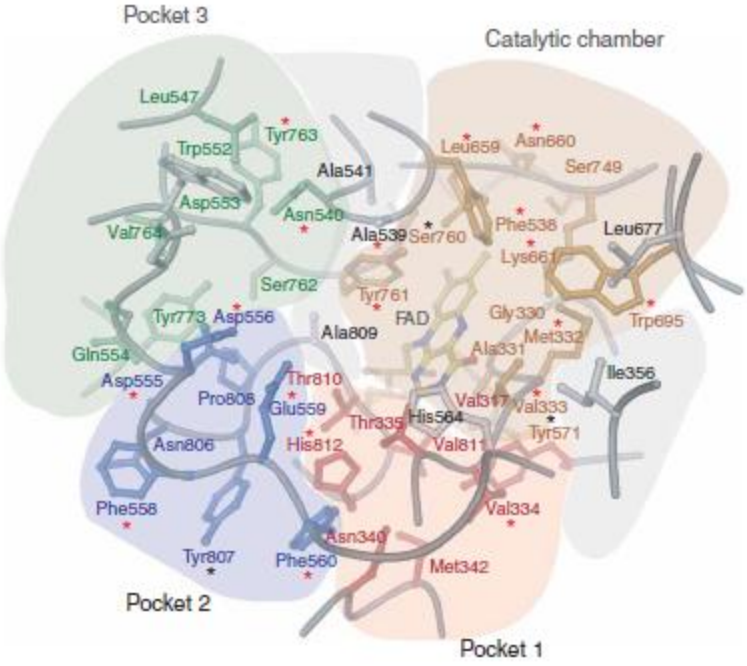

Figure 7.8. Location of the various pockets within the active site cavity.

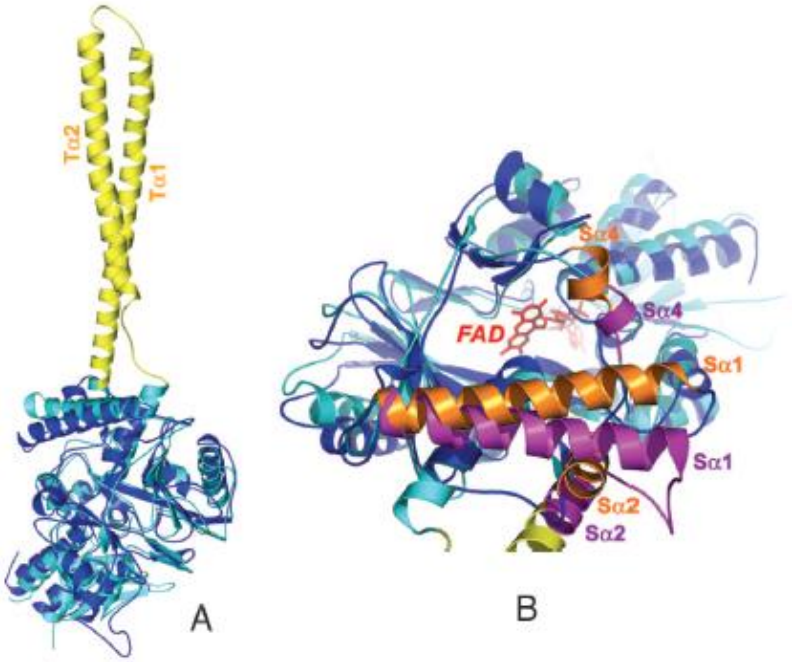

Figure 7.9. A) Superposition of LSD1 (cyan) on the structure of PAO (blue). The Tower domain of LSD1 is colored in yellow. B) Superposition of the AOL domain of LSD1(cyan and purple) on the structure of PAO (blue and orange) highlighting the differences in the catalytic cavity.

Although the similarity is evident in the FAD-binding subdomain, the structure of LSD1 substrate-binding subdomain differs from that of PAO in several aspects (Fig. 7.9A and B). LSD1 comprises a long insertion between Sα2 and Sα3 and contains a large catalytic cavity between the FAD- and substrate-binding subdomains with a volume of 1.245 $Å^3$. In contrast, the catalytic center of PAO is located in a narrow U-shaped tunnel with a significantly smaller volume (716 $Å^3$).[456] The difference in the shape of the substrate-binding site reflects the different substrate specificities of the two enzymes; indeed the substrates of LSD1 are methylated histone peptides which are bulkier than the linear-shaped substrates of PAO, like spermidine.[457] Furthermore the two diagonally interacting helices, Sα1 and Sα3, form a highly acidic flat surface at the entrance of the catalytic cavity, serving as an additional binding site for the basic histone H3 tail. Most of the residues forming this surface and the catalytic cavity are highly conserved not only among LSD1 orthologs in different species but also in LSD2, a close homolog of LSD1.[449]

The **tower domain** is formed by two long α-helices, TαA and TαB, which pack against each other without coiling, forming a left-handed superhelix. The sequence of the Tower domain reveals a repeating pattern of seven residues, $(abcdefg)_n$, the characteristic of coiled-coil proteins with hydrophobic amino acids predominating at positions *a* and *d* of the heptad repeat (Figure 7.10). A deletion mutant of LSD1 (LSD1ΔTower), in which the Tower domain was deleted and replaced by a pentaglycine loop, wasn't able to reduce the methylation level at K4. This result support the notion that the Tower domain is indispensable for the histone demethylase activity of LSD1. The Tower domain of LSD1 may also act as an adaptor to recruit other proteins. One of these proteins, CoREST, endows LSD1 with the ability to demethylate nucleosomal substrates and protects LSD1 from proteasomal degradation.[180] The Tower domain of LSD1 is, by itself, sufficient for a stable interaction with CoREST. The fact that LSD1ΔTower does not interact with CoREST indicates that the SWIRM and AOL domains of LSD1 do not significantly contribute to the interaction with CoREST. Based on these observations it is possible to conclude that the tower domain of LSD1 contains the binding site for CoREST.

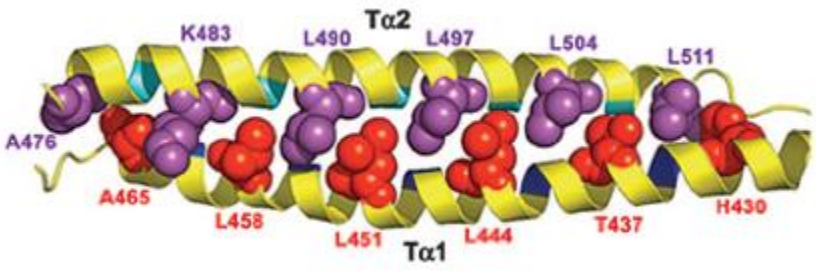

Figure 7.10. Ribbon diagram of the coiled coil of the Tower domain. The amino acids at the d positions of the heptad repeat of the two helices are in space-filling representation and colored in red (Tα1) and purple (Tα2), respectively.

7.2.1.2.2. The role of LSD1 in gene activation and repression

LSD1 transcriptional regulation remains confuse, essentially because LSD1 associates with different complexes and it can function as co-repressor or co-activator in a target specific manner. LSD1 has been found in different transcriptional complexes involved in transcription repression such as CoREST and NuRD. Consistent with its role in transcription repression, LSD1 demethylates monomethyl and dimethyl histone H3 lysine 4 (H3K4me1 and H3K4me2), which are marks of active chromatin transcription state. LSD1 has also been found to have a role in transcriptional activation as exemplified by the nuclear hormone receptors induced transcription (Figure 7.11).[498]

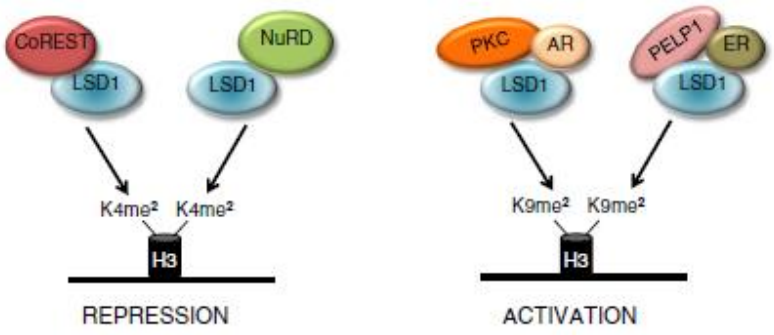

Figure 7.11. LSD1-associated complexes and their demethylation targets.

Recent studies report LSD1 in transcriptional activation mediated by nuclear receptors (the androgen and estrogen receptors, AR and ER) functioning as an H3K9 demethylase.[451,452] This function was firstly described by Metzger et al. who showed that activation of AR target genes requires LSD1-dependent histone H3K9 demethylation. They demonstrated that, following hormone treatment, AR and LSD1 colocalize on promoters and stimulate H3K9 demethylation without altering the H3K4 methylation status and promote ligand dependent transcription of AR target genes resulting in enhanced tumor cell growth.[445] Consistently, LSD1 knock-down resulted in decreased activation of AR-responsive promoters. Recently, a genome-wide analysis of LSD1 promoter occupancy following estrogen treatment of MCF7 cells has revealed striking results regarding the activatory role of LSD1.[451] LSD1 occupies nearly 20 % of the total assayed promoters and 84 % of these promoters are associated with RNA polymerase II and additionally with activation markers such as dimethyl-H3K4 and acetyl-H3K9 suggesting that LSD1 is extensively involved in gene activation. The dual role of LSD1 in gene repression and activation is also demonstrated by the fine regulation of growth hormone expression during pituitary development.[447] Activation of growth hormone expression is regulated by the transcriptional activator pituitary transcription factor 1 (Pit1) during the early phases through recruitment of a LSD1-containing mixed lineage leukemia 1 (MLL1) coactivator complex. Pit1 is later replaced by zinc finger E-box binding homeobox 1 (ZEB1), a transcriptional repressor which recruits a co-repressor complex containing

C-terminal binding protein (CtBP), CoREST and LSD1, switching off growth hormone expression. Until now it is not clear how LSD1 functions as a H3K9 demethylase in association with AR, ER or other transcription factors. Alternatively and more likely, other H3K9-specific histone demethylases could be recruited by LSD1 or by a LSD1-associated protein. In this case, LSD1 might act as a docking or adaptor module for different coactivator complexes that might contain a demethylase specific for H3K9. Indeed, it was observed that some chromatin-remodeling complexes contain both LSD1 and a H3K9 demethylase of the Jumonji-containing class JMJD2C.[458] JMJD2C assembles into the AR complex and collaborates in AR-target-gene transcription together with LSD1. In addition to its transcriptional regulation of individual genes, LSD1 plays an important role in interchromosomal interaction and nuclear rearrangement. Hu et al. showed that upon treatment of estrogen, LSD1 is recruited to distinct interchromatin granules, long thought to serve as "storage" site for the splicing machinery, some transcription elongation factors and various chromatin remodeling complexes, enhancing nuclear receptor-induced transcription.[459]

LSD1, as already mentioned, was originally identified as a component of transcriptional repressor complexes comprising transcriptional corepressor protein (CoREST) and HDAC1/2. In association with the transcription factor repressor element 1-silencing transcription factor (REST), the LSD1-CoREST-HDAC core mediates long-term repression of neuronal genes in nonneuronal cells and in neuronal precursors. The LSD1-CoREST-HDAC core is functionally and structurally conserved and was shown to be also involved in various biological processes.[460] In hematopoiesis, the LSD1-CoREST-HDAC core associates with growth factor independent 1 transcription repressor (Gfi-1) repressing Gfi-1 target genes.[461] LSD1-CoREST-HDAC core is also involved in silencing mature B-cell genes through direct interaction with the transcriptional repressor B lymphocyte-induced maturation protein-1 (Blimp-1).[462] Moreover, LSD1 can directly interact with p53 to confer p53-mediated transcriptional repression, such as the repression of the alpha-fetoprotein (AFP), whereas the well known p53 target gene p21 can be actively transcribed without recruitment of LSD1. This finding suggests that LSD1 is targeted to chromatin by p53 but likely in a gene-specific manner.[463] Liu et al. have reported that the amine oxidase domain of LSD1 is important in suppressing SALL4-mediated reporter transcription. The stem cell protein SALL4 plays a critical role in hematopoiesis by regulating the cell fate. This study revealed that LSD1 may negatively regulate SALL4-mediated transcription, and the dynamic regulation of SALL4-associated epigenetic factors cooperatively modulates early hematopoietic precursor proliferation.[464] Another important indication of LSD1 involvement in gene repression is that the DNA methylase regulator DNMT3L recognizes histone H3 tails that are unmethylated at H3K4. This finding suggests the importance of LSD1 in the formation and propagation of heterochromatin through LSD1-dependent H3K4 demethylation and following *de novo* DNA methylation.[465]

In 2010 Lin and colleagues first investigated the interaction between LSD1 and the transcription factor SNAIL1 that has a key roles in development and oncogenesis. On the basis of a weak sequence similarity between SNAIL1 and the histone H3 N-terminal tail they proposed that SNAIL1 could bind to LSD1 in the same site of the histone H3 substrate. This model for SNAIL1-LSD1 interactions implied that SNAIL1 should inhibit LSD1 enzymatic activity.[466] Consistently, Baron et al. found that a 20-amino-acid peptide corresponding to SNAIL1 N-terminal residues effectively inhibits LSD1-CoREST.[467] Moreover to explain the mechanism of SNAIL1 recognition by LSD1 they determined the crystal structure of the ternary complex LSD1-CoREST/SNAIL1 peptide at 3.0 Å resolution (Figure 7.12).[467] The peptide occupies the open cleft that has been shown to form the binding site for the H3 tail.[468] The comparative analysis of the H3 and SNAIL1 complexes clearly indicates that Arg7 of SNAIL1 occupies the same position and establishes similar interactions (with Cys360, Asp375, and Glu379) as Arg8 of H3. In conclusion SNAIL1 N-terminal residues act as a mimic of H3 being able to effectively bind to the enzyme active-site cleft. Alignment of the N-terminal sequences of the common SNAG domain of SNAIL1 and H3 reveals that the residues that are key for binding to LSD1, as gathered from the SNAIL1/LSD1/CoREST crystal structure, are conserved among almost all SNAIL1-related proteins. This feature predicts that other transcription factors of the SNAIL/Scratch family are likely to associate to LSD1 (and possibly LSD2) following the same molecular mechanism highlighted by SNAIL1. SNAIL1 directly interacts with the LSD1 histone demethylase and recruits the LSD1 complex to the E-cadherin and other epithelial gene promoters, resulting in downregulation of the active H3K4m2 mark and promoter activity. LSD1 serves as an essential effector of SNAIL1-dependent transcriptional repression of epithelial genes, suggesting that the LSD1 complex could be a potential therapeutic target for Epithelial-mesenchymal transition (EMT) and tumor invasion.[469,470]

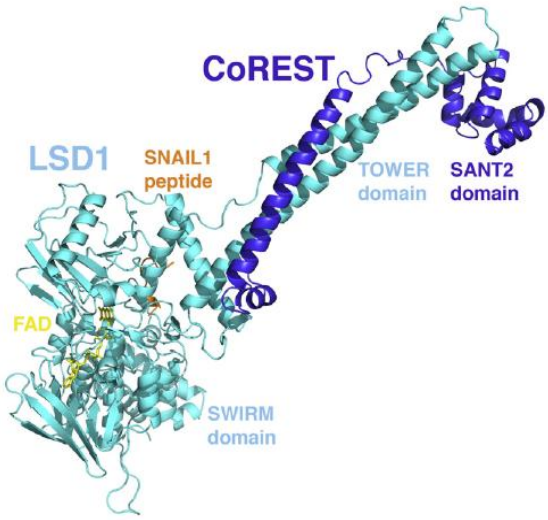

Figure 7.12. Ribbon representation of the ternary complex of LSD1 (cyan), CoREST (blue), and the SNAIL1 peptide (orange).The cofactor FAD is in yellow sticks.

7.2.1.2.3. LSD1 and cancer

LSD1 has been reported to be associated with cancer only few years ago and it has been found to possess oncogenic properties in several cancers ranging from prostate,[471] bladder,[472] neuroblastomas,[473] lung cancers,[474] sarcomas and hepato-carcinomas.[475] LSD1 inhibition reduces or blocks cell growth in many of these tumors, while its over-expression has been found to contribute to human carcinogenesis through chromatin modification.[476] Recent advances in leukemia biology come from studies that investigated on genetic and epigenetic abnormalities in leukemic cells.[477] The role of LSD1 as essential regulator of leukemia stem cells (LSC) potential has been described in a mouse and human models of human MLL-AF9 leukemia.[478] The extent of LSD1 knockdown significantly correlated with loss of the LSC potential of acute myeloid leukemia (AML) cells through impairment of differentiation and apoptosis. Cells without active LSD1 are unable to form colonies (consistent with loss of LSC potential) exhibit differentiated cell morphology and are not able to cause leukemia when introduced into mice.[479] It is clearly demonstrated that in AML demethylation by LSD1 is related with activation of LSC associated to oncogenic target genes. The mechanisms by which LSD1 functions at its target genes and the protein complexes recruited by LSD1 at these loci require further investigations.[480] In T-cell acute lymphoblastic leukemia (T-ALL), Notch mediated regulation of its targets is the first example of the dual role of LSD1 as activator or repressor; it is known that the DNA-binding factor CSL binds and represses Notch targets in the absence of Notch, while the presence of Notch converts CSL in a transcriptional activator. The finding that LSD1 interacts with CSL explains the mechanism through which Notch determines gene repression by removing the H3K4me2 marks at Notch targets in the absence of Notch. Indeed, a functional switch of LSD1 activity is observed upon Notch activation. In the absence of Notch, LSD1 triggers H3K4me2 demethylation while in its presence the enzyme acts preferentially on H3K9me2 leading to activation of target genes. Thus, LSD1 inhibition in T-ALL reproduces cell growth arrest and alteration of growth, and a phenotype was previously attributed to Notch silencing.[481] High levels of LSD1 protein have been found in several types of solid tumors and are associated with poor prognosis. This is the reason why LSD1 has been proposed as a biomarker for neuroblastoma, non-small cell lung carcinomas (NSCLC), breast and prostate cancers. In NSCLC it has been shown that down regulation of LSD1 expression by the pharmacological inhibitor pargyline or by specific siRNAs determines suppression of cell growth, migration and invasion. Similarly, LSD1 immuno-reactivity is increased in a substantial fraction of hepato-carcinomas (HCC), and LSD1 knockdown in HCC cells decreases substantial cell proliferation. [471-473]

7.2.1.3. LSD2

LSD2 (AOF1 or KDM1B) has been recently identified as a homolog of LSD1 and it demethylates H3K4me2/1 like LSD1. In LSD2 the SWIRM domain is involved in an interaction with glyoxylate reductase 1 homolog (GLYR1; also known as NPAC), which positively stimulates demethylase activity. This interaction is mediated through a unique coiled loop that is not found in the SWIRM domain of LSD1, thus NPAC does not associate with LSD1. Apart from sharing the AOL and SWIRM domains, LSD1 and LSD2 have different domain architectures, associate with different proteins and show different genomic distribution profiles. One of the most striking differences is that LSD1 forms part CoREST complex and this interaction is due to the presence of a coiled-coil 'Tower' domain inserted into the AOL domain of LSD1. LSD2 does not have a Tower domain but instead has an a unique N-terminal zinc finger domain of unknown function (Figure 7.13).[482-484]

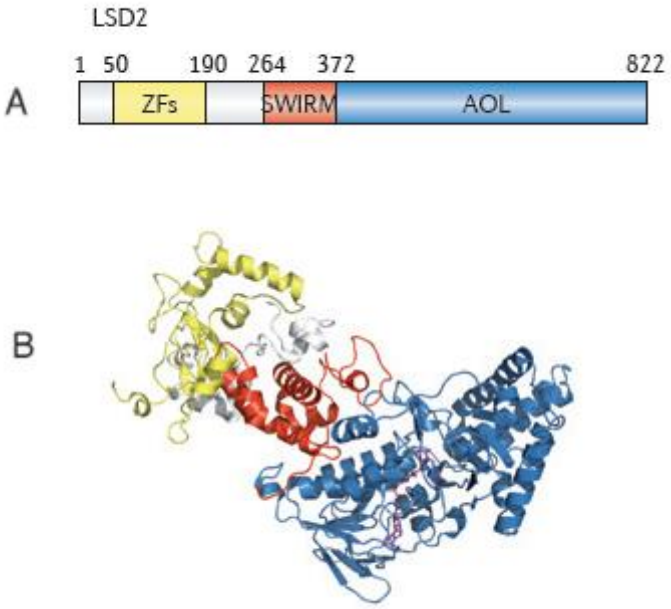

Figure 7.13. (A) Ribbon diagram of the LSD2 structure. (B) Domain organization of LSD2.

A genome-wide mapping analysis has revealed that LSD2 primarily resides in the intragenic regions of actively expressed genes. LSD2 may activate its target genes, possibly via its association with transcriptional elongation factors.[485] LSD2 seems to be not essential for mouse development. However, the DNA methylation of several imprinted genes is lost in oocytes from LSD2-deleted females. Consequently, the embryos derived from these oocytes exhibited biallelic expression or silencing (i.e., loss of monoallelic expression) of the affected imprinted genes and died before midgestation.[486] The molecular mechanism underlying the functional link between H3K4 demethylation and DNA methylation for expression of imprinted genes remains to be investigated.

7.2.2. The Jumonji C domain-containing demethylases

The second family of histone lysine demethylases is characterized by the presence of the catalytic Jumonji C (JmjC) domain. The first JmjC domain protein was identified in a gene trap screen for factors involved in neural tube formation. The homozygous mutant mice showed abnormal groove formation on the neural plate and a defect in neural tube closure. Takeuchi et al. called this mutation jumonji (Jmj), since homozygous mutant mice usually form an additional groove at the future midbrain–hindbrain boundary that intersects the normal neural groove, resulting in a ‘‘cross’’-shaped cut on the neural plate (in Japanese jumonji means cruciform).[487] The Jumonji protein family demethylases is named this way because it contains the conserved JmjC catalytic domain that was first identified in the so called Jumonji protein JARID2.[488] The JmjC domain is present in 31 human proteins, about 20 have been published to demethylate specific lysines in the histone (Table 7.2). Depending on the homology of the JmjC domain and the presence of other domains, these histone lysine demethylases can be divided into seven subfamilies (Figure 7.14).[489]

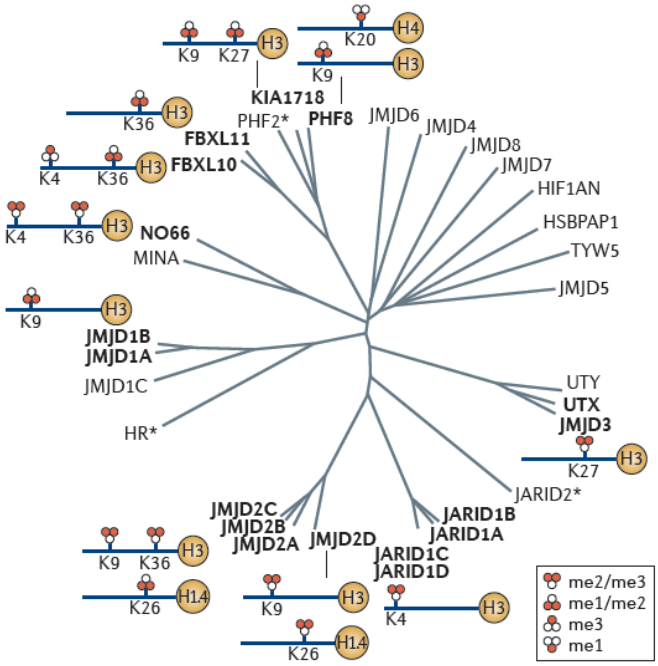

Figure 7.14. Phylogenetic tree of Jumonji C (JmjC) domain-containing proteins. Proteins demonstrated to be histone lysine demethylases are marked in bold and their histone residue and methylation-level specificities are indicated. Proteins with a non-canonical amino acid at a position involved in cofactor binding are marked with an asterisk and may be catalytically inactive.

7.2.2.1. Catalytic mechanism and structural studies

In contrast to the flavin-dependent demethylases LSD1/2, which require the presence of an intermediate iminium cation in their catalytic cycle, the demethylases containing a JmjC domain act via a fundamentally different reaction mechanism. This also allows the removal of a trimethyl mark, which is not possible for LSD1-type demethylases due to chemical reasons.[490] Jumonji-type demethylases belong to

the cupin superfamily of oxygenases and contain an Fe^{2+} ion in their catalytic domain and use α-ketoglutarate as co-substrate. The proposed mechanism of action of JmjC domain containing demethylases is commonly assumed to be similar to that of other Fe(II)-containing and α-ketoglutarate-dependent hydroxylases. A plausible sequence of reaction steps is outlined in Figure 7.15.[491,492]

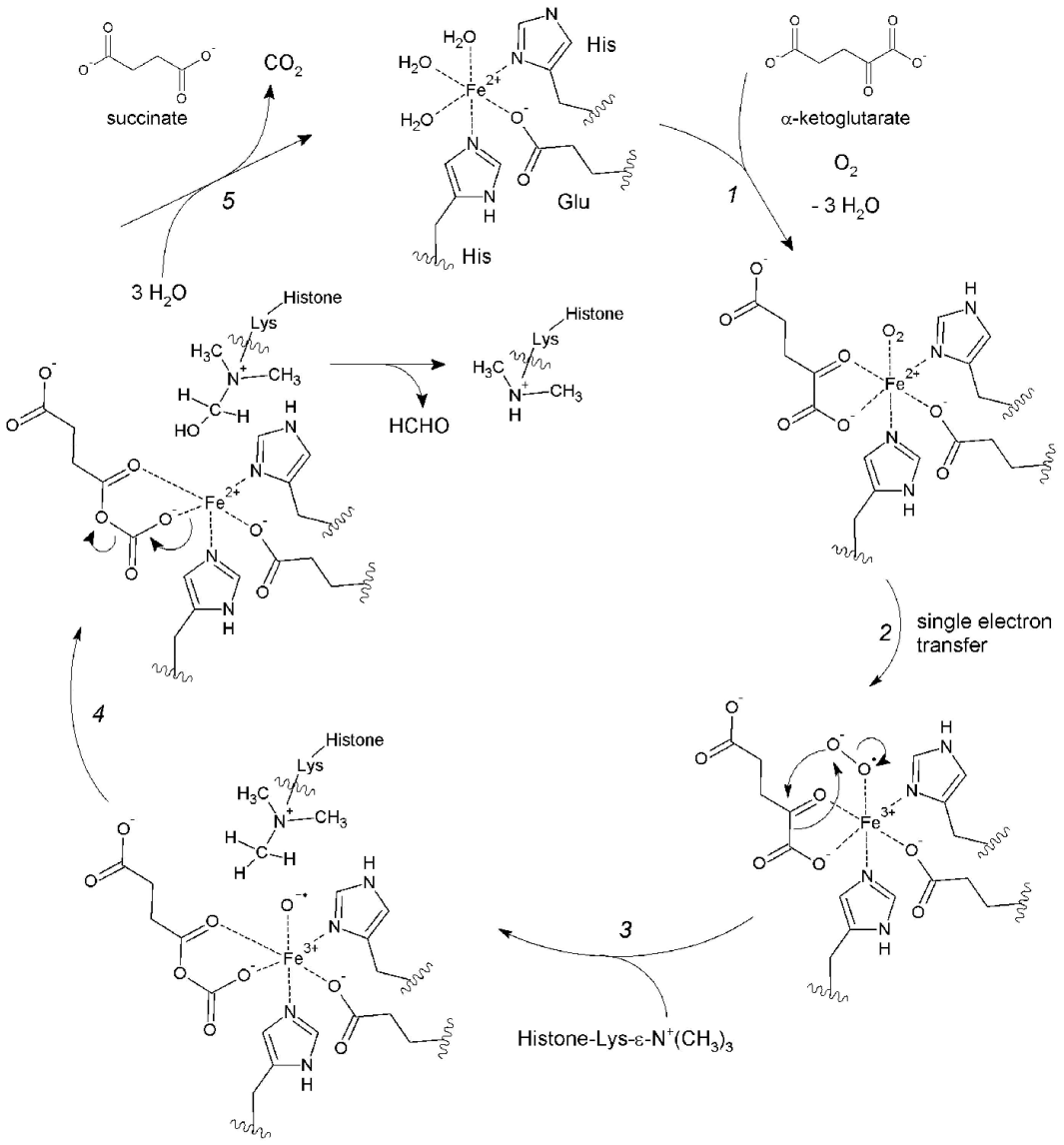

Figure 7.15. Catalytic mechanism of JumonjiC domain ontaining demethylases.

The catalytically active iron ion in the unbound state is in the 2^+ oxidation state and coordinated by two histidine residues, a glutamate residue, and three molecules of water. Initially, the co-substrate α-ketoglutarate as well as dioxygen are coordinated onto the iron center, displacing the water ligands (step 1). Most likely, a single electron transfer occurs next from the iron(II) ion onto the coordinated oxygen yielding a reactive peroxide radical anion species (step 2). This can, in turn, attack the α-ketoglutarate ligand leading to a mixed anhydride bound to the remaining

iron(III)-hydroxyl radical anion (step 3). This highly reactive hydroxyl radical is able to activate the stable C-H bond in the adjacent methyl group of the substrate methyllysine and to form hydroxymethyllysine via abstraction of a proton and subsequent transfer of the hydroxyl group onto the methyl carbon atom (step 4) leaving behind a coordinative gap on the central iron (II) ion. Upon dissociation of the bound mixed anhydride from the central iron, it decomposes into carbon dioxide and succinate as byproducts (step 5). Binding of three molecules of water regenerates the original catalytic species. This reaction cycle could, in principle, be repeated resulting in removal of one methyl group after the other.[491]

Crystal structures have been described for α-ketoglutarate histone demethylases with different selectivities. In Figure 7.16, the crystal structures of JMJD2A and PHF8 are reported.[493-495] These structures reveal the target lysine residue to be bound in an extended form in a relatively wide cleft formed primarily by the side chains of hydrophobic residues, which position the Nε-methyl group adjacent to the active site Fe(II). Variations in the size of the active site region binding the Nε-methyl group are proposed, in part, to confer methylation state selectivity; the degree of selectivity varies with the particular enzyme or subfamily.

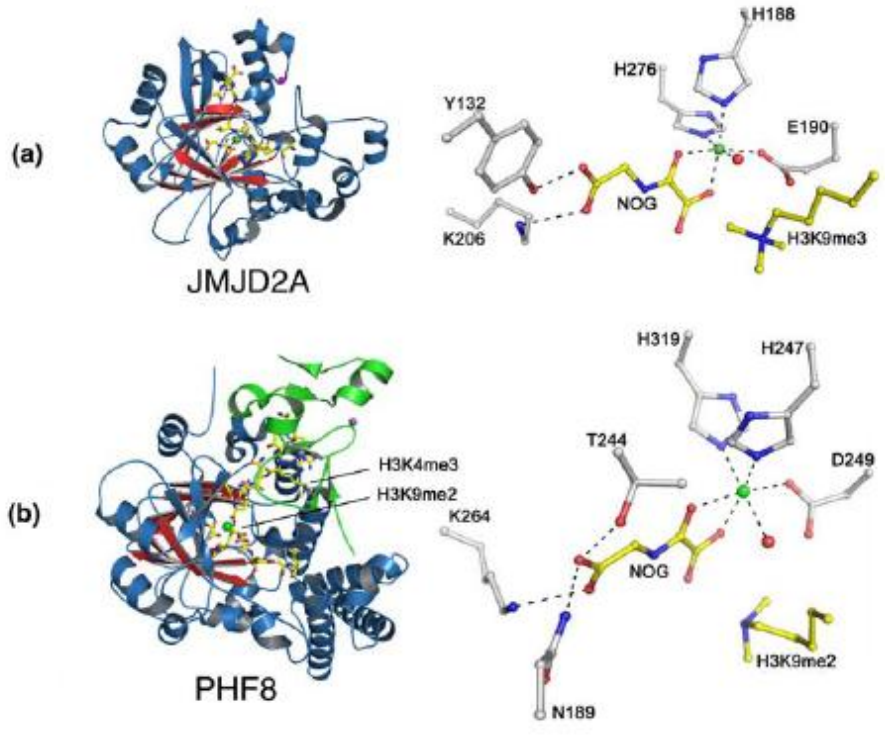

Figure 7.16. Crystal structures of α-ketoglutarate histone demethylases. a) Catalytic domain of the histone demethylase JMJD2A in complex with a fragment of H3K9me3. b) Catalytic and methyl-lysine binding PHD (green) domains of PHF8 in complex with H3K4me3 and H3K9me2 substrate fragment.

The crystal structure of the catalytic core of JMJD2A shows that, although the JmjC domain contains the sites of interaction for the two cofactors, Fe(II) and α-ketoglutarate, additional domains are needed for catalytic activity. In the JMJD2 family, two regions within the N terminus and a region immediately upstream of the JmjC domain complete the catalytic centre.[496,497] In contrast to LSD1, the structure of the JmjC demethylase JMJD2A shows that the binding pocket specifically recognizes and fits trimethylated Lys residues. H3K36me3 and H3K9me3 are both substrates for JMJD2A, but they are bound in different conformations with a broad conformation for H3K9me3 and a more tightly bent, U-shaped conformation for H3K36me3.[498] The structural data of JMJD2A in complex with different H3 peptides further shows that it is the sequence of the H3 peptide surrounding the Lys residues that is important for substrate specificity: for H3K9me3, the preferred substrate of JMJD2A, two nearby Gly residues seem to be important for acquiring the required conformation, whereas two Gly residues and a Pro residue provide binding specificity for H3K36me3. Other Lys residues that lack these adjacent amino acids in their primary structure cannot access the catalytic centre.

The importance of binding domains was first illustrated for the histone demethylases PHF8. In addition to JmjC catalytic domain, PHF8 has a plant homeobox domain that binds to the Nε-trimethylated form of lysine 4 of histone H3; this interaction increases the activity of the catalytic domain with regards to demethylation of Nε-dimethylated lysine9 histone H3.[499] Crystallographic analyses have revealed the structural basis for this activation process (Figure 7.16b).[494]

7.2.2.2. FBXL subfamily

The first JmjC domain-containing protein shown to be a histone lysine demethylase was FBXL11 (F-box and leucine-rich repeat protein 11). FBXL11 and FBLX10 have been demonstrated to catalyze H3K36me2/me1 demethylation.[500] In addition, mammalian FBXL10 has been suggested to act as an H3K4me3 demethylase, but this activity is still controversial.[501] FBXL10 besides having the catalytic JmjC domain, contain an F-box (which is a signature domain for a component of SCF (SKP1–cullin-1–F-box) E3 ligases) and a CXXC DNA-binding domain. The recent demonstration that FBXL10 regulates the expression of Polycomb target genes suggests that FBXL10 might contribute to tumorigenesis through the regulation of these genes.[502]

Moreover retroviral insertional mutagenesis within the FBXL10 gene has been shown to cause lymphoma in BLM (Bloom syndrome RecQ protein-like-3 DNA helicase)-deficient mice so indicating FBLX10 as a candidate tumour suppressor.[503] Other studies have proposed FBXL10, along with FBXL11, as a putative proto-oncogene.[504] Expression data from human cancers show over-expression of FBXL10 in lymphomas and adenocarcinomas,[504] but reduced expression of FBLX10 and FBXL11 in prostate cancer and in the most aggressive of the primary brain tumours, the glioblastoma multiform, respectively.[505]

7.2.2.3. JMJD1 subfamily

JMJD1A is a histone demethylase specific for H3K9me2/me1.[506] Two JMJD1A homologues exist in human cells: JMJD1B and JMJD1C. JMJD1A has a characteristic LXXLL motif that is involved in nuclear receptor interactions.[507] The expression of JMJD1A has been implicated in demethylation of H3K9me2 of androgen receptor (AR) target genes.[506] Indeed, JMJD1A was found to interact with the AR in a ligand-dependent manner.

Studies of knockout mice have demonstrated important roles for JMJD1 in germ cell development and metabolism.[508,509] JMJD1A knockout mice also exhibit an adult onset obesity phenotype and, in this context, JMJD1A has been implicated in the transcriptional control of metabolic genes in muscle and adipose tissues.[508] JMJD1A is highly and dynamically expressed during spermatogenesis, and male JMJD1A genetrap mice are infertile, with small testes and a severe reduction in sperm count. This defect has been linked to JMJD1A positively regulating expression of genes involved in sperm chromatin condensation and maturation through demethylation of H3K9me2/me1.[509] During hypoxia JMJD1A stimulates the expression of HIF target genes such as adrenomedullin (ADM). Krieg et al. showed that the expression of ADM is regulated by JMJD1A under hypoxia in colon cancer, and that ADM facilitates the growth of colon carcinoma cells. However, the regulatory mechanisms of JMJD1A and its target gene ADM during hypoxia have not yet been elucidated in hepatocellular carcinoma (HCC) and breast cancer cells.[510,511] Frequent deletion of 5q31 locating *JMJD1B* gene or reduced expression of JMJD1C in various malignancies suggest possible roles of JMJD1 proteins in tumor suppression.[512]

7.2.2.4. JMJD2 subfamily

JMJD2 subfamily, containing four expressed members JMJD2A to JMJD2D, are selective for the demethylation of the tri- and di-Nε- methylation states of specific lysines on histone H3. Interestingly, different members of this family have slightly different substrate preferences.[513] Thus, JMJD2D can demethylate H3K9me2 and H3K9me3 but not H3K36me2 and H3K36me3. Sequence alignment of JMJD2A and JMJD2D shows that a variable Ser/Ala position in the binding pocket is responsible for this different selectivity, and by generating Ser288Ala and Ala291Ser mutations in JMJD2A and JMJD2D, respectively, it is possible to switch the substrate specificity of the two enzymes.[496] Strong genetic data have linked the loss of H3K9 trimethylation to the development of cancer in various mouse models, thus a decrease in H3K9me3 levels can accelerate carcinogenesis in a mouse model of T cell lymphoma.[514] Given that the JMJD2 family of proteins are H3K9me3 and H3K9me2 demethylases, it is plausible that overexpression of these proteins would result in similar effects. Furthermore several studies have shown that JMJD2C is required for growth in an array of different cancer cell lines, including squamous cell carcinoma,[515] prostate carcinoma,[458] breast carcinoma[516] and diffuse large B cell lymphoma.[517] Introduction of JMJD2C gene in normal breast MCF10A cells could

increase the capacity to generate mammospheres, a phenotype of cancer stem cells, suggesting that GASC1 acts as a transforming gene.[516] The involvement of JMJD2C in tumorigenesis has been supported further by a recent study demonstrating the functional interaction between JMJD2C and AR in prostate carcinoma.[458] It was already known the cooperation between LSD1 and JMJD1A for the transcriptional activation of AR responsive genes, and for proliferation of prostate cancer cells. Although LSD1 and JMJD1A only demethylate H3K9me2/1, JMJD2C is especially capable of efficiently demethylating H3K9me3, inducing a robust cooperative stimulation of AR transcriptional activity. Thus, specific modulation of JMJD2C activity alone, or in combination with LSD1, may be a promising therapeutic strategy to control AR activity in tissues where AR has a key physiological role.

7.2.2.5. JARID1 subfamily

The members of the JARID1 subfamily (JARID1A-D) are able to demethylase tri- and dimethylated H3K4. Despite the fact that other members of JARID1 family catalyze the demethylation of the same histone mark, they appear to have unique functional properties probably due to their divergent expression profiles and presence in distinct protein complexes.

JARID1A has a role in the regulation of circadian clock length that is not the result of its catalytic demethylase activity but possibly depends on JARID1A mediated inhibition of histone deacetylase HDAC1.[517,518] JARID1A forms a complex with CLOCK and BMAL1, transcription factors that are key in the regulation of animal circadian rhythms. In mammalian cells, deletion of JARID1A causes a reduction in the activation of circadian genes and a shortening of the circadian rhythm. These changes in gene expression are accompanied by reduced histone H3K9 acetylation and can be rescued by catalytically inactive JARID1A.[518] Moreover JARID1A has been shown to be a key effector of retinoblastoma protein (pRB) mediated cell cycle withdrawal and differentiation by interacting with the tumor suppressor pRB.[519]

A recent study found that it is overexpressed in gastric cancer and that its inhibition leads to cellular senescence of gastric and cervical cancer cells by derepressing cyclin dependent kinase inhibitors like p27, p21 and p16.[520] Enhanced JARID1A expression was found to contribute to drug tolerance in a non-small cell lung carcinoma (NSCLC) cell-system. These drug-tolerant NSCLC cells display reduced levels of H3K4me2 and H3K4me3 which is reminiscent of the prognostic value of reduced H3K4me3 in NSCLC.[521] This also indicates that acquired drug resistances are accompanied by epigenetic changes, and combining a chromatin modifying agent with a single rationally targeted agent would prevent the development of drug resistance.

JARID1B, which targets H3K4me2 and H3K4me3, is mainly associated with transcription start sites (TSSs) and coding regions in embryonic stem (ES) cells.[522] Knockdown of JARID1B results in an average 2.2 fold increase of H3K4me3 at JARID1B targets. However, only 3.4% of JARID1B target genes are differentially expressed following its depletion in these cells. Nonetheless, depletion of JARID1B

results in a failure to properly initiate ectodermal differentiation *in vitro*. Thus, it has been hypothesized that the function of JARID1B is to maintain H3K4me3 at low or intermediate levels at its target genes, thereby fine-tuning transcription levels and ensuring the proper execution of differentiation programmes.[522] This protein is overexpressed in various different cancers, including breast, prostate and bladder carcinoma.[523-525] It has been reported that JARID1B is required for the growth of a breast cancer cell line and for the continuous growth of melanoma.[526,527]
JARID1C has been implicated in X-linked mental retardation and epilepsy.[528] Its role in the pathogenesis of human papillomavirus (HPV)-associated cancers has been very recently identified by a genome-wide siRNA screen showing JARID1C as one of the E2-dependent regulators of HPV oncogene expression.[529]

7.2.2.6.UTX- JMJD3 subfamily

The JmjC domain-containing proteins, UTX (ubiquitously transcribed tetratricopeptide repeat, X chromosome) and JMJD3, can specifically remove di- and trimethyl marks from H3K27 and, thereby counteract PcG-mediated histone modification by EZH2. JMJD3 is recruited to promoters that have increased H3K4me3 levels following lipopolysaccharide (LPS) treatment of macrophages.[530,531] Interestingly, most of the promoters bound by JMJD3 are not associated with H3K27me3 before JMJD3 binding, and only a minor fraction of the H3K27me3 positive promoters that are bound by JMJD3 shows decreased levels of H3K27me3 after LPS treatment. Moreover, JMJD3 depletion only affects the expression of relatively few genes and does not result in an increase of H3K27me3. Thus, JMJD3 might instead serve as a safeguard against further H3K27 methylation, thereby ensuring the activation of target genes in response to LPS treatment.[531] UTX is associated with MLL3/4 complexes and was the first reported mutated histone demethylase gene associated with cancer.[532,533] Biallelic somatic mutations of UTX in several human cancers (with highest prevalence in multiple myeloma) clearly suggested UTX role as a tumor suppressor gene.[534]

7.2.2.7. The PHF2- PHF8 subfamily

The PHF2/PHF8 subfamily includes PHF2, PHF8 and KIAA1718; they have a plant homeo domain (PHD)-type zinc finger motif in addition to a JmjC domain (Figure 7.17).[535]

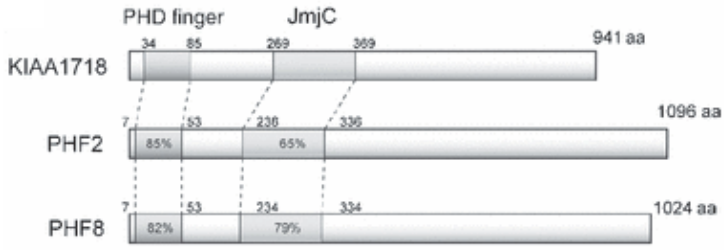

Figure 7.17. Schematic representation of mouse KIAA1718 and the PHF2/PHF8 protein family. The percentage identity is indicated in the aligned sequences for the PHD finger and jumonjiC domains.

PHF8 targets H3K9me1 and H3K9me2, whereas its close relative KIAA1718 catalyses demethylation of both mono-and dimethylated H3K9 and H3K27.[499] This difference in substrate specificity has been ascribed to different distances between the JmjC and PHD finger domains. Both enzymes associate with H3K4me3 through their PHD domain, but PHF8 has a shorter, more flexible linker that assumes a bent conformation, allowing its JmjC domain to interact with and demethylate H3K9me1 and H3K9me2. For KIAA1718, the linker is longer and more rigid, resulting in an extended conformation that renders it inactive towards H3K9me1 and H3K9me2 in the presence of nearby H3K4me3, and leads to selectivity towards H3K27me1 and H3K27me2 *in vitro*.[536]

In this model for substrate recognition by PHF8 and KIAA1718, the presence of H3K4me3 seems to lead demethylase activity towards Lys27 and Lys9 residues on the same tail *in vitro*. However, in a study of the *C. elegans* homologue of KIAA1718 (ceKDM7A), the PHD domain of ceKDM7A binds to H3K4me3 on one H3 tail and to the substrate H3K9me2 or H3K27me2 on another H3 tail. Moreover, the PHD domain of ceKDM7A and its binding to H3K4me3 is required for the *in vivo* demethylase activity towards both H3K27me2 and H3K9me2, suggesting that the presence of H3K4me3 does not necessarily lead to preferential demethylation of H3K27me2 by ceKDM7A *in vivo*.[537]

PHF8 also binds to H3K4me3-positive genes but not necessarily to regions that carry its target histone modifications. The loss of PHF8 most often affects the expression of genes to which it binds, but the expression of 95% of PHF8 target genes remains unchanged. Furthermore, the depletion of PHF8 does not lead to detectable changes in H3K9me2 levels and only produces minor changes in H3K9me1 and H4K20me1 levels associated with target genes.[538]

In 2010, Huang et al. demonstrate that KIAA1718 plays an important role in neural differentiation, using a mouse embryonic stem cell (ESC) differentiation system. The

neural promoting effect is mediated by FGF4, a molecule involved in neural differentiation. How KIAA1718 is recruited to the promoter region of FGF4 gene remains to be determined.[539] It is possible that KIAA1718 is recruited by a protein complex that contains DNA- or histone-binding activities, but it is also possible that KIAA1718 is recruited by pre-existing epigenetic marks. Since H3K9me2 and H3K27me2 are important epigenetic marks associated with transcription repression, a histone demethylase for these two marks may have many biological functions. However, futher studies using transgenic and knockout mouse models are needed to reveal other biological functions of KIAA1718.

7.2.3. KMD Inhibitors

7.2.3.1. LSD1 inhibitors

The first generation of LSD1 inhibitors that were discovered, was based on its homology with monoamine oxidases, which also use FAD as cofactor. Since MAO enzymes are established targets for the treatment of neurological disorders, a large number of inhibitors have been synthesized and tested for specificity towards MAO enzymes. MAO inhibitors were tested for their ability to inhibit LSD1 and tranylcypromine and phenelzine were shown to inhibit LSD1 activity with the highest potency (IC_{50}=21 μM) (Figure 7.18). In addition, chemically synthesized propargyl lysine-derivatised histone H3 tail peptide could irreversibly inhibit LSD1. Recently, polyamine analogues (bisguanidine and biguanidine types) have also been characterized as potent non-competitive inhibitors of LSD1 (Figure 7.19).

Anti-MAO-Based Small Molecules

Due to the high sequence similarity between LSD1 and MAO, some known anti-MAO agents were tested against LSD1. Pargyline (**1**), a propargylamine-based anti-MAO initially suggested as a valuable LSD1 inhibitor prototype, failed in further studies to inhibit the lysine demethylase.[540] Phenelzine (**2**), an anti-MAO agent bearing a hydrazine moiety, has a potency against LSD1 (K_i= 17.6 μM), similar to that displayed versus MAOs.[541] Tranylcypromine (*trans*-2-phenylcyclopropyl-1-amine, *trans*-2-PCPA, **3**) was reported to inhibit LSD1 with a K_i value ranging from 477 to 22 μM, depending on the type of assay and condition used for testing.[542,543] Nevertheless, *trans*-2-PCPA became a useful lead to develop highly potent small-molecule inhibitors of LSD1. Interestingly, the introduction of a bulky branched substituent at the 4 position of the benzene ring, able to occupy the wide space present in the LSD1 cavity surrounding the FAD cofactor and the AO domain, furnished tranylcypromine-based compounds such as **4**-**9** endowed with high potency against LSD1 and weak or no activity against MAOs.[544,545] Compounds **4** and **5** were also reported to be active against a panel of cancer cell lines (HeLa cervix cancer, PC3 prostate cancer, KYSE150 esophagus cancer) with growth inhibition 50% (GI_{50}) values ranging from 6.0 to 67 μM,[544] whereas **8** was able to inhibit cell growth and

induce differentiation in murine acute promyelocytic leukemia (APL) blasts as a single agent and in APL-derived NB4 cells in synergy with retinoic acid (RA).[545]

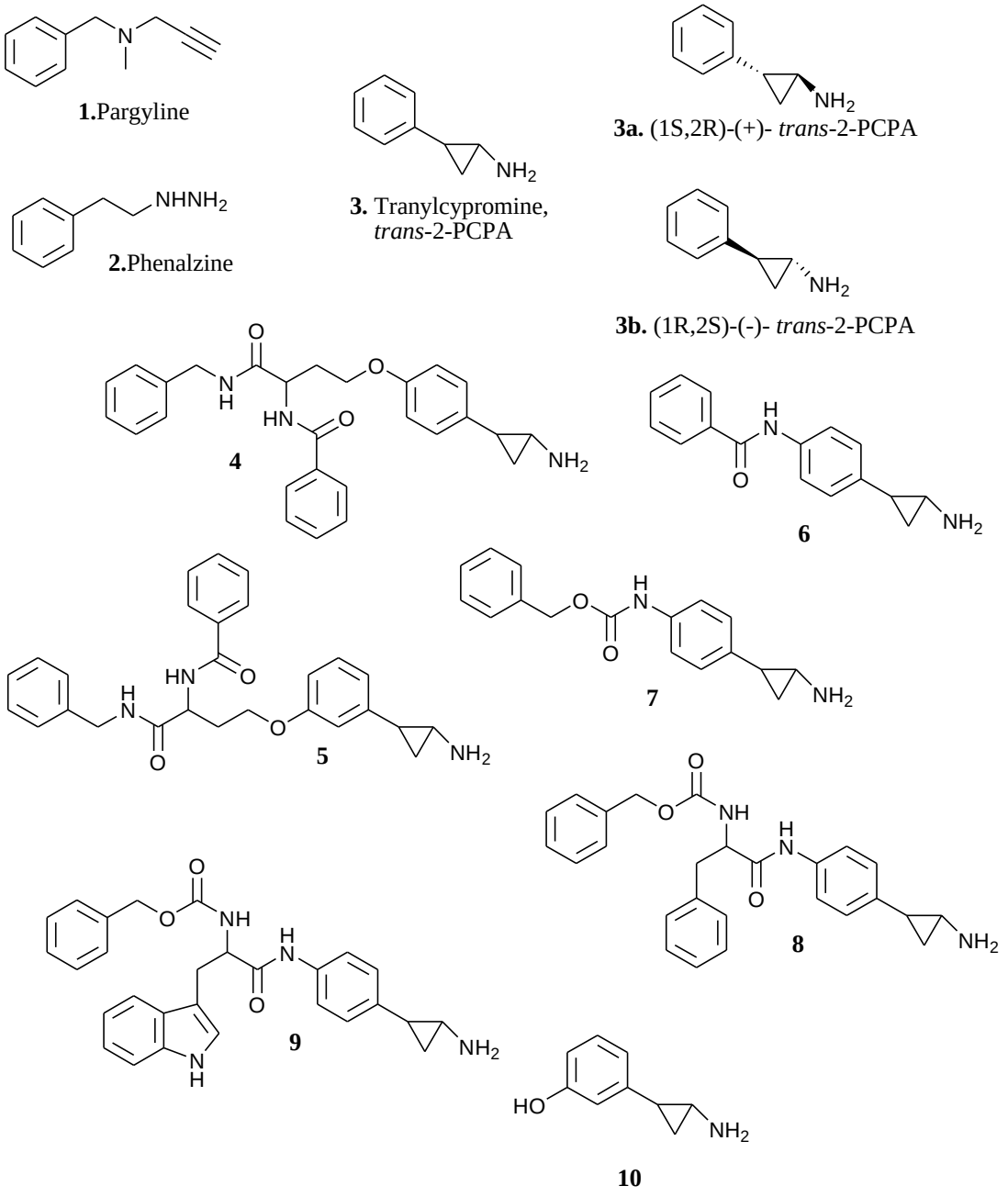

Figure 7.18. Anti-MAO- Based small molecules.

As *trans*-2-PCPA is the racemic mixture of 2 enantiomers, (+)-*trans*-2-PCPA and (–)-*trans*-2-PCPA, Mai and colleagues prepared large amounts of *trans*- and *cis*-2-PCPA, separated the 2 *trans*- and 2 *cis*-enantiomers, and tested them against LSD1 and MAOs, determining their binding to FAD through X-ray crystallography.[544] They reporter that the 2 *trans*-enantiomers of 2-PCPA were slightly more potent than the 2 *cis* congeners against LSD1, with (–)-*trans*-2-PCPA (**3b**) being 1.7- fold more efficient than (+)-*trans*-2-PCPA (**3a**). Conversely, against MAO-B, (+)-*trans*-2-

PCPA was 20-fold more potent than the corresponding (–) enantiomer, highlighting the crucial role of stereochemistry in MAO-B inhibition by *trans*-2-PCPA. Recently, a novel PCPA derivative named OG-L002 (**10**) has been identified to be a highly specific LSD1 inhibitor ($IC_{50}\approx$ 0.02 μM), showing a >36-fold selectivity over MAOases.[545]

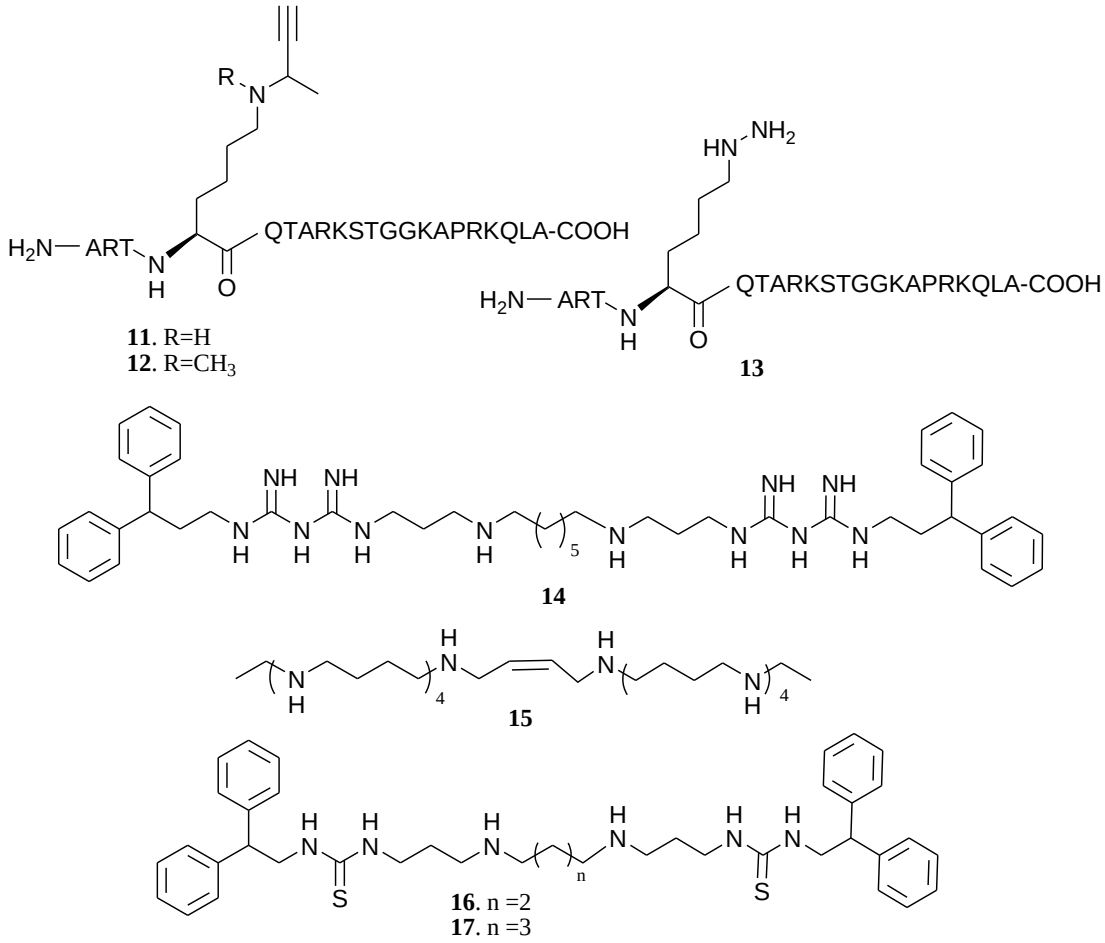

Figure 7.19. Substrates analogues and polyamines.

Substrates analogues

In search of more selective inhibitors, a series of peptide-based inhibitors, such as compounds with the propargylamine or hydrazine functionality were synthesized in the context of a histone H3 peptide. H3-tail peptides require at least 15 amino acid residues for efficient reaction (Figure 7.19). Based on this observation the propargyl-Lys-derivatized peptide **11** was designed as a mechanism-based LSD1 inhibitor. This compound **11** exhibited K_i= 16.6 and then 0.77 μM against LSD1, showing a clear time and concentration dependent inhibition of the enzyme. X-ray crystal structure of the LSD1/**12** complex suggested that LSD1 inactivation involves amine oxidation followed by Michael addition of the $FADH_2$ N^5 to the propargylic imine.[546] The analog bearing a hydrazine (**13**) exhibit the most potent LSD1 inhibitory activity

(K_i=4.35 nM).[547] However, poor membrane permeability limited the usage of these peptide-based inhibitors in cellular assays.

Polyamines

LSD1 was identified in part because its C-terminal domain shares significant sequence homology with the polyamine oxidases APAO and SMO.[548] APAO and SMO are not inhibited by the classical MAO inhibitor pargyline but several groups have identified polyamine analogues that act as inhibitors of these two polyamine oxidases.[549] A series of (bis)guanidines and (bis)biguanides, previously synthesized as potential antitrypanosomal agents, were tested as inhibitors of LSD1 (Figure 7.19).[550] Huang et al. reported that ,within a series of compounds, analog **14** showed high noncompetitive LSD1 inhibition at < 2.5 μM and was able to induce the reexpression of aberrantly silenced tumor suppressor genes in colon cancer cells *in vitro*, together with an increase of H3K4me2 and acetyl-H3K9 marks, and a decrease of the repressive H3K9me1 and H3K9me2 marks. The same effects on recombinant LSD1 as well as human colon cancer HCT116 and RKO cell growth were observed for compound **15**.[551] The series of polyamine analogues was further expanded with some (bis)urea and (bis)thiourea derivatives among them **16** and **17** were also able to inhibit the growth of Calu-6 non-small cell lung carcinoma cells *in vitro.*[552]

7.2.3.2. JmjC demethylases inhibitors

Several inhibitors of JmjC demethylases have been reported (Figure 7.20), but few have sufficient potency and selectivity to be considered lead structures for drug development. JmjC demethylases could be expected to share some similarities with HDACs, whose substrates also present a lysine side chain with its N-terminus in the proximity of a bivalent metal ion. HDAC inhibitors are, however, poor inhibitors of the JMJD2 family of demethylases.[553] The α-ketoglutarate analogue, N-oxalylglycine (NOG **19**), could weakly inhibit JMJD2C and the catalytic core of JMJD2A.[554] JMJD2A was also found to be specifically inhibited by disruption of its Zn-binding site by Zn-ejecting compounds such as disufiram (**21**) and ebselen (**22**).[555] Interestingly, Zn-ion ejection seemed to be selective for the JMJD2 subfamily as other KDMs do not contain a Zn-binding site near their catalytic domain.
Besides NOG, another α-KG analog, the oncometabolite α-hydroxyglutarate (α-HG **20**) was found to inhibit JMJD2A, JMJD2C and JHDM1A with IC_{50} values ranging from 24 μM to 106 μM.[556] A screen using known inhibitors from other Fe^{2+}/α-KG dependent oxygenases identified 2,4-pyridinedicarboxylic acid (**23**), which showed potent inhibitory activity on JMJD2E (IC_{50}=1.4 μM).[553] High-throughput screening also identified PDCA-related compound 5-carboxy-8-hydroxyquinoline (**24**), which has a greater potency for JMJD2E (IC_{50}=200 nM).[557]

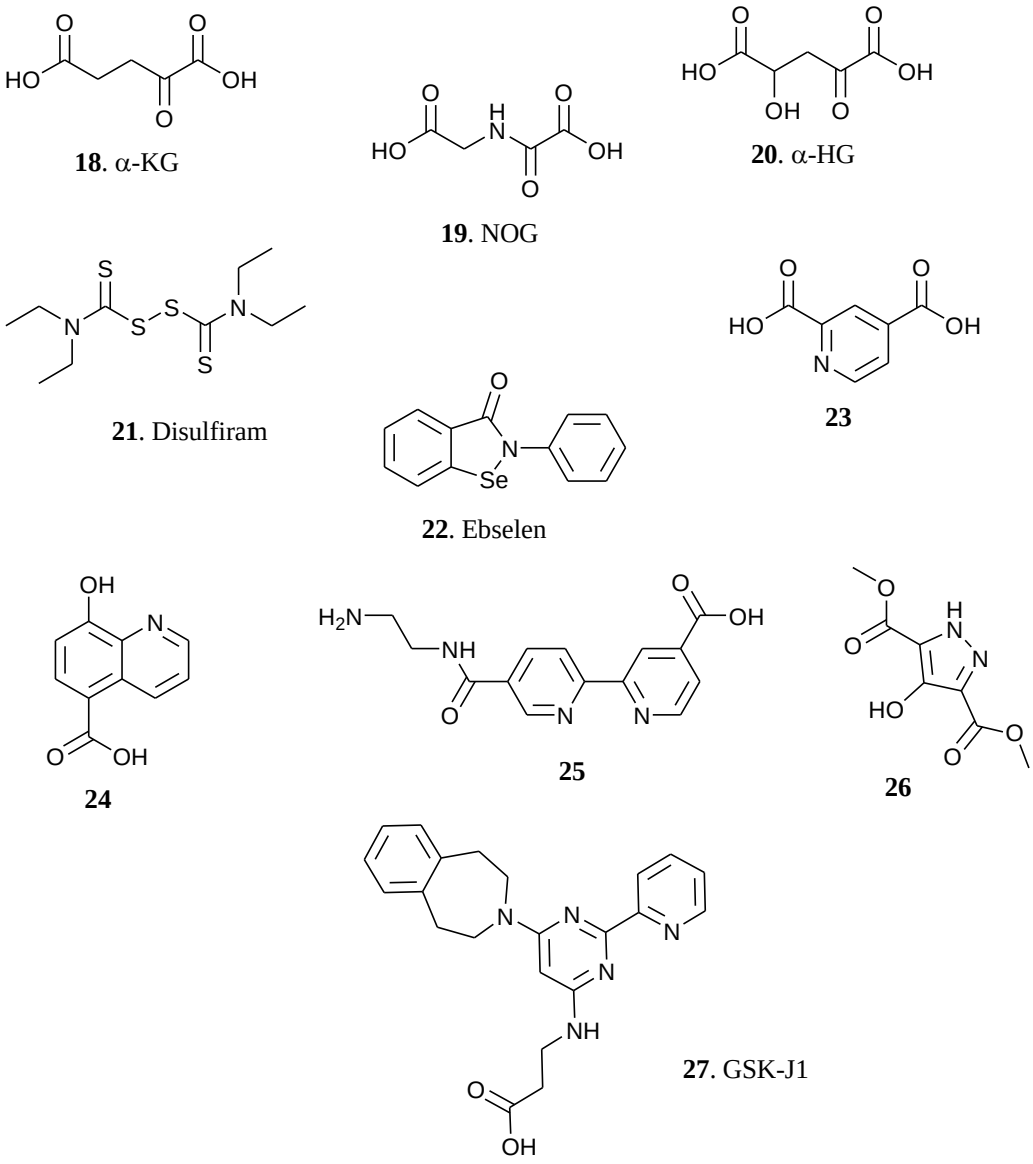

Figure 7.20. JmjC demethylases inhibitors.

Another family of pyridine-based compounds, with a 4-carboxy-2,2'-bipyridyl scaffold (**25**) have also been reported to show enhanced inhibitory activity toward JMJD2 subfamily of demethylases.[558] Structural characterization validated that this bipyridine compound also functions through α-KG competition. The carboxylate group of the compound is positioned to interact with the same manner observed for α-KG, whereas the active site Ni^{2+} cation was chelated through both pyridinyl nitrogen atoms. Based on the crystal structure of JMJD2A and on homology model of JMJD2C, Hamada and colleagues designed a series of hydroxamate analogs bearing a tertiary amine and identified analog **26** to be a potent and selective JMJD2 inhibitor, showing 500-fold greater JMJD2C inhibitory activity over NOG.[559] One of the most encouraging potential lead compounds reported is GSK-J1 (**27**), which is an inhibitor of the JMJD3 subfamily. This compound has an IC_{50} of 60 nM and is remarkably selective for the JMJD3 subfamily, although the JARID1 subfamily was

not included in the selectivity studies, despite being the closest subfamily to JMJD3. The propanoic acid of GSK-J1, mimicking α-KG, binds competitively to the 2-oxoglutarate cofactor and has the functionality to chelate the active site metal. This chelating interaction is likely to be a significant factor that contributes to the affinity of the inhibitor, and it is encouraging to see that specificity is possible for molecules that bind to the highly conserved features within the JmjC demethylase family and oxygenase superfamily.[560]

8. Selective non-nucleoside inhibitors of human DNA methyltransferases analogs of SGI-1027*

8.1. Research project

Reactivation of silenced tumor suppressor genes by 5- azacytidine (Vidaza) and its congener 5-aza-2-deoxycytidine (decitabine) has provided an alternate approach to cancer therapy. As reported previously (See Sec. 2.6.1.1.), these drugs selectively and rapidly induce degradation of the maintenance DNA methyltransferase 1 (DNMT1) by a proteasomal pathway. Although 5-azacytidine and 5-aza-2-deoxycytidine have been used for nearly 25 years as DNA hypomethylating agents in experimental systems and more recently for treating some cancer patients, their relative instability and toxicity due to incorporation into DNA have limited their clinical applications.

Some compounds have been reported as non-nucleoside DNMTi (See Sec. 2.6.2.), but typically they share low potency and/or low selectivity for DNMTs, and their mechanism of inhibition is unknown. Among them SGI-1027 (Figure 8.1, **1**), identified in a series of quinoline-based compounds developed as anticancer drugs, has attracted our attention because of its high potency in both enzyme and cell assays.[110]

Quinolinium bisquaternary salts related to SGI-1027 are known to bind reversibly in the minor groove of DNA as shown by NMR (nuclear magnetic resonance) and X-ray crystallographic studies.[561,562] Originally, the bisquaternary salts were developed as anticancer drugs,[563] in which the quaternary functions is required for their activity and for DNA binding but their mechanism of action was not defined. The nonquaternized, weakly basic compound SGI-1027, it is reported to bind reversibly but less strongly to DNA [IC_{50}= 0.51 μmol/L for binding to poly(dA-dT) determined by fluorescence quenching assay] and is indefinitely stable in aqueous solution. It is highly lipophilic (C_{log}= 5.93) and has a low polar surface area of 116 indicating a good distribution and cell uptake abilities. SGI-1027 exhibits poor solubility and excellent stability in rat and human plasma and microsomes (at 1 μmol/L).[110] In 2009, Datta et al. reported that SGI-1027 has a really prominent inhibitory effect on mammalian DNMTs (IC_{50}= 6-12.5 μmol/L), displaying comparable inhibitory activity toward DNMT1, DNMT3A, and DNMT3B.[110]

SGI-1027 (**1)** shows four fragments (4-aminoquinoline + 4-aminobenzoic acid + 1,4-phenylenediamine + 2,4-diamino-6-methylpyrimidine) linked in sequence with *para*/*para* orientation, we prepared a series of regioisomers of **1** by shifting each fragment's linkage from *para* to *meta* or *ortho* position, so obtaining compounds **2-9** (Figure 8.1). In addition, we prepared two related compounds (**10**, **11**) showing either a bis-quinoline or bis-pyrimidine structure and two truncated compounds (**12**, **13**) lacking the "right" pyrimidine or the "left" quinolone portion, respectively (Figure 8.1).

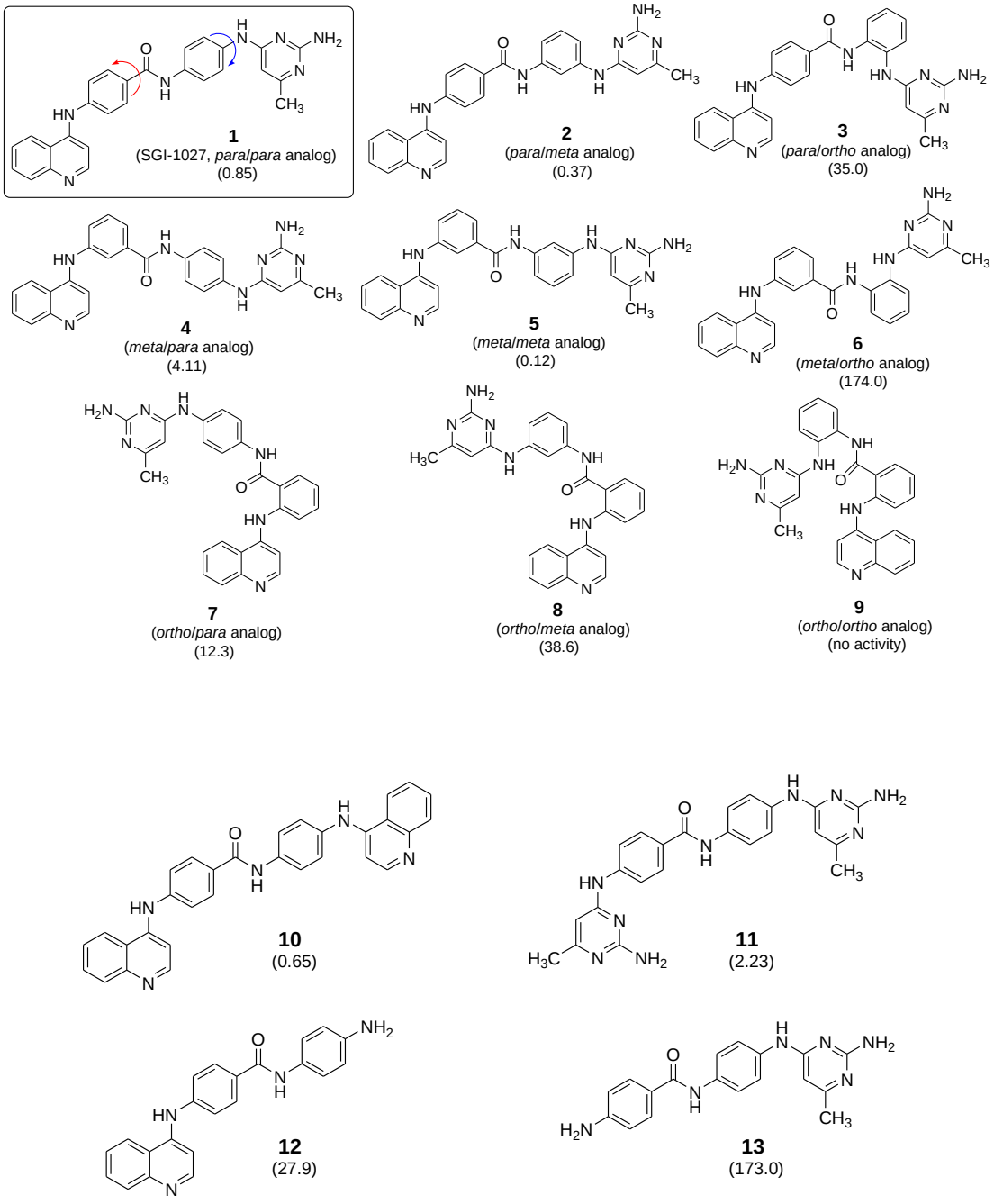

Reference drugs: SAH (0.28), sinefungin (7.4)

Figure 8.1. Chemical structures of SGI-1027 (1) and the related analogs 2-13. Their IC_{50} values (μM) from nanoscale HTS against human DNMT1 are reported into brackets.

8.2. Chemistry

Compounds **1-9** were prepared by coupling the 2-, 3-, or 4-(quinolin-4-ylamino)benzoic acid **14a-c** with the N^4-(2-, 3-, or 4-aminophenyl)-6-methylpyrimidine-2,4-diamine **15a-c**, in the presence of benzotriazol-1-yl-oxytripyrrolidinophosphonium hexafluorophosphate (PyBOP) and triethylamine, in dry *N,N*-dimethylformamide as solvent (Scheme 1). The intermediate compounds **14a-c** were prepared by reaction between 4-chloroquinoline with the appropriate ethyl 2-, 3-, or 4-aminobenzoate and 37% hydrochloric acid in ethanol at 80 °C. The obtained ethyl benzoates **16a-c** underwent basic hydrolysis using 2N potassium hydroxide to afford the corresponding acids **14a-c**. The same reaction conducted with 4-chloro-6-methylpyrimidin-2-amine and the opportune 2-, 3-, or 4-nitroanilines in the presence of 37% hydrochloric acid and ethanol at 80 °C furnished the nitro-intermediates **17a-c** which were in turn reduced with stannous chloride dihydrate and 37% hydrochloric acid in ethanol to the corresponding anilines **15a-c**.

Scheme 1

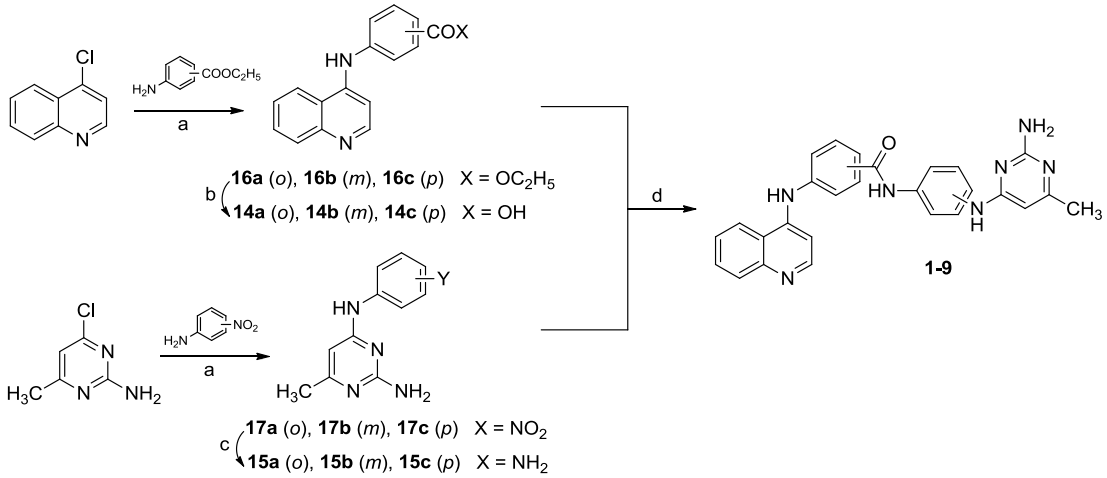

Reagents and conditions: (a): 37% HCl, CH_3CH_2OH, 80 °C, 2 h; (b): 2N KOH, CH_3CH_2OH; (c): stannous chloride dihydrate, 37% HCl, CH_3CH_2OH, 1 h, 80 °C; (d): $(C_2H_5)_3N$, PyBOP, anhydrous DMF, N_2 atmosphere, room temperature, 1 h.

The bisquinoline **10** was obtained by treating 4-chloroquinoline with 4-nitroaniline and, after reduction of the nitro group of the resulting intermediate **18** to the corresponding aniline **19**, by coupling **19** with **16c** (Scheme 2A). Treatment of 4-chloro-6-methylpyrimidin-2-amine with ethyl 4-aminobenzoate afforded the intermediate ester **20**, which was hydrolyzed to the acid **21** and then was coupled with **17c** to furnish the bispyrimidine **11** (Scheme 2B). The truncated compounds **12** and **13** were prepared by reaction of **16c** with 4-phenylendiamine (**12**), or by reaction of **17c** with 4-nitrobenzoic acid and subsequent reduction of the nitro group of the intermediate **22** to the corresponding amine (**13**) (Scheme 3).

Scheme 2

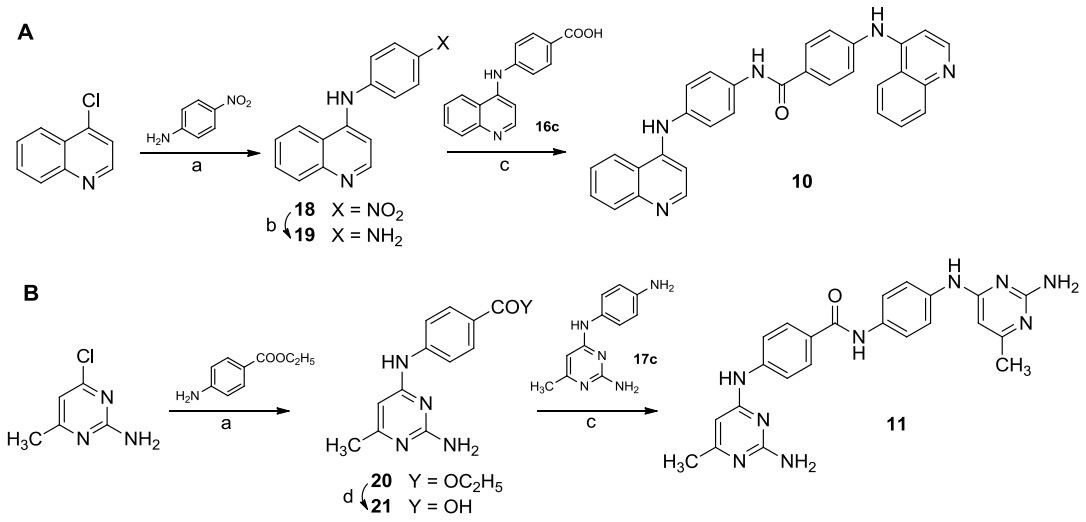

Reagents and conditions: (a): 37% HCl, CH_3CH_2OH, 80 °C, 2 h; (b): stannous chloride dihydrate, 37% HCl, CH_3CH_2OH, 80 °C, 1 h; (c): $(C_2H_5)_3N$, PyBOP, anhydrous DMF, N_2 atmosphere, room temperature, 1 h; (d): 2 N KOH, CH_3CH_2OH.

Scheme 3

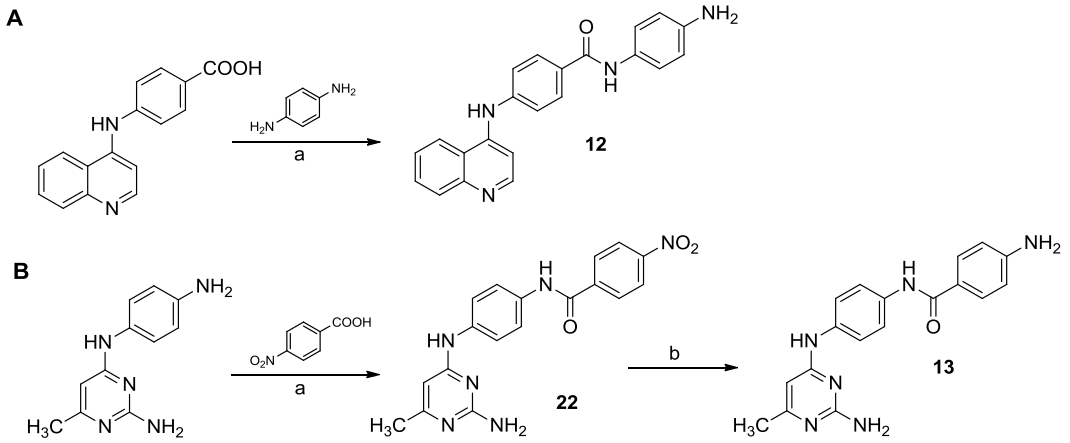

Reagents and conditions: (a): $(C_2H_5)_3N$, PyBOP, anhydrous DMF, N_2 atmosphere, room temperature, 1 h; (b): stannous chloride dihydrate, 37% HCl, CH_3CH_2OH, 80 °C, 1 h.

The chemical and physical data of final compounds **1-13** and those of the intermediate compounds **14-22** are shown in Table 8.1 and 8.2 respectively.

Table 8.1. Chemical and physical properties of compounds **1-13**.

Cpd	molecolar structure	mp, °C	recrystall. solvent	Yield %
SGI-1027 1	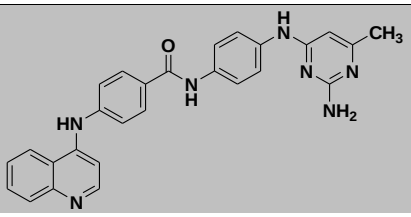	>300	C	79
2	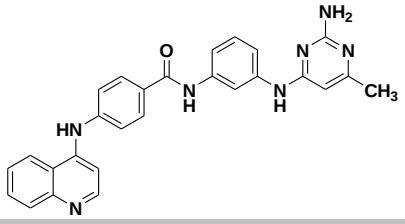	270-275	C	81
3	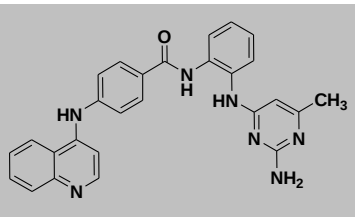	200-205	B	72
4	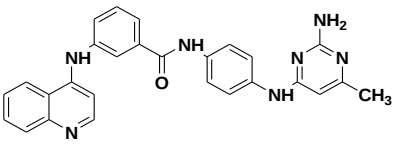	>300	C	83
5	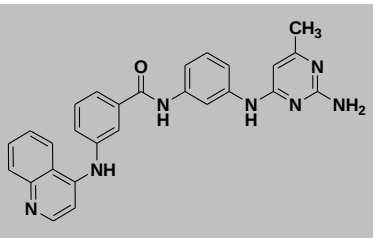	270-272	C	80
6	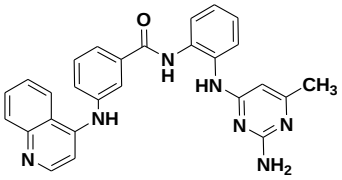	170-172	A	66
7	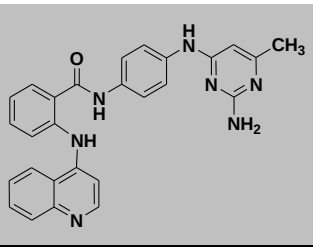	274-279	C	78

8	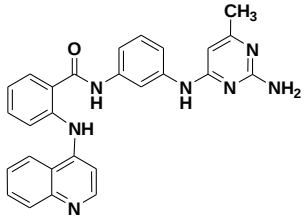	158-161	A	74
9	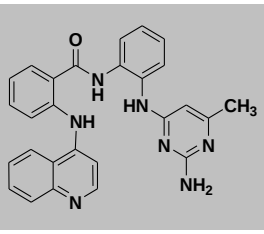	252-255	C	68
10	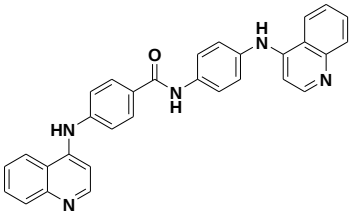	>300	C	77
11	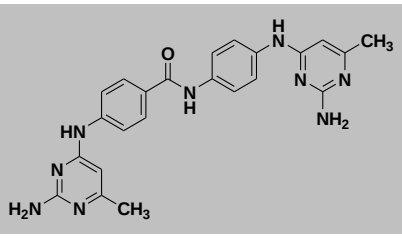	>300	C	73
12	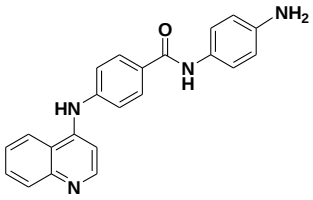	264-267	C	83
13	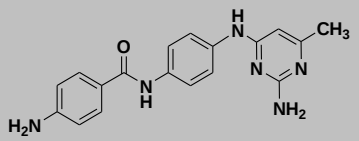	>300	C	75

A: acetonitrile; B: acetonitrile/metanol; C: metanol

Table 8.2. Chemical and physical properties of compounds **14-22**.

Cpd	molecolar structure	mp, °C	recrystall. solvent	Yield %
14	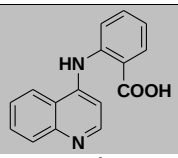	>300	D	88
14b	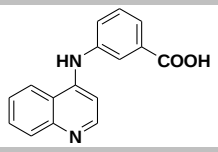	>300	D	90
14c	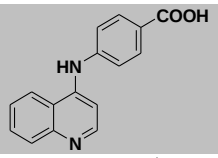	>300	D	85
15	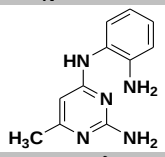	213-215	C	64
15b	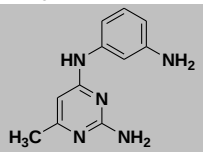	140-142	B	73
15c	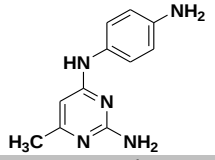	88-90	A	79
16	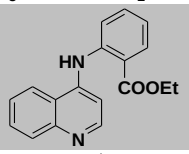	235-237	C	71
16b	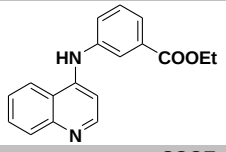	260-263	D	80
16c	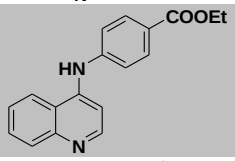	262-265	D	83
17	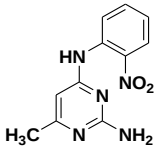	251-253	D	63

17b	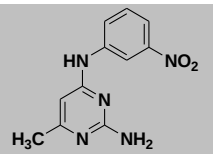	290-292	D	72
17c	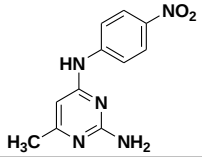	>300	D	67
18	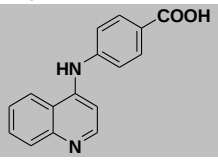	>300	D	74
19	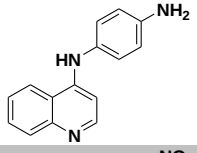	168-170	B	77
20	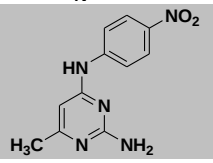	238-240	C	65
21	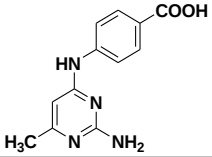	>300	D	87
22	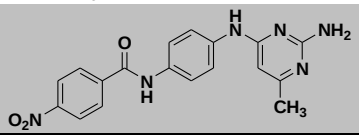	>300	D	76

A: acetonitrile; B: acetonitrile/metanol; C: metanol

8.3. Experimental section

Chemistry. Melting points were determined on a Buchi 530 melting point apparatus and are uncorrected. ^{1}H NMR and ^{13}C NMR spectra were recorded at 400 MHz on a Bruker AC 400 spectrometer; chemical shifts are reported in δ (ppm) units relative to the internal reference tetramethylsilane (Me_4Si). EIMS spectra were recorded with a Fisons Trio 1000 spectrometer; only molecular ions (M+) and base peaks are given. All compounds were routinely checked by TLC, ^{1}H NMR and ^{13}C NMR spectra. TLC was performed on aluminum-backed silica gel plates (Merck DC, Alufolien Kieselgel 60 F254) with spots visualized by UV light. All solvents were reagent grade and, when necessary, were purified and dried by standard methods. Concentration of solutions after reactions and extractions involved the use of a rotary evaporator operating at reduced pressure of ca. 20 Torr. Organic solutions were dried over anhydrous sodium sulfate. Elemental analysis has been used to determine purity of the described compounds, that is >95%. Analytical results are within ± 0.40% of the theoretical values. All chemicals were purchased from Aldrich Chimica, Milan (Italy), or from Alfa Aesar, Milan (Italy), and were of the highest purity.

General Procedure for the Synthesis of the Ester Intermediates 16a-c, 20, and the Nitro Intermediates 17a-c, 18. Example: Synthesis of Ethyl 3-(Quinolin-4-ylamino)benzoate (16b). 4-Chloroquinoline (6.11 mmol, 1 g), ethyl 3-aminobenzoate (6.11 mmol, 1 g) and catalytic amount (4 drops) of 37% hydrochloric acid are refluxed for 2 h. The reaction was allowed to cool down to room temperature and the precipitated solid was filtered off, washed with water (3 × 5 mL) and recrystallized by methanol to afford pure **16b** as hydrochloride salt. ^{1}H NMR (DMSO-d_6, 400 MHz, δ; ppm) δ 1.34 (t, 3H, J = 7.2 Hz, -COOCH$_2$C*H$_3$*), 4.36 (q, 2H, J = 7.2 Hz, -COOC*H$_2$*CH$_3$), 6.88 (d, 1H, J = 5.2 Hz, quinoline proton), 7.74 (m, 2H, benzene protons), 7.84 (t, 1H, J = 7.4 Hz, benzene proton), 8.00 (d, 1H, J = 8.2 Hz, quinoline proton), 8.06-8.12 (m, 3H, quinoline and benzene protons), 8.56 (d, 1H, J = 8.2 Hz, quinoline proton), 8.81 (d, 1H, J = 5.2 Hz, quinoline proton), 11.08 (bs, 1H, -N*H*), 14.68 (bs, 1H, H^+) ppm; ^{13}C NMR (DMSO-d_6, 100 MHz, δ; ppm) δ 14.1, 60.9, 112.8, 114.2, 119.9, 121.6, 122.1, 124.2, 125.7, 129.2, 129.6, 130.9, 133.7, 138.7, 142.3, 149.7, 151.6, 165.9 ppm; MS (EI), m/z $[M]^+$ $C_{18}H_{16}N_2O_2$ calcd 292.1212, found 292.1218.

General Procedure for the Synthesis of the Acid Intermediates 14a-c, 21. Example: Synthesis of 3-(Quinolin-4-ylamino)benzoic acid (14b). A solution of ethyl 3-(quinolin-4-ylamino)benzoate **16b** (1.71 mmol, 0.5 g) and 2N KOH (6.84 mmol, 0.38 g) in ethanol (15 mL) was stirred overnight at room temperature. Then the solvent was evaporated, and 2N HCl was slowly added untill the aqueous phase reached the pH value of 5.0. The colorless solid was filtered, washed with water and recrystallized by methanol to obtain pure **14b**. ^{1}H NMR (DMSO-d_6, 400 MHz, δ; ppm) δ 7.00 (d, 1H, J = 5.2 Hz, quinoline proton), 7.51-7.58 (m, 2H, quinoline and benzene protons), 7.63 (d, 1H, benzene proton), 7.68-7.75 (m, 2H, quinoline and

benzene protons), 7.90-7.93 (m, 2H, quinoline and benzene protons), 8.39 (d, 1H, *J* = 8.0 Hz, quinoline proton), 8.51 (d, 1H, *J* = 5.2 Hz, quinoline proton), 9.17 (bs, 1H, NH) ppm; ^{13}C NMR (DMSO-d_6, 100 MHz, δ; ppm) δ 112.8, 119.5 (2C), 120.2, 121.6, 124.2, 125.7, 129.2, 129.6, 131.1 (2C), 138.7, 149.7, 151.1, 151.6, 169.3 ppm; MS (EI), m/z $[M]^+$ $C_{16}H_{12}N_2O_2$ calcd 264.0899, found 264.0902.

General Procedure for the Synthesis of the Anilines 15a-c, 19 and 13. Example: Synthesis of *N*^{4}-(3-Aminophenyl)-6-methylpyrimidine-2,4-diamine (15b). To a cooled solution of 6-methyl-*N*^{4}-(3-nitrophenyl)pyrimidine-2,4-diamine **17b** (1.63 mmol, 0.5 g) and stannous chloride dihydrate (8.15 mmol, 1.84 g) in ethanol (10 mL), 37 % hydrochloric acid solution (0.3 mL) was slowly added at 0 °C. The reaction was then kept at 80 °C for 1 h. Afterwards, the reaction was quenched at room temperature by 2N sodium carbonate solution (20 mL) and mixture was extracted with ethyl acetate (3 × 30 mL), washed with brine (3 × 30 mL), then dried with anhydrous sodium sulfate, filtered and concentrated under reduced pressure. The crude solid was recrystallized by cyclohexane to give the pure product **15b**. ^{1}H NMR (DMSO-d_6, 400 MHz, δ; ppm) δ 2.06 (s, 3H, -C*H*$_3$), 4.92 (bs, 2H, -N*H*$_2$-aniline), 5.87 (s, 1H, pyrimidine proton), 5.97 (bs, 2H, -N*H*$_2$-pyrimidine), 6.19 (d, 1H, *J* = 8.0 Hz, aniline proton), 6.80 (d, 1H, *J* = 8.0 Hz, aniline proton), 6.87-6.91 (m, 2H, aniline protons), 8.64 (bs, 1H, -N*H*) ppm; ^{13}C NMR (DMSO-d_6, 100 MHz, δ; ppm) δ 23.9, 93.8, 102.7, 105.0, 107.8, 130.3, 143.2, 147.8, 163.1, 164.5, 170.2 ppm; MS (EI), m/z $[M]^+$ $C_{11}H_{13}N_5$ calcd 215.1171, found 215.1167.

General Procedure for the Synthesis of the Compounds 1-12 and 22. Example: Synthesis of *N*-(3-(2-Amino-6-methylpyrimidin-4-ylamino)phenyl)-3-(quinolin-4-ylamino)benzamide (5). Triethylamine (3.04 mmol, 0.42 mL) and benzotriazol-1-yl-oxytripyrrolidinophosphonium hexafluorophosphate (PyBOP) (0.91 mmol, 0.47 g) were added to a solution of 3-(quinolin-4-ylamino)benzoic acid **14b** (0.76 mmol, 0.2 g) in anhydrous *N*,*N*-dimethylformamide (5 mL) under nitrogen atmosphere. The resulting mixture was stirred for 30 minutes at room temperature, afterwards *N*^{4}-(3-aminophenyl)-6-methylpyrimidine-2,4-diamine **15b** (0.76 mmol, 0.16 g) was added under nitrogen atmosphere and the reaction was stirred overnight. The reaction was quenched with water (50 mL) and extracted with ethyl acetate (3 × 30 mL). The combined organic extracts were dried and the residue obtained upon evaporation of solvent was purified by column chromatography (SiO_2 eluting with ethyl acetate/methanol 10/1) to provide pure **5**. ^{1}H NMR (DMSO-d_6, 400 MHz, δ; ppm) δ 2.10 (s, 3H, -C*H*$_3$), 5.94 (s, 1H, pyrimidine proton), 6.07 (bs, 2H, -N*H*$_2$-pyrimidine), 7.06 (d, 1H, *J* = 4.8 Hz, quinoline proton), 7.26 (t, 1H, *J* = 8.0 Hz, benzene proton), 7.35 (d, 1H, *J* = 7.6 Hz, quinoline proton), 7.55-7.61 (m, 4H, benzene and quinoline protons), 7.72-7.75 (m, 2H, benzene protons), 7.91 (d, 1H, *J* = 8.0 Hz, quinoline proton), 7.95 (s, 1H, benzene proton), 8.03 (s, 1H, benzene proton), 8.42 (d, 1H, *J* =8.4 Hz, quinoline proton), 8.52 (d, 1H, *J* = 5.6 Hz, quinoline proton), 9.04 (bs, 1H, -N*H*-pyrimidine), 9.16 (bs, 1H, -N*H*-quinoline), 10.18 (s, 1H, -CON*H*-) ppm; ^{13}C

NMR (DMSO-d_6, 100 MHz, δ; ppm) δ 23.9, 93.8, 108.0, 111.6, 111.8, 112.8, 113.4, 117.5, 121.2, 121.6, 124.2, 125.7, 129.2, 129.6, 129.7, 133.9, 135.0, 136.7, 138.7, 142.5, 142.6, 149.7, 151.6, 163.1, 164.5, 164.7, 170.2 ppm; MS (EI), m/z $[M]^+$ $C_{27}H_{23}N_7O$ calcd 461.1964, found 461.1969.

***N*-(4-(2-Amino-6-methylpyrimidin-4-ylamino)phenyl)-4-(quinolin-4-ylamino) benzamide (1, SGI-1027).** ^{1}H NMR (DMSO-d_6, 400 MHz, δ; ppm) δ 2.10 (s, 3H, -C*H*$_3$), 5.88 (s, 1H, pyrimidine proton), 6.14 (bs, 2H, -N*H*$_2$-pyrimidine), 7.21 (d, 1H, *J* = 5.4 Hz, quinoline proton), 7.48-7.81 (m, 8H, benzene and quinoline protons), 7.93-8.03 (m, 3H, benzene and quinoline protons), 8.42 (d, 1H, *J* =8.4 Hz, quinoline proton), 8.52 (d, 1H, *J* = 5.6 Hz, quinoline proton), 8.97 (bs, 1H, -N*H*-pyrimidine), 9.25 (bs, 1H, -N*H*-quinoline), 10.06 (bs, 1H, -CON*H*-) ppm; ^{13}C NMR (DMSO-d_6, 100 MHz, δ; ppm) δ 23.9, 93.8, 111.4 (2C), 112.8, 117.7 (2C), 121.6, 122.4 (2C), 124.2 (2C), 125.7, 127.9, 129.2, 129.6, 130.2 (2C), 136.5, 138.7, 149.3, 149.7, 151.6, 163.1, 164.5, 164.7, 170.2 ppm; MS (EI), m/z $[M]^+$ $C_{27}H_{23}N_7O$ calcd 461.1964, found 461.1969.

***N*-(3-(2-Amino-6-methylpyrimidin-4-ylamino)phenyl)-4-(quinolin-4-ylamino)benzamide (2).** ^{1}H NMR (DMSO-d_6, 400 MHz, δ; ppm) δ 2.10 (s, 3H, -C*H*$_3$), 5.95 (s, 1H, pyrimidine proton), 6.07 (bs, 2H, -N*H*$_2$-pyrimidine), 7.21-7.25 (m, 2H, benzene and quinoline protons), 7.37 (d, 1H, *J* = 8.2 Hz, benzene proton), 7.50-7.61 (m, 4H, benzene and quinoline protons), 7.75 (t, 1H, *J* = 7.4 Hz, quinoline proton), 7.93-8.03 (m, 4H, benzene and quinoline protons), 8.42 (d, 1H, *J* =8.4 Hz, quinoline proton), 8.52 (d, 1H, *J* = 5.6 Hz, quinoline proton), 9.03 (bs, 1H, -N*H*-pyrimidine), 9.25 (bs, 1H, -N*H*-quinoline), 10.05 (bs, 1H, -CON*H*-) ppm; ^{13}C NMR (DMSO-d_6, 100 MHz, δ; ppm) δ 23.9, 93.8, 108.0, 111.4 (2C), 111.6, 112.8, 113.4, 121.6, 124.2 (2C), 125.7, 129.2, 129.6, 129.7, 130.2 (2C), 136.7, 138.7, 142.6, 149.3, 149.7, 151.6, 163.1, 164.5, 164.7, 170.2 ppm; MS (EI), m/z $[M]^+$ $C_{27}H_{23}N_7O$ calcd 461.1964, found 461.1969.

***N*-(2-(2-Amino-6-methylpyrimidin-4-ylamino)phenyl)-4-(quinolin-4-ylamino)benzamide (3).** ^{1}H NMR (DMSO-d_6, 400 MHz, δ; ppm) δ 2.09 (s, 3H, -C*H*$_3$), 5.88 (s, 1H, pyrimidine proton), 6.31 (bs, 2H, -N*H*$_2$-pyrimidine), 7.18-7.22 (m, 2H, benzene and quinoline protons), 7.37-7.50 (m, 4H, 7.58-7.65 (m, 2H benzene and quinoline protons), 7.72-7.77 (m, 2H, benzene protons), 7.94-7.96 (m, 2H, quinoline protons), 8.37 (d, 1H, *J* = 7.6 Hz, quinoline proton), 8.55 (bs, 1H, -N*H*-pyrimidine), 8.58 (d, 1H, *J* = 4.8 Hz, quinoline proton), 9.25 (bs, 1H, -N*H*-quinoline), 10.15 (bs, 1H, -CON*H*-) ppm; ^{13}C NMR (DMSO-d6, 100 MHz, δ; ppm) δ 23.9, 93.8, 111.4 (2C), 112.8, 118.9, 121.6, 122.8, 124.2 (2C), 125.5, 125.7, 126.1, 129.2, 129.6, 130.2 (2C), 137.9, 138.7, 147.6, 149.3, 149.7, 151.6, 163.1, 164.5, 170.2, 172.5 ppm; MS (EI), m/z $[M]^+$ $C_{27}H_{23}N_7O$ calcd 461.1964, found 461.1969.

***N*-(4-(2-Amino-6-methylpyrimidin-4-ylamino)phenyl)-3-(quinolin-4-ylamino)benzamide (4).** ^{1}H NMR (DMSO-d_6, 400 MHz, δ; ppm) δ 2.08 (s, 3H, -

C*H*$_3$), 5.87 (s, 1H, pyrimidine proton), 6.10 (bs, 2H, -N*H*$_2$-pyrimidine), 7.06 (d, 1H, *J* = 5.6 Hz, quinoline proton), 7.54-7.74 (m, 9H, benzene and quinoline protons), 7.90 (d, 1H, *J* = 8.4 Hz quinoline proton), 8.01 (s, 1H, benzene proton), 8.46 (d, 1H, *J* = 8.4 Hz, quinoline proton), 8.51 (d, 1H, *J* = 4.0 Hz, quinoline proton), 9.01 (bs, 1H, -N*H*-pyrimidine), 9.28 (bs, 1H, -N*H*-quinoline), 10.30 (s, 1H, -CON*H*-) ppm; ^{13}C NMR (DMSO-d_6, 100 MHz, δ; ppm) δ 23.9, 93.8, 111.8, 112.8, 117.5, 117.7 (2C), 121.2, 121.6, 122.4 (2C), 124.2, 125.7, 127.9, 129.2, 129.6, 133.9, 135.0, 136.5, 138.7, 142.5, 149.7, 151.6, 163.1, 164.5, 164.7, 170.2 ppm; MS (EI), m/z $[M]^+$ $C_{27}H_{23}N_7O$ calcd 461.1964, found 461.1969.

***N*-(2-(2-Amino-6-methylpyrimidin-4-ylamino)phenyl)-3-(quinolin-4-ylamino)benzamide (6).** ^{1}H NMR (DMSO-d_6, 400 MHz, δ; ppm) δ 2.05 (s, 3H, -C*H*$_3$), 5.86 (s, 1H, pyrimidine proton), 6.23 (bs, 2H, -N*H*$_2$-pyrimidine), 7.04 (d, 1H, *J* = 5.6 Hz, quinoline proton), 7.20 (m, 2H, benzene and quinoline protons), 7.51-7.74 (m, 7H, benzene and quinoline protons), 7.90-7.92 (m, 2H, benzene and quinoline protons), 8.40 (d, 1H, *J* = 8.4 Hz, quinoline proton), 8.47 (bs, 1H, -N*H*-pyrimidine), 8.51 (d, 1H, *J* = 5.4 quinoline proton), 9.11 (bs, 1H, -N*H*-quinoline), 10.19 (bs, 1H, -CON*H*-) ppm; ^{13}C NMR (DMSO-d_6, 100 MHz, δ; ppm) δ 23.9, 93.8, 111.8, 112.8, 117.5, 118.9, 121.2, 121.6, 122.8, 124.2, 125.5, 125.7, 126.1, 129.2, 129.6, 133.9, 135.0, 137.9, 138.7, 142.5, 147.6, 149.7, 151.6, 163.1, 164.5, 164.7, 170.2 ppm; MS (EI), m/z $[M]^+$ $C_{27}H_{23}N_7O$ calcd 461.1964, found 461.1969.

***N*-(4-(2-Amino-6-methylpyrimidin-4-ylamino)phenyl)-2-(quinolin-4-ylamino)benzamide (7).** ^{1}H NMR (DMSO-d_6, 400 MHz, δ; ppm) δ 2.07 (s, 3H, -C*H*$_3$), 5.85 (s, 1H, pyrimidine proton), 6.08 (bs, 2H, -N*H*$_2$-pyrimidine), 7.15 (d, 1H, *J* = 5.4 Hz, quinoline proton), 7.26 (t, 1H, *J* = 6.8 Hz, quinoline proton), 7.48-7.75 (m, 9H, benzene and quinoline protons), 7.92 (m, 2H, quinoline protons), 8.16 (d, 1H, *J* = 8.0 Hz, quinoline proton), 8.55 (d, 1H, *J* = 4.0 Hz, quinoline proton), 8.95 (bs,1H, -N*H*-pyrimidine), 10.26 (bs, 1H, -N*H*- quinoline), 10.41 (bs, 1H, -CONH-) ppm; ^{13}C NMR (DMSO-d_6, 100 MHz, δ; ppm) δ 23.9, 93.8, 112.8, 116.4, 117.7 (2C), 117.9, 118.8, 121.6, 122.4 (2C), 124.2, 125.7, 127.9, 128.3, 129.2, 129.6, 132.9, 136.5, 138.7, 149.7, 151.6, 151.9, 163.1, 164.5, 167.5, 170.2 ppm; MS (EI), m/z $[M]^+$ $C_{27}H_{23}N_7O$ calcd 461.1964, found 461.1969.

***N*-(3-(2-Amino-6-methylpyrimidin-4-ylamino)phenyl)-2-(quinolin-4-ylamino)benzamide (8).** ^{1}H NMR (DMSO-d_6, 400 MHz, δ; ppm) δ 2.08 (s, 3H, -C*H*$_3$), 5.91 (s, 1H, pyrimidine proton), 6.05 (bs, 2H, -N*H*$_2$-pyrimidine), 7.12-7.28 (m, 3H, benzene and quinoline protons), 7.61-7.73 (m, 3H, benzene and quinoline protons), 7.71-7.76 (m, 3H, benzene protons), 7.91-7.96 (m, 2H, benzene and quinoline protons), 8.16 (d, 1H, *J* = 8.0 Hz, quinoline proton), 8.55 (d, 1H, *J* = 4.8 Hz, quinoline proton), 9.02 (bs, 1H, -N*H*-pyrimidine), 10.10 (bs, 1H, -N*H*-quinoline), 10.40 (bs, 1H, -CON*H*-) ppm; ^{13}C NMR (DMSO-d_6, 100 MHz, δ; ppm) δ 23.9, 93.8, 108.0, 111.6, 112.8, 113.4, 116.4, 117.9, 118.8, 121.6, 124.2, 125.7, 128.3, 129.2, 129.6, 129.7, 132.9, 136.7, 138.7, 142.6, 149.7, 151.6, 151.9, 163.1,

164.5, 167.5, 170.2 ppm; MS (EI), m/z $[M]^+$ $C_{27}H_{23}N_7O$ calcd 461.1964, found 461.1969.

***N*-(2-(2-Amino-6-methylpyrimidin-4-ylamino)phenyl)-2-(quinolin-4-ylamino)benzamide (9).** ^{1}H NMR (DMSO-d_6, 400 MHz, δ; ppm) δ 2.01 (s, 3H, -C*H*$_3$), 5.81 (s, 1H, pyrimidine proton), 6.27 (s, 2H, -N*H*$_2$-pyrimidine), 7.12-7.24 (m, 4H, benzene and quinoline protons), 7.48 (d, 1H, *J* = 7.6 Hz, benzene proton), 7.54-7.61 (m, 3H, benzene protons), 7.71-7.76 (m, 2H, benzene and quinoline protons), 7.92-7.97 (m, 2H, benzene and quinoline protons), 8.08 (d, 1H, *J* = 8.8 Hz, quinoline protons), 8.57 (m, 2H, quinoline and -N*H*-pyrimidine protons), 10.44 (bs, 1H, -N*H*-quinoline), 10.57 (bs, 1H, -CON*H*-) ppm; ^{13}C NMR (DMSO-d_6, 100 MHz, δ; ppm) δ 23.9, 93.8, 112.8, 116.4, 117.9, 118.8, 118.9, 121.6, 122.8, 124.2, 125.5, 125.7, 126.1, 128.3, 129.2, 129.6, 132.9, 137.9, 138.7, 147.6, 149.7, 151.6, 151.9, 163.1, 164.5, 167.5, 170.2 ppm; MS (EI), m/z $[M]^+$ $C_{27}H_{23}N_7O$ calcd 461.1964, found 461.1969.

4-(Quinolin-4-ylamino)-*N*-(4-(quinolin-4-ylamino)phenyl)benzamide (10). ^{1}H NMR (DMSO-d_6, 400 MHz, δ; ppm) δ 6.83 (d, 1H, *J* = 6.0 Hz, quinoline proton), 7.20 (d, 1H, *J* = 4.8 Hz, quinoline proton), 7.42 (d, 2H, *J* = 8.8 Hz, benzene protons), 7.53 (d, 2H, *J* = 8.4 Hz, benzene protons), 7.60-7.68 (m, 2H, quinoline protons), 7.79 (t, 1H, *J* = 7.2 Hz, quinoline proton), 7.83 (t, 1H, *J* = 7.2 Hz, quinoline proton), 7.94-7.97 (m, 4H, benzene and quinoline protons), 8.07 (d, 2H, *J* = 7.6 Hz, benzene protons), 8.45-8.49 (m, 2H, quinoline protons), 8.57-8.61 (m, 2H, quinoline protons), 9.49 (bs, 1H, -N*H*-quinoline), 9.82 (bs, 1H, -N*H*-quinoline), 10.35 (bs, 1H, -CON*H*-) ppm; ^{13}C NMR (DMSO-d_6, 100 MHz, δ; ppm) δ 111.4 (2C), 112.8 (2C), 117.7 (2C), 121.6 (2C), 122.4 (2C), 124.2 (3C), 125.7 (2C), 127.9, 129.2 (2C), 129.6 (2C), 130.2 (2C), 138.7 (2C), 141.5, 149.3, 149.7 (2C), 151.6 (2C), 164.7 ppm; MS (EI), m/z $[M]^+$ $C_{31}H_{23}N_5O$ calcd 481.1903, found 481.1908.

4-(2-Amino-6-methylpyrimidin-4-ylamino)-*N*-(4-(2-amino-6-methylpyrimidin-4-ylamino) phenyl)benzamide (11). ^{1}H NMR (DMSO-d_6, 400 MHz, δ; ppm) δ 2.09 (s, 3H, -C*H*$_3$), 2.13 (s, 3H, -C*H*$_3$), 5.86 (s, 1H, pyrimidine proton), 5.95 (s, 1H, pyrimidine proton), 6.10 (bs, 2H, -N*H*$_2$-pyrimidine), 6.26 (bs, 2H, -N*H*$_2$-pyrimidine), 7.65 (m, 4H, benzene protons), 7.89 (m, 4H, benzene protons), 8.91 (bs, 1H, -N*H*-pyrimidine), 9.32 (bs, 1H, -N*H*-pyrimidine), 9.96 (bs, 1H, -CON*H*-) ppm; ^{13}C NMR (DMSO-d_6, 100 MHz, δ; ppm) δ 23.9 (2C), 93.8 (2C), 111.4 (2C), 117.7 (2C), 122.4 (2C), 124.2, 127.9, 130.2 (2C), 136.5, 144.3, 163.1 (2C), 164.5, 164.7, 167.0, 167.7, 170.2 ppm; MS (EI), m/z $[M]^+$ $C_{23}H_{23}N_9O$ calcd 441.2026, found 441.2023.

***N*-(4-Aminophenyl)-4-(quinolin-4-ylamino)benzamide (12).** ^{1}H NMR (DMSO-d_6, 400 MHz, δ; ppm) δ 4.91 (bs, 2H, -N*H*$_2$-benzene), 6.56 (d, 2H, *J* = 7.6 Hz, benzene protons), 7.18 (d, 1H, *J* = 4.8 Hz, quinoline proton), 7.38 (d, 2H, *J* = 8.4 Hz, benzene protons), 7.46 (d, 2H, *J* = 8.4 Hz, benzene protons), 7.60 (t, 1H, *J* = 7.2 Hz, quinoline proton), 7.74 (t, 1H, *J* = 7.2 Hz, quinoline proton), 7.93 (d, 1H, *J* = 8.0 Hz, quinoline

proton), 7.97 (d, 2H, *J* = 8.4 Hz, benzene protons), 8.38 (d, 1H, *J* = 8.4 Hz, quinoline proton), 8.57 (d, 1H, *J* = 4.4 Hz, quinoline proton), 9.20 (bs, 1H, -N*H*-quinoline), 9.79 (bs, 1H, -CON*H*-) ppm; ^{13}C NMR (DMSO-d_6, 100 MHz, δ; ppm) δ 111.4 (2C), 112.8, 116.5 (2C), 121.6, 122.4 (2C), 124.2 (2C), 125.7, 127.9, 129.2, 129.6, 130.2 (2C), 138.7, 144.0, 149.3, 149.7, 151.6, 164.7 ppm; MS (EI), m/z $[M]^+$ $C_{22}H_{18}N_4O$ calcd 354.1481, found 354.1486.

4-Amino-*N*-(4-(2-amino-6-methylpyrimidin-4-ylamino)phenyl)benzamide (13). ^{1}H NMR (DMSO-d_6, 400 MHz, δ; ppm) δ 2.06 (s, 3H, -CH_3), 5.71 (bs, 2H, -NH_2-benzene), 5.85 (s, 1H, pyrimidine proton), 6.08 (bs, 2H, -NH_2-pyrimidine), 6.60 (d, 2H, *J* = 8.4 Hz, benzene protons), 7.59-7.64 (m, 4H, benzene protons), 7.71 (d, 2H, *J* = 8.4 Hz, benzene protons), 8.88 (bs, 1H, -N*H*-pyrimidine), 9.66 (bs, 1H, -CON*H*-) ppm; ^{13}C NMR (DMSO-d_6, 100 MHz, δ; ppm) δ 23.9, 93.8, 114.3 (2C), 117.7 (2C), 122.4 (2C), 124.2, 127.9, 130.2 (2C), 136.5, 151.8, 163.1, 164.5, 164.7, 170.2 ppm; MS (EI), m/z $[M]^+$ $C_{18}H_{18}N_6O$ calcd 334.1542, found 334.1545.

8.4. Biological evaluation, results and discussion

8.4.1. Nanoscale DNMT1 pre-screen

Compounds **1-13** were tested in 10-dose IC_{50} mode with 2-fold serial dilution at starting concentration of 500 μM against human DNMT1, using poly(dI-dC) (0.001 mg/mL) as substrate in the presence of AdoMet (1 μM) as cofactor. Control compounds, AdoHcy (S-(5'-adenosyl)-l-homocysteine) and sinefungin, were tested in 10-dose IC_{50} mode with 3-fold serial dilution starting at 100 μM. Their IC_{50} values (μM) from nanoscale HTS against human DNMT1 are reported in Figure 8.2. Compounds **2**, **4** and **5**, obtained by replacing either or both the *para* with the *meta* linkages in the **1** structure, emerged as highly efficient DNMT1 inhibitors; whereas the *ortho* regioisomers were less potent (**3**, **6**-**8**) or totally inactive (**9**). The bisquinoline **10** displayed similar potency as SGI-127 (**1)** against DNMT1, while the bispyrimidine **11** was less efficient, and the truncated compounds **12** and **13** showed a severe drop of inhibition (Figure 8.2).

8.4.2. DNMT1, DNMT3A2/3L, PRMT1 and GLP assays

To perform wider and more accurate assays against DNMTs, the most potent compounds **2**, **4**, **5**, **10** and **11,** in comparison with **1**, were tested against human DNMT1 using a hemimethylated substrate and human DNMT3A2/DNMT3L complex using an unmethylated substrate (Figure 8.2b). Under these assay conditions, the *meta*/*meta* analog **5** (IC_{50}= 9 μM) displayed a 4-fold higher activity than **1** against DNMT1, while the *para*/*meta* (**2**) and the *meta*/*para* (**4**) analogs were 2.5- and 7.6-fold less potent, respectively. The bisquinoline **10** showed the same DNMT1 inhibiting activity as **1**, while the bispyrimidine **11** was 2-fold less active. Against DNMT3A2/DNMT3L, all the inhibitors were more efficient than against DNMT1, and **5** was again the most potent with IC_{50} = 2.8 μM, compared to lead

compound **1** [IC_{50}= 10 µM]. Among the remaining compounds, **11** and **2** were 2-fold less potent than **1**, and lower activities were registered with **10** and **4** (Figure 8.2b).

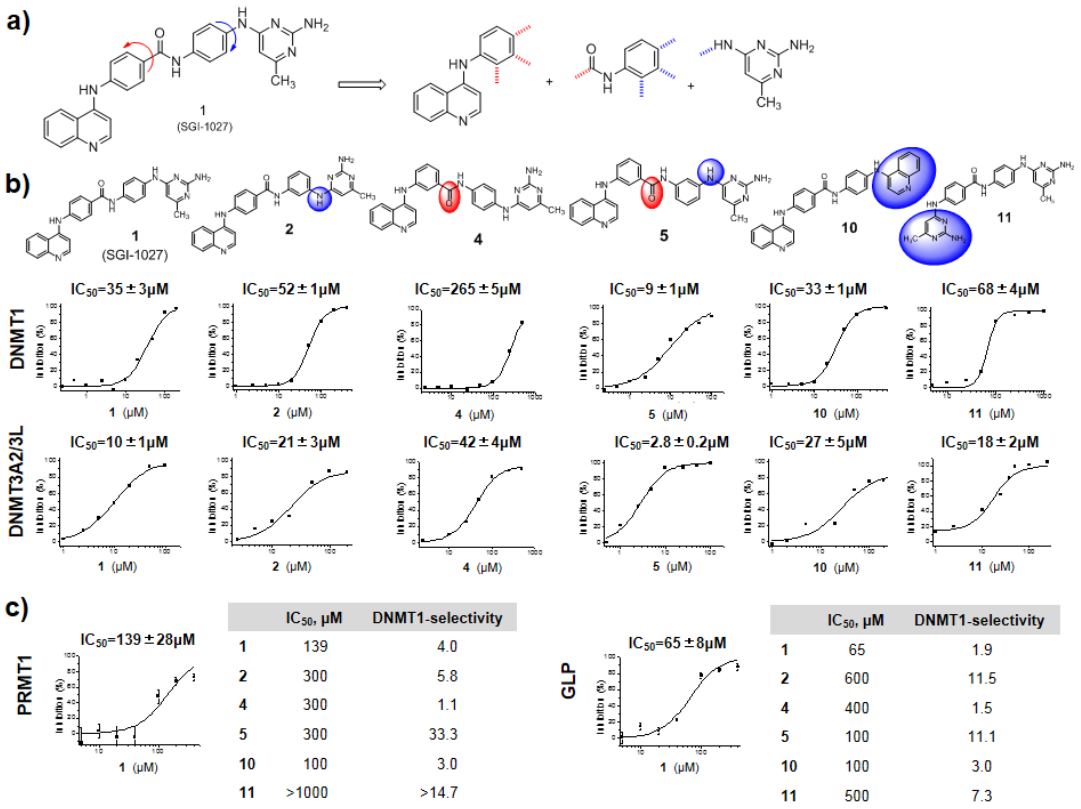

	IC_{50}, µM	DNMT1-selectivity
1	139	4.0
2	300	5.8
4	300	1.1
5	300	33.3
10	100	3.0
11	>1000	>14.7

	IC_{50}, µM	DNMT1-selectivity
1	65	1.9
2	600	11.5
4	400	1.5
5	100	11.1
10	100	3.0
11	500	7.3

Figure 8.2. Novel quinoline-based non-nucleoside DNMTi. (a) Design of **1** regioisomers. (b) Inhibitory activities of **1**, **2**, **4**, **5**, **10** and **11** against human DNMT1 (hemimethylated substrate) and the DNMT3A2/DNMT3L complex (unmethylated substrate). (c) Inhibitory activities of **1**, **2**, **4**, **5**, **10** and **11** against PRMT1 and GLP. The DNMT1-selectivity (as PRMT or GLP/DNMT1 IC_{50} ratio) for each compound is reported.

To determine the specificity of **1**, **2**, **4**, **5**, **10** and **11** for DNMTs among other AdoMet-dependent enzymes, these compound were tested against PRMT1, a protein arginine methyltransferase,[564] and G9a-like protein (GLP), a histone H3 lysine 9 methyltransferase.[436] Under the tested conditions, the new derivatives displayed very low (or none) PRMT1 and GLP inhibiting activities, resulting in all cases more DNMTs-selective than **1**, that shared only 4- and 1.9-fold lower activities against PRMT1 and GLP, respectively, when compared with DNMTs inhibition. In contrast, **5** was 33- and 11-fold less potent against PRMT1 and GLP than against DNMT1 (Figure 8.2c).

8.4.2.1.Methods

Protein purification. Expression and purification of human DNMT1 *N*-terminal deletion of 600 residues (residues 601-1600) and human DNMT3A2/DNMT3L complex have been described.[565] Recombinant rat PRMT1[564] and human G9a-like protein (GLP) C-terminal fragment containing both the ankyrin

repeats and catalytic SET domain (residues 734-1235; pXC758) were purified as described.[566]

DNMT1 inhibition assay. For DNMT1, methyl transfer activity inhibition assays were performed in 20 μL reactions containing 4.6 mM [methyl-^{3}H]-AdoMet (10.0 Ci/mmol; Perkin Elmer), 1 mM DNA oligonucleotides, 0.2 μM DNMT1, 1 mM EDTA and 50 mM Tris-HCl pH 7.5. The DNA substrates were 36-base pair hemi-methylated $(GAC)_{12}$. Enzymes were pre-incubated with AdoMet and various concentrations of inhibitors for 5 min at 37 ^oC before the addition of substrate DNA. After 15 min incubation, the reactions were terminated by the addition of 1% sodium dodecyl sulfate and 1 mg/mL of protease K and heat at 50 ^oC for 15 min. The reaction mixtures were spotted on DE81 paper circles (Whatman), washed with 5 ml of cold 0.2 M NH_4HCO_3 (twice), 5 mL of deionized water (twice) and 5 mL of ethanol (once). The dried circles were subjected to liquid-scintillation counting with Cytoscint scintillant. All curves were fit individually using Origin 7.5 software (OriginLab).

DNMT3A inhibition assay. For DNMT3a2/3L complex, the inhibition assays were performed 20 μL reactions containing 4.6 mM [methyl-^{3}H]-AdoMet, 1.0 mM DNA oligonucleotides, 0.3 μM enzyme, 0.5 mM tris(2-carboxyethyl)phosphine (TCEP), 2.5% (v/v) glycerol and 50 mM Tris–HCl pH 7.5. The DNA substrates were 28-base pair containing two CpG sites: 5'-ACA GTA CGT CAA GAT CTT GAC GTA CTG T-3' and the complimentary strand.

PRMT1 and GLP inhibition assays. For histone methylation inhibitions, the assays were performed in 20 μL reactions containing 4.6 mM [methyl-^{3}H]-AdoMet, 50 μg/mL histone from calf thymus (SIGMA), 12 μg/mL (0.3 μM) PRMT1 or 10 μg/mL (0.17 μM) GLP, 100 mM KCl, 5 mM dithiothreitol (DTT) and 50 mM Tris-HCl pH 8.5. Enzymes were pre-incubated with AdoMet and various concentrations of inhibitors for 5 min at 37 ^oC (for PRMT1) or 30 ^oC (for GLP) before the addition of histone substrates. After incubation (6.5 min for PRMT1 or 5 min for GLP), the reactions were terminated by the addition of 20% trichloroacetic acid (TCA, Fisher Scientific). The reaction mixtures were spotted on GF/A paper circles (Whatman), washed three times with 3 mL of 10% TCA and once with 3 ml of ethanol. The dried circles were subjected to liquid-scintillation counting with Cytoscint scintillant. All curves were fit individually using Origin 7.5 software (OriginLab).

*8.4.3. Docking studies of **1** and **5** in DNMT1 alone and in DNMT1/DNA complex structures*

Mechanism of action of 5. To better understand the mechanism of inhibition of our compounds against DNMT1, **1** and **5** were docked in two different DNMT1 structures available in Protein Data Bank (PDB), first using DNMT1 (residues 600-1600) crystallized in complex with the cofactor analog sinefungin (PDB 3SWR, Hashimoto and Cheng, unpublished data), and then using DNMT1 (residues 646-1600) in complex with both AdoMet and a 19-base pair DNA duplex (PDB 3PTA).[62]

These two structures share a similar overall three-dimensional arrangement with some conformational differences mainly in the DNA binding CXXC domain region (residues 646–692, Figure 8.3).

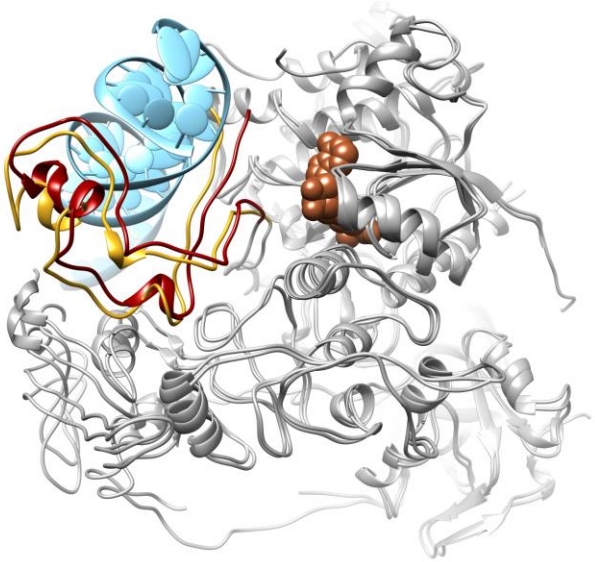

Figure 8.3. Superimposition of the DNMT1 structures crystallized in complex (PDB 3PTA) and unliganded to DNA (PDB 3SWR). Both the catalytic regions are depicted as grey ribbons, in the 3PTA structure SAH, the CXXC domain and the DNA are depicted as brown spheres, red ribbons and cyan ribbons and ellipsoids, respectively. In the 3SWR structure the CXXC domain is represented as red ribbons.

Docking results achieved on the DNMT1 structure alone (unbound to DNA) revealed that both **1** and **5** were able to spam between the AdoMet binding site and the CXXC region (Figure 8.4a), inserting their 4-aminoquinoline fragments in a lipophilic region normally occupied by AdoMet, and establishing with their 2,4-diamino-6-methylpyrimidine terminal heads a number of hydrogen-bonds at the CXXC domain region. In particular, **5** is able to establish hydrophobic contacts with I1167, M1169, P1225, I1247 and T-shaped interaction with F1145, thus clarifying why **5** is more potent than its structural congener **1**. Indeed, substitution of the quinoline ring with a smaller pyrimidine one (**11**) or with a hydrogen (**13**) would cause the loss of the interactions within the cleft thus explaining the drop in inhibitory potency. Moreover, the attached central fragments (4-aminobenzoic acid + 1,4-phenylenediamine of **1** and 3-aminobenzoic acid + 1,3-phenylenediamine of **5**) are embedded in a region in which cation-π and π-π interactions are established with R1574 and W1170, respectively. The intrinsic rigidity of these fragments allows to project the 2,4-diamino-6-methylpyrimidine terminal at the crevice between CXXC and methyltransferase domains. In this position, the terminal hydrophilic heads of **1** and **5** H-bond with M694 (backbone CO) and N1568 (side-chain) and with M694 and P692 (backbone COs) and D1571 (side-chain), respectively. Comparison between the two predicted complexes would suggest that in **5** the 4 ligand fragments are optimally assembled so as to maximize the interactions in this enzyme region, thus clarifying why **5** is more active than its structural parent compound **1**. Almost the same binding

orientation was obtained when docking **1** in the enzyme/DNA structure in line with experimental data demonstrating that this ligand inhibits DNMT1 by competing with AdoMet but not with the substrate DNA (Figure 8.4b). On the contrary, the same calculations did not succeed in suggesting a well-defined binding pose for **5**; indeed, when superimposing the coordinates of **5**, achieved in the absence of DNA, in the DNMT1/DNA complex it seems clear that the subtle rearrangements of the CXXC domain induced by the presence of DNA would sterically hamper **5** to spam from the AdoMet interaction site to the cleft between CXXC and methyltransferase domains (Figure 8.4b). These data allow postulating that, differently from **1**, **5** binds the enzyme when the DNA is absent thereby inhibiting the enzyme by competing with this target substrate. Competition experiments performed with **5** and DNMT1 by varying concentration of either DNA or AdoMet confirmed that the mechanism of inhibition of **5** was competitive with the DNA substrate and not with the AdoMet cofactor (Figure 8.4c).

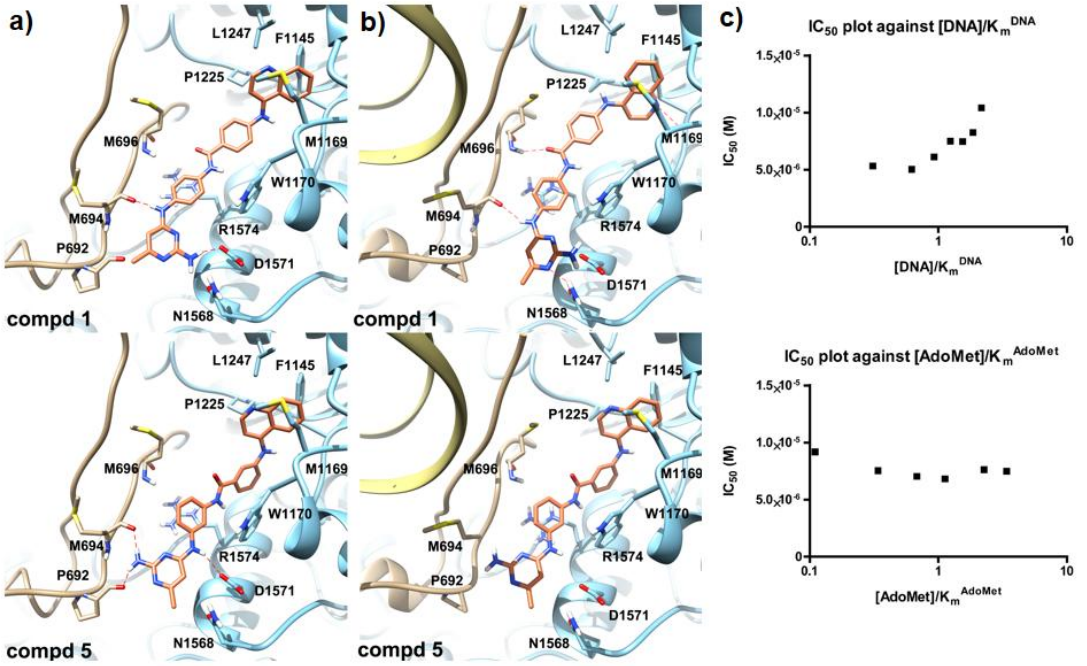

Figure 8.4. Binding mode and mechanism of action of compound 5. (a) Binding modes of **1** (top) and **5** (bottom) to DNA-unliganded DNMT1 (PDB 3SWR). (b) Binding modes of **1** (top) and **5** (bottom) to DNA/DNMT1 complex (PDB 3PTA). (c) Competition experiments performed with **5** and DNMT1 by varying DNA (top) or AdoMet (bottom) concentrations.

8.4.3.1.Methods

Molecular modelling. Prior to docking calculations, the Epik software was used to calculate the most relevant ionization and tautomeric state of compounds **1** and **5**. Then the Glide program of the Schröedinger package was used to dock these compounds into the two selected DNMT1 X-ray structures (PDBs 3SWR, Hashimoto and Cheng, unpublished results, and 3PTA). The receptor grid generation was performed for the box with a center in the putative binding sites of the two structures.

The size of the box was determined automatically. The extra precision mode (XP) of Glide was used for docking. The ligand scaling factor was set to 1.0. The geometry of the ligand binding site of the complex between **1** and **5** and the DNMT1 structures was then optimized. The binding site was defined as **1** or **5** and all amino acid residues located within 8 Å from the ligands. All the receptor residues located within 2 Å from the binding site were used as a shell. The following parameters of energy minimization were used: OPLS2005 force field was used. Water was used as an implicit solvent, and a maximum of 5000 iterations of the Polak-Ribier conjugate gradient minimization method was used with a convergence threshold of 0.01 kJ mol^{-1} $Å^{-1}$. All complex pictures were rendered employing the UCSF Chimera software.

Competition studies. In AdoMet-competition assays, AdoMet (0.6TBq/mmol) was varied between 0.5 μM and 15 μM with an isotopic dilution of 1*:1 at a fixed DNA duplex concentration of 1.0 μM. For each AdoMet concentration, the tested compound concentration was adjusted between its IC_{10} and its IC_{80}. In DNA-competition assays, the DNA duplex concentration was varied between 0.05 μM and 1.0 μM whereas AdoMet (0.6TBq/mmol) concentration was hold at 15 μM with an isotopic dilution of 1*:2. For each DNA duplex concentration, the tested compound concentration was adjusted between its IC_{10} and its IC_{80}. For each substrate concentration, the IC_{50} of tested compound was calculated by non-linear regression fitting with sigmoidal dose-response (variable slope). For each compound concentration, K_m^{app} and V_m^{app} of each substrate were approximated by non-linear fitting of the data with the Michaelis-Menten equation on GraphPad Prism 4.03.

8.4.4. Effects of quinoline-based DNMTi in a panel of cancer cell lines

To study the effects in a cellular context, the DNMTi **1**, **2**, **4**, **5**, **10** and **11** were tested in a panel of cancer cells (histiocytic lymphoma U-937, breast cancer MDA-MB-231, Burkitt's lymphoma RAJI and prostate cancer PC-3). Trypan blue exclusion assays were carried out to determine their effects on cell proliferation and viability. The effect of the tested compounds in peripheral blood mononuclear cells (PBMCs) was also determined to assess for differential toxicity. In full agreement with their DNMT inhibition potency, compounds **1**, **2** and **5** displayed the highest antiproliferative effects and the strongest cell death induction in all the cancer cells tested (Figure 8.5a-d). Compounds **4**, **10** and **11** showed both lower activity and cytotoxicity in these assays (Figure 8.1). Compounds **1** and **5** showed comparable potency against tumor cells, but **5** was the less toxic in PBMCs (Figure 8.5e, f). Nuclear morphological changes were further observed by fluorescence microscopy after Hoechst and propidium iodide (PI) staining in both U-937 and RAJI cells treated with increasing doses of **5**, to assess levels of necrosis and apoptosis induced by the compound (Figure 8.5g). In U-937 cells, **5** displayed massive apoptosis at 10 μM followed by necrosis at 25μM, while in RAJI cells **5** mainly let to necrosis at 25 μM without triggering any apoptotic response at lower concentrations.

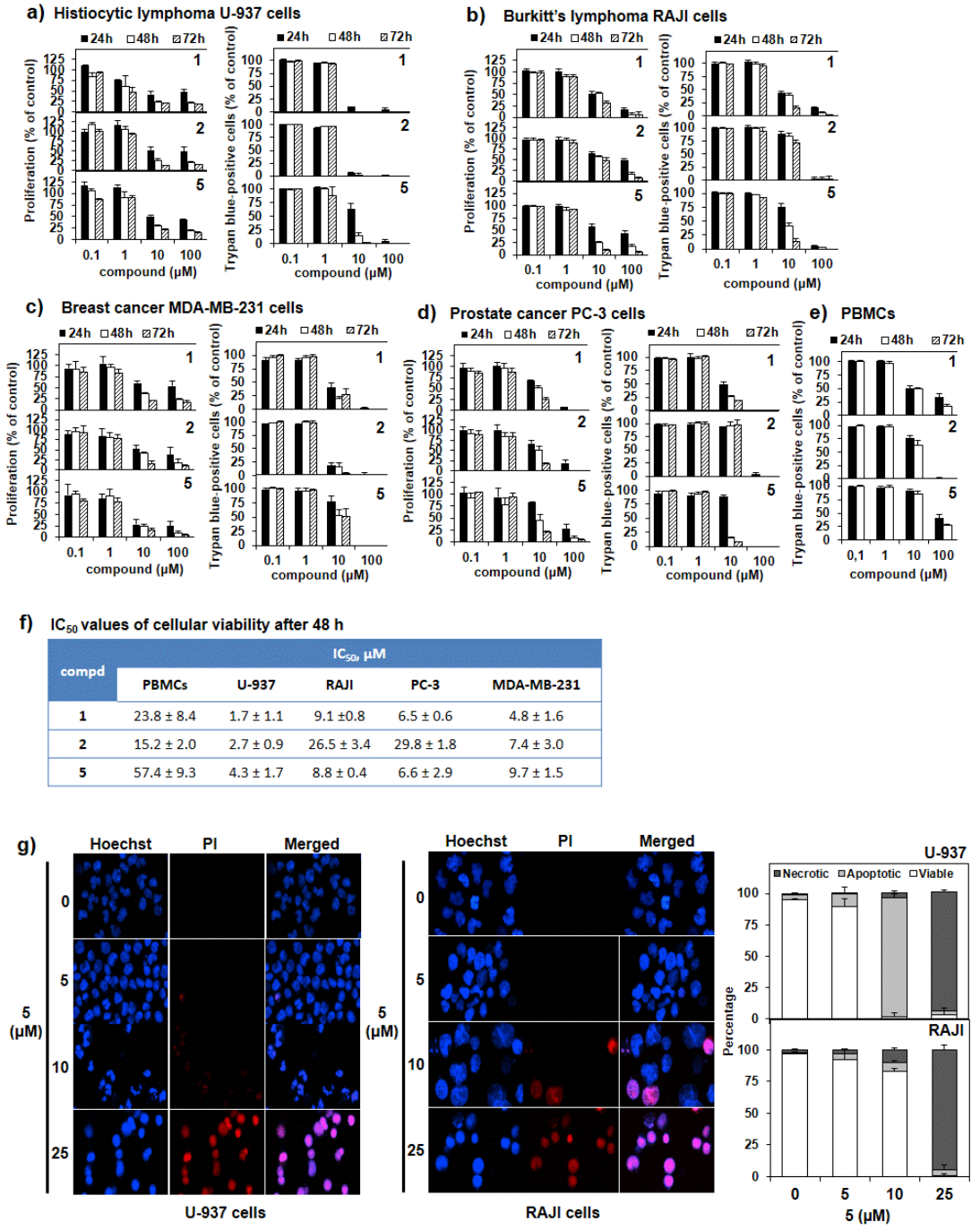

compd	IC_{50}, μM				
	PBMCs	U-937	RAJI	PC-3	MDA-MB-231
1	23.8 ± 8.4	1.7 ± 1.1	9.1 ±0.8	6.5 ± 0.6	4.8 ± 1.6
2	15.2 ± 2.0	2.7 ± 0.9	26.5 ± 3.4	29.8 ± 1.8	7.4 ± 3.0
5	57.4 ± 9.3	4.3 ± 1.7	8.8 ± 0.4	6.6 ± 2.9	9.7 ± 1.5

Figure 8.5. Cellular studies on quinoline-based DNMTi. (a-e) Antiproliferative effects (left) and cell death induction (right) of **1**, **2** and **5** on U-937 (a), RAJI (b), MDA-MB-231 (c), PC-3 (d) and PBM (e) cells. (f) IC_{50} values of cell viability relative to the above cells treated with **1**, **2** and **5** for 48 h. (g) Nuclear morphology analysis after Hoechst and PI staining in U-937 and RAJI cells treated with increasing doses of **5** for 72 h. Data represent the mean (±SD) of at least three independent experiments. Pictures are representative of three independent experiments.

8.4.4. 1. Effects of 2 and 5 in medulloblastoma stem cells (MbSCs)

Further results were collected to evaluate the effect of the compound **2** and **5** on murine stem tumor medulloblastoma (MBSC), which express high levels of DNMT.[567] When tested in mouse MbSCs, expressing high levels of DNMTs, compound **5** arrested the cell clonogenic activity and induced cell adhesion and differentiation, significantly impairing MbSC growth rate, evaluated by quantification of PCNA levels and MTT assay (Figure 8.6a, b). MbSCs dfferentiation was evaluated by βIII-tubulin and phase contrast images (Figure 8.6c, d). In these assays, **5** displayed the highest growth arrest, while **2** showed higher differentiation already after treatment with lower doses. To the best of our knowledge, these are the first examples of non-nucleoside DNMTi tested in cancer stem cells (CSCs).

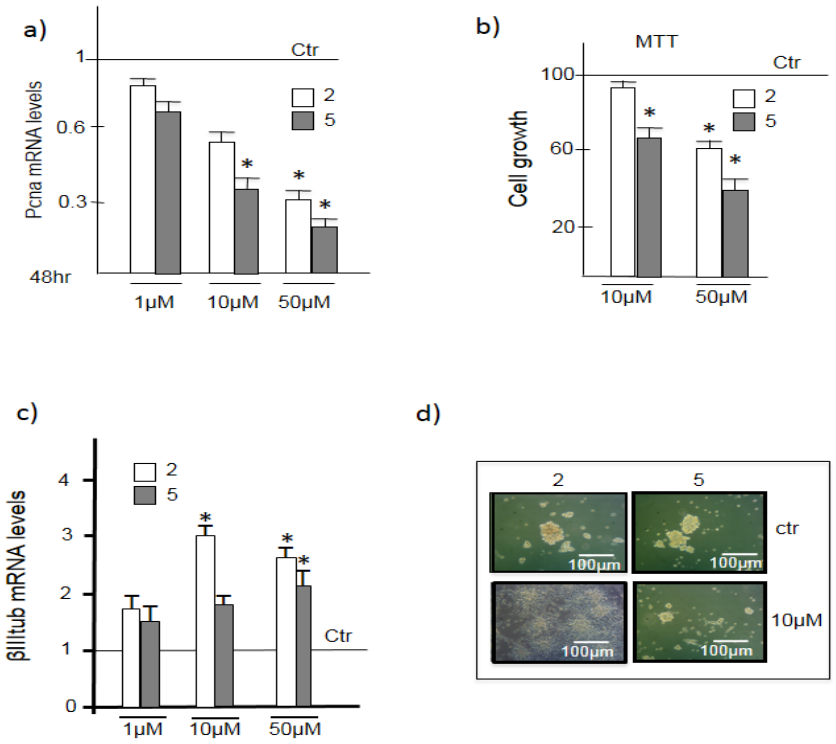

Figure 8.6. Effects of **2** and **5** in MbSCs. (a) PCNA mRNA levels and (b) MTT assay of MbSCs after 48 h of **2** and **5** treatment or DMSO as control (Ctr). *P<0.05 versus untreated cells (ctr). (c) mRNA levels of βIII-tubulin (βIIItub) in **2**- and **5**-treated MbSCs for 48 h. DMSO was used as control.*P<0.05 versus untreated cells (ctr). (d) Representative bright field images of MbSCs after **2** or **5** (48 h, 10 μM) or DMSO as control.

8.4.4.2. Methods

U-937, RAJI, PC-3, MDA-MB-231 and PBM cellular assays. U-937 (histiocytic lymphoma), RAJI (Burkitt's lymphoma), PC-3 (prostate cancer), MDA-MB-231 (breast cancer) cell lines were purchased from Deutsche Sammlung für Mikroorganismen und Zellkulturen (DSZM). Cells were cultured in RPMI 1640

(Lonza), supplemented with 10% fetal calf serum (Lonza) and 1% antibiotic antimycotic (Lonza). Peripheral blood mononuclear cells (PBMCs) were isolated and cultured as previously reported by our collaborators.[568] Cells in exponential growth phase were treated with compounds at the indicated concentrations. Proliferation and viability were assessed by trypan blue exclusion analysis at the indicated time points. Morphological determination of apoptosis and necrosis was performed as described previously.[569]

Stem cell cultures and treatments. Medulloblastoma cancer stem cells (MbSCs) were isolated and cultivated as already described.[569] More in detail, MbSCs were isolated from fresh tumor specimens from Ptch1+/-. Cells were obtained after mechanical and enzymatic dissociation and cultured in serum-free DMEM-F12 plus glucose 0.6%, insulin 25 mg/mL, *N*-acetyl-L-cystein 60 mg/mL, heparin 2 mg/mL, B271X, EGF 20 ng/mL and bFGF 20 ng/mL. MbSCs were also treated to differentiate in vitro after withdrawal of EGF/bFGF and addition of differentiating factors (Platelet Derived Growth Factor, PDGF) for 48 h. Compounds **2** and **5** were resuspended in DMSO at 1 mM. Cells were treated with increasing concentration of **2** or **5** (1, 10 and 50 µM) for 48 h and DMSO was used as control. Unless otherwise indicated, media and supplements were purchased from Gibco-Invitrogen (Life Science) and chemicals were from Sigma-Aldrich (St. Louis, MO).

MTT assay. MbSC were treated with 1, 10 and 50 µM of compound **2** or **5** for 48 h. Growth of drug-treated cells relative to untreated cells was measured by MTT assay. Each sample was measured in triplicates and repeated at least three times.

8.4.5. Conclusion

Through chemical manipulation applied on the structure **1** we identified compound **5**, a novel non-nucleoside DNMTi more potent of **1** and more selective towards other AdoMet-dependent methyltransferases (PRMT1, GLP). Differently from **1**, competitive with AdoMet, **5** was found to be competitive with DNA for its DNMT1 inhibition. Tested on a panel of cancer cells (leukemia U937, breast cancer MDA-MB-231, Burkitt's lymphoma RAJI, and prostate cancer PC-3) as well as on PBMCs, **5** displayed comparable activity as **1** and less toxicity. In MbSCs, at 10 μM **5** significantly blocked proliferation but required higher doses (50 μM) to induce differentiation, while the related compound **2**, less potent as antiproliferative agent, showed high differentiating activity. The anticancer activity displayed by **2** and **5** in the tested cancer cells including CSCs suggests their use as potent and selective non-nucleoside DNMTi for cancer therapy.

* Adapted with the permission from Valente, S., Liu, Y., Schnekenburger, M., Zwergel, C., Cosconati, S., Gros, C., Tardugno, M., Labella, D., Florean, C., Minden, S., Hashimoto, H., Chang,Y., Zhang, X., Kirsch, G., Novellino, E., Arimondo, P.B., Miele, E., Ferretti, E., Gulino, A., Diederich, M., Cheng, X., Mai, A. Selective non-nucleoside inhibitors of human dna methyltransferases active in cancer including cancer stem cells, *J. Med. Chem.*, accepted.[570]

9. Quinazoline analogues as Novel DNA methyltransferase 3A inhibitors*

9.1. Research project

DNMT3A and DNMT3B are *de novo* methyltransferases, adding methyl groups in unmethylated genomic sequences at CpG dinucleotides, and are highly expressed in early embryonic cells, downregulated after differentiation and in adult somatic tissues, and overexpressed in cancer.[571,572] During our investigation of small molecule epigenetic modulators, we recently described various series of compounds able to inhibit protein/histone methyltransferases, a subfamily of AdoMet-dependent methyltransferases catalyzing the (poly)methylation of arginine (Arg) or lysine (Lys) residues in both histone and in non-histone proteins.[573,574] In particular, chemical manipulation of BIX-012946 (1) (Figure 9.1), a specific G9a/G9a-like protein (GLP) histone H3 Lys9 (H3K9) methyltransferase inhibitor, led to E67[575] (2) (Figure 9.1), bearing a 5-amminopentyloxy substituent at the C7 position of the quinazoline ring with enhanced G9a/GLP inhibitory activity *in vitro* and reduced toxicity *in vivo*. X-ray crystal structures of 1 and 2 complexed with GLP [564,575,576] showed that for both compounds the quinazoline scaffold, linked to the C4-(1-benzyl-4-piperidinylamino) and the C2-diazepane (1) or C2-(3-dimethylaminopropylamino) (2) moieties, resembles the bound conformation of histone H3 Lys4 to Arg8, while the C6-(5-aminopentyloxy) chain of 2 mimics the target Lys9 of histone H3 in the substrate peptide binding groove. For both compounds, the C6-methoxy group is inserted into a shallow surface pocket mimicking the H3A7 side chain, and is crucial for binding to H3K9 modification enzymes (methyltransferases as well as demethylases), discriminating them from other enzymes, such as for example H3K4 methyltransferases and demethylases.[564,575,576]

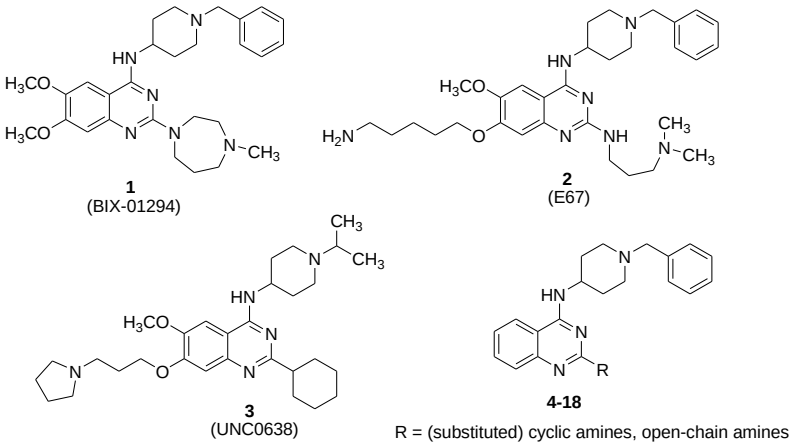

Figure 9.1. Known quinazolines (**1**-**3**) as G9a/GLP inhibitors, and novel 6,7-desmethoxyquinazolines **4**-**18**.

Chemical changes performed by other authors on **1** led to UNC0638 [577] (Figure 9.1, **3**), a potent and selective G9a/GLP inhibitor featuring the 1-*iso*-propyl-4-piperidinylamino moiety at C4, the cyclohexyl group at C2, the 3-(1-pyrrolidino)propyloxy chain at C7, and the methoxy group at C6 position of the quinazoline ring. Compound **3** showed nanomolar potency against G9a, excellent cell permeability and robust on-target activity in cells.[577] Interestingly, compound **3** was found to be inactive against other histone lysine methyltransferases, but displayed high micromolar activity against DNMT1.[577] This suggested that the quinazoline moiety, used to develop lysine methyltransferase and demethylase inhibitors, could also be suitable to design, with appropriate substitutions, compounds able to inhibit DNMTs. In addition, we thought that such quinazoline-based compounds lacking the C6 methoxy group should be devoid of anti-H3K9 methyltransferase activity. Thus, we prepared the series of 6,7-desmethoxy quinazolines **4-18** (Figure 9.1) by maintaining the 1-benzyl-4-piperidinylamino moiety (typical of **1** and **2**) at the C4 position of the quinazoline ring and changing the substituent at C2, spanning from differently sized cyclic amines (containing or not heteroatoms and/or lipophilic groups) to open-chain amines. Compounds **4-18** were tested against hDNMT1, catalytic hDNMT3A and hGLP, to assess their activities and selectivity. Molecular modeling studies were performed on the most potent **4** and **14** compounds, using the DNMT3A crystal structure,[54] to gain insight on their binding modes. In addition, cellular studies were carried out to determine their anticancer effects.

9.2. Chemistry

The synthetic route followed for the preparation of **4-18** is depicted in Scheme 1. The 2,4- dichloroquinazoline **19** [578] was treated with 4-amino-1-benzylpiperidine at room temperature providing the 4-substituted intermediate **20**, which underwent C2-chloro displacement at the quinazoline ring with the proper amines at 110 °C in a sealed tube to provide the desired 2,4-disubstituted quinazolines.

Scheme 1

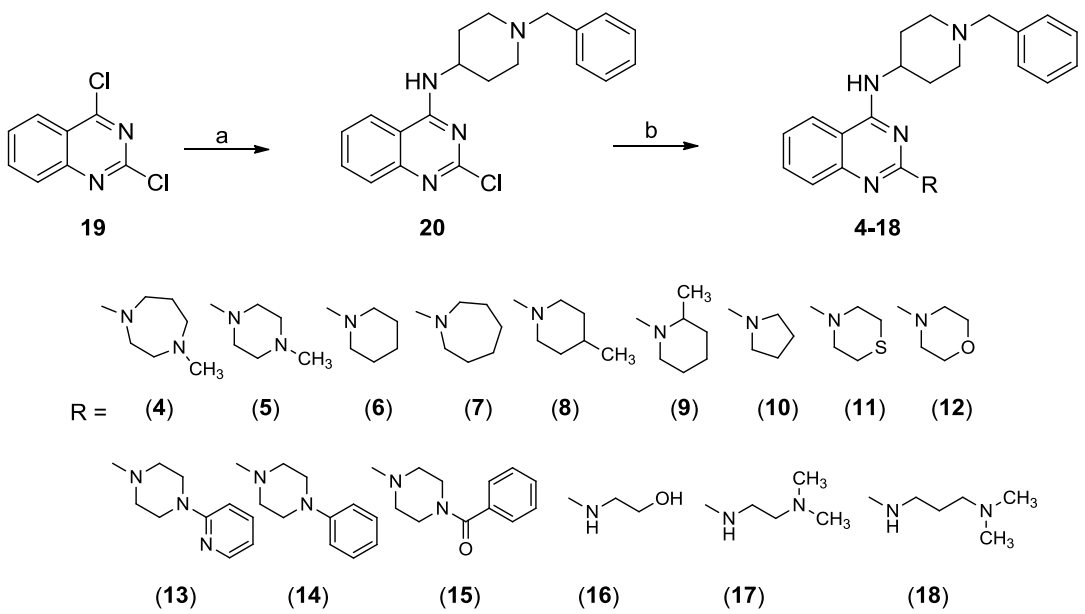

Reagents and conditions: (a) 4-amino-1-benzylpiperidine, dry THF, room temperature; (b) various amines, 110 °C, sealed tube.

The chemical and physical data of the intermediate **20** and those of the final compounds **4-18** are shown in Table 9.1 and 9.2, respectively.

Table 9.1. Chemical and physical properties of compound **20**.

Cpd	molecolar structure	mp, °C	recrystall. solvent	Yield %
20	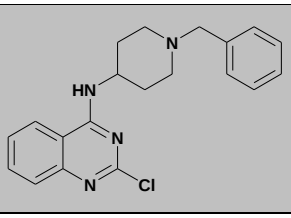	158-160	A	86
A: benzene/cyclohexane				

Table 9.2. Chemical and physical properties of compound **4-18**.

Cpd	molecolar structure	mp, °C	recrystall. solvent	Yield %
4	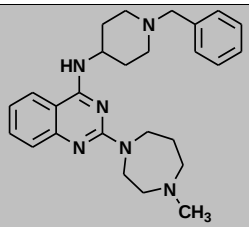	96-98	A	65
5	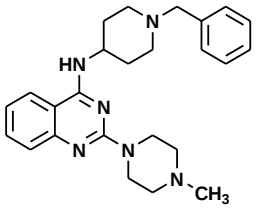	114-118	A	68
6	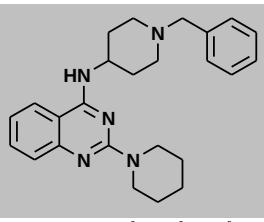	118-120	A	61
7	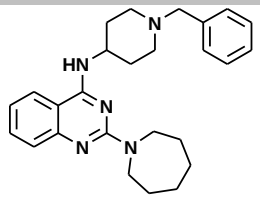	119-122	A	71
8	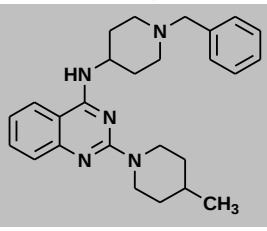	106-108	B	57
9	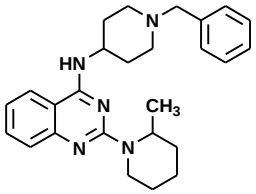	128-129	A	45
10	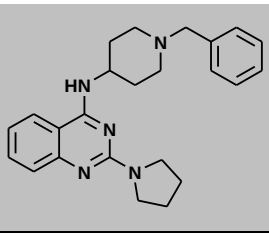	112-115	B	68

11	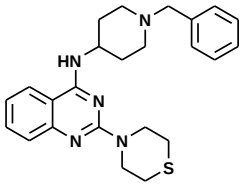	155-157	A	59
12	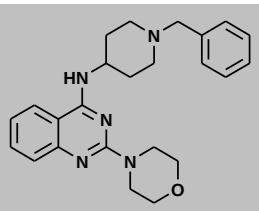	110-112	B	70
13	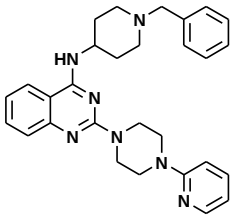	98-100	B	58
14	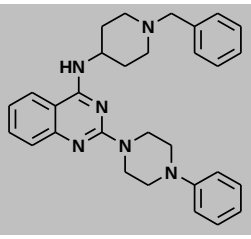	143-145	A	63
15	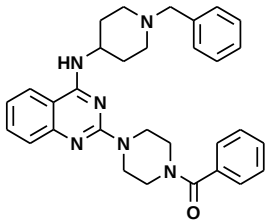	213-215	C	50
16	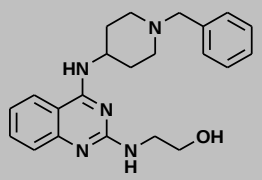	116-118	B	61
17	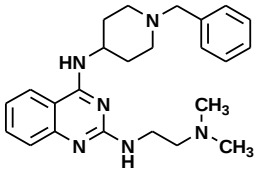	120-122	A	51

18	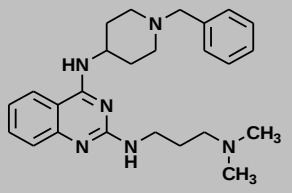	Oil	-	51

A: cyclohexane; B: petroleum ether; C: acetonitrile

9.3. Experimental section

Chemistry. Melting points were determined on a Buchi 530 melting point apparatus. ^{1}H- and ^{13}C-NMR spectra were recorded at 400 MHz on a Bruker AC 400 spectrometer; chemical shifts are reported in δ (ppm) units relative to the internal reference tetramethylsilane (Me_4Si). All compounds were routinely checked by TLC and ^{1}H-NMR. TLC was performed on aluminium-backed silica gel plates (Merck DC, Alufolien Kieselgel 60 F254) with spots visualized by UV light. Mass spectra were recorded on a API-TOF Mariner by Perspective Biosystem (Stratford, Texas, USA), samples were injected by an Harvard pump using a flow rate of 5-10 μL/min, infused in the Electrospray system. All solvents were reagent grade and, when necessary, were purified and dried by standard methods. Concentration of solutions after reactions and extractions involved the use of a rotary evaporator operating at reduced pressure of ~ 20 Torr. Organic solutions were dried over anhydrous sodium sulphate. Elemental analysis has been used to determine purity of the described compounds, that is > 95%. Analytical results are within ± 0.4% of the theoretical values. All chemicals were purchased from Aldrich Chimica, Milan (Italy), or from Lancaster Synthesis GmbH, Milan (Italy), and were of the highest purity.

Preparation of *N*-(1-benzylpiperidin-4-yl)-2-chloroquinazolin-4-amine (20). 2,4-dichloroquinazoline **19** [578] (1 eq, 6.2 mmol, 1.2 g) was dissolved in dry tetrahydrofuran (THF, 50 mL) and 4-amino-1- benzylpiperidine (2.5 eq, 15.4 mmol, 2.9 mL) was added to the clear solution. The mixture was stirred at room temperature and the reaction was completed after 30 min. The resulting white salt in suspension was filtered off and washed with dry THF. The filtrate and the washings were concentrated in vacuum and the crude solid triturated with petroleum ether, collected by filtration, washed with petroleum ether and dried to give **20** as a pure white solid. ^{1}H-NMR ($CDCl_3$): δ 1.65-1.69 (m, 2H, C*H*-piperidine ring), 2.14-2.16 (m, 2H, C*H*-piperidine ring), 2.26-2.31 (m, 2H, C*H*-piperidine ring), 2.90-2.93 (m, 2H, C*H*-piperidine ring), 3.58 (s, 2H, CH_2Ph), 4.33 (m, 1H, NHC_4-*H*-piperidine ring), 5.78 (d, 1H, N*H*), 7.29-7.36 (m, 5H, C*H*-phenyl ring), 7.66-7.68 (t, 1H, C_6-*H* quinazoline ring), 7.74-7.76 (m, 3H, $C_{5,7,8}$-*H* quinazoline ring). ^{13}C-NMR ($CDCl_3$) δ 30.3, 51.8, 56.8, 64.6, 114.2, 122.5, 126.6, 127.2, 127.6, 128.4, 128.8, 133.1, 138.6, 150.7,

157.6, 160.3 ppm. HR-MS (ESI) calculated for $C_{20}H_{22}ClN_4$ $[M + H]^+$, 353.1533; found, 353.1537.

General Procedure for the Preparation of 4-(1-Benzylpiperidin-4-yl)-2-(cyclo/alkylamino)quinazolin-4-amines (4-21). Example: *N*-(1-Benzylpiperidin-4-yl)-2- morpholinoquinazolin-4-amine (12). A mixture of *N*-(1-benzylpiperidin-4-yl)-2-chloroquinazolin-4-amine **23** (1 eq, 0.6 mmol, 0.2 g) and morpholine (5 eq, 2.8 mmol, 0.25 mL) was placed in a sealed tube and stirred at 110 °C for 1 h. After cooling to room temperature, 5 mL of water were added and the resulting precipitate was filtered and washed with water. The obtained solid residue was recrystallized from petroleum ether to provide pure **12** as a white solid. ^{1}H-NMR ($CDCl_3$): δ 1.71-1.76 (m, 2H, C*H*-piperidine ring), 2.14-2.31 (m, 4H, C*H*-piperidine ring), 2.96 (m, 2H, C*H*-piperidine ring), 3.61 (s, 2H, CH_2Ph), 3.80-3.87 (m, 8H, C*H*-morpholine ring), 4.18 (m, 1H, NHC4-*H*-piperidine), 5.56 (d, 1H, N*H*), 7.11 (m, 1H, C_6-*H* quinazoline ring), 7.31-7.38 (m, 5H, C-*H* phenyl ring), 7.50-7.53 (m, 3H, $C_{5,7,8}$-*H* quinazoline ring). ^{13}C-NMR ($CDCl_3$) δ 30.3, 48.7, 51.9, 56.8, 64.7, 66.3, 110.3, 123.0, 127.2, 127.7, 127.8, 128.4, 128.8, 132.7, 138.6, 152.3, 160.1, 184.6 ppm. HR-MS (ESI) calculated for $C_{24}H_{30}N_{5O}$ $[M + H]^+$, 404.2450; found, 404.2446.

***N*-(1-Benzylpiperidin-4-yl)-2-(4-methyl-1,4-diazepan-1-yl)quinazolin-4-amine (4).** ^{1}H-NMR (DMSO) δ 1.63-1.65 (m, 2H, C*H*-piperidine ring), 1.86 (m, 2H, C*H*-diazepan ring), 1.94-1.97 (m, 2H, C*H*-piperidine ring), 2.05 (m, 2H, C*H*-piperidine ring), 2.24 (s, 3H, N-CH_3), 2.43-2.44 (m, 2H C*H*-diazepane ring), 2.58 (m, 2H, C*H*-diazepane ring), 2.86-2.88 (m, 2H, C*H*-piperidine ring), 3.48 (s, 2H, CH_2Ph), 3.76-3.79 (m, 2H, C*H*-diazepane ring), 3.84 (m, 2H, C*H*-diazepane ring), 4.02 (m, 1H, NHC*H*-piperidine), 7.00 (t, 1H, C*H* quinazoline ring), 7.22-7.27 (m, 2H, C*H* phenyl ring), 7.32-7.36 (m, 4H, C*H* phenyl ring and N*H*), 7.44-7.48 (m, 1H, C*H* quinazoline ring), 7.51-7.53 (d, 1H, C*H* quinazoline ring), 8.02-8.04 (d, 1H, C*H*, quinazoline ring). ^{13}C-NMR (DMSO) δ 26.5, 30.2, 46.8, 51.6, 51.9, 56.9, 57.5, 59.2, 61.9, 64.8, 110.4, 123.1, 127.3, 127.7, 127.8, 128.4, 128.8, 132.8, 138.5, 152.1, 160.1, 184.5 ppm. HR-MS (ESI) calculated for $C_{26}H_{35}N_6$ $[M + H]^+$, 431.2923; found, 431.2928.

***N*-(1-Benzylpiperidin-4-yl)-2-(4-methylpiperazin-1-yl)quinazolin-4-amine (5).** ^{1}H-NMR ($CDCl_3$) δ 1.62-1.64 (m, 2H, C*H*-piperidine ring), 2.11 (m, 2H, C*H*-piperidine ring), 2.22 (m, 2H, C*H*-piperidine ring), 2.34 (s, 3H, N-CH_3), 2.49 (m, 4H, C*H*-piperazine ring), 2.87-2.90 (m, 2H, C*H*-piperidine ring), 3.54 (s, 2H, CH_2Ph), 3.91 (m, 4H, C*H*-piperazine ring), 4.13 (m, 1H, NHC_4-*H*-piperidine), 5.45 (s, 1H, N*H*), 7.05 (m, 1H, C*H* quinazoline ring), 7.32-7.33 (m, 5H, C*H* phenyl ring), 7.42-7.49 (m, 3H, C*H* quinazoline ring). ^{13}C-NMR ($CDCl_3$) δ 30.3, 46.6, 51.9, 52.0, 56.8, 57.2, 64.7, 110.3, 123.1, 127.3, 127.6, 127.9, 128.5, 128.8, 132.3, 138.5, 152.8, 160.4, 184.6 ppm. HR-MS (ESI) calculated for $C_{25}H_{33}N_6$ $[M + H]^+$, 417.2767; found, 417.2761.

***N*-(1-Benzylpiperidin-4-yl)-2-(piperidin-1-yl)quinazolin-4-amine (6).** ^{1}H-NMR ($CDCl_3$) δ 1.68-1.72 (m, 8H, C*H*-piperidine rings), 2.14-2.17 (m, 2H, C*H*-piperidine ring), 2.24-2.29 (m, 2H, C*H*-piperidine ring), 2.93 (m, 2H, C*H*-piperidine ring), 3.59

(s, 2H, C*H*$_2$Ph), 3.89-3.90 (m, 4H, C*H*-piperidine ring at C_2), 4.16 (m, 1H, NHC$_4$-*H*-piperidine), 5.52 (s, 1H, N*H*), 7.05 (m, 1H, C*H* quinazoline ring), 7.33-7.38 (m, 5H, C-*H* phenyl ring), 7.49-7.53 (m, 3H, C-*H* quinazoline ring). ^{13}C-NMR ($CDCl_3$) δ 24.5, 25.5, 30.3, 51.8, 54.8, 56.8, 64.8, 110.1, 123.3, 127.3, 127.7, 127.8, 128.5, 128.8, 132.7, 138.9, 152.3, 160.2, 184.5 ppm. HR-MS (ESI) calculated for $C_{25}H_{32}N_5$ $[M + H]^+$, 402.2658; found, 402.2664.

2-(Azepan-1-yl)-*N*-(1-benzylpiperidin-4-yl)quinazolin-4-amine (7). ^{1}H-NMR ($CDCl_3$) δ 1.57-1.67 (m, 6H, C*H* azepane and piperidine rings), 1.82 (m, 4H, C*H*-azepane ring), 2.15-2.25 (m, 4H, C*H*-piperidine ring), 2.90-2.93 (m, 2H, C*H*-piperidine ring), 3.57 (s, 2H, C*H*$_2$Ph), 3.83-3.85 (m, 4H, C*H* azepane ring), 4.14-4.16 (m, 1H, NHC$_4$-*H*-piperidine), 5.40 (s, 1H, N*H*), 7.03 (m, 1H, C-*H* quinazoline ring), 7.34-7.37 (m, 5H, C*H* phenyl ring), 7.47-7.51 (m, 3H, C-*H* quinazoline ring). ^{13}C-NMR ($CDCl_3$) δ 26.8, 28.0, 30.3, 51.9, 54.2, 56.7, 64.7, 110.3, 123.4, 127.3, 127.7, 127.9, 128.7, 128.9, 132.9, 138.6, 152.5, 160.5, 184.3 ppm. HR-MS (ESI) calculated for $C_{26}H_{34}N_5$ $[M + H]^+$, 416.2814; found, 416.2819.

***N*-(1-Benzylpiperidin-4-yl)-2-(4-methylpiperidin-1-yl)quinazolin-4-amine (8).** ^{1}H-NMR ($CDCl_3$) δ 0.97-0.99 (d, 3H, CHC*H3*), 1.19-1.23 (m, 2H, C*H*-piperidine ring at C2), 1.65-1.76 (m, 5H, C*H*-piperidine rings), 2.15-2.26 (m, 4H, C*H*-piperidine ring), 2.90-2.94 (m, 4H, C*H*-piperidine rings), 3.58 (s, 2H, C*H*$_2$Ph), 4.15 (m, 1H, NHC$_4$- *H*-piperidine), 4.86-4.89 (m, 2H, C*H*-piperidine ring at C_2), 5.40 (s, 1H, N*H*), 7.05 (m, 1H, C-*H* quinazoline ring), 7.30-7.37 (m, 5H, C*H*-phenyl ring), 7.46-7.52 (m, 3H, C-*H* quinazoline ring). ^{13}C-NMR ($CDCl_3$) δ 20.4, 30.2, 32.3, 34.3, 51.9, 52.3, 56.5, 64.9, 110.6, 123.5, 127.6, 127.9, 127.8, 128.4, 128.8, 132.5, 138.6, 152.3, 160.4, 184.7 ppm. HR-MS (ESI) calculated for $C_{26}H_{34}N_5$ $[M + H]^+$, 416.2814; found, 416.2808.

***N*-(1-Benzylpiperidin-4-yl)-2-(2-methylpiperidin-1-yl)quinazolin-4-amine (9).** ^{1}H-NMR ($CDCl_3$) δ 1.22-1.24 (d, 3H, CHC*H*$_3$), 1.53-1.54 (m, 2H, C*H* piperidine ring at C2), 1.64-1.77 (m, 6H, C*H* piperidine rings), 2.14-2.27 (m, 4H, C*H*-piperidine ring), 2.91-3.02 (m, 3H, C*H*-piperidine rings), 3.59 (s, 2H, C*H*$_2$Ph), 4.15 (m, 1H, NHC$_4$-*H* piperidine), 4.77-4.81 (m, 1H, C*H*-piperidine ring at C_2), 5.21 (s, 1H, N*H*), 7.06 (m, 1H, C-*H* quinazoline ring), 7.31-7.39 (m, 5H, C-*H* phenyl ring), 7.50-7.52 (m, 3H, C-*H* quinazoline ring). ^{13}C-NMR ($CDCl_3$) δ 18.6, 23.3, 25.7, 30.2, 33.8, 51.9, 52.3, 56.8, 62.6, 64.5, 110.3, 123.2, 127.0, 127.2, 127.5, 128.1, 128.8, 132.7, 138.8, 152.3, 160.2, 184.5 ppm. HR-MS (ESI) calculated for $C_{26}H_{34}N_5$ $[M + H]^+$, 416.2814; found, 416.2818.

***N*-(1-Benzylpiperidin-4-yl)-2-(pyrrolidin-1-yl)quinazolin-4-amine (10).** ^{1}H-NMR ($CDCl_3$) δ 1.62-1.66 (m, 2H, C*H*-piperidine ring), 1.98-2.00 (m, 4H, C*H*-pyrrolidine ring), 2.17-2.27 (m, 4H, C*H*-piperidine ring), 2.91 (m, 2H, C*H* piperidine ring), 3.57 (s, 2H, C*H*$_2$Ph), 3.67 (m, 4H, C*H*-pyrrolidine ring), 4.19-4.20 (m, 1H, NHC$_4$- *H*-piperidine), 5.30 (s, 1H, N*H*), 7.03 (m, 1H, C-*H* quinazoline ring), 7.28 (m, 2H, C*H*-

phenyl ring), 7.36 (m, 3H, C*H*-phenyl ring), 7.44-7.50 (m, 3H, C-*H* quinazoline ring). ^{13}C-NMR ($CDCl_3$) δ 25.5, 30.5, 51.9, 54.5, 56.9, 64.8, 110.6, 123.0, 127.2, 127.6, 127.9, 128.4, 128.6, 132.7, 138.5, 152.4, 160.5, 184.3 ppm. HR-MS (ESI) calculated for $C_{24}H_{30}N_5$ $[M + H]^+$, 388.2501; found, 388.2507.

***N*-(1-Benzylpiperidin-4-yl)-2-thiomorpholinoquinazolin-4-amine (11).** ^{1}H-NMR ($CDCl_3$) δ 1.71-1.73 (m, 2H, C*H*-piperidine ring), 2.15-2.17 (m, 2H, C*H*-piperidine ring), 2.26-2.32 (m, 2H, C*H*-piperidine ring), 2.69-2.71 (m, 4H, C*H*-thiomorpholine ring), 2.95-2.98 (m, 2H, C*H*-piperidine ring), 3.61 (s, 2H, CH_2Ph), 4.14-4.17 (m, 1H, NHC_4-*H*-piperidine), 4.23-4.25 (m, 4H, C*H*-thiomorpholine ring), 5.53 (s, 1H, N*H*), 7.09-7.12 (m, 1H, C-*H* quinazoline ring), 7.28-7.38 (m, 5H, C*H*-phenyl ring), 7.50-7.54 (m, 3H, C-*H* quinazoline ring). ^{13}C-NMR ($CDCl_3$) δ 27.7, 30.5, 51.7, 53.6, 56.8, 64.5, 110.7, 123.5, 127.2, 127.7, 127.9, 128 HR-MS (ESI) calculated for $C_{24}H_{30}N_5S$ $[M + H]^+$, 420.2222; found, 420.2229.

***N*-(1-Benzylpiperidin-4-yl)-2-(4-(pyridin-2-yl)piperazin-1-yl)quinazolin-4-amine (13).** ^{1}H-NMR (DMSO) δ 1.65-1.67 (m, 2H, C*H*-piperidine ring), 1.95-1.98 (m, 2H, C*H*-piperidine ring), 2.10-2.13 (m, 2H, C*H*-piperidine ring), 2.87-2.90 (m, 2H, C*H*-piperidine ring), 3.51 (s, 2H, CH_2Ph), 3.57-3.60 (m, 4H, C*H*-piperazine ring), 3.87 (m, 4H, C*H* piperazine ring), 4.08 (m, 1H, NHC_4-*H*-piperidine), 6.65-6.67 (t, 1H, C-*H* pyridine ring), 6.87-6.89 (d, 1H, C-*H* pyridine ring), 7.07 (t, 1H, C-*H* quinazoline ring), 7.29-7.33 (m, 6H, C*H*-phenyl ring and N*H*), 7.53 (m, 2H, C-*H* quinazoline and pyridine rings), 7.63-7.64 (d, 1H, C-*H* quinazoline ring), 8.07-8.09 (d, 1H, C6-*H* pyridine ring), 8.13-8.14 (d, 1H, C-*H* quinazoline ring). ^{13}C-NMR (DMSO) δ 30.3, 48.5, 49.5, 51.9, 56.8, 64.8, 106.2, 110.3, 117.9, 123.3, 127.3, 127.7, 127.8, 128.4, 128.8, 132.6, 138.2, 138.7, 148.1, 152.3, 158.3, 160.2, 184.3 ppm. HR-MS (ESI) calculated for $C_{29}H_{34}N_7$ $[M + H]^+$, 480.2876; found, 480.2871.

***N*-(1-Benzylpiperidin-4-yl)-2-(4-phenylpiperazin-1-yl)quinazolin-4-amine (14).** ^{1}H-NMR ($CDCl_3$) δ 1.68-1.71 (m, 2H, C*H*-piperidine ring), 2.17-2.20 (m, 2H, C*H*-piperidine ring), 2.26-2.32 (m, 2H, C*H*-piperidine ring), 2.94-2.97 (m, 2H, C*H* piperidine ring), 3.30 (m, 4H, C*H*-piperazine ring), 3.61 (s, 2H, CH_2Ph), 4.08 (m, 4H, C*H*-piperazine ring), 4.21 (m, 1H, NHC_4-*H*-piperidine), 5.45 (s, 1H, N*H*), 6.89-6.93 (m, 1H, C-*H* phenyl ring), 7.01-7.03 (m, 2H, C-*H* phenyl ring), 7.11 (m, 1H, C-*H* quinazoline ring), 7.28-7.41 (m, 7H, C-*H* phenyl rings), 7.49-7.54 (m, 3H, C-*H* quinazoline ring). ^{13}C-NMR ($CDCl_3$) δ 30.3, 49.4, 51.9, 56.6, 64.7, 110.5, 114.7, 121.6, 123.1, 127.2, 127.7, 127.9, 128.5, 128.8, 129.5, 132.7, 138.6, 149.8, 152.5, 160.2, 184.7 ppm. HR-MS (ESI) calculated for $C_{30}H_{35}N_6$ $[M + H]^+$, 479.2923; found, 479.2928.

***N*-(1-Benzylpiperidin-4-yl)-2-(4-benzoylpiperazin-1-yl)quinazolin-4-amine (15).** ^{1}H-NMR (DMSO) δ 1.63-1.65 (m, 2H, C*H*-piperidine ring), 1.90-1.93 (m, 2H, C*H*-piperidine ring), 2.07 (m, 2H, C*H*-piperidine ring), 2.83-2.86 (m, 2H, C*H*-piperidine ring), 3.32 (m, 2H, C*H*-piperazine ring), 3.47 (s, 2H, CH_2Ph), 3.69-3.78 (m, 6H, C*H*-

piperazine ring), 4.05 (m, 1H, NHC_4-*H*-piperidine), 7.08 (m, 1H, C-*H* quinazoline ring), 7.24-7.32 (m, 6H, C*H*-phenyl ring and N*H*), 7.45-7.52 (m, 6H, C*H*-phenyl and quinazoline rings), 7.64-7.66 (m, 1H, C-*H* quinazoline ring), 8.07-8.09 (d, 1H, C-*H* quinazoline ring). ^{13}C-NMR (DMSO) δ 30.5, 50.1, 51.3, 51.9, 56.8, 64.9, 110.7, 123.0, 127.2, 127.3, 127.7, 127.8, 128.4, 128.5, 128.8, 129.5, 132.6, 135.2, 138.6, 152.5, 160.3, 168.9, 184.5 ppm. HR-MS (ESI) calculated for $C_{31}H_{35}N_6O$ $[M + H]^+$, 507.2872; found, 507.2879.

***N*-(1-Benzylpiperidin-4-yl)-2-(ethanolamino)quinazolin-4-amine (16).** ^{1}H-NMR ($CDCl_3$) δ 1.60-1.65 (m, 2H, C*H*-piperidine ring), 2.09-2.12 (m, 2H, C*H*-piperidine ring), 2.20-2.23 (m, 2H, C*H*-piperidine ring), 2.89-2.92 (m, 2H, C*H*-piperidine ring), 3.52 (s, 2H, CH_2Ph), 3.62-3.73 (m, 2H, $NHCH_2CH_2OH$), 3.87 (t, 2H, $NHCH_2CH_2OH$), 4.16 (m, 1H, NHC-*H*-piperidine), 5.37-5.42 (s, 1H, N*H*), 5.48-5.51 (s, 1H, $NHCH_2CH_2OH$), 7.10-7.12 (m, 1H, C-*H* quinazoline ring), 7.30-7.36 (m, 5H, C*H*-phenyl ring), 7.50-7.56 (m, 3H, C-*H* quinazoline ring). ^{13}C-NMR ($CDCl_3$) δ 30.1, 46.0, 51.7, 56.8, 61.1, 64.5, 109.2, 121.3, 125.2, 126.1, 127.0, 128.4, 128.6, 131.0, 138.3, 149.8, 158.5, 177.7 ppm. HR-MS (ESI) calculated for $C_{22}H_{28}N_5O$ $[M + H]^+$, 378.2294; found, 378.2299.

***N*^{4}-(1-Benzylpiperidin-4-yl)-*N*^{2}-(2-(dimethylamino)ethyl)quinazoline-2,4-diamine (17).** ^{1}H-NMR (DMSO) δ 1.63-1.69 (m, 2H, C*H*-piperidine ring), 1.88 (m, 2H, C*H*-piperidine ring), 2.01-2.07 (m, 2H, C*H*-piperidine ring), 2.13-2.17 (s, 6H, $N(CH_3)_2$), 2.38-2.42 (t, 2H, $NHCH_2CH_2N(CH_3)_2$), 2.85-2.88 (m, 2H, C*H*-piperidine ring), 3.30-3.34 (t, 2H, $NHCH_2CH_2N(CH_3)_2$), 3.42 (s, 2H, CH_2Ph), 4.17-4.18 (m, 1H, NHC_4-*H*-piperidine), 6.21-6.24 (s, 1H, $NHCH_2CH_2N(CH_3)_2$), 6.98-7.01 (m, 1H, C-*H* quinazoline ring), 7.32-7.39 (m, 6H, C-*H* phenyl ring and N*H*), 7.44-7.47 (m, 2H, C-*H* quinazoline ring), 8.00-8.03 (m, 1H, C-*H* quinazoline ring). ^{13}C-NMR (DMSO) δ 30.0, 46.6, 46.7, 51.7, 56.8, 60.5, 64.5, 109.2, 121.4, 125.2, 126.1, 127.0, 128.2, 128.5, 131.0, 138.3, 149.8, 158.5, 177.6 ppm. HR-MS (ESI) calculated for $C_{24}H_{33}N_6$ $[M + H]^+$, 405.2767; found, 405.2761.

***N*^{4}-(1-Benzylpiperidin-4-yl)-*N*^{2}-(3-(dimethylamino)propyl)quinazoline-2,4-diamine (18).** Oil. Yield: 59%. ^{1}H-NMR ($CDCl_3$) δ 1.64-1.66 (m, 2H, $CH_2CH_2N(CH_3)_2$), 1.82 (m, 2H, C*H*-piperidine ring), 2.10-2.14 (m, 2H, C*H*-piperidine ring), 2.20-2.267 (m, 8H, $NHCH_2CH_2CH_2N(CH_3)_2$ and C*H*-piperidine ring), 2.40-2.44 (m, 4H, $CH_2CH_2N(CH_3)_2$ and C*H*-piperidine ring), 2.90-2.93 (m, 2H, C*H*-piperidine ring), 3.53-3.57 (m, 4H, CH_2Ph and $NHCH_2CH_2CH_2N(CH_3)_2$), 4.19-4.22 (m, 1H, NHC_4-*H*-piperidine), 5.51 (s, 1H, N*H*), 7.10-7.12 (m, 1H, C-*H* quinazoline ring), 7.30-7.36 (m, 5H, C-*H* phenyl ring), 7.48-7.54 (m, 3H, C-*H* quinazoline ring). ^{13}C-NMR ($CDCl_3$) δ 26.5, 30.3, 40.2, 46.5, 51.8, 55.3, 56.4, 64.7, 109.3, 121.3, 125.4, 126.1, 127.0, 128.2, 128.7, 131.3, 138.1, 149.8, 158.4, 177.5 ppm. HR-MS (ESI) calculated for $C_{25}H_{35}N_6$ $[M + H]^+$, 419.2923; found, 419.2928.

9.4 Biological evaluation, results and discussion

9.4.1. DNMT1, DNMT3A and GLP assays

Human DNMT1 and human DNMT3A catalytic domain (hDNMT3A) were used as enzyme sources to test **4**-**18**, in comparison with **1** as reference drug. In Table 9.3 the percent of inhibition of DNMT1 (at 100 μM) and DNMT3A (at 100, 33, 10, and 3.3 μM) for **4**-**18** are reported.

Table 9.3. Percent of inhibition of **4**-**18** against hDNMT1 and hDNMT3A.[a]

Compound	% inhibition				
	hDNMT1	hDNMT3A			
	100 μM	100 μM	32 μM	10 μM	3.2 μM
4	NA[b]	67 ± 3	55 ± 3	39 ± 2	16 ± 4
5	NA	30 ± 8	14 ± 3	0	ND[c]
6	NA	57 ± 8	33 ± 6	14 ± 6	11 ± 5
7	NA	57 ± 3	32 ± 3	16 ± 2	7 ± 2
8	NA	53 ± 3	35 ± 5	14 ± 2	7 ± 1
9	NA	47 ± 5	14 ± 7	5 ± 2	1 ± 0.5
10	47 ± 2	66 ± 4	43 ± 6	21 ± 8	8 ± 4
11	NA	42 ± 3	ND	8 ± 2	ND
12	NA	0	ND	ND	ND
13	NA	62 ± 3	52 ± 5	19 ± 13	8 ± 0.4
14	NA	63 ± 4	54 ± 3	40 ± 4	13 ± 2
15	NA	0	ND	ND	ND
16	NA	0	ND	ND	ND
17	NA	0	ND	ND	ND
18	NA	0	ND	ND	ND
1	35 ± 8	0	ND	ND	ND

[a] Values are means of two to six experiments ± standard errors. [b] NA, not active (% inhibition < 30%).[c] ND, not determined.

Most of the tested compounds were unable to significantly inhibit DNMT1 at 100 μM, with the exception of the *N*-(1-benzylpiperidin-4-yl)-2-(pyrrolidin-1 yl)quinazolin-4-amine **10**, that showed at 100 μM almost 50% DNMT1 inhibition. For comparison SGI-1027, known DNMT1 inhibitor,[110] gave 95% of DNMT1 inhibition at 100 μM. Surprisingly, the majority of the synthesized quinazolines (**4**, **6-10**, **13** and **14**) selectively inhibited catalytic human DNMT3A with an inhibition at 100 μM ranging from 47 to 70% (Table 9.3). EC_{50} values for the most potent compounds (**4**, **10**, **13** and **14**) are reported in Table 9.4.

Table 9.4. EC_{50} values for **4**, **10**, **13** and **14** against DNMT3A.[a]

Compound	EC_{50} (μM)
4	10.2 (7.8 to 13.2)
10	35.4 (22.0 to 56.8)
13	12.2 (8.6 to 15.8)
14	8.7 (8.9 to 11.0)

[a]Values are means of at least three experiments.

Comparing chemical structures of active versus inactive quinazolines, it is clear that the C2 position of the quinazoline scaffold should be substituted with a large hydrophobic moiety, typically a diazepane (**4**) or piperazine carrying an aryl (phenyl, pyridyl) ring decreasing its basicity (**13**, **14**), or an azacycloalkane such as piperidine (**6**) eventually carrying a methyl group at C4 position (**8**), azepane (**7**), or pyrrolidine (**10**) to obtain the highest inhibition. The presence of a heteroatom different from N (i.e., S or O) in the C2-ring decreased the DNMT3A inhibitory activity of the compound (**11**) or abrogated it completely (**12**). Increasing the hydrophilic status of the molecules, either by adding a carbonyl group (**15**) at the C2 substituent or by introducing hydroxy- (**16**) or dimethylamino- (**17**, **18**) alkylamino open side chains at C2 gave scarcely active (**16**) or totally inactive (**15**, **17**, **18**) compounds.

Compounds **4**, **10**, **13**, and **14** were tested at 8 μM against the H3K9 methyltransferase GLP in comparison with **1**, used as reference drug, to determine if the absence of the C6/C7 dimethoxy substitution could abolish the inhibitory effect of such derivatives against H3K9 methyltransferases (Figure 9.2). As expected, in opposition to BIX-10294 (**1**), **4** was totally inactive against GLP, and **10**, **13** and **14** showed scarce GLP inhibition.

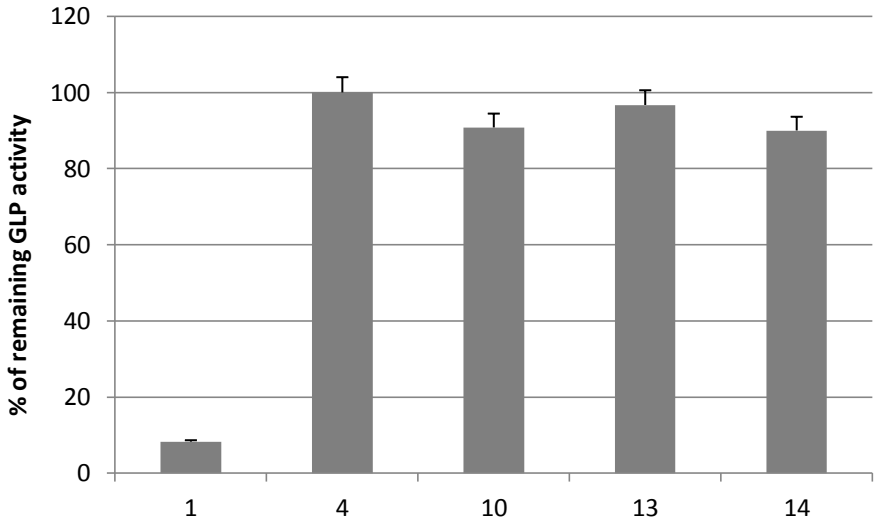

Figure 9.2. Inhibition of GLP by **1**, **4**, **10**, **13** and **14** (measured at 8 μM).

9.4.1.1. Methods

DNMT1 Assay. His-DNMT1 (182kDa, human) was cloned, expressed and purified as described by Lee et al.[579] The DNMT1 assay was performed according to Gros et al.[580] Briefly, the reaction was started by addition of 90 nM of DNMT1 on a mix containing the tested compound (up to 1% DMSO), 1 µM of a AdoMet/[methyl-^{3}H]-AdoMet mix in a ratio of 3-to-1 (isotopic dilution 1*:3) and 0.3 µM of biotinylated DNA duplex in 10 µL final volume. The reaction was incubated at 37 °C for 2 h in reaction buffer (20 mM HEPES pH 7.2, 1 mM EDTA, 50 mM KCl, 25 µg/mL BSA). 8 µL are then transferred into a streptavidin-coated Flashplate PLUS (PerkinElmer) containing 190 µL of 20 µM AdoHcy (Sigma-Aldrich) in 50 mM Tris-HCl pH 7.4. The Flashplate was agitated at room temperature for 1 h, washed three times with 200 µL of 0.05% Tween-20 in 50 mM Tris-HCl pH 7.4, and read in 200 µL of 50 mM Tris-HCl pH 7.4 on TopCount NXT (PerkinElmer). Percentages of inhibition were calculated with the same formula as in DNMT3A assay.

DNMT3A assay. DNMT3A enzyme inhibition was adapted from the restriction-based fluorescence assay protocol described in Ceccaldi et al.[581] Briefly, a 5'-labelled biotin oligonucleotide is hybridized to its complementary strand labelled with 6-carboxyfluorescein at the 3'-end into a 384 well microplate (black Optiplates; Perkin Elmer) pre-coated with avidin. The duplex contains a unique CpG site overlapping with a restriction site of a methylation sensitive restriction enzyme. The C-terminal catalytic domain of human DNMT3A (residues 623-908), produced as described,[54] was added in each well (200 ng/well) and mixed with the chemical compounds at desired concentrations and freshly prepared AdoMet (20 µM final concentration) to start the reaction in a total volume of 50 µL. After 1 hour incubation at 37 °C each well were washed three times with PBS, 0.05% Tween-20, 500 mM NaCl and three more times with PBST. Specific fluorescent signals were detected with the methylation-sensitive restriction enzyme HpyCH4IV (NEB) as described and measured on a Perkin Elmer Envision detector. The percentage of inhibition is reported. The formula used to calculate the percentage of inhibition is [(X-Y)/ X] x 100, where X is the signal determined in the absence of the inhibitor and Y is the signal obtained in the presence of the inhibitor. The concentration at which 50% of efficacy of inhibition is observed (EC_{50}) was determined by analysis of a concentration range of the tested compound in triplicates. The non-linear regression fittings with sigmoidal dose-response (variable slope) were performed with GraphPad Prism 4.03 (GraphPad Software).

GLP Assay. Recombinant human G9a-like protein (GLP) C-terminal fragment containing both the ankyrin repeats and catalytic SET domain (residues 734-1235; pXC758) were purified as described.[566] For histone methylation inhibition, the assay was performed in 20 µL reaction containing 4.6 mM [methyl-^{3}H]-AdoMet, 50 µg/mL histone from calf thymus (SIGMA), 10 µg/mL (0.17 µM) GLP, 100 mM KCl, 5 mM dithiothreitol (DTT) and 50 mM Tris-HCl pH 8.5. GLP was pre-incubated with

AdoMet and 8 µM inhibitors for 5 min at 30 °C before the addition of the histone substrate. After incubation (5 min), the reaction was terminated by the addition of 20% trichloroacetic acid (TCA, Fisher Scientific). The reaction mixture was spotted on GF/A paper circles (Whatman), washed three times with 3 mL of 10% TCA and once with 3 mL of ethanol. The dried circles were subjected to liquid-scintillation counting with Cytoscint scintillant.

9.4.2. Molecular Modeling Studies

Molecular modeling studies were performed to explain the reasons behind the DNMT3A inhibitory activity of the newly discovered analogues of **1**. In particular, the most potent and structurally diverse DNMT3A inhibitors **4** and **14** were docked into the active site of the enzyme using the Glide software which has been already successfully used to suggest a binding conformation for other DNMT3A inhibitors.[582] To this end, the 2.89 Å resolution X-ray crystal structure of the catalytic hDNMT3A-hDNMT3L tetrameric complex bound to *S*-adenosyl- L-homocysteine (AdoHcy) was used (PDB code 2QRV).[54] Docking simulations achieved for **4** placed the ligand in the enzyme's binding cleft of AdoHcy with a calculated docking score of -7.232 kcal/mol (Figures 9.3a and 9.3b).

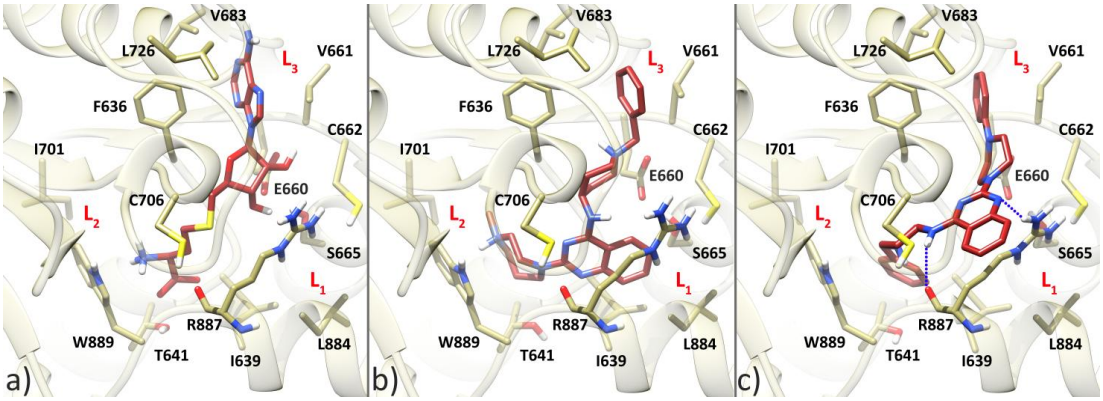

Figure 9.3. Experimental (a) and theoretical (b and c) binding mode of AdoHcy (a), **4** (b) and **14** (c) in the DNMT3A active site. Protein is depicted as light yellow ribbons and sticks while ligands are depicted as red sticks. Hydrogen-bonds are depicted as dashed blue lines.

In this conformation, the quinazoline core scaffold is embedded in a rather lipophilic and narrow cleft made up by I639, S665, and L884 (Figure 9.3b, highlighted as L_1). Indeed, the limited room available in the aforementioned cleft would not allow hosting of the C6- and C7-methoxy groups of **1** thus explaining why the latter compound is inactive against DNMT3A. The achieved binding pose also allowed explaining the contribution to ligand binding of the C2- and C4-substituents. In particular, the C2-diazepane moiety takes favorable hydrophobic contact with T641 and I701 residues (herein referred to as L_2) explaining why substitution of the C2 position with neutral azacycloalkane rings (**6-10**) by favorably filling the L_2 cleft still results in effective DNMT3A inhibitors. Interestingly, unlike **6-10**, **4** bears a

protonated nitrogen (N4 of the diazepane ring) that is able to engage with the adjacent W889 forming a cation-π interaction which was also detected, through X-ray studies,[54] for the terminal positively charged nitrogen atom of AdoHcy in the interaction with DNMT3A (Figure 9.3a). In agreement with this binding orientation, the absence of hydrophobic and/or cation-π interactions in this region is detrimental for enzyme inhibition (**11**, **12, 16-18**). Regarding the C4 substituent, the 1-benzyl-4-piperidinylamino group is optimally oriented to engage a long-range ionic interaction with E660 so that the terminal aromatic ring is able to form a well-oriented T-shaped charge-transfer interaction with F636 and additional hydrophobic contacts in the cleft made up by V661, C662, V683, and L726 (herein referred to as L_3). Also in this case, the same contacts were already detected for the adenine ring of AdoHcy in its interaction with the enzyme (Figure 9.3a).[54] Interestingly, docking results achieved for **14** (docking score -6.353 kcal/mol) placed the ligand in a reverted binding pose in which the C2 and C4 substituents are now lodged in the L_3 and L_2 pockets, respectively. Such a binding position places the conformationally rigid C-2 phenylpiperazinyl moiety of **14** so as to recapitulate the interaction pattern established by the C4-substituent of **4** and the adenine ring of AdoHcy with the enzyme (Figures 9.3c, 9.3b and 9.3a, respectively). Accordingly, increasing of the steric demands of the C4-substituent (**15-18**) should disrupt the interactions with the L_3 pocket thus being detrimental for the ligand inhibitory potency. On the other hand, the L_2 pocket is now favorably contacted by the C2 1-benzyl-4-piperidinylamino moiety of **14** through a parallel displaced π-π interaction with W889 aromatic ring. In this position, the above mentioned L_1 pocket does not seem to be contacted by the ligand quinazoline ring that is now forming a hydrogen-bond between its N1 atom and R887 side chain; the latter residue is also forming an additional hydrogen-bond through its backbone carbonyl oxygen with the ligand exocyclic NH in C4.

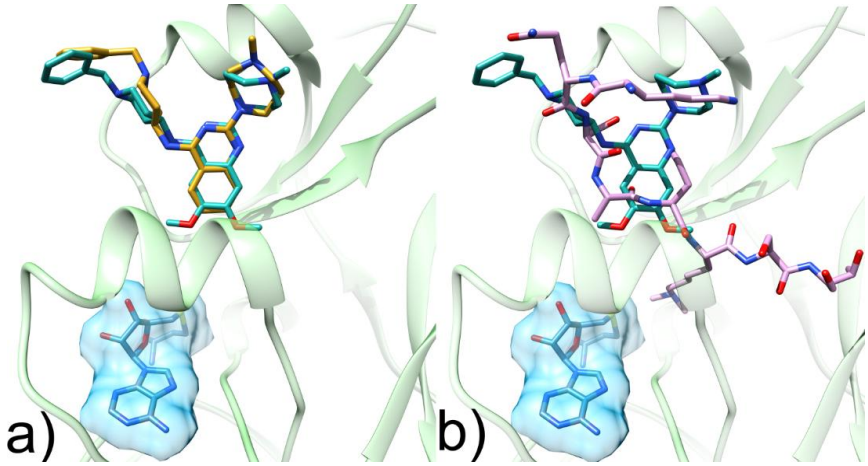

Figure 9.4. a) Binding mode of **4** (yellow sticks) in the GLP binding site (green ribbons) as predicted by Glide. The co-crystal ligand **1** (cyan sticks) was also reported for comparison as well as the co-factor analogue S-adenosyl-L-homocysteine (blue sticks and surface). b) Superimposition of the experimental binding pose of the dimethylated H3K9 peptide (pink sticks, PDB code 2RFI) and **1** (cyan sticks) in the GLP binding site (green ribbons).

To rationalize the lack of inhibition potency of the analogues of **1** against GLP, compound **4** was docked into the X-ray structure of the enzyme obtained in complex with **1** (PDB code 3FPD). Glide results indicated that **4** is indeed able to recapitulate the experimental binding position of **1** (Figure 9.4a). Interestingly, in the latter compound the C6- and C7- methoxy groups are demonstrated to play a critical role in the ligand inhibition as they provide further interactions to better mimic the substrate/GLP recognition (Figure 9.4b) thus explaining why their absence in **4** results in no GLP inhibition.[436]

9.4.2.1. Methods

Docking Studies. Prior to docking calculations, the Epik software was used to calculate the most relevant ionization and tautomeric state of compounds **4** and **14**. Then the Glide program of the Schrodinger package was used to dock **4** and **14** to the DNMT3A structure (PDB 2QRV). The receptor grid generation was performed for the box with a center in the putative binding site. The size of the box was determined automatically. The extra precision mode (XP) of Glide was used for docking. The ligand scaling factor was set to 1.0. The geometry of the ligand binding site of the complex between 10 and the receptor was then optimized. The binding site was defined as 10 and all amino acid residues located within 8 Å from the ligand. All the receptor residues located within 2 Å from the binding site were used as a shell. The OPLS2005 force field was used for energy minimization. Water was used as an implicit solvent, and a maximum of 5000 iterations of the Polak–Ribier conjugate gradient minimization method was used with a convergence threshold of 0.01 kJ mol^{-1} $Å^{-1}$. All complex pictures were rendered employing the UCSF Chimera software.

9.4.3. Studies on different cancer cell lines

Next we investigated the effects of the most active DNMTi **4**, **6**-**8**, **10** and **14** on proliferation and viability of U-937 and RAJI lymphoma cells (Figure 9.5a,b). In order to assess the differential toxicity of these DNMTi, we then tested their effects on peripheral blood mononuclear cells (PBMCs) (Figure 9.5c). Globally, all compounds were cytotoxic as they decreased cell proliferation as a consequence of a loss of cell viability. IC_{50} values of **4**, **6**- **8**, **10** and **14** on the cell viability at 48 h on PBMCs and on lymphoma cells are reported in Table 9.5. In agreement with its DNMT inhibitory potential, compound **14** is the most potent compound in cancer cells.

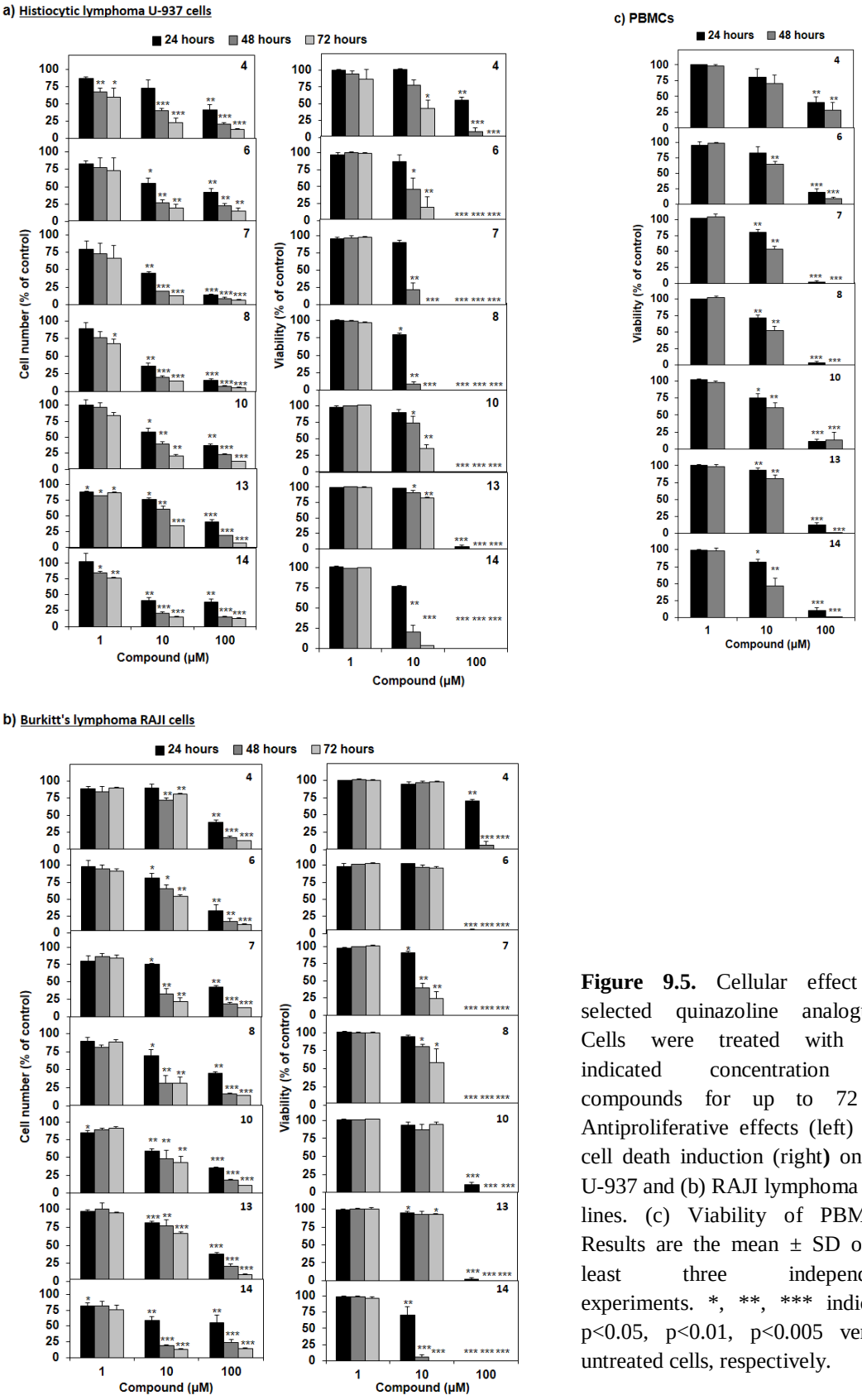

Figure 9.5. Cellular effect of selected quinazoline analogues. Cells were treated with the indicated concentration of compounds for up to 72 h. Antiproliferative effects (left) and cell death induction (right**)** on (a) U-937 and (b) RAJI lymphoma cell lines. (c) Viability of PBMCs. Results are the mean ± SD of at least three independent experiments. *, **, *** indicate $p<0.05$, $p<0.01$, $p<0.005$ versus untreated cells, respectively.

Table 9.5. Effect of selected quinazolines **4**, **6-8**, **10**, **13** and **14** on PBMC and human lymphoma U-937 and RAJI cell viability at 48h.

Compound	IC_{50} (mean ± SD, μM)		
	PBMCs	U-937	RAJI
4	31.6 ± 5.8	16.6 ± 3.8	21.1 ± 2.5
6	18..9 ± 3.2	10.0 ± 4.0	31.0 ± 1.2
7	11.2 ± 2.3	5.6 ± 0.1	5.9 ± 4.3
8	10.0 ± 4.3	5.2 ± 0.6	24.1 ± 2.2
10	24.2 ± 6.9	14.7 ± 3.8	18.7 ± 4.3
13	11.2 ± 2.2	18.8 ± 1.2	19.7 ± 1.4
14	9.5 ± 1.2	4.4 ± 1.4	3.4 ± 0.3

9.4.3.1. Methods

Cellular Assays. U-937 and RAJI cell lines were purchased from Deutsche Sammlung für Mikroorganismen und Zellkulturen (DSZM). Cells were maintained in RPMI 1640 (Lonza) supplemented with 10% fetal calf serum (Lonza) and 1% antibiotic–antimycotic (Lonza). Peripheral blood mononuclear cells (PBMCs) were purified and processed as previously described.[567] Cells were treated with compounds at the indicated concentrations in exponential growth phase. Proliferation and viability were assessed by trypan blue exclusion analysis at the indicated time points.

9.4.4. Conclusion

Quinazoline is a known valuable scaffold for designing histone H3K9 methyltransferase inhibitors and, when properly substituted (a methoxy group at C6 and a methoxy/aminoalkyloxy group at C7 position, a 1-alkyl-4-piperidinylamino moiety at C4 and a bulky (aza)cycloalkane at C2) provided highly potent G9a/GLP inhibitors such as **1**-**3**. Since compound **3** has been reported to be inactive towards other protein lysine methyltransferases but able to inhibit DNMT1 at high micromolar concentration, we explored the possibility to design new quinazoline derivatives as novel DNMT inhibitors. Such compounds should be related to **1-3** regarding to C2 and C4-substitution, but lacking the C6/C7 dimethoxy group, crucial for the interaction with G9a/GLP enzymes. The obtained compounds **4-21** were tested against human DNMT1 and C-terminal human DNMT3A and, surprisingly, they showed little (if any) inhibiting activity against DNMT1, excepted compound **10**, but were in some cases (**4**, **6-8**, **13** and **14**) potent and selective inhibitors of DNMT3A. Structure-activity relationship (SAR) data, supported by molecular modeling studies performed on the DNMT3A crystal structure (PDB 2QRV), highlighted the crucial role of the insertion of a large hydrophobic moiety (azacycloalkane, diazepane) or a poorly basic piperazine group at the C2 position of the quinazoline scaffold to obtain potent inhibitors. The most efficient DNMT3A

inhibitors **4**, **13** and **14**, in opposite to **1**, failed in inhibiting GLP at 8 μM. When tested in human lymphoma U-937 and RAJI cells, compounds **4**, **6**-**8** and **14** displayed high antiproliferative and cell death induction properties already at 10 μM concentration, they being less able to decrease viability in PBMCs, taken as model for differential toxicity. In agreement with the anti-DNMT3A activity, **14** was the most potent in lymphoma cells too, and it represents our lead compound for further optimization.[583]

*Adapted with the permission from Rotili, D., Tarantino, D., Marrocco, B., Gros, C., Masson, V., Gregoire, J-M., Ausseil, F., Chang, Y., Labella, D., Cosconati, S., Di Maro, S., Novellino, E., Schnekenburger, M., Grandjenette, C., Bouvy, C., Diederich, M., Cheng, X., Arimondo, P. B., Mai. A. Identification of quinazoline analogues as novel dna methyltransferase 3a inhibitors. *J. Med. Chem.* submitted.[583]

10. *tert*-Butylcarbamate-containing histone deacetylase inhibitors*

10.1. Research project

Overexpression of specific HDACs has been observed in many types of cancer, and often correlates with poor prognosis.[584] HDAC inhibition induced by HDAC inhibitors (HDACi) may regulate gene expression, both directly and indirectly, by hyperacetylation of histones and/or transcription factors such as NF-κB, STAT1, STAT3, YY1, E2F, and Rb. In cancer cells, HDACi induce cell-cycle arrest by up-regulation of p21 and/ or down-regulation of cyclins, suppress angiogenesis by decreased expression of pro-angiogenic factors (VEGF, HIF-1a), and modulate the release of cytokines (TNF-α, interleukin-1).[585] Thus, HDACi and their development have become the subject of intense interest by both academic and industrial scientists, and many of them have now entered the clinical arena (see Sec. 6.2.7).
According to the well-known pharmacophore model for HDACi, a deacetylase inhibitor should bear a CAP group to interact with the rim of the catalytic tunnel of the enzyme, a connection unit, linking the CAP to a hydrophobic spacer (HS) and lying into the tunnel, and an enzyme inhibiting group (EIG), able to complex the zinc ion, crucial for the catalysis at the bottom of the tunnel. From 2001, our research group has described various chemically different series of HDACi, aroylpyrrolylhydroxamates (APHAs) and (aryloxopropenyl)pyrrolylhydroxamates **1**,[586] aroyl/arylamino-, (phenyloxopropenyl)-, (amidopropenyl)cinnamyl and -pyridinylpropenoic hydroxamates **2**,[587] and uracil-based hydroxamates and 2-aminoanilides (UBHAs) **3**,[588] fitting with this pharmacophore model (Figure 10.1).

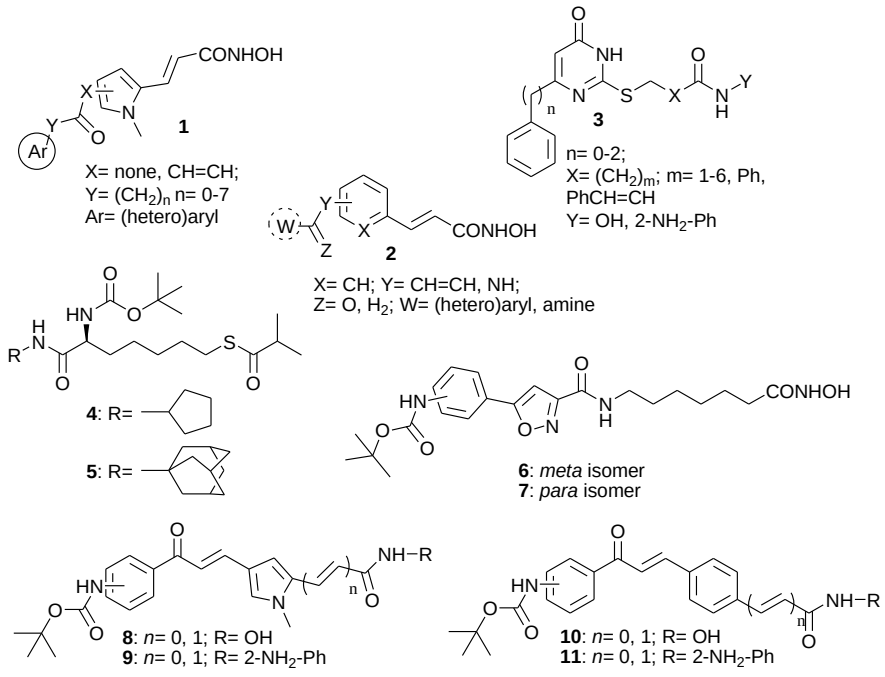

Figure 10.1. Design of novel HDAC inhibitors.

Some analogues of **1**, namely MC1575 and MC1568, displayed class-II-selective HDAC inhibitory activity, and have been used as valuable tools to dissect the role of class II HDACs in a number of different biological contexts.[355] Some derivatives of **2** and **3** showed high anticancer effects. Recently, several authors highlighted structurally different HDACi bearing the N-tert-butyloxycarbonyl (Boc)-amino group at the CAP moiety (compounds **4-7**; Figure 10.1). Such compounds showed anti-HDAC6 specific activity and synergistic inhibition of HCT116 cancer cell growth when used in combination with paclitaxel, inhibition of the estrogen-stimulated growth of human breast cancer MCF7 cells, and block the proliferation of a panel of pancreatic cancer cell lines.[589] Thus, we designed and synthesized a series of analogues of **1** and **2** containing this chemical feature at the CAP benzene ring, and carrying as EIG either the hydroxamate (**8**, **10**) or the 2- aminoanilide (**9**, **11**) moiety (Figure 10.1). All the new derivatives **8-11** were tested at 5 μM against human recombinant (hr) HDAC1 and HDAC4, and for selected compounds IC_{50} values were determined against all the HDAC1-11 isoforms. Compounds **8-11** were also assayed in human leukemia U937 cells to determine their effects on cell cycle, apoptosis induction, and granulocytic differentiation after treatment for 30 h. The most pro-apoptotic derivatives were then tested in three different cancer cell lines to assess their antiproliferative activities, and the most potent compound was further characterized (antiproliferative activity against a wider panel of cancer cells, histone H3 acetylation, clonogenic assay) as a valuable anticancer agent.[590]

10.2. Chemistry

The synthetic route followed for the preparation of **8-11** is reported in Scheme 1. Aldol condensation of commercially available ethyl 4-formyl-1-methyl-1H-pyrrole-2-carboxylate **12a** or ethyl 3-(4-formyl-1-methyl-1H-pyrrol-2-yl)acrylate **12b**[591] with 3- or 4-tert-butoxycarbonylaminoacetophenones **13a,b** was carried out in dry ethanol in the presence of sodium ethylate and afforded the pyrrole-containing ethyl esters **14a-d** (Scheme 1). The same reaction performed starting from ethyl 4-formylbenzoate or ethyl-(4-formylphenyl)acrylate **15a**,**b** furnished the ethyl benzoates/cinnamates **16a-d**. The esters **14** and **16** were then hydrolyzed with lithium hydroxide in tetrahydrofuran/water to afford the corresponding carboxylic/acrylic acids **17** and **18**, key intermediates for the synthesis of the related hydroxamates (reaction with ethyl chloroformate/triethylamine followed by addition of *O*-(2-methoxy-2-propyl)hydroxylamine and final acidic treatment with the Amberlyst 15) **8**, **10** or 2'-aminoanilides [treatment with benzotriazole-1 yloxytris(dimethylamino)phosphonium hexafluorophosphate (BOP reagent, Castro's reagent), ortho-phenylendiamine, and $(C_2H_5)_3N$ in dry N,N-dimethylformamide] **9**, **11**. Chemical and physical data of compounds **8-11** are listed in Table 10.1. Chemical and physical data of the intermediate compounds **14**, **16-18** are listed in table 10.2.

Scheme 1

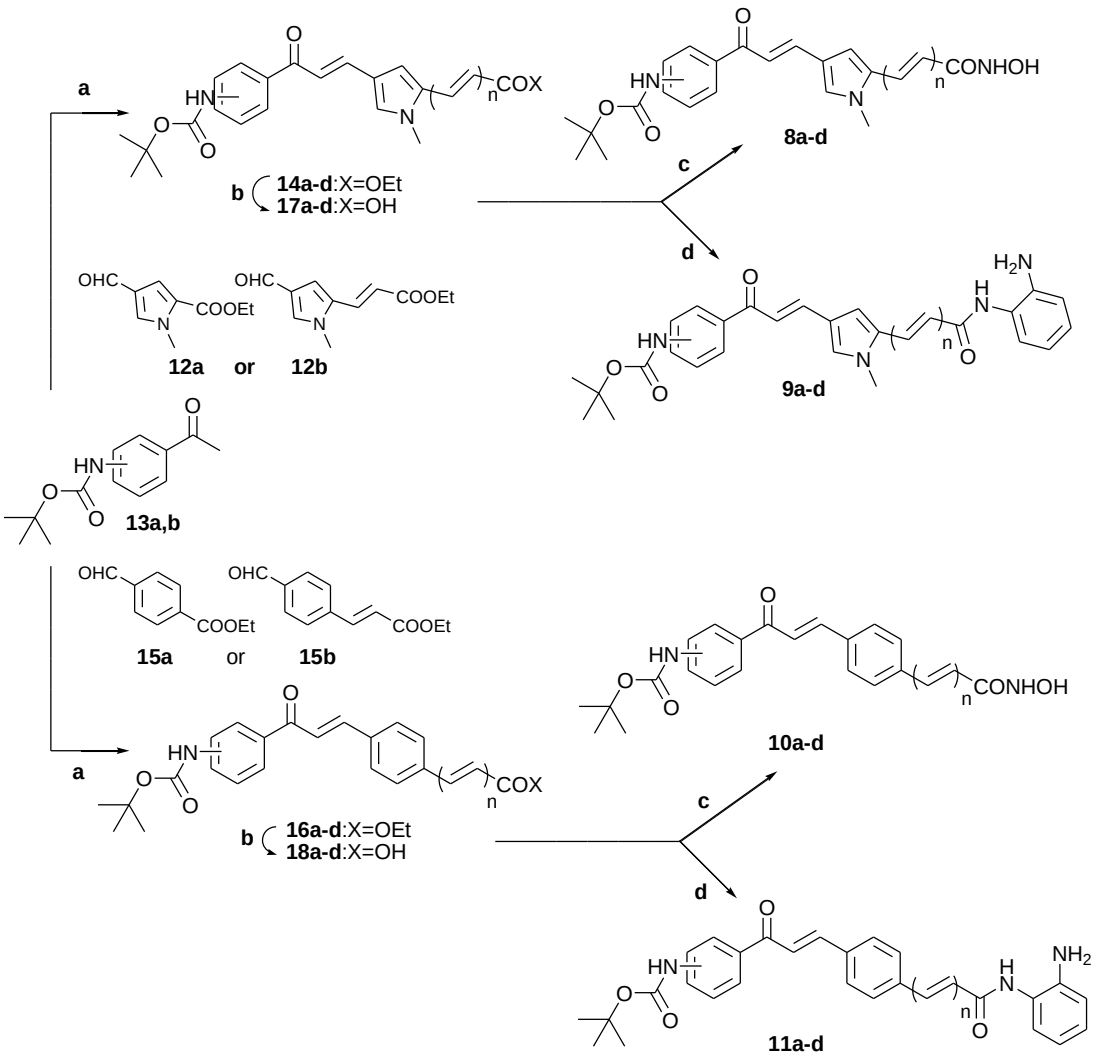

Reagents and conditions: a) C_2H_5ONa, anhyd. C_2H_5OH, RT, 2 h; b) LiOH, THF/H_2O, overnight; c) 1. $ClCOOC_2H_5$, $(C_2H_5)_3N$, anhyd. THF, 0°C, 30 min, 2. $CH_3O(CH_3)_2ONH_2$, anhyd. THF, 0°C, 1 h, 3. Amberlyst 15, CH_3OH, RT, 1.5 h; d) 1. $(C_2H_5)_3N$, BOP reagent, anhyd. DMF, $N_{2(g)}$, RT, 2. o-phenylendiamine, anhyd. DMF, $N_{2(g)}$, RT, 1 h.

Table 10.1. Chemical and physical properties of compounds **8-11**.

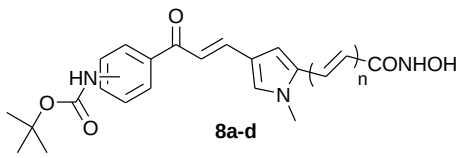

8a-d

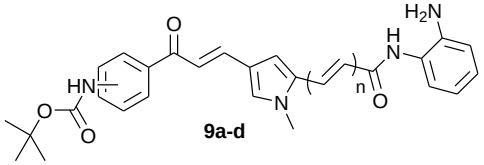

9a-d

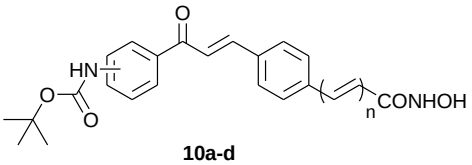

10a-d

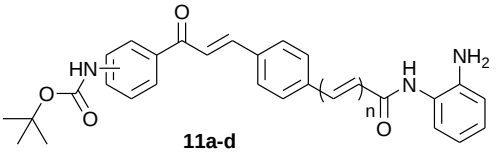

11a-d

Cpd	NH-BOC	*n*	mp, °C	recrystall. solvent	Yield %
8a	3	0	121-123	A	77
8b	4	0	102-104	A	75
8c	3	1	120-122	A	73
8d	4	1	122-124	A	75
9a	3	0	185-187	B	69
9b	4	0	119-121	A	88
9c	3	1	162-164	B	72
9d	4	1	220-222	C	87
10a	3	0	125-127	B	82
10b	4	0	190-192	A	75
10c	3	1	162-164	A	78
10d	4	1	180-182	A	81
11a	3	0	210-212	C	67
11b	4	0	194-196	B	74
11c	3	1	205-207	C	74
11d	4	1	123-125	A	59

A: toluene; B: acetonitrile; C: methanol

Table 10.2. Chemical and physical data of compounds **14**, **16**-**18**.

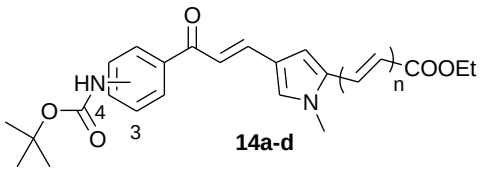

14a-d

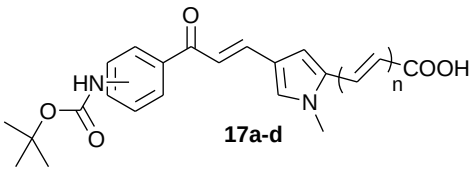

17a-d

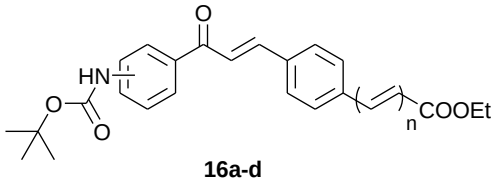

16a-d

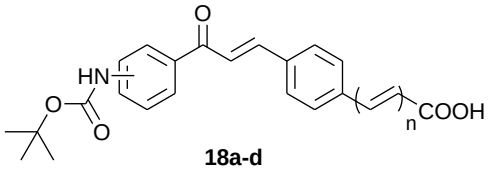

18a-d

Cpd	NH-BOC	*N*	mp, °C	recrystall. solvent	Yield %
14a	3	0	97-99	D	78
14b	4	0	110-112	D	76
14c	3	1	115-117	E	75
14d	4	1	120-122	E	73
16a	3	0	172-174	B	78
16b	4	0	180-182	B	81
16c	3	1	167-169	B	73
16d	4	1	179-181	B	77
17a	3	0	199-201	C	73
17b	4	0	135-137	A	75
17c	3	1	209-211	C	72
17d	4	1	190-192	B	74
18a	3	0	216-218	C	76
18b	4	0	227-229	C	77
18c	3	1	212-214	C	73
18d	4	1	222-224	B	75

A: toluene; B: acetonitrile; C: methanol; D: cyclohexane; E: cyclohexane/toluene

10.3. Experimental section

Chemistry. Melting points were determined on a Büchi 530 melting point apparatus and are uncorrected. ^{1}H NMR and ^{13}C NMR spectra were recorded at 400 MHz on a Bruker AC 400 spectrometer; chemical shifts (δ) are reported in ppm relative to the internal reference tetramethylsilane. EIMS data were recorded with a Fisons Trio 1000 spectrometer; only molecular ions $[M]^{+}$ and base peaks are given. All compounds were routinely checked by TLC, ^{1}H NMR and ^{13}C NMR spectra. TLC was performed on aluminum-backed silica gel plates (Merck DC, Alufolien Kieselgel 60 F_{254}) with spots visualized by UV light. All solvents were reagent grade and, when necessary, were purified and dried by standard methods. Concentration of solutions after reactions and extractions involved the use of a rotary evaporator operating at reduced pressure of ~20 Torr. Organic solutions were dried over anhydrous Na_2SO_4. All chemicals were purchased from Aldrich Chimica, Milan (Italy) or from Alfa Aesar, Milan (Italy), and were of the highest purity.

General procedure for the synthesis of the esters 14 and 16. Example: Synthesis of ethyl 3-(4-(3-(4-((tert-butoxycarbonyl)amino) phenyl)-3-oxoprop-1-enyl)phenyl)acrylate (16 d): tert-Butyl 4-acetylphenylcarbamate **13b** (2.12 mmol, 0.5 g) and ethyl 3-(4-formylphenyl) acrylate **15b** (2.12 mmol, 0.433 g) were added to a solution of Na^{0} (2.54 mmol, 0.05 g) in C_2H_5OH (5 mL). The resulting mixture was stirred at room temperature for 4 h. The reaction was quenched with H_2O (30 mL) and extracted with EtOAc (3x50 mL). The combined organic extracts were washed with saturated NaCl solution (3x50 mL), dried with Na_2SO_4, and concentrated to obtain a residue that was purified by column chromatography (SiO_2 eluting with EtOAc/*n*-hexane 1:2) to give the compound **16d** as a pale-yellow solid. ^{1}H NMR ($CDCl_3$, 400 MHz): δ=1.33-1.37 (t, 3H,$OCH_2C\mathit{H}_3$), 1.54 (s, 9H, $C(C\mathit{H}_3)_3$), 4.25-4.31 (q, 2H, $OC\mathit{H}_2CH_3$), 6.47-6.51 (d, 1H, CH=C*H*COOEt), 6.76 (bs, 1H, $(CH_3)_3CON\mathit{H}$), 7.50- 7.71 (m, 8H, benzene protons, C*H*=CHCOOEt and PhCOC*H*=CH), 7.77- 7.81 (d, 1H, PhCOCH=C*H*), 8.00-8.02 ppm (d, 2H, benzene protons); ^{13}C NMR ($CDCl_3$): δ=28.5 (3C), 79.5, 118.9, 121.4, 122.1 (2C), 126.3 (4C), 130.1 (2C), 133.5, 134.4 (2C), 141.7, 144.0, 145.2, 153.9, 161.6, 189.7 ppm; MS (EI) calcd for $C_{25}H_{27}NO_5$ m/z $[M]^{+}$: 421.1889, found: 421.1885.

General procedure for the synthesis of the acids 17 and 18. Example: Synthesis of 3-(4-(3-(4-((tert-butoxycarbonyl)amino)phenyl)- 3-oxoprop-1-enyl)-1-methyl-1H-pyrrol-2-yl)acrylic acid (17 d): A solution of ethyl 3-(4-(3-(4-((tert-butoxycarbonyl)amino)phenyl)-3- oxoprop-1-enyl)-1-methyl-1H-pyrrol-2-yl)acrylate **14d** (0.82 mmol, 0.35 g) and 2N KOH (1.64 mmol, 0.092 g) in C_2H_5OH (15 mL) was stirred overnight at room temperature. Then the solvent was evaporated and 2N HCl was slowly added till the aqueous phase reached pH 5.0. The colorless solid was filtered and washed first with H_2O and then with a mixture of $(C_2H_5)_2O$/petroleum ether 1:1 to afford pure **17d**. ^{1}H NMR ([D_6]DMSO, 400 MHz): δ=1.46 (s, 9H, $C(C\mathit{H}_3)_3$), 3.87 (s, 3H, $C\mathit{H}_3$), 6.34 (d, 1H, CH=C*H*COOH), 7.11 (s, 1H, pyrrole-β

proton), 7.26-7.37 (m, 3H, benzene protons and PhCOC*H*=CH), 7.57-7.63 (m, 4H, pyrrole-a proton, benzene protons, PhCOCH=C*H* and CH=C*H*COOH), 8.08-8.09 (m, 1H, benzene proton), 9.52 (bs, 1H, $(CH_3)_3CONH$), 13.0 ppm (bs, 1H, COO*H*); ^{13}C NMR ([D_6]DMSO, 400 MHz): δ=28.5 (3C), 34.0, 79.5, 104.8, 108.0, 121.6, 122.1 (2C), 123.2, 127.4, 130.1 (2C), 130.6, 133.5, 138.8, 141.7, 145.2, 153.9, 170.6, 189.7 ppm; MS (EI) calcd for $C_{22}H_{24}N_2O_5$ m/z $[M]^+$: 396.1685, found: 396.1690.

General procedure for the synthesis of the hydroxamic acids 8,10. Example: Synthesis of tert-butyl-(3-(3-(5-(hydroxycarbamoyl)-1-methyl-1H-pyrrol-3-yl)acryloyl)phenyl)carbamate (8 a): $(C_2H_5)_3N$ (0.12 mmol, 0.017 mL) and $ClCOOC_2H_5$ (0.11 mmol, 0.015 mL) were slowly added to a cooled (0 °C) solution of 4-(3-(3- ((tert-butoxycarbonyl)amino)phenyl)-3-oxoprop-1-enyl)-1-methyl- 1H-pyrrole-2-carboxylic acid **17a** (0.092 mmol, 0.034 g) in anhydrous THF (5 mL), and the mixture was stirred for 45 min at room temperature under N_2 atmosphere. Afterward, the solid was filtered, washed with anhydrous THF (3 x 5 mL) and then O-(2-methoxy-2-propyl)hydroxylamine (0.27 mmol, 0.02 mL) was added, and the resulting mixture was stirred for 15 min at room temperature. After this time the solvent was removed under vacuum, the residue was diluted in CH_3OH (10 mL), and Amberlyst 15 ion-exchange resin (0.36 g) was added. The mixture was stirred at room temperature for 1 h. After that, the resin was filtered and the filtrate was concentrated under reduced pressure to give crude **8a**, which was purified by recrystallization. ^1H NMR ([D_6]DMSO, 400 MHz): δ=1.50 (s, 9H, C(C*H*$_3$)$_3$), 3.94 (s, 3H, C*H*$_3$), 7.04 (s, 1H, pyrrole-β proton), 7.26-7.67 (m, 6H, benzene proton, PhCOC*H*=CH and PhCOCH=C*H*), 8.09 (s, 1H, pyrrole-α proton), 8.99 (bs, 1H, $(CH_3)_3CONH$), 9.56 (bs, 1H, CONHO*H*), 10.95 ppm (bs, 1H, CON*H*OH); ^{13}C NMR ([D_6]DMSO, 400 MHz): δ=28.5 (3C), 32.9, 79.5, 111.0, 118.7, 122.1 (2C), 126.1, 127.4, 130.1 (2C), 132.0, 133.5, 141.7, 145.2, 153.9, 163.0, 189.7 ppm; MS (EI) calcd for $C_{20}H_{23}N_3O_5$ m/z $[M]^+$: 385.1638, found: 385.1632.

General procedure for the synthesis of the 2'-aminoanilides 9,11. Example: Synthesis of tert-butyl-(3-(3-(5-((2-aminophenyl)carbamoyl)-1-methyl-1H-pyrrol-3-yl)acryloyl)phenyl)carbamate (9 a): $(C_2H_5)_3N$ (1.6 mmol, 0.22 mL) and benzotriazole-1-yloxytris(dimethylamino) phosphonium hexafluorophosphate (BOP reagent) (0.48 mmol, 0.21 g) were added to a solution of 4-(3-(3-((tert-butoxycarbonyl) amino)phenyl)-3-oxoprop-1-enyl)-1-methyl-1H-pyrrole-2-carboxylic acid **17a** (0.4 mmol, 0.32 g) in anhydrous DMF (5 mL) under N_2 atmosphere. The resulting mixture was stirred for 30 min at room temperature; afterward 1,2-phenylenediamine (0.44 mmol, 0.05 g) was added under N_2 atmosphere and the reaction was stirred overnight. The reaction was quenched with H_2O (50 mL) and extracted with EtOAc (3x30 mL). The combined organic extracts were dried and the residue obtained upon evaporation of solvent was purified by column chromatography (SiO_2 eluting with EtOAc/n-hexane 1:1) to give pure **9a**. ^1H NMR ([D_6]DMSO, 400 MHz): δ= 1.48 (s, 9H, C(C*H*$_3$)$_3$), 3.87 (s, 3H, C*H*$_3$), 4.89 (bs, 2H, N*H*$_2$), 6.59-6.61 (m, 1H, benzene proton), 6.75-6.77 (d, 1H, benzene proton),

6.96-6.98 (m, 1H, benzene proton), 7.14-7.16 (d, 1H, benzene proton), 7.26-7.66 (m, 7H, benzene protons, pyrrole α and -β protons, PhCOC*H*=CH and PhCOCH=C*H*), 8.09 (s, 1H, benzene proton), 9.35 (bs, 1H, $(CH_3)_3CONH$), 9.52 ppm (bs, 1H, CON*H*); ^{13}C NMR ([D_6]DMSO, 400 MHz): δ=28.5 (3C), 32.9, 79.5, 111.0, 116.5, 118.7, 119.0, 119.6, 122.4, 122.9, 125.2, 125.5, 126.1, 127.4 (2C), 129.5, 132.0, 136.4, 138.1, 141.8, 145.2, 153.9, 162.7, 189.7 ppm; MS (EI) calcd for $C_{26}H_{28}N_4O_4$ m/z $[M]^+$: 460.2111, found: 460.2118.

***tert*-Butyl-(4-(3-(5-(hydroxycarbamoyl)-1-methyl-1H-pyrrol-3-yl)acryloyl) phenyl)carbamate (8 b):** ^1H NMR ([D_6]DMSO, 400 MHz): δ= 1.50 (s, 9H, $C(CH_3)_3$), 3.94 (s, 3H, CH_3), 7.04 (s, 1H, pyrrole- β proton), 7.26-7.67 (m, 6H, benzene protons, PhCOC*H*=CH and PhCOCH=C*H*), 8.09 (s, 1H, pyrrole-α proton), 8.99 (bs, 1H, $(CH_3)_3CONH$), 9.56 (bs, 1H, CONHO*H*), 10.95 ppm (bs, 1H, CON*H*OH); ^{13}C NMR ([D_6]DMSO, 400 MHz): δ=28.5 (3C), 32.9, 79.5, 111.0, 118.7, 122.1 (2C), 126.1, 127.4, 130.1 (2C), 132.0, 133.5, 141.7, 145.2, 153.9, 163.0, 189.7 ppm; MS (EI) calcd for $C_{20}H_{23}N_3O_5$ m/z $[M]^+$: 385.1638, found: 385.1632.

***tert*-Butyl-(3-(3-(5-(3-(hydroxyamino)-3-oxoprop-1-enyl)-1-methyl-1H-pyrrol-3-yl)acryloyl)phenyl)carbamate (8 c):** ^1H NMR ([D_6]DMSO, 400 MHz): δ=1.50 (s, 9H, $C(CH_3)_3$), 3.94 (s, 3H, CH_3), 7.04 (s, 1H, pyrrole-β proton), 7.26-7.67 (m, 7H, benzene protons, PhCOC*H*=CH and PhCOCH=C*H*, CH=C*H*CONHOH), 8.09-8.3 (m, 2H, pyrrole-α proton, C*H*=CHCONHOH), 8.99 (bs, 1H, $(CH_3)_3CONH$), 9.56 (bs, 1H, CONHO*H*), 10.95 ppm (bs, 1H, CON*H*OH); ^{13}C NMR ([D_6]DMSO, 400 MHz): δ=28.5 (3C), 34.0, 79.5, 104.8, 108.0, 119.6, 123.2, 124.9, 125.5, 127.4 (2C), 129.5, 130.6, 134.8, 136.4, 138.1, 145.2, 153.9, 161.6, 189.7 ppm; MS (EI) calcd for $C_{22}H_{25}N_3O_5$ m/z $[M]^+$: 411.1794, found: 411.1788.

***tert*-Butyl-(4-(3-(5-(3-(hydroxyamino)-3-oxoprop-1-enyl)-1-methyl-1H-pyrrol-3-yl)acryloyl)phenyl)carbamate (8 d):** ^1H NMR ([D_6]DMSO, 400 MHz): δ=1.48 (s, 9H, $C(CH_3)_3$), 3.8 (s, 3H, CH_3), 6.98 (s, 1H, pyrrole-β proton), 7.16-7.7 (m, 7H, benzene protons, PhCOC*H*=CH and PhCOCH=C*H*, CH=C*H*CONHOH), 8.09–8.3 (m, 2H, pyrrole-α proton, C*H*=CHCONHOH), 9.02 (bs, 1H, $(CH_3)_3CONH$), 9.43 (bs, 1H, CONHO*H*), 10.97 ppm (bs, 1H, CON*H*OH); ^{13}C NMR ([D_6]DMSO, 400 MHz): δ=28.5 (3C), 34.0, 79.5, 104.8, 108.0, 122.1 (2C), 123.2, 124.9, 127.4, 130.1 (2C), 130.6, 133.5, 134.8, 141.7, 145.2, 153.9, 161.6, 189.7 ppm; MS (EI) calcd for $C_{22}H_{25}N_3O_5$ m/z $[M]^+$: 411.1794, found: 411.1788.

***tert*-Butyl-(3-(3-(4-(hydroxycarbamoyl)phenyl)acryloyl) phenyl)-carbamate (10 a):** ^1H NMR ([D_6]DMSO, 400 MHz): δ=1.47 (s, 9H, $C(CH_3)_3$), 7.44-7.48 (m, 1H, COC*H*=CH), 7.50-8.03 (m, 8H, benzene protons, PhCOCH=C*H*), 8.10-8.14 (m, 1H, benzene proton), 9.09 (bs, 1H, $(CH_3)_3CONH$), 9.53 (bs, 1H, CONHO*H*), 11.30 ppm (bs, 1H, CON*H*OH); ^{13}C NMR ([D_6]DMSO, 400 MHz): δ=28.5 (3C), 79.5, 119.6, 121.4, 125.5, 126.5 (2C), 127.4 (3C), 129.5, 133.4, 136.4, 138.1, 138.6, 145.2, 153.9,

163.0, 189.7 ppm; MS (EI) calcd for $C_{21}H_{22}N_2O_5$ m/z $[M]^+$: 382.1529, found: 382.1535.

***tert*-Butyl-(4-(3-(4-(hydroxycarbamoyl)phenyl)acryloyl) phenyl)- carbamate (10 b):** ^{1}H NMR ([D$_6$]DMSO, 400 MHz): δ=1.49 (s, 9H, C(C*H*$_3$)$_3$), 6.65-8.11 (m, 10H, benzene protons, PhCOCH=C*H* and COC*H*=CH), 9.10 (bs, 1H, (CH$_3$)$_3$CON*H*), 9.84 (bs, 1H, CONHO*H*), 11.39 ppm (bs, 1H, CON*H*OH); ^{13}C NMR ([D$_6$]DMSO, 400 MHz): δ= 28.5 (3C), 79.5, 121.4, 122.1 (2C), 126.5 (2C), 127.4 (2C), 130.1 (2C), 133.4, 133.5, 138.6, 141.7, 145.2, 153.9, 163.0, 189.7 ppm; MS (EI) calcd for $C_{21}H_{22}N_2O_5$ m/z $[M]^+$: 382.1529, found: 382.1535.

***tert*-Butyl-(3-(3-(4-(3-(hydroxyamino)-3-oxoprop-1-enyl)-phenyl)-acryloyl) phenyl) carbamate (10 c):** ^{1}H NMR ([D$_6$]DMSO, 400 MHz): δ=1.48 (s, 9H, C(C*H*$_3$)$_3$), 6.52-6.56 (d, 1H, CH=C*H*CONH), 7.47-7.50 (d, 1H, PhCOC*H*=CH), 7.63-7.96 (m, 10H, benzene protons, C*H*= CHCONH and PhCOCH=C*H*), 9.12 (bs, 1H, (CH$_3$)$_3$CON*H*), 9.55 (bs, 1H, CONHO*H*), 10.79 ppm (bs, 1H, CON*H*OH); ^{13}C NMR ([D$_6$]DMSO, 400 MHz): δ=28.5 (3C), 79.5, 118.9, 119.6, 121.4, 125.5, 126.3 (4C), 127.4, 129.5, 134.4 (2C), 136.4, 138.1, 144.0, 145.2, 153.9, 161.6, 189.7 ppm; MS (EI) calcd for $C_{23}H_{24}N_2O_5$ m/z $[M]^+$: 408.1685, found: 408.1691.

***tert*-Butyl-(4-(3-(4-(3-(hydroxyamino)-3-oxoprop-1-enyl)phenyl)acryloyl) phenyl)carbamate (10 d):** ^{1}H NMR ([D$_6$]DMSO, 400 MHz): d=1.47 (s, 9H, C(C*H*$_3$)$_3$), 6.52-6.55 (d, 1H, CH=C*H*CONH), 7.45-7.47 (d, 1H, PhCOC*H*=CH), 7.49-8.09 (m, 10H, benzene protons, C*H*=CHCONH and PhCOCH=C*H*), 9.10 (bs, 1H, (CH$_3$)$_3$CON*H*), 9.80 (bs, 1H, CONHO*H*), 10.78 ppm (bs, 1H, CON*H*OH); ^{13}C NMR ([D$_6$]DMSO, 400 MHz): d=28.5 (3C), 79.5, 118.9, 121.4, 122.1 (2C), 126.3 (4C), 130.1 (2C), 133.5, 134.4 (2C), 141.7, 144.0, 145.2, 153.9, 161.6, 189.7 ppm; MS (EI) calcd for $C_{23}H_{24}N_2O_5$ m/z $[M]^+$: 408.1685, found: 408.1691.

***tert*-Butyl-(4-(3-(5-((2-aminophenyl)carbamoyl)-1-methyl-1Hpyrrol-3-yl)acryloyl)phenyl)carbamate (9 b):** ^{1}H NMR ([D$_6$]DMSO, 400 MHz): δ=1.49 (s, 9H, C(C*H*$_3$)$_3$), 3.91 (s, 3H, C*H*$_3$), 4.89 (bs, 2H, N*H*$_2$), 6.49-6.51 (m, 1H, benzene proton), 6.56-6.63 (d, 1H, benzene proton), 6.75-6.81 (m, 1H, benzene proton), 6.92-6.94 (d, 1H, benzene proton), 7.31-7.64 (m, 7H, benzene protons, pyrrole α and β protons, PhCOC*H*=CH and PhCOCH=C*H*), 8.08-8.09 (d, 1H, benzene proton), 9.35 (bs, 1H, (CH$_3$)$_3$CON*H*), 9.52 ppm (bs, 1H, CON*H*); ^{13}C NMR ([D$_6$]DMSO, 400 MHz): δ=28.5 (3C), 32.9, 79.5, 111.0, 116.5, 118.7, 119.0, 122.1 (2C), 122.4, 122.9, 125.2, 126.1, 127.4, 130.1 (2C), 132.0, 133.5, 141.7, 141.8, 145.2, 153.9, 162.7, 189.7 ppm; MS (EI) calcd for $C_{26}H_{28}N_4O_4$ m/z $[M]^+$: 460.2111, found: 460.2118.

***tert*-Butyl-(3-(3-(5-(3-(2-aminophenylamino)-3-oxoprop-1-enyl)-1-methyl-1H-pyrrol-3-yl)acryloyl)phenyl)carbamate (9 c):** ^{1}H NMR ([D$_6$]DMSO, 400 MHz): δ=1.48 (s, 9H, C(C*H*$_3$)$_3$), 3.79 (s, 3H, C*H*$_3$), 4.89 (bs, 2H, N*H*$_2$), 6.57-6.59 (m, 1H, benzene proton), 6.72-6.75 (d, 3H, CH=C*H*CONH, benzene protons), 6.88-6.90 (m, 1H, benzene proton), 7.15 (s, 1H, pyrrole-α proton), 7.33-7.35 (m, 1H, benzene

proton) 7.42-7.72 (m, 6H, benzene protons, pyrrole-β proton, C*H*=CHCONH, PhCOC*H*=CH, PhCOCH=C*H*), 8.12 (s, 1H, benzene proton), 9.34 (bs, 1H, $(CH_3)_3CONH$), 9.52 ppm (bs, 1H, CON*H*); ^{13}C NMR ([D_6]DMSO, 400 MHz): δ=28.5 (3C), 34.0, 79.5, 104.8, 108.0, 116.5, 119.0, 119.6, 122.4, 122.9, 123.2, 124.9, 125.2, 125.5, 127.4 (2C), 129.5, 130.6, 134.8, 136.4, 138.1, 141.8, 145.2, 153.9, 166.7, 189.7 ppm; MS (EI) calcd for $C_{28}H_{30}N_4O_4$ m/z $[M]^+$: 486.2267, found: 486.2261.

***tert*-Butyl-(4-(3-(5-(3-(2-aminophenylamino)-3-oxoprop-1-enyl)-1-methyl-1H-pyrrol-3-yl)acryloyl)phenyl)carbamate (9 d):** ^1H NMR ([D_6]DMSO, 400 MHz): δ=1.49 (s, 9H, $C(CH_3)_3$), 3.78 (s, 3H, CH_3), 4.93 (bs, 2H, NH_2), 6.55-6.59 (m, 1H, benzene proton), 6.71-6.75 (d, 3H, CH=C*H*CONH, benzene protons), 6.88-6.91 (m, 1H, benzene proton), 7.17 (s, 1H, pyrrole-α proton), 7.34-7.36 (m, 1H, benzene proton) 7.52-7.74 (m, 5H, benzene proton, pyrrole-β proton, C*H*=CHCONH, PhCOC*H*=CH, PhCOCH=C*H*), 8.04-8.06 (d, 2H, benzene protons), 9.34 (bs, 1H, $(CH_3)_3CONH$), 9.52 ppm (bs, 1H, CON*H*); ^{13}C NMR ([D_6]DMSO, 400 MHz): δ=28.5 (3C), 34.0, 79.5, 104.8, 108.0, 116.5, 119.0, 122.1 (2C), 122.4, 122.9, 123.2, 124.9, 125.2, 127.4, 130.1 (2C), 130.6, 133.5, 134.8, 141.7, 141.8, 145.2, 153.9, 166.7, 189.7 ppm; MS (EI) calcd for $C_{28}H_{30}N_4O_4$ m/z $[M]^+$: 486.2267, found: 486.2261.

***tert*-Butyl-(3-(3-(4-((2-aminophenyl)carbamoyl)phenyl)acryloyl)-phenyl)carbamate (11a):** ^1H NMR ([D_6]DMSO, 400 MHz): δ=1.49 (s, 9H, $C(CH_3)_3$), 4.93 (bs, 2H, NH_2), 6.58-6.61 (m, 1H, benzene proton), 6.77-6.79 (d, 1H, benzene proton), 6.96-6.99 (m, 1H, benzene proton), 7.16-7.18 (d, 1H, benzene proton), 7.63-7.65 (d, 2H, benzene protons), 7.69-7.74 (d, 1H, PhCOC*H*=CH), 7.96-8.23 (m, 5H, benzene protons and PhCOCH=C*H*), 8.15-8.23 (d, 2H, benzene protons), 9.75 (bs, 1H, $(CH_3)_3CONH$), 9.83 ppm (bs, 1H, CON*H*); ^{13}C NMR ([D_6]DMSO, 400 MHz): δ=28.5 (3C), 79.5, 116.5, 119.0, 119.6, 121.4, 122.4, 122.9, 125.2, 125.5, 126.5 (2C), 127.4 (3C), 129.5, 133.4, 136.4, 138.1, 138.6, 141.8, 145.2, 153.9, 164.8, 189.7 ppm; MS (EI) calcd for $C_{27}H_{27}N_3O_4$ m/z $[M]^+$: 457.2002, found: 457.2008.

tert-Butyl-(4-(3-(4-((2-aminophenyl)carbamoyl)phenyl)acryloyl)-phenyl)carbamate (11b): ^1H NMR ([D_6]DMSO, 400 MHz): δ=1.49 (s, 9H, $C(CH_3)_3$), 4.93 (bs, 2H, NH_2), 6.58-6.61 (m, 1H, benzene proton), 6.77-6.79 (m, 1H, benzene proton), 6.96-6.99 (m, 1H, benzene proton), 7.16-7.18 (m, 1H, benzene proton), 7.63-7.65 (d, 2H, benzene protons), 7.69-7.74 (d, 1H, PhCOC*H*=CH), 7.96-8.23 (m, 5H, benzene protons and PhCOCH=C*H*), 8.15–8.23 (d, 2H, benzene protons), 9.75 (bs, 1H, $(CH_3)_3CONH$), 9.83 ppm (bs, 1H, CON*H*); ^{13}C NMR ([D_6]DMSO, 400 MHz): δ=28.5 (3C), 79.5, 116.5, 119.0, 121.4, 122.1 (2C), 122.4, 122.9, 125.2, 126.5 (2C), 127.4 (2C), 130.1 (2C), 133.4, 133.5, 138.6, 141.7, 141.8, 145.2, 153.9, 164.8, 189.7 ppm; MS (EI) calcd for $C_{27}H_{27}N_3O_4$ m/z $[M]^+$: 457.2002, found: 457.2008.

tert-Butyl-(3-(3-(4-(3-(2-aminophenylamino)-3-oxoprop-1-enyl)-phenyl)acryloyl)phenyl)carbamate (11c): ^{1}H NMR ([D$_6$]DMSO, 400 MHz): d=1.49 (s, 9H, C(C*H*$_3$)$_3$), 4.95 (bs, 2H, N*H*$_2$), 6.59-6.63 (m, 1H, benzene proton), 6.73-6.75 (m, 1H, benzene proton), 6.83-6.85 (d, 1H, PhCOC*H*=CH), 6.97-6.99 (m, 1H, benzene proton), 7.18-7.20 (m, 1H, benzene proton), 7.33-7.35 (d, 1H, PhCOC*H*=CH), 7.44-7.47 (t, 1H, benzene proton), 7.73-8.19 (m, 8H, benzene protons, PhCOCH=C*H* and PhCOCH=C*H*), 8.30-8.31 (m, 1H benzene proton), 9.57 (bs, 1H, (CH$_3$)$_3$CON*H*), 9.75 ppm (bs, 1H, CON*H*); ^{13}C NMR ([D$_6$]DMSO, 400 MHz): d=28.5 (3C), 79.5, 116.5, 118.9, 119.0, 119.6, 121.4, 122.4, 122.9, 125.2, 125.5, 126.3 (4C), 127.4, 129.5, 134.4 (2C), 136.4, 138.1, 141.8, 144.0, 145.2, 153.9, 166.7, 189.7 ppm; MS (EI) calcd for $C_{29}H_{29}N_3O_4$ m/z [M]$^+$: 483.2158, found: 483.2165.

tert-Butyl-(4-(3-(4-(3-(2-aminophenylamino)-3-oxoprop-1-enyl)-phenyl)acryloyl)phenyl)carbamate (11d): ^{1}H NMR ([D$_6$]DMSO, 400 MHz): d=1.47 (s, 9H, C(C*H*$_3$)$_3$), 4.55 (bs, 2H, N*H*$_2$), 6.56-6.91 (m, 5H, CH=C*H*CONH, benzene protons), 7.33-8.10 (m, 11H, PhCOC*H*=CH, C*H*=CHCONH, PhCOCH=C*H* and benzene protons), 9.30 (bs, 1H, (CH$_3$)$_3$CON*H*), 9.80 ppm (bs, 1H, CONH); ^{13}C NMR ([D$_6$]DMSO, 400 MHz): d=28.5 (3C), 79.5, 116.5, 118.9, 119.0, 121.4, 122.1 (2C), 122.4, 122.9, 125.2, 126.3 (4C), 130.1 (2C), 133.5, 134.4 (2C), 141.7, 141.8, 144.0, 145.2, 153.9, 166.7, 189.7 ppm; MS (EI) calcd for$C_{29}H_{29}N_3O_4$ m/z [M]$^+$: 483.2158, found: 483.2165.

10.4. Biological evaluation, results and discussion

10.4.1. Human recombinant HDAC1 and HDAC4 assays

Compounds **8-11** were tested at 5 μM against hrHDAC1 (substrate: histone H3) and hrHDAC4 (substrate: the non-histone trifluoroacetyllysine derivative),[592] and the results are summarized in Table 10.3. Among the hydroxamates **8** and **10**, the benzene compounds **10** showed, in general, similar or better potency against HDAC1 than the corresponding pyrrole analogues (with the exception of **10d**) but lower than SAHA and, with some exceptions (**10c** and **8c**), than MS-275, used as reference drugs. Typically, 3-NH-Boc-substituted compounds were more efficient than their 4-NH-Boc counterparts, and the arylcarbonyl hydroxamates were less potent than the arylacrylic analogues, at least in the pyrrole series **8**. However, **10a-c** and the pyrrole **8a** displayed higher potency than SAHA against HDAC4. Regarding the 2'-aminoanilides **9** and **11**, both the pyrrole and benzene derivatives showed low inhibitory potency against HDAC1 if compared with the related hydroxamates, but against HDAC4 the pyrrole compounds **9** (with the exception of **9a**) were more potent than the corresponding hydroxamates, thus being quite HDAC4-selective. Against HDAC4 the benzene anilides **11**, despite a drop of potency when compared with the related hydroxamates, maintained 36- 41% inhibition at 5 μM. In relation particularly to the pyrrole series **9**, the introduction of the Boc-amino substituent at

the 3-position of the benzene ring seemed to be preferred, and the insertion of a double bond between the carbonyl function and the 2'-aminoanilide moiety led to more potent compounds (**9c**,**d**).

Table 10.3. hrHDAC1 and hrHDAC4 inhibitory activity of compounds **8-11.**

Compound	Inhibition (%)[a]	
	HDAC1	HDAC4
8a	37 ± 0.8	71 ± 4
8b	24 ± 1	21 ± 2
8c	65 ± 3	60 ±3
8d	59 ± 2	51 ± 2
9a	22 ± 2	43 ± 2
9b	11 ± 1	32 ± 2
9c	31 ± 1.2	64 ± 3
9d	25 ± 2.1	6 ± 2.2
10a	43 ± 1.8	83 ± 4.4
10b	37 ± 1.1	8.3 ± 5.2
10c	65 ± 2.4	76 ± 3.2
10d	35 ± 1.8	63 ± 2.5
11a	14 ± 0.9	38 ± 1.4
11b	10 ± 0.3	36 ± 2.4
11c	9 ± 0.2	41 ± 1.4
11d	11 ± 0.9	40 ± 1.3
SAHA	87 ± 2.2	63 ± 1.3
MS-275	54 ± 2.1	10 ± 1.4

[a]Percent inhibition at 5 μM; data represent mean values ± SD of at least three separate experiments

10.4.1.1.Methods

The HDAC Fluorescent Activity Assay for HDAC1 and HDAC4 is based on the Fluor de Lys Substrate and Developer combination (BioMol), and has been carried out according to the supplier's instructions and as previously reported.[586e] First, the inhibitors and purified recombinant HDAC1 or HDAC4 enzymes have been pre-incubated at room temperature for 15 min before the addition of the substrate which is the Fluor de Lys substrate, which comprises an acetylated lysine side chain. For the HDAC4 assay, the HDAC4-selective, non-histone substrate reported by Lahm et al.[592] was used. Full-length HDAC1 and HDAC4 with C-terminal His tags were expressed using baculovirus systems. Deacetylation sensitizes the substrates that, in the second step, treated with the developer produce a fluorophore. Fluorescence was detected with a TECAN Infinite M200 station.

*10.4.2. Effect of compounds **8-11** on α-tubulin acetylation in human leukemia U937 cells as an indication of HDAC6 inhibition*

Western blot analyses in human leukemia U937 cells were performed on **8-11** (5 μM, 24h) to detect their effects on the acetylation level of α-tubulin, a marker of HDAC6 inhibition. MS-275 and SAHA (5 μM, 24h) were used as reference drugs. Data depicted in Figure 10.2 show that both pyrrole (**8**) and benzene (**10**) hydroxamates were able to strongly increase α-tubulin acetylation, with **10** more efficient than **8**. In contrast, the 2'-aminoanilides **9** and **11** (including the reference MS-275) yielded a signal similar or slightly higher than the control (DMSO).

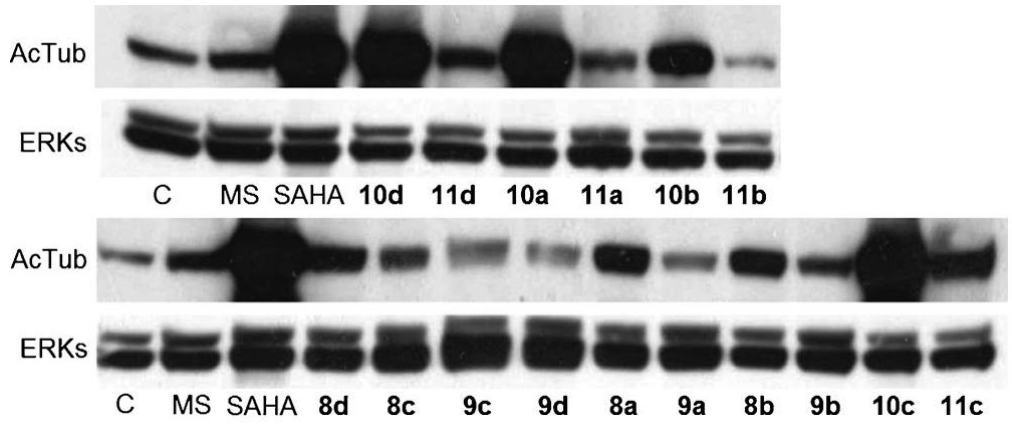

Figure 10.2. Effects of compounds **8-11**, MS-275 (MS), and SAHA (5 μM, 24 h) on α-tubulin acetylation (AcTub) in human U937 leukemia cells. Western blot analyses were performed with specific antibodies. ERK proteins were used for equal loading. Blots representative of two independent experiments with similar results are shown.

10.4.2.1. Methods

For determination of the acetylation levels of α-tubulin in U937 cells and histone H3 in HT29 cells, 25 μg of total protein extracted from the cells were separated on 10 and 13.5% polyacrylamide gels, respectively, and blotted as previously described.[586e] Immunodetection was performed using antibodies directed to acetylated α-tubulin (Sigma-Aldrich), total ERKs (Santa Cruz Biotechnology), acetyl (Lys 9/14)-histone H3 (Ac-H3, Millipore), and β-actin (Sigma-Aldrich). Anti-mouse or anti-rabbit immunoglobulin G (IgG)–horseradish peroxidase (HRP)-conjugated antibodies (Amersham Biosciences) were used as secondary antibodies at 1:10000 dilution. Antibody binding was visualized by enhanced chemiluminescence according to manufacturer's specification and recorded on autoradiography film (Amersham Biosciences).

*10.4.3. Profiling of selected compounds **8b** and **10c** on HDAC1-11 isoforms*

Two selected compounds, **8b** and **10c**, chosen because of their effect on tubulin acetylation and their high pro-apoptotic properties in U937 cells (See Sec. 10.4.5), were tested against all the HDAC1-11 isoforms in ten-dose IC_{50} mode with three fold serial dilution starting from 50 μM solutions (Table 10.4). From these data, the tert-butyl-(3-(3-(4-(3-(hydroxyamino)-3-oxoprop-1-en-1-yl)phenyl)acryloyl)phenyl) carbamate **10c** was generally more potent than the tert-butyl (4-(3-(5-(hydroxycarbamoyl)-1- methyl-1H-pyrrol-3-yl)acryloyl)phenyl)carbamate **8b** against HDACs (with the exception of HDAC5), and was less efficient than SAHA, used as reference drug. Compound **10c** displayed single-digit micromolar inhibition of HDAC1, -2, -4, -8, and -10, and nanomolar activity against HDAC6 (IC_{50}=10.2 nM). Compound **8b** was also highly potent against HDAC6, with an IC_{50} value similar to SAHA (IC_{50} **8b**= 27.9 nM; IC_{50} SAHA= 28.6 nM), confirming the western blot data on acetyl-α-tubulin, and because of its low activities against the other HDAC isoforms, it is extremely HDAC6-selective.

Table 10.4. Inhibition of HDAC1-11 isoforms by compounds **8b** and 1**0c** and SAHA.

HDACs	IC_{50} (μM)		
	8 b	**10 c**	**SAHA**
1	54.8	2.9	0.26
2	28% [a]	2.1	0.92
3	82.2	10.8	0.35
4	74.4	3.2	0.49
5	70.6	101.0	0.38
6	0.03	0.01	0.03
7	30% [a]	34% [a]	0.34
8	19.8	1.2	0.24
9	99.9	68.8	0.32
10	NA [b]	5.1	0.46
11	16% [a]	12.0	0.36

[a] Percent inhibition at 50 μM; [b] Not active.

10.4.3.1. Methods

Individual IC_{50} values for each HDAC isozyme were measured with the homogeneous fluorescence release HDAC assay. Purified recombinant enzymes were incubated with serial diluted inhibitors at the indicated concentration. The deacetylase activities of HDACs 1, 2, 3, 6, and 10 were measured by assaying enzyme activity using AMC-K(Ac)GL substrate and AMC-K(TFA)GL substrate for HDACs 4, 5, 7, 8, 9, and 11 as previously described.[592] Deacetylated AMC-KGL was sensitive toward lysine peptidase, and free fluorogenic 4-methylcoumarin-7-amide (MCA) was generated, which can be excited at 355 nm and observed at 460 nm. The data was analyzed on a plate to plate basis in relationship to the control and imported into analytical software (GraphPad Prism).

*10.4.4. Binding studies of **10c** in the HDAC6 binding site*

To better rationalize the enhanced inhibitory activity against HDAC6 of the newly discovered compounds, molecular modeling studies were undertaken. As the X-ray structure of HDAC6 has not been solved, a homology-based model of its major functional domain (second catalytic subunit CDII, G482- G801)[593] was constructed. In this step, multiple HDAC X-ray templates and subsequent multiple-threading alignments were employed following the I-TASSER methodology.[594] Interestingly, the same methodology has been already applied by Kozikowski and co-workers to propose viable ligand-HDAC6 theoretical complexes.[595] The resulting HDAC6 model was then used to dock compound **10c**, which is among the most active and selective HDAC6 inhibitors described herein. Analysis of the modeled enzyme binding cavity revealed that its outer portion is lined by five loops that could rearrange upon ligand binding. Therefore, to allow for a certain amount of protein plasticity during the docking calculation an induced-fit docking approach (IFD) was used. In the best ranking binding pose predicted by the IFD (Figure 10.3), **10c** is well inserted in the enzyme binding cavity with its hydroxamate group coordinating the zinc ion. Moreover, the rigid aromatic spacer is embedded in an aromatic cage formed by H500, F620, and F680 engaging favorable charge-transfer interactions and hydrophobic contacts with P501. On the other hand, the tert-butylcarbamate group at position 3 of the terminal phenyl ring extends toward the outer portion of the binding gorge contacting one of the loops lining the rim of the catalytic tunnel (residues G677–G686). In this position the latter group hydrogen bonds with the F199 backbone CO group and engages in hydrophobic contacts with the M682 side chain.

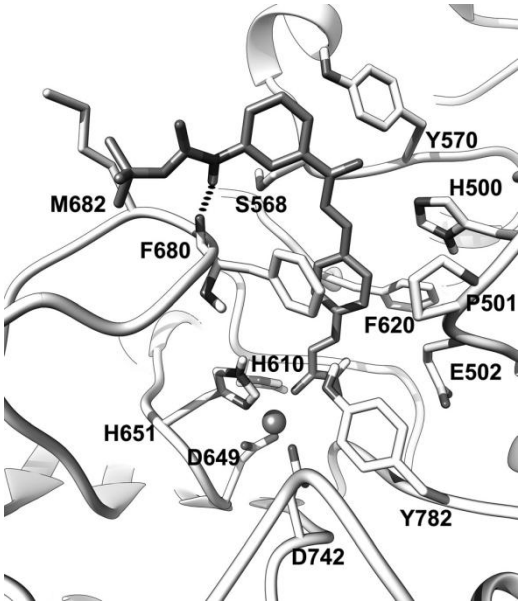

Figure 10.3. Predicted binding pose of **10c** in the HDAC6 homology model. The ligand is represented as dark-gray sticks, whereas the enzyme is represented as white sticks. Hydrogen bonds are displayed as black dashed lines.

Analysis of the results obtained for **10d** (Figure 10.4) revealed that the ligand is unable to form the aforementioned hydrogen bond interaction with the enzyme while the hydrophobic contacts with M682 are maintained. According to these calculations, the Boc-unsubstituted N-hydroxy- 3-(4-(3-oxo-3-phenylprop-1-en-1-yl)phenyl)acrylamide would be unable to establish the same interaction pattern contacts with the outer portion of the enzyme. These data would explain why **10c** (IC_{50}= 0.01 μM) is a more potent HDAC6i than its close analogue **10d** or the Boc-unsubstituted prototype (IC_{50}=0.04 μM and 0.5 μM, respectively).

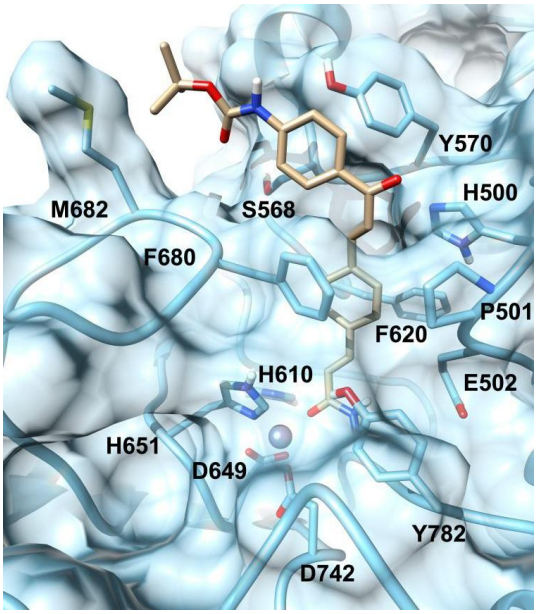

Figure 10.4. Predicted binding pose of **10d** in the HDAC6 homology model. The ligand is represented as brown sticks while the enzyme as cyan sticks and surface.

10.4.4.1. Methods

The human HDAC6 homology model was obtained using the I-TASSER approach.[594] In particular the sequence of the second catalytic subunit of HDAC6 (Q9UBN7), retrieved from the Uniprot server (http://www.uniprot.org), was used as the input for the ITASSER method. The position of the zinc ion and the conformation of the chelating residues were extracted from the resolved structure of human HDAC7 complexed with SAHA (PDB ID: 3C0Z).[596] The constructed model was then processed using the Protein Preparation Wizard panel of the Schrödinger 2012 molecular modeling package. In particular, using the preprocess and analyze structure tool, the bond orders were assigned, all the hydrogen atoms were added, and the disulfide bonds were assigned. Using Epik 2.0 a prediction of the heterogroups ionization and tautomeric states was performed. An optimization of the hydrogen bonding network was performed using the H-bond assignment tool. Finally, using the impref utility, the positions of the hydrogen atoms were optimized by keeping all the heavy atoms in place. Ligand files (**10c** and **10d**) were prepared employing the Builder tool and generated with the Ligprep module within Schrödinger 2012

molecular modeling package. Partial ligand charges were calculated by means of the Jaguar suite (Jaguar 4.1; Schrödinger, Inc.) within the same package. The electrostatic potential was computed using 6-31G* basis set. Ligands were submitted as starting geometries to IFD calculations (Schrödinger Suite 2012) using Glide (Glide 5.7; Schrödinger Suite 2012). In the first IFD stage, a softened-potential docking was performed using GlideSP (Standard Precision) mode generating 20 initial poses. For each one, a full circle of protein refinement was performed using Prime (Prime 3.0; Schrödinger Suite 2011). Residues of the protein within 5.0 Å of ligand poses were refined, and side chains were conformationally changed and subsequently minimized. Ligands were re-docked with GlideXP included in IFD to generate poses. All ligand–protein complex pictures were rendered employing the UCSF Chimera software.

*10.4.5. Effect of compounds **8-11** on cell-cycle distribution, apoptosis induction, and granulocytic differentiation in human U937 leukemia cells*

Compounds **8-11** were tested at 5 μM for 30 h in U937 cells to determine their effects on cell cycle, apoptosis induction, and granulocytic differentiation (Figure 10.5, 10.6a,b). SAHA and MS-275 (5 μM) were used as reference drugs. Among the hydroxamates **8**, **10**, the compounds **8a**, **8b**, and **10c** displayed an arrest in the G_1 phase similar to (**10c**) or higher than (**8a**, **8b**) MS-275. Compound **8c** blocked the cycle at the S phase, similar to SAHA. In relation to the 2'-aminoanilides, the benzene compounds **11a** and **11b** showed a block at the G_1 phase similar to MS-275, whereas the remaining derivatives produced a weaker effect (Figure 10.5).

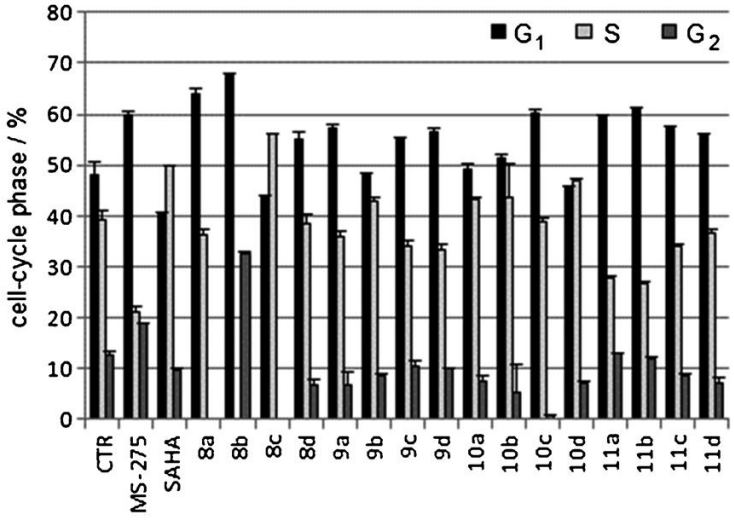

Figure 10.5. Cell-cycle analysis in human U937 leukemia cells treated with compounds **8-11**, SAHA, and MS-275 at 5 μM for 30 h.

Taking into account the pre-G_1 peak as an index of pro-apoptotic properties of the compounds, Figure 10.6a shows that the hydroxamates **8a-c** and **10c**,**d** exhibited 15-21% apoptotic induction in this assay, with **8b** and **10c** being more potent than

SAHA (percent pre-G_1 peak: 18.4 (**8b**), 21.4 (**10c**), and 16.9% (SAHA). The expression of the surface antigen CD11c was determined as a marker of granulocytic differentiation in U937 leukemia cells. The cells were treated with **8**-**11** at 5 μM for 30 h, and then the percentage values of CD11c-positive/propidium iodide (PI)-negative cells were determined. In this assay, both the pyrrole hydroxamates (**8c**,**d**) and 2-aminoanilides (**9c**,**d**) were able to induce cytodifferentiation effects more potently than MS-275, one of the most efficient cytodifferentiating agents among the HDAC inhibitors described in literature.[588b,597] In particular, **9c** and **9d** displayed respectively 90.9 and 76.1% of CD11c+/PI-cells (Figure 10.6b).

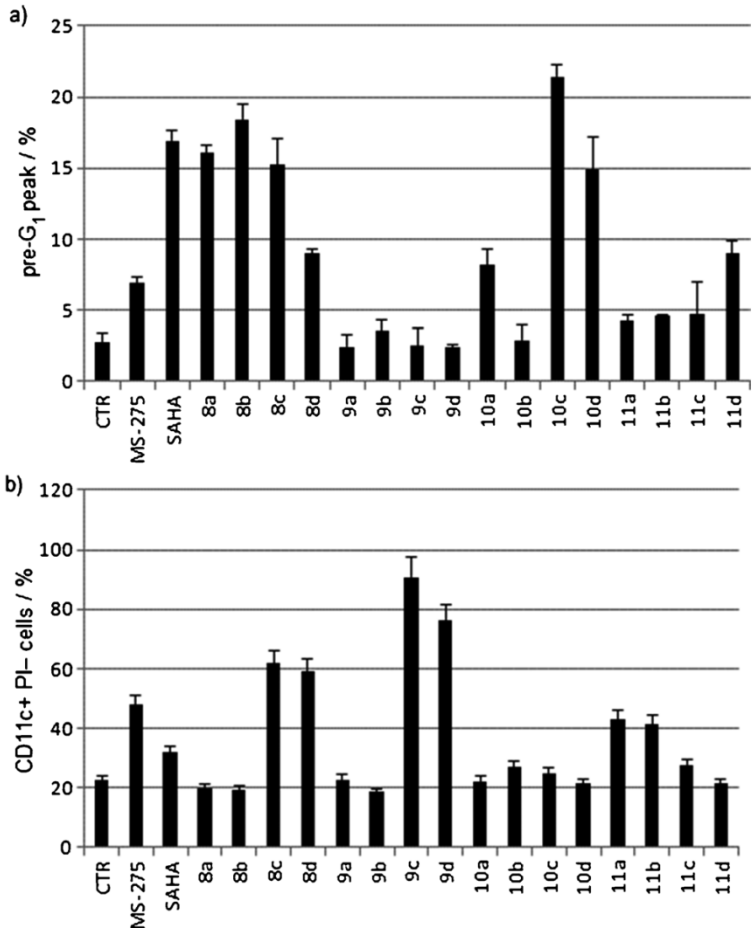

Figure 10.6. a) apoptosis induction, b) granulocytic differentiation in human U937 leukemia cells treated with compounds **8**-**11**, SAHA, and MS-275 at 5 μM for 30 h.

10.4.5.1. Methods

Cell-cycle analysis of U937 cells. $2.5x10^5$ treated and untreated cells were collected, fixed, and resuspended in 500 μL of a hypotonic buffer (0.1% Triton X-100, 0.1% sodium citrate, 50 μg mL^{-1} propidium iodide (PI), RNase A). Cells were incubated in the dark for 30 min. Samples were acquired on a FACS-Calibur flow cytometer using Cell Quest software and analyzed with standard procedures using Cell Quest

software (Becton Dickinson) and ModFit LT version 3 Software (Verity) as previously reported.[598] All the experiments were performed three times.

Granulocytic differentiation on U937 cells. Granulocytic differentiation of U937 cells was carried out as previously described.[598] Briefly, treated and untreated cells were harvested and resuspended in 10 μL phycoerythrin-conjugated CD11c (CD11c–PE). Control samples were incubated with 10 μL PE-conjugated mouse IgG1, incubated for 30 min at 4 °C in the dark, washed in PBS, and resuspended in 500 μL PBS containing PI (0.25 μg mL^{-1}). Samples were analyzed by FACS with Cell Quest technology (Becton Dickinson). PI+ cells were excluded from the analysis.

10.4.6. Antiproliferative activities of selected compounds in a panel of different cancer cell lines

Selected pro-apoptotic compounds (**8a**, **8b**, **10c** and **10d**) were first tested in three different human cancer cell lines (colon carcinoma HCT116, non-small-cell lung adenocarcinoma A549, and chronic myeloid leukemia K562), using the CellTiter-Glo luminescent cell viability assay, to determine their antiproliferative effects after 72 h of treatment (Table 10.5). The benzene hydroxamates **10c** and **10d** showed the highest antiproliferative activities in these assays, with IC_{50} values ranging from 0.6 to 4.1 μM.

Table 10.5. In vitro antiproliferative effects of selected compounds against cancer cell lines.

Compound	IC_{50} (μM)[a]		
	HTC116	A549	K562
8 a	3.6	12.2	1.5
8 b	9.7	18.8	3.1
10 c	1.0	4.1	0.6
10 d	1.3	3.1	1.6

[a]Concentration of test compound required for 50% inhibition of cell viability. Performed in replicate ($n \geq 2$); values are the mean (SD < 30% of the mean). HTC116: human colon carcinoma, A549: human non small-cell lung adenocarcinoma, K562: chronic myeloid leukemia.

Thus, we selected the tert-butyl-3-(3-(4-(3-(hydroxyamino)- 3-oxoprop-1-en-1-yl)phenyl)acryloyl)phenylcarbamate **10c** to extend the characterization against a panel of different cancer cells (colon carcinoma HT29, melanoma M14, nonsmall-cell lung adenocarcinoma H1299, breast adenocarcinoma MCF7, ovarian carcinoma HEY, glioblastoma U87, neuroblastoma LAN-5 and SH-SY5Y, pancreatic carcinoma PANC-1, prostate carcinoma PC3, and ovarian carcinoma SKOV3 cancer cells) after 48h treatment, using the 3-(4,5-dimethylthiazol-2-yl)-2,5-diphenyltetrazolium bromide (MTT) method (Table 10.6). In these assays, the two

neuroblastoma LAN-5 and SH-SY5Y cell lines were the most sensitive, with **10c** displaying sub-micromolar antiproliferative activities, followed by H1229 and HT29 carcinoma cells (**10c** active at single-digit micromolar range), whereas the other screened cell lines were less susceptible to the treatment.

Table 10.6. In vitro antiproliferative activity of **10c** against a panel of cancer cell lines.

Cell line	IC_{50} (μM)[a]
Colon carcinoma HT29	3.2
Melanoma M14	21
Non-small-cell lung adenocarcinoma H1299	2.2
Breast carcinoma MCF7	21
Ovarian carcinoma HEY	20
Ovarian carcinoma SKOV3	40
Glioblastoma U87	13
Neuroblastoma LAN- 5	0.4
Neuroblastoma SH- SY5Y	0.6
Pancreatic carcinoma PANC-1	28
Prostate carcinoma PC3	24.5

[a]Concentration of **10c** required for 50% inhibition of cell viability. Determined by MTT assay; cells were treated with **10c** ranging from 0.1 to 100 μM for 48h. The results are reported as the average of two or three independent experiment (SD < 30% of the mean).

*10.4.6.1. Effects of **10c** in HT29 cells*

Choosing colon HT29 as a representative cancer cell line, the effect of **10c** on acetylation level of histone H3 (10 μM, 24 h) was detected by western blot analysis. SAHA was used at 50 μM as reference drug. As depicted in Figure 10.7, an increased acetylation at Lys 9/14 of histone H3 was observed after exposure to **10c** when compared with untreated cells.

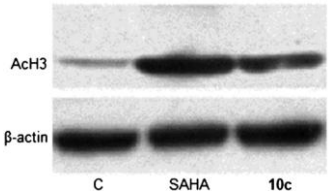

Figure 10.7. Western blot analysis of acetylated histone H3 on Lys 9/14 (Ac-H3) in protein extracts obtained after treatment of HT29 cells with **10c** (10 μM) and SAHA (50 μM) for 24 h. β-Actin is shown as loading and transferring control. A blot representative of two independent experiments with similar results is shown.

To further characterize the antiproliferative effect of **10c** in HT29 cells, experiments were performed by treating cells for 24 h with the compound (0.5, 1, and 5 μM) and assessing cell proliferation both at the end of treatment and from 24 to 96 h after the end of treatment (Figure 10.8).

As reported in Figure 10.8, **10c** induced a dose-dependent decrease of cell survival up to 16% (5 μM, 96 h after the end of treatment). SAHA, tested at the same conditions, was less effective.

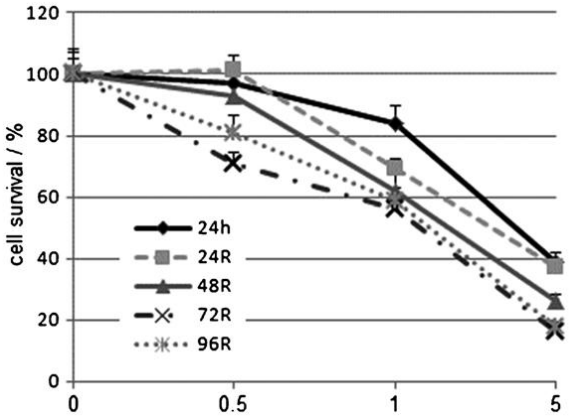

Figure 10.8. Percentage of cell survival after treatment with **10c** at doses ranging from 0.5 to 5 μM for 24 h. Analysis was performed at the end of treatment (24 h), and 24 (24R), 48 (48R), 72 (72R), and 96 h (96R) after the end of treatment (R= recovery). The results are reported as (viability of treated cells)/(viability of control cells)×100, and represent the average ± SD of three independent experiments.

Finally, we assessed the ability of HT29 cells to form colonies after treatment with **10c** (0.5, 1.0, and 5.0 mm, for 24 h). As reported in Figure 10.9, a dose-dependent decrease in colony-forming potential was evident in HT29 cells after **10c** treatment. In particular, an approximate 60% reduction was observed after exposure to 5 μM **10c** for 24 h as compared with control untreated cells.

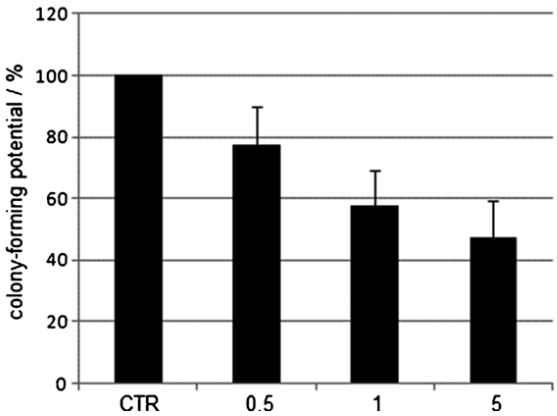

Figure 10.9. In vitro clonogenic ability of HT29 cells after treatment with **10c** at doses ranging from 0.5 to 5 μM for 24 h.

10.4.6.2. Methods

Antiproliferative effects of compounds 8 and 10 on a wide panel of cancer cell lines.: The antiproliferative effect of selected **8** and **10** compounds was evaluated against K562, A549, and HCT116 cell lines using the CellTiter-Glo luminescent cell

viability assay (Promega) according to the manufacturer's instructions. K562, A549, and HCT116 cells were incubated for 72 h with various inhibitor concentrations. An equivalent of the CellTiter-Glo reagent was then added, the solution was mixed for 2 min in order to induce cell lysis, and the luminescence was recorded after a further 10 min. IC_{50} values were calculated using GraphPad software.

The antiproliferative effect of **10c** on a wider panel of cancer cell lines was evaluated by 3-(4,5-dimethylthiazol-2-yl)-2,5-diphenyltetrazolium bromide (MTT, mitochondrial respiration analysis, Sigma-Aldrich). Briefly, exponentially growing tumor cells were seeded (3×10^3 cells per well) in sextuplicate in 96-well culture plates (Nunc), and 24 h later cells were treated with **10c** at concentrations ranging from 0.1 to 100 μM for 24 or 48 h. Cells were also treated with 1% DMSO, as control. Recovery experiments were performed by treating cells for 24 h with the compound and assessing cell proliferation both at the end of treatment and from 24 to 96 h after the washout of the drug. Cell viability was evaluated by adding MTT to each well at a final concentration of 0.5 mg mL^{-1} and after 4 h of incubation at 37 °C, the formazan salt was dissolved with 200 μL isopropyl alcohol. The absorbance of each well was measured with an ELISA reader (DASIT) at λ 570 nm and the viability was calculated for each concentration of **10c** used as ($OD_{treated\ cells}$)/($OD_{control\ cells}$)×100. The concentration of **10c** that causes a 50% of cell viability inhibition (IC_{50}) was also calculated.

In vitro colony-forming assay. Suspensions from treated (0.5- 5 μM **10c**, 24 h) and untreated HT29 cells were seeded into 60 mm Petri dishes (Nunc, Mascia Brunelli) for 10 days. Colonies were stained with 2% methylene blue in 95% ethanol and counted (1 colony >50 cells). The surviving fractions were calculated as the ratio of number of colonies per number of plated cells ×100.

10.4.7. Conclusion

Using HDAC6-selective inhibitors **4**-**7**, which bear the NH-Boc group at the CAP moiety and show growth inhibition of colon HCT116, estrogen-stimulated breast MCF7, and a panel of pancreatic carcinoma cell lines as a structural basis, we designed, new pyrrole- and benzene-containing hydroxamates (**8**, **10**) and 2'-aminoanilides (**9**, **11**). These compounds (**8**, **10**, **9**, **11**) are substituted with a NH-Boc group either at the 3- or 4-position of the benzoyl group and are therefore analogues of compounds **1**, **2** previously described by us and endowed with anticancer properties. When tested against HDAC1 and -4, the 3-NH-Boc-substituted compounds seemed to be more potent than the corresponding 4-NH-Boc counterparts. The benzene hydroxamates **10** displayed higher inhibition than the related pyrrole analogues **8**, and exhibited a great decrease in activity when changed into 2'-aminoanilides (**11**). In the pyrrole series a similar decrease of potency from hydroxamates **8** to anilides **9** was not registered. Both the pyrrole (**8**) and benzene (**10**) hydroxamates increased the acetylation level of α-tubulin in human leukemia

U937 cells, a marker of HDAC6 inhibition, whereas both the anilides (**9**, **11**) did not. Two compounds, **8b** and **10c**, were tested on all the HDAC1-11 isoforms, and in agreement with previous data, **10c** was more potent than **8b** in ten of the eleven tested isoforms, and both compounds showed HDAC6 inhibition at a nanomolar level, **8b** being three fold less potent than **10c** but extremely more selective because of its low potency against the other enzymes. In comparison with other known HDAC6-selective inhibitors, such as the Boc-containing compounds **4-7**,[589] the tetrahydropyrido[4,3-*b*]indole derivative tubastatin A,[595] or the macrocyclic hydroxamates (S)-**9**, (S)-**34**, and (S)-**35**,[599] compounds **8b** and **10c** displayed similar potency and/or selectivity, despite some chemical differences shown mainly at the CAP and HS level in the structures. In U937 cells, **8b** and **10c** (5 μM, 30 h) induced greater apoptosis (18.4 and 21.4%) than SAHA (16.9 %), and the pyrrole 2'-aminoanilides **9c** and **9d** (5 μM, 30 h) showed the highest cytodifferentiating effect (76.1 and 90.9 %). When tested against a wide panel of different cancer cell lines, **10c** showed low or single-digit micromolar antiproliferative effect, probably related to its ability to inhibit HDAC1 and -2, largely overexpressed in cancer (see Sec. 6.2.5.) Remarkably, against neuroblastoma LAN-5 and SH-SY5Y cell lines **10c** exerted growth inhibition at nanomolar level, suggesting an additional role for HDAC6 inhibition in neurologic diseases.[600] In colon HT29 cell line, chosen as a representative cell line, **10c** increased the level of histone H3 acetylation (10 μM, 24 h), and decreased up to 60% the colony-forming potential in a dose-dependent manner. Further studies with **10c** in vivo are required to assess its potential use as anticancer agent.

11. Pan-inhibitors simultaneously targeting Jumonji C and lysine specific demethylases*

11.1. Research project

In contrast to lysyl-acetylation, which normally correlates with transcriptional activation, lysyl-methylation correlates with both activation and repression depending on the context, including lysine residue location and the extent (me1, me2, or me3) of methylation. In general, methylation of histone H3 at Lys residues 9 or 27 (H3K9 or H3K27) or histone H4 at Lys 20 (H4K20) is associated with repression, whereas H3K4, H3K36 and H3K79 methylation correlates with enhanced transcription.[444] Lysine methylation was once thought to be irreversible, however, the identification, first, of the lysine specific demethylases (LSDs) followed by the Jumonji C (JmjC) demethylases has led to the proposal that it is dynamic. The human LSDs (LSD1 and LSD2) demethylate histone substrates using a flavin adenine dinucleotide (FAD)-dependent amine oxidase type mechanism. (See Sec. 7.2.1.2.). For mechanistic reasons, the LSDs demethylate only mono-and dimethylated lysines. LSD1 is specific for H3K4me1/me2 as a component of the CoREST co-repressor complex, but in presence of the androgen receptor (AR) its specificity changes from H3K4 to H3K9, thus, LSD1 can act either as a transcriptional corepressor or coactivator depending on its binding partners and substrates. Pathologically, LSD1 was found to be oncogenic and/or overexpressed in several cancers ranging from leukemias to solid tumors.

The JmjC enzymes belong to the cupin superfamily of oxygenases and contain an Fe^{2+} ion in their catalytic domain and use α-ketoglutarate as co-substrate (See Sec. 7.2.2.1). In contrast to the LSDs, the JmjC KDMs can demethylate all three lysine methylation states. JmjC demethylases are overexpressed in multiple types of cancer cells,and some JmjC demethylases have been involved in neural development and/or function and are associated with non-cancer diseases including X-linked mental retardation, autism and midline defects.

In addition to histones, LSD1 and some JmjCs interact with non-histone proteins that also contribute to transcriptional and/or non-transcriptional related processes.

In human prostate cancers, LSD1 and the JmjC KDM4A/C are co-expressed and co-localize with androgen receptor (AR). Recently, KDM4A/C inhibitors were found not to inhibit prostate (LNCaP and PC3) and colon (HCT116) cancer cell growth in isolation, but displayed anti-proliferative effects in combination with NCL-2, an LSD1 inhibitor,[559] suggesting a potential for synergy in LSD and JmjC KDM inhibition.[601]

It is now clear that in multifactorial diseases such as cancer, central nervous system disorders, diabetes, or immunoinflammatory diseases, which involve multiple altered cellular pathways and signals, the use of single-target drugs (the “one drug, one

target" concept) can result in unsatisfactory treatment outcomes.[602] Combination therapies employing two or more drugs, can be more efficient in controlling such complex disease systems and less prone to resistance.[603] An alternative strategy to combination therapy is to develop a single chemical entity that is able to modulate multiple targets simultaneously (designed multiple ligands, DMLs).[604,605] The overall goal of the DML approach is to enhance the efficacy and/or improve the safety of therapy respect to drug combination. Additional advantages of DMLs are the reduction of pill burden for patients, due to the administration of a single compound, a lower risk of drug-drug interactions, and improvement in medication adherence. Building on previous works,[544,573,576] here are described pan-demethylase inhibitors **1-6** (Figure 11.1) that simultaneously inhibit both LSD1 and JmjC KDMs. Compounds **1-6** were designed by coupling tranylcypromine (**7**),[544] a known LSD1 inhibitor, and 4-carboxy-4'-carbomethoxy-2,2'-bipyridine **8**[553]or 5-carboxy-8-hydroxyquinoline (**9**, 5-carboxy-8HQ),[606] two 2OG competitive templates developed for JmjC inhibition (Figure 11.1). The molecular weight of these pan-demethylase inhibitors is acceptable because they result from combination of low molecular weight molecules.

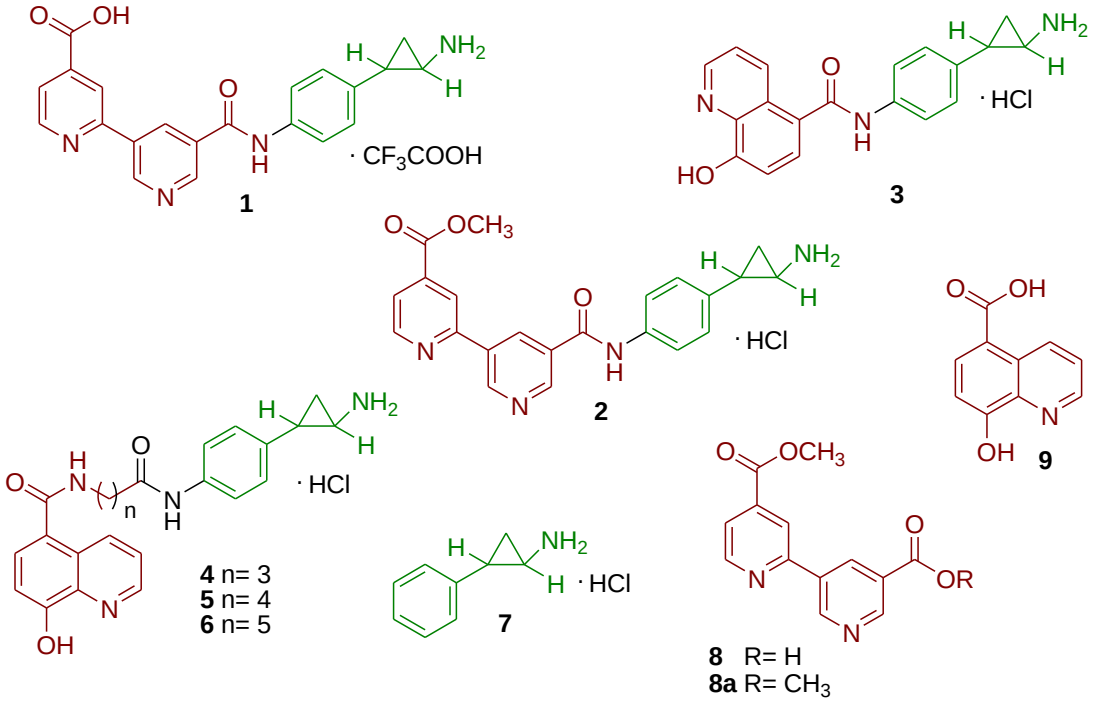

Figure 11.1. Structures of the new pan-demethylase inhibitors **1-6** and of the single-family target inhibitors **7-9**.

The compounds were designed based on known inhibition results and crystallographic analyses of both the LSDs and JmjC KDMs. Based on manual docking studies (Figure 11.2), we proposed that conjugation of tranylcypromine to the carboxylate group of either 4-carboxy-4'-carbomethoxy-2,2'-bipyridine **8** [553] or 5-carboxy-8-hydroxyquinoline **9** [606] (to form compounds **1**, **2** and **3-6** respectively),

would give compounds that are capable of binding to both the LSD and KDM4 active sites.

Based on the LSD1 structure (PDB 2XAJ),[544] the bipyridyl (for **1**) and hydroxyquinoline (for **3**) rings are predicted to protrude into the LSD1 substrate binding pocket, with the tranylcypromine moiety conjugating to FAD, as occurs during inhibition by tranylcypromine **7** alone (Figure 11.2A). Analysis of the active site of KDM4A (PDB 3PDQ) leads to the proposal that both compounds **1** and **3** can chelate the protein-bound iron via their bipyridyl and hydroxyquinoline groups respectively, as observed for a known bipyridyl inhibitorand 5-carboxy-8HQ **9**. Moreover, the primary amines of **1** and **3** may be involved in hydrogen bonding and/or electrostatic interactions with KDM4A (Figure 11.2B).

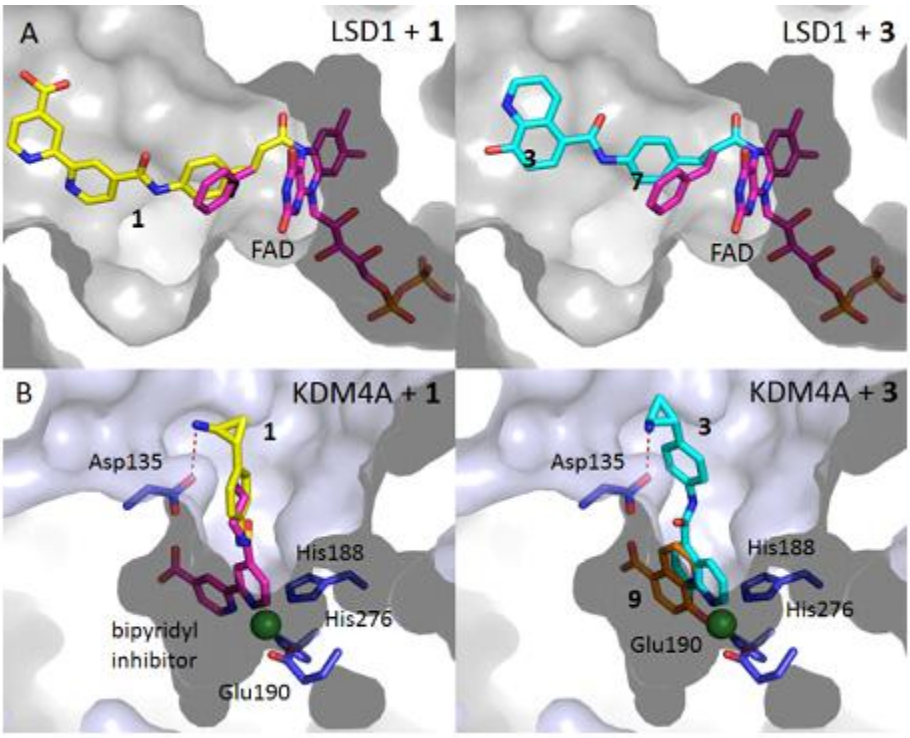

Figure 11.2. Manual docking of compounds **1** and **3** in LSD1 and KDM4A active sites: (A) **1** (yellow, left) and **3** (cyan, right) docked into the active site of LSD1. (B) **1** (yellow, left) and **3** (cyan, right) docked into the active site of KDM4A. A known bipyridyl inhibitor is shown in pink (left) and the 5-carboxy-8HQ **9** in orange (right).

11.2. Chemistry

Compounds **1** and **2** (Scheme 1A) were prepared by coupling 4-carboxy-4'-carbomethoxy-2,2'-bipyridine **8**[553] with *trans*-*N*-Boc-2-(4-aminophenyl) cyclopropylamine **10**[544] using HOBt/EDCI to give amide **11**; ester hydrolysis to give **12** followed by *N*-Boc deprotection with CF_3CO_2H gave initial target **1** (Scheme 1, all hybrid compounds were prepared as *trans* racemates). Alternatively, **11** was directly cleaved in 4N HCl to give ester **2**. To prepare 8-hydroxyquinoline compounds **3**-**6** (Scheme 1B), 5-carboxy-8HQ **9**[606] as its *O*-MOM-protected

derivative (**13**) was condensed with **10**, and intermediate **14** was treated with 4N HCl to provide **3**. Reaction of **13** with the requisite methyl-ω-aminoalkanoate hydrochlorides[607] gave methyl esters **15-17**, which after alkaline hydrolysis were condensed with **10** to give the intermediates **18-20**. Subsequent acid deprotection of **18-20** afforded final compounds **4-6**. Alternatively, intermediates **15-17** were MOM group deprotected to give the 8HQ methyl esters **21-23**, which were hydrolyzed to give acids **24-26**.

Scheme 1

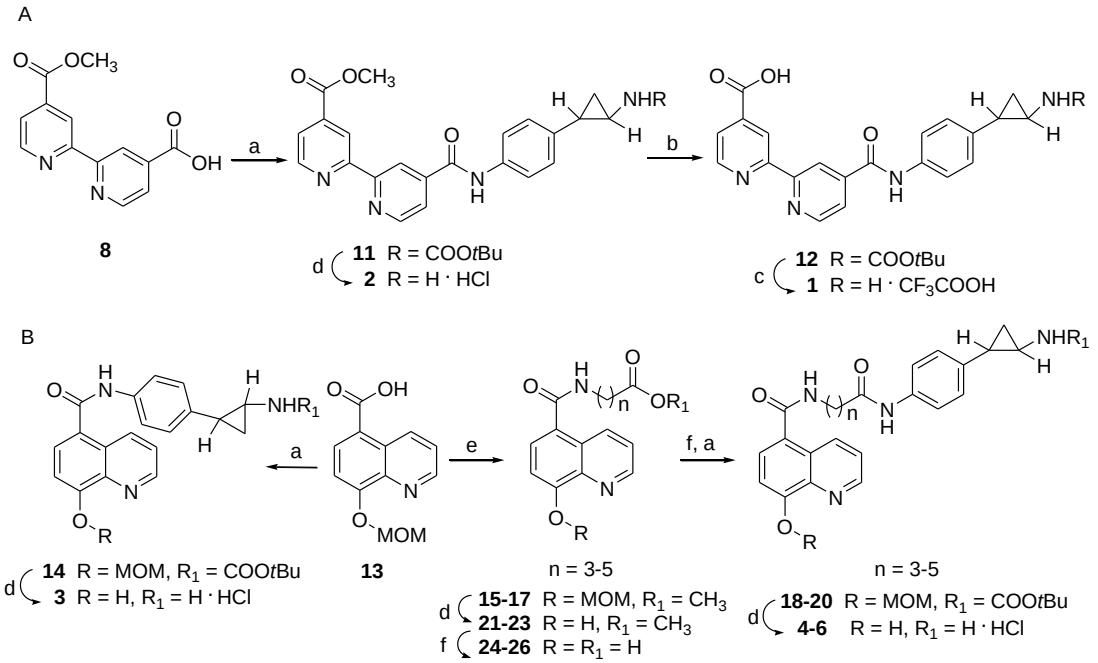

Reagents and conditions: a) racemic *trans-N*-Boc-2-(4-aminophenyl)cyclopropylamine **10**, HOBt, EDCI, Et_3N, DMF, room temperature; b) 0.2N NaOH, MeOH, RT; c) CF_3COOH, 0 °C to room temperature; d) 4N HCl in 1,4-dioxane, THF/MeOH, room temperature; e) methyl ω-aminoalkanoate hydrochloride, HOBT, EDCI, Et_3N, DCM, room temperature; f) 2N LiOH, THF, room temperature.

The chemical and physical data of the intermediate 11-26 and final compounds 1-6 are reported in Table 11.1 and 11.2, respectively.

Table 11.1. Chemical and physical data of intermediates **11-26**.

Cpd	mp, °C	recrystall. Solvent	Yield %
11	196-199	A	80
12	>250	A	89
13	157-159	B	75
14	188-191	C	67
15	115-117	D	83
16	96-98	D	52
17	121-123	D	66
18	184-186	D	88
19	111-114	E	74
20	69-72	E	74
21	185-186	C	77
22	175-177	C	95
23	164-166	C	97
24	217-218	A	86
25	207-209	A	96
26	187-189	C	66
A: ethanol; B: acetonitrile/cyclohexane; C: acetonitrile; D: benzene/cyclohexane; E: cyclohexane			

Table 11.2. Chemical and physical data of intermediates **1-6**.

Cpd	mp, °C	recrystall. Solvent	Yield %
1	>250	A	90
2	>250	A	61
3	>250	A	71
4	>250	A	85
5	>250	A	65
6	>250	A	89
A: tetrahydrofuran/methanol			

11.3. Experimental section

Chemistry. Melting points were determined on a Buchi 530 melting point apparatus. ^{1}H-NMR and ^{13}C-NMR spectra were recorded at 400 MHz using a Bruker AC 400 spectrometer; chemical shifts are reported in δ (ppm) units relative to the internal reference tetramethylsilane (Me_4Si). Mass spectra were recorded on a API-TOF Mariner by Perspective Biosystem (Stratford, Texas, USA), samples were injected by an Harvard pump using a flow rate of 5-10 μL/min, infused in the Electrospray system. All compounds were routinely checked by TLC and ^{1}H NMR. TLC was performed on aluminum-backed silica gel plates (Merck DC, Alufolien Kieselgel 60 F_{254}) with spots visualized by UV light or using a $KMnO_4$ alkaline solution. All solvents were reagent grade and, when necessary, were purified and dried by standard methods. Concentration of solutions after reactions and extractions involved the use of a rotary evaporator operating at reduced pressure of ~ 20 Torr. Organic solutions were dried over anhydrous sodium sulfate. Elemental analysis has been used to determine purity of the described compounds, that is >95%. Analytical results are within 0.40% of the theoretical values. All chemicals were purchased from Sigma Aldrich, Milan (Italy) or from TCI Europe, Zwijndrecht (Belgium), and were of the highest purity. As a rule, samples prepared for physical and biological studies were dried in high vacuum over P_2O_5 for 20h at temperatures ranging from 25 to 40 °C, depending on the sample melting point.

***trans*-Methyl-4'-((4-(2-((*tert*-Butoxycarbonyl)amino)cyclopropyl)phenyl) carbamoyl) -[2,2'-bipyridine]-4-carboxylate (11).** The reagents HOBT (62 mg, 0.39 mmol), EDCI (75 mg, 0.39 mmol) and Et_3N (0.15 mL, 1.11 mmol) were added in sequence to a mixture of compound **8**[553] (101 mg, 0.39 mmol) and *trans-tert*-butyl 2-(4-aminophenyl)cyclopropylcarbamate **10**[546] (81 mg, 0.33 mmol) in dry DMF (2.1 mL), and the resulting solution was stirred at room temperature overnight. The reaction was quenched with brine (5 mL) and concentrated under reduced pressure, and the aqueous phase was extracted with AcOEt (4×30 mL). The combined organic phases were washed with $NaHCO_3$ saturated solution (2×7 mL) and brine (5 mL). The organic phases were collected, dried over anhydrous Na_2SO_4, filtered and concentrated *in vacuo* to give a crude product that was purified by column chromatography on silica gel (eluent: $CHCl_3$/MeOH 100/1) to give compound **11**. ^{1}H-NMR (DMSO-d_6) δ_H/ppm: 1.10 (m, 2H, -CH_2- cyclopropane ring), 1.43 (s, 9H, $NHCO_2C(CH_3)_3$), 1.91 (m, 1H, -C*H*- cyclopropane ring), 2.62 (m, 1H, -C*H*- cyclopropane ring), 3.98 (s, 3H, CO_2CH_3), 7.12 (d, 2H, benzene ring), 7.24 (bs, 1H, CHN*H*CO_2tBu), 7.70 (d, 2H, benzene ring), 7.97 (m, 2H, bipyridine rings), 8.89 (s, 2H, bipyridine rings), 8.93 (m, 1H, bipyridine ring), 8.98 (m, 1H, bipyridine ring), 10.64 (bs, 1H, ArN*H*CO). ^{13}C-NMR (DMSO-d_6) δ_C/ppm: 15.6, 22.4, 29.3, 31.3, 49.7, 81.2, 117.8, 118.2, 121.1, 121.8, 122.6, 126.5, 132.4, 137.6, 142.8, 149.2, 150.0, 154.8, 155.3, 156.0, 159.2, 166.7, 168.8. MS, m/z: 489 $[M+H]^+$.

General Procedure for the Synthesis of *trans*-Methyl 4'-((4-(2-Aminocyclopropyl)phenyl)carbamoyl)-[2,2'-bipyridine]-4-carboxylate hydrochloride (2), *trans*-*N*-(4-(2-Aminocyclopropyl)phenyl)-8-hydroxyquinoline-5-carboxamide hydrochloride (3) and *trans*-*N*-(ω-((4-(2-Aminocyclopropyl)phenyl)amino)-ω-oxoalkyl)-8-hydroxyquinoline-5-carboxamide hydrochlorides (4-6). Example: *trans*-*N*-(4-((4-(2-Aminocyclopropyl)phenyl)amino)-4-oxobutyl)-8-hydroxyquinoline-5-carboxamide hydrochloride (4). Compound **18** (100 mg, 0.18 mmol, 1.0 eq) was dissolved in a mixture of dry THF/MeOH (1.4 mL/1.4 mL) and the solution stirred at 0 °C, then 4N HCl in 1,4-dioxane (3.65 mL, 14.58 mmol) was added dropwise and the mixture was allowed to warm at room temperature. After 3 hours, the suspension was cooled at 0 °C, and 4N HCl in 1,4-dioxane (1.82 mL, 7.29 mmol) was added dropwise again. After 8 hours, when conversion was complete, the suspension was filtered and washed with dry THF and then with dry Et_2O to afford compound **4** as a yellow hygroscopic solid. ^{1}H-NMR (DMSO-d_6) δ_H/ppm: 1.15 (m, 1H, -C*H*H- cyclopropane ring), 1.35 (m, 1H, -C*H*H- cyclopropane ring), 1.90 (m, 2H, $CH_2CH_2CH_2$), 2.28 (m, 1H, -C*H*- cyclopropane ring), 2.42 (m, 2H, CH_2CH_2CO), 2.74 (m, 1H, -CH- cyclopropane ring), 7.06 (d, 2H, benzene ring), 7.30 (d, 1H, quinoline ring), 7.52 (d, 2H, benzene ring), 7.87 (m, 2H, quinoline ring), 8.47 (bs, 3H, $CHNH_2{\cdot}HCl$), 8.65 (bs, 1H, $CONHCH_2$), 9.02 (d, 1H, quinoline ring), 9.24 (d, 1H, quinoline ring), 10.01 (s, 1H, ArN*H*CO), 11.40 (bs, 1H, quinoline OH). ^{13}C-NMR (DMSO-d_6) δ_C/ppm: 14.9, 22.8, 26.2, 28.5, 34.1, 40.1, 112.4, 119.7, 124.5, 126.7, 128.2, 128.5, 130.5, 131.1, 133.6, 135.3, 138.9, 150.3, 157.7, 162.1, 180.6. MS (relative to free amine), m/z: 405 $[M+H]^+$.

***trans*-Methyl 4'-((4-(2-Aminocyclopropyl)phenyl)carbamoyl)-[2,2'-bipyridine]-4-carboxylate hydrochloride (2).** ^{1}H-NMR (DMSO-d_6) δ_H/ppm: 1.22 (m, 1H, -CH*H*- cyclopropane ring), 1.39 (m, 1H, -CH*H*- cyclopropane ring), 2.34 (m, 1H, -C*H*- cyclopropane ring), 2.81 (m, 1H, -C*H*- cyclopropane ring), 3.97 (s, 3H, CO_2CH_3), 7.19 (d, 2H, benzene ring), 7.76 (d, 2H, benzene ring), 7.99 (m, 2H, bipyridine rings), 8.43 (bs, 3H, $CHNH_2{\cdot}HCl$), 8.89 (s, 2H, bipyridine rings), 8.94 (d, 1H, bipyridine ring), 8.98 (d, 1H, bipyridine ring), 10.71 (bs, 1H, ArN*H*CO). ^{13}C-NMR (DMSO-d_6) δ_C/ppm: 14.5, 22.4, 28.3, 52.0, 117.6, 118.1, 120.8, 122.1, 123.0, 125.8, 133.4, 137.5, 144.1, 149.9, 150.5, 155.2, 156.8, 158.2, 165.3, 166.4. MS (relative to free amine), m/z: 389 $[M+H]^+$.

***trans*-*N*-(4-(2-Aminocyclopropyl)phenyl)-8-hydroxyquinoline-5-carboxamide hydrochloride (3).** ^{1}H-NMR (DMSO-d_6) δ_H/ppm: 1.23 (m, 1H, -C*H*H- cyclopropane ring), 1.38 (m, 1H, -C*H*H- cyclopropane ring), 2.32 (m, 1H, -C*H*- cyclopropane ring), 2.80 (m, 1H, -CH- cyclopropane ring), 7.17 (d, 2H, benzene ring), 7.28 (d, 1H, quinoline ring), 7.72 (d, 2H, benzene ring), 7.79 (m, 1H, quinoline ring), 7.94 (d, 1H, quinoline ring), 8.38 (bs, 3H, $CHNH_2{\cdot}HCl$), 9.00 (m, 2H, quinoline ring), 10.47 (s, 1H, ArN*H*CO). ^{13}C-NMR (DMSO-d_6) δ_C/ppm: 14.8, 22.6, 28.2, 113.8, 121.7, 125.7,

126.8, 128.0, 129.1, 130.2, 130.9, 134.1, 135.8, 137.9, 152.1, 159.3, 165.1. MS (relative to free amine), m/z: 320 $[M+H]^+$.

***trans*-*N*-(5-((4-(2-Aminocyclopropyl)phenyl)amino)-5-oxopentyl)-8-hydroxyquinoline-5-carboxamide hydrochloride (5).** ^{1}H-NMR (DMSO-d_6) δ_H/ppm: 1.17 (m, 1H, -C*H*H- cyclopropane ring), 1.33 (m, 1H, -C*H*H- cyclopropane ring), 1.64 (m, 4H, $CH_2CH_2CH_2CH_2$), 2.26 (m, 1H, -C*H*- cyclopropane ring), 2.36 (t, 2H, CH_2CH_2CO), 2.75 (m, 1H, -CH- cyclopropane ring), 7.07 (d, 2H, benzene ring), 7.21 (d, 1H, quinoline ring), 7.53 (d, 2H, benzene ring), 7.78 (m, 2H, quinoline ring), 8.35 (bs, 3H, $CHNH_2{\cdot}HCl$), 8.57 (bs, 1H, $CONHCH_2$), 8.97 (d, 1H, quinoline ring), 9.06 (d, 1H, quinoline ring), 9.92 (s, 1H, ArN*H*CO), 11.10 (bs, 1H, quinoline OH). ^{13}C-NMR (DMSO-d_6) δ_C/ppm: 14.5, 22.3, 23.1, 28.0, 29.4, 38.3, 39.0, 114.4, 121.9, 125.4, 126.6, 127.9, 128.8, 130.5, 131.1, 134.7, 135.4, 138.9, 151.7, 159.3, 162.4, 179.7. MS (relative to free amine), m/z: 419 $[M+H]^+$.

***trans*-*N*-(6-((4-(2-Aminocyclopropyl)phenyl)amino)-6-oxohexyl)-8-hydroxyquinoline-5-carboxamide hydrochloride (6).** ^{1}H-NMR (DMSO-d_6) δ_H/ppm: 1.18 (m, 1H, -C*H*H- cyclopropane ring), 1.38 (m, 3H, -C*H*H- cyclopropane ring and $-CH_2$- aliphatic chain), 1.61 (m, 4H, aliphatic chain), 2.32 (m, 3H, -C*H*- cyclopropane ring and CH_2CH_2CO), 2.75 (m, 1H, -CH- cyclopropane ring), 3.33 (t, 2H, $NHCH_2CH_2$), 7.06 (d, 2H, benzene ring), 7.33 (d, 1H, quinoline ring), 7.52 (d, 2H, benzene ring), 7.85 (d, 1H, quinoline ring), 7.89 (m, 1H, quinoline ring), 8.43 (bs, 3H, $CHNH_2{\cdot}HCl$), 8.62 (bs, 1H, $CONHCH_2$), 9.03 (d, 1H, quinoline ring), 9.24 (d, 1H, quinoline ring), 9.92 (s, 1H, ArN*H*CO). ^{13}C-NMR (DMSO-d_6) δ_C/ppm: 14.3, 22.2, 25.2, 25.7, 28.1, 29.5, 38.4, 39.5, 114.3, 121.5, 125.8, 126.9, 127.7, 128.7, 130.4, 131.3, 134.5, 135.3, 138.8, 151.7, 159.5, 162.7, 179.8. MS (relative to free amine), m/z: 433 $[M+H]^+$.

4'-((4-(2-((*tert*-Butoxycarbonyl)amino)cyclopropyl)phenyl)carbamoyl)-[2,2'-bipyridine]-4-carboxylic acid (12). Compound **11** (111 mg, 0.227 mmol, 1.0 eq) was suspended in 4 mL of MeOH and cooled in an ice bath, then NaOH (27.3 mg, 0.682 mmol, 3.0 eq) in water (0.7 mL) was added dropwise and the mixture was allowed to stir at room temperature. After 9 hours the organic solvent was removed *in vacuo* and the aqueous phase, cooled at 0 °C, was acidified to pH 2 with a solution of 0.5N $KHSO_4$. The obtained suspension was filtered to afford the desired compound **12** (89%) as a yellow solid. ^{1}H-NMR (DMSO-d_6) δ_H/ppm: 1.11 (m, 2H, -C*H*$_2$- cyclopropane ring), 1.39 (s, 9H, $NHCO_2C(CH_3)_3$), 1.90 (m, 1H, -C*H*- cyclopropane ring), 2.62 (m, 1H, -C*H*- cyclopropane ring), 7.12 (d, 2H, benzene ring), 7.24 (bs, 1H, $CHNHCO_2tBu$), 7.70 (d, 2H, benzene ring), 7.95 (m, 2H, bipyridine rings), 8.88 (s, 2H, bipyridine rings), 8.94 (m, 2H, bipyridine ring), 10.64 (bs, 1H, ArN*H*CO), 13.89 (bs, 1H, COO*H*). ^{13}C-NMR (DMSO-d_6) δ_C/ppm: 14.1, 21.9, 27.8, 32.7, 80.3, 117.6, 118.2, 118.4, 120.1, 121.5, 124.4, 125.3, 134.0, 137.4, 144.9, 149.1, 149.9, 154.9, 155.4, 155.9, 159.5, 164.8, 170.1. MS, m/z: 475 $[M+H]^+$.

***trans*-4'-((4-(2-Aminocyclopropyl)phenyl)carbamoyl)-[2,2'-bipyridine]-4-carboxylic acid trifluoroacetate (1).** Trifluoroacetic acid (1.04 mL, 13.54 mmol, 230 eq) was added to **12** (28.2 mg, 0.059 mmol, 1.0 eq) placed in an ice bath, and the mixture was allowed to stir at room temperature. After 5 hours the solvent was removed at low temperature under reduced pressure, then the solid was stirred as suspension in dry Et_2O for 1 hour and filtered to provide the desired compound **1** (90%) as a dark red solid. ^{1}H-NMR (DMSO-d_6) δ_H/ppm: 1.23 (m, 1H, -C*H*H- cyclopropane ring), 1.33 (m, 1H, -C*H*H- cyclopropane ring), 2.28 (m, 1H, -C*H*- cyclopropane ring), 2.84 (m, 1H, -C*H*- cyclopropane ring), 7.20 (d, 2H, benzene ring), 7.74 (d, 2H, benzene ring), 7.96 (m, 2H, bipyridine rings), 8.26 (bs, 3H, N*H*$_2^+$CF$_3$COO*H*), 8.88 (s, 2H, bipyridine rings), 8.94 (m, 2H, bipyridine ring), 10.69 (bs, 1H, ArN*H*CO). ^{13}C-NMR (DMSO-d_6) δ_C/ppm: 14.9, 22.6, 28.2, 117.3, 117.9, 118.7, 120.7, 121.2, 124.1, 125.5, 134.5, 138.7, 144.9, 149.2, 149.8, 155.2, 156.1, 159.8, 162.2, 164.9, 170.4. MS (relative to free amine), m/z: 375 $[M+H]^+$.

8-(Methoxymethoxy)quinoline-5-carboxylic acid (13). 8-Hydroxyquinoline-5-carboxylic acid (2.41 g, 12.8 mmol, 1 eq) was added portion wise to a stirring suspension of 60% NaH (1.28 g, 31.9 mmol, 2.5 eq) in dry THF (30 mL) at 0 °C, and the resulting mixture was stirred under inert atmosphere (N_2) for 30 min. Then MOM-Br (2.5 mL, 30.6 mmol, 2.4 eq) dissolved in dry THF (20 mL) was added dropwise, and the suspension was allowed to warm to room temperature under inert atmosphere (N_2). After 4 hours, a solution of LiOH (1.22 g, 51.0 mmol, 4.0 eq) in water (25.5 mL) was added at 0 °C, and the resulting mixture was stirred at room temperature overnight. The reaction mixture was acidified with glacial acetic acid to pH 4 and then extracted with DCM (5×90 mL); the organic phases were collected, dried over anhydrous Na_2SO_4, filtered and the solvent removed under reduced pressure to give compound **13** (98%) as a white solid. ^{1}H-NMR (CD_3OD) δ_H/ppm: 2.09 (s, 3H, CH_2OCH_3), 4.08 (s, 2H, OCH_2OCH_3), 5.97 (d, 1H, quinoline ring), 6.18 (m, 1H, quinoline ring), 6.83 (d, 1H, quinoline ring), 7.39 (d, 1H, quinoline ring), 8.06 (d, 1H, quinoline ring). ^{13}C-NMR (CD_3OD) δ_C/ppm: 55.1, 95.3, 104.5, 119.0, 122.7, 126.5, 131.3, 133.1, 140.0, 148.1, 159.7, 167.5. MS**,** m/z: 234 $[M+H]^+$.

***trans-tert*-Butyl(2-(4-(8-(Methoxymethoxy)quinoline-5-carboxamido)phenyl) cyclopropyl) carbamate (14).** Compound **14** was prepared following the same procedure used for **11**, starting from **13** and **10**. ^{1}H-NMR ($CDCl_3$) δ_H/ppm: 1.19 (m, 2H, -CH_2- cyclopropane ring), 1.49 (s, 9H, $NHCO_2C(CH_3)_3$), 2.07 (m, 1H, -C*H*- cyclopropane ring), 2.74 (m, 1H, -C*H*- cyclopropane ring), 3.61 (s, 3H, CH_2OCH_3), 5.58 (s, 2H, OCH_2OCH_3), 7.21 (d, 2H, benzene ring), 7.44 (d, 1H, quinoline ring), 7.56 (m, 3H, quinoline ring and benzene ring), 7.67 (s, 1H, CON*H*Ar), 7.80 (d, 1H, quinoline ring), 8.93 (d, 1H, quinoline ring), 9.04 (d, 1H, quinoline ring). ^{13}C-NMR ($CDCl_3$) δ_C/ppm: 15.2, 23.3, 29.0, 32.8, 55.4, 80.5, 95.1, 107.8, 121.8, 125.3, 126.0, 127.7, 128.3, 130.0, 131.4, 133.8, 136.5, 138.1, 151.5, 156.4, 161.2, 164.4. MS**,** m/z: 464 $[M+H]^+$.

General Procedure for the Synthesis of 8-(Methoxymethoxy)quinoline-5-carboxyamidoalkyl Methyl Esters (15-17). Example: Methyl 4-({[8-(Methoxymethoxy)quinolin-5-yl]carbonyl}amino)butanoate (15). The reagents HOBT (382 mg, 2.40 mmol), EDCI (460 mg, 2.40 mmol) and Et_3N (1.12 mL, 8 mmol) were added in sequence to a mixture of **13** (560 mg, 2.40 mmol) and methyl 4-aminobutanoate hydrochloride (306 mg, 2 mmol) in dry DCM (12 mL), and the solution was stirred at room temperature. After overnight stirring, the reaction mixture was diluted with DCM (90 mL) and the organic phase washed with Na_2CO_3 (2×50 mL) and brine (2×50 mL), dried over anhydrous Na_2SO_4, filtered and concentrated *in vacuo* to give a residue that was purified by column chromatography on silica gel (eluent: DCM/MeOH 35/1). The collected fractions were evaporated and the resulting crude was finally recrystallized from benzene/cyclohexane to afford compound **15** (83%) as a white solid. ^{1}H-NMR ($CDCl_3$) δ_H/ppm: 2.04 (m, 2H, $NCH_2CH_2CH_2$), 2.52 (t, 2H, $CH_2CH_2CO_2Me$), 3.61 (m, 5H, $NHCH_2CH_2$ and CO_2CH_3), 3.70 (s, 3H, OCH_2OCH_3), 5.56 (s, 2H, OCH_2OCH_3), 6.32 (bs, 1H, $CONHCH_2$), 7.39 (d, 1H, quinoline ring), 7.53 (m, 1H, quinoline ring), 7.66 (d, 1H, quinoline ring), 8.91 (d, 1H, quinoline ring), 9.01 (d, 1H, quinoline ring). ^{13}C-NMR ($CDCl_3$) δ_C/ppm: 22.8, 29.5, 40.3, 50.7, 55.4, 92.7, 107.8, 126.3, 129.7, 130.1, 131.3, 131.9, 137.5, 151.3, 163.4, 165.0, 176.1. MS, m/z: 333 $[M+H]^+$.

Methyl 5-({[8-(Methoxymethoxy)quinolin-5-yl]carbonyl}amino)pentanoate (16). ^{1}H-NMR ($CDCl_3$) δ_H/ppm: 1.77 (m, 4H, $CH_2CH_2CH_2CH_2$), 2.44 (t, 2H, $CH_2CH_2CO_2Me$), 3.53 (m, 2H, $NHCH_2CH_2$), 3.60 (s, 3H, CO_2CH_3), 3.71 (s, 3H, OCH_2OCH_3), 5.56 (s, 2H, OCH_2OCH_3), 6.16 (bs, 1H, $CONHCH_2$), 7.39 (d, 1H, quinoline ring), 7.53 (m, 1H, quinoline ring), 7.67 (d, 1H, quinoline ring), 8.89 (d, 1H, quinoline ring), 9.00 (d, 1H, quinoline ring). ^{13}C-NMR ($CDCl_3$) δ_C/ppm: 22.3, 30.1, 32.4, 39.7, 52.6, 56.6, 92.7, 111.2, 128.1, 128.7, 130.2, 132.1, 133.7, 137.9, 155.3, 163.4, 164.1, 176.7. MS, m/z: 347 $[M+H]^+$.

Methyl 6-({[8-(Methoxymethoxy)quinolin-5-yl]carbonyl}amino)hexanoate (17). ^{1}H-NMR ($CDCl_3$) δ_H/ppm: 1.50 (m, 2H, aliphatic chain), 1.72 (m, 4H, aliphatic chain), 2.38 (t, 2H, $CH_2CH_2CO_2Me$), 3.55 (m, 2H, $NHCH_2CH_2$), 3.60 (s, 3H, CH_2OCH_3), 3.69 (s, 3H, CO_2CH3), 5.56 (s, 2H, OCH_2OCH_3), 6.06 (bs, 1H, $CONHCH_2$), 7.39 (d, 1H, quinoline ring), 7.53 (m, 1H, quinoline ring), 7.65 (d, 1H, quinoline ring), 8.87 (d, 1H, quinoline ring), 9.01 (d, 1H, quinoline ring).^{13}C-NMR ($CDCl_3$) δ_C/ppm: 24.3, 25.2, 30.1, 32.9, 41.6, 51.7, 57.6, 93.2, 109.8, 123.2, 128.9, 129.6, 131.2, 132.3, 135.2, 153.8, 161.1, 162.8, 175.8. MS, m/z: 361 $[M+H]^+$.

General Procedure for the Synthesis of *trans*-*tert*-Butyl (2-(4-(ω-(8-(Methoxymethoxy)quinoline-5-carboxamido)alkylamido)phenyl)cyclopropyl) carbamate (18-20). Example: *trans*-*tert*-Butyl (2-(4-(6-(8-(Methoxymethoxy)quinoline-5-carboxamido)hexanamido)phenyl)cyclopropyl)carbamate (20). LiOH (102 mg, 4.26 mmol) dissolved in water (3 mL) was added to a stirred solution of **17** (360 mg, 1.07 mmol) in THF (4 mL) placed on an ice bath, and the resulting mixture was

stirred at room temperature overnight. The reaction was acidified with glacial acetic acid to pH 4-5, then diluted with DCM (50 mL) and extracted; the aqueous phase was further extracted with DCM (9×50 mL). The organic phases were collected, dried over anhydrous Na_2SO_4, filtered and concentrated *in vacuo* to afford the 5-({[8-(methoxymethoxy)quinolin-5-yl]carbonyl}amino)hexanoic acid (300 mg, 85%) as a white solid that was used in the next step without further purification. HOBT (92 mg, 0.58 mmol), EDCI (110 mg, 0.58 mmol) and Et_3N (0.24 mL, 1.70 mmol) were added in sequence to a mixture of 5-({[8-(methoxymethoxy)quinolin-5-yl]carbonyl}amino)hexanoic acid (190 mg, 0.58 mmol) and *trans-tert*-butyl 2-(4-aminophenyl)cyclopropylcarbamate **10**[544] (132 mg, 0.53 mmol) in dry DMF (4.2 mL) and the resulting solution was stirred at room temperature. After 18 h the solvent was evaporated under reduced pressure and the residue partitioned between AcOEt (100 mL) and brine (20 mL). The organic phase was further washed with $NaHCO_3$ saturated solution (2 × 40 mL) and the aqueous phases back-extracted with AcOEt (40 mL). The organic phases were collected, dried over anhydrous Na_2SO_4, filtered and concentrated *in vacuo* to give a crude product that was purified by column chromatography on silica gel (eluent: $CHCl_3$/MeOH 30/1) to give compound **20** (74%) as a yellow foam. ^{1}H-NMR ($CDCl_3$) δ_H/ppm: 1.15 (m, 2H, -C*H*$_2$- cyclopropane ring), 1.47 (s, 9H, $NCO_2C(CH_3)_3$), 1.53 (m, 2H, aliphatic chain), 1.72 (m, 2H, aliphatic chain), 1.81 (m, 2H, aliphatic chain), 2.02 (m, 1H, -C*H*- cyclopropane ring), 2.40 (t, 2H, CH_2CH_2CO), 2.68 (m, 1H, -C*H*- cyclopropane ring), 3.57 (m, 5H, $NHCH_2CH_2$ and CH_2OCH_3), 4.88 (bs, 1H, $CHNHCO_2tBu$), 5.55 (s, 2H, OCH_2OCH_3), 6.28 (bs, 1H, $CONHCH_2$), 7.07 (d, 2H, benzene ring), 7.35 (m, 2H, quinoline ring and ArNHCO), 7.40 (d, 2H, benzene ring), 7.50 (m, 1H, quinoline ring), 7.65 (d, 1H, quinoline ring), 8.87 (d, 1H, quinoline ring), 9.00 (d, 1H, quinoline ring). ^{13}C-NMR ($CDCl_3$) δ_C/ppm: 16.3, 21.7, 24.6, 26.7, 29.1, 29.7, 32.5, 37.6, 39.3, 53.8, 79.1, 89.4, 107.5, 124.6, 127.3, 127.8, 128.2, 129.3, 132,5, 133.6, 135.0, 139.2, 140.6, 151.0, 153.3, 159.8, 162.7, 182.9. MS, m/z: 577 $[M+H]^+$.

***trans-tert*-Butyl (2-(4-(4-(8-(Methoxymethoxy)quinoline-5-carboxamido)butanamido)phenyl)cyclopropyl)carbamate (18).** ^{1}H-NMR ($CDCl_3$) δ_H/ppm: 1.14 (m, 2H, -C*H*$_2$- cyclopropane ring), 1.47 (s, 9H, $NCO_2C(CH_3)_3$), 2.02 (m, 1H, -C*H*- cyclopropane ring), 2.09 (m, 2H, $CH_2CH_2CH_2$), 2.53 (t, 2H, CH_2CH_2CONH), 2.69 (m, 1H, -C*H*- cyclopropane ring), 3.59 (s, 3H, CH_2OCH_3), 3.66 (m, 2H, $NHCH_2CH_2$), 4.89 (bs, 1H, $CHNHCO_2tBu$), 5.54 (s, 2H, OCH_2OCH_3), 6.65 (bs, 1H, $CONHCH_2$), 7.08 (d, 2H, benzene ring), 7.32 (d, 1H, quinoline ring), 7.50 (m, 3H, benzene ring and quinoline ring), 7.65 (d, 1H, quinoline ring), 8.46 (bs, 1H, ArNHCO), 8.89 (d, 1H, quinoline ring), 9.00 (d, 1H, quinoline ring). ^{13}C-NMR ($CDCl_3$) δ_C/ppm: 16.0, 22.1, 26.8, 27.5, 32.3, 35.8, 39.0, 53.5, 80.2, 95.5, 107.4, 119.6, 126.6, 126.9, 128.3, 129.3, 131.5, 133.9, 135.1, 137.7, 141.8, 148.8, 155.9, 159.5, 165.6, 184.4. MS, m/z: 549 $[M+H]^+$.

***trans-tert*-Butyl (2-(4-(5-(8-(Methoxymethoxy)quinoline-5-carboxamido)pentanamido)phenyl)cyclopropyl)carbamate (19).** ^{1}H-NMR

($CDCl_3$) δ_H/ppm: 1.15 (m, 2H, -C*H*$_2$- cyclopropane ring), 1.47 (s, 9H, $NHCO_2C(CH_3)_3$), 1.78 (m, 2H, aliphatic chain) 1.87 (m, 2H, aliphatic chain), 2.02 (m, 1H, -C*H*- cyclopropane ring), 2.09 (m, 2H, $CH_2CH_2CH_2$), 2.49 (t, 2H, CH_2CH_2CO), 2.68 (m, 1H, -C*H*- cyclopropane ring), 3.58 (m, 5H, $NHCH_2CH_2$ and CH_2OCH_3), 4.87 (bs, 1H, N*H*CO_2tBu), 5.56 (s, 2H, OCH_2OCH_3), 6.41 (bs, 1H, CON*H*CH_2), 7.07 (d, 2H, benzene ring), 7.38 (d, 1H, quinoline ring), 7.45 (m, 3H, benzene ring and quinoline ring), 7.64 (bs, 1H, ArN*H*CO), 7.68 (d, 1H, quinoline ring), 8.85 (d, 1H, quinoline ring), 9.00 (d, 1H, quinoline ring). ^{13}C-NMR ($CDCl_3$) δ_C/ppm: 15.8, 21.7, 21.9, 27.8, 29.1, 29.8, 37.7, 39.4, 53.0, 80.1, 93.8, 106.9, 123.4, 126.6, 127.0, 127.5, 128.4, 130.0, 131.8, 136.1, 137.7, 138.1, 149.7, 156.5, 161.2, 164.4, 182.2. MS, m/z: 563 $[M+H]^+$.

General Procedure for the Synthesis of ω-(8-Hydroxyquinoline-5-carboxamido)alkyl Methyl Esters (21-23). Example: Methyl 5-(8-Hydroxyquinoline-5-carboxamido)pentanoate (22). Compound **16** (150 mg, 0.43 mmol, 1.0 eq) was dissolved in a mixture of dry THF/MeOH (2 mL/2 mL) and the solution was stirred at 0 °C, then 4N HCl in 1,4-dioxane (6.5 mL, 25.98 mmol, 60 eq) was added dropwise, and the mixture was allowed to warm to room temperature. After 6 hours, when conversion was complete, the suspension was filtered and washed with dry Et_2O to give compound **22** (95%) as a yellow solid. ^{1}H-NMR (DMSO-d_6) δ_H/ppm: 1.60 (m, 4H, $CH_2CH_2CH_2CH_2$), 2.38 (t, 2H, $CH_2CH_2CO_2Me$), 3.32 (m, 2H, $NHCH_2CH_2$), 3.60 (s, 3H, CO_2CH_3), 7.44 (d,1H, quinoline ring), 7.92 (d, 1H, quinoline ring), 8.00 (m, 1H, quinoline ring), 8.70 (bs, 1H, CON*H*CH_2), 9.08 (d, 1H, quinoline ring), 9.39 (m, 1H, quinoline ring), 12.17 (bs, 1H, ArO*H*). ^{13}C-NMR (DMSO-d_6) δ_C/ppm: 22.9, 29.7, 32.8, 40.1, 50.8, 111.6, 126.5, 128.5, 131.6, 132.0, 134.9, 140.2, 153.0, 161.2, 163.8, 175.9. MS, m/z: 303 $[M+H]^+$.

Methyl 6-(8-Hydroxyquinoline-5-carboxamido)hexanoate (23). ^{1}H-NMR (DMSO-d_6) δ_H/ppm: 1.37 (m, 2H, aliphatic chain), 1.59 (m, 4H, aliphatic chain), 2.33 (t, 2H, $CH_2CH_2CO_2Me$), 3.30 (m, 2H, $NHCH_2CH_2$), 7.28 (d, 1H, quinoline ring), 7.82 (d, 1H, quinoline ring), 7.87 (m, 1H, quinoline ring), 8.57 (bs, 1H, CON*H*CH_2), 9.02 (d, 1H, quinoline ring), 9.18 (d, 1H, quinoline ring), 11.35 (bs, 1H, ArO*H*). ^{13}C-NMR (DMSO-d_6) δ_C/ppm: 24.5, 26.4, 30.0, 32.7, 40.4, 51.5, 109.5, 122.6, 130.4, 130.8, 133.0, 133.7, 134.0, 152.5, 160.8, 163.0, 174.1. MS, m/z: 317 $[M+H]^+$.

Methyl 4-(8-Hydroxyquinoline-5-carboxamido)butanoate (21). ^{1}H-NMR (DMSO-d_6) δ_H/ppm: 1.84 (m, 2H, $CH_2CH_2CH_2$), 2.42 (t, 2H, $CH_2CH_2CO_2Me$), 3.61 (s, 3H, CO_2CH_3), 7.09 (d, 1H, quinoline ring), 7.62 (m, 1H, quinoline ring), 7.69 (d, 1H, quinoline ring), 8.43 (bs, 1H, CON*H*CH_2), 8.87 (m, 2H, quinoline ring), 10.21 (bs, 1H, ArO*H*). ^{13}C-NMR (DMSO-d_6) δ_C/ppm: 23.6, 30.0, 39.7, 50.2, 107.7, 126.8, 129.8, 130.0, 133.1, 133.8, 136.8, 151.2, 162.7, 164.9, 176.0. MS**,** m/z: 289 $[M+H]^+$.

General Procedure for the Synthesis of ω-(8-Hydroxyquinoline-5-carboxamido)alkanoic acids (24-26). Example: 5-(8-Hydroxyquinoline-5-

carboxamido)pentanoic acid (25). A solution of LiOH (47 mg, 1.11 mmol, 3.0 eq) in water (0.6 mL) was added to a stirred solution of compound **22** (112 mg, 0.37 mmol, 1.0 eq) in THF (1.3 mL) placed on an ice bath, and the resulting mixture was stirred at room temperature overnight. The solvent was removed, $NaHCO_3$ saturated solution (10 mL) was added and the aqueous phase was washed with AcOEt (3 × 10 mL). The aqueous solution was acidified with glacial acetic acid to pH 4, then extracted with AcOEt (5×20 mL). The organic phases were collected, dried over anhydrous Na_2SO_4, filtered and concentrated *in vacuo* to afford compound **25** (96%) as an off yellow solid. ^{1}H-NMR (DMSO-d_6) δ_H/ppm: 1.58 (m, 4H, aliphatic chain), 2.30 (t, 2H, $CH_2CH_2CO_2H$), 7.08 (d, 1H, quinoline ring), 7.62 (m, 1H, quinoline ring), 7.68 (d, 1H, quinoline ring), 8.41 (bs, 1H, $CONHCH_2$), 8.84 (d, 1H, quinoline ring), 8.88 (d, 1H, quinoline ring), 10.17 (bs, 1H, ArOH), 11.98 (bs, 1H, CH_2CO_2H). ^{13}C-NMR (DMSO-d_6) δ_C/ppm: 22.6, 29.8, 33.3, 39.9, 111.1, 126.3, 128.4, 128.7, 131.8, 132.7, 136.0, 151.0, 160.1, 162.9, 177.9. MS, m/z: 289 $[M+H]^+$.

5-(8-Hydroxyquinoline-5-carboxamido)hexanoic acid (26). ^{1}H-NMR (DMSO-d_6) δ_H/ppm: 1.38 (m, 2H, aliphatic chain), 1.57 (m, 4H, aliphatic chain), 2.23 (t, 2H, $CH_2CH_2CO_2H$), 7.08 (d, 1H, quinoline ring), 7.62 (m, 1H, quinoline ring), 7.69 (d, 1H, quinoline ring), 8.41 (bs, 1H, $CONHCH_2$), 8.83 (d, 1H, quinoline ring), 8.88 (d, 1H, quinoline ring), 10.16 (bs, 1H, ArOH), 12.00 (bs, 1H, CH_2CO_2H). ^{13}C-NMR (DMSO-d_6) δ_C/ppm: 24.3, 27.2, 29.0, 34.5, 40.1, 110.4, 125.8, 128.8, 129.1, 131.9, 132.5, 133.9, 153.4, 158.5, 162.3, 175.5. MS, m/z: 303 $[M+H]^+$.

5-(8-Hydroxyquinoline-5-carboxamido)butanoic acid (24). ^{1}H-NMR (DMSO-d_6) δ_H/ppm: 1.79 (m, 2H, $CH_2CH_2CH_2$), 2.32 (m, 2H, $CH_2CH_2CO_2H$), 7.08 (d, 1H, quinoline ring), 7.62 (m, 1H, quinoline ring), 7.69 (d, 1H, quinoline ring), 8.44 (bs, 1H, $CONHCH_2$), 8.84 (d, 1H, quinoline ring), 8.89 (d, 1H, quinoline ring), 10.20 (bs, 1H, ArOH), 12.05 (bs, 1H, CH_2CO_2H). ^{13}C-NMR (DMSO-d_6) δ_C/ppm: 23.2, 33.2, 39.5, 110.8, 126.0, 128.5, 128.7, 131.9, 132.2, 135.5, 151.0, 159.7, 162.9, 178.8. MS, m/z: 275 $[M+H]^+$.

11.4. Biological evaluation, results and discussion

11.4.1. KDM inhibitory assays

Compounds **1-6** were tested against LSD1 and a subfamily representative panel of JmjC KDMs including KDM4. In LSD1 inhibition assays, the tested compounds all showed single-digit (**1**, **5**, **6**) or submicromolar (**2-4**) IC_{50} values, with similar or increased potencies respect to the reference **7** (Table 11.3, 11.4). Compounds **1-3** were also tested against MAO-A and MAO-B to assess their selectivity towards LSD1: at the tested conditions, **1** and **3** were definitively more effective in inhibiting LSD1 than MAOs, while **2** was less potent against MAO-B but showed similar inhibitory potency against MAO-A respect to LSD1, analogously to what observed with other tranylcypromine- based compounds (Table 11.3).[544] Inhibition of the JmjC KDMs by the hybrid compounds **1-6** (Table 11.4) was then investigated, using **8** and **9** as

references. Interestingly, both 8HQ (compounds **3-6**) and bipyridine (compound **1**) hybrid inhibitors showed similar potencies against JmjC KDMs as the reference compounds **8** and **9**, demonstrating that the conjugation of tranylcypromine does not adversely affect activity. Compound **1** displayed low-or sub-micromolar activity against all the tested JmjCs, thus being the most potent of the series. Importantly, when tested against the hypoxia inducible factor hydroxylases FIH and PHD2, the former of which is closely related to the JmjC KDMs, **1** showed no/weak inhibition, revealing high KDM-selectivity. Consistent with previous SAR for the bipyridine derivatives, the free acid is required for high potency against JmjC KDMs as the ester "pro-drug" form (**2**) weakens the potency. Single digit (9 out of 10) values were obtained for **2-6** against KDM4, the KDM subfamily that has been shown to work synergistically with LSD1 (Table 11.3, 11.4).[559]

Table 11.3. Inhibition of both LSD1 enzyme by pan-demethylase inhibitors **1-6**. Compound **7-9** are used as refence

cpd	**IC_{50}, µM**		
	LSD1 (KDM1)	MAO A	MAO B
1	2.2	35.4	47.0
2	<1	<1	43.3
3	<1	8.9	81.0
4	<1		
5	1.6		
6	1.0		
7	2.1	4.5	2.5
8	>100		
9	ND[a]		

Inhibition assays were performed in duplicate. The errors in determinations of IC_{50}s are within ±10% of their values. [a]ND, Not Detectable. Compound **9** interferes with the peroxidase used in the coupled enzymatic assay and the inhibition could not be reliably measured.

Table 11.4. Inhibition of JmjC enzymes by pan-demethylase inhibitors **1**-**6**. The KDM subfamily of each enzyme is reported among brackets. Single family-specific target inhibitors **7**-**9** were used as references.

cpd	IC_{50}, μM							
	FBXL11 (KDM2/7)	JMJD1A (KDM3)	JMJD2C (KDM4)	JMJD2E (KDM4)	JARID1C (KDM5)	JMJD3 (KDM6)	FIH	PHD2
1	0.22	0.14	0.07	0.42	0.19	2.7	>100	278
2	12.2	37	2.7	16	8.5	76		
3	7.8	31	1.2	3.9	26	27	25	8.5
4	12	12	4.5	5.5	35	18		
5	8.2	9.7	3.1	3.5	21	14		
6	12	9.1	2.5	5.1	37	16		
7	>100	>100	>100	>100	>100	>100		
8	4.8	1.1	3.5	5.0	0.03	11.2		
9	15	0.17	0.6	0.3	25	0.14		

Inhibition assays were performed in duplicate. The errors in determinations of IC_{50}s are within ±10% of their values.

11.4.1.1. Methods

LSD1 assay. His-tagged recombinant form of human LSD1 comprising residues 171-836 was copurified with a glutathione transferase-tagged CoREST protein (residues 308-440) as described.[544] The potency of the inhibitors was evaluated by measuring their IC_{50} using a coupled enzymatic assay monitoring hydrogen peroxide formation. A peptide corresponding to the *N*-terminal 21 amino acids of H3 monomethylated on Lysine 4 was used as substrate at the fixed concentration of 29 μM (five-fold the K_m). The reaction mixture contained 50 mM Hepes pH 7.5, 0.1 mM 4-aminoantipyrine, 1 mM 3,5- dichloro-2-hydroxybenzenesulfonic acid, 2.8 μM horseradish peroxidase, 1 μM LSD1/CoREST. The enzyme was incubated for five minutes at room temperature before measuring the enzymatic activity.

MAO-A and MAO-B assays. Recombinant human MAO-A and -B were expressed in *P. pastoris* and purified as described.[544] IC_{50} values were measured with the peroxidase-coupled assay using benzylamine (MAO-B) and kynuramine (MAO-A) as substrates, at the fixed concentration of 333 μM (1.5 fold the K_m). The protein

(16.7 nM) was titrated with increasing concentrations of inhibitor (5 minute incubation at room temperature). The reaction mixture contained 50 mM Hepes pH 7.5, 0.025% (w/v) reduced Triton-X100, 0.1 mM Amplex Red, 2.8 μM horseradish peroxidase, 16 nM enzyme.

JmjC inhibitory assays. *Materials.* Anti-histone H3 (dimethyl K9) (Abcam), antihistone H3 (trimethyl K9) (Abcam), anti-histone H3 (dimethyl K4) (Abcam), anti-histone H3 (trimethyl K4) (Diagenode) goat anti-mouse Alexafluor 488 (Invitrogen) or goat anti-rabbit Alexafluor 488 (Invitrogen).
2OG oxygenase enzyme assay. All recombinant 2OG oxygenase enzymes were produced as described.[628] The IC50 values of inhibitors against JmjC containing KDMs were determined using AlphaScreen as described.[608] RapidFire mass spectrometry based assay methods were used for PHD2 and FIH.

*11.4.2. Effects of **2** and **3** on histone methylation in HeLa cells*

We then investigated whether the pan-demethylase inhibitors **1**, **2** and **3** affect selected global histone methylation states in HeLa cells, using immunofluorescence based methods (Figure 11.3).

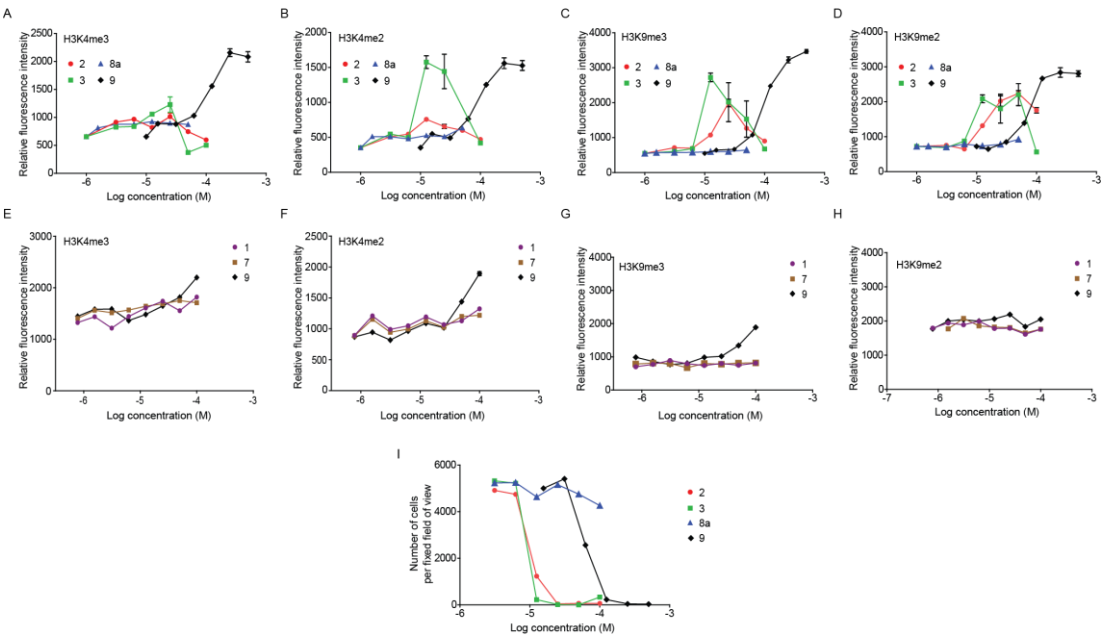

Figure 11.3. Detection of changes in the global histone methylation levels in HeLa cells after treatment with **1**, **2**, **3**, **7**, **8a** and **9** over 72 h using an immunofluorescence-based assay (A-H). Cytotoxicity of compounds **2**, **3** and **8a** at high doses is shown as number of cells per fixed field of view (I).

Compounds **7** for LSD1, and **8a**[558] (a pro-drug form of **8**,[490] Figure 11.1) and **9** for JmjC enzymes, were used as references. The hybrid inhibitors **2** and **3** caused substantial, dose-dependent increases of methyl marks at lower concentrations than **9**, whereas **7** caused essentially no changes in the overall methylation levels (including H3K4 methylations), in agreement with previous studies.[479,609,610] The

lack of effects on H3K4me3 may reflect the weaker inhibition of H3K4 demethylases (JARID/KDM5) over H3K9me3 KDMs (KDM4), coupled to the simultaneous effect of inhibiting the H3K4me2 selective demethylase LSD1 (Table 11.3, 11.4) or more complex effects due to inhibition of multiple targets. The 2,2'-bipyridine derivative **2** caused a H3K9me2/3-specific dose-dependent hypermethylation effect, whereas **8a** and **7** alone had no effect. This observation suggests that the "hybridization" of the bipyridyl and tranylcypromine motif has a synergistic effect, with respect to inhibition of LSD1 and KDM4/3 families. There was a general decrease in the immunofluorescence signal at higher doses where toxicity was observed (Figure 11.3I).

11.4.2.1.Methods

Cell culturing. HeLa cells were maintained in OptiMEM media supplemented with 0.5% foetal calf serum and 1% penicillin-streptomycin. Cells (1500 cells per well) were seeded into 96-well optical grade plate (Becton Dickinson) and left overnight to adhere. Test compounds were diluted in culture medium at a concentration of 100 μM, further serially diluted at a ratio of 1:2 (1% DMSO final), and incubated on the adhered HeLa cells. Media containing inhibitors was replaced every 24 h for 3 day period.

Immunostaining. Cells were rinsed with phosphate buffered saline (PBS) and fixed in 4% paraformaldehyde (20 min) and permeabilised with 0.5% TritonX-100 (10 min), followed by another PBS rinse. The cells were blocked (30 min) with 3% foetal calf serum diluted in PBS and further incubated overnight in primary antibody (1:500) diluted in blocking solution. Cells were rinsed three times with PBS, followed by incubation with the secondary antibody for 1 hour. After PBS rinses (×3), cells were stained with DAPI.

Image acquisition and analysis. The Pathway (Beckton Dickinson), an automated high-content imaging platform, was used to image the immunostained cells in the 96-well plate configuration. For each well, the system acquired a 3-by-3 tile-scanned image for Alexafluor 488 and DAPI. During analysis, the Pathway's software used the DAPI staining to identify nuclei as regions-of-interests (ROI). For each nucleus, the software extracted the average intensity of the histone staining, followed by the average intensity of all the nuclei in that particular well. The number of remaining cells and average nuclear size of each well was also calculated from the DAPI image. These three parameters from each well were then plotted against the corresponding concentration to obtain a dose response curve, which was plotted in GraphPad Prism 5.

11.4.3. Effects of pan-KDM inhibitors in human prostate LNCaP and colon HCT116 cancer cells

Compounds **1**-**6** (50 μM) were tested in human prostate LNCaP and colon HCT116 cancer cells to investigate their effects on cell cycle (after 30 h), apoptosis (after 30 h) and differentiation (after 48 h), using **7**-**9** as references. In LNCaP cells, **2**, **3** and **6** caused a strong G1 phase arrest (≥ 90%) with a substantial fraction of the cells in pre-G1 stage consistent with apoptosis induction, especially for **2** and **3** (Figure 11.4A). In HCT116 cells, the pan-inhibitors **3** and **5** and the JmjC selective inhibitor **9** displayed cell cycle alteration when compared to controls; however, as with the LNCaP cells, only compounds **2** and **3** induced the pre-G1 phase accumulation (Figure 11.4B). Dose-response curves for apoptosis in LNCaP and HCT116 cells were detected after treatment of cells for 48 h with **2** and **3** at doses from 10 to 100 μM (Figure 11.4C). When compared in independent experiments to a combination of the single-family target inhibitors **7** and **8**, **2** and **3** showed much more efficacy in inducing apoptosis both in LNCaP and HCT116 cells (at 50 μM for 24 h; Figure 11.5). To assess their differential toxicity, compounds **2** and **3** were also tested (50 μM, 24 h) in mesenchymal progenitor (MePR) cells [611]: in this non-cancer cell line **2** increased the pre-G1 peak percentage from 8.4 to 12.8% respect to the control, while with **3** the same value was under the control value (4.2%), suggesting a cancer cell-selective apoptotic induction for the two pan-KDM inhibitors (Figure 11.5).

A)

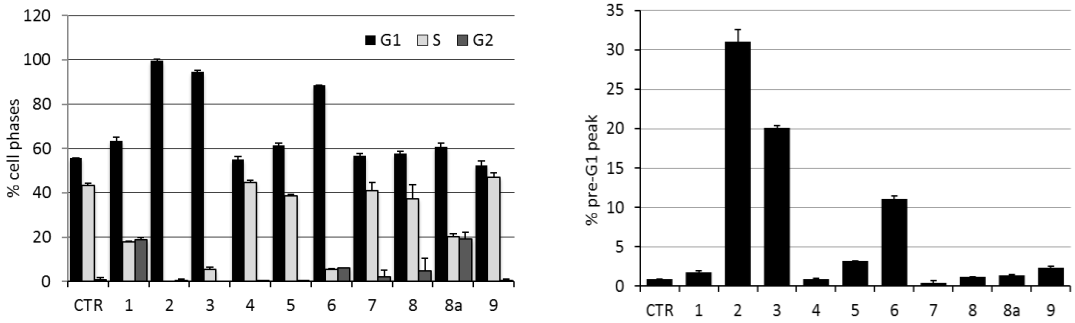

B)

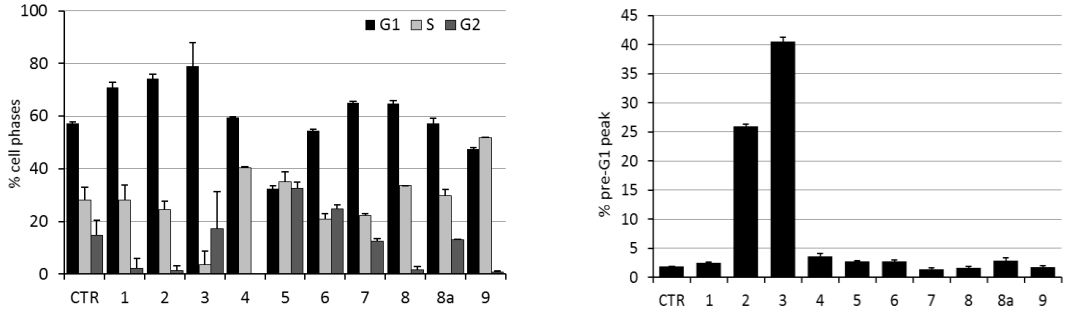

C)

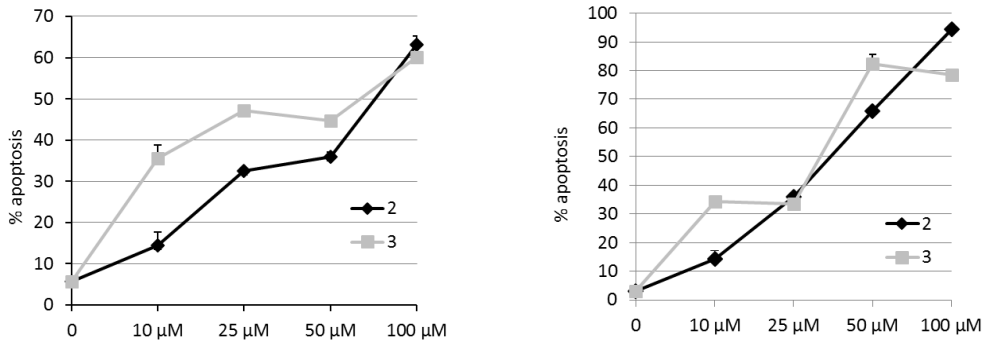

Figure 11.4. Effects of pan-demethylase inhibitors **1**-**6** in LNCaP and in HCT116 cells. Cell cycle effect (left) and percentage of cells at pre-G1 peak (right) of **1**-**9** (50 µM, 30 h) in LNCaP (A) and HCT116 (B) cells. (C) dose-response curves with **2** and **3** for apoptosis (48h) in LNCaP (left) and HCT116 (right) cells.

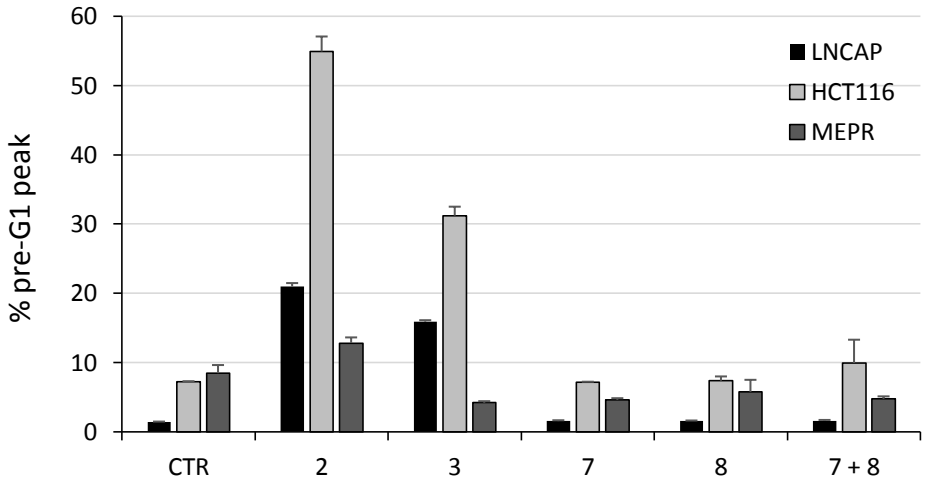

Figure 11.5. Comparison of effects on pre-G1 peak accumulation for **2**, **3**, **7**, **8** and combination of **7** plus **8** (50 µM, 24 h) in LNCaP, HCT116, and MePR cells.

Despite differences in number of cells in pre-G1 phase, among Figure 11.4 and 11.5, compounds **2** and **3** induced cell death in cancer specific manner. These differences, however, could be due to cell populations (ie, the value of percentage of pre-G1 for the untreated HCT116 cells was around 2% in Figure 11.4 and around 8% in Figure 11.5). Also times of induction (30 h in Figure 11.4 and 24 h in Figure 11.5) could justify the differences among percentages in data.

Effects on cell proliferation and migration were detected by treating LNCaP and HCT116 cells with 50µM **2** and **3** up to 72 h, using the HDAC inhibitor SAHA as a positive control. In LNCaP cells, **2** showed similar growth arrest as SAHA, while **3** was less effective (Figure 11.6A, left). Differently from SAHA, neither **2** or **3** was

able to stop migration in this cell line (Figure 11.6A, right). In HCT116 cells, strong antiproliferative effects for **2** and **3** were detected even after 6 h (Figure 11.6B, left), while the corresponding SAHA effect appeared only at 72 h. In this cell line, **2** and SAHA strongly hampered migration, while **3** had no effect (Figure 11.6B, right).

A)

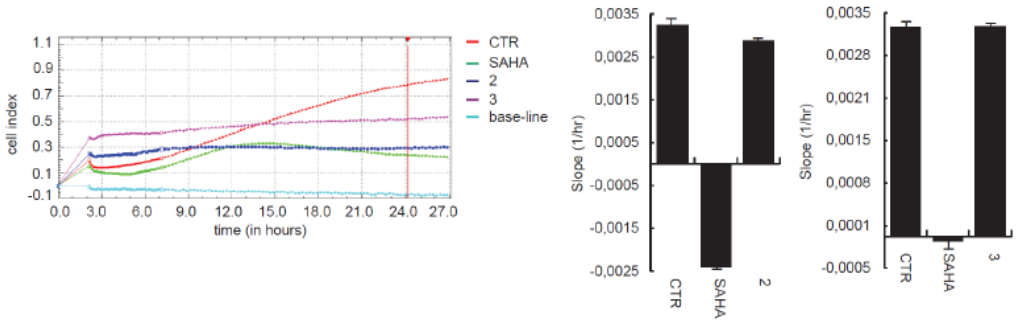

B)

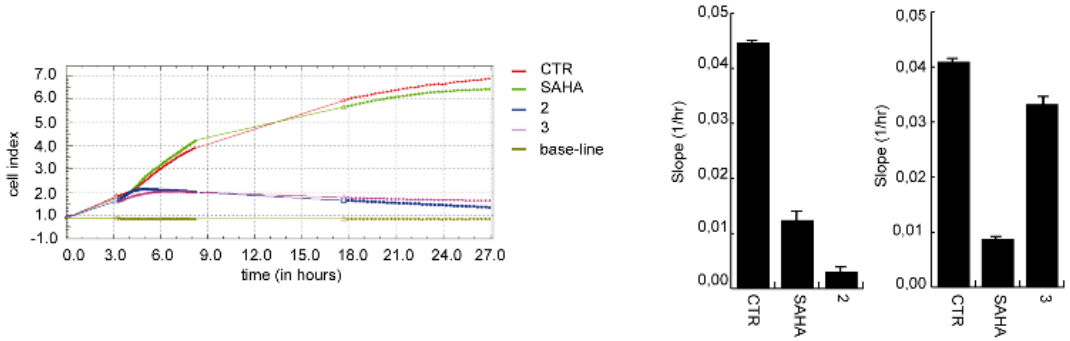

Figure 11.6. Proliferation curves and cell migration relative to LNCaP (A) and HCT116 (B) cell lines after 24h. The HDAC inhibitor SAHA is used as a reference drug. Left: proliferation curves after 24h. Control (untreated cells) in red, cells treated with SAHA (5 μM) in green, cells treated with **2** (50μM) in blue, cells treated with **3** (50 μM) in violet, in blue (LNCaP, A) or yellow-green (HCT116, B) the base lines. Right: cell migration after 24 h. Histograms have been represented by slope relative to the control (untreated cells), cells treated SAHA (5 μM), cells treated with **2** (50 μM) and cells treated with **3** (50 μM). Data show the mean value from three parallel experiments with error bars showing the standard deviations on top of each column.

Western blot analysis using mark-specific antibodies supported the proposal that the effects of **2** and **3** in LNCaP and HCT116 cells are due to both LSD1 and JmjC inhibition. Figure 11.7 shows increased H3K4me2/3 and H3K9me3 methylation after treatment with 50 μM **2** and **3**.

A) LNCaP cells

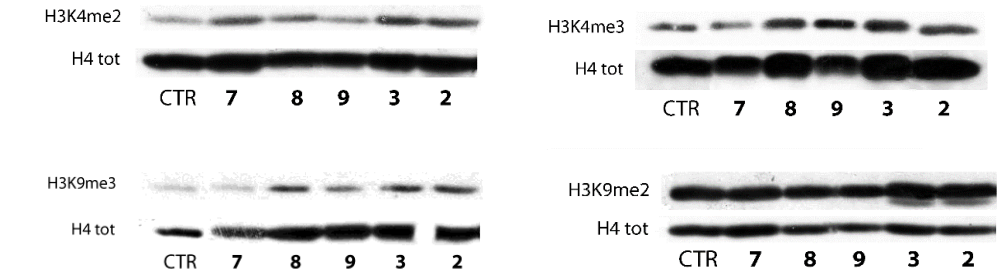

B) HCT116 cells

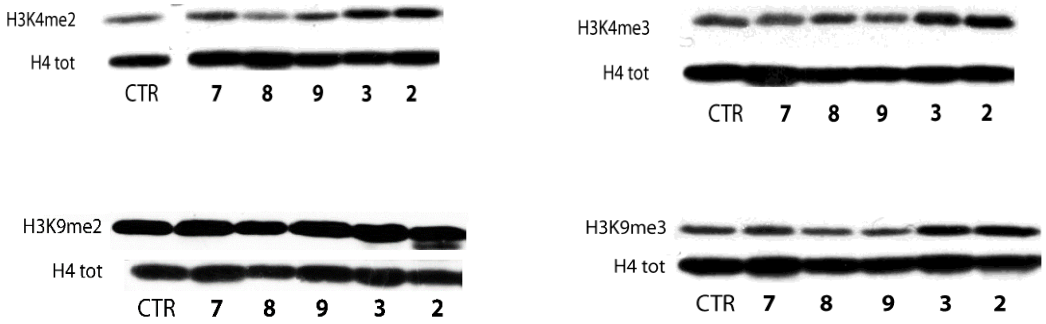

Figure 11.7. Western blot analyses of H3K4me2/3 and H3K9me2/3 methylation after treatment of LNCaP (A) and HCT116 (B) cells with **2**, **3** and the references **7**-**9**.

11.4.3.1. Methods

Cell lines. HCT116 (human colorectal carcinoma cell line-ATCC) were grown at 37 °C in air and 5% CO_2 in DMEM medium (Euroclone) and LNCaP (human prostate cancer cell line-ATCC) in RPMI medium (Euroclone). Both media were supplemented with 10% heat-inactivated FBS (Euroclone), 1% glutamine (Lonza), 1% penicillin/streptomycin (Euroclone) and 0.1% gentamycin (Lonza).

Cell cycle analysis. 2.5×10^5 cells (HCT116 and LNCaP) were collected by centrifugation after 48 h of stimulation with reference or testing compounds at 50 µM. The cells were resuspended in 500 µL of hypotonic buffer (0.1% NP-40, 0.1% sodium citrate, 50 µg/mL PI, RNAse A) and incubated in the dark for 30 min. The analysis was performed by FACS-Calibur (Becton Dickinson) using the Cell Quest Pro software (Becton Dickinson) and ModFit LT version 3 software (Verity). Pre-G1 picks were analyzed as indicative of sub-G1 apoptotic population. The experiments were performed in triplicate and shown data represent independent media values.

Dose-dependent apoptosis evaluation. 2.5×10^5 HCT116 and LNCaP cells were treated for 48 h with increasing doses (10, 25, 50, 100 µM) of **2** and **3**. Cell cycle distribution of 10,000 cells was analyzed with a FACS-Calibur flow cytometer

(Becton Dickinson) by ModFit version 3 Technology (Verity). Pre-G1 picks were analyzed as indicative of sub-G1 apoptotic population. All the experiments were performed at least 3 times and values were expressed in mean ± SD.

Histone Extraction. After stimulation with compounds, cells (HCT116 and LNCaP) were collected by centrifugation and washed two times with PBS. Then the samples were resuspended in Triton extraction buffer (PBS containing 0.5% Triton X 100 (v/v), 2 mM PMSF, 0.02% (w/v) NaN_3), and the lysis was performed for 10 min at 4 °C. Next, samples were centrifugated at 2000 rpm for 10 min at 4 °C, and the pellets were washed in TEB (half the volume). After a new centrifugation under the same conditions, the samples were re-suspended in 0.2 N HCl and the acidic histone extraction was carried out overnight at 4 °C. The supernatant was recovered by centrifugation and the protein content was quantified with BCA™ Protein Assay (Pierce).

Western blot analysis. Histone extracts (10 μg) were denatured and boiled in buffer (0.25 M Tris-HCl pH 6.8, 8% SDS, 40% glycerol, 5% 2-mercaptoethanol, bromophenol blue 0.05%) for 3 min before electrophoresis. Proteins were subjected to SDS-PAGE (15% polyacrylamide gels) in Tris-glycine-SDS (25 mM Tris, 192 mM glycine, 0.1% SDS). After electrophoresis, proteins were transferred to nitrocellulose membranes (Biorad Mini-protean gel and Transblot Turbo, Transfer System Biorad). The membranes were stained with Ponceau red, before to start with blocking (5% non-fat dry milk in TBS 1x/Tween 0.1%), and then incubated with the primary antibodies overnight at 4 °C. The employed antibodies were H3K4me2 and H3K4me3, H3K9me2 and H3K9me 3 (Abcam); total H4 (Cell Signalling) was used to normalize for equal loading of histone extracts.

Determining cell proliferation with the xCELLigence system. Tumour cell proliferation was monitored with the xCELLigence system (Roche). LNCaP and HCT116 cells were suspended in DMEM and RPMI media respectively and added into a 96 well microtiter plate that is specifically designed to measure cellular impedance (E-Plate, Roche). The measured impedance, which is dependent on the level of confluence, was expressed as an arbitrary unit called Cell Index. The Cell Index at each time point is defined as (Rn-Rb)/(15X), where Rn is the cell-electrode impedance of the well when it contains cells and Rb is the background impedance of the well with the media alone. xCELLigence monitors cellular events in real time measuring electrical impedance across interdigitated micro-electrode integrated on the bottom of tissue culture E-Plates. The impedance measurement provides quantitative information about the biological status of the cells, including cell number, viability, and morphology. For experiments, LNCaP and HCT116 cell lines were starved in DMEM/10% FBS and RPMI/10% FBS, respectively, overnight before being seeded on an EPlate 96. Two hours after seeding, scalar cell concentrations were added in triplicate. Dynamic CI values were monitored in 30-

minute intervals from the time of plating until the end of the experiment. CI values were calculated and plotted on the graph. Standard deviation of tetraplicates of wells for the two types cells with different treatments were analysed with the RTCA Software.

Cell migration assay. The kinetic information about cell migration by dynamically recording the whole cell migration process in real time without labelling cells, has been performed with the Roche xCELLigence Real-Time Cell Analyzer (RTCA) DP instrument. The RTCA DP instrument uses the CIM (cellular invasion/migration)-Plate 16 featuring microelectronic sensors integrated into the underside of the microporous polyethylene terephthalate (PET) membrane of a Boyden-like chamber. In this way cells migrate from the upper chamber through the membrane into the bottom chamber in response to the chemoattractant (foetal bovine serum) so contacting and adhering to the electronic sensors on the underside of the membrane, resulting in an increase of the impedance. The impedance increase is proportional to increasing numbers of migrated cells on the underside of the membrane. Moreover cell-index values reflecting impedance changes are recorded by RTCA DP instrument. The CIM-Plate has been assembled by placing the top chamber into the bottom chamber and snapping the two together. Serum-free medium has been placed in the top chamber to hydrate and pre-incubate the membrane for 1 h in the CO_2 incubator at 37 °C before obtaining a background measurement. LNCaP and HCT116 cells were resuspended at the indicated concentration in serum-free medium. Once the CIM-Plate has equilibrated, it has been placed in the RTCA DP station and the background cell index values have been measured. The CIM-Plate was then removed from the RTCA DP station and then cells have been added to the top chamber at the desired concentration. The CIM-Plate was placed in the RTCA DP station and migration has been monitored every 2 minutes for several hours. Cells have been analysed in absence or presence of 10% FBS in the bottom chamber. Cell migration was detected by automated real time monitoring and the low and high seeding densities were quantitatively monitored and reflected by the cell index values.

11.4.4. Conclusion

In conclusion, we have shown that "pan-KDM" inhibitors can be obtained by coupling the chemical features of tranylcypromine, a known LSD1 inhibitor, with the 2,2'-bipyridine or 5-carboxy-8HQ scaffolds, two 2OG competitive moieties developed for JmjC inhibition. Such compounds are able to inhibit LSD1 as well as JmjC enzymes while have little or no effect against other tested 2OG enzymes lacking KDM activity. It is also interesting that the tranylcypromine-moieties act as covalently binding inhibitors, whereas the JmjC inhibitor scaffolds bind reversibly. The application of such LSD/JmjC hybrid inhibitors to cells enables simultaneous increases in levels of H3K4me2/3 and H3K9me2/3 as well as high growth arrest and apoptosis (**2** and **3**) in LNCaP prostate and HCT116 colon cancer cells, whereas the

related family-specific single-target inhibitors **7**-**9** as well as a combination of **7** plus **8** were inactive. When tested in MePR non-cancer cells to assess their differential toxicity, **2** and **3** showed very low (**2**) or no (**3**) ability to increase the pre-G1 accumulation. It should be noted that since a single KDM may target multiple substrates, different biological effects depending on the context could manifest. More generally, the results demonstrate that hybrid molecules inhibiting different classes of histone modifying enzymes have substantial potential as functional probes or histone methylation, and we suggest that combining other types of inhibitors targeting histone modifying enzymes may be productive with respect to regulating the expression of specific sets of genes. Our pan-demethylase inhibitors may also be useful for medicinal chemistry efforts relating to cancer, in line with SAHA, which likely owes its anticancer activity to its pan-HDAC inhibitor profile.[612]

*Adapted with the permission from Rotili, D., Tomassi, S., Conte, M., Benedetti, R., Tortorici, M., Ciossani, G., Valente, S., Marrocco, B., Labella, D., Novellino, E., Mattevi, A., Altucci, L., Tumber, A., Yapp, C., King, O. N. F., Hopkinson, R. J., Kawamura, A., Schofield, C. J., Mai. A. Pan-histone demethylase inhibitors simultaneously targeting Jumonji C and lysine specific demethylases display high anticancer activities. *J. Med. Chem.*, accepted.[612]

12. From BIX-01294 to a selective inhibitor of Jumonji demethylases*

12.1. Research project

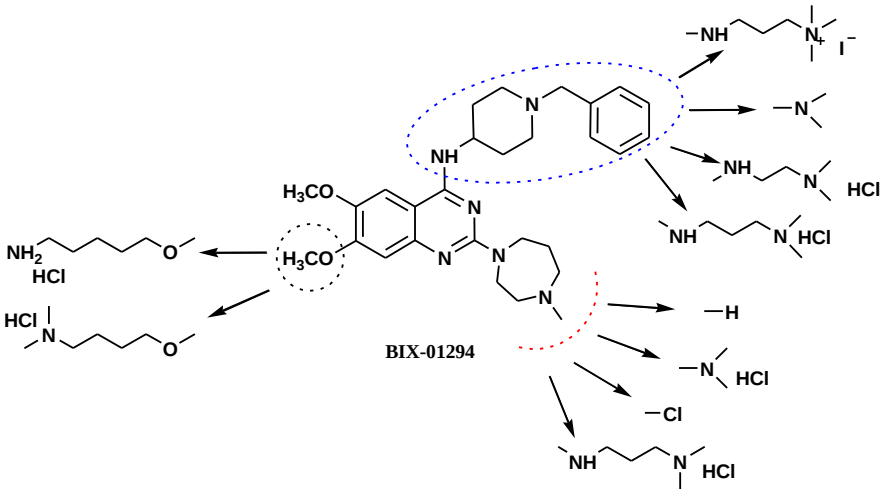

Figure 12.1. BIX-01294 and its analogs.

BIX-01294 (a diazepin-quinazolin-amine derivative; Figure 12.1) inhibits activities of G9a[613] and G9a-like protein (GLP) lysine methyltransferase by mimicking the bound conformation of histone H3 Lys4 to Arg8, residues N-terminal to the target lysine 9 of histone H3, in the substrate peptide-binding groove.[565] Addition of a lysine or methyl-lysine mimic to BIX-01294 enhances its potency of inhibition of G9a and GLP due to the insertion of the mimics into the target lysine-binding channel.[575,577,614,615] It is interesting to note that both lysine methyltransferases and demethylases recognize lysines in methylated and unmethylated states, whether they are substrates or reaction products. We therefore explore whether BIX analogs can function as selective inhibitors of human KIAA1718 (a H3K9me2 demethylase, also known as JHDM1D), in comparison with their inhibitions of human GLP (a H3K9 methyltransferase, also known as EHMT1) whose loss-of-function mutations cause the 9q34 subtelomeric deletion syndrome[616] and human JARID1C (a H3K4me3 demethylase, also known as SMCX) mutations of which affect its demethylase activity are found in X-linked mental retardation patients.[528,617] KIAA1718 belongs to a small family of Jumonji proteins with three members (PHF2, PHF8 and KIAA1718) (See Sec. 7.2.2.7). Each of these proteins harbors two domains in its respective N-terminal half: a PHD domain that binds tri-methylated histone H3 lysine 4 (H3K4me3), a modification associated with transcriptional activation, and their linked Jumonji domains which remove methyl marks (H3K9me2, H3K27me2, or H4K20me1) that are associated with transcriptional repression.[497] KIAA1718 removes methyl marks from dimethylated H3 lysine 9 (H3K9me2) and/or lysine 27

(H3K27me2),[497,534,539] which shares an ARKS sequence. By using a structure activity relationship (SAR) approach we have designed a new set of inhibitor, starting from the BIX-01294 structure, which selectively inhibited KIAA1718 but not GLP (Figure 12.1).

12.2. Chemistry

The derivatives **1-5** have been prepared as reported in Scheme 1. The dichloroquinazoline derivative **11,** prepared as reported previously,[618] was treated with dimethylamine at room temperature providing the 4-substituted intermediate **12**. This latter was converted into **13** by the mean of a further treatment with dimethylamine at 110 °C in a sealed tube. The intermediate **13** was then converted into the phenol derivative **14** by debenzylation with trifluoroacetic acid under reflux conditions. The same reaction has been performed to convert **12** into its debenzylated derivative **19**. The two phenol compounds **14** and **19** undergo to a Mitsunobu reaction with the Boc-protected 5-aminopentan-1-ol to provide the derivatives **16** and **20**, respectively, that were finally converted into the final derivatives **3** and **4**, respectively, by deprotection and salification with HCl. Compound **20** has also been treated with the commercially available N^1,N^1-dimethylpropane-1,3-diamine at 110 °C in a sealed tube to give the intermediate **21**, that was finally deprotected with HCl to give **5**. By the means of a Mitsunobu reaction with the 4-bromobutanol the intermediate **14** was also converted into the corresponding bromoalkyl ether **15** that was finally transformed into the final compound **2** by treatment with dimethylamine at 110 °C in a sealed tube and subsequent salification with HCl. By a catalytic hydrogenation **12** was also converted into its debenzylated and dechlorinated intermediate **17** that, after alkylation under Mitsunobu conditions with the Boc-protected 5-aminopentan-1-ol and subsequent deprotection/salification with HCl, gave the final compound **1**. The derivatives **6-10** have been prepared as reported in Scheme 2. The intermediates **28-30** were obtained after treatment of the dichloroquinazoline **11** with the proper amines, followed by trifluoroacetic acid mediated deprotection and subsequent Mitsunobu reaction with the Boc-protected 5-aminopentan-1-ol. The final compounds **8-10** were then obtained by deprotection/salification with HCl of the intermediates **28-30**. The compound **6** was obtained by treatment of **30** with N^1,N^1-dimethylpropane-1,3-diamine at 110 °C in a sealed tube to give the intermediate **31** and final deprotection with HCl. By reaction at room temperature with iodomethane, starting from **29**, was obtained the ammonium salt **32** that was finally converted into the compound **7** by HCl-mediated deprotection/salification.

Scheme 1

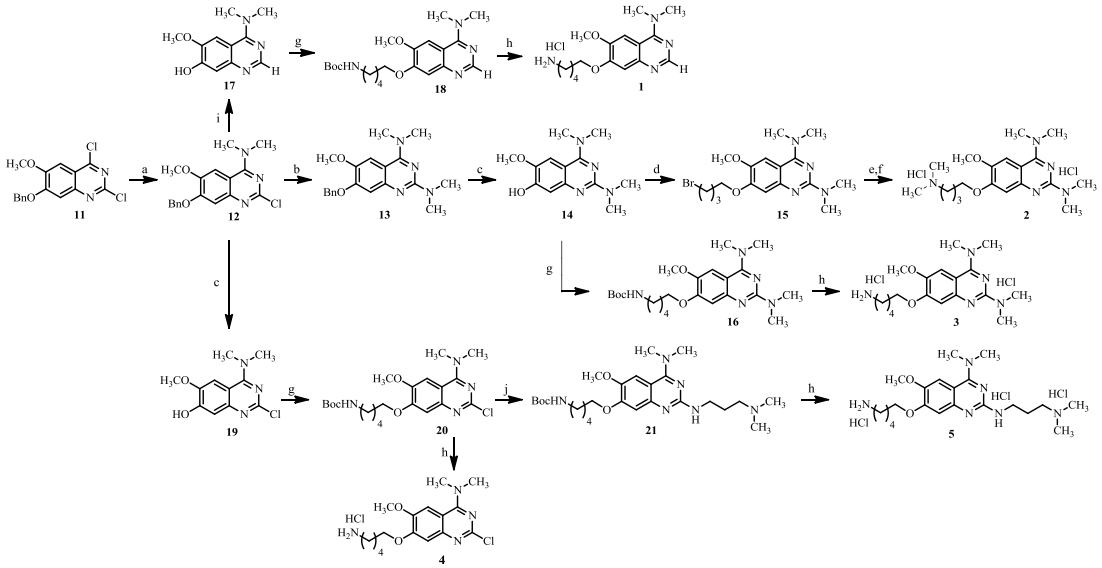

Reagents and conditions: (a) Dimethylamine 2M in THF, dry THF, rt; (b) dimethylamine 2M in THF, dry THF, 110 °C, sealed tube; (c) TFA, reflux; (d) 4-bromo-1-butanol, PPh_3, DIAD, dry THF, N_2, rt; (e) dimethylamine 2M in THF, dry THF, 110 °C sealed tube; (f) HCl 2N in diethyl ether, dry THF, rt; (g) 5-(Boc-amino)-1-pentanol, PPh_3, DIAD, dry THF, N_2, rt; (h) HCl 4N in dioxane, dry THF or dry THF-MeOH (1:1), rt; (i) H_2, Pd-C, dry THF-MeOH (2:1), 1 atm, rt; (j) 3-(dimethylamino)-1-propylamine, 110 °C, sealed tube.

Scheme 2

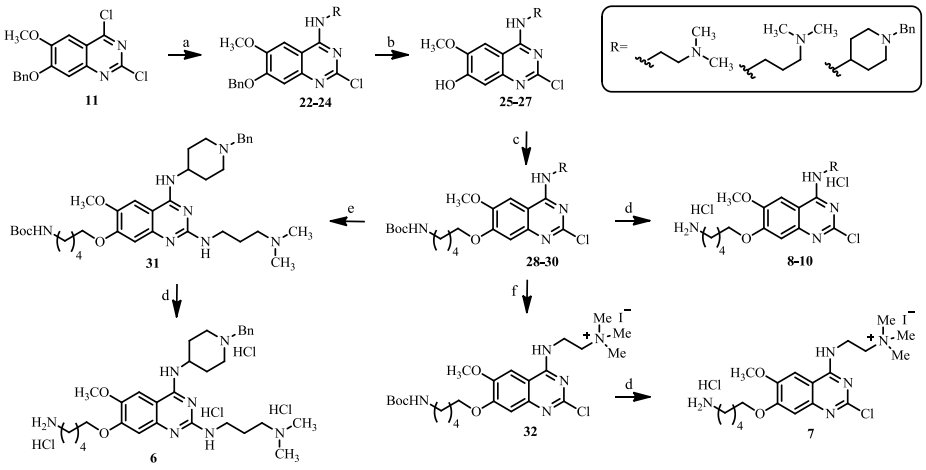

Reagents and conditions: (a) Various amines, dry THF, rt; (b) TFA, reflux; (c) 5-(Boc-amino)-1-pentanol, PPh_3, DIAD, dry THF, N_2, rt; (d) HCl 4N in dioxane, dry THF or dry THF-MeOH (1:1), rt; (e) 3-(dimethylamino)-1-propylamine, 110 °C, sealed tube; (f) MeI, dry THF, rt.

The chemical and physical data of the intermediate **11-32** and final compounds **1-10** are reported in Table 12.1 and 12.2, respectively.

Table 12.1. Chemical and physical data of compounds **11-32.**

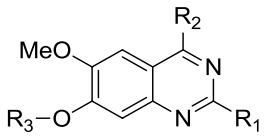

Cpd	R_1	R_2	R_3	mp, °C	recrystall. solvent	Yield %
12	Cl		Bn	151-153	A	89
13			Bn	112-113	B	88
14			H	149-151	A	80
15			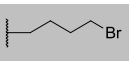	oil	-	70
16			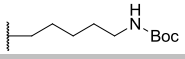	oil	-	67
17	H		H	210-213	C	75
18	H		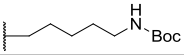	oil	-	70
19	Cl		H	219-221	C	80
20	Cl		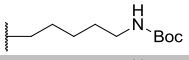	oil	-	65
21	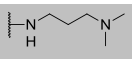		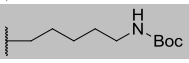	87-90	D	75
22	Cl	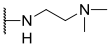	Bn	132-134	B	89
23	Cl	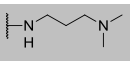	Bn	135-138	B	91
24	Cl	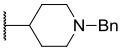	Bn	155-158	A	90
25	Cl	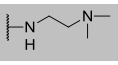	H	160-163	A	80
26	Cl	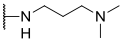	H	95-99	E	81
27	Cl	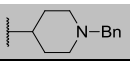	H	189-191	F	78
28	Cl	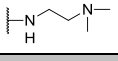	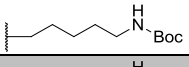	130-132	B	66
29	Cl	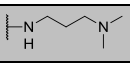	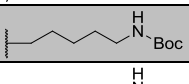	oil	-	67
30	Cl	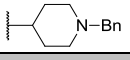	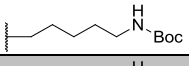	88-90	D	68
31	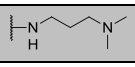	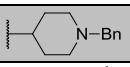	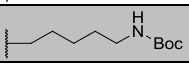	44-47	D	71
32	Cl	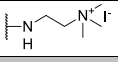	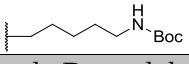	159-162	A	83

A: acetonitrile; B: benzene; C: methanol; D: cyclohexane; E: cyclohexane/benzene; F: acetonitrile/methanol .

Table 12.2. Chemical and physical data of final compounds **1-10.**

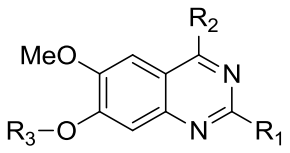

Cpd	R_1	R_2	R_3	mp, °C	recrystal. solvent	Yield %
1	H		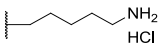	>250	C	93
2	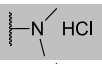		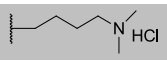	>250	C	94
3	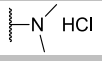		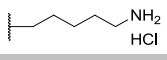	>250	C	95
4	Cl		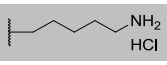	>250	C	94
5	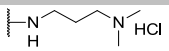		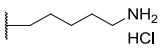	>250	C	92
6	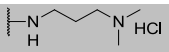	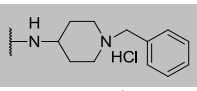	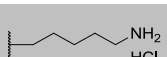	>250	C	96
7	Cl	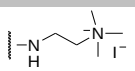	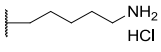	>250	C	93
8	Cl	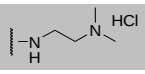	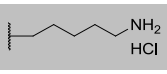	>250	C	97
9	Cl	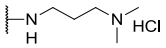	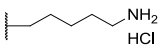	>250	C	95
10	Cl	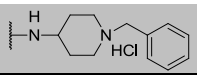	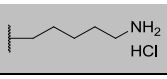	>250	C	96

A: acetonitrile; B: benzene; C: methanol; D: cyclohexane; E: cyclohexane/benzene; F: acetonitrile/methanol .

12.3. Experimental section

Chemistry. Melting points were determined on a Buchi 530 melting point apparatus and are uncorrected. ^{1}H-NMR and ^{13}C-NMR spectra were recorded at 400 MHz on a Bruker AC 400 spectrometer; chemical shifts are reported in δ (ppm) units relative to the internal reference tetramethylsilane (Me_4Si). EIMS spectra were recorded with a Fisons Trio 1000 spectrometer; only molecular ions (M^+) and base peaks are given. All compounds were routinely checked by TLC and ^{1}H NMR. TLC was performed on aluminum-backed silica gel plates (Merck DC, Alufolien Kieselgel 60 F254) with spots visualized by UV light. All solvents were reagent grade and, when necessary, were purified and dried by standard methods. Concentration of solutions after reactions and extractions involved the use of a rotary evaporator operating at reduced pressure of ca. 20 Torr. Organic solutions were dried over anhydrous sodium sulfate. Analytical results are within ± 0.40% of the theoretical values. All chemicals were purchased from Aldrich Chimica, Milan (Italy), or from Alfa Aesar, Milan (Italy), and were of the highest purity.

General procedure for the synthesis of the 4-Amino-quinazoline derivatives (12, 22-24). Example: 7-(Benzyloxy)-2-chloro-6-methoxy-*N*,*N*-dimethylquinazolin-4-amine (12).To 7-(benzyloxy)-2,4-dichloro-6-methoxyquinazoline **11** (650 mg, 1.939 mmol) dissolved in dry THF (12.5 mL) was added a solution of dimethylamine 2M in THF (2.90 mL, 5.817 mmol); the mixture was stirred at room temperature and the reaction was completed after 1h and 10 min. The resulting solid in suspension was filtered off and washed with THF. The filtrate and washings were concentrated in vacuum and the residual solid triturated from petroleum ether, collected by filtration, washed with petroleum ether and dried to give pure **3** as a white solid (75%). ^{1}H-NMR ($CDCl_3$, 400 MHz, δ; ppm) 3.36 (s, 6H, N-(CH_3)$_2$), 4.01 (s, 3H, OCH_3), 5.27 (s, 2H, CH_2-benzyl protons), 7.21 (s, 1H, *H* quinazoline ring), 7.29 (s, 1H, *H* quinazoline ring), 7.34-7.36 (m, 1H, *H* phenyl ring), 7.40-7.42 (d, 2H, *H* phenyl ring), 7.47-7.49 (d, 2H, *H* phenyl ring). ^{13}C-NMR ($CDCl_3$) δ 40.7 (2C), 56.2, 71.2, 103.3, 107.8, 117.3, 127.2 (2), 127.7, 129.0 (2), 141.2, 148.9, 152.5, 156.1, 160.3, 179.6. MS (EI): *m*/*z* $[M]^+$: 343.11.

Procedure for the preparation of the 7-(Benzyloxy)-6-methoxy-N^2,N^2,N^4,N^4-tetramethylquinazoline-2,4-diamine (13).A solution of dimethylamine 2M in THF (2.25 mL) was added to 7-(benzyloxy)-2-chloro-6-methoxy-*N*,*N*-dimethylquinazolin-4-amine **12** (200 mg, 0.582 mmol) in a sealed tube and the resulting mixture was stirred at 110 °C for 26h. After cooling to room temperature the reaction was quenched with 10 mL of water, then extracted with ethyl acetate (3 x 10 mL). The collected organic phases were washed with brine (1 x 5 mL), dried over sodium sulfate and concentrated to give pure **13** which was directly used in the following step without further purification. ^{1}H-NMR (DMSO-d_6, 400 MHz, δ; ppm) 3.11 (s, 6H, N-(CH_3)$_2$), 3.18 (s, 6H, N-(CH_3)$_2$), 3.82 (s, 3H, OCH_3), 5.20 (s, 2H, CH_2-benzyl protons), 6.90 (s, 1H, *H* quinazoline ring), 7.20 (s, 1H, *H* quinazoline ring), 7.36-7.38 (m, 1H, *H* phenyl ring), 7.42-7.44 (d, 2H, *H* phenyl ring), 7.47-7.49 (d, 2H, *H* phenyl ring). ^{13}C-NMR (DMSO) δ 40.3 (2C), 40.7 (2C), 56.2, 71.2, 103.5, 107.8, 113.3, 127.2(2C), 127.7, 129.0 (2C), 141.2, 148.9, 150.6, 159.9¸179.3, 183.2 MS (EI): *m*/*z* $[M]^+$: 352.19.

General procedure for the synthesis of the *Tert*-butyl-(5-((4-(amino substituted)-2-((3-(dimethylamino)propyl)amino)-6-methoxyquinazolin-7-yl)oxy)pentyl)carbamates (21, 31).Example: *Tert*-butyl-(5-((4-(dimethylamino)-2-((3-(dimethylamino)propyl)amino)-6-methoxyquinazolin-7-yl)oxy)pentyl)carbamate (21). A mixture of *tert*-butyl (5-((2-chloro-4-(dimethylamino)-6-methoxyquinazolin-7-yl)oxy)pentyl)carbamate **20** (180 mg, 0.410 mmol) and 3-dimethylaminopropylamine (0.36 mL) was placed in a sealed tube and stirred at 110 °C for 7 h. After cooling to room temperature, 10 mL of water were added and the aqueous phase was extracted with ethyl acetate (3 x 10 mL), the combined organic phases were then washed with brine (1 x 5 mL) and dried over sodium sulfate. After evaporation in vacuum the crude was purified by aluminum oxide chromatographic column eluting with AcOEt: MeOH 25:1 to provide the

desired compound **21**. ^{1}H-NMR (DMSO-d_6, 400 MHz, δ; ppm) 1.64-1.77 (m, 2H, -NHCH$_2$C*H$_2$*CH$_2$N(CH$_3$)$_2$, 2.15 (s, 6H, -NHCH$_2$CH$_2$C*H$_2$*N(C*H$_3$*)$_2$), 2.28 (t, 2H, -NHCH$_2$CH$_2$C*H$_2$*N(CH$_3$)$_2$), 2.93 (q, 2H, -C*H$_2$*NH-Boc), 3.13 (s, 6H, -N(C*H$_2$*)$_3$), 3.27-3.29 (t, 2H, -NHC*H$_2$*CH$_2$CH$_2$N(CH$_3$)$_2$), 3.80 (s, 3H, -OC*H$_3$*), 4.02 (t, 2H, -OC*H$_2$*), 6.33 (t, 1H, -N*H*CH$_2$CH$_2$CH$_2$N(CH$_3$)$_2$), 6.74 (s, 1H, *H* quinazoline ring) 6.79 (s, 1H, -N*H*-Boc), 7.15 (s, 1H, *H* quinazoline ring).

General procedure for the synthesis of the 7-Hydroxy quinazoline derivatives (14, 19, 25-27). Example: 2-Chloro-4-(3-(dimethylamino)propylamino)-6-methoxyquinazolin-7-ol (26). A solution of 7-(benzyloxy)-2-chloro-*N*-(3-(dimethylamino)propyl)-6-methoxyquinazolin-4-amine **23** (400 mg, 0.996 mmol) in trifluoroacetic acid (5.5 mL) was refluxed at 115°C for 1.5 h. The trifluoroacetic acid was removed by evaporation, the reaction was left to reach 0 °C, quenched with water (6 mL) and a saturated solution of Na_2CO_3 was then slowly added until pH 9.5-10 to give a white suspension. The resulting precipitate was collected, the aqueous layer was extracted with a mixture of $CHCl_3$: *i*-PrOH 4:1 (3 x 20 mL) and the combined organic phases were dried over sodium sulfate. After evaporation in vacuum the obtained solid was reunited with the first one, triturated from petroleum ether/diethyl ether (1:1) and then filtered to give the pure compound **26** (80%). ^{1}H-NMR (DMSO-d_6, 400 MHz, δ; ppm) 1.74-1.80 (m, 2H, NHCH$_2$C*H$_2$*CH$_2$), 2.17 (s, 6H, N-(C*H$_3$*)$_2$), 2.30-2.34 (t, 2H, NHCH$_2$CH$_2$C*H$_2$*), 3.46-3.51 (m, 2H, NHC*H$_2$*CH$_2$CH$_2$), 3.89 (s, 3H, OC*H$_3$*), 6.89 (s, 1H, *H* quinazoline ring), 7.57 (s, 1H, *H* quinazoline ring), 8.36 (s, 1H, N*H*), 10.32 (bs, 1H, O*H*). ^{13}C-NMR (DMSO) δ 26.6, 43.2, 45.9 (2C), 56.2, 56.5, 99.5, 110.6, 110.7, 147.3¸150.3, 155.1¸155.8, 158.9. MS (EI): *m*/*z* $[M]^+$: 310.12.

General procedure for the preparation of the 4-(dimethylamino)-6-methoxyquinazolin-7-ol (17). To a solution of the compound **12** (545 mg, 1.585 mmol) in a mixture of dry THF: dry MeOH (2:1) (38 mL: 19 mL) was added Pd-C 10% wt (0.168 g) at room temperature and 1 atm H_2 till the reaction was completed (3h). The reaction was then filtered to remove palladium, the solvent was distilled to give a crude yellow solid that was triturated from a mixture THF: MeOH (2:1), collected by filtration, washed with diethyl ether and dried to give the desired compound **17.** ^{1}H-NMR (DMSO-d_6, 400 MHz, δ; ppm) 3.56 (s, 6H, N-(C*H$_3$*)$_2$), 3.94 (s, 3H, OC*H$_3$*), 7.29 (s, 1H, *H* quinazoline ring), 7.57 (s, 1H, *H* quinazoline ring), 8.65 (s, 1H, *H* quinazoline ring), 11.51-11.67 (bs, 1H, O*H*). ^{13}C-NMR (DMSO) δ 40.7 (2C), 56.2, 103.8, 112.5, 118.8, 148.1, 151.1¸ 154.7, 155.0, 178.1. MS (EI): *m*/*z* $[M]^+$: 219.10.

General procedure for the synthesis of *NH*-Boc quinazoline derivatives (16,18,20,28-30). Example: *Tert*-butyl 5-(4-(1-benzylpiperidin-4-ylamino)-2-chloro-6-methoxyquinazolin-7-yloxy)pentylcarbamate (30). Triphenylphosphine (1.845 g, 7.04 mmol) and 5-(Boc-amino)-1-pentanol (1.040 g, 5.12 mmol) were added to a solution of 4-(1-benzylpiperidin-4-ylamino)-2-chloro-6-

methoxyquinazolin-7-ol **27** (0.510 g, 1.28 mmol) in dry THF (22mL) under nitrogen atmosphere; afterwards DIAD (1.293 g, 6.4 mmol) was added dropwise at 0 °C. Then the reaction was left to reach room temperature and stirred for 2h. The solvent was removed to give a residue that was purified by chromatographic column on silica gel eluting with $CHCl_3$:MeOH 30:1 to provide pure **30**. ^{1}H-NMR ($CDCl_3$, 400 MHz, δ; ppm) 1.54 (s, 9H, C(C*H*$_3$)$_3$), 1.57-1.61 (m, 4H, OCH$_2$CH$_2$C*H*$_2$C*H*$_2$), 1.72-1.73 (m, 4H, OCH$_2$C*H*$_2$CH$_2$CH$_2$C*H*$_2$), 2.15-2.16 (m, 2H, C*H*$_2$ piperidine ring), 2.34-2.37 (m, 2H, C*H*$_2$ piperidine ring), 2.99-3.02 (m, 2H, C*H*$_2$ piperidine ring), 3.17-3.18 (m, 2H, C*H*$_2$ piperidine ring), 3.65 (s, 2H, C*H*$_2$-benzyl protons), 4.00 (s, 3H, OC*H*$_3$), 4.11-4.14 (t, 2H, OC*H*$_2$), 4.33-4.35 (bs, 1H, N*H*COOC(CH$_3$)$_3$), 4.57-4.59 (bs, 1H, N*H*), 5.38-5.40 (m, 1H, *H* piperidine ring), 6.79 (s, 1H, *H* quinazoline ring), 7.11 (s, 1H, *H* quinazoline ring), 7.28 (d, 2H, *H* phenyl ring), 7.32 (m, 1H, *H* phenyl ring), 7.37-7.39 (d, 2H, *H* phenyl ring). ^{13}C-NMR ($CDCl_3$) δ 23.1, 28.5 (3C), 29.4, 30.0, 30.4 (2C), 41.9, 49.4 (2C), 53.1, 56.2, 60.4, 69.2 , 79.5, 99.2, 107.1 , 111.0, 127.3, 128.5 (2C), 128.9 (2C), 135.6, 147.4, 151.5 ,155.8, 156.0, 158.9, 159.6. MS (EI): *m*/*z* [*M*]$^+$: 583.29.

Preparation of 3-(7-(5-(*tert*-butoxycarbonyl)pentyloxy)-2-chloro-6-methoxyquinazolin-4-ylamino)-*N*,*N*,*N*-trimethylpropan-1-aminium iodide (32). To a solution of the NH-Boc intermediate **28** (0.400 g, 0.808 mmol) in dry THF (5 mL) was slowly added iodomethane (4.04 mmol, 0.573 g), then the reaction was stirred at room temperature for 1 hour. The solvent was distilled and the crude product was purified by aluminum oxide chromatographic column eluting with $CHCl_3$: MeOH: TEA ,30: 1: 0.1, to provide pure **32.** ^{1}H-NMR ($CDCl_3$, 400 MHz, δ; ppm) 1.45 (s, 9H, C(C*H*$_3$)$_3$), 1.52-1.55 (m, 4H, OCH$_2$CH$_2$C*H*$_2$C*H*$_2$), 1.90-1.92 (m, 4H, NHCH$_2$CH$_2$C*H*$_2$ and OCH$_2$CH$_2$CH$_2$CH$_2$C*H*$_2$), 2.40 (m, 2H, NHCH$_2$CH$_2$C*H*$_2$), 3.35 (s, 9H, N(C*H*$_3$)$_3$), 3.71-3.73 (m, 2H, NHC*H*$_2$CH$_2$CH$_2$), 3.85-3.86 (m, 2H, NHC*H*$_2$CH$_2$CH$_2$), 3.99-4.01 (t, 2H, OC*H*$_2$), 4.12 (s, 3H, OC*H*$_3$), 4.61 (bs, 1H, N*H*COOC(CH$_3$)$_3$), 7.05 (s, 1H, *H* quinazoline ring), 7.86 (s, 1H, *H* quinazoline ring), 8.22 (bs, 1H, N*H*). ^{13}C-NMR ($CDCl_3$) δ 22.3, 23.1, 28.5 (3C), 29.4, 30.0, 41.9, 44.0, 54.7 (3C), 56.2, 64.4, 69.2, 79.5, 99.2, 107.1, 111.0, 147.4, 151.5, 155.8, 156.0, 158.9, 159.6. MS (EI): *m*/*z* [*M*]$^+$: 637.19.

Preparation of the derivative 7-(4-Bromobutoxy)-6-methoxy-N^2,N^2,N^4,N^4-tetramethylquinazoline-2,4-diamine (15). Triphenylphosphine (770 mg, 2.93 mmol) and 4-bromo-1-butanol (327 mg, 2.13 mmol) were added to a solution of 2,4-dimethylammino-2-chloro-6-methoxyquinazolin-7-ol **14** (140 mg, 0.533 mmol) in dry THF (6.5 mL) under nitrogen atmosphere; afterwards DIAD (539.6 mg, 0.525 mL, 2.67 mmol) was added dropwise at 0 °C. Then the reaction was left to reach room temperature and stirred for 36 h. The solvent was removed to give a residue that was purified by chromatographic column on silica gel eluting with $CHCl_3$:MeOH 60:1 to give pure **15**. ^{1}H-NMR ($CDCl_3$, 400 MHz, δ; ppm) 2.09 (m, 4H, OCH$_2$C*H*$_2$C*H*$_2$CH$_2$Br), 3.20 (s, 12H, N(C*H*$_3$)$_2$), 3.51-3.58 (t, 2H,

$OCH_2CH_2CH_2CH_2Br$), 3.91 (s, 3H, OCH_3), 4.23 (m, 2H, $OCH_2CH_2CH_2CH_2Br$), 7.17 (s, 1H, *H* quinazoline ring), 7.28 (s, 1H, *H* quinazoline ring).

Preparation of the derivative 7-(4-(dimethylamino)butoxy)-6-methoxy-N^2,N^2,N^4,N^4-tetramethylquinazoline-2,4-diamine dihydrochloride (2). To the intermediate 7-(4-bromobutoxy)-6-methoxy-N^2,N^2,N^4,N^4-tetramethylquinazoline-2,4-diamine **15** (108 mg, 0.271 mmol) in dry DMF (1 mL) was added a 2.0 M dimethylamine solution in THF (2 mL), then the mixture was heated in a sealed tube under stirring at 110 °C for 4 hour. The reaction was quenched with water (15 mL), then extracted with ethyl acetate (3 x 15 mL). The collected organic phases were washed with saturated sodium chloride solution (2 x 5 mL) and dried over sodium sulfate. The solvent was removed to give a crude residue that was purified by aluminum oxide chromatographic column eluting with AcOEt:MeOH 25:1 to provide the pure 7-(4-(dimethylamino)butoxy)-6-methoxy-N^2,N^2,N^4,N^4-tetramethylquinazoline-2,4-diamine. The 7-(4-(dimethylamino)butoxy)-6-methoxy-N^2,N^2,N^4,N^4-tetramethylquinazoline-2,4-diamine (0.14 mmol, 50 mg) was then dissolved in dry THF (1 mL) and to the solution was added HCl 2M in diethyl ether (1 mL). After 2 hours of stirring at room temperature the solid in suspension was filtered, washed with dry diethyl ether to give the desired dihydrochloride salt **2**. ^{1}H-NMR (DMSO-d_6, 400 MHz, δ; ppm) 1.84 (m, 4H, $CH_2CH_2CH_2CH_2O$), 2.72 (s, 6H, $CH_2N(CH_3)_2$), 3.12 (m, 2H, $CH_2N(CH_3)_2$), 3.25 (s, 6H, $N(CH_3)_2$), 3.44 (s, 6H, $N(CH_3)_2$), 3.85 (s, 3H, OCH_3), 4.10 (m, 2H, OCH_2), 7.44 (s, 1H, *H* quinazoline ring), 7.81 (s, 1H, *H* quinazoline ring), 10.57 (bs, 1H, $CH_2{}^+HN(CH_3)_2$), 12.20 (bs, 1H, $^+HN(CH_3)_2$). ^{13}C-NMR (DMSO-d_6) δ 24.1, 27.4, 40.3 (2C), 40.7 (2C), 45.9 (2C), 56.2, 59.1, 68.9, 103.5, 107.8, 113.3, 148.9, 150.6, 159.9, 179.3, 183.2. MS (EI): *m*/*z* $[M]^+$: 433.20.

General procedure for the synthesis of hydrochlorides derivatives (1-10). Example: 7-(5-Aminopentyloxy)-2-chloro-*N*-(2-(dimethylamino)ethyl)-6-methoxyquinazolin-4-amine dihydrochloride (8). The compound **28** (50 mg, 0.104 mmol) was dissolved in a mixture dry THF: dry MeOH (1:1) and to the solution was added HCl 4N in dioxane (1.55 mL, 6.23 mmol). After stirring at room temperature for 1 day the reaction mixture was filtered and the solid was washed with dry diethyl ether to give the desired hydrochloride salt **8**. ^{1}H-NMR (DMSO-d_6, 400 MHz, δ; ppm) 1.49-1.51 (m, 2H, $CH_2CH_2CH_2O$), 1.63-1.66 (m, 2H, $CH_2CH_2CH_2CH_2O$), 1.79-1.83 (m, 2H, CH_2CH_2O), 2.80-2.82 (m, 2H, $H_3N^+CH_2CH_2$), 2.87-2.88 (ss, 6H, $^+HN(CH_3)_2$), 3.40-3.41 (m, 2H, $NHCH_2CH_2$), 3.87-3.89 (m, 2H, $NHCH_2CH_2$), 3.94 (s, 3H, OCH_3), 4.10-4.13 (m, 2H, $CH_2CH_2CH_2O$), 7.11 (s, 1H, *H* quinazoline ring), 7.88-7.95 (s, m, 4H, H_3N^+, *H* quinazoline ring), 9.04 (t, 1H, $HNCH_2$), 10.38 (bs, 1H, $^+HN(CH_3)_2$). ^{13}C-NMR (DMSO-d_6) δ 23.1, 29.4, 32.8, 42.1, 45.6 (2C), 47.1, 56.2, 58.1, 69.2, 99.2, 107.1, 111.0, 147.4, 151.5, 155.8, 158.9, 159.6. MS (EI): *m*/*z* $[M]^+$: 453.15.

7-(5-aminopentyloxy)-6-methoxy-*N*,*N*-dimethylquinazolin-4-amine hydrochloride (1). ^{1}H-NMR (DMSO-d_6, 400 MHz, δ; ppm) 1.50-1.52 (m, 2H, $CH_2CH_2CH_2O$), 1.61-1.67 (m, 2H, $CH_2CH_2CH_2CH_2O$), 1.82-1.86 (m, 2H, CH_2CH_2O), 2.80-2.82 (m, 2H, $H_3N^+CH_2CH_2$), 3.56 (s, 6H, $N(CH_3)_2$), 3.95 (s, 3H, OCH_3), 4.14-4.18 (t, 2H, $CH_2CH_2CH_2O$), 7.41 (s, 1H, *H* quinazoline ring), 7.60 (s, 1H, *H* quinazoline ring), 7.87-7.94 (m, 3H, H_3N^+), 8.72 (s, 1H, *H* quinazoline ring). ^{13}C NMR (DMSO-d_6) δ 23.1, 29.4, 32.8, 40.7 (2C), 42.1, 56.2, 69.2, 103.5, 108.9¸119.2, 148.2, 152.3, 155.0, 159.2, 178.1. (EI): *m*/*z* $[M]^+$: 340.17.

7-(5-Aminopentyloxy)-6-methoxy-N^2,N^2,N^4,N^4-tetramethylquinazoline-2,4-diamine dihydrochloride (3).^{1}H-NMR (DMSO-d_6, 400 MHz, δ; ppm) 1.50 (m, 2H, $CH_2CH_2CH_2O$), 1.64 (m, 2H, $CH_2CH_2CH_2CH_2O$), 1.81 (m, 2H, CH_2CH_2O), 1.99 (m, 2H, $NHCH_2CH_2$), 2.74 (s, 6H, $^+HN(CH_3)_2$), 2.80 (m, 2H, $H_3N^+CH_2CH_2$), 3.11 (m, 2H, $CH_2CH_2N(CH_3)_2H^+$), 3.47 (s, 6H, $N(CH_3)_2$), 3.49 (m, 2H, $NHCH_2CH_2CH_2$), 3.86 (s, 3H, OCH_3), 4.09 (m, 2H, $CH_2CH_2CH_2O$), 7.15 (s, br, 1H $NHCH_2CH_2CH_2$), 7.45 (s, 1H, *H* quinazoline ring), 7.93 (m, 4H, *H* quinazoline ring and H_3N^+), 10.6 (s, br, $^+HN(CH_3)_2$), 12,8 (s br, 1H, HN^+ quinazoline ring). ^{13}C-NMR (DMSO-d_6) δ 23.1, 29.4, 32.8, 40.3 (2C), 40.7 (2C), 42.1, 56.2, 69.2, 103.5, 107.8, 113.3, 148.9, 150.6, 159.9, 179.3, 183.2. (EI): *m*/*z* $[M]^+$: 419.19.

7-(5-Aminopentyloxy)-2-chloro-6-methoxy-N,N-dimethylquinazolin-4-amine hydrochloride (4). ^{1}H-NMR (DMSO-d_6, 400 MHz, δ; ppm) 1.47-1.51 (m, 2H, $CH_2CH_2CH_2O$), 1.62-1.66 (m, 2H, $CH_2CH_2CH_2CH_2O$), 1.80-1.83 (m, 2H, CH_2CH_2O), 2.79-2.83 (m, 2H, $H_3N^+CH_2CH_2$), 3.34 (s, 6H, $N(CH_3)_2$), 3.90 (s, 3H, OCH_3), 4.11-4.15 (t, 2H, $CH_2CH_2CH_2O$), 7.15 (s, 1H, quinazoline ring), 7.43 (s, 1H, quinazoline ring), 7.87-7.95 (m, 3H, H_3N^+). ^{13}C-NMR (DMSO-d_6) δ 23.1, 29.4, 32.8, 40.7 (2C), 42.1, 56.2 , 69.2, 103.3, 107.8, 117.3, 148.9, 152.5, 156.1, 160.3, 179.6. (EI): *m*/*z* $[M]^+$: 374.13.

7-(5-Aminopentyloxy)-N^2-(3-(dimethylamino)propyl)-6-methoxy-N^4,N^4-dimethylquinazoline-2,4-diamine trihydrochloride (5). ^{1}H-NMR (DMSO-d_6, 400 MHz, δ; ppm) 1.50 (m, 2H, $CH_2CH_2CH_2O$), 1.65 (m, 2H, $CH_2CH_2CH_2CH_2O$), 1.81 (m, 2H, CH_2CH_2O), 2.80 (m, 2H, $H_3N^+CH_2CH_2$), 3.26 (s, 6H, $N(CH_3)_2$), 3.45 (s, 6H, $N(CH_3)_2$), 3.87 (s, 3H, OCH_3), 4.08 (m, 2H, $CH_2CH_2CH_2O$), 7.15 (s, 1H, $NHCH_2$), 7.45 (s, 1H, quinazoline ring), 7.76 (s, 1H, quinazoline ring), 7.99 (s br, 3H, H_3N^+), 12,1 (s br, 1H, HN^+ quinazoline ring). ^{13}C-NMR (DMSO-d_6) δ 23.1, 26.6 , 29.4, 32.8, 40.7 (2C), 42.1, 42.8, 45.9 (2C), 56.2, 56.5, 69.2, 101.9, 105.4, 112.2, 147.5, 148.1, 158.3, 176.3, 177.9. (EI): *m*/*z* $[M]^+$: 476.24.

7-(5-Aminopentyloxy)-N^4-(1-benzylpiperidin-4-yl)-N^2-(3-(dimethylamino)propyl)-6-methoxyquinazoline-2,4-diamine trihydrochloride (6).^{1}H-NMR (DMSO-d_6, 400 MHz, δ; ppm) 1.47-1.52 (m, 2H, $CH_2CH_2CH_2O$), 1.62-1.66 (m, 2H, $CH_2CH_2CH_2CH_2O$), 1.80-1.82 (m, 2H, $H_3N^+CH_2CH_2$), 2.00 (m, 2H, piperidine ring), 2.00-2.03 (m, 4H, CH_2CH_2O and CH_2 piperidine ring), 2.77-2.85

(m, 8H, N(CH_3)$_2$ and propyl protons), 3.15-3.18 (m, 2H, CH_2N(CH$_3$)$_2$), 3.32-3.40 (m, 4H, piperidine ring), 3.50-3.65 (m, 2H, NHCH_2), 3.89 (s, 3H, OCH_3), 4.07-4.09 (t, 2H, CH$_2$CH$_2$CH_2O), 4.34 (s, 2H, CH_2-benzyl protons), 4.51-4.52 (m, 1H, piperidine ring), 7.03 (s, 1H, NHCH$_2$), 7.48 (s, 1H, quinazoline ring), 7.69 (s, 1H, quinazoline ring), 7.93-8.00 (m, 2H, phenyl ring), 8.12-8.35 (m, 5H, benzenic protons and NH_2), 9.33-9.37 (s, 1H, NH-piperidine), 10.89-10.96 (bs, 1H, H_3N^+), 11.23-11.34 (bs, 1H, ^+HNbn), 12.78-12.90 (bs, 1H, ^+HN(CH$_3$)$_2$). ^{13}C-NMR (DMSO-d$_6$) δ 23.1, 26.6, 29.4, 30.4 (2C), 32.8, 42.1, 42.8, 45.9 (2C), 49.4 (2C), 53.1, 56.2, 56.5, 60.4, 69.2, 97.8, 104.7 , 105.9, 127.3, 128.5 (2C), 128.9 (2C), 135.6, 146.5, 146.6, 157.2, 157.6. 176.0. (EI): *m*/*z* [*M*]$^+$: 657.31.

3-(7-(5-aminopentyloxy)-2-chloro-6-methoxyquinazolin-4-ylamino)-*N*,*N*,*N*-trimethylpropan-1-aminium iodide hydrochloride (7). ^{1}H-NMR (DMSO-d$_6$, 400 MHz, δ; ppm) 1.48-1.50 (m, 2H, CH_2CH$_2$CH$_2$O), 1.62-1.66 (m, 2H, CH_2CH$_2$CH$_2$CH$_2$O), 1.78-1.82 (m, 2H, CH_2CH$_2$O), 2.12-2.13 (m, 2H, NHCH$_2$CH_2), 3.09(s, 9H, N(CH_3)$_3$), 3.45-3.49 (m, 2H, NHCH$_2$CH$_2$CH_2), 3.58-3.60 (m, 2H, H$_3$N$^+$CH_2CH$_2$), 3.79 -3.82 (m, 2H, NHCH_2CH$_2$CH$_2$), 3.93 (s, 3H, OCH_3), 4.09-4.11 (m, 2H, CH$_2$CH$_2$CH_2O), 7.10 (s, 1H, quinazoline ring), 7.87-7.95 (m, 3H, quinazoline ring and NH_2), 9.13 (s, 1H, NH-CH$_2$), 10.12-10.16 (bs, 1H, $^+H_3$N). ^{13}C-NMR (DMSO-d$_6$) δ 22.3 , 23.1, 29.4, 32.8, 42.1, 44.0, 54.7 (3C), 56.2, 64.4, 69.2, 99.2, 107.1, 111.0, 147.4, 151.5, 155.8, 158.9, 159.6. (EI): *m*/*z* [*M*]$^+$: 573.11.

7-(5-aminopentyloxy)-2-chloro-*N*-(3-(dimethylamino)propyl)-6-methoxyquinazolin-4-amine dihydrochloride (9). ^{1}H-NMR (DMSO-d$_6$, 400 MHz, δ; ppm) 1.49-1.50 (m, 2H, CH_2CH$_2$CH$_2$O), 1.62-1.65 (m, 2H, CH_2CH$_2$CH$_2$CH$_2$O), 1.78-1.82 (m, 2H, CH_2CH$_2$O), 2.03-2.07 (m, 2H, m, 2H, NHCH$_2$CH_2), 2.77-2.83 (m, 8H, CH$_2$N(CH_3)$_2$ and CH_2N(CH$_3$)$_2$), 3.15-3.17 (m, 2H, H$_3$N$^+$CH_2CH$_2$), 3.56-3.58 (m, 2H, NHCH_2CH$_2$), 3.91 (s, 3H, OCH_3), 4.09-4.12 (m, 2H, CH$_2$CH$_2$CH_2O), 7.46 (s, 1H, quinazoline ring), 7.84-7.88 (m, 4H, quinazoline ring and H_3N^+), 8.88 (s, 1H, NH-CH_2), 10.21-10.23 (bs, 1H, ^+HN(CH$_3$)$_2$). ^{13}C NMR (DMSO-d$_6$) δ 23.1, 26.6, 29.4¸32.8, 42.1, 43.2, 45.9 (2C), 56.2, 56.5, 69.2, 99.2, 107.1, 111.0, 147.4, 151.5, 155.8, 158.9, 159.6. (EI): *m*/*z* [*M*]$^+$: 467.16.

7-(5-aminopentyloxy)-*N*-(1-benzylpiperidin-4-yl)-2-chloro-6-methoxyquinazolin-4-amine dihydrochloride (10). ^{1}H-NMR (DMSO-d$_6$, 400 MHz, δ; ppm) 1.47-1.49 (m, 2H, CH_2CH$_2$CH$_2$O), 1.61-1.63 (m, 2H, CH_2CH$_2$CH$_2$CH$_2$O), 1.78-1.80 (m, 2H, CH_2CH$_2$O), 2.11 (m, 4H, CH_2 piperidine ring), 2.80-2.82 (m, 2H, H$_3$N$^+$CH_2CH$_2$), 3.14 (m, 2H, CH_2 piperidine ring), 3.37-3.39 (m, 2H, CH_2 piperidine ring), 3.91 (s, 3H, OCH_3), 4.09-4.11 (m, 2H, CH$_2$CH$_2$CH_2O), 4.28-4.30 (m, 3H, CH_2-benzyl ring and CH piperidine ring), 7.07 (s, 1H, quinazoline ring), 7.47-7.48 (m, 3H, quinazoline ring and phenyl ring), 7.65-7.66 (m, 2H, phenyl ring), 7.83 (m, 3H, *H* phenyl ring and NH_2), 8.45-8.46 (s, 1H, NH-piperidine), 10.89-11.12 (bs, 1H, H_3N^+), 11.34 (bs, 1H, ^+HN piperidine ring). ^{13}C-NMR (DMSO-d$_6$) δ 23.1, 29.4, 30.4 (2C), 32.8, 42.1, 49.4 (2C), 53.1, 56.2, 60.4,

69.2, 99.2, 107.1, 111.0, 127.3, 128.5 (2C), 128.9 (2C), 135.6, 147.4, 151.5, 155.8, 158.9, 159.6. (EI): *m*/*z* $[M]^+$: 555.19.

12.4. Biological evaluation, results and discussion

*12.4.1. Inhibition of KIAA1718 by BIX and its analog **6***

First, we found that BIX-01294 inhibits the demethylation activity of KIAA1718 Jumonji domain (residues 92-488) with an IC_{50} (half-maximal inhibitory concentration) value of approximately 16.5 μM, using a histone H3K9me2 peptide (residues 1-24) as substrate, by a mass spectrometry-based demethylation assay[497] (Figure 12.2, right). Next, we tested the BIX analog **6** (Figure 12.2, left), which was originally generated with improved inhibition for GLP,[575] with the replacement of the O6-methoxy group with a 5-aminopentyloxy substituent at position 7 of the quinazoline ring and the diazepane ring with a 3-dimethylaminopropyl group at position 2. The cumulative effect of these changes in **6** decreases its IC_{50} by a factor of approximately 4.5 in comparison to that of BIX.

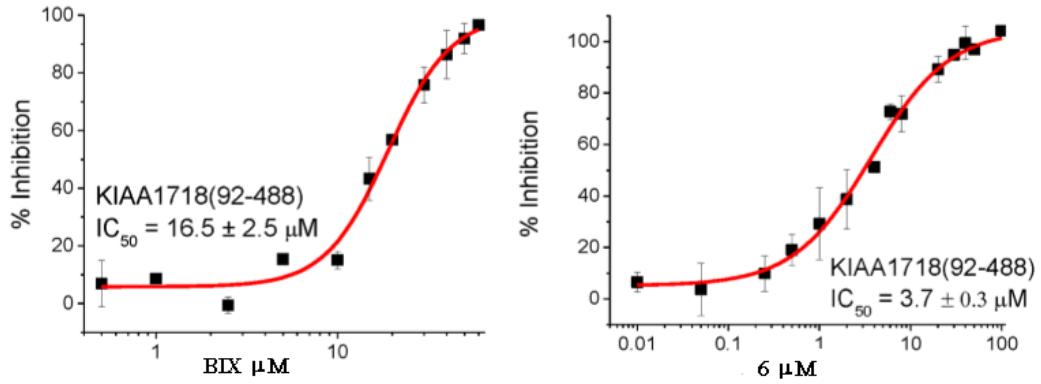

Figure 12.2. The inhibition (IC_{50} values) of compounds BIX-01294 and **6** against demethylation reaction by KIAA1718 (Jumonji domain) is plotted against various concentrations of inhibitor.

12.4.1.1. Methods

Protein purification and expression. KIAA1718 and PHF8 proteins, used in this study, were expressed and purified as described.[497] Briefly, the plasmid encoding the GST tagged fusion proteins were transformed into *E. coli* BL21 DE3 codon plus cells and grown in auto induction media[619] at 37°C. The proteins were purified by three-column chromatography (GST, Hi-TrapSP and S200). The GST tag was removed by thrombin cleavage. The purified KIAA1718 (residues 92-488) was concentrated to approximately 10-15 mg ml^{-1} in 20 mM BisTris pH 5.5, 5% glycerol, 200 mMNaCl and 1 mMdithiothreitol.

KIAA1718 assay. We tested the compounds BIX-01294 and **6** under the conditions of 2.5 μM enzyme and 5 μM H3(1-24)K9me2 peptide substrate in 50 mM HEPES pH 7.0, 1 mM α-KG, 50 μM $Fe(NH_4)_2(SO_4)_2$ and 2 mM ascorbic acid. The enzyme

and the respective inhibitor were preincubated for 10 min at room temperature (approximately 21 °C). Adding substrate H3 peptide initiated reaction for 10 min at 37 °C and subjected to mass spectrometry-based inhibition assay as previously described.[566]

*12.4.2. Structure of KIAA1718 Jumonji domain bound with **6***

We co-crystallized KIAA1718 Jumonji domain with **6**, which was dissolved in aqueous buffer, in the presence of α-ketoglutarate and Ni^{2+} ion. The structure was solved at a resolution of 2.8 Å. The first 22 residues (amino acids 92-113) and the last 9 residues (amino acids 480-488) of KIAA1718 were not observed.

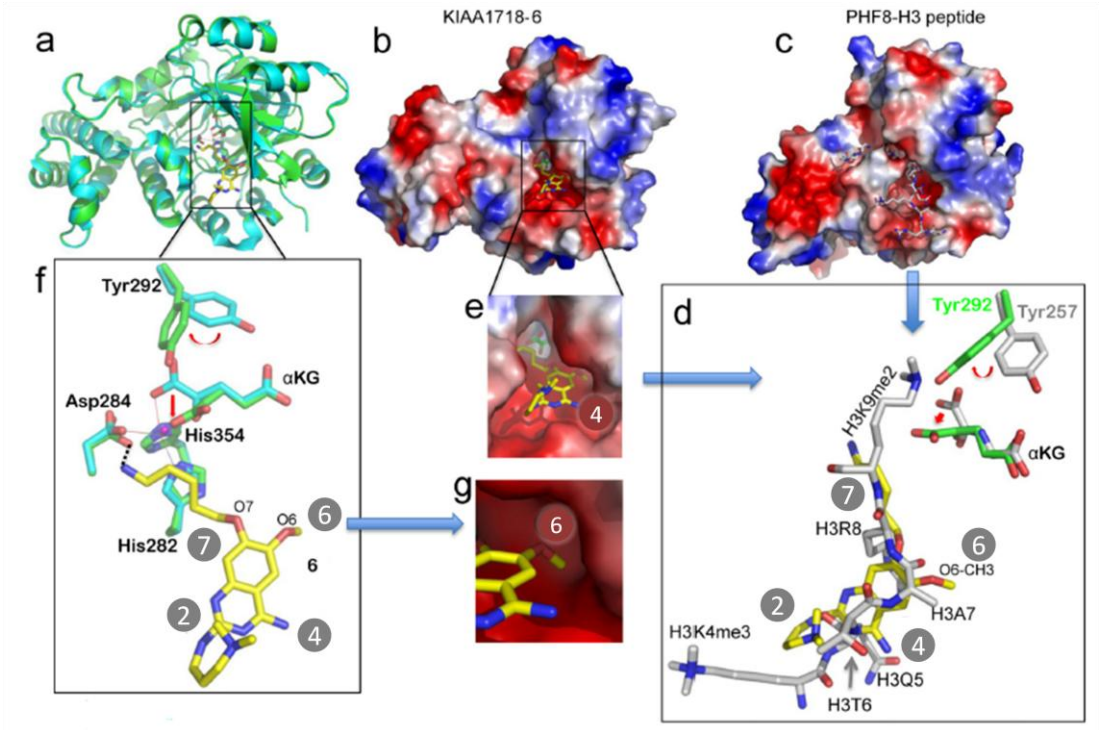

Figure 12.3. Structure of KIAA1718-**6** complex.
(a) Superimposition of KIAA1718 Jumonji domain structures with bound **6** (colored in green) and in the absence of bound substrate (cyan; PDB 3KVA). (b, c) Surface representation of the KIAA1718 Jumonji domain with **6** bound in the acidic substrate peptide binding groove (b), which is occupied by a histone peptide in the closely related PHF8 structure (c; PDB 3KV4). The surface charge at neutral pH is displayed as red for negative, blue for positive, and white for neutral. (d) Superimposition of H3 peptide (grey; taken from PDB 3KV4) and **6** (yellow). The inhibitor occupies the space of bound histone H3 peptide from Lys4 (main chain) to Lys9 (main chain). The corresponding tyrosine (Tyr292 in KIAA1718 and Tyr257 in PHF8) adopts different rotamer conformation resulting in a different mode of binding of α-ketoglutarate (αKG). (e) Enlarged view of **6** binding site with α-ketoglutarate (green) in the bottom of the pocket. (f) Network of interactions centered on the amino group of 5-aminopentyloxy moiety at position 7 of **6**. The metal ion (in small ball) is coordinated by side chains of His282, Asp284, His354 and two oxygen atoms of α-ketoglutarate. (g) The methyl group of the methoxy at site 6 of compound **6**, mimics the side chain of histone H3 Ala7 (see panel d), is bound in a shallow surface pocket of KIAA1718.

The protein component of the structure is highly similar to that of KIAA1718 in the absence of bound peptide substrate (Figure 12.3a; PDB 3KVA) and that of PHF8 in the presence of bound H3 peptide substrate (Figure 12.3c; PDB 3KV4), with a root mean squared deviation (rmsd) of approximately 0.3 Å and 1.3 Å, respectively, when comparing 366 pairs of Cα atoms (residues 114-479).

Compound **6** lies in a location occupied by the histone H3 peptide in the PHF8-peptide complex and occupies approximately the same space as that by histone H3 lysine 4 (main chain) to lysine 9 (Figure 12.3d), with a total of buried interface area of 422 $Å^2$. The acidic binding pocket is wide open and the α-ketoglutarate can be seen at the bottom of the pocket (Figure 12.3e). The 5-aminopentyloxy moiety at position 7 of the quinazoline ring is extended near the metal cofactor in the active site, with the aliphatic chain stacking with the planar surface of His282 and the terminal amino group forming a weak hydrogen bond with one of the carboxyl oxygen atoms of Asp284 (3.4 Å) (Figure 12.3f). The side chains of His282 and Asp284, together with His354, coordinate the binding of the metal ion. The *N*,*N*-dimethylpropylamine side chain at position 2 is near the acidic entrance of the substrate binding groove on the protein surface (Figure 12.3e) and the terminal dimethylated amino group folds back and stacks with the planar surface of the quinazoline ring (Figure 12.3f). The methyl group of the methoxy at position 6 is inserted into a shallow surface pocket of an inner wall formed by Gln200 and Thr279 (Figure 12.3g), mimicking the side chain of histone H3Ala7 (H3A7; Figure 12.3d). The O6 methyoxy-H3A7 mimic has also been observed in the interactions of **6** as well as BIX with GLP methyltransferase.[566,574] Thus, we suggest the O6 methyoxy at position 6 is an important discriminator of H3K9 enzymes (methylase and demethylases) vs. H3K4 enzyme(s) (see below). The *N*-benzyl-4-amino-piperidine moiety at position 4 is not observed in the structure. We could however model the moiety in the current structure without steric clashes with the protein by pointing the moiety to the solvent (Figure 12.4).

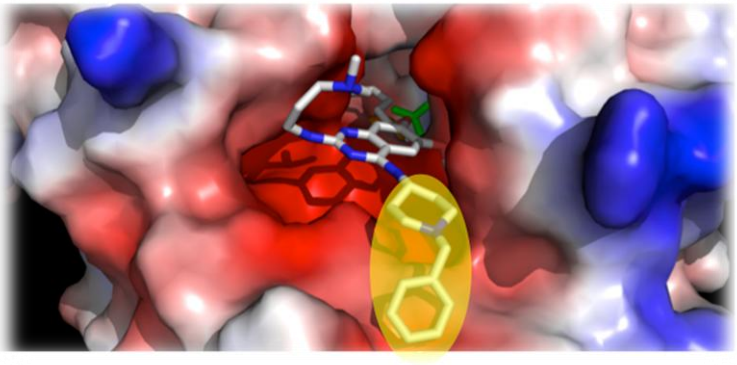

Figure 12.4. A model of the complete molecule **6** inside KIAA1718, in yellow it is show the suppose binding mode of the N-benzyl-4-amino-piperidine moiety.

12.4.2.1. Methods

The crystals were grown at 16 °C by hanging drop vapor diffusion method. The concentrated KIAA1718 (92-488) protein solution (~10 mg ml^{-1}) was mixed with 5 mM α-ketoglutarate, 4 mM $NiCl_2$ and 1 mM compound **6** (dissolved in aqueous buffer) prior to the setting up for crystallization. The well solution contained 15-20% (v/v) polyethylene glycol 5KMME, 0.2M $CaCl_2$, 0.1M BisTris pH 6.4.
The X-ray diffraction data[576] were collected at the Advanced Photon Source, Argonne National Laboratory, SERCAT beamline (22-BM). Diffraction data were processed scaled by HKL2000. We used PHENIX for molecular replacement, using a previously solved KIAA1718 (residues 92-488) structure (PDB 3KVA) as the initial model, and refinement. Coot was used for graphic model building. PRODRG server generated the initial model of compound **6**. The ReadySet software integrated in PHENIX generated the structural restraints for the inhibitor molecule. PyMOL (DeLano Scientific) was used to prepare the structural figures.

12.4.3. Generation of selective KIAA1718 inhibitors

In order to draw preliminary structure activity relationships keeping intact the 6 methoxy group we modified the positions 2, 4 and 7 of the quinazoline ring. As we can see from Table 12.3, in position 7 the 5-aminopentyloxy moiety is always better in terms of inhibitory potency than its closer homologues and than its methylated counterparts. As suggested by X-ray and docking inspections, the removal of the N-benzylpiperidine at position 4 didn't lead to any loss of activity. Indeed, the derivative **5** showed almost the same % of KIAA1718 inhibition of the prototype **6**. The same inhibitory potency was also observed by removing the dimethylammino-propylamino side chain at position 2 as exemplified by the derivative **10**. On the other hand, the double removal of the substituents at both positions 2 and 4 always led to a decrease of potency.

Table 12.3. Percent of inhibition of **1**-**10** against KIAA1718.

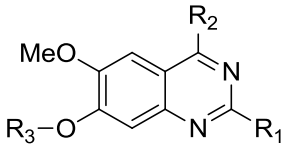

Cpd	R1	R2	R3	% KIAA1718 Inhibition @ 10 µM
1	H		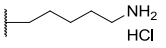	22
2	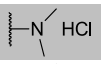		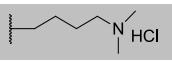	17.4
3			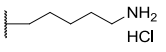	23
4	Cl		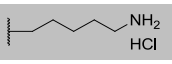	21
5	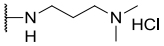		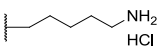	77
6	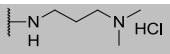	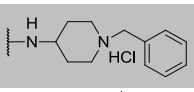	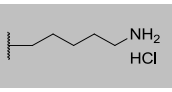	79
7	Cl	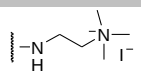	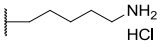	58
8	Cl	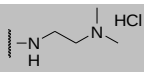	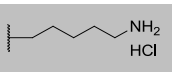	69
9	Cl	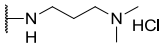	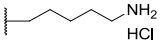	73
10	Cl	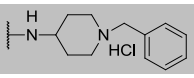	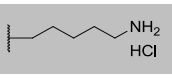	76

The IC_{50} values determinations confirmed the results obtained at fixed doses. Indeed, the removal of the substituent at either positions 2 or 4 led to two derivatives **10** and **5** with IC_{50} values 2.4 and 3.4 µM, respectively, equal or even slightly better than that of the prototype **6** (IC_{50}= 3.7 µM). Only the removal of both branches at the same time led to a drop of inhibitory potency of about 5-fold as proved by the compound **3** which has an IC_{50} 19 µM (Figure 12.5).

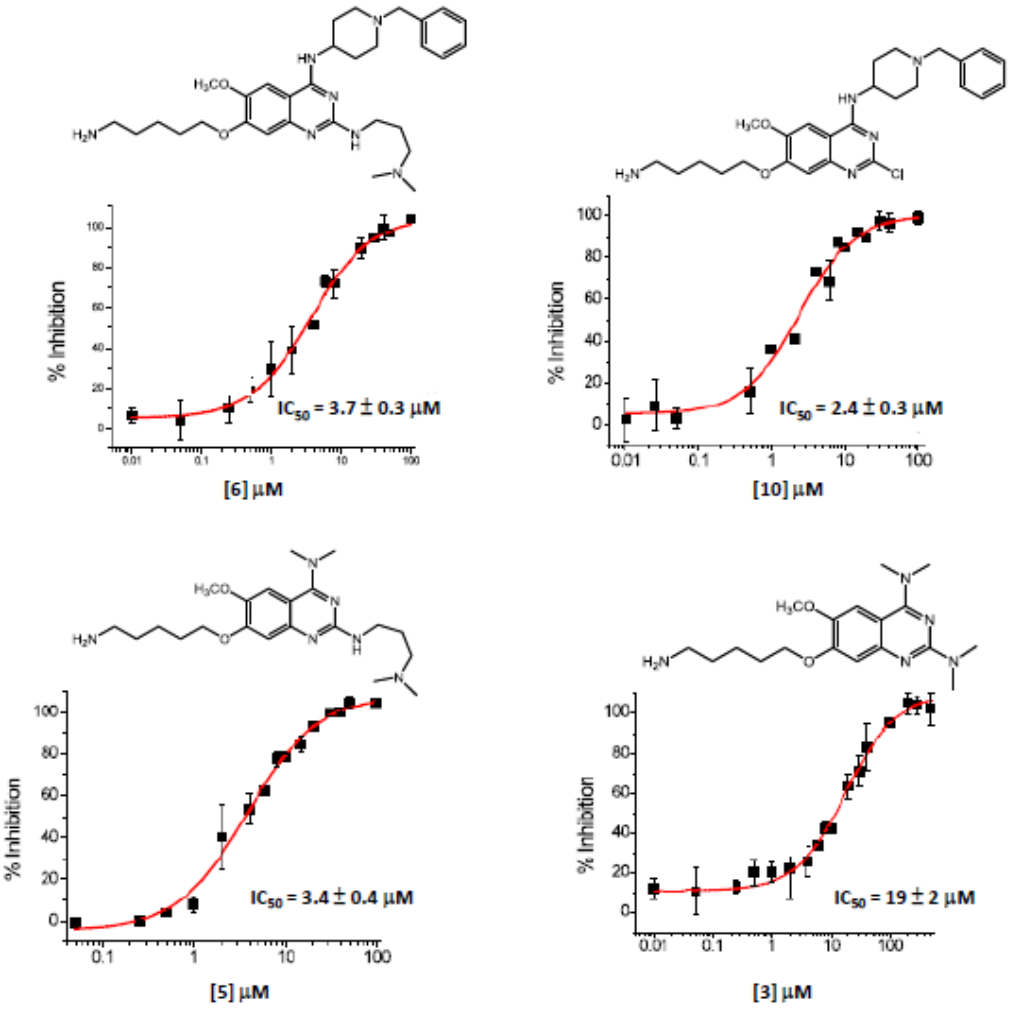

Figure 12.5. IC_{50} values of compounds **3**, **5**, **6**, **10** against demethylation reaction by KIAA1718.

We then decided to evaluate the effects of the removal of the substituents at positions 2 and 4 on the inhibition of GLP methyltransferase, considering that compound **6** was originally designed to improve the potency against H3K9 methyltransferase activities of G9a and GLP (with an IC_{50} value of 50 nM).[575] Surprisingly, as shown in Figure 12.6 both derivatives with only one branch missing (**5**, **10**) and the derivative without the two branches (**3**) were completely inactive against GLP at least at 10 µM concentration and more importantly in this way they revealed to be selective inhibitors of KIAA1718.

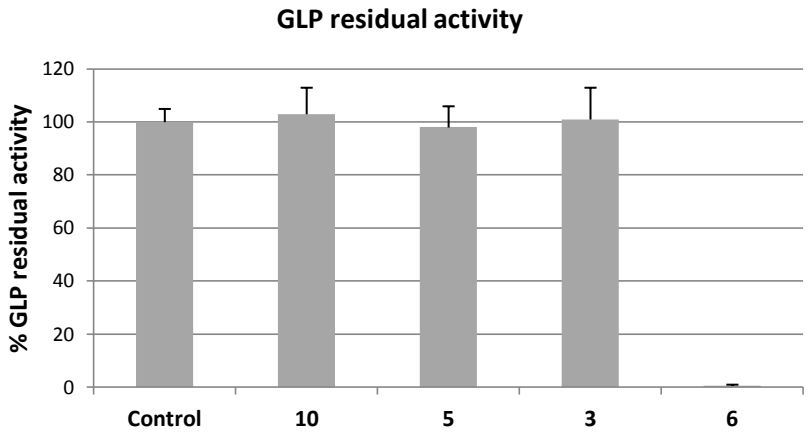

Figure 12.6. Effect of compounds **10**, **5**, **3**, **6** on methylation reaction by GLP (SET domain) at fixed dose of 10 μM.

After the finding that simplified analogues of **6** were able to discriminate between histone lysine 9 methyltransferases such as GLP and histone lysine 9 demethylases such as KIAA1718, we decided to test the new analogs against other two jumonji demethylases. One, PHF8, that belongs to the same subfamily of KIAA (KDM7) and works on the same substrate, the dimethylated lysine 9 of the histone H3, and another one JARID1C that belongs to another subfamily (KDM5) and demethylates the tri-methylated lysine 4 of the histone H3. All the derivatives displayed about an 80% inhibition of PHF8 (Figure 12.7, left). As evident from the activity data (Figure 12.7, right), neither BIX nor its analogs (**6**, **5**) can significantly inhibit JARID1C demethylation activity on the H3K4me3 peptide substrates. This is consistent with the fact that recognition of H3K4 and H3K9 methylation marks involves different sets of backbone and side chain interactions, the BIX analogs tested in this work were originally designed to mimic H3K9 binding. Both graphs demonstrate a subfamily selectivity in the inhibition of jumonji histone demethylases by our compounds.

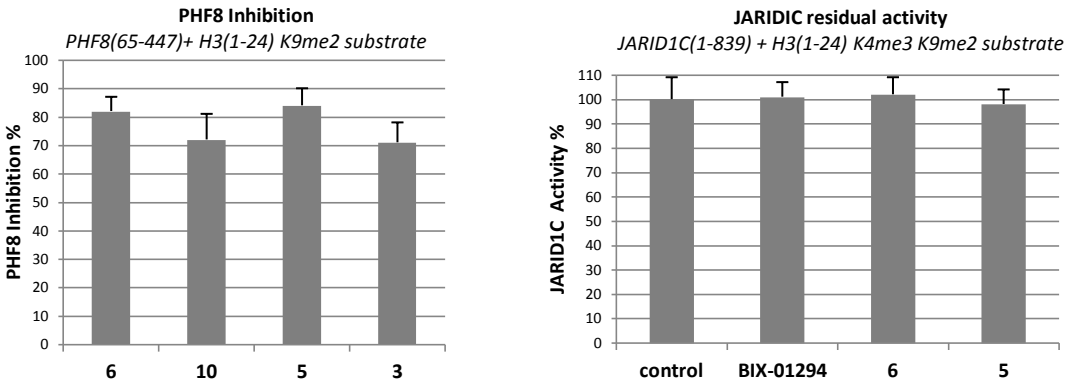

Figure 12.7. Percentage of inhibition of the H3K9me2 demethylation activities of PHF8 Jumonji domain (residues 65-447) on H3(1-24)K9me2. H3K4me3 demethylation activity of JARID1C(1-839) on H3(1-24)K4me3K9me2 substrate.In both assays are used 10 μM inhibitors.

12.4.3.1. Methods

Percentage of inhibition of the H3K9me2 demethylation activities of KIAA1718 Jumonji domain and PHF8 Jumonji domain was determined under the conditions of 2.5 μM enzyme, 5 μM substrate H3 ((1-24) K9me2) and 10 μM inhibitors. Enzymes were pre-incubated with the inhibitors for 10 min at room temperature (approximately 21 °C) prior to the addition of substrate peptide. The reactions were then incubated at 37 °C for 10 min (KIAA1718) or 60 min (PHF8).

To determinate the inhibition of **3**, **5**, **6** and **10** against methylation reaction by GLP we used the following conditions:0.1 μM enzyme and 5 μM H3 peptide (residues 1-15) in 20 mM Tris 8.0, 5 mM dithiothreitol (DTT) and 100 μM S-adenosyl-L-methionine (AdoMet). GLP was pre-incubated with varying 10 μM of inhibitors for 5 min at room temperature (approximately 21 °C). Adding substrate H3 peptide initiated reaction for 5 min at 30° C.

H3K4me3 demethylation activity of JARID1C (1-839) on H3(1-24)K4me3, K9me2 substrate was determined, under these conditions: 0.25 μM enzyme, 10 μM peptide substrate and 10 μM inhibitor in 50 mM MES pH 6.8. Enzyme was pre-incubated with inhibitor at room temperature (~ 21 °C) prior to the addition of substrate peptide and the reactions were lasted for 10 min at 37 °C.

12.4.4. Conclusion

Here we show that BIX-01294, a H3K9 peptide mimic small molecule compound, can inhibit both H3K9 methyltransferase (GLP: IC_{50}= 0.25 μM) and demethylase (KIAA1718: IC_{50}=16.5 μM). Supported by crystallographic and docking studies we have increased the inhibitory potency against the lysine 9 methyltransferase GLP of about 13-fold developing the derivative **6**. By deleting the benzylated six-membered piperidine ring moiety, as suggested by the co-crystal structure of KIAA1718-**6** complex, we have obtained some simplified analogues such as the compound **5** that is more selective against KIAA1718 (and his subfamily PHF8) than GLP of almost 13 fold (GLP: IC_{50}= 75 μM, KIAA1718: IC_{50}= 3.4 μM). This reversal of selectivity is only due to the severe loss in activity against GLP without affecting inhibition against KIAA1718. Therefore, the current structure of KIAA1718-**6** complex provides new avenues for further improving the potency and selectivity of the inhibitor by strengthening KIAA1718-**6** interactions. For example, the *N*,*N*-dimethylpropylamine side chain at position 2 has little contact with the protein and replacement with group(s) that maximize the interaction near the entrance of the substrate binding groove may increase the potency against KIAA1718.
To best of our knowledge, compound **5** is the first examples of subfamily-selective small molecule inhibitors of jumonji demethylases which don't chelate the Fe^{2+} cofactor of these enzymes. Iterative cycles of crystallography, synthesis, and bioassay will ultimately aid successful design of selective and potent epigenetic inhibitors of histone lysine demethylases.

*Adapted with the permission from Upadhyay, A. K., Rotili, D., Han, J. W., Hu, R., Chang, Y., Labella, D., Zhang, X., Yoon, Y. S., Mai, A., Cheng, X. An analog of BIX-01294 selectively inhibits a family of histone H3 lysine 9 Jumonji demethylases. *J. Mol. Biol.* **2012,** 416, 319-327.[576]

13. *In vitro* assays to determine Sirtuin deacylation activity

Consistent with the diverse cellular functions of sirtuins, different peptide substrates have been identified as targets for deacylation by the various sirtuin enzymes. Activation of these enzymes has been thought to provide protection from certain neurodegenerative diseases and metabolic disorders, and the inhibition of the enzymes may inhibit progression of cancer.[224] Identification of small-molecule modulators (activators or inhibitors) of this class of enzymes could lead to the development of novel therapeutic agents. Therefore, it is important to develop powerful screening methods to investigate activities, substrate specificities or the effectiveness of potential activators and inhibitors. In the literature several assays for sirtuin enzymes have been reported. Early approaches monitored the release of radioactive products derived from either ^{3}[H]-acetylated substrates or ^{14}[C]-NAD^{+} and ^{32}[P]-NAD^{+}, respectively.[620-623] Later developments mainly utilized fluorescence detection, for example the commercially available Fluor de Lys^{TM}-assay. It is based on the deacetylation of acetylated tetrapeptides labeled with 7-amino-4-methylcoumarin at the C-terminus. An alternative method using Z-Mal as a substrate was shown by Heltweg et al..[624] Other approaches include the separation of acetylated peptides and their respective deacetylated products by high performance liquid chromatography (HPLC) or mass spectrometry (MS) after enzymatic reaction.[625] Furthermore, Marcotte et al. reported on a fluorescence resonance energy transfer (FRET)-based assay using peptides modified with a quencher at the N-terminus and a fluorophore at the C-terminus.[626] Liu and coworkers used Caliper´s sipper chips to realize a microfluidic mobility shift assay for the determination of K_m and IC_{50} values. They also employed luciferase in a bioluminescence assay based upon quantitation of remaining NAD^{+}.[627] Moreover, the deacetylation of proteins has been studied by means of an enzyme-linked immunosorbent assay (ELISA).[628] Scriba´s group demonstrated the determination of kinetic and inhibition parameters of hSIRT1 and hSIRT2 establishing a validated capillary electrophoresis (CE) method. As substrates 9-fluorenylmethoxycarbonyl (Fmoc)-labeled peptides were synthesized and evaluated.[629] More recently, Denu´s group developed a spectroscopic assay capable of determining steady-state kinetic parameters and continuous product monitoring. Formed nicotinamide is converted on a microplate by additional enzymatic and oxidative steps yielding NAD(P)$^{+}$.[630] Moreover, a fluorogenic assay based on the quantification of remaining NAD^{+} was published. In this approach the remaining cofactor is converted to a highly fluorescent compound with a two-step fluorogenic reaction.[631]

During my stay at the University of Bayreuth, laboratory of Prof. Steegborn, my goal was to learn and apply the FdL assay, continuous microplate assay and a MS-based assay to investigate the potential effect of small molecules that can regulate Sirtuin activity.

13.1. Fluorescence assay of SIRT protein deacetylases

One of the traditional assays for the in vitro measurement of histone deacetylase/deacylase activity is the widely used "Fluor-de-Lys" assay. The assay is based on peptidic substrates that contain an ε-acylated lysine residue followed by a 4-methylcoumarin-7-amide (MCA) moiety at their carboxytermini. The assay is a two-step enzymatic reaction (Figure 13.1).[632] In the first reaction catalyzed by histone deacetylases, acetate is released from ε-acetylated lysine moieties. In the second reaction, the deacetylated peptides are recognized as substrates by trypsin, which cleaves only after deacetylation and then after lysine residues. The assay is highly sensitive and does not demand the consumption of expensive material such as histones. However, since the peptidic substrates used so far are only poor substrates to trypsin, relatively high concentrations of the latter are required to drive the (second) reaction to completion within a short period of time.

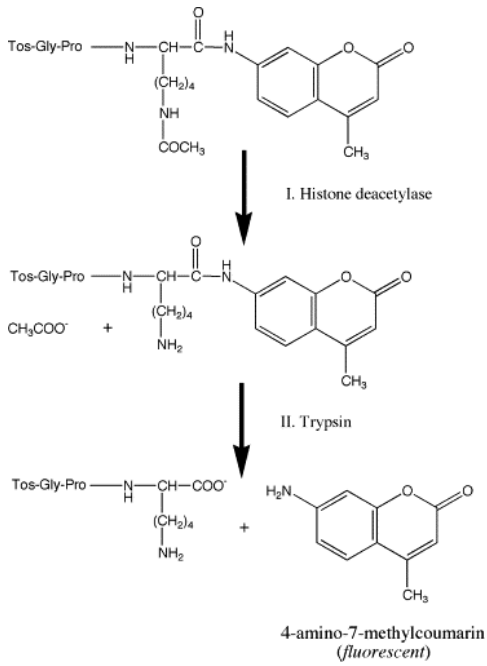

Figure 13.1. Principle of the fluorescence deacetylase assay. The assay comprises two steps. In step I the ε-acetylated lysyl moieties of the peptidic substrate is deacetylated. In step II deacetylated substrate molecules are cleaved by trypsin which at the same time releases fluorescent 7-amino-4-methylcoumarin. Fluorescence measurement is done at λ_{ex}=390 nm and λ_{em}=460 nm.

This assay can be easily used for high-throughput-screening but can cause artifact. For example Sirt1 activation by some compounds in Fluor de Lys assays does not correlate with activity measured using nonfluorescent peptides or full-length proteins. Indeed, the putative Sirt1 activator resveratrol requires the AMC portion of the Fluor de Lys substrate to observe activation.[223]

We use this assay to test a series of EX-527 analogs against human SIRT1. The protein was already provided in lab, but the compounds didn´t show any effect.

13.1.1. Materials and methods

The SIRT inhibition assay was performed using human recombinant SIRT1 produced in *E. coli*. Compounds were tested using a SIRT1 Fluorescent Activity Assay Kit (Enzo Life Science, Plymouth Meeting, PA). The procedure includes two steps: in the first part 0.1 mM SIRT1 substrate, a p53-derived fluorophore-labeled peptide (FdL-1 substrate peptide, Enzo), was incubated with 0.3 μg of protein, 0.5 mM NAD^+ in the presence of 10/50 μM compounds and 1% (v/v) DMSO or DMSO without compound as a control, for 30 minutes at 37 °C, in a total volume of 50 μL. In the second stage samples were incubated with Developer II for 45 minutes at room temperature. Developer II includes nicotinamide (NAM), a sirtuin inhibitor that stops the SIRT1 activity, and trypsin, which releases the fluorophor, thus producing the fluorescent signal. The fluorescence was measured on a FluoDia T70 (*Photal*) microplate reader, with excitation set at 360 nm and emission detection set at 460 nm.

13.2. Continuous microplate assay

In 2009, Smith and colleagues reported another spectroscopic assay, the continuous microplate assay, that is using an enzyme-coupled system in which NAM is converted to nicotinic acid and ammonia by nicotinamidase (Figure 13.2).[629] Almost all of the assays, known until this study, required unnatural fluorescent or radioactive substrates, additional enzymatic steps for detection of the deacetylation reaction, and specialized equipment. Furthermore, all previously reported sirtuin assays were endpoint assays. The continuos microplate assay allows to measure sirtuin activity with native substrates, does not use radioactive or fluorescent labels, requires no special instrumentation other than a common spectrophotometer, and measures sirtuin activity continuously. This assay is also a rapid method because it doesn't need any additional workup steps to detect enzymatic activity.[629]
This assay is based on the reaction shown in Figure 13.2.[629] Sirtuins catalyze protein deacetylation using NAD^+ as a cosubstrate forming deacetylated peptide/protein, O-acetyl-ADP-ribose (OAADPr), and NAM. Sirtuins stoichiometrically use NAD^+ such that one molecule of NAM is formed from NAD^+ for every lysine residue deacetylated. Nicotinamidase hydrolyzes NAM in nicotinic acid and ammonia. The ammonia is transferred to α-ketoglutarate via glutamate dehydrogenase, yielding to glutamate and the oxidation of NAD(P)H to $NAD(P)^+$. NAD(P)H consumption oxidation is measured spectrophotometrically at 340 nm.
This test still has disadvantages: it suffers from interference of absorbing and/or fluorescent compounds, furthermore compounds intended to modulate sirtuin activity could interfere with coupled enzymes (e.g. GW5074 is a GDH inhibitor) and, more importantly, this assay is not very sensitive.
The continuous microplate assay was used to test the potential activity of some SRT1720 analogs on human SIRT3, but no significant result were found.

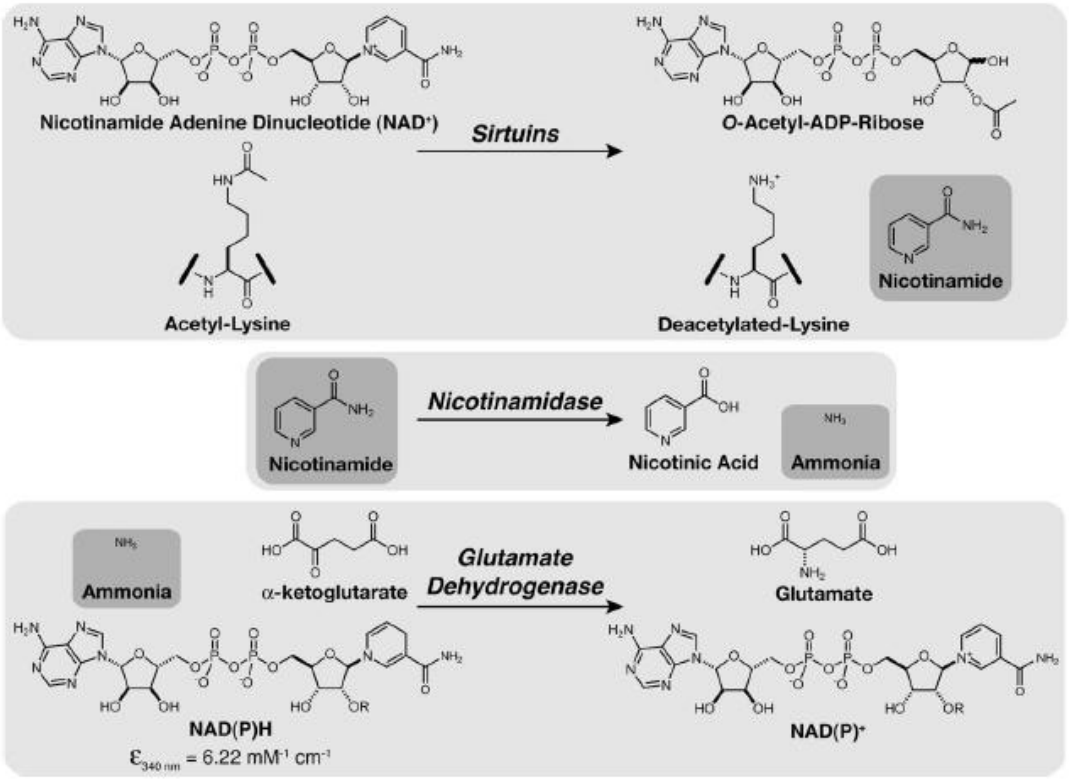

Figure 13.2. Scheme of the nicotinamidase/ glutamate dehydrogenase enzyme couple assay.

13.2.2. Materials and methods

Materials. Chemicals were purchased from *Sigma-Aldrich, Roth* and *Applichem.* Buffers were prepared with ddH_2O. The peptide (ACS2_2, TRSG-acetylK- VMRRL) was synthesized by *GL Biochem.* Human Sirt3 (aa 114- 380) was available in lab and at least affinity purified and gelfiltrated. The protein possessed an N-terminal hexa-histidine tag and a TEV protease cleavage site for tag removal.

Continuous Deacetylation Assay. Reaction mixture, total volume 100 µL, consisted of 2 µM hSirt3, 200 µM substrate peptide (ACS2_2), 0.5 mM NAD^+, 3.5 mM α-ketoglutarate, 2 µM nicotinamidase, 2 U/mL GDH and 0.5 mM NADPH, in 20 mM sodium phosphate buffer pH 7.7, in the presence of 10/100 µM compounds in 2% DMSO. All assay components except compound and NAD^+ where preincubated for 5 minutes and the reaction was initiated by addition of NAD^+. The consumption of NADPH was followed as a decrease in absorption at a wavelength of 340 nm, in a 96-well plate and monitored using a LAMBDA-Scan spectrophotometer (*MWG Biotech*). The assays were performed for 1 hour at room temperature with measurement intervals of 1 min. Activity was determined by linear fitting of the initial rate of the reaction.

13.3. Identification of small molecules as SIRT5 inhibitors through MS-Based Deacylation Assay

Recently, Sirt5 was found to possess potent and unique demalonylase and desuccinylase activities and CPS1 is the most important substrate.[223] Du et al. show that while CPS1 is both acetylated and succinylated at three lysine residues (K44, K287, and K1291), in the absence of SIRT5 succinylation of K1291 increases, whereas succinylation of K44 and K287 or acetylation of K44, K287, and K1291 remain unchanged. These new succinylation data suggests that SIRT5 regulates the enzymatic activity of CPS1 by desuccinylating K1291. Because acetylation and succinylation can occur on the same CPS1 lysine residues, further studies are needed to resolve which modification is regulatory. The preference for succinyl and malonyl groups is due to the presence of an arginine residue (Arg^{105}) and tyrosine residue (Tyr^{102}) in the acyl pocket of Sirt5 (Figure 13.3).[623]

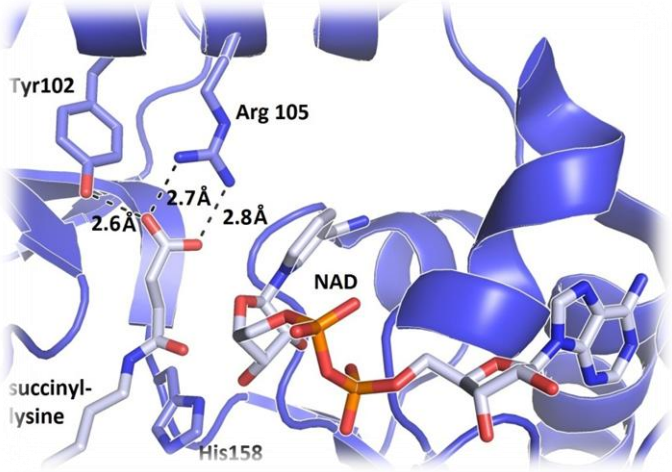

Figure 13.3. Sirt5-succinyl peptide-NAD ternary structure showing that the succinyl group interact with Tyr^{102} and Arg^{105}.

Sirt5 deficiency in mice leads to hyperammonemia after a period of caloric restriction. This effect is due to the lack of Sirt5-dependent deacylation and thereby activation of its first identified physiological substrate carbamoyl phosphate synthetase 1 (CPS1). Sirt5 activity is triggered by higher NAD^+ availability in times of nutrient deprivation, when amino acids are catabolized as an alternative energy source and CPS1 is needed to detoxicate the by-product ammonia through catalyzing the first step of the urea cycle.[230,259]

Inhibitors that are specific for a particular Sirtuin isoform will be very useful for investigating the therapeutic potential of the specific Sirtuin and their biological function. The major obstacle in the development of small molecules that can regulate Sirtuin activity is the fact that some human Sirtuins have very weak enzymatic activity, not always the proper Sirtuin substrate is known, and suitable assays are either not available or difficult to perform.

In order to overcome the limitations of the *in vitro* assays described above, it is possible to use a deacylation assay based on the direct and label-free relative quantification of substrate and product using LC-MS.[257]

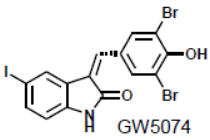

GW5074

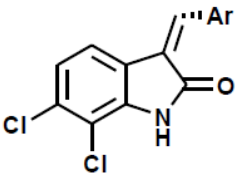

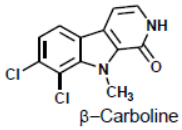

β–Carboline

Cpd	Ar	E/Z ratio
UBCS_0159	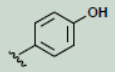	57:43
UBCS_0160	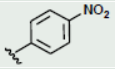	57:43
UBCS_0161		100:0
UBCS_0162		100:0
UBCS_0163	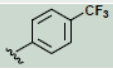	60:40
UBCS_0164	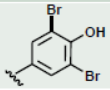	30:70

Cpd	Ar	E/Z ratio
UBCS_0165		0:100
UBCS_0166	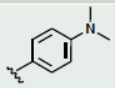	82:18
UBCS_0167		54:46
UBCS_0168	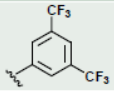	69:31
UBCS_0169	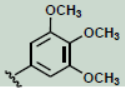	50:50

Figure 13.4. Novel 3-Arylidenindolin-2-ones.

The aim of this project was to identify a potent and selective inhibitor for the human isoform Sirt5. Until now just few modulators have been reported for Sirt5. Thiosuccinyl peptides are the only know selective and potent Sirt5 inhibitors. The thioacetylated peptides can undergo the first step of the sirtuin-catalyzed deacylation reaction, forming the covalent thioalkyl-imidate intermediate that stops any futher reaction. Despite this first success, peptide derivative inhibitors are generally pharmacologically limited due to their size, biostability and poor membrane permeability.[634]

In a recent study, carried out by our collaborators Suenkel et al., it has been found that GW5074 (Figure 13.4), an indole derivative, is able to inhibit Sirt5 desuccinylation activity with an IC_{50} of 20 μM; so a first pharmacological scaffold has been identified in order to develop Sirt5 specific inhibitors.[404]
In 2010, Prof. Bracher and his team from Ludwidg-Maximilians-Universität München, presented novel Sirt inhibitors based on a 6,7-dichloro-2-oxindole scaffold with low micromolar activity. To prepare this series of derivatives, they combined structural elements of the alkaloid β-Carboline (with antiproliferative and antiviral activity) with those of the Sirtuin inhibitor GW5074 (Figure 13.4).[635] Due to the

structure similarity with GW5074, we decided to test these series of analogs (Figure 13.4) in order to find a more selective and potent inhibitor of human Sirt5.
GW5074 disturbs signal in FdL assay and it is known to inhibit the glutamate dehydrogenase (GDH), which makes this compound incompatible with the continuous assays, so we tested this series of analogs on hSirt5 in a MS-based assay using, as substrate, the succinylated peptide Peroxiredoxin 1 (succPRX1: SKEYFS-succinylLys-QK).

13.3.1. Materials and methods

13.3.1.1. Expression and purification of human Sirt5 (34-302)

Heterologous overexpression of protein. The human Sirt5 construct used in this study (already provided by the lab of Prof. Clemens Steegborn) comprises amino acids 34-302 cloned in pET151/D-TOPO vector harboring a N-terminal 6x His tag and a TEV protease cleavage site. Sirt5 protein was expressed in *E. coli* BL21DE3 Rosetta 2 cells. Cells were cultured at 37 °C to an OD_{600} of 0.6, in LB media (containing 100 µg/ml Ampicillin and 34 µg/ml Chloramphenicol). Expression was induced by adding 0.5 mM isopropylthiogalactopyranoside (IPTG), and culturing continued overnight at 20 °C/140 RPM in a shaker (Infors HT, Switzerland). After overnight protein expression, the cells were harvested by centrifugation at 5.000 RPM at 4 °C for 20 minutes, cell pellets were resuspended in lysis buffer (50 mM Tris/HCl pH 7.8, 200 mM NaCl) supplemented with 0.5 mM phenylmethylsulfonylfluorid (PMSF) and stored at – 80 °C until required.

Cell lysis. Frozen cells were thawed and resuspended on ice in lysis buffer. During resuspension, 0.04 mg lyzosyme were added to 1 g cells and incubated for 20 minute. Cells lysis was further performed mechanically using a a Microfluidizer (Microfluidics, USA) maintained at 4° C. The lysed cells were centrifuged at 18.000 RPM for 45 minutes in a refrigerated Beckman Coulter Avanti J-26XP centrifuge fitted with a JA-30.50 Ti rotor (Beckman Coulter, USA) to remove cell debris.

Purification of protein

Affinity chromatography. Purification of recombinant protein containing His-tag was performed using TALON resin (Clontech, USA). For every liter of *E. coli* culture, 1 ml bed volume of resin was used. Prior to usage, the resin was washed and equilibrated twice with 10 bed volumes of lysis buffer. The cleared *E. coli* supernatant containing the recombinant protein in lysis buffer was incubated with the resin at 4 °C for 1 hour by stirring for efficient binding of the protein to the resin. After the incubation, the flowthrough was collected by gravity flow using a glass column (Bio-Rad, USA) and the column washed with 10 bed volumes of wash buffer A and 10 bed volumes of buffer B, then eluted with elution buffer (buffer compositions see below). The samples were run on SDS-PAGE to access the size and purity of the protein before performing additional purification steps.

Buffer compositions. Lysis buffer: 50 mM Tris, pH 7.5, 300 mM NaCl, 0.2 mM PMSF, protease inhibitor (Roche cOmplete EDTA free). Wash buffer: buffer A) 50 mM Tris/HCl pH 7.8, 500 mM NaCl; buffer B) 50 mM Tris/HCl pH 7.8, 200 mM NaCl, 5 mM imidazole. Elution buffer: 50 mM Tris/HCl pH 7.8, 200 mM NaCl, 250 mM imidazole.

Size exclusion chromatography. Elution samples from the affinity chromatography were pooled, concentrated using an Amicon centrifugal concentrator (Millipore, USA) to 5 ml and applied on to a preequilibrated Superose 12 size exclusion column (GE Healthcare, USA) and eluted with 20 mM Tris/HCl pH 7.8, 150 mM NaCl Following chromatography, the samples were run on SDS-PAGE to access their purity; appropriate fractions were pooled and concentrated.

Determination of protein concentration

Protein concentrations were either determined by Bradford-assay or based on Lambert-Beer's law. For those purposes, absorptions were measured using a Cary® 50 UV-Vis spectrophotometer (*Varian*). Bradford-assay was performed by mixing 200 µL Bradford-reagent (*Bio-rad*), 790 µL ddH_2O with 10 µL protein solution and determination of absorption at 595 nm to calculate protein concentration via **equation 1**, which is based on experimental data with standard proteins.[636]

$$C\ \left[\frac{mg}{mL}\right] = \frac{(37.4 \cdot\ A_{595} - 0.74) \cdot 1000}{V_{Protein}} \cdot \frac{2}{3} \div 1000$$

Equation 1. C:concentration A_{595}: Absorption at 595 nm $V_{protein}$: Volume of protein solution used for measurement

Determination of protein concentration based on Lambert-Beer's law was done by measuring absorption at 280 nm and calculating protein concentration using **equation 2**, including the protein's theoretical absorption coefficient at 280 nm.

$$C[mM] = \frac{A_{280}}{\varepsilon_{280}} \cdot 1000$$

Equation 2. C: concentration [mM] A_{280}: absorption at a wavelength of 280 nm ε_{280}: absorption coefficient at a wavelength of 280 nm [$M^{-1}cm^{-1}$] d: thickness of cuvette (1 cm)

Absorption coefficients at 280 nm were calculated from the amino acid sequence using Protparam 67.

13.3.1.2. Mass-spectrometry based deacylation assay

Direct measurement of desuccinylation by Sirt5 was done by a MS-based deacylation assay already established in Prof. Steegborn lab.[257] We decided to test the series of 3-Arylidenindolin-2-ones (Figure 13.4) at two concentration, 10 and 100 µM. The reaction mixture, containing 0.05 mM succPRX1 and hSirt5 0.01 mg/ml, was incubated at 37 °C and reaction was started by adding 2.5 mM NAD^+ and different

compound concentrations in 20mM Tris/HCl pH 7.8 and 150mM NaCl. The reaction was stopped with trifluoroacetic acid (0.25% final concentration) at four time points within 20 min incubation. Samples were diluted with 0.1 % formic acid, to achieve the final peptide concentration of 1μM, and were filtered by using a AcroPrep™ Advance 96-well Filter Plates. After filtration samples were analyzed to detect the ratio of the succinylated and desuccinylated peptide species, with a LC-MS system by using a linear gradient from 0% to 45% buffer B in 20 min (buffer A: 0.1%TFA, buffer B: Acetonitrile, 0.1%TFA). To determine the peak areas Skyline software was used (MacCoss lab, Seattle). Skyline determined two transitions for the peptide that contained the succinylated lysine (succPRX1: SKEYFS-succinylLys-QK) and one for the desuccinylated peptide (PRX1: SKEYFSKQ). Sirt5 activity was calculated by linear regression analysis of time series using *Excel 2010*. In all MS based assays the relative amount of deacylated peptide in percent (= Deacetylation [%]) was calculated according to **equation 3**. For the analysis the value for deacylation [%] of the sample, where the putative inhibitor was absent, was set as 100 % to get relative values for deacylation.

$$Deacylation\ [\%] = \frac{Area_{deacylated\ peptide}}{Area_{\ deacylated\ peptide} + Area_{acylated\ perptide}} \cdot 100 \qquad \textbf{Equation 3}$$

13.3.2. Results

Testing Sirt5 activity was initially performed with a MS-based assay using a succCPS1 substrate, but no good signals for the peptides were detectable in MS-spectra, possibly due to the high hydrophobicity of the CPS1-peptide. We then decided to use as substrate a succylated peptide derived from peroxiredoin1 (succPRX1). In Figure 13.5 the effect of GW5074 derivates on Sirt5 is shown. The best compounds that show a relative Sirt5 dessucinylation activity similar to GW5074, are the following: UBCS_164, bearing the same aromatic substitution of the parent compound, UBCS_165 characterized by the 2,4-dimethylpyrrole and UBCS_167 having the p-Fluor on the aromatic ring (Figure 13.4). To evaluate the selectivity of these promising analogs, we decided to test UBCS_164, 165,167 and the parent compound GW5074 (at 10 and 100 μM) on the human Sirtuin 1, 2 and 3 (Figure 13.6). In the assay, for better comparison, we kept NAD^+ and substrate concentration constant (See Sec. 13.3.1.2.*)*, and we used 0.02 mg/ml of each enzyme. For the different isoform Sirt1, 2 and 3, we used the *in vitro* substrates p53short (RHK-acetylK-LMFK), α-Tubulin (MPSD-acetylK-TIG) and ACS2_2 (TRSG-acetylK- VMRRL) respectively.

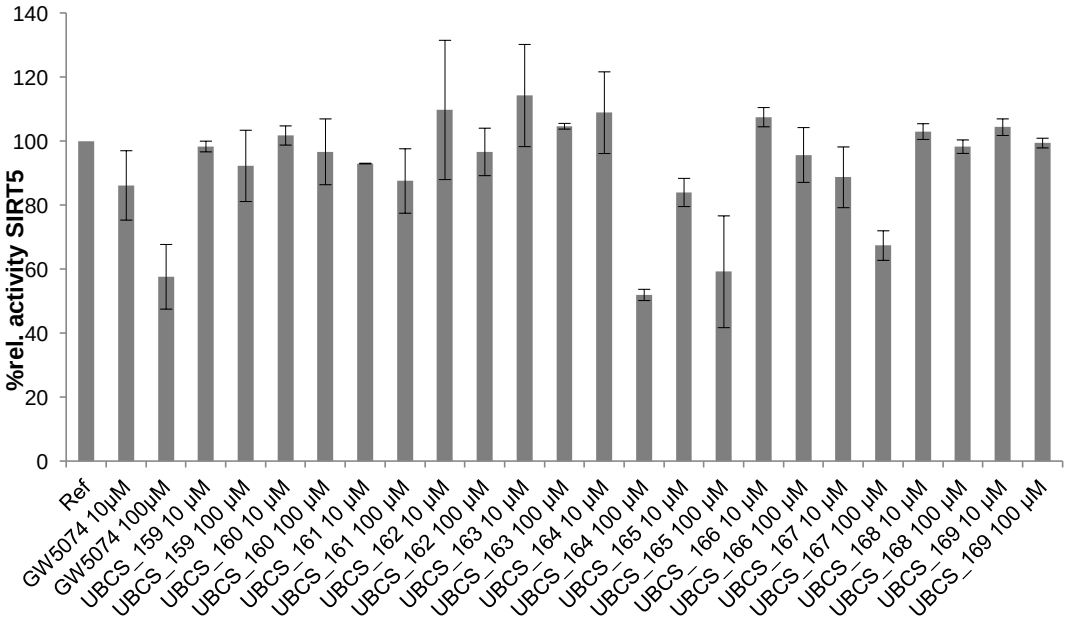

Figure 13.5. Relative Sirt5 desuccinylation activity in presence of 10 and 100 µM compound. Relative activities were calculated by determining the linear slope of each assay at four time points within 20 min incubation. Error bars are the variation of three independent assays.

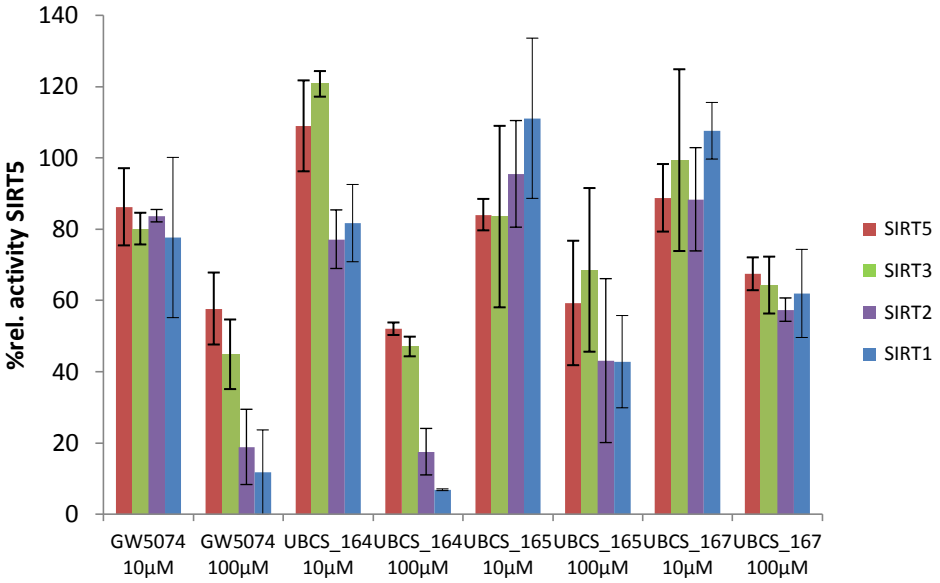

Figure 13.6. Relative deacylation activity on different Sirtuin isoforms.

13.3.3. Conclusion

As shown in Figure 13.5, the compound UBCS_164 exhibits an activity against Sirt5 comparable to the lead compound GW5074. From this first comparison we can conclude that by changing the halogen substitution of the oxindole scaffold from position 5 to both position 6 and 7 no gain in the inhibition is observed. No Sirt5 inhibition is shown when the two bromide are removed from the aromatic ring as for UBCS_159 and when a steric hindrance at position 3, 4, 5 of the phenyl group is present, as in UBCS_169. Particularly interesting are the results obtained by testing the GW5074 analogs on the different Sirtuin isoform (Figure 13.6). The parent compound GW5074 show at 100 μM a strong inhibition of Sirt1 that decrease in order against Sirt2, 3 and 5; we can observe the same trends for UBCS_164. The compounds UBCS_165 and 167, bearing the 2, 4-dimethylpyrrole and the p-Fluor on the aromatic ring, respectively, show almost the same inhibition for all four Sirtuin isoform. In conclusion we cannot gain selectivity just by changing the halogen substitution on the oxindole scaffold, but we can modulate the potency and selectivity of the compounds in particularly by changing the benzyliden substitution. For a better potency it seems that the benzylidene ring needs to have a 4-phenol or a good hydrogen bond donator, flanked by a halogen substitute.

14. References

1. Waddington, C.H. The epigenotype. *Endeavour* **1942**, 1, 18-20.
2. Goldberg A.D., Allis C.D., Bernstein E. Epigenetics: a landscape takes shape. *Cell.* **2007**, 128, 635-8.
3. Jones, P.A., Baylin, S.B. The fundamental role of epigenetic events in cancer. *Nat. Rev. Genet.* **2002**, 3, 415-428.
4. Jones, P.A., Martienssen, R.. A blueprint for a human epigenome project: the AACR human epigenome workshop. *Cancer Res.* **2005**, 65, 11241-11246.
5. Yoo, C.B., Jones, P.A. Epigenetic therapy of cancer: past, present and future. *Nat. Rev. Drug Discov*. **2006**, 5, 37-50.
6. Jones, P.A., Baylin, S. B. A decade of exploring the cancer epigenome - biological and translational implications. *Nature Reviews Cancer* **2011**, 11, 726-734.
7. Kouzarides, T. Chromatin Modifications and Their Function. *Cell* **2007**, 128, 693-705.
8. Bird A. Perceptions of epigenetics *Nature* **2007**,447.
9. Dennis C. Altered states. *Nature* **2003**, 421, 686-688.
10. Maier S., Olek A. Diabetes: A candidate disease for efficient DNA methylation profiling. *J Nutr Sci* **2002**, 132, 2440-2443.
11. Lister, R., Pelizzola, M., Dowen, R. H., Hawkins, R.D., Hon, G., Tonti-Filippini, J., Nery, J.R., Lee, L., Ye, Z., Ngo, Q. M., Edsall, L., Antosiewicz-Bourget, J., Stewart, R., Ruotti, V., Millar, A. H., Thomson, J.A., Ren,B., Ecker, J.R. Human DNA methylomes at base resolution show widespread epigenomic differences. *Nature* **2009**, 462, 315-322.
12. Laurent, L., Wong, E., Li, G., Huynh, T., Tsirigos, A., Ong, C. T., Low, H. M., Kin Sung, K. W., Rigoutsos, I., Loring, J., Wei, C.L. Dynamic changes in the human methylome during differentiation. *Genome Res.* **2010**, 20, 320-321.
13. Portela, A., Esteller, M. Epigenetic modifications and human disease. *Nat. Biotechnol.* **2010**, 28, 1057-1068.
14. Doi, A., Park, I.-H., Wen, B., Murakami, P., Aryee, M. J., Irizarry, R., Herb, B., Ladd-Acosta, C., Rho, J., Loewer, S., Miller, J., Schlaeger, T., Daley, G.Q., Feinberg, A.P. Differential methylation of tissue- and cancer-specific CpG island shores distinguishes human induced pluripotent stem cells, embryonic stem cells and fibroblasts. *Nat. Genet.* **2009,** 41, 1350-1353.
15. Irizarry, R. A., Ladd-Acosta, C., Wen, B., Wu, Z., Montano, C., Onyango, P., Cui, H., Gabo, K., Rongione, M., Webster, M., Ji, H., Potash, J. B., Sabunciyan, S., Feinberg, A. P. The human colon cancer methylome shows similar hypo- and hypermethylation at conserved tissue-specific CpG island shores. *Nat. Genet.* **2009,** 41, 178-186.
16. Razin, A., Riggs, A.D. DNA methylation and gene function. *Science* **1980**, 210, 604-610.

17. Comb, M., Goodman, H.M. CpG methylation inhibits proenkephalin gene expression and binding of the transcription factor AP-2. *Nucleic Acids Res.* **1990**, 18, 3975-3982.
18. Inamdar, N.M.; Ehrlich, K.C.; Ehrlich, M. CpG methylation inhibits binding of several sequence specific DNA-binding proteins from pea, wheat, soybean and cauliflower. *Plant Mol. Biol.* **1991**, *17*, 111-123.
19. Ehrlich, M. DNA methylation in cancer: too much, but also too little. *Oncogene* **2002**, 21, 5400-5413.
20. Robertson, K.D., Jones, P.A. DNA methylation: past, present and future directions. *Carcinogenesis* **2000**, 21, 461-467.
21. Yan, J.; Zierath, J. R.; Barres, R. Evidence for non-CpG methylation in mammals. *Exp. Cell Res.* **2011**, *317*, 2555–2561.
22. Klimasauskas, S., Kumar, S., Roberts, R. J., Cheng, X. HhaI methyltransferase flips its target base out of the DNA helix. *Cell* **1994**, 76, 357-369.
23. Svedruzic, Z.M., Reich, N.O. Mechanism of allosteric regulation of DNMT1's processivity. *Biochemistry* **2005**, 44, 14977-14988.
24. Okano, M., Bell, D. W., Haber, D. A., Li, E. DNA methyltransferases DNMT3A and DNMT3B are essential for de novo methylation and mammalian development. *Cell* **1999**, 99, 247-257.
25. Leonhardt, H., Page, A.W., Weier, H.U., Bestor, T.H. A targeting sequence directs DNA methyltransferase to sites of DNA replication in mammalian nuclei. *Cell* **1992**, 71, 865-873.
26. Okano, M., Xie, S., Li, E. Cloning and characterization of a family of novel mammalian DNA (cytosine-5) methyltransferases. *Nat. Genet.* **1998**, 19, 219-220.
27. Lauster, R., Trautner, T.A., Noyer-Weidner, M. Cytosine-specific type II DNA methyltransferases. A conserved enzyme core with variable target recognizing domains. *J. Mol. Biol.* **1989**, 206, 305-312.
28. Robertson, K.D. DNA methylation, methyltransferases, and cancer. *Oncogene* **2001**, 20, 3139-3155.
29. Bestor, T.H., Verdine, G.L. DNA methyltransferases. *Curr. Opin. Cell Biol.* **1994**, 6, 380-389.
30. Bestor, T.H., Laudano, A., Mattaliano, R., Ingram, V. Cloning and sequencing of a cDNA encoding DNA methyltransferase of mouse cells. The carboxylterminal domain of the mammalian enzymes is related to bacterial restriction methyltransferases. *J. Mol. Biol.* **1988**, 203, 971-983.
31. Bestor, T.H. Cloning of a mammalian DNA methyltransferase. *Gene* **1988**, 74, 9-12.
32. Robertson, K.D., Uzvolgyi, E., Liang, G., Talmadge, C., Sumegi, J., Gonzales, F.A., Jones, P. A. The human DNA methyltransferases (DNMTs) 1, 3A and 3B: coordinate mRNA expression in normal tissues and overexpression in tumors. *Nucleic Acids Res.* **1999**, 27, 2291-2298.

33. Mertineit, C., Yoder, J.A., Taketo, T., Laird, D.W., Trasler, J. M., Bestor, T.H. Sex-specific exons control DNA methyltransferase in mammalian germ cells. *Development* **1998**, 125, 889-897.
34. Pradhan, S., Talbot, D., Sha, M., Benner, J., Hornstra, L., Li, E., Jaenisch, R., Roberts, R.J. Baculovirus-mediated expression and characterization of the full-length murine DNA methyltransferase. *Nucleic Acids Res.* **1997**, 25, 4666-4673.
35. Pradhan, S., Bacolla, A., Wells, R.D., Roberts, R.J. Recombinant human DNA (cytosine-5) methyltransferase. I. Expression, purification, and comparison of de novo and maintenance methylation. *J. Biol. Chem.* **1999**, 274, 33002-33010.
36. Prokhortchouk, E., Defossez, P.A. The cell biology of DNA methylation in mammals, *Biochim. Biophys. Acta* **2008**, 1783, 2167-2173.
37. Takashima, S., Takehashi, M., Lee, J., Chuma, S., Okano, M., Hata, K., Suetake, I., Nakatsuji, N., Miyoshi, H., Tajima, S., Tanaka, Y., Toyokuni, S., Sasaki, H., Kanatsu-Shinohara, M., Shinohara, T. Abnormal DNA methyltransferase expression in mouse germ-line stem cells results in spermatogenic defects. *Biol. Reprod.* **2009**, 81, 155-164.
38. Chen, T., Hevi, S., Gay, F., Tsujimoto, N., He, T., Zhang, B., Ueda, Y., Li, E. Complete inactivation of DNMT1 leads to mitotic catastrophe in human cancer cells. *Nat. Genet.* **2007**, 39, 391-396.
39. Gaudet, F., Hodgson, J.G., Eden, A., Jackson-Grusby, L., Dausman, J., Gray, J.W., Leonhardt, H., Jaenisch, R. Induction of tumors in mice by genomic hypomethylation. *Science* **2003**, 300, 489-492.
40. Eden, A., Gaudet, F., Waghmare, A., Jaenisch, R. Chromosomal instability and tumors promoted by DNA hypomethylation. *Science* **2003**, 300, 455.
41. Chik, F., Szyf, M. Effects of specific DNMT gene depletion on cancer cell transformation and breast cancer cell invasion; toward selective DNMT inhibitors. *Carcinogenesis* **2011**, 32, 224-232.
42. Sharif, J., Koseki, H., Recruitment of DNMT1 roles of the SRA protein Np95 (UHRF1) and other factors. *Prog. Mol. Biol. Transl. Sci.* **2011**, 101, 289-310.
43. Iida, T., Suetake, I., Tajima, S., Morioka, H., Ohta, S., Obuse, C., Tsurimoto, T. PCNA clamp facilitates action of DNA cytosine methyltransferase 1 on hemimethylated DNA. *Genes Cells* **2002**, 7, 997-1007.
44. Lan, J., Hua, S., He, X., Zhang, Y. DNA methyltransferases and methyl-binding proteins of mammals. *Acta Biochim. Biophys. Sin. (Shanghai)* **2010**, 42, 243-252.
45. Jones, P.A., Liang, G. Rethinking how DNA methylation patterns are maintained. *Nat. Rev. Genet.* **2009**, 10, 805-811.
46. Goll, M. G., Bestor, T. H. Eukaryotic cytosine methyltransferases *Annu. Rev. Biochem.* **2005**, 74, 481-514.
47. Schaefer, M., Lyko, F. Solving the DNMT2 enigma. *Chromosoma* **2010**, 119, 35-40.

48. Squires, J.E., Patel, H.R., Nousch, M., Sibbritt, T., Humphreys, D.T., Parker, B.J., Suter, C.M., Preiss, T. Widespread occurrence of 5-methylcytosine in human coding and non-coding RNA. *Nucleic Acids Res.* **2012**, 40, 5023-5033.
49. Hermann, A., Gowher, H., Jeltsch, A. Biochemistry and biology of mammalian DNA methyltransferases. *Cell. Mol. Life Sci.* **2004**, 61, 2571-2587.
50. Espada, J., Esteller, M. DNA methylation and the functional organization of the nuclear compartment. *Semin. Cell Dev. Biol.* **2010**, 21, 238-246.
51. Hansen, R. S., Wijmenga, C., Luo, P., Stanek, A. M., Canfield, T. K., Weemaes, C. M., Gartler, S. M. The DNMT3B DNA methyltransferase gene is mutated in the ICF immunodeficiency syndrome. *Proc. Natl. Acad. Sci. U. S. A.* **1999**, 96, 14412-14417.
52. Deplus, R., Brenner, C., Burgers, W. A., Putmans, P., Kouzarides, T., de Launoit, Y., Fuks, F. DNMT3L is a transcriptional repressor that recruits histone deacetylase. *Nucleic Acids Res.* **2002**, 30, 3831-3838.
53. Margot, J. B., Ehrenhofer-Murray, A. E., Leonhardt, H. Interactions within the mammalian DNA methyltransferase family. *BMC Mol. Biol.* **2003**, 4, 7.
54. Jia, D., Jurkowska, R. Z., Zhang, X., Jeltsch, A., Cheng, X. Structure of DNMT3A bound to DNMT3L suggests a model for *de novo* DNA methylation. *Nature* **2007**, 449, 248-251.
55. Jurkowska, R. Z., Anspach, N., Urbanke, C., Jia, D., Reinhardt, R., Nellen, W., Cheng, X., Jeltsch, A. Formation of nucleoprotein filaments by mammalian DNA methyltransferase DNMT3A in complex with regulator DNMT3L. *Nucleic Acids Res.* **2008**, 36, 6656-6663.
56. Ge, Y. Z., Pu, M. T., Gowher, H., Wu, H. P., Ding, J. P., Jeltsch, A., Xu, G. L. Chromatin targeting of *de novo* DNA methyltransferases by the PWWP domain. *J. Biol. Chem.* **2004**, 279, 25447-25454.
57. Fatemi, M, Hermann, A., Gowher, H., Jeltsch, A. DNMT3a and DNMT1 functionally cooperate during *de novo* methylation of DNA. *Eur. J. Biochem.* **2002**, 269, 4981-4984.
58. Kim, G. D, Ni, J., Kelesoglu, N., Roberts, R. J., Pradhan, S. Co-operation and communication between the human maintenance and *de novo* DNA (cytosine-5) methyltransferases. *EMBO J.* **2002**, 21, 4183-4195.
59. ,Xu, F., Mao, C., Ding, Y., Rui, C., Wu, L., Shi, A., Zhang, H., Zhang, L., Xu, Z. Molecular and enzymatic profiles of mammalian DNA methyltransferases: structures and targets for drugs. *Curr. Med. Chem.* **2010**, 17, 4052-4071.
60. Goyal, R., Reinhardt, R., Jeltsch, A. Accuracy of DNA methylation pattern preservation by the DNMT1 methyltransferase. *Nucleic Acids Res.* **2006**, 34, 1182-1188.
61. Rhee, I., Bachman, K. E., Park, B. H., Jair, K. W., Yen, R. W., Schuebel, K. E., Cui, H., Feinberg, A. P., Lengauer, C., Kinzler, K. W., Baylin, S. B., Vogelstein, B. DNMT1 and DNMT3B cooperate to silence genes in human cancer cells. *Nature* **2002**, 416, 552-556.

62. Song J, Rechkoblit O., Bestor T. H., Patel D. J. Structure of DNMT1-DNA complex reveals a role for autoinhibition in maintenance dna methylation. *Science* **2011**, 331, 1036-1040.
63. Qureshi, I. A., Mehler, M. F., Advances in epigenetics and epigenomics for neurodegenerative diseases. *Curr. Neurol. Neurosci. Rep.* **2011**, 11, 464-473.
64. Fuso, A., Nicolia, V., Cavallaro, R. A., Scarpa, S. DNA methylase and demethylase activities are modulated by one-carbon metabolism in Alzheimer's disease modelsl. *J. Nutr. Biochem.* **2011**, 22, 242-251.
65. Higuchi, F., Uchida, S., Yamagata, H., Otsuki, K., Hobara, T., Abe, N., Shibata, T., Watanabe, Y. State-dependent changes in the expression of DNA methyltransferases in mood disorder patients. *J. Psychiatr. Res.* **2011**, 45, 1295-1300.
66. Lopez-Pedrera, C.,Perez-Sanchez, C., Ramos-Casals, M., Santos-Gonzalez, M., Rodriguez-Ariza, A., Cuadrado, M. J. Cardiovascular risk in systemic autoimmune diseases: epigenetic mechanisms of immune regulatory functions. *Clin. Dev. Immunol.* **2012**, 2012, 1-10.
67. Sacconi, S., Camano, P., de Greef, J. C., Lemmers, R. J., Salviati, L., Boileau, P., Lopez de Munain, A. A., Van der Maarel, S. M., Desnuelle, C. Patients with a phenotype consistent with facioscapulohumeral muscular dystrophy display genetic and epigenetic heterogeneity. *J. Med. Genet.* **2011**, 49, 41-46.
68. Bressler, J., Shimmin, L. C., Boerwinkle, E., Hixson, J. E. Global DNA methylation and risk of subclinical atherosclerosis in young adults: the pathobiological determinants of atherosclerosis in youth (PDAY) study. *Atherosclerosis* **2011**, 219, 958-962.
69. Rodriguez, J., Frigola, J., Vendrell, E., Risques, R. A., Fraga, M .F., Morales, C., Moreno, V., Esteller, M., Capella, G., Ribas, M., Peinado, M. A. Chromosomal instability correlates with genome-wide DNA demethylation in human primary colorectal cancers. *Cancer Res.* **2006**, 66, 8462-9468.
70. Farinha, N.J., Shaker, S., Lemaire, M., Momparler, L., Bernstein, M., Momparler, R. L. Activation of expression of p15, p73 and E-cadherin in leukemic cells by different concentrations of 5-aza-20-deoxycytidine (decitabine). *Anticancer Res.* **2004**, 24, 75-78.
71. Gore, S. D., Baylin, S., Sugar, E., Carraway, H., Miller, C. B., Carducci, M., Grever, M.; Galm, O., Dauses, T., Karp, J. E., Rudek, M. A., Zhao, M., Smith, B. D., Manning, J., Jiemjit, A., Dover, G., Mays, A., Zwiebel, J., Murgo, A., Weng, L. J., Herman, J. G. Combined DNA methyltransferase and histone deacetylase inhibition in the treatment of myeloid neoplasms. *Cancer Res.* **2006**, 66, 6361-6369.
72. Jung, Y., Park, J., Kim, T., Park, J. H., Jong, H. S., Im, S. A., Robertson, K., Bang, Y. J., Kim, T. Y. Potential advantages of DNA methyltransferase 1 (DNMT1)-targeted inhibition for cancer therapy. *J. Mol. Med.* **2007**, 85, 1137-1148.

73. Suzuki, M.; Sunaga, N.; Shames, D. S.; Toyooka, S.; Gazdar, A. F.; Minna, J. D. RNA interference-mediated knockdown of DNA methyltransferase 1 leads to promoter demethylation and gene re-expression in human lung and breast cancer cells. *Cancer Res.* **2004**, *64*, 3137–3143.
74. Mund, C., Brueckner, B., Lyko, F. Reactivation of epigenetically silenced genes by DNA methyltransferase inhibitors: basic concepts and clinical applications. *Epigenetics* **2006**, 1, 7-13.
75. Wijermans, P. W., Lubbert, M., Verhoef, G., Klimek, V., Bosly, A. An epigenetic approach to the treatment of advanced MDS; the experience with the DNA demethylating agent 5-aza-20-deoxycytidine (decitabine) in 177 patients. *Ann. Hematol.* **2005**, 84, 9-17.
76. Lemaire, M., Momparler, L. F., Raynal, N. J., Bernstein, M. L., Momparler, R. L. Inhibition of cytidine deaminase by zebularine enhances the antineoplastic action of 5-aza-2'- deoxycytidine. *Cancer Chemother. Pharmacol.* **2009**, 63, 411-416.
77. Yang, A. S., Estecio, M. R., Garcia-Manero, G., Kantarjian, H. M., Issa, J. P. Comment on "Chromosomalinstability and tumors promoted by DNA hypomethylation" and "Induction of tumors in nice by genomic hypomethylation". *Science* **2003**, 302, 1153.
78. Brueckner, B., Rius, M., Markelova, M. R., Fichtner, I., Hals, P. A., Sandvold, M. L., Lyko, F. Delivery of 5-azacytidine to human cancer cells by elaidic acid esterification increases therapeutic drug efficacy. *Mol. Cancer Ther.* **2010**, 9, 1256-1264.
79. Yoo, C.B., Jeong, S., Egger, G., Liang, G., Phiasivongsa, P., Tang, C., Redkar, S., Jones, P. A. Delivery of 5-aza-2'-deoxycytidine to cells using oligodeoxynucleotides. *Cancer Res.* **2007**, 67, 6400-6408.
80. http://clinicaltrials.gov/show/NCT01696032
81. Shen, L., Kantarjian, H., Guo, Y., Lin, E., Shan, J., Huang, X., Berry, D., Ahmed, S., Zhu, W., Pierce, S. DNA Methylation Predicts Survival and Response to Therapy in Patients with Myelodysplastic Syndromes. *J. Clin. Oncol.* **2010**, 28, 605-613.
82. Walter, E. D. Genistein (an isoflavone glucoside) and its aglucone, genistein, from soybeans. *J. Am. Chem. Soc.* **1941**, 63, 3273-3276.
83. Yang, C. S., Wang, X., Lu, G., Picinich, S. C. Cancer prevention by tea: animal studies, molecular mechanisms and human relevance. *Nat. Rev. Cancer* **2009**, 9, 429-439.
84. Yang S.C., Fang M., Lambert J.D., Yan P., Huang T.H.M Reversal of hypermethylation and reactivation of genes by dietary polyphenolic compounds. *Nutr Rev* **2008**, 66, 18-20.
85. Lee W.J., Shim J.Y., Zhu B.T. Mechanisms for the inhibition of DNA methyltransferases by tea catechins and bioflavonoids. *Mol Pharmacol.* **2005**, 68, 1018-1030.

86. Hoshino, O., Murakata, M., Yamada, K. A convenient synthesis of a bromotyrosine derived metabolite, psammaplin A, from psammaplysilla sp. *Bioorg. Med. Chem. Lett.* **1992**, 2, 1561-1562.
87. Pina, I. C., Gautschi, J. T., Wang, G. Y., Sanders, M. L., Schmitz, F. J., France, D., Cornell-Kennon, S., Sambucetti, L. C., Remiszewski, S. W., Perez, L. B., Bair, K. W., Crews, P. Psammaplins from the sponge Pseudoceratina purpurea: inhibition of both histone deacetylase and DNA methyltransferase. *J. Org. Chem.* **2003**, 68, 3866-3873.
88. Godert, A. M., Angelino, N., Woloszynska-Read, A., Morey, S. R., James, S. R., Karpf, A. R., Sufrin, J. R. An improved synthesis of psammaplin A. *Bioorg. Med. Chem. Lett.* **2006**, 16, 3330-3333.
89. Baud, M. G., Leiser, T., Haus, P., Samlal, S., Wong, A. C., Wood, R. J., Petrucci, V., Gunaratnam, M., Hughes, S. M., Buluwela, L., Turlais, F., Neidle, S., Meyer- Almes, F. J., White, A. J., Fuchter, M. J. Defining the mechanism of action and enzymatic selectivity of psammaplin A against its epigenetic targets. *J. Med. Chem.* **2012**, 55, 1731-1750.
90. Liu, Z., Xie, Z., Jones, W., Pavlovicz, R. E., Liu, S., Yu, J., Li, P. K., Lin, J., Fuchs, J. R., Marcucci, G., Li, C., Chan, K. K. Curcumin is a potent DNA hypomethylation agent. *Bioorg. Med. Chem. Lett.* **2009**, 19, 706-709.
91. Burgos-Morón, E., Calderón-Montaño, J.M., Salvador, J., Robles, A., López-Lázaro, M., The dark side of curcumin. *International Journal of Cancer* **2010**, 126, 1771–1775.
92. Reuter S, Gupta S.C., Park B., Goel A., Aggarwal B.B. Epigenetic changes induced by curcumin and other natural compounds. *Genes Nutr*. **2011**, 6, 93-108
93. Nagaraju G.P., Zhu S., Wen J., Farris A.B., Adsay V.N., Diaz R., Snyder J.P., Mamoru S., El-Rayes B.F. Novel synthetic curcumin analogues EF31 and UBS109 are potent DNA hypomethylating agents in pancreatic cancer. *CancerLetters*, **2013**, 341, 195-203
94. Kuck, D., Singh, N., Lyko, F., Medina-Franco, J. L. Novel and selective DNA methyltransferase inhibitors: docking-based virtual screening and experimental evaluation. *Bioorg. Med. Chem.* **2010**, 18, 822-829.
95. Kuck, D., Caulfield, T., Lyko, F., Medina-Franco, J. L. Nanaomycin A selectively inhibits DNMT3B and reactivates silenced tumor suppressor genes in human cancer cells. *Mol. Cancer Ther.* **2010**, 9, 3015-3023.
96. Siedlecki, P., Garcia Boy, R., Musch, T., Brueckner, B., Suhai, S., Lyko, F., Zielenkiewicz, P. Discovery of two novel, small-molecule inhibitors of DNA methylation. *J. Med. Chem*. **2006**, 49, 678-683.
97. Brueckner, B., Garcia Boy, R., Siedlecki, P., Musch, T., Kliem, H. C., Zielenkiewicz, P., Suhai, S., Wiessler, M., Lyko, F. Epigenetic reactivation of tumor suppressor genes by a novel small-molecule inhibitor of human DNA Methyltransferases. *Cancer Res*. **2005**, 65, 6305-6311.

98. Stresemann, C., Brueckner, B., Musch, T., Stopper, H., Lyko, F. Functional diversity of DNA methyltransferase inhibitors in human cancer cell lines. *Cancer Res*. **2006**, 66, 2794-2800.
99. Mai, A., Altucci, L. Epi-drugs to fight cancer: from chemistry to cancer treatment, the road ahead. *Int. J. Biochem. Cell Biol.* **2009**, 41, 199-213.
100. Cornacchia, E., Golbus, J., Maybaum, J., Strahler, J., Hanash, S., Richardson, B. Hydralazine and procainamide inhibit T cell DNA methylation and induce autoreactivity. *J. Immunol*. **1988**, 140, 2197-2200.
101. Segura-Pacheco, B., Trejo-Becerril, C., Perez-Cardenas, E., Taja-Chayeb, L., Mariscal, I., Chavez, A., Lizano, M., Duenas-Gonzalez, A. Reactivation of tumor suppressor genes by the cardiovascular drugs hydralazine and procainamide and their potential use in cancer therapy. *Clin. Cancer Res*. **2003**, 9, 1596-1603.
102. Deng, C., Lu, Q., Zhang, Z., Rao, T., Attwood, J., Yung, R., Richardson, B. Hydralazine may induce autoimmunity by inhibiting extracellular signal-regulated kinase pathway signaling. *Arthritis Rheum*. **2003**, 48, 746-756.
103. Brueckner, B., Kuck, D., Lyko, F. DNA methyltransferase inhibitors for cancer therapy. *Cancer J*. **2007**, 13, 17-22.
104. Chuang, J. C., Yoo, C. B., Kwan, J. M., Li, T. W., Liang, G., Yang, A. S., Jones, P. A. Comparison of biological effects of Non-Nucleoside DNA methylation inhibitors versus 5-Aza-2′-Deoxycytidine. *Mol. Cancer Ther*. **2005**, 4, 1515-1520.
105. Coronel, J., Cetina, L., Pacheco, I., Trejo-Becerril, C., Gonzalez- Fierro, A., de la Cruz-Hernandez, E., Perez-Cardenas, E., Taja-Chayeb, L., Arias-Bofill, D., Candelaria, M., et al. A double-blind, placebo-controlled, randomized phase III trial of chemotherapy plus epigenetic therapy with hydralazine valproate for advanced cervical cancer: preliminary results. *Med Oncol* **2010**, 28, 540-546.
106. Candelaria, M., Herrera, A., Labardini, J., Gonzalez-Fierro, A., Trejo-Becerril, C., Taja-Chayeb, L., Perez-Cardenas, E., de la Cruz-Hernandez, E., Arias-Bofill, D., Vidal, S., et al. Hydralazine and magnesium valproate as epigenetic treatment for myelodysplastic syndrome: preliminary results of a Phase-II trial. *Ann. Hematol*. **2011**, 90, 379-387.
107. Zambrano, P., Segura-Pacheco, B., Perez-Cardenas, E., Cetina, L., Revilla-Vazquez, A., Taja-Chayeb, L., Chavez-Blanco, A., Angeles, E., Cabrera, G., Sandoval, K., Trejo-Becerril, C., Chanona-Vilchis, J., Duenas-Gonzalez, A. A phase I study of hydralazine to demethylate and reactivate the expression of tumor suppressor genes, *BMC Cancer* **2005**, 5, 44.
108. Villar-Garea, A., Fraga, M. F., Espada, J., Esteller, M. Procaine is a DNA-demethylating agent with growth-inhibitory effects in human cancer cells. *Cancer Res*. **2003**, 63, 4984-4989.
109. Stresemann, C., Brueckner, B., Musch, T., Stopper, H., Lyko, F. Functional diversity of DNA methyltransferase inhibitors in human cancer cell lines. *Cancer Res*. **2006**, 66, 2794-2800.

110. Datta, J., Ghoshal, K., Denny, W. A., Gamage, S. A., Brooke, D. G., Phiasivongsa, P., Redkar, S., Jacob, S. T. A new class of quinoline-based DNA hypomethylating agents reactivates tumor suppressor genes by blocking DNA methyltransferase 1 activity and inducing its degradation. *Cancer Res*. **2009**, 69, 4277-4285.
111. Chen, S.M., Leupin, W., Rance, M., Chazin, W.J. Two dimensional NMR studies of d(GGTTAATGCGGT). (ACCGCATTAACC) complexed with the minor groove binding drug SN-6999. *Biochemistry*, **1992**, 31, 4406-4413.
112. Adams, A., Leong, C., Denny, W.A., Guss, J.M. Structures of two minor-groove-binding quinolinium quaternary salts complexed with d(CGCGAATTCGCG)(2) at 1.6 and 1.8 Angstrom resolution. *Acta Crystallogr D Biol Crystallogr* **2005**, 61,1348-1353.
113. Wu, J., Grunstein, M. 25 Years after the nucleosome model: chromatin modifications. *Trends Biochem. Sci*. **2000**, 25, 612-623.
114. Luger, K., Mader, A.W., Richmond, R.K., Sargent, D.F., Richmond, T.J. Crystal structure of the nucleosome core particle at 2,8 Å resolution. *Nature* **1997**, 389, 251-260.
115. Jendwein, T., Allis, C.D. Translating the histone code. *Science* **2001**, 293, 1074-1080.
116. Gaspar-Maia, A., Alajem, A., Meshorer, E., Ramalho-Santos, M. Open chromatin in pluripotency and reprogramming. *Nature Reviews Molecular Cell Biology* **2011**, 12, 36-47.
117. Petty, E. and Pillus, L. Balancing chromatin remodeling and histone modifications in transcription. *Trends in Genetics* **2013**, 29, 621-629.
118. Clapier, C. R. and Cairns, R. B. The biology of chromatin remodeling complexes. *Annual Review of Biochemistry* **2009**, 78, 273-304.
119. Dawson, M.A. and Kouzarides, T. Cancer epigenetics: from mechanism to therapy. *Cell* **2012**, 150, 12-27.
120. Turner, B. M. Histone acetylation and an epigenetic code. *BioEssay* **2000**, 22, 836-845.
121. Xu, Y.Z., Kanagaratham, C. and Radzioch D. *Biochemistry, Genetics and Molecular Biology*. "Chromatin Remodelling", ISBN 978-953-51-1087-3, April 17, **2013**.
122. Wolffe, A.P. and Hayes, J.J. Chromatin disruption and modification. *Nucleic Acid Res* **1999**, 27,711-720.
123. Hecht, A., Laroche, T., Strahl-Bolsinger, S., Gasser, S.M., Grunstein, M. Histone H3 and H4 N-termini interact with SIR3 and SIR4 proteins: a molecular model for the formation of heterochromatin in yeast. *Cell* **1995**, 80,583-592.
124. Edmonson, D.G., Smith, M.M., Roth, S.Y. Repression domain of the yeast global repressor Tup1 interacts directly with histones H3 and H4. *Genes Dev*. **1996**, 10, 1247-1259.

125. Metzger, E., Imhof, A., Patel, D., Kahl, P., Hoffmeyer, K., Friedrichs, N., Muller, J.M., Greschik, H., Kirfel, J., Ji, S. Phosphorylation of histone H3T6 by PKCbeta(I) controls demethylation at histone H3K4. *Nature* **2010**, 464, 792-796.
126. Baek, S.H. When signaling kinases meet histones and histone modifiers in the nucleus. *Mol Cell.* **2011**, 42, 274-284.
127. Thorne, A. W., Sautiere, P., Briand, G., Crane-Robinson, C. The structure of ubiquitinated histone H2B. *The EMBO Journal* **1987**, 6, 1005-1010.
128. Osley, M. A. Regulation of histone H2A and H2B ubiquitylation. *Briefings in Functional Genomics & Proteomics* **2006**, 5, 179-189.
129. Wang, H., Wang, L., Erdjument-Bromage, H., Vidal, M., Tempst, P., Jones, R. S., Zhang, Y. Role of histone H2A ubiquitination in Polycomb silencing. *Nature* **2004**, 431, 873-878.
130. Fierz, B., Chatterjee, C., McGinty, R. K., Bar-Dagan, M., Raleigh, D. P., Muir, T. W. Histone H2B ubiquitylation disrupts local and higher-order chromatin compaction. *Nature Chemical Biology* **2011**, 7, 113-119.
131. Johnsen, S. A. The enigmatic role of H2Bub1 in cancer. *FEBS Letters* **2012**, 586, 1592-1601.
132. Kim, J., Guermah, M., McGinty, R. K., Lee, J. S., Tang, Z., Milne, T. A., ... & Roeder, R. G. RAD6-mediated transcription-coupled H2B ubiquitylation directly stimulates H3K4 methylation in human cells. *Cell* **2009**, 137, 459-471.
133. Shema, E., Tirosh, I., Aylon, Y., Huang, J., Ye, C., Moskovits, N., Oren, M. The histone H2B-specific ubiquitin ligase RNF20/hBRE1 acts as a putative tumor suppressor through selective regulation of gene expression. *Genes & Development* **2008**, 22, 2664-2676.
134. Moyal, L., Lerenthal, Y., Gana-Weisz, M., Mass, G., So, S., Wang, S. Y., Shiloh, Y. Requirement of ATM-dependent monoubiquitylation of histone H2B for timely repair of DNA double-strand breaks. *Molecular Cell* **2011**, 41, 529-542.
135. Groth, A., Rocha, W., Verreault, A., Almouzni, G. Chromatin challenges during DNA replication and repair. *Cell* **2007**, 128, 721-733.
136. Shahbazian, M.D,, Grunstein, M. Functions of site-specific histone acetylation and deacetylation. *Annu Rev Biochem* **2007**, 76, 75-100.
137. Davie, J.R. Covalent modifications of histones expression from chromatin templates. *Curr Opin Genet Dev* **1998**, 8, 173-178.
138. Davie, J.R., Spencer, V.A. Control of histone modifications. *J Cell Biochem* **1999**,141-148.
139. Turner, B.M. Histone acetylation and epigenetic code. *Bioessays* **2000**, 22, 836-845.
140. Brownell, J. E., Allis, C. D. Special HATs for special occasions: linking histone acetylation to chromatin assembly and gene activation. *Curr. Opin. Genes Dev.**199***6, 6, 176-184
141. Lee, K. K., Workman, J. L. Histone acetyltransferase complexes: one size doesn't fit all. *Nat Rev Mol Cell Biol* **2007**, 8, 284-295

142. Gu, W., Roeder, R. G. Activation of p53 sequencespecific DNA binding by acetylation of the p53 C-terminal domain. *Cell* **1997**, 90, 595-606.
143. Dornan, D., Shimizu, H., Perkins, N. D., Hupp, T. R. DNA-dependent acetylation of p53 by the transcription coactivator p300. *J. Biol. Chem.* **2003** ,278, 13431-13441.
144. Zhang, Y.; Fang, H.; Jiao, J., Xu, W. The structure and function of histone deacetylases: the target for anti-cancer therapy. *Curr. Med.Chem.* **2008**, 15, 2840-2849
145. de Ruijter, A.J., van Gennip, A.H., Caron, H.N., Kemp, S., van Kuilenburg, A.B., Histone deacetylases (HDACs): characterization of the classical HDAC family. *Biochem. J.* **2003**, 370, 737-749.
146. Gregoretti, I.V., Lee, Y.M., Goodson, H.V. Molecular evolution of the histone deacetylase family: functional implications of phylogenetic analysis. *J. Mol. Biol.* **2004**, 338, 17-31.
147. Kao, H.Y., Lee, C.H., Komarov, A. Isolation and characterization of mammalian HDAC10, a novel histone deacetylase. *J Biol Chem* **2002**, 277, 187-193.
148. Gao, L., Cueto, M.A., Asselbergs, F., Ataoja, P. Cloning and functional characterization of HDAC11, a novel member of the human histone deacetylase family. *J Biol Chem* **2002**, 277, 25748-25755.
149. Grozinger, C.M., Hassig, C.A., Schreiber, S.L. Three proteins define a class of human histone deacetylases related to yeast Hda1p. *Proc Natl Acad Sci USA* **1999**, 96, 4868-4873.
150. Yang, X. J., Seto, E. The Rpd3/Hda1 family of lysine deacetylases: from bacteria and yeast to mice and men. *Nat Rev Mol Cell Biol* **2008**, 9, 206-218.
151. Marks, P. A., Xu, W. S. Histone deacetylase inhibitors: potential in cancer therapy. *J. Cell. Biochem.* **2009**, 107, 600-608
152. Huang, Y., Myers, S.J., Dingledine, R. Transcriptional repression by REST: recruitment of Sin3A and histone deacetylase to neuronal genes. *Nat. Neurosci*. **1999**, 2, 867-872.
153. Ahringer, J. NuRD and SIN3 histone deacetylase complexes in development. *Trends Genet.*, **2000**, 16, 351-356.
154. McKinsey, T.A., Zhang, C.L., Lu, J., Olson, E.N. Signal-dependent nuclear export of a histone deacetylase regulates muscle differentiation. *Nature* **2000**, 408, 106-111.
155. Verdin, E., Dequiedt, F., Kasler, H.G. Class II histone deacetylases: versatile regulators. *Trends Genet.* **2003**; 19, 286-293.
156. Berdeaux, R., Goebel, N., Banaszynski, L., Takemori, H., Wandless, T., Shelton, G.D., Montminy, M. SIK1 is a class II HDAC kinase that promotes survival of skeletal myocytes. *Nat. Med.* **2007**, 13, 597-603.
157. Chang, S., Bezprozvannaya, S., Li, S., Olson, E.N. An expression screen reveals modulators of class II histone deacetylase phosphorylation. *Proc. Natl. Acad. Sci. USA* **2005**, 102, 8120-8125.

158. Bertos, N.R., Wang, A.H., Yang, X.Y. Class II histone deacetylases: structure, function and regulation. *Biochem Cell Biol* **2001**, 79, 243-252.
159. Yang, X.Y., Seto, E. Collaborative spirit of histone deacetylases in regulating chromatin structure and gene expression. *Curr Opin Genet Dev* **2000**,13,143-153.
160. Frye, RA. Phylogenetic classification of prokaryotic and eukaryotic Sir2-like proteins. *Biochem Biophys Res Commun* **2000**, 273, 793-798.
161. Chang, J.H., Kim, H.C., Hwang, K.Y., Lee, J.W., Jackson, S.P., Bell, S.D., Cho, Y. Structural basis for the NAD^+-dependent deacetylase mechanism of Sir 2. *J Biol Chem* **2002**, 277, 34489-34498.
162. Brunmeir, R., Lagger, S., Seiser, C. Histone deacetylase HDAC1/HDAC2-controlled embryonic development and cell differentiation. *Int J Dev Biol* **2009**, 53, 275-289.
163. Jurkin, J., Zupkovitz, G., Lagger, S., Grausenburger, R., Hagelkruys, A., Kenner, L., Seiser, C. Distinct and redundant functions of histone deacetylases HDAC1 and HDAC2 in proliferation and tumorigenesis. *Cell Cycle* **2011**, 10,406-412.
164. Weichert, W., Roske, A., Niesporek, S., Noske, A., Buckendahl, A.C., Dietel, M., Gekeler, V., Boehm, M., Beckers, T., Denkert, C. Class I histone deacetylase expression has independent prognostic impact in human colorectal cancer: specific role of class I histone deacetylases in vitro and in vivo. *Clin. Cancer Res.* **2008**, 14, 1669-1677.
165. Rikimaru, T., Taketomi, A., Yamashita, Y., Shirabe, K., Hamatsu, T., Shimada, Y., Maehara, M. Clinical significance of histone deacetylase 1 expression in patients with hepatocellular carcinoma. *Oncology* **2007**, 72, 69-74.
166. Glaser, K.B., Li, J., Staver, M.J., Wie, R.Q., Albert, D.H., Davidsen, S.K. Role of class I and class II histone deacetylases in carcinoma cells using siRNA. *Biochem. Biophys. Res. Commun.* **2003,**; 310,529-536.
167. Senese, S., Zaragoza, K., Minardi, S., Muradore, I., Ronzoni, S., Passafaro, A., Bernard, L., Draetta, G.F., Alcalay, M., Seiser, C., Chiocca, S. Role for histone deacetylase 1 in human tumor cell proliferation. *Mol. Cell. Biol.* **2007**, 27, 4784-4795.
168. Huang, B.H., Laban, M., Leung, C.H., Lee, L., Lee, C.K., Salto-Tellez, M., Raju, G.C., Hooi, S.C. Inhibition of histone deacetylase 2 increasesapoptosis and p21Cip1/WAF1 expression, independent of histone deacetylase 1. *Cell Death Differ.* **2005**, 12, 395-404.
169. Harms, K.L., Chen, X. Histone deacetylase 2 modulates p53transcriptional activities through regulation of p53-DNA binding activity. *Cancer Res.* **2007**, 67, 3145-3152.
170. Taplick, J., Kurtev, V., Kroboth, K., Posch, M., Lechner, T., Seiser, C. Homooligomerisation and nuclear localisation of mouse histone deacetylase 1. *J Mol Biol* **2001**, 308, 27-38.

171. Luo, Y., Jian, W., Stavreva, D., Fu, X., Hager, G., Bungert, J., Huang, S., Qiu, Y. Transregulation of histone deacetylase activities through acetylation. *J Biol Chem* **2009**, 284, 34901-34910.
172. Yamaguchi, T., Cubizolles, F., Zhang, Y., Reichert, N., Kohler, H., Seiser, C., Matthias P. Histone deacetylases 1 and 2 act in concert to promote the G1-to-S progression. *Genes Dev* **2010**, 24, 455-469.
173. He, S., Sun, J.M., Li, L., Davie, J.R. Differential intranuclear organization of transcription factors Sp1 and Sp3. *Mol Biol Cell* **2005**, 16, 4073-4083.
174. Wysocka, J., Myers, M. P., Laherty, C. D., Eisenman, R. N., Herr, W. Human Sin3 deacetylase and trithorax-related Set1/Ash2 histone H3-K4 methyltransferase are tethered together selectively by the cell-proliferation factor HCF-1. *Genes & development* **2003**, 17, 896-911.
175. Fleischer, T. C., Yun, U. J., Ayer, D. E. Identification and characterization of three new components of the mSin3A corepressor complex. *Molecular and cellular biology* **2003**, 23, 3456-3467.
176. Hayakawa, T., Nakayama, J. Physiological roles of class I HDAC complex and histone demethylase. *J Biomed Biotechnol* **2011**, 129383.
177. Denslow, S.A., Wade, P.A: The human Mi-2/NuRD complex and gene regulation. *Oncogene* **2007**, 26,5433-5438.
178. Wang, Y., Zhang, H., Chen, Y.P., Sun, Y.M., Yang, F., Yu, W.H., Liang, J., Sun, L.Y., Yang, X.H., Shi, L., Li, R.F., Li, Y.Y., Zhang, Y., Li, Q., Yi, X., Shang, Y.F. LSD1 is a subunit of the NuRD complex and targets the metastasis programs in breast cancer. Cell **2009**; 138, 660-672.
179. Lee, M.G., Wynder, C., Cooch, N., Shiekhattar, R. An essential role for CoREST in nucleosomal histone 3 lysine 4 demethylation. *Nature* **2005**, 437,432-435.
180. Shi, Y.J., Matson, C., Lan, F., Iwase, S., Baba, T., Shi, Y. Regulation of LSD1 histone demethylase activity by its associated factors. *Mol Cell* **2005**, 19,857-864.
181. Guan, J.S., Haggarty, S.J., Giacometti, E., Dannenberg, J.H., Joseph, N., Gao, J., Nieland, T.J., Zhou, Y., Wang, X., Mazitschek, R., Bradner, J.E., DePinho, R.A., Jaenisch, R., Tsai, L.H. HDAC2 negatively regulates memory formation andsynaptic plasticity. *Nature* **2009**, 459, 55-60.
182. Karolczak-Bayatti, M., Sweeney, M., Cheng, J., Edey, L., Robson, S. C., Ulrich, S. M., Europe-Finner, G. N. Acetylation of heat shock protein 20 (Hsp20) regulates human myometrial activity. *Journal of Biological Chemistry* **2011**, 286, 34346-34355.
183. Bhaskara, S., Knutson, S. K., Jiang, G., Chandrasekharan, M. B., Wilson, A. J., Zheng, S., Hiebert, S. W. Hdac3 is essential for the maintenance of chromatin structure and genome stability. *Cancer cell* **2010**,18, 436-447.
184. Moser, M. A., Hagelkruys, A., Seiser, C. Transcription and beyond: the role of mammalian class I lysine deacetylases. *Chromosoma* **2013**,1-12.

185. Waltregny, D., Glenisson, W., Tran, S. L., North, B. J., Verdin, E., Colige, A., Castronovo, V. Histone deacetylase HDAC8 associates with smooth muscle α-actin and is essential for smooth muscle cell contractility. *FASEB J* **2005**, 19, 966-968.
186. Wolfson, N. A., Pitcairn, C. A., Fierke, C. A. HDAC8 substrates: histones and beyond. *Biopolymers* **2013**, 99, 112-126.
187. Hu, E., Chen, Z., Fredrickson, T., Zhu, Y., Kirkpatrick, R., Zhang, G. F., Winkler, J. Cloning and characterization of a novel human class I histone deacetylase that functions as a transcription repressor. *Journal of Biological Chemistry* **2000**, 275, 15254-15264.
188. Waltregny, D., de Leval, L., Glénisson, W., Ly Tran, S., North, B. J., Bellahcène, A., Castronovo, V. Expression of histone deacetylase 8, a class I histone deacetylase, is restricted to cells showing smooth muscle differentiation in normal human tissues. *The American journal of pathology* **2004**, 165, 553-564.
189. Parra, M., Verdin, E. Regulatory signal transduction pathways for class IIa histone deacetylases. *Current opinion in pharmacology* **2010**, 10, 454-460.
190. McKinsey, T.A. Derepression of pathological cardiac genes by members of the CaMkinase superfamily. *Cardiovasc Res* **2007**, 73, 667-677.
191. Backs, J., Backs, T., Bezprozvannaya, S., McKinsey, T.A., Olson, E.N. Histone deacetylase 5 acquires calcium/calmodulindependent kinase II responsiveness by oligomerization with histone deacetylase 4. *Mol Cell Biol* **2008,**; 28, 3437-3445.
192. Bolger, T.A., Yao, T.P. Intracellular trafficking of histone deacetylase 4 regulates neuronal cell death. *J Neurosci* **2005**, 25, 9544-9553.
193. Soriano, F. X., Chawla, S., Skehel, P., Hardingham, G. E. SMRT-mediated co-shuttling enables export of class IIa HDACs independent of their CaM kinase phosphorylation sites. *Journal of neurochemistry* **2013**, 124, 26-35.
194. Martin, M., Kettmann, R., Dequiedt, F. Class IIa histone deacetylases: regulating the regulators. *Oncogene* **2007**, 26, 5450-5467.
195. Martin, M., Kettmann, R., Dequiedt, F. Class IIa histone deacetylases: conducting development and differentiation. *Int J Dev Biol* **2009**, 53, 291-301.
196. Potthoff, M.J., Olson, E.N. MEF2: a central regulator of diverse developmental programs. *Development* **2007**, 134, 4131-4140.
197. Morin, R.D., Mendez-Lago, M., Mungall, A.J., Goya, R., Mungall, K.L., Corbett, R.D., Johnson, N.A., Severson, T.M., Chiu, R., Field, M. Frequent mutation of histone-modifying genes in non-Hodgkin lymphoma. *Nature* **2011**, 476, 298-303.
198. Pasqualucci, L., Dominguez-Sola, D., Chiarenza, A., Fabbri, G., Grunn, A., Trifonov, V., Kasper, L.H., Lerach, S., Tang, H., Ma, J. Inactivating mutations of acetyltransferase genes in B-cell lymphoma. *Nature* **2011**, 471, 189-195.

199. Lu, J., McKinsey, T.A., Zhang, C.L., Olson,E.N. Regulation of skeletal myogenesis by association of the MEF2 transcription factor with class II histone deacetylases. *Mol. Cell* **2000**, 6, 233-244.
200. Wang, A.H., Yang, X.J. Histone deacetylase 4 possesses intrinsic nuclear import and export signals. *Mol. Cell Biol.* **2001**, 21, 5992-6005.
201. Han, A., He, J., Wu, Y., Liu, J.O., Chen, L. Mechanism of recruitment of class II histone deacetylases by myocyte enhancer factor-2. *J. Mol. Biol.* **2005**, 345, 91-102.
202. Jayathilaka, N., Han, A., Gaffney, K. J., Dey, R., Jarusiewicz, J. A., Noridomi, K., Chen, L. Inhibition of the function of class IIa HDACs by blocking their interaction with MEF2. *Nucleic acids research* **2012**, 40, 5378-5388.
203. Vega, R. B., Matsuda, K., Oh, J.; Barbosa, A. C., Yang, X., Meadows, E., McAnally, J., Pomajzl, C., Shelton, J. M., Richardson, J. A. Histone deacetylase 4 controls chondrocyte hypertrophy during skeletogenesis. *Cell* **2004**, 119, 555-566.
204. Chauchereau, A., Mathieu, M., de Saintignon, J., Ferreira, R., Pritchard, L. L., Mishal, Z., Dejean, A., Harel-Bellan, A. HDAC4 mediates transcriptional repression by the acute promyelocytic leukaemia-associated protein PLZF. *Oncogene* **2004**, 23, 8777-8784.
205. Chang, S., McKinsey, T. A., Zhang, C. L., Richardson, J. A., Hill, J. A., Olson, E. N. Histone deacetylases 5 and 9 govern responsiveness of the heart to a subset of stress signals and play redundant roles in heart development. *Mol. Cell. Biol.* **2004**, 24, 8467-8476.
206. Zhang, C. L., McKinsey, T. A., Chang, S., Antos, C. L., Hill, J. A., Olson, E. N. Class II histone deacetylases act as signal-responsive repressors of cardiac hypertrophy. *Cell* **2002**, 110, 479-488.
207. Dequiedt, F., Kasler, H., Fischle, W., Kiermer, V., Weinstein, M., Herndier, B. G., Verdin, E. HDAC7, a thymus-specific class II histone deacetylase, regulates Nur77 transcription and TCR mediated apoptosis. *Immunity* **2003**, 18, 687-698.
208. Chang, S., Young, B. D., Li, S., Qi, X., Richardson, J. A., Olson, E. N. Histone deacetylase 7 maintains vascular integrity by repressing matrix metalloproteinase 10. *Cell* **2006**, 126, 321- 334.
209. Zhu, C., Chen, Q., Xie, Z., Ai, J., Tong, L., Ding, J., Geng, M. The role of histone deacetylase 7 (HDAC7) in cancer cell proliferation: regulation on c-Myc. *J Mol Med (Berl)* **2011**, 89, 279-289.
210. Zhang, G., Wang, Z. RNA interference of HDAC7 expression in hepatocellular carcinoma. *Journal of Central South University. Medical sciences* **2010**, 35, 718-724.
211. Bradner, J. E., West, N., Grachan, M. L., Greenberg, E. F., Haggarty, S. J., Warnow, T., Mazitschek, R. Chemical phylogenetics of histone deacetylases. *Nature chemical biology* **2010**, 6, 238-243.

212. Hubbert, C., Guardiola, A., Shao, R., Kawaguchi, Y., Ito, A., Nixon, A., Yoshida, M., Wang, X.F., Yao, T.P. HDAC6 is a microtubule-associated deacetylase, *Nature* **2002**, 417, 455-458.
213. Kovacs, J.J., Murphy, P.J., Gaillard, S., Zhao, X., Wu, J.T., Nicchitta, C.V., Yoshida, M., Toft, D.O., Pratt, W.B., Yao, T.P. HDAC6 regulates Hsp90 acetylation and chaperone-dependent activation of glucocorticoid receptor. *Mol. Cell* **2005**, 18, 601-607.
214. Namdar, M., Perez, G., Ngo, L., Marks, P. A. Selective inhibition of histone deacetylase 6 (HDAC6) induces DNA damage and sensitizes transformed cells to anticancer agents. *Proceedings of the National Academy of Sciences* **2010**, 107, 20003-20008.
215. Kawaguchi, Y., Kovacs, J.J., McLaurin, A., Vance, J.M., Ito, A., Yao, T.P. The deacetylase HDAC6 regulates aggresome formation and cell viability in response to misfolded protein stress. *Cell* **2003**, 115, 727-738.
216. Pandey, U.B., Nie, Z., Batlevi, Y., McCray, B.A., Ritson, G.P., Nedelsky, N.B., Schwartz, S.L., Di Prospero, N.A., Knight, M.A., Schuldiner, O., Padmanabhan, R., Hild M. HDAC6 rescues neurodegeneration and provides an essential link between autophagy and the UPS. *Nature* **2007**, 447, 859-863.
217. Lee, J. H., Jeong, E. G., Choi, M. C., Kim, S. H., Park, J. H., Song, S. H., Park, J., Bang, Y. J., Kim, T. Y. Inhibition of histone deacetylase 10 induces thioredoxin-interacting protein and causes accumulation of reactive oxygen species in SNU-620 human gastric cancer cells. *Mol. Cells* **2010**, 30, 107-112.
218. Villagra, A., Sotomayor, E.M., Seto, E. Histone deacetylases and the immunological network: implications in cancer and inflammation. *Oncogene* **2010**, 29,157-173.
219. Deubzer, H. E., Schier, M. C., Oehme, I., Lodrini, M., Haendler, B., Sommer, A., Witt, O. HDAC11 is a novel drug target in carcinomas. *International Journal of Cancer* **2012**.
220. Shore, D., Squire, M., Nasmyth, K.A. Characterization of two genes required for the position-effect control of yeast mating-type genes. *EMBO J*. **1984**, 3, 2817-2823.
221. Tissenbaum, H.A., Guarente, L. Increased dosage of a sir-2 gene extends lifespan in Caenorhabditis elegans. *Nature* **2001**, 410, 227-230.
222. Rogina, B., Helfand, S.L. Sir2 mediates longevity in the fly through a pathway related to calorie restriction. *Proc Natl Acad Sci U S A* **2004**,101, 15998-16003.
223. Du, J., Zhou, Y., Su, X., Yu, J. J., Khan, S., Jiang, H., Lin, H. Sirt5 is a NAD-dependent protein lysine demalonylase and desuccinylase. *Science*. **2011**, 334, 806-809.
224. Michan, S., Sinclair, D. Sirtuins in mammals: insights into their biological function. *Biochem. J*. **2007**, 404, 1-13.
225. Martínez-Redondo, P., Vaquero, A. The diversity of histone versus nonhistone Sirtuin substrates. *Genes & Cancer* **2013**.

226. Aquilano, K., Vigilanza, P., Baldelli, S., Pagliei, B., Rotilio, G., Ciriolo,M.R. Peroxisome proliferator-activated receptor gamma co-activator 1alpha (PGC-1alpha) and sirtuin 1 (SIRT1) reside in mitochondria: possible direct function in mitochondrial biogenesis. *J. Biol. Chem.* **2010**, 285, 21590-21599.
227. Tanno, M., Sakamoto, J., Miura, T., Shimamoto, K., Horio, Y. Nucleocytoplasmic shuttling of the NAD^+-dependent histone deacetylase SIRT1. *J. Biol. Chem.* **2007**, 282, 6823-6832.
228. Vaquero, A., Scher, M. B., Lee, D. H., Sutton, A., Cheng, H. L., Alt, F. W., Reinberg, D. SirT2 is a histone deacetylase with preference for histone H4 Lys 16 during mitosis. *Genes Dev.* **2006**, 20, 1256-1261.
229. Huang, J. Y., Hirschey, M. D., Shimazu, T., Ho, L., Verdin, E. Mitochondrial sirtuins. *Biochim. Biophys. Acta* **2010**, 1804, 1645-1651.
230. Gertz, M., Steegborn, C. Function and regulation of the mitochondrial Sirtuin isoform Sirt5 in Mammalia. *Biochimica et Biophysica Acta (BBA)-Proteins and Proteomics* **2010**, 1804,1658-1665.
231. Mostoslavsky, R., Chua, K. F., Lombard, D. B., Pang, W. W., Fischer, M. R., Gellon, L., Alt, F. W. Genomic instability and aging-like phenotype in the absence of mammalian SIRT6. *Cell* **2006**, 124, 315-329.
232. Ford, E., Voit, R., Liszt, G., Magin, C., Grummt, I., Guarente, L. Mammalian Sir2 homolog SIRT7 is an activator of RNA polymerase I transcription. *Genes Dev.***2006**, 20, 1075-1080.
233. Vaziri, H., Dessain, S. K., Eaton, E. N., Imai, S. I., Frye, R. A., Pandita, T. K., Weinberg, R. A. hSIR2 (SIRT1) functions as an NAD-dependent p53 deacetylase. *Cell* **2001**, 107, 149-159.
234. Herranz, D., Serrano, M. SIRT1: recent lessons from mouse models. *Nature Reviews Cancer* **2010**, *10*, 819-823.
235. Rodgers, J. T., Lerin, C., Haas, W., Gygi, S. P., Spiegelman, B. M., Puigserver, P. Nutrient control of glucose homeostasis through a complex of PGC-1α and SIRT1. *Nature* **2005**, 434, 113-118.
236. Bordone, L., Motta, M. C., Picard, F., Robinson, A., Jhala, U. S., Apfeld, J., Guarente, L. Sirt1 regulates insulin secretion by repressing UCP2 in pancreatic β cells. *PLoS biology* **2005**, 4, e31.
237. Chen, D., Steele, A. D., Lindquist, S., Guarente, L. Increase in activity during calorie restriction requires Sirt1. *Science* **2005**, 310, 1641-1641.
238. Li, X., Zhang, S., Blander, G., Tse, J.G., Krieger, M., Guarente, L. SIRT1 deacetylates and positively regulates the nuclear receptor LXR. *Mol. Cell* **2007**, 28, 91-106.
239. Vaquero, A., Sternglanz, R., Reinberg, D. NAD^+-dependent deacetylation of H4 lysine 16 by class III HDACs. *Oncogene* **2007**, 26, 5505-5520.
240. North, B.J., Marshall, B.L., Borra, M.T., Denu, J.M., Verdin, E. The human Sir2 ortholog, SIRT2, is an NAD^+-dependent tubulin deacetylase. *Mol. Cell* **2003**, 11,437-444.

241. North, B.J., Verdin, E. Mitotic regulation of SIRT2 by cyclin-dependent kinase 1-dependent phosphorylation. *J. Biol. Chem* **2007**, 282,19546-19555.
242. Inoue, T., Nakayama, Y., Yamada, H., Li, Y.C., Yamaguchi, S. SIRT2 downregulation confers resistance to microtubule inhibitors by prolonging chronic mitotic arrest. *Cell Cycle* **2009**, 8, 1279-1291.
243. Tang, B.L., Chua, C.E. SIRT2, tubulin deacetylation, and oligodendroglia differentiation. *Cell Motil. Cytoskeleton* **2008**, 65, 179-182.
244. Wu, F., Schweizer, C., Rudinskiy, N., Taylor, D.M., Kazantsev, A., Luthi-Carter, R., Fraering, P.C. Novel gamma-secretase inhibitors uncover a common nucleotide-binding site in JAK3, SIRT2, and PS1. *FASEB J.* **2010**, 24, 2464-2474.
245. Lombard, D.B., Alt, F.W., Cheng, H.L., Bunkenborg, J., Streeper, R.S., Mostoslavsky, R., Kim, J., Yancopoulos, G., Valenzuela, D., Murphy, A. Mammalian Sir2 homolog SIRT3 regulates global mitochondrial lysine acetylation. *Mol Cell Biol* **2007**, 27, 8807-8814.
246. Hebert, A.S., Dittenhafer-Reed, K.E., Yu, W., Bailey, D.J., Selen, E.S., Boersma, M.D., Carson, J.J., Tonelli, M., Balloon, A.J., Higbee, A.J. Calorie restriction and SIRT3 trigger global reprogramming of the mitochondrial protein acetylome. *Mol Cell* **2013**, 49, 186-199.
247. Hirschey, M.D., Shimazu, T., Goetzman, E., Jing, E., Schwer, B., Lombard, D.B., Grueter, C.A., Harris, C., Biddinger, S., Ilkayeva, O.R. SIRT3 regulates mitochondrial fatty-acid oxidation by reversible enzyme deacetylation. *Nature* **2010**, 464, 121-125.
248. Schwer, B., Bunkenborg, J., Verdin, R.O., Andersen, J.S., Verdin, E. Reversible lysine acetylation controls the activity of the mitochondrial enzyme acetyl-CoA synthetase 2. *Proc Natl Acad Sci U S A* **2006**, 103, 10224-10229.
249. Cimen, H., Han, M.J., Yang, Y., Tong, Q., Koc, H., Koc, E.C. Regulation of succinate dehydrogenase activity by SIRT3 in mammalian mitochondria. *Biochemistry* **2010**, 49, 304-311.
250. Hallows, W.C., Yu, W., Smith, B.C., Devires, M.K., Ellinger, J.J., Someya, S., Shortreed, M.R., Prolla, T., Markley, J.L., Smith, L.M., Zhao, S., Guan, K.L., Denu, J.M. Sirt3 promotes the urea cycle and fatty acid oxidation during dietary restriction. *Mol. Cell* **2011**, 41, 139-149.
251. Dölle, C., Rack, J. G., Ziegler, M. NAD and ADP-ribose metabolism in mitochondria. *FEBS Journal* **2013**.
252. Haigis, M. C., Mostoslavsky, R., Haigis, K. M., Fahie, K., Christodoulou, D. C., Murphy, A. J., Guarente, L. SIRT4 inhibits glutamate dehydrogenase and opposes the effects of calorie restriction in pancreatic β cells. *Cell* **2006**, 126, 941-954.
253. Ahuja, N., Schwer, B., Carobbio, S., Waltregny, D., North, B. J., Castronovo, V., Verdin, E. Regulation of insulin secretion by SIRT4, a mitochondrial ADP-ribosyltransferase. *Journal of Biological Chemistry* **2007**, 282, 33583-33592.

254. Nasrin, N., Wu, X., Fortier, E., Feng, Y., Bare, O. C., Chen, S., Bordone, L. SIRT4 regulates fatty acid oxidation and mitochondrial gene expression in liver and muscle cells. *Journal of Biological Chemistry* **2010**, 285, 31995-32002.
255. Laurent, G., German, N. J., Saha, A. K., de Boer, V. C., Davies, M., Koves, T. R., Haigis, M. C. SIRT4 coordinates the balance between lipid synthesis and catabolism by repressing malonyl CoA decarboxylase. *Molecular cell* **2013**, 50, 686-698.
256. Nakagawa, T., Lomb, D.J., Haigis, M.C., Guarente, L. SIRT5 Deacetylates carbamoyl phosphate synthetase 1 and regulates the urea cycle. *Cell* **2009**, 137,560-570.
257. Fischer, F., Gertz, M., Suenkel, B., Lakshminarasimhan, M., Schutkowski, M., Steegborn, C. Sirt5 deacylation activities show differential sensitivities to nicotinamide inhibition. *PLoS One* **2012**, 7, e45098.
258. Nakamura, Y., Ogura, M., Ogura, K., Tanaka, D., Inagaki, N. SIRT5 deacetylates and activates urate oxidase in liver mitochondria of mice. *FEBS Lett* **2012**, 586, 4076-4081.
259. Wu, X.W., Muzny, D.M., Lee, C.C., Caskey, C.T. Two independent mutational events in the loss of urate oxidase during hominoid evolution. *J Mol Evol* **1992**, 34, 78-84.
260. Verdin, E., Hirschey, M. D., Finley, L. W. S., Haigis, M. C. Sirtuin regulation of mitochondria: energy production, apoptosis, and signaling. *Trends Biochem. Sci.* **2010**, 35, 669-675.
261. Carafa, V., Nebbioso, A., Altucci, L. Sirtuins and disease: the road ahead. *Frontiers in pharmacology* **2012**, 3.
262. Michishita, E., McCord, R.A., Berber, E., Kioi, M., Padilla-Nash, H., Damian, M., Cheung, P., Kusumoto, R., Kawahara, T.L., Barrett, J.C., Chang, H.Y., Bohr, V.A., Ried, T., Gozani, O., Chua, K.F. SIRT6 is a histone H3 lysine 9 deacetylase that modulates telomeric chromatin. *Nature* **2008**, 452, 492-496.
263. Mao, Z., Hine, C., Tian, X., Van Meter, M., Au, M., Vaidya, A., Seluanov, A., Gorbunova, V. SIRT6 promotes DNA repair under stress by activating PARP1. *Science* **2011**, 332, 1443-1446.
264. Gil, R., Barth, S., Kanfi, Y., Cohen, H. Y. SIRT6 exhibits nucleosome-dependent deacetylase activity. *Nucleic acids research* **2013**, 41, 8537-8545.
265. Jiang, H., Khan, S., Wang, Y., Charron, G., He, B., Sebastian, C., Du, J., Kim, R., Ge, E., Mostoslavsky, R., Hang, H.C., Hao, Q., Lin, H. SIRT6 regulates TNF-α secretion through hydrolysis of long-chain fatty acyl lysine. *Nature* **2013**, 496, 110-113.
266. Zhong, L., D'Urso, A., Toiber, D., Sebastian, C., Henry, R.E., Vadysirisack, D.D., Guimaraes, A., Marinelli, B., Wikstrom, J.D., Nir, T., Clish, C.B., Vaitheesvaran, B., Iliopoulos, O., Kurland, I., Dor, Y., Weissleder, R., Shirihai, O.S., Ellisen, L.W., Espinosa, J.M., Mostoslavsky, R. The histone deacetylase Sirt6 regulates glucose homeostasis via Hif1alpha. *Cell* **2010**, 140, 280-293.

267. Sebastián, C., Zwaans, B. M., Silberman, D. M., Gymrek, M., Goren, A., Zhong, L., Mostoslavsky, R. The histone deacetylase SIRT6 is a tumor suppressor that controls cancer metabolism. *Cell* **2012**, 151, 1185-1199.
268. McCord, R. A., Michishita, E., Hong, T., Berber, E., Boxer, L. D., Kusumoto, R., Chua, K. F. SIRT6 stabilizes DNA-dependent protein kinase at chromatin for DNA double-strand break repair. *Aging (Albany NY)* **2009**, 1, 109.
269. Barber, M.F., Michishita-Kioi, E., Xi, Y., Tasselli, L., Kioi, M., Moqtaderi, Z., Tennen, R.I., Paredes, S., Young, N.L., Chen, K. SIRT7 links H3K18 deacetylation to maintenance of oncogenic transformation. *Nature* **2012**, 487, 114-118.
270. Kim, J.K., Noh, J.H., Jung, K.H., Eun, J.W., Bae, H.J., Kim, M.G., Chang, Y.G., Shen, Q., Park, W.S., Lee, J.Y. Sirtuin7 oncogenic potential in human hepatocellular carcinoma and its regulation by the tumor suppressors MiR-125a-5p and MiR-125b. *Hepatology* **2013**, 57, 1055-1067.
271. Chen, S., Seiler, J., Santiago-Reichelt, M., Felbel, K., Grummt, I., Voit, R. Repression of RNA polymerase I upon stress is caused by inhibition of RNA-dependent deacetylation of PAF53 by SIRT7. *Molecular cell* **2013**, 52, 303-313.
272. Vakhrusheva, O., Smolka, C., Gajawada, P., Kostin, S., Boettger, T., Kubin, T., Bober, E. Sirt7 increases stress resistance of cardiomyocytes and prevents apoptosis and inflammatory cardiomyopathy in mice. *Circulation research* **2008**, 102, 703-710.
273. Pereira, C. V., Lebiedzinska, M., Wieckowski, M. R., Oliveira, P. J.. Regulation and protection of mitochondrial physiology by sirtuins. *Mitochondrion* **2012**, 12, 66-76.
274. Sanders, B. D., Jackson, B., Marmorstein, R. Structural basis for sirtuin function: What we know and what we don't. *Biochimica et Biophysica Acta (BBA)-Proteins and Proteomics* **2010**, 1804,1604-1616.
275. Chakrabarty, S. P., Balaram, H. Reversible binding of zinc in *Plasmodium falciparum* Sir2: structure and activity of the apoenzyme. *Biochim. Biophys. Acta* **2010**, 1804, 1743-1750.
276. Min, J., Landry, J., Sternglanz, R., Xu, R.M. Crystal structure of a SIR2 homolog-NAD complex, *Cell* **2001**, 105, 269-279.
277. Prasad, G. S., Sridhar, V., Yamaguchi, M., Hatefi, Y., Stout, C. D. Crystal structure of transhydrogenase domain III at 1.2 Å resolution. *Nat. Struct. Biol.* **1999**, 6, 1126-1131.
278. Hawse, W.F., Hoff, K.G., Fatkins, D.G., Daines, A., Zubkova, O.V., Schramm, V.L., Zheng, W., Wolberger, C. Structural Insights into Intermediate Steps in the Sir2 Deacetylation Reaction. *Structure* **2008**, *16*, 1368-1377.
279. Fraga, M.F., Ballestar, E., Villar-Garea, A., Boix-Chornet, M., Espada, J., Schotta, G., Bonaldi, T., Haydon, C., Ropero, S., Petrie, K., Iyer, N.G., Perez-Rosado, A., Calvo, E., Lopez, J.A., Cano, A., Calasanz, M.J., Colomer, D., Piris, M.A., Ahn, N., Imhof, A., Caldas, C., Jenuwein, T., Esteller, M. Loss of

acetylation at Lys16 and trimethylation at Lys20 of histone H4 is a common hallmark of human cancer. *Nat. Genet.* **2005**, 37, 391-400.

280. Choi, J.H., Song, Y.S., Yoon, J.S., Song, K.W., Lee, Y.Y. Enhancer of zeste homolog 2 expression is associated with tumor cell proliferation and metastasis in gastric cancer. *Apmis* **2010**, 118, 196-202.

281. Zhang, Z., Yamashita, H., Toyama, T., Sugiura, H., Ando, Y., Mita, K., Hamaguchi, M., Hara, Y., Kobayashi, S., Iwase, H. Quantitation of HDAC1 mRNA expression in invasive carcinoma of the breast. *Breast Cancer Res. Treat*. **2005**, 94, 11-16.

282. Fritzsche, F.R., Weichert, W., Roske, A., Gekeler, V., Beckers, T., Stephan, C., Jung, K., Scholman, K., Denkert, C., Dietel, M., Kristiansen, G. Class I histone deacetylases 1, 2 and 3 are highly expressed in renal cell cancer. *BMC Cancer* **2008**, 8, 381.

283. Adams, H., Fritzsche, F.R., Dirnhofer, S., Kristiansen, G., Tzankov, A. Class I histone deacetylases 1, 2 and 3 are highly expressed in classical Hodgkin's lymphoma. *Expert Opin. Ther. Targets* **2010**, 14, 577-584.

284. Jung, K.H., Noh, J.H., Kim, J.K., Eun, J.W., Bae, H.J., Xie, H.J., Chang, Y.G., Kim, M.G., Park, H., Lee, J.Y., Nam, S.W. HDAC2 overexpression confers oncogenic potential to human lung cancer cells by deregulating expression of apoptosis and cell cycle proteins. *J. Cell. Biochem.* **2012**, 113, 2167-2177.

285. Oehme, I., Deubzer, H.E., Wegener, D., Pickert, D., Linke, J.P., Hero, B., Kopp-Schneider, A., Westermann, F., Ulrich, S.M., von Deimling, A., Fischer, M., Witt, O. Histone deacetylase 8 in neuroblastoma tumorigenesis. *Clin. Cancer Res.* **2009**, 15, 91-99.

286. Park, S.Y., Jun, J.A., Jeong, K.J., Heo, H.J., Sohn, J.S., Lee, H.Y., Park, C.G., Kang, J. Histone deacetylases 1, 6 and 8 are critical for invasion in breast cancer. *Oncol. Rep.* **2011**, 25, 1677-1681.

287. Xie, H.J., Noh, J.H., Kim, J.K., Jung, K.H., Eun, J.W., Bae, H.J., Kim, M.G., Chang, Y.G., Lee, J.Y., Park, H., Nam, S.W. HDAC1 inactivation induces mitotic defect and caspaseindependent autophagic cell death in liver cancer. *PLoS One* **2012**, 7, 34265.

288. Sun, J.Y., Xu, L., Tseng, H., Ciccarelli, B., Fulciniti, M., Hunter, Z.R., Maghsoudi, K., Hatjiharissi, E., Zhou, Y., Yang, G., Zhu, B., Liu, X., Gong, P., Ioakimidis, L., Sheehy, P., Patterson, C.J., Munshi, N.C., O'Connor, O.A., Treon, S.P. Histone deacetylase inhibitors demonstrate significant preclinical activity as single agents, and in combination with bortezomib in Waldenstrom's macroglobulinemia. Clin. *Lymphoma. Myeloma Leuk.* **2011**, 11, 152-156.

289. Ozdag, H., Teschendorff, A.E., Ahmed, A.A., Hyland, S.J., Blenkiron, C., Bobrow, L., Veerakumarasivam, A., Burtt, G., Subkhankulova, T., Arends, M.J., Collins, V.P., Bowtell, D., Kouzarides, T., Brenton, J.D., Caldas, C. Differential expression of selected histone modifier genes in human solid cancers. *BMC Genomics* **2006**, 7, 90.

290. Stark, M., Hayward, N. Genome-wide loss of heterozygosity and copy number analysis in melanoma using high-density single-nucleotide polymorphism arrays. *Cancer Res.* **2007**, 67, 2632-2642.
291. Sjoblom, T., Jones, S., Wood, L.D., Parsons, D.W., Lin, J., Barber, T.D., Mandelker, D., Leary, R.J., Ptak, J., Silliman, N., Szabo, S., Buckhaults, P., Farrell, C., Meeh, P., Markowitz, S.D., Willis, J., Dawson, D., Willson, J.K., Gazdar, A.F., Hartigan, J., Wu, L., Liu, C., Parmigiani, G., Park, B.H., Bachman, K.E., Papadopoulos, N., Vogelstein, B., Kinzler, K.W., Velculescu, V.E. The consensus coding sequences of human breast and colorectal cancers. *Science* **2006**, 314, 268-274.
292. Milde, T., Oehme, I., Korshunov, A., Kopp-Schneider, A., Remke, M., Northcott, P., Deubzer, H.E., Lodrini, M., Taylor, M.D., von Deimling, A., Pfister, S., Witt, O. HDAC5 and HDAC9 in medulloblastoma: novel markers for risk stratification and role in tumor cell growth. *Clin. Cancer Res.* **2010**, 16, 3240-3252.
293. Lachenmayer, A., Toffanin, S., Cabellos, L., Alsinet, C., Hoshida, Y., Villanueva, A., Minguez, B., Tsai, H.W., Ward, S.C., Thung, S., Friedman, S.L., Llovet, J.M. Combination therapy for hepatocellular carcinoma: additive preclinical efficacy of the HDAC inhibitor panobinostat with sorafenib. *J. Hepatol.* **2012**, 56, 1343-1350.
294. Weichert, W. HDAC expression and clinical prognosis in human malignancies. *Cancer Lett.* **2009**, 280, 168-176.
295. Moreno, D.A., Scrideli, C.A., Cortez, M.A., de Paula Queiroz, R., Valera, E.T., da Silva Silveira, V., Yunes, J.A., Brandalise, S.R., Tone, L.G. Differential expression of HDAC3, HDAC7 and HDAC9 is associated with prognosis and survival in childhood acute lymphoblastic leukaemia. *Br. J. Haematol.* **2010**, 150, 665-673.
296. Skov, V., Larsen, T.S., Thomassen, M., Riley, C.H., Jensen, M.K., Bjerrum, O.W., Kruse, T.A., Hasselbalch, H.C. Increased gene expression of histone deacetylases in patients with Philadelphia-negative chronic myeloproliferative neoplasms. *Leuk. Lymphoma.* **2012**, 53, 123-129.
297. Lee, Y.S., Lim, K.H., Guo, X., Kawaguchi, Y., Gao, Y., Barrientos, T., Ordentlich, P., Wang, X.F., Counter, C.M., Yao, T.P. The cytoplasmic deacetylase HDAC6 is required for efficient oncogenic tumorigenesis. *Cancer Res.* **2008**, 68, 7561-7569.
298. Sakuma, T., Uzawa, K., Onda, T., Shiiba, M., Yokoe, H., Shibahara, T., Tanzawa, H. Aberrant expression of histone deacetylase 6 in oral squamous cell carcinoma. *Int. J. Oncol.* **2006**, 29, 117-124.
299. Zhang, Z., Yamashita, H., Toyama, T., Sugiura, H., Omoto, Y., Ando, Y., Mita, K., Hamaguchi, M., Hayashi, S., Iwase, H. HDAC6 expression is correlated with better survival in breast cancer. *Clin. Cancer Res.* **2004**, 10, 6962-6968.

300. Saji, S., Kawakami, M., Hayashi, S., Yoshida, N., Hirose, M., Horiguchi, S., Itoh, A., Funata, N., Schreiber, S.L., Yoshida, M., Toi, M. Significance of HDAC6 regulation via estrogen signaling for cell motility and prognosis in estrogen receptorpositive breast cancer. *Oncogene* **2005**, 24, 4531-4539.
301. Gao, L., Alumkal, J. Epigenetic regulation of androgen receptor signaling in prostate cancer. *Epigenetics* **2010**, 5, 100-104.
302. Hsieh, T.H., Tsai, C.F., Hsu, C.Y., Kuo, P.L., Lee, J.N., Chai, C.Y., Hou, M.F., Chang, C.C., Ko, Y.C., Tsai, E.M. Phthalates stimulate the epithelial to mesenchymal transition through an HDAC6-dependent mechanism in human breast epithelial stem cells. *Toxicol. Sci.* **2012**, 128, 365-376.
303. Kaluza, D., Kroll, J., Gesierich, S., Yao, T.P., Boon, R.A., Hergenreider, E., Tjwa, M., Rossig, L., Seto, E., Augustin, H.G., Zeiher, A.M., Dimmeler, S., Urbich, C. Class IIb HDAC6 regulates endothelial cell migration and angiogenesis by deacetylation of cortactin. *Embo J.* **2011**, 30, 4142-4156.
304. Li, D., Xie, S., Ren, Y., Huo, L., Gao, J., Cui, D., Liu, M., Zhou, J. Microtubule-associated deacetylase HDAC6 promotes angiogenesis by regulating cell migration in an EB1-dependent manner. *Protein Cell* **2011**¸2, 150-160.
305. Aldana-Masangkay, G.I., Rodriguez-Gonzalez, A., Lin, T., Ikeda, A.K., Hsieh, Y.T., Kim, Y.M., Lomenick, B., Okemoto, K., Landaw, E.M., Wang, D., Mazitschek, R., Bradner, J.E., Sakamoto, K.M. Tubacin suppresses proliferation and induces apoptosis of acute lymphoblastic leukemia cells. *Leuk. Lymphoma* **2011**, 52, 1544-1555.
306. Santo, L., Hideshima, T., Kung, A.L., Tseng, J.C., Tamang, D., Yang, M., Jarpe, M., van Duzer, J.H., Mazitschek, R., Ogier, W.C., Cirstea, D., Rodig, S., Eda, H., Scullen, T., Canavese, M., Bradner, J., Anderson, K.C., Jones, S.S., Raje, N. Preclinical activity, pharmacodynamic, and pharmacokinetic properties of a selective HDAC6 inhibitor, ACY-1215, in combination with bortezomib in multiple myeloma. *Blood* **2012**, 119, 2579-2589.
307. Chen, W. Y., Wang, D. H., Yen, R. C., Luo, J., Gu, W., Baylin, S. B. Tumor suppressor HIC1 directly regulates SIRT1 to modulate p53-dependent DNA-damage responses. *Cell*. **2005**, 123,437-448.
308. Zhang, Y., Zhang, M., Dong, H., Yong, S., Li, X., Olashaw, N., Zhang, X. Deacetylation of cortactin by SIRT1 promotes cell migration. *Oncogene* **2009**, 28, 445-460.
309. Suzuki, K., Hayashi, R., Ichikawa, T., Imanishi, S., Yamada, T., Inomata, M., Tobe, K. SRT1720, a SIRT1 activator, promotes tumor cell migration, and lung metastasis of breast cancer in mice. *Oncol Rep*. **2012**, 27, 1726-1732.
310. Noguchi, A., Li, X., Kubota, A., Kikuchi, K., Kameda, Y., Zheng, H., Takano, Y. SIRT1 expression is associated with good prognosis for head and neck squamous cell carcinoma patients. *Oral Surg Oral Med Oral Pathol Oral Radiol*. **2013**, 115,385-392.

311. Hiratsuka, M., Inoue, T., Toda, T., Kimura, N., Shirayoshi, Y., Kamitani, H., Oshimura, M. Proteomics-based identification of differentially expressed genes in human gliomas:down-regulation of SIRT2 gene. *Biochem Biophys Res Commun*. **2003**, 309,558-566.
312. Peters, C.J., Rees, J.R., Hardwick, R.H. Oesophageal Cancer Clinical and Molecular Stratification (OCCAMS) Study Group. A 4-gene signature predicts survival of patients with resected adenocarcinoma of the esophagus, junction, and gastric cardia. *Gastroenterology*. **2010**, 139,1995-2004.
313. Kim, H. S., Vassilopoulos, A., Wang, R. H., Lahusen, T., Xiao, Z., Xu, X., Deng, C. X. SIRT2 maintains genome integrity and suppresses tumorigenesis through regulating APC/C activity. *Cancer Cell*. **2011**, 20, 487-499.
314. He, X., Nie, H., Hong, Y., Sheng, C., Xia, W., Ying, W. SIRT2 activity is required for the survival of C6 glioma cells. *Biochem Biophys Res Commun*. **2012**, 417, 468-472.
315. Li, Y., Matsumori, H., Nakayama, Y., Osaki, M., Kojima, H., Kurimasa, A., Inoue, T. SIRT2 down-regulation in HeLa can induce p53 accumulation via p38 MAPK activation-dependent p300 decrease, eventually leading to apoptosis. *Genes Cells*. **2011**, 16, 34-45.
316. Finley, L. W., Carracedo, A., Lee, J., Souza, A., Egia, A., Zhang, J., Haigis, M. C. SIRT3 opposes reprogramming of cancer cell metabolism through HIF1alpha destabilization. *Cancer Cell*. **2011**, 19, 416-428.
317. Lai, C. C., Lin, P. M., Lin, S. F., Hsu, C. H., Lin, H. C., Hu, M. L., Yang, M. Y. Altered expression of SIRT gene family in head and neck squamous cell carcinoma. *Tumour Biol*. **2013**, 34, 1847-1854.
318. Roth M, Chen WY. Sorting out functions of sirtuins in cancer. *Oncogene*. **2013**.
319. Alhazzazi, T. Y., Kamarajan, P., Joo, N., Huang, J. Y., Verdin, E., D'Silva, N. J., Kapila, Y. L. Sirtuin-3 (SIRT3), a novel potential therapeutic target for oral cancer. *Cancer* **2011,** 117, 1670-1678.
320. Ashraf, N., Zino, S., Macintyre, A., Kingsmore, D., Payne, A. P., George, W. D., Shiels, P. G. Altered sirtuin expression is associated with node-positive breast cancer. *Br J Cancer*. **2006**, 95, 1056-1061.
321. Jeong, S. M., Xiao, C., Finley, L. W., Lahusen, T., Souza, A. L., Pierce, K., Haigis, M. C. SIRT4 has tumor-suppressive activity and regulates the cellular metabolic response to DNA damage by inhibiting mitochondrial glutamine metabolism. *Cancer Cell*. **2013**, 23, 450-463.
322. Newman, J.C., He, W., Verdin, E. Mitochondrial protein acylation and intermediary metabolism: regulation by sirtuins and implications for metabolic disease. *J Biol Chem* **2012**, 287, 42436-42443.
323. Yang, B., Zwaans, B.M., Eckersdorff, M., Lombard, D.B. The sirtuin SIRT6 deacetylates H3 K56Ac in vivo to promote genomic stability. *Cell Cycle*. **2009**, 8, 2662-2663.

324. Das, C., Lucia, M. S., Hansen, K. C., Tyler, J. K. CBP/p300-mediated acetylation of histone H3 on lysine 56. *Nature* **2009**, 459, 113-117.
325. Van Meter, M., Mao, Z., Gorbunova, V., Seluanov, A. SIRT6 overexpression induces massive apoptosis in cancer cells but not in normal cells. *Cell cycle* **2011**, 10, 3153-3158.
326. Bauer, I., Grozio, A., Lasigliè, D., Basile, G., Sturla, L., Magnone, M., Nencioni, A. The NAD^+-dependent histone deacetylase SIRT6 promotes cytokine production and migration in pancreatic cancer cells by regulating Ca^{2+} responses. *Journal of Biological Chemistry* **2012**, 287, 40924-40937.
327. Kim, J. K., Noh, J. H., Jung, K. H., Eun, J. W., Bae, H. J., Kim, M. G., Nam, S. W. SIRT7 oncogenic potential in human hepatocellular carcinoma and its regulation by the tumor suppressors mir-125a-5p and mir-125b. *Hepatology* **2013**, 57, 1055-1067.
328. De Nigris, F., Cerutti, J., Morelli, C., Califano, D., Chiariotti, L., Viglietto, G., Fusco, A. Isolation of a SIR-like gene, SIR-T8, that is overexpressed in thyroid carcinoma cell lines and tissues. *Br J Cancer* **2002**, 86, 917-923.
329. Barber, M. F., Michishita-Kioi, E., Xi, Y., Tasselli, L., Kioi, M., Moqtaderi, Z., Chua, K. F. SIRT7 links H3K18 deacetylation to maintenance of oncogenic transformation. *Nature* **2012**, 487, 114-118.
330. Buglio, D., Khaskhely, N.M., Voo, K.S., Martinez-Valdez, H., Liu, Y.J., Younes, A. HDAC11 plays an essential role in regulating OX40 ligand expression in Hodgkin lymphoma. *Blood* **2011**, 117, 2910-2917.
331. Finnin, M. S., Donigian, J. R., Cohen, A., Richon, V. M., Rifkind, R. A., Marks, P. A., Pavletich, N. P. Structures of a histone deacetylase homologue bound to the TSA and SAHA inhibitors. *Nature* **1999**, 401, 188-193.
332. Tsuji, N., Kobayashi, M., Nagashima, K., Wakisaka, Y., Koizumi, K. A new antifungal antibiotic, trichostatin. *J Antibiot* **1976**; 29, 1-6.
333. Tsuji, N., Kobayashi, M. Trichostatin C, a glucopyranosyl hydroxamate. *J Antibiot* **1978**, 31, 939-944.
334. Yoshida, M., Nomura, S., Beppu, T. Effects of trichostatins on differentiation of murine erythroleukemia cells. *Cancer Res* **1987**, 47,3688-3691.
335. Yoshida, M., Horinouchi, S., Beppu, T. Trichostatin and trapoxin: novel chemical probes for the role of histone acetylation in chromatin structure and function. *Bioessays* **1995**, 17, 423-430.
336. Yoshida, M., Kijima, M., Akita, M., Beppu, T. Potent and specific inhibition of mammalian histone deacetylase both *in vivo* and *in vitro* by trichostatin A. *J Biol Chem* **1990**, 265, 17174-17179.
337. Sauve, A. A., Youn, D. Y. Sirtuins: NAD^+dependent deacetylase mechanism and regulation. *Current opinion in chemical biology* **2012**, 16, 535-543.
338. Hoff, K. G., Avalos, J. L., Sens, K., Wolberger, C. Insights into the Sirtuin Mechanism from Ternary Complexes Containing NAD^+ and Acetylated Peptide. *Structure* **2006**, 14,1231-1240.
339. http://clinicaltrials.gov/

340. Yeo, W., Chung, H. C., Chan, S. L., Wang, L. Z., Lim, R., Picus, J., Goh, B. C. Epigenetic therapy using belinostat for patients with unresectable hepatocellular carcinoma: a multicenter phase I/II study with biomarker and pharmacokinetic analysis of tumors from patients in the Mayo Phase II Consortium and the Cancer Therapeutics Research Group. *Journal of Clinical Oncology* **2012**, 30, 3361-3367.
341. Giaccone, G., Rajan, A., Berman, A., Kelly, R. J., Szabo, E., Lopez-Chavez, A., Loehrer, P. J. Phase II study of belinostat in patients with recurrent or refractory advanced thymic epithelial tumors. *Journal of Clinical Oncology* **2011**, 29, 2052-2059.
342. Hainsworth, J. D., Infante, J. R., Spigel, D. R., Arrowsmith, E. R., Boccia, R. V., Burris, H. A. A phase II trial of panobinostat, a histone deacetylase inhibitor, in the treatment of patients with refractory metastatic renal cell carcinoma. *Cancer Invest.* **2011**, 7, 451-455.
343. Dokmanovic, M., Clarke, C., Marks, P. A. Histone deacetylase inhibitors: overview and perspectives. *Molecular cancer research* **2007**, 5, 981-989.
344. Barbetti, V., Gozzini, A., Rovida, E., Morandi, A., Spinelli, E., Fossati, G., Santini, V. Selective anti-leukaemic activity of low-dose histone deacetylase inhibitor ITF2357 on AML1/ETO-positive cells. *Oncogene* **2008**, 27, 1767-1778.
345. Guerini, V., Barbui, V., Spinelli, O., Salvi, A., Dellacasa, C., Carobbio, A., Rambaldi, A. The histone deacetylase inhibitor ITF2357 selectively targets cells bearing mutated JAK2(V617F). *Leukemia* **2008**, 22, 740-747.
346. Viviani, S., Bonfante, V., Fasola, C., Valagussa, P., Gianni, A.M. Phase II study of the histone-deacetylase inhibitor ITF2357 in relasped/refractory Hodgkin's lymphoma patients. *J Clin Oncol*. **2008**, 7, 47.
347. Adimoolam, S., Sirisawad, M., Chen, J., Thiemann, P., Ford, J. M., Buggy, J. J. HDAC inhibitor PCI-24781 decreases RAD51 expression and inhibits homologous recombination. *Proc Natl Acad Sci U S A*. **2007**, 104, 19482-19487.
348. Undevia, S. D., Janisch, L., Schilsky, R. L., Loury, D., Balasubramanian, S., Mani, C., Ratain, M. J. Phase I study of the safety, pharmacokinetics (PK) and pharmacodynamics (PD) of the histone deacetylase inhibitor (HDACi) PCI-24781. *J Clin Oncol*. **2008**, 26, S14514.
349. Arts, J., Angibaud, P., Marien, A., Floren, W., Janssens, B., King, P., Van Dun, J., Janssen, L., Geerts, T., Tuman, R. R306465 is a novel potent inhibitor of class I histone deacetylases with broadspectrum antitumoral activity against solid and haematological malignancies. *Br. J. Cancer* **2007**, 97, 1344-1353.
350. Mithraprabhu, S., Khong, T., Jones, S. S., Spencer, A. Histone deacetylase (HDAC) inhibitors as single agents induce multiple myeloma cell death principally through the inhibition of class I HDAC. *British journal of haematology* **2013**.
351. Mandl-Weber, S., Meinel, F.G., Jankowsky, R., Oduncu, F., Schmidmaier, R., Baumann, P. The novel inhibitor of histone deacetylase resminostat

(ras2410) inhibits proliferation and induces apoptosis in multiple myeloma (mm) cells. *Br. J. Haematol.* **2010**, 149, 518-528.

352. Brunetto, A.T., Ang, J.E., Lal, R., Olmos, D., Frentzas, S., Mais, A., Hauns, B., Mollenhauer, M., Lahu, G., de Bono, J.S. A first-in-human phase I study of 4sc-201, an oral histone deacetylase (hdac) inhibitor, in patients with advanced solid tumors. *J. Clin. Oncol.* **2009**, 27, 3530.
353. Bitzer, M., Horger, M., Ganten, T.M., Lauer, U.M., Woerns, M.A., Siveke, J.T., Dollinger, M.M., Gerken, G., Wege, H., Giannini, E.G., Hentsch, B. Efficacy, safety, tolerability, and pk of the hdac inhibitor resminostat in sorafenib-refractory hepatocellular carcinoma (hcc): Phase II shelter study. *J. Clin. Oncol.* **2012**, 30, 4115.
354. Grassadonia, A., Cioffi, P., Simiele, F., Iezzi, L., Zilli, M., Natoli, C. Role of Hydroxamate-Based Histone Deacetylase Inhibitors (Hb-HDACIs) in the Treatment of Solid Malignancies. *Cancers* **2013**, 5, 919-942.
355. A) Massa, S., Mai, A., Sbardella, G., Esposito, M., Ragno, R., Loidl, P., Brosch, G. 3-(4-Aroyl-1*H*-pyrrol-2-yl)-*N*-hydroxy-2-propenamides, a New Class of Synthetic Histone Deacetylase Inhibitors. *J. Med. Chem.* **2001**, 44, 2069-2072. B) Mai, A., Massa, S., Cerbara, I., Valente, S., Ragno, R., Bottoni, P., Scatena, R., Loidl, P., Brosch, G. 3-(4-Aroyl-1-methyl-1*H*-2- pyrrolyl)-N-hydroxy-2-propenamides as a New Class of Synthetic Histone Deacetylase Inhibitors. 2. Effect of Pyrrole C2 and/or C4 Substitutions on Biological Activity. *J. Med. Chem*. **2004**, 47, 1098-1109. C) Mai, A., Valente, S., Nebbioso, A., Simeoni, S., Ragno, R., Massa, S., Altucci, L. New pyrrole-based histone deacetylase inhibitors: Binding mode, enzyme-and cell-based investigations. *The International Journal of Biochemistry & Cell Biology* **2009**, 41, 235-247.
356. Illi, B., Russo, C. D., Colussi, C., Rosati, J., Pallaoro, M., Spallotta, F., Rotili, D., Valente, S., Ragone, G., Martelli, F., Biglioli, P., Steinkuhler, C., Gallinari, P., Mai, A., Capogrossi M. C., Gaetano, C. Nitric oxide modulates chromatin folding in human endothelial cells via protein phosphatase 2A activation and class II histone deacetylases nuclear shuttling. *Circulation research* **2008**, 102, 51-58.
357. Venza, I., Visalli, M., Oteri, R., Cucinotta, M., Teti, D., Venza, M. Class II-specific histone deacetylase inhibitors MC1568 and MC1575 suppress IL-8 expression in human melanoma cells. *Pigment cell & melanoma research* **2013**.
358. Closse, A.; Huguenin, R. Isolation and structural clarification of chlamydocin. *Helv. Chim. Acta* **1974**, 57, 533-545.
359. Singh, S. B., Zink, D. L., Polishook, J. D., Dombrowski, A. W., Darkin-Rattray, S. J., Schmatz, D. M., Goetz, M. A. Apicidins: novel cyclic tetrapeptides as coccidiostats and antimalarial agents from *Fusarium pallidoroseum*. *Tetrahedron Lett.* **1996**, 37, 8077-8080.
360. Colletti, S. L., Myers, R. W., Darkin-Rattray, S. J., Gurnett, A. M., Dulski, P. M., Galuska, S., Meinke, P. T. Broad spectrum antiprotozoal agents that inhibit

histone deacetylase: structure-activity relationships of apicidin. Part 1. *Bioorg. Med. Chem. Lett.* **2001**, 11, 107-111.

361. Komatsu, Y., Tomizaki, K., Tsukamoto, M., Kato, T. Cyclic Hydroxamic-acid-containing Peptide 31, a potent synthetic histone deacetylase inhibitor with antitumor activity. *Cancer Res.* **2001**, 61, 4459- 4466.
362. Ueda, H., Nakajima, H., Hori, Y., Fujita, T., Nishimura, M., Goto, T., Okuhara, M. FR901228, a novel antitumor bicyclic depsipeptide produced by Chromobacterium violaceum n^{o}. 968. *J Antibiot.* **1994**, 47, 301-310.
363. Furumai, R., Matsuyama, A., Kobashi, N., Lee, K.H., Nishiyama, M., Nakajima, H., Tanaka, A., Komatsu, Y., Nishino, N., Yoshida, M., Horinouchi, S. FK228 (depsipeptide) as a natural prodrug that inhibits class I histone deacetylases. *Cancer Res.* **2002**, 62, 4916-4921.
364. Mwakwari, S. C., Patil, V., Guerrant, W., Oyelere, A. K. Macrocyclic histone deacetylase inhibitors. *Current topics in medicinal chemistry* **2010**, 10, 1423.
365. Chen, J. S., Faller, D. V. Short-chain fatty acid inhibitors of histone deacetylases: promising anticancer.*Curr. Cancer Drug Targets* **2003**, 3, 219-236.
366. Watson, J., Glasg, M. B. Butyric acid in the treatment of cancer. *Lancet* **1933**, 746-748.
367. Kim, S. W., Hooker, J. M., Otto, N., Win, K., Muench, L., Shea, C., Fowler, J. S. Whole-body pharmacokinetics of HDAC inhibitor drugs, butyric acid, valproic acid and 4-phenylbutyric acid measured with carbon-11 labeled analogs by PET. *Nuclear medicine and biology* **2013**, 40, 912-918.
368. Gottlicher, M., Minucci, S., Zhu, P., Kramer, O.H., Schimpf, A., Giavara, S., Sleeman, J.P., Lo Coco, F., Nervi, C., Pelicci, P.G., Heinzel, T. Valproic acid defines a novel class of HDAC inhibitors inducing differentiation of transformed cells. *EMBO J* **2001**, 20, 6969-6978.
369. Ververis, K., Hiong, A., Karagiannis, T. C., Licciardi, P. V. Histone deacetylase inhibitors (HDACIs): multitargeted anticancer agents. *Biologics: targets & therapy* **2013**, 7, 47.
370. Soriano, A. O., Yang, H., Faderl, S., Estrov, Z., Giles, F., Ravandi, F., Garcia-Manero, G. Safety and clinical activity of the combination of 5-azacytidine, valproic acid, and all-trans retinoic acid in acute myeloid leukemia and myelodysplastic syndrome. *Blood.* **2007**, 110, 2302-2308.
371. Candelaria, M., Gallardo-Rincón, D., Arce, C., Cetina, L., Aguilar-Ponce, J. L., Arrieta, O., Duenas-Gonzalez, A. A phase II study of epigenetic therapy with hydralazine and magnesium valproate to overcome chemotherapy resistance in refractory solid tumors. *Ann Oncol.* **2007**, 18, 1529-1538.
372. Suzuki, T., Ando, T., Tsuchiya, K., Fukazawa, N., Saito, A., Mariko, Y., Nakanishi, O. Synthesis and histone deacetylase inhibitory activity of new benzamide derivatives. *Journal of medicinal chemistry* **1999**, 42, 3001-3003.
373. Saito, A., Yamashita, T., Mariko, Y., Nosaka, Y., Tsuchiya, K., Ando, T., Suzuki, T., Tsuruno, T., Nakanishi, O. A synthetic inhibitor of histone

deacetylase, MS-27-275, with marked in vivo antitumor activity against human tumors. *Proc. Natl. Acad.Sci. U.S.A.* **1999**, 96, 4592-4597.

374. Kummar, S., Gutierrez, M., Gardner, E. R., Donovan, E., Hwang, K., Chung, E. J., Murgo, A. J. Phase I trial of MS-275, a histone deacetylase inhibitor, administered weekly in refractory solid tumors and lymphoid malignancies. *Clin Cancer Res*. **2007**, 13, 5411-5417.
375. Gore, L., Rothenberg, M. L., O'Bryant, C. L., Schultz, M. K., Sandler, A. B., Coffin, D., Eckhardt, S. G. A phase I and pharmacokinetic study of the oral histone deacetylase inhibitor, MS-275, in patients with refractory solid tumors and lymphomas. *Clin Cancer Res*. **2008**, 14, 4517-4525.
376. Gojo, I., Jiemjit, A., Trepel, J. B., Sparreboom, A., Figg, W. D., Rollins, S., Karp, J. E. Phase 1 and pharmacologic study of MS-275, a histone deacetylase inhibitor, in adults with refractory and relapsed acute leukemias. *Blood*. **2007**, 109, 2781-2790.
377. Wozniak, A., O'Shaughnessy, J., Fiorica, J., Grove, W. Phase II trial of CI-994 in patients (pts) with advanced nonsmall cell lung cancer (NSCLC). *Proc Am Soc Clin Oncol.* **1999**, 18.
378. Copley-Merriman, K., Von Pawel, J.,Shepherd F. Randomized phase 2 study of the oral histone deacetylase inhibitor CI-994 plus gemcitabine vs placebo plus gemcitabine in second-line nonsmall cell lung cancer (NSCLC): health-related quality of life results. *Proc Am Soc Clin Oncol* **2002**, 21, 324.
379. Le Tourneau, C., Siu, L.L. Promising antitumor activity with MGCD0103, a novel isotypeselective histone deacetylase inhibitor. *Expert Opin Investig Drugs* **2008**, 17, 1247-1254.
380. Jackson, M. D., Schmidt, M. T., Oppenheimer, N. J., Denu, J. M. Mechanism of nicotinamide inhibition and transglycosidation by Sir2 histone/protein deacetylases. *J. Biol. Chem.* **2003**, 278, 50985-50998.
381. Fatkins, D. G., Zheng, W. Substituting Nε-thioacetyl-lysine for Nε-acetyl-lysine in peptide substrates as a general approach to inhibiting human NAD^+-dependent protein deacetylases. *International journal of molecular sciences* **2008**, 9, 1-11.
382. Smith, B.C., Denu, J.M. Mechanism-based inhibition of Sir2 deacetylases by thioacetyl-lysine peptide. *Biochemistry* **2007**, 46, 14478-14486.
383. Kiviranta, P.H., Suuronen, T., Wallén, E.A., Leppänen, J., Tervonen, J., Kyrylenko, S., Salminen, A., Poso, A., Jarho, E.M. N(epsilon)-thioacetyl-lysine-containing tri-, tetra-, and pentapeptides as SIRT1 and SIRT2 inhibitors. *J Med Chem.* **2009**, 52, 2153-2156.
384. Suzuki, T., Asaba, T., Imai, E., Tsumoto, H., Nakagawa, H., Miyata, N. Identification of a cell-active non-peptide sirtuin inhibitor containing N-thioacetyl lysine. *Bioorganic & medicinal chemistry letters* **2009**, 19, 5670-5672.
385. Grozinger, C. M., Chao, E. D., Blackwell, H. E., Moazed, D., and Schreiber, S. L. Identification of a class of small molecule inhibitors of the sirtuin family of

NAD-dependent deacetylases by phenotypic screening. *J. Biol. Chem.* **2001**, 276, 38837-38843.

386. Ota, H., Tokunaga, E., Chang, K., Hikasa, M., Iijima, K., Eto, M., Kaneki, M. Sirt1 inhibitor, Sirtinol, induces senescence-like growth arrest with attenuated Ras-MAPK signaling in human cancer cells. *Oncogene* **2006**, 25, 176-185.

387. Orecchia, A., Scarponi, C., Di Felice, F., Cesarini, E., Avitabile, S, Mai, A., Failla, C. M. Sirtinol treatment reduces inflammation in human dermal microvascular endothelial cells. *PLoS One* **2011**, 6, e24307.

388. A) Mai, A., Massa, S., Lavu, S., Pezzi, R., Simeoni, S., Ragno, R., Sinclair, D. A. Design, synthesis, and biological evaluation of sirtinol analogues as class III histone/protein deacetylase (Sirtuin) inhibitors. *J. Med. Chem. 2005*, 48, 7789-7795. B) Lara, E., Mai, A., Calvanese, V., Altucci, L., Lopez-Nieva, P., Martinez-Chantar, M. L., Fraga, M. F. Salermide, a Sirtuin inhibitor with a strong cancer-specific proapoptotic effect. *Oncogene* **2009**, 28, 781-791.

389. Heltweg, B., Gatbonton, T., Schuler, A. D., Posakony, J., Li, H., Goehle, S., Bedalov, A. Antitumor activity of a smallmolecule inhibitor of human silent information regulator 2 enzymes. *Cancer. Res.* **2006**, 66, 4368-4377.

390. Medda, F., Russell, R. J., Higgins, M., McCarthy, A. R., Campbell, J., Slawin, A. M., Westwood, N. J. Novel cambinol analogs as sirtuin inhibitors: synthesis, biological evaluation, and rationalization of activity. *J. Med. Chem.* **2009**, 52, 2673-2682.

391. Howitz, K.T., Bitterman, K.J., Cohen, H.Y., Lamming, D.W., Lavu, S., Wood, J.G., Zipkin, R.E., Chung, P., Kisielewski, A., Zhang, L.L., Scherer, B., Sinclair, D.A. Small molecule activators of sirtuins extend Saccharomyces cerevisiae lifespan, *Nature* **2003**, 425, 191-196.

392. Trapp, J., Meier, R., Hongwiset, D., Kassack, M. U., Sippl, W., Jung, M. Structure- activity studies on suramin analogues as inhibitors of NAD^+-dependent histone deacetylases (sirtuins). *ChemMedChem* **2007**, 2, 1419-1431.

393. Schuetz, A., Min, J., Antoshenko, T., Wang, C. L., Allali-Hassani, A., Dong, A., Plotnikov, A. N. Structural basis of inhibition of the human NAD^+-dependent deacetylase SIRT5 by suramin. *Structure* **2007**, 15, 377-389.

394. Bedalov, A., Gatbonton, T., Irvine, W. P., Gottschling, D. E., Simon, J. A. Identification of a small molecule inhibitor of Sir2p. *Proc. Natl. Acad. Sci. USA* **2001**, 98, 15113-15118.

395. Posakony, J., Hirao, M., Stevens, S., Simon, J. A., Bedalov, A. Inhibitors of Sir2: evaluation of splitomicin analogues. *Journal of medicinal chemistry* **2004**, 47, 2635-2644.

396. Napper, A. D., Hixon, J., McDonagh, T., Keavey, K., Pons, J. F., Barker, J., Curtis, R. Discovery of indoles as potent and selective inhibitors of the deacetylase SIRT1. *Journal of medicinal chemistry* **2005**, 48, 8045-8054.

397. Solomon, J. M., Pasupuleti, R., Xu, L., McDonagh, T., Curtis, R., DiStefano, P. S., Huber, L. J. Inhibition of SIRT1 catalytic activity increases p53

acetylation but does not alter cell survival following DNA damage. *Molecular and cellular biology* **2006**, 26, 28-38.

398. Gertz, M., Fischer, F., Nguyen, G. T. T., Lakshminarasimhan, M., Schutkowski, M., Weyand, M., Steegborn, C. Ex-527 inhibits Sirtuins by exploiting their unique NAD^+-dependent deacetylation mechanism. *Proceedings of the National Academy of Sciences* **2013**, 110, 2772-2781.
399. Outeiro, T.F., Kontopoulos, E., Altmann, S.M., Kufareva, I., Strathearn, K.E., Amore, A.M., Volk, C.B., Maxwell, M.M., Rochet, J.C., McLean, P.J., Young, A.B., Abagyan, R., Feany, M.B., Hyman, B.T., Kazantsev, A.G. Sirtuin 2 inhibitors rescue alphasynuclein- mediated toxicity in models of Parkinson's disease. *Science* **2007**, 317, 516-519.
400. Garske, A.L., Smith, B.C., Denu, J.M. Linking SIRT2 to Parkinson's disease. *ACS Chem. Biol.* **2007**, 2, 529-532.
401. Jin, L., Galonek, H., Israelian, K., Choy, W., Morrison, M., Xia, Y., Westphal, C. H. Biochemical characterization, localization, and tissue distribution of the longer form of mouse SIRT3. *Protein Science* **2009**, 18,514-525.
402. Nguyen, G. T. T., Schaefer, S., Gertz, M., Weyand, M., Steegborn, C. Structures of human sirtuin 3 complexes with ADP-ribose and with carba-NAD^+ and SRT1720: binding details and inhibition mechanism. *Acta Crystallographica Section D: Biological Crystallography* **2013**, 69, 1423-1432.
403. Trapp, J., Jochum, A., Meier, R., Saunders, L., Marshall, B., Kunick, C., Jung, M. Adenosine mimetics as inhibitors of NAD^+-dependent histone deacetylases, from kinase to sirtuin inhibition. *Journal of medicinal chemistry* **2006**, 49, 7307-7316.
404. Suenkel, B., Fischer, F., Steegborn, C. Inhibition of the human deacylase Sirtuin 5 by the indole GW5074. *Bioorg. Med. Chem. Lett.*, **2013**, 23, 143-147.
405. Murray, K. The occurrence of ε-*N*-methyl lysine in histones. *Biochemistry* **1964**, 3, 10-15.
406. Paik, W. K., Kim, S. ε-*N*-dimethyllysine in histones. *Biochem.Biophys. Res. Commun.* **1967**, 27, 479-483.
407. Gershey, E. L., Haslett, G. W., Vidali, G., Allfrey, V. G. Chemical studies of histone methylation. Evidence for the occurrence of 3-methylhistidine in avian erythrocyte histone fractions. *J. Biol. Chem.* **1969**, 244, 4871-4877.
408. Greer, E. L., Shi, Y. Histone methylation: a dynamic mark in health, disease and inheritance. *Nature Reviews Genetics* **2012**, 13, 343-357.
409. Suzuki, T., Terashima, M., Tange, S., Ishimura, A. Roles of histone methyl-modifying enzymes in development and progression of cancer. *Cancer science* **2013,** 104, 795-800.
410. Shi, Y., Lan, F., Matson, C., Mulligan, P., Whetstine, J. R., Cole, P. A., Shi, Y Histone demethylation mediated by the nuclear amine oxidase homolog LSD1. *Cell* **2004**, 119, 941-953.

411. Zhang, Y. and D. Reinberg. Transcription regulation by histone methylation: interplay between different covalent modifications of the core histone tails. *Genes Dev* **2001**, 15, 2343-2360.
412. Krivtsov, A.V., Armstrong, S.A. MLL translocations, histone modifications and leukaemia stem-cell development. *Nat Rev Cancer* **2007**, 7, 823-833.
413. Li, Z., Luo, R. T., Mi, S., Sun, M., Chen, P., Bao, J., Thirman, M. J. Consistent deregulation of gene expression between human and murine MLL rearrangement leukemias. *Cancer Res* **2009**, 69, 1109-1116.
414. Kroon, E., Krosl, J., Thorsteinsdottir, U., Baban, S., Buchberg, A.M., Sauvageau, G. Hoxa9 transforms primary bone marrow cells through specific collaboration with Meis1a but not Pbx1b. *EMBO J* **1998**,17, 3714-3725.
415. Okada, Y., Feng, Q., Lin, Y., Jiang, Q., Li, Y., Coffield, V. M., Zhang, Y. hDOT1L links histone methylation to leukemogenesis. *Cell* **2005**, 12, 167-178.
416. Balakrishnan, A., Bleeker, F.E., Lamba, S., Rodolfo, M., Daniotti, M., Scarpa, A., van Tilborg, A.A., Leenstra, S., Zanon, C., Bardelli, A. Novel somatic and germline mutations in cancer candidate genes in glioblastoma, melanoma, and pancreatic carcinoma. *Cancer Res.* **2007**, 67, 3545-3550.
417. Madan, V., Madan, B., Brykczynska, U., Zilbermann, F., Hogeveen, K., Dohner, K., Dohner, H., Weber, O., Blum, C., Rodewald, H.R., Sassone-Corsi, P., Peters, A.H., Fehling, H.J. Impaired function of primitive hematopoietic cells in mice lacking the Mixed-Lineage-Leukemia homolog MLL5. *Blood* **2009**, 113, 1444-1454.
418. Strahl, B.D., Grant, P.A., Briggs, S.D., Sun, Z.W., Bone, J.R., Caldwell, J.A., Allis, C. D. Set2 is a nucleosomal histone H3-selective methyltransferase that mediates transcriptional repression. *Mol Cell Biol* **2002**, 22, 1298-306.
419. Nimura, K., Ura, K., Shiratori, H., Ikawa, M., Okabe, M., Schwartz, R. J., & Kaneda, Y. A histone H3 lysine 36 trimethyltransferase links Nkx2-5 to Wolf–Hirschhorn syndrome. *Nature* **2009**, 460, 287-291.
420. Rayasam, G. V., Wendling, O., Angrand, P. O., Mark, M., Niederreither, K., Song, L., Losson, R.. NSD1 is essential for early post-implantation development and has a catalytically active SET domain. *EMBO J* **2003**, 22, 3153-3163.
421. Wang, G.G., Cai, L., Pasillas, M.P., Kamps, M.P. NUP98-NSD1 links H3K36 methylation to Hox-A gene activation and leukaemogenesis. *Nat Cell Biol* **2007**, 9, 804-812.
422. Kim, J. Y., Kee, H. J., Choe, N. W., Kim, S. M., Eom, G. H., Baek, H. J., Seo, S. B. Multiple myeloma- related WHSC1/MMSET isoform RE-IIBP is a histone methyltransferase with transcriptional repression activity. *Mol Cell Biol* **2008**, 28, 2023-2034
423. Marango, J., Shimoyama, M., Nishio, H., Meyer, J. A., Min, D. J., Sirulnik, A., Licht, J. D. The MMSET protein is a histone methyltransferase with characteristics of a transcriptional corepressor. *Blood* **2008**, 111, 3145-3154.

424. Angrand, P. O., Apiou, F., Stewart, A. F., Dutrillaux, B., Losson, R., Chambon, P.NSD3, a new SET domain-containing gene, maps to 8p12 and is amplified in human breast cancer cell lines. *Genomics* **2001**, 74, 79-88.
425. Rosati, R., La Starza, R., Veronese, A., Aventin, A., Schwienbacher, C., Vallespi, T., Mecucci, C. NUP98 is fused to the NSD3 gene in acute myeloid leukemia associated with t(8;11)(p11.2;p15). *Blood* **2002,** 99, 3857-3860.
426. Kirmizis, A., Bartley, S. M., Kuzmichev, A., Margueron, R., Reinberg, D., Green, R., & Farnham, P. J. Silencing of human polycomb target genes is associated with methylation of histone H3 Lys 27. *Genes Dev*. **2004,** 18,1592-1605.
427. Saramäki, O. R., Tammela, T. L., Martikainen, P. M., Vessella, R. L., & Visakorpi, T. The gene for polycomb group protein enhancer of zeste homolog 2 (EZH2) is amplified in late-stage prostate cancer. *Genes Chromosom. Cancer* **2006**, 45, 639-645.
428. Kleer, C. G., Cao, Q., Varambally, S., Shen, R., Ota, I., Tomlins, S. A., Chinnaiyan, A. M. EZH2 is a marker of aggressive breast cancer and promotes neoplastic transformation of breast epithelial cells. *Proc. Natl Acad. Sci. USA* **2003**, 100, 11606-11611.
429. Morin, R. D., Johnson, N. A., Severson, T. M., Mungall, A. J., An, J., Goya, R., Paul, J.E., Boyle, M., Woolcock, B.W., Kuchenbauer, FYap, ., D., Humphries, R.K., Griffith, O.L., Shah, S., Zhu, H., Kimbara, M., Shashkin, P., Charlot, J.F., Tcherpakov, M., Corbett, R., Marra, M.A. Somatic mutations altering EZH2 (Tyr641) in follicular and diffuse large B-cell lymphomas of germinal-center origin. *Nat.Genet.* **2010**, 42, 181-185.
430. Tachibana, M., Ueda, J., Fukuda, M., Takeda, N., Ohta, T., Iwanari, H., Shinkai, Y. Histone methyltransferases G9a and GLP form heteromeric complexes and are both crucial for methylation of euchromatin at H3-K9. *Genes Dev*. **2005**, 19, 815-826.
431. Wu, H., Chen, X., Xiong, J., Li, Y., Li, H., Ding, X., Liu, S., Chen, S., Gao, S., Zhu, B. Histone methyltransferase G9a contributes to H3K27 methylation in vivo. *Cell Res* **2011**, 21, 365-367.
432. Weiss, T., Hergeth, S., Zeissler, U., Izzo, A., Tropberger, P., Zee, B.M., Dundr, M., Garcia, B.A., Daujat, S., Schneider, R. Research histone H1 variant-specific lysine methylation by G9a/KMT1C and Glp1/KMT1D. *Epigenetics Chromatin* **2010**, 3, 7.
433. Rountree, M.R., Selker, E.U. DNA methylation and the formation of heterochromatin in Neurospora crassa. *Heredity* **2010**, 105, 38-44.
434. Estève, P. O., Chin, H. G., Smallwood, A., Feehery, G. R., Gangisetty, O., Karpf, A. R., Pradhan, S. Direct interaction between DNMT1 and G9a coordinates DNA and histone methylation during replication. *Genes Dev* **2006**, 20, 3089-3103.
435. Chen, M. W., Hua, K. T., Kao, H. J., Chi, C. C., Wei, L. H., Johansson, G., Kuo, M. L. H3K9 histone methyltransferase G9a promotes lung cancer invasion

and metastasis by silencing the cell adhesion molecule Ep-CAM. *Cancer Res* **2010**, 70, 7830-7840.

436. Shinkai, Y., Tachibana, M. H3K9 methyltransferase G9a and the related molecule GLP. *Genes & development* **2011**, 25, 781-788.

437. Lehnertz, B., Ueda, Y., Derijck, A.A., Braunschweig, U., Perez-Burgos, L., Kubicek, S., Chen, T., Li, E., Jenuwein, T., Peters, A.H.Suv39h-mediated histone H3 lysine 9 methylation directs DNA methylation to major satellite repeats at pericentric heterochromatin. *Curr Biol* **2003**, 13, 1192-1200.

438. Rice, J. C., Briggs, S. D., Ueberheide, B., Barber, C. M., Shabanowitz, J., Hunt, D. F., Allis, C. D. Histone methyltransferases direct different degrees of methylation to define distinct chromatin domains. *Mol. Cell* **2003**, 12, 1591-1598.

439. Kim, K. C., Geng, L., Huang, S. Inactivation of a histone methyltransferase by mutations in human cancers. *Cancer Res.* **2003**, 63, 7619-7623.

440. Rea, S., Eisenhaber, F., O'Carroll, D., Strahl, B. D., Sun, Z. W., Schmid, M., Jenuwein, T. Regulation of chromatin structureby site-specific histone H3 methyltransferases, *Nature* **2000**, 406, 593-599.

441. Nielsen, S. J., Schneider, R., Bauer, U. M., Bannister, A. J., Morrison, A., O'Carroll, D., Kouzarides, T. Rb targets histone H3 methylation and HP1 to promoters. *Nature* **2001**, 412, 561-565.

442. Du, Y., Carling, T., Fang, W., Piao, Z., Sheu, J. C., Huang, S. Hypermethylation in human cancers of the RIZ1 tumor suppressor gene, a member of a histone/ protein methyltransferase superfamily. *Cancer Res.* **2001**, 61, 8094-8099.

443. Tokumaru, Y., Nomoto, S., Jerónimo, C., Henrique, R., Harden, S., Trink, B., Sidransky, D. Biallelic inactivation of the RIZ1 gene in human gastric cancer. *Oncogene* **2003**, 22, 6954-6958.

444. Varier, R. A., Timmers, H. T. Histone lysine methylation and demethylation pathways in cancer. *Biochimica et Biophysica Acta (BBA)-Reviews on Cancer* **2011**, 1815, 75-89.

445. Metzger, E., Wissmann, M., Yin, N., Muller, J.M., Schneider, R., Peters, A.H., Gunther, T., Buettner, R., Schule, R. LSD1 demethylates repressive histone marks to promote androgen receptor- dependent transcription. *Nature* **2005**, 437, 436-439.

446. Huang, J., Sengupta, R., Espejo, A. B., Lee, M. G., Dorsey, J. A., Richter, M., Berger, S. L.. p53 is regulated by the lysine demethylase LSD1. *Nature* **2007**, 449, 105-108.

447. Wang, J., Hevi, S., Kurash, J. K., Lei, H., Gay, F., Bajko, J., Chen, T. The lysine demethylase LSD1 (KDM1) is required for maintenance of global DNA methylation. *Nature Genet.* **2009**, 41, 125-129.

448. Kontaki, H., Talianidis, I. Lysine methylation regulates E2F1-induced cell death. *Mol. Cell* **2010**, 39, 152-160.

449. Karytinos, A., Forneris, F., Profumo, A., Ciossani, G., Battaglioli, E., Binda, C., Mattevi, A. A novel mammalian flavin-dependent histone demethylase. *Journal of Biological Chemistry* **2009**, 284, 17775-17782.
450. Forneris, F., Binda, C., Battaglioli, E., Mattevi, A. LSD1: oxidative chemistry for multifaceted functions in chromatin regulation. *Trends in biochemical sciences* **2008**, 33, 181-189.
451. Garcia-Bassets, I., Kwon, Y. S., Telese, F., Prefontaine, G. G., Hutt, K. R., Cheng, C. S., Rosenfeld, M. G. Histone methylation-dependent mechanisms impose ligand dependency for gene activation by nuclear receptors. *Cell* **2007**, 128, 505-518.
452. Forneris, F., Binda, C., Vanoni, M. A., Battaglioli, E., Mattevi, A. Human histone demethylase LSD1 reads the histone code. *Journal of Biological Chemistry* **2005**, 280, 41360-41365.
453. Culhane, J. C., Cole, P. A. LSD1 and the chemistry of histone demethylation. *Current opinion in chemical biology* **2007**, 11, 561-568.
454. Chen, Y., Yang, Y., Wang, F., Wan, K., Yamane, K., Zhang, Y., Lei, M. Crystal structure of human histone lysine-specific demethylase 1 (LSD1). *Proc. Natl. Acad. Sci.* **2006**,103,13956-13961.
455. Stavropoulos, P., Blobel, G., Hoelz, A. Crystal structure and mechanism of human lysine-specific demethylase-1. *Nature structural & molecular biology* **2006**, 13, 626-632.
456. Binda, C., Coda, A., Angelini, R., Federico, R., Ascenzi, P., Mattevi, A. A 30 Å long U-shaped catalytic tunnel in the crystal structure of polyamine oxidase. *Structure* **1999**, 7, 265-276.
457. Binda, C., Angelini, R., Federico, R., Ascenzi, P., Mattevi, A. Structural bases for inhibitor binding and catalysis in polyamine oxidase. *Biochemistry* **2001**, 40, 2766-2776.
458. Wissmann, M., Yin, N., Müller, J. M., Greschik, H., Fodor, B. D., Jenuwein, T., Schüle, R. Cooperative demethylation by JMJD2C and LSD1 promotes androgen receptor-dependent gene expression. *Nature cell biology* **2007**, 9, 347-353.
459. Hu, Q., Kwon, Y. S., Nunez, E., Cardamone, M. D., Hutt, K. R., Ohgi, K. A., Fu, X. D. Enhancing nuclear receptor-induced transcription requires nuclear motor and LSD1-dependent gene networking in interchromatin granules. *Proc Natl Acad Sci U S A* **2008**, 105, 19199-19204.
460. Dallman, J. E., Allopenna, J., Bassett, A., Travers, A., & Mandel, G. A conserved role but different partners for the transcriptional corepressor CoREST in fly and mammalian nervous system formation. *J Neurosci* **2004**, 24, 7186-7193.
461. Saleque, S., Kim, J., Rooke, H. M., Orkin, S. H. Epigenetic regulation of hematopoietic differentiation by Gfi-1 and Gfi-1b is mediated by the cofactors CoREST and LSD1. *Mol Cell* **2007**, 27, 562-572.

462. Su, S. T., Ying, H. Y., Chiu, Y. K., Lin, F. R., Chen, M. Y., Lin, K. I. Involvement of histone demethylase LSD1 in Blimp-1-mediated gene repression during plasma cell differentiation. *Mol Cell Biol* **2009**, 29, 1421-1431.
463. Tsai, W. W., Nguyen, T. T., Shi, Y., & Barton, M. C. p53-targeted LSD1 functions in repression of chromatin structure and transcription in vivo. *Mol Cell Biol* **2008**, 28, 5139-5146.
464. Liu, L., Souto, J., Liao, W., Jiang, Y., Li, Y., Nishinakamura, R., Yang, J. Histone lysine-specific demethylase 1 (LSD1) protein is involved in Sal-like Protein 4 (SALL4)-mediated transcriptional repression in hematopoietic stem cells. *Journal of Biological Chemistry* **2013**, 288, 34719-34728.
465. Ooi, S. K., Qiu, C., Bernstein, E., Li, K., Jia, D., Yang, Z., Bestor, T. H. DNMT3L connects unmethylated lysine 4 of histone H3 to de novo methylation of DNA. *Nature* **2007**, 448, 714-717.
466. Lin, T., Ponn, A., Hu, X., Law, B. K., Lu, J. Requirement of the histone demethylase LSD1 in Snai1-mediated transcriptional repression during epithelial-mesenchymal transition. *Oncogene* **2010**, *29*, 4896-4904.
467. Baron, R., Binda, C., Tortorici, M., McCammon, J. A., Mattevi, A. Molecular mimicry and ligand recognition in binding and catalysis by the histone demethylase LSD1-CoREST complex. *Structure* **2011**, 19, 212-220.
468. Forneris, F., Binda, C., Adamo, A., Battaglioli, E., Mattevi, A. Structural basis of LSD1-CoREST selectivity in histone H3 recognition. *Journal of Biological Chemistry* **2007**, 282, 20070-20074.
469. Barrallo-Gimeno, A., Nieto, M.A. Evolutionary history of the Snail/ Scratch superfamily. *Trends Genet.* **2009**, 25, 248-252.
470. Peinado, H., Olmeda, D., Cano, A. Snail, Zeb and bHLH factors in tumour progression: an alliance against the epithelial phenotype?. *Nature Reviews Cancer* **2007**, 7, 415-428.
471. Kahl, P., Gullotti, L., Heukamp, L. C., Wolf, S., Friedrichs, N., Vorreuther, R., Buettner, R. Androgen receptor coactivators lysine-specific histone demethylase 1 and four and a half LIM domain protein 2 predict risk of prostate cancer recurrence. *Cancer research* **2006**, 66, 11341-11347.
472. Kauffman, E. C., Robinson, B. D., Downes, M. J., Powell, L. G., Lee, M. M., Scherr, D. S., Mongan, N. P. Role of androgen receptor and associated lysine-demethylase coregulators, LSD1 and JMJD2A, in localized and advanced human bladder cancer. *Mol. Carcinog.* **2011**, 50, 931-944.
473. Schulte, J. H., Lim, S., Schramm, A., Friedrichs, N., Koster, J., Versteeg, R., Kirfel, J. Lysine-specific demethylase 1 is strongly expressed in poorly differentiated neuroblastoma: implications for therapy. *Cancer Res.* **2009**, 69, 2065-2071.
474. Lv, T., Yuan, D., Miao, X., Lv, Y., Zhan, P., Shen, X., & Song, Y. Over-expression of LSD1 promotes proliferation, migration and invasion in non-small cell lung cancer *PLoS One* **2012**, 7, e35065.

475. Zhao, Z. K., Dong, P., Gu, J., Chen, L., Zhuang, M., Lu, W. J., Liu, Y. B. Overexpression of LSD1 in hepatocellular carcinoma: a latent target for the diagnosis and therapy of hepatoma. *Tumor Biology* **2013**, 34, 173-180.
476. Hayami, S., Kelly, J. D., Cho, H. S., Yoshimatsu, M., Unoki, M., Tsunoda, T., Hamamoto, R. Overexpression of LSD1 contributes to human carcinogenesis through chromatin regulation in various cancers. *Int. J. Cancer* **2011**, 128, 574-586.
477. L.P. Vu, L. Luciani, S.D. Nimer Histone-modifying enzymes: their role in the pathogenesis of acute leukemia and their therapeutic potential *Int. J. Hematol.* **2013**, 1-12.
478. Lokken, A. A., Zeleznik-Le, N. J. Breaking the LSD1/KDM1A addiction: therapeutic targeting of the epigenetic modifier in AML. *Cancer Cell* **2012**, 21, 451-453.
479. Harris, W. J., Huang, X., Lynch, J. T., Spencer, G. J., Hitchin, J. R., Li, Y., Somervaille, T. C. The histone demethylase KDM1A sustains the oncogenic potential of MLL-AF9 leukemia stem cells. *Cancer Cell* **2012**, 21, 473-487.
480. Amente, S., Lania, L., Majello, B. The histone LSD1 demethylase in stemness and cancer transcription programs. *Biochimica et Biophysica Acta (BBA)-Gene Regulatory Mechanisms* **2013**, 1829, 981-986.
481. Yatim, A., Benne, C., Sobhian, B., Laurent-Chabalier, S., Deas, O., Judde, J. G., Benkirane, M. NOTCH1 nuclear interactome reveals key regulators of its transcriptional activity and oncogenic function. *Mol. Cell* **2012**, 48, 445-458.
482. Yang ,Z., Jiang, J., Stewart, D.M., Qi, S., Yamane, K., Li, J., Zhang, Y., Wong, J. AOF1 is a histone H3K4 demethylase possessing demethylase activity-independent repression function. *Cell Res* **2010**, 20**,** 276-287.
483. Højfeldt, J. W., Agger, K., Helin, K. Histone lysine demethylases as targets for anticancer therapy. *Nature Reviews Drug Discovery* **2013**.
484. Fang, R., Chen, F., Dong, Z., Hu, D., Barbera, A. J., Clark, E. A., Shi, Y. G. LSD2/KDM1B and its cofactor NPAC/ GLYR1 endow a structural and molecular model for regulation of H3K4 demethylation. *Mol. Cell* **2013**, 49, 558-570.
485. Fang, R., Barbera, A.J., Xu, Y., Rutenberg, M., Leonor, T., Bi, Q., Lan, F., Mei, P., Yuan, G.C., Lian, C., Shi, Y.G. Human LSD2/KDM1b/AOF1 regulates gene transcription by modulating intragenic H3K4me2 methylation. *Mol Cell* **2010**, 39**,** 222-233.
486. Ciccone, D.N., Su, H., Hevi, S., Gay, F., Lei, H., Bajko, J., Xu, G., Li, E., Chen, T. KDM1B is a histone H3K4 demethylase required to establish maternal genomic imprints. *Nature* **2009**, 46, 415-418.
487. Takeuchi, T., Yamazaki, Y., Katoh-Fukui, Y., Tsuchiya, R., Kondo, S., Motoyama, J., Higashinakagawa, T. Gene trap capture of a novel mouse gene, jumonji, required for neural tube formation. *Genes Dev.* **1995**, 9, 1211-1222.

488. Tsukada, Y. I., Fang, J., Erdjument-Bromage, H., Warren, M. E., Borchers, C. H., Tempst, P., Zhang, Y. Histone demethylation by a family of JmjC domain-containing proteins. *Nature* **2005**, 439, 811-816.
489. Arrowsmith, C.H., Bountra, C., Fish, P.V., Lee, K., Schapira, M.. Epigenetic protein families: a new frontier for drug discovery. *Nat. Rev. Drug Discov.* **2012**, 11, 384-400.
490. McDonough, M. A., Loenarz, C., Chowdhury, R., Clifton, I. J., & Schofield, C. J. Structural studies on human 2-oxoglutarate dependent oxygenases. *Current opinion in structural biology* **2010**, 20,659-672.
491. Hoffmann, I., Roatsch, M., Schmitt, M. L., Carlino, L., Pippel, M., Sippl, W., Jung, M. The role of histone demethylases in cancer therapy. *Molecular Oncology* **2012**, 6, 683-703.
492. Ng, S.S., Kavanagh, K.L., McDonough, M.A., Butler, D., Pilka, E.S., Lienard, B.M.R., Bray, J.E., Savitsky, P., Gileadi, O., von Delft, F., Oppermann, U. Crystal structures of histone demethylase JMJD2A reveal basis for substrate specificity. *Nature* **2007**, 448, 87-91.
493. Han, Z., Liu, P., Gu, L., Zhang, Y., Li, H., Chen, S., Chai, J. Structural basis for histone demethylation by JHDM1. *Front Sci* **2007**, 1, 52-61.
494. Yue, W.W., Hozjan, V., Ge, W., Loenarz, C., Cooper, C.D.O., Schofield, C.J., Kavanagh, K.L., Oppermann, U., McDonough, M.A. Crystal structure of the PHF8 Jumonji domain, an Ne-methyl lysine demethylase. *FEBS Lett* **2010**, 584, 825-830.
495. Chen, Z., Zang, J., Whetstine, J., Hong, X., Davrazou, F., Kutateladze, T. G., Zhang, G. Structural insights into histone demethylation by JMJD2 family members. *Cell* **200**6, 125, 691-702.
496. Couture, J. F., Collazo, E., Ortiz-Tello, P. A., Brunzelle, J. S. Trievel, R. C. Specificity and mechanism of JMJD2A, a trimethyllysine-specific histone demethylase. *Nature Struct. Mol. Biol.* **2007**, 14, 689-695.
497. Horton, J.R., Upadhyay, A.K., Qi, H.H., Zhang, X., Shi, Y., Cheng, X. Enzymatic and structural insights for substrate specificity of a family of jumonji histone lysine demethylases. *Nat Struct Mol Biol* **2010**, 17, 38-43.
498. He, J., Kallin, E. M., Tsukada, Y. I., Zhang, Y. The H3K36 demethylase Jhdm1b/Kdm2b regulates cell proliferation and senescence through p15Ink4b. *Nat Struct Mol Biol* **2008**, 15, 1169-1175.
499. Lagarou, A., Mohd-Sarip, A., Moshkin, Y. M., Chalkley, G. E., Bezstarosti, K., Demmers, J. A., Verrijzer, C. P. dKDM2 couples histone H2A ubiquitylation to histone H3 demethylation during Polycomb group silencing. *Genes & development* **2008**, 22, 2799-2810.
500. Frescas, D., Guardavaccaro, D., Bassermann, F., Koyama-Nasu, R., Pagano, M. JHDM1B/FBXL10 is a nucleolar protein that represses transcription of ribosomal RNA genes. *Nature* **2007**, 450, 309-313.

501. Wu, X., Johansen, J. V. & Helin, K. Fbxl10/Kdm2b recruits Polycomb repressive complex 1 to CpG islands and regulates H2A ubiquitylation. *Mol. Cell* **2013**, 49, 1134-1146.
502. Farcas, A. M., Blackledge, N. P., Sudbery, I., Long, H. K., McGouran, J. F., Rose, N. R., Klose, R. J. KDM2B links the Polycomb Repressive Complex 1 (PRC1) to recognition of CpG islands. *Elife* **2012**, 1, e00205.
503. Suzuki, T., Minehata, K. I., Akagi, K., Jenkins, N. A., Copeland, N. G. Tumor suppressor gene identification using retroviral insertional mutagenesis in Blm-deficient mice. *EMBO l* **2006**, *25*, 3422-3431.
504. Pfau, R., Tzatsos, A., Kampranis, S. C., Serebrennikova, O. B., Bear, S. E., & Tsichlis, P. N.. Members of a family of JmjC domain-containing oncoproteins immortalize embryonic fibroblasts via a JmjC domain-dependent process. *Proc Natl Acad Sci U S A.*, **2008**, 105, 1907-1912.
505. Frescas, D., Guardavaccaro, D., Kuchay, S. M., Kato, H., Poleshko, A., Basrur, V., Pagano, M.. KDM2A represses transcription of centromeric satellite repeats and maintains the heterochromatic state. *Cell Cycle* **2008**, 7, 3539-3547.
506. Yamane, K., Toumazou, C., Tsukada, Y. I., Erdjument-Bromage, H., Tempst, P., Wong, J., & Zhang, Y. JHDM2A, a JmjC-containing H3K9 demethylase, facilitates transcription activation by androgen receptor. *Cell* **2006**, 125, 483-495.
507. Heery, D. M., Kalkhoven, E., Hoare, S., Parker, M. G. A signature motif in transcriptional co-activators mediates binding to nuclear receptors. *Nature* **1997**, 387, 733-736.
508. Inagaki, T., Tachibana, M., Magoori, K., Kudo, H., Tanaka, T., Okamura, M., Sakai, J. Obesity and metabolic syndrome in histone demethylase JHDM2a-deficient mice. *Genes to Cells* **2009**, 14, 991-1001.
509. Liu, Z., Zhou, S., Liao, L., Chen, X., Meistrich, M., Xu, J. Jmjd1a demethylase-regulated histone modification is essential for cAMP-response element modulator-regulated gene expression and spermatogenesis. *Journal of Biological Chemistry* **201**0, 285, 2758-2770.
510. Krieg, A. J., Rankin, E. B., Chan, D., Razorenova, O., Fernandez, S., Giaccia, A. J.. Regulation of the histone demethylase JMJD1A by hypoxia-inducible factor 1α enhances hypoxic gene expression and tumor growth. *Molecular and cellular biology* **2010**, 30, 344-353.
511. Park, S. J., Kim, J. G., Son, T. G., Yi, J. M., Kim, N. D., Yang, K., Heo, K. The histone demethylase JMJD1A regulates adrenomedullin-mediated cell proliferation in hepatocellular carcinoma under hypoxia. *Biochemical and biophysical research communications* **2013**, 434, 722-727.
512. Hu, Z., Gomes, I., Horrigan, S. K., Kravarusic, J., Mar, B., Arbieva, Z., Westbrook, C. A. A novel nuclear protein, 5qNCA (LOC51780) is a candidate for the myeloid leukemia tumor suppressor gene on chromosome 5 band q31. *Oncogene* **2001**, 20, 6946-6954.

513. Brauchle, M., Yao, Z., Arora, R., Thigale, S., Clay, I., Inverardi, B., Ruffner, H. Protein complex interactor analysis and differential activity of KDM3 subfamily members towards H3K9 methylation. *PloS one* **2013**, 8, e60549.
514. Braig, M., Lee, S., Loddenkemper, C., Rudolph, C., Peters, A. H., Schlegelberger, B., Schmitt, C. A. Oncogene-induced senescence as an initial barrier in lymphoma development. *Nature* **2005**, 436, 660-665.
515. Cloos, P. A., Christensen, J., Agger, K., Maiolica, A., Rappsilber, J., Antal, T., Helin, K. The putative oncogene *GASC1* demethylates tri- and dimethylated lysine 9 on histone H3. *Nature* **2006**, 442, 307-311.
516. Liu, G., Bollig-Fischer, A., Kreike, B., van de Vijver, M. J., Abrams, J., Ethier, S. P., Yang, Z. Q. Genomic amplification and oncogenic properties of the GASC1 histone demethylase gene in breast cancer. *Oncogene* **2009**, 28, 4491-4500.
517. Rui, L., Emre, N. C., Kruhlak, M. J., Chung, H. J., Steidl, C., Slack, G., Staudt, L. M. Cooperative epigenetic modulation by cancer amplicon genes. *Cancer Cell* **2010**, 18, 590-605 .
518. Di Tacchio, L., Le, H. D., Vollmers, C., Hatori, M., Witcher, M., Secombe, J., Panda, S. Histone lysine demethylase JARID1a activates CLOCK-BMAL1 and influences the circadian clock. *Science* **2011**, 333, 1881-1885.
519. Benevolenskaya, E.V., Murray, H.L., Branton, P., Young, R.A., Kaelin, W.G., Binding of pRB to the PHD protein RBP2 promotes cellular differentiation. *Mol Cell* **2005**, 18, 623-635.
520. Zeng, J., Ge, Z., Wang, L., Li, Q., Wang, N., Björkholm, M., Xu, D. The histone demethylase RBP2 Is overexpressed in gastric cancer and its inhibition triggers senescence of cancer cells. *Gastroenterology* **2010**, 138, 981-992.
521. Sharma, S. V., Lee, D. Y., Li, B., Quinlan, M. P., Takahashi, F., Maheswaran, S., Settleman, J. A chromatin-mediated reversible drug-tolerant state in cancer cell subpopulations. *Cell* **2010**, 141, 69-80.
522. Schmitz, S. U., Albert, M., Malatesta, M., Morey, L., Johansen, J. V., Bak, M., Helin, K. Jarid1b targets genes regulating development and is involved in neural differentiation. *EMBO J.* **2011**, 30, 4586-4600.
523. Lu, P. J., Sundquist, K., Baeckstrom, D., Poulsom, R., Hanby, A., Meier-Ewert, S., Taylor-Papadimitriou, J. A novel gene (PLU-1) containing highly conserved putative DNA/chromatin binding motifs is specifically up-regulated in breast cancer. *Journal of Biological Chemistry* **1999**, 274, 15633-15645.
524. Hayami, S., Yoshimatsu, M., Veerakumarasivam, A., Unoki, M., Iwai, Y., Tsunoda, T., Hamamoto, R. Overexpression of the JmjC histone demethylase KDM5B in human carcinogenesis: involvement in the proliferation of cancer cells through the E2F/RB pathway. *Mol Cancer* **2010**, 9, 59.
525. Xiang, Y., Zhu, Z., Han, G., Ye, X., Xu, B., Peng, Z., Chen, C. D. JARID1B is a histone H3 lysine 4 demethylase up-regulated in prostate cancer. *Proceedings of the National Academy of Sciences* **2007**, 104, 19226-19231.

526. Yamane, K., Tateishi, K., Klose, R. J., Fang, J., Fabrizio, L. A., Erdjument-Bromage, H., Zhang, Y. PLU-1 is an H3K4 demethylase involved in transcriptional repression and breast cancer cell proliferation. *Molecular cell* **2007**, 25, 801-812.
527. Roesch, A., Fukunaga-Kalabis, M., Schmidt, E. C., Zabierowski, S. E., Brafford, P. A., Vultur, A., Herlyn, M. A temporarily distinct subpopulation of slow-cycling melanoma cells is required for continuous tumor growth. *Cell* **2010**, 141, 583-594.
528. M. Tahiliani, P. Mei, R. Fang, T. Leonor, M. Rutenberg, F. Shimizu, J. Li, A. Rao, Y. Shi, The histone H3K4 demethylase SMCX links REST target genes to X-linked mental retardation. *Nature* **2007**, 447, 601-605.
529. J.A. Smith, E.A. White, M.E. Sowa, M.L. Powell, M. Ottinger, J.W. Harper, P.M. Howley, Genome-wide siRNA screen identifies SMCX, EP400, and Brd4 as E2- dependent regulators of human papillomavirus oncogene expression. *Proceedings of the National Academy of Sciences* **2010**, 107, 3752-3757.
530. De Santa, F., Totaro, M. G., Prosperini, E., Notarbartolo, S., Testa, G., Natoli, G. The histone H3 lysine-27 demethylase Jmjd3 links inflammation to inhibition of polycomb-mediated gene silencing. *Cell* **2007**, 130, 1083-1094.
531. De Santa, F., Narang, V., Yap, Z. H., Tusi, B. K., Burgold, T., Austenaa, L., Natoli, G. Jmjd3 contributes to the control of gene expression in LPS-activated macrophages. *The EMBO journal* **2009**, 28, 3341-3352.
532. Lee, M. G., Villa, R., Trojer, P., Norman, J., Yan, K. P., Reinberg, D., Shiekhattar, R. Demethylation of H3K27 regulates polycomb recruitment and H2A ubiquitination. *Science* **2007**, 318, 447-450.
533. Issaeva, I., Zonis, Y., Rozovskaia, T., Orlovsky, K., Croce, C. M., Nakamura, T., Canaani, E. Knockdown of ALR (MLL2) reveals ALR target genes and leads to alterations in cell adhesion and growth. *Molecular and cellular biology* **2007**, 27, 1889-1903.
534. van Haaften, G., Dalgliesh, G. L., Davies, H., Chen, L., Bignell, G., Greenman, C., Wong, J. Somatic mutations of the histone H3K27 demethylase gene UTX in human cancer. *Nature genetics* **2009**, 41, 521-523.
535. Yokoyama, A., Okuno, Y., Chikanishi, T., Hashiba, W., Sekine, H., Fujiki, R., Kato, S. KIAA1718 is a histone demethylase that erases repressive histone methyl marks. *Genes to Cells* **2010**, 15, 867-873.
536. Kooistra, S. M., Helin, K. Molecular mechanisms and potential functions of histone demethylases. *Nature reviews Molecular cell biology* **2012**, 13, 297-311.
537. Yang, Y., Hu, L., Wang, P., Hou, H., Lin, Y., Liu, Y., Xu, Y. Structural insights into a dual-specificity histone demethylase ceKDM7A from Caenorhabditis elegans. *Cell research* **2010**, 20, 886-898.
538. Qi, H. H., Sarkissian, M., Hu, G. Q., Wang, Z., Bhattacharjee, A., Gordon, D. B., Shi, Y. Histone H4K20/H3K9 demethylase PHF8 regulates zebrafish brain and craniofacial development. *Nature* **2010**, 466, 503-507.

539. Huang, C., Xiang, Y., Wang, Y., Li, X., Xu, L., Zhu, Z., Chen, C. D. Dual-specificity histone demethylase KIAA1718 (KDM7A) regulates neural differentiation through FGF4. *Cell research* **2010**, 20, 154-165.
540. Lee, M.G., Wynder, C., Schmidt, D.M., McCafferty, D.G., Shiekhattar, R. Histone H3 lysine 4 demethylation is a target of nonselective antidepressive medications. *Chem Biol.* **2006**,13, 563-567.
541. Culhane, J.C., Wang, D., Yen, P.M., Cole, P.A. Comparative analysis of small molecules and histone substrate analogues as LSD1 lysine demethylase inhibitors. *J Am Chem Soc.* **2010**, 132, 3164-3176.
542. Yang, M., Culhane, J. C., Szewczuk, L. M., Jalili, P., Ball, H. L., Machius, M., Yu, H. Structural basis for the inhibition of the LSD1 histone demethylase by the antidepressant trans-2-phenylcyclopropylamine. *Biochemistry* **2007**,46, 8058-8065.
543. Ueda, R., Suzuki, T., Mino, K., Tsumoto, H., Nakagawa, H., Hasegawa, M., Miyata, N. Identification of cell-active lysine specific demethylase 1–selective inhibitors. *J Am Chem Soc.* **2009**,131, 17536-17537.
544. Binda, C., Valente, S., Romanenghi, M., Pilotto, S., Cirilli, R., Karytinos, A., Mai, A. Biochemical, structural, and biological evaluation of tranylcypromine derivatives as inhibitors of histone demethylases LSD1 and LSD2. *J Am Chem Soc.* **2010**, 132, 6827-6833.
545. Liang, Y., Quenelle, D., Vogel, J. L., Mascaro, C., Ortega, A., Kristie, T. M. A novel selective LSD1/KDM1A inhibitor epigenetically blocks herpes simplex virus lytic replication and reactivation from latency. *MBio* **2013**, 4, e00558-12.
546. Szewczuk, L.M., Culhane, J.C., Yang, M., Majumdar, A., Yu, H., Cole, P.A. Mechanistic analysis of a suicide inactivator of histone demethylase LSD1. *Biochemistry* **2007**;46, 6892-902.
547. Yang, M., Culhane, J. C., Szewczuk, L. M., Gocke, C. B., Brautigam, C. A., Tomchick, D. R., Yu, H. Structural basis of histone demethylation by LSD1 revealed by suicide inactivation. *Nature Structural and Molecular Biology* **2007**, 14, 535-539.
548. Wang, Y., Murray-Stewart, T., Devereux, W., Hacker, A., Frydman, B., Woster, P. M., Casero, R. A. Properties of purified recombinant human polyamine oxidase, PAOh1/SMO. *Biochemical and biophysical research communications* **2003**, 304, 605-611.
549. Bi, X., Lopez, C., Bacchi, C.J., Rattendi, D., Woster, P.M. Novel alkylpolyaminoguanidines and alkylpolyaminobiguanides with potent antitrypanosomal activity. *Bioorg Med Chem Lett.* **2006**,16, 3229-32.
550. Sharma, S. K., Hazeldine, S., Crowley, M. L., Hanson, A., Beattie, R., Varghese, S., Woster, P. M. Polyamine-based small molecule epigenetic modulators. *MedChemComm* **2012**, 3, 14-21.
551. Huang, Y., Stewart, T. M., Wu, Y., Baylin, S. B., Marton, L. J., Perkins, B., Casero, R. A. Novel oligoamine analogues inhibit lysine-specific demethylase 1

and induce reexpression of epigenetically silenced genes. *Clin Cancer Res.* **2009**,15, 7217-7228.

552. Sharma, S. K., Wu, Y., Steinbergs, N., Crowley, M. L., Hanson, A. S., Casero Jr, R. A., Woster, P. M. (Bis)urea and (bis)thiourea inhibitors of lysine-specific demethylase 1 as epigenetic modulators. *J Med Chem.* **2010**, 53, 5197-5212.

553. Rose, N. R., Ng, S. S., Mecinović, J., Liénard, B. M., Bello, S. H., Sun, Z., Schofield, C. J. Inhibitor Scaffolds for 2-Oxoglutarate-Dependent Histone Lysine Demethylases. *J Med Chem.* **2008**, 51, 7053-7056.

554. Chen, Z., Zang, J., Kappler, J., Hong, X., Crawford, F., Wang, Q., Zhang, G. Structural basis of the recognition of a methylated histone tail by JMJD2A. *Proc Natl Acad Sci USA* **2007**, 104, 10818-10823.

555. Sekirnik, R., Rose, N. R., Thalhammer, A., Seden, P. T., Mecinović, J., Schofield, C. J. Inhibition of the histone lysine demethylase JMJD2A by ejection of structural Zn (II). *ChemComm* **2009**, 42, 6376.

556. Chowdhury, R., Yeoh, K. K., Tian, Y. M., Hillringhaus, L., Bagg, E. A., Rose, N. R., Leung, I. K., Li, X. S., Woon, E. C., Yang, M.,Mcdonough, M. A., King, O. N., Clifton, I. J., Klose, R. J., Claridge, T. D., Ratcliffe, P. J., Schofield, C. J., Kawamura, A. The oncometabolite 2-hydroxyglutarate inhibits histone lysine demethylases. *EMBO Reports* **2011**, 12, 463-469.

557. King, O. N., Li, X. S., Sakurai, M., Kawamura, A., Rose, N. R., Ng, S. S., Quinn, A. M., Rai, G., Mott, B. T., Beswick, P., Klose, R. J., Oppermann, U., Jadhav, A., Heightman, T. D., Maloney, D. J., Schofield, C. J., Simeonov, A. Quantitative High-Throughput Screening Identifies 8-Hydroxyquinolines As Cell-Active Histone Demethylase Inhibitors. *Plos One* **2010**, 5, e15535.

558. Chang, K. H., King, O. N., Tumber, A., Woon, E. C., Heightman, T. D., Mcdonough, M. A., Schofield, C. J., Rose, N. R. Inhibition of histone demethylases by 4-carboxy-2,2'-bipyridyl compounds *Chemmedchem* **2011**, 6, 759-764.

559. Hamada, S., Suzuki, T., Mino, K., Koseki, K., Oehme, F., Flamme, I., Ozasa, H., Itoh, Y., Ogasawara, D., Komaarashi, H., Kato, A., Tsumoto, H., Nakagawa, H., Hasegawa, M., Sasaki, R.,Mizukami, T., Miyata, N. Design, synthesis, enzyme inhibitory activity, and effect on human cancer cells of a novel series of jumonji domain-containing protein 2 histone demethylase inhibitors. *J Med Chem.* **2010**, 53, 5629-5638.

560. Kruidenier, L., Chung, C. W., Cheng, Z., Liddle, J., Che, K., Joberty, G., Bantscheff, M., Bountra, C., Bridges, A., Diallo, H., Eberhard, D., Hutchinson, S., Jones, E., Katso, R., Leveridge, M., Mander, P. K., Mosley, J., Ramirez-Molina, C., Rowland, P., Schofield, C. J., Sheppard, R. J., Smith, J. E., Swales, C., Tanner, R., Thomas, P., Tumber, A., Drewes, G., Oppermann, U., Patel, D. J., Lee, K., Wilson, D. M. A selective jumonji H3K27 demethylase inhibitor modulates the proinflammatory macrophage response. *Nature* **2012**, 488, 404-408.

561. Chen, S. M., Leupin, W., Rance, M., Chazin, W. J. Two-dimensional NMR studies of d (GGTTAATGCGGT). cntdot. d (ACCGCATTAACC) complexed with the minor groove binding drug SN-6999. *Biochemistry* **1992**, 31, 4406-4413.

562. Adams, A., Leong, C., Denny, W.A., Guss, J.M. Structures of two minor-groove-binding quinolinium quaternary salts complexed with d(CGCGAATTCGCG)(2) at 1.6 and 1.8 Angstrom resolution. *Acta Crystallogr D Biol Crystallogr* **2005**, 61,1348-1353.

563. Denny, W.A., Atwell, G.J., Baguley, B.C., Cain, B.F. Potential antitumor agents. 29. Quantitative structure-activity relationships for the antileukemic bisquaternary ammonium heterocycles. *J Med Chem* **1979**, 22, 134-150.

564. Zhang, X.; Cheng, X. Structure of the predominant protein arginine methyltransferase PRMT1 and analysis of its binding to substrate peptides. *Structure* **2003**, 11, 509-520.

565. Hashimoto, H.; Liu, Y.; Upadhyay, A. K.; Chang, Y.; Howerton, S. B.; Vertino, P. M.; Zhang, X.; Cheng, X. Recognition and potential mechanisms for replication and erasure of cytosine hydroxymethylation. *Nucleic Acids Res*. **2012**, *40*, 4841-4849.

566. Chang, Y.; Zhang, X.; Horton, J. R.; Upadhyay, A. K.; Spannhoff, A.; Liu, J.; Snyder, J. P.; Bedford, M. T.; Cheng, X. Structural basis for G9a-like protein lysine methyltransferase inhibition by BIX-01294. *Nat. Struct. Mol. Biol*. **2009**, *16*, 312-317.

567. Schnekenburger, M., Grandjenette, C., Ghelfi, J., Karius, T., Foliguet, B., Dicato, M., Diederich, M. Sustained exposure to the DNA demethylating agent, 2′-deoxy-5-azacytidine, leads to apoptotic cell death in chronic myeloid leukemia by promoting differentiation, senescence, and autophagy. *Biochem. Pharmacol*. **2011**, 81, 364-378.

568. Charlet, J., Schnekenburger, M., Brown, K. W., Diederich, M. DNA demethylation increases sensitivity of neuroblastoma cells to chemotherapeutic drugs. *Biochem. Pharmacol*. **2012**, 83, 858-865.

569. Dudley, K. J., Revill, K., Whitby, P., Clayton, R. N., Farrell, W. E. Genome-wide analysis in a murine Dnmt1 knockdown model identifies epigenetically silenced genes in primary human pituitary tumors. *Molecular Cancer Research* **2008**, 6, 1567-1574.

570. Valente, S., Liu, Y., Schnekenburger, M., Zwergel, C., Cosconati, S., Gros, C., Tardugno, M., Labella, D., Florean, C., Minden, S., Hashimoto, H., Chang,Y., Zhang, X., Kirsch, G., Novellino, E., Arimondo, P.B., Miele, E., Ferretti, E., Gulino, A., Diederich, M., Cheng, X., Mai, A. Selective non-nucleoside inhibitors of human dna methyltransferases active in cancer including cancer stem cells, *J Med Chem,* accepted.

571. You, J. S., Jones, P. A. Cancer genetics and epigenetics: two sides of the same coin? *Cancer Cell* **2012,** 22, 9-20.

572. Gros, C., Fahy, J., Halby, L., Dufau, I., Erdmann, A., Gregoire, J. M., Ausseil, F., Vispe, S., Arimondo, P. B. DNA methylation inhibitors in cancer: recent and future approaches. *Biochimie* **2012,** 94, 2280-2296.
573. Mai, A., Cheng, D., Bedford, M. T., Valente, S., Nebbioso, A., Perrone, A., Brosch, G., Sbardella, G., De Bellis, F., Miceli, M., Altucci, L. Epigenetic multiple ligands: mixed histone/protein methyltransferase, acetyltransferase, and class III deacetylase (sirtuin) inhibitors. *J. Med. Chem.* **2008,** 51, 2279-2290.
574. Cheng, D., Valente, S., Castellano, S., Sbardella, G., Di Santo, R., Costi, R., Bedford, M. T., Mai, A. Novel 3,5-bis(bromohydroxybenzylidene)piperidin-4-ones as coactivator-associated arginine methyltransferase 1 inhibitors: enzyme selectivity and cellular activity. *J. Med. Chem.* **2011,** 54, 4928-4932.
575. Chang, Y., Ganesh, T., Horton, J. R., Spannhoff, A., Liu, J., Sun, A., Zhang, X., Bedford, M. T., Shinkai, Y., Snyder, J. P., Cheng, X. Adding a lysine mimic in the design of potent inhibitors of histone lysine methyltransferases. *J. Mol. Biol.* **2010,** 400, 1-7.
576. Upadhyay, A. K., Rotili, D., Han, J. W., Hu, R., Chang, Y., Labella, D., Zhang, X., Yoon, Y. S., Mai, A., Cheng, X. An analog of BIX-01294 selectively inhibits a family of histone H3 lysine 9 Jumonji demethylases. *J. Mol. Biol.* **2012,** 416, 319-327.
577. Vedadi, M., Barsyte-Lovejoy, D., Liu, F., Rival-Gervier, S., Allali-Hassani, A., Labrie, V., Wigle, T. J., Dimaggio, P. A., Wasney, G. A., Siarheyeva, A., Dong, A., Tempel, W., Wang, S. C., Chen, X., Chau, I., Mangano, T. J., Huang, X. P., Simpson, C. D., Pattenden, S. G., Norris, J. L., Kireev, D. B., Tripathy, A., Edwards, A., Roth, B. L., Janzen, W. P., Garcia, B. A., Petronis, A., Ellis, J., Brown, P. J., Frye, S. V., Arrowsmith, C. H., Jin, J. A chemical probe selectively inhibits G9a and GLP methyltransferase activity in cells. *Nat. Chem. Biol.* **2011,** 7, 566-574.
578. DeRuiter, J., Brubaker, A. N., Millen, J., Riley, T. N. Design and synthesis of 2-(arylamino)- 4(3*H*)-quinazolinones as novel inhibitors of rat lens aldose reductase. *J. Med. Chem.* **1986,** 29, 627-629.
579. Lee, B. H., Yegnasubramanian, S., Lin, X., Nelson, W. G. Procainamide is a specific inhibitor of DNA methyltransferase 1. *J. Biol. Chem.* **2005**, 280, 40749-40756.
580. Gros, C., Chauvigné, L., Poulet, A., Menon, Y., Ausseil, F., Dufau, I., Arimondo, P. B. Development of a universal radioactive DNA methyltransferase inhibition test for high-throughput screening and mechanistic studies. *Nucleic Acids Res.* **2013**, 41, e185.
581. Ceccaldi, A., Rajavelu, A., Champion, C., Rampon, C., Jurkowska, R., Jankevicius, G., Senamaud-Beaufort, C., Ponger, L., Gagey, N., Ali, H. D., Tost, J., Vriz, S., Ros, S., Dauzonne, D., Jeltsch, A., Guianvarc'h, D., Arimondo, P. B. C5-DNA methyltransferase inhibitors: from screening to effects on zebrafish embryo development. *ChemBioChem* **2011**, 12, 1337-1345.

582. Yoo, J., Choi, S., Medina-Franco, J. L. Molecular modeling studies of the novel inhibitors of DNA methyltransferases SGI-1027 and CBC12: implications for the mechanism of inhibition of DNMTs. *PloS One* **2013,** 8, e62152.

583. Rotili, D., Tarantino, D., Marrocco, B., Gros, C., Masson, V., Gregoire, J-M., Ausseil, F., Chang, Y., Labella, D., Cosconati, S., Di Maro, S., Novellino, E., Schnekenburger, M., Grandjenette, C., Bouvy, C., Diederich, M., Cheng, X., Arimondo, P. B., Mai. A. Identification of Quinazoline Analogues as Novel DNA methyltransferase 3A Inhibitors. *J Med Chem* submitted.

584. a) Mai, A., Small-molecule chromatin-modifying agents: therapeutic applications. *Epigenomics* **2010**, 2, 307-324; b) Conte, M., Altucci, L. Molecular pathways: the complexity of the epigenome in cancer and recent clinical advances. *Clin. Cancer Res.* **2012**, 18, 5526-5534.

585. Spiegel, S., Milstien, S., Grant, S. Endogenous modulators and pharmacological inhibitors of histone deacetylases in cancer therapy. *Oncogene* **2011**, 31, 537-551.

586. a) Mai, A., Massa, S., Ragno, R., Esposito, M., Sbardella, G., Nocca, G., Brosch, G. Binding mode analysis of 3-(4-benzoyl-1-methyl-1 H-2-pyrrolyl)-N-hydroxy-2-propenamide: a new synthetic histone deacetylase inhibitor inducing histone hyperacetylation, growth inhibition, and terminal cell differentiation. *J Med Chem* **2002**, *45*(9), 1778-1784. b) Mai, A., Massa, S., Ragno, R., Cerbara, I., Jesacher, F., Loidl, P., Brosch, G. 3-(4-Aroyl-1-methyl-1 H-2-pyrrolyl)-N-hydroxy-2-alkylamides as a new class of synthetic histone deacetylase inhibitors. 1. Design, synthesis, biological evaluation, and binding mode studies performed through three different docking procedures. *J Med Chem* **2003**, 46, 512-524. c) Ragno, R., Mai, A., Massa, S., Cerbara, I., Valente, S., Bottoni, P.,Brosch, G. 3-(4-Aroyl-1-methyl-1 H-pyrrol-2-yl)-N-hydroxy-2-propenamides as a new class of synthetic histone deacetylase inhibitors. 3. discovery of novel lead compounds through structure-based drug design and docking studies. *J Med Chem* **2004**, 47, 1351-1359. d) Mai, A., Massa, S., Valente, S., Simeoni, S., Ragno, R., Bottoni, P., Brosch, G. Aroyl-Pyrrolyl Hydroxyamides: Influence of pyrrole C4-phenylacetyl substitution on histone deacetylase inhibition. *ChemMedChem* **2006**, 1, 225-237. e) Valente, S., Tardugno, M., Conte, M., Cirilli, R., Perrone, A., Ragno, R., Mai, A. Novel cinnamyl hydroxyamides and 2-aminoanilides as histone deacetylase inhibitors: apoptotic induction and cytodifferentiation activity. *ChemMedChem* **2011**, 6, 698-712.

587. a) Mai, A., Massa, S., Pezzi, R., Valente, S., Loidl, P., Brosch, G. Synthesis and biological evaluation of 2-, 3-, and 4-acylaminocinnamyl-nhydroxyamides as novel synthetic HDAC inhibitors. *Medicinal Chemistry* **2005**, 1, 245-254; b) Varasi, M., Thaler, F., Abate, A., Bigogno, C., Boggio, R., Carenzi, G., Mai A., Mercurio, C. Discovery, synthesis, and pharmacological evaluation of spiropiperidine hydroxamic acid based derivatives as structurally novel histone deacetylase (HDAC) inhibitors. *J Med Chem* **2011**, 54, 3051-3064;

588. a) Mai, A., Jelicic, K., Rotili, D., Di Noia, A., Alfani, E., Valente, S., Migliaccio, G. Identification of two new synthetic histone deacetylase inhibitors that modulate globin gene expression in erythroid cells from healthy donors and patients with thalassemia. *Mol. Pharmacol.* **2007**, 72, 1111-1123; b) Mai, A., Perrone, A., Nebbioso, A., Rotili, D., Valente, S., Tardugno, M., Massa S., De Bellis L., Altucci, L. Novel uracil-based 2-aminoanilide and 2-aminoanilide-like derivatives: Histone deacetylase inhibition and in-cell activities. *Bioorg. Med. Chem. Lett.* **2008**, 18, 2530-2535.

589. Itoh, Y., Suzuki, T., Kouketsu, A., Suzuki, N., Maeda, S., Yoshida, M., Miyata, N. Design, synthesis, structure-selectivity relationship, and effect on human cancer cells of a novel series of histone deacetylase 6-selective inhibitors. *Journal of medicinal chemistry* **2007**, 50, 5425-5438.

590. Valente, S., Trisciuoglio, D., Tardugno, M., Benedetti, R., Labella, D., Secci, D., Mercurio, C., Boggio, R., Tomassi, S., Di Maro, S, Novellino, E., Altucci, L., Del Bufalo, D., Mai, A., Cosconati, S. tert-Butylcarbamate-containing histone deacetylase inhibitors: apoptosis induction, cytodifferentiation, and antiproliferative activities in cancer cells. *ChemMedChem* **2013**, 8, 800-811.

591. Mai, A., Massa, S., Pezzi, R., Simeoni, S., Rotili, D., Nebbioso, A., Brosch, G. Class II (IIa)-selective histone deacetylase inhibitors. 1. Synthesis and biological evaluation of novel (aryloxopropenyl) pyrrolyl hydroxyamides. *Journal of medicinal chemistry*, **2005**, 48, 3344-3353.

592. Lahm, A., Paolini, C., Pallaoro, M., Nardi, M. C., Jones, P., Neddermann, P., Gallinari, P. Unraveling the hidden catalytic activity of vertebrate class IIa histone deacetylases. *Proceedings of the National Academy of Sciences* **2007**, 104, 17335-17340.

593. Zou, H., Wu, Y., Navre, M., Sang, B. C. Characterization of the two catalytic domains in histone deacetylase 6. *Biochemical and biophysical research communications* **2006**, 341, 45-50.

594. Roy, A., Kucukural, A., Zhang, Y. I-TASSER: a unified platform for automated protein structure and function prediction. *Nature protocols* **2010**, 5, 725-738.

595. Butler, K. V., Kalin, J., Brochier, C., Vistoli, G., Langley, B., Kozikowski, A. P. Rational design and simple chemistry yield a superior, neuroprotective HDAC6 inhibitor, tubastatin A. *Journal of the American Chemical Society* **2010**, 132, 10842-10846.

596. Schuetz, A., Min, J., Allali-Hassani, A., Schapira, M., Shuen, M., Loppnau, P., Vedavi M. Arrowsmith, C. H. Human HDAC7 harbors a class IIa histone deacetylase-specific zinc binding motif and cryptic deacetylase activity. *Journal of Biological Chemistry* **2008**, 283, 11355-11363.

597. Hess-Stumpp, H., Bracker, T. U., Henderson, D., Politz, O. MS-275, a potent orally available inhibitor of histone deacetylases the development of an anticancer agent. *The international journal of biochemistry & cell biology* **2007**, 39, 1388-1405.

598. Nebbioso, A., Clarke, N., Voltz, E., Germain, E., Ambrosino, C., Bontempo, P., Altucci, L. Tumor-selective action of HDAC inhibitors involves TRAIL induction in acute myeloid leukemia cells. *Nature medicine* **2004**, 11, 77-84.
599. Auzzas, L., Larsson, A., Matera, R., Baraldi, A., Deschênes-Simard, B., Giannini, G., Hanessian, S. Non-natural macrocyclic inhibitors of histone deacetylases: design, synthesis, and activity. *Journal of medicinal chemistry* **2010**, 53, 8387-8399.
600. Li, Y., Shin, D., & Kwon, S. H. Histone deacetylase 6 plays a role as a distinct regulator of diverse cellular processes. *FEBS Journal* **2013**, 280, 775-793.
601. Rotili, D., Mai, A. Targeting histone demethylases: a new avenue for the fight against cancer. *Genes Cancer* **2011**, 2, 663-679.
602. Sams-Dodd, F. Target-based drug discovery: is something wrong? *Drug Discov. Today* **2005**, 10,139-147.
603. Rather, M. A., Bhat, B. A., Qurishi, M. A. Multicomponent phytotherapeutic approach gaining momentum: Is the "one drug to fit all" model breaking down?. *Phytomedicine* **2013**, 21, 1-14.
604. Morphy, R., Rankovic, Z. Designed Multiple Ligands. An Emerging Drug Discovery Paradigm. *J.Med. Chem*. **2005**, 48, 6523-6543.
605. Zimmerman, G. R., Lehar, J., Keith, C. T. Multi-target therapeutics: when the whole is greater than the sum of the parts. *Drug Discov. Today* **2007**, 12, 34-42.
606. Hopkinson, R. J., Tumber, A., Yapp, C., Chowdhury, R., Aik, W., Che, K. H., Li, X. S., Kristensen,J. B. L., King, O. N. F., Chan, M. C., Yeoh, K. K., Choi, H., Walport, L. J., Thinnes, C. C., Bush, J. T., Lejeune, C., Rydzik, A. M., Rose, N. R., Bagg, E. A., McDonough, M. A., Krojer, T. J., Yue, W. W., Ng, S. S., Olsen, L., Butler, E. S., Opperman, U., Muller, S., Klose, R. J., Ratcliffe, P. J., Schofield, C. J., Kawamura, A. 5-Carboxy-8-hydroxyquinoline is a broad spectrum 2-oxoglutarate oxygenase inhibitor which causes iron translocation. *Chem. Sci*. **2013**, 4, 3110-3117.
607. Gros, L, Lorente, S. O., Jimenez, C. J., Yardley, V., Rattray, L., Wharton, H., Little, S., Croft, S. L., Ruiz-Perez, L. M., Gonzalez-Pacanowska, D., Gilbert, I. H. Evaluation of azasterols as anti-parasitics. *J. Med. Chem*. **2006**, 49, 6094-6103.
608. Rose, N. R., Woon, E. C., Tumber, A., Walport, L. J., Chowdhury, R., Li, X. S., King, O. N., Lejeune, C., Ng, S. S., Krojer, T., Chan, M. C., Rydzik, A. M., Hopkinson, R. J., Che, K. H., Daniel, M., Strain-Damerell, C., Gileadi, C., Kochan, G., Leung, I. K., Dunford, J., Yeoh, K. K., Ratcliffe, P. J., Burgess-Brown, N., von Delft, F.; Muller, S., Marsden, B., Brennan, P. E., McDonough, M. A., Oppermann, U., Klose, R. J., Schofield, C. J., Kawamura, A. Plant growth regulator daminozide is a selective inhibitor of human KDM2/7 histone demethylases. *J. Med. Chem*. **2012**, 55, 6639-6643.
609. Kerenyi, M. A., Shao, Z., Hsu, Y. J., Guo, G., Luc, S., O'Brien, K., Fujiwara, Y., Peng, C., Nguyen, M., Orkin, S. H. Histone demethylase Lsd1 represses

hematopoietic stem and progenitor cell signatures during blood cell maturation. *Elife* **2013**, 2, e00633.

610. Schenk, T., Chen, W. C., Gollner, S., Howell, L., Jin, L., Hebestreit, K., Klein, H. U., Popescu, A. C., Burnett, A., Mills, K., Casero, R. A. Jr., Marton, L., Woster, P., Minden, M. D., Dugas, M., Wang, J. C., Dick, J. E., Muller-Tidow, C., Petrie, K., Zelent, A. Inhibition of the LSD1 (KDM1A) demethylase reactivates the all-trans-retinoic acid differentiation pathway in acute myeloid eukemia. *Nat. Med*. **2012**, 18, 605-611.
611. Miceli, M., Franci, G., Dell'Aversana, C., Ricciardiello, F., Petraglia, F., Carissimo, A., Perone, L., Maruotti, G. M., Savarese, M., Martinelli, P., Cancemi, M., Altucci, L. MePR: a novel human mesenchymal progenitor model with characteristics of pluripotency. *Stem Cells Dev*. **2013**, 22, 2368-2383.
612. Rotili, D., Tomassi, S., Conte, M., Benedetti, R., Tortorici, M., Ciossani, G., Valente, S., Marrocco, B., Labella, D., Novellino, E., Mattevi, A., Altucci, L., Tumber, A., Yapp, C., King, O. N. F., Hopkinson, R. J., Kawamura, A., Schofield, C. J., Mai. A. Pan-histone demethylase inhibitors simultaneously targeting Jumonji C and lysine specific demethylases display high anticancer activities. *J Med Chem*, accepted.
613. Kubicek, S., O'Sullivan, R. J., August, E. M., Hickey, E. R., Zhang, Q., Teodoro, M. L., Jenuwein, T. Reversal of H3K9me2 by a small-molecule inhibitor for the G9a histone methyltransferase. *Molecular cell* **2007**, 25, 473-481.
614. Liu, F., Chen, X., Allali-Hassani, A., Quinn, A. M., Wasney, G. A., Dong, A., Jin, J. Discovery of a 2, 4-diamino-7-aminoalkoxyquinazoline as a potent and selective inhibitor of histone lysine methyltransferase G9a. *Journal of medicinal chemistry* **2009**, 52, 7950-7953.
615. Liu, F., Barsyte-Lovejoy, D., Allali-Hassani, A., He, Y., Herold, J. M., Chen, X., Jin, J. Optimization of cellular activity of G9a inhibitors 7-aminoalkoxy-quinazolines. *Journal of medicinal chemistry* **2011**, 54, 6139-6150.
616. Kleefstra, T., Brunner, H. G., Amiel, J., Oudakker, A. R., Nillesen, W. M., Magee, A., van Bokhoven, H. Loss-of-function mutations in euchromatin histone methyl transferase 1 (EHMT1) cause the 9q34 subtelomeric deletion syndrome. *The American Journal of Human Genetics* **2006**, 79, 370-377.
617. Iwase, S., Lan, F., Bayliss, P., de la Torre-Ubieta, L., Huarte, M., Qi, H. H., Shi, Y. The X-linked mental retardation gene SMCX/JARID1C defines a family of histone H3 lysine 4 demethylases. *Cell* **2007**, 128, 1077-1088.
618. Lee, J. H., Lee, B. S., Shin, H., Chi, D. Y. Acetonitrile-mediated synthesis of 2, 4-dichloroquinoline from 2-ethynylaniline and 2, 4-dichloroquinazoline from anthranilonitrile. *Synlett*, **2006**, 65-68.
619. Studier, F. W. Protein production by auto-induction in high density shaking cultures. *Protein Expr Purif* **2005**, 41, 207-234.
620. Hirao, M., Posakony, J., Nelson, M., Hruby, H., Jung, M., Simon, J. A., Bedalov, A. Identification of selective inhibitors of NAD^+-dependent

deacetylases using phenotypic screens in yeast. *Journal of Biological Chemistry* **2003**, 278, 52773-52782.

621. Kaeberlein, M., McDonagh, T., Heltweg, B., Hixon, J., Westman, E. A., Caldwell, S. D., Kennedy, B. K. Substrate-specific activation of sirtuins by resveratrol. *Journal of Biological Chemistry* **2005**, 280, 17038-17045.
622. Borra, M. T., Langer, M. R., Slama, J. T., Denu, J. M. Substrate specificity and kinetic mechanism of the Sir2 family of NAD^+-dependent histone/protein deacetylases. *Biochemistry* **2004**, 43, 9877-9887.
623. Borra, M. T., Denu, J. M. Quantitative assays for characterization of the sir2 family of NAD^+-dependent deacetylases. *Methods in enzymology* **2003**, 376, 171-187.
624. Heltweg, B., Trapp, J., Jung, M. In vitro assays for the determination of histone deacetylase activity. *Methods* **2005**, 36, 332-337.
625. de Boer, V. C., de Goffau, M. C., Arts, I. C., Hollman, P. C., Keijer, J. SIRT1 stimulation by polyphenols is affected by their stability and metabolism. *Mechanisms of ageing and development* **2006**, 127, 618-627.
626. Marcotte, P. A., Richardson, P. R., Guo, J., Barrett, L. W., Xu, N., Gunasekera, A., Glaser, K. B. Fluorescence assay of SIRT protein deacetylases using an acetylated peptide substrate and a secondary trypsin reaction. *Analytical biochemistry* **2004**, 332, 90-99.
627. Liu, Y., Gerber, R., Wu, J., Tsuruda, T., McCarter, J. D. High-throughput assays for sirtuin enzymes: a microfluidic mobility shift assay and a bioluminescence assay. *Analytical biochemistry* **2008**, 378, 53-59.
628. Fan, Y., Ludewig, R., Imhof, D., Scriba, G. K. Development of a capillary electrophoresis-based assay of sirtuin enzymes. *Electrophoresis* **2008**, 29, 3717-3723.
629. Fan, Y., Ludewig, R., Scriba, G. K. 9-Fluorenylmethoxycarbonyl-labeled peptides as substrates in a capillary electrophoresis-based assay for sirtuin enzymes. *Analytical biochemistry* **2009**, 387, 243-248.
630. Smith, B. C., Hallows, W. C., Denu, J. M. A continuous microplate assay for sirtuins and nicotinamide-producing enzymes. *Analytical biochemistry* **2009**, 394, 101-109.
631. Feng, Y., Wu, J., Chen, L., Luo, C., Shen, X., Chen, K., Liu, D. A fluorometric assay of SIRT1 deacetylation activity through quantification of nicotinamide adenine dinucleotide. *Analytical biochemistry* **2009**, 395, 205-210.
632. Wegener, D., Hildmann, C., Riester, D., Schwienhorst, A. Improved fluorogenic histone deacetylase assay for high-throughput-screening applications. *Analytical biochemistry* **2003**, 321, 202-208.
633. Lakshminarasimhan, M., Rauh, D., Schutkowski, M., & Steegborn, C. (2013). Sirt1 activation by resveratrol is substrate sequence-selective. *Aging (Albany NY)*, *5*(3), 151.
634. He B, Du J, Lin H., Thiosuccinyl Peptides as Sirt5-Specific Inhibitors. *Journal of the American Chemical Society* **2012**, 134, 1922-1925.

635. Huber, K., Schemies, J., Uciechowska, U., Wagner, J. M., Rumpf, T., Lewrick, F., Bracher, F. Novel 3-arylideneindolin-2-ones as inhibitors of NAD^+-dependent histone deacetylases (sirtuins). *Journal of medicinal chemistry* **2009**, 53, 1383-1386.
636. Bradford, M. M. A rapid and sensitive method for the quantitation of microgram quantities of protein utilizing the principle of protein-dye binding. *Analytical biochemistry* **1976**, 72, 248-254.

15. Acknowledgements

First and foremost I want to thank my supervisor Prof. Antonello Mai. It has been an honor to be his Ph.D. student. He has introduced me to "the wonderland of Epigenetics" since I was a graduate student. I appreciate all his contributions of time, ideas, and funding to make my Ph.D. experience productive and stimulating. I would also like to express my sincere thanks to Dr. Dante Rotili and Dr. Sergio Valente for all them constant support and excellent scientific discussions.

I am thankful to Prof. Clemens Steegborn, for providing me the opportunity to work in his laboratory with exciting research topics. I would also like to thank all the members of the biochemistry department, University of Bayreuth, Germany for all the support and a good working atmosphere.

I will always be grateful to "Neverlab" group members, past and present, for their unconditional help, insightful discussions, and friendship. In particular, I would like to thank Maria Tardugno, Stefano Tomassi, Clemens Zwergel, Paolo Mellini and Biagina Marrocco and Alessia Lenoci for their help for my research.

Finally I wish to thank my family and friends for their infinite love and support that made all of the above possible.

“Imagination is more important than knowledge.
Knowledge is limited.
Imagination encircles the world.”